

**UCLA**

**UCLA Electronic Theses and Dissertations**

**Title**

Photochemistry and Kinetic Analysis of Radical Pairs from  $\alpha$ -Aryl-Substituted Ketones in Solution and in Nanocrystalline Suspensions

**Permalink**

<https://escholarship.org/uc/item/4ws623sf>

**Author**

Park, Jin

**Publication Date**

2018

Peer reviewed|Thesis/dissertation

UNIVERSITY OF CALIFORNIA

Los Angeles

Photochemistry and Kinetic Analysis of Radical Pairs from  $\alpha$ -Aryl-Substituted Ketones in  
Solution and in Nanocrystalline Suspensions

A dissertation submitted in partial satisfaction of the requirements for the degree  
Doctor of Philosophy in Chemistry

by

Jin Hong Park

2018

© Copyright by

Jin Hong Park

2018

## ABSTRACT OF THE DISSERTATION

Photochemistry and Kinetic Analysis of Radical Pairs from  $\alpha$ -Aryl-Substituted Ketones in  
Solution and in Nanocrystalline Suspensions

by

Jin Hong Park

Doctor of Philosophy in Chemistry

University of California, Los Angeles, 2018

Professor Miguel A. Garcia-Garibay, Chair

Through years of development and refinement, solid-state photochemistry has been proven to be a powerful tool in many fields of science. This is because in comparison to solution-state photochemistry, molecules that react in the solid-state are trapped in their crystal cavity, which limits the number of reactive chemical pathways that these reactants are able to explore. In many cases, this phenomenon induces desirable reaction characteristics such as high stereospecificity and regiospecificity and high product yield due to the minimal formation of side products. However, the utility of solid-state photochemistry has been limited because of a lack of

readily accessible methods to analyze and observe reactions in the solid-state. Although literature precedence reveals significant efforts to understand the mechanistic aspects of solid-state photochemical reactions, primarily by comparison of crystallographic data of the reactants and products, the use of pulsed-laser techniques to analyze the formation of excited states and transient intermediates is currently limited by challenges arising from the optical properties of bulk solids. Therefore, in order to develop a more powerful method to extract kinetic information of photochemical solid-state reactions, our research group has developed the use of nanocrystalline suspensions as a means to overcome the physical limitations of bulk solids. We have shown that nanocrystals suspended in water approach the properties of supramolecular systems and reduce many of the challenges associated with the high optical densities, light scattering and birefringence of solids. By taking advantage of a one-way flow system the use of nanocrystalline suspension also limits the potential interference from photoproduct build-up. Thus, in order to further elucidate a useful method for determining kinetic information, this dissertation offers a novel perspective to enhance the field of solid-state photochemistry via reporting the photochemistry and kinetic analysis of various  $\alpha$ -phenyl substituted ketones in solution and in nanocrystalline suspensions.

Chapter one serves as an overview of solid-state photochemistry and the overall development of the field by highlighting important milestones throughout history. It will also mention and credit recent efforts as well as the limitations regarding the extraction of kinetic information of photochemical reactions in the solid-state.

Chapter two addresses the nanosecond electronic spectra and kinetics of the triplet radical pairs from various crystalline  $\alpha$ ,  $\alpha'$ ,  $\alpha''$ ,  $\alpha'''$ -tetraarylacetonones by taking advantage of aqueous nanocrystalline suspensions. The compounds selected were  $\alpha$ ,  $\alpha'$ ,  $\alpha''$ ,  $\alpha'''$ -tetraarylacetonones

para substituted with -proton, -methyl, -chloro, -fluoro, and methoxy in order to alter the electronic density of the ketone. After showing that all tetraarylacetonates react efficiently by a photodecarbonylation reaction in the crystalline state, we were able to detect the intermediate diphenylmethyl radical pairs and show that the solid-state spectra of the radical pairs are very similar to those detected in solution. This work also demonstrates that detection of the radical pairs can be performed consistently for several derivatives. In addition, our studies indicate that the kinetics for all of the derivatives in the nanocrystalline suspensions exhibit a biexponential decay. (DOI: 10.1021/jacs.7b04449)

Chapter three further expands the scope of these tetraarylacetonates by exploring the kinetics of the intersystem crossing rates of diphenylmethyl radical pairs generated upon photolysis. Specifically, we designed tetraarylacetonates with various bulky substituents at the *para*-phenyl positions to explore how the bulkiness will alter the lifetime of the triplet diphenylmethyl radical pairs in the solid. The current hypothesis is that the extra bulk would increase the degrees of freedom inside the crystal; this would allow the triple radical species of the diphenylmethyl radical pairs to rotate more freely increasing the fluidity and thus allowing a more favorable intersystem crossing step. The current data supports this hypothesis where the lifetimes of the -H, -Me, -tBu *para*-phenyl substituted acetones decrease from 70  $\mu\text{s}$  > 50  $\mu\text{s}$  > 32  $\mu\text{s}$  with additional bulk.

Chapter four describes the study of kinetics on non-symmetrical  $\alpha$ -alkyl,  $\alpha$ -aryl substituted ketones to demonstrate if the kinetics of triple radical pairs of different stability will have an impact on the solid-state lifetime. To our surprise, the data indicates that the lifetimes of the studied ketones exhibit similar lifetimes. In addition, this work proposes that the quantum yield of all the derivatives are at around 30% conversion. Therefore, by combining the knowing

that this photoreaction yields a single photoproduct, a more possible mechanistic pathway for the photodecarbonylation of  $\alpha$ -alkyl,  $\alpha$ -aryl substituted ketones is one that would also include a pathway to funnel back to the starting compound. (Manuscript ID: Ja-2018-032479)

Chapter five explains the work done on probing the lifetimes of ketones with a diphenylmethyl handle at one  $\alpha$  position and alkyl, aryl substituents at the other  $\alpha$  position. Upon irradiation, these ketones will absorb a photon and reach the excited state. At this stage, the ketones can undergo an intersystem crossing from the singlet to the triplet state. The ketones then undergo an initial  $\alpha$ -cleavage of the weaker carbon-carbon bond to form the first triplet radical pair. Next, if a second  $\alpha$ -cleavage is favorable, the ketone will undergo a second carbon-carbon homolytic cleavage, ultimately forming a new triplet radical pair. However, in the event that the second  $\alpha$ -cleavage is unfavorable, the triplet radical undergoes an intersystem crossing to the singlet radical pair which instantaneously leads to the recombination of the initial carbon-carbon bond cleavage to form the starting material. For this study, most of the ketones were specifically engineered to not be able to reach the second  $\alpha$ -cleavage step forcing the diphenylmethyl-acyl radical pair to regenerate the starting ketone. By detecting the lifetime of the diphenylmethyl radical, this work confirms that these ketones after irradiation are indeed reacting to regenerate the starting compound in the solid-state and not simply unreacted starting material.

The dissertation of Jin Hong Park is approved.

Neil Garg

Nanthia Suthana

Miguel A. Garcia-Garibay, Committee Chair

University of California, Los Angeles

2018



*To my family, friends, and especially my parents for their endless support, love, and sacrifice*

## Table of contents

<b>Chapter 1. Solid-State Organic Photochemistry and Nanocrystalline suspensions.....</b>	<b>1</b>
1.1 Overview and Background.....	2
1.2 Solid-State Photochemistry and the Topochemical Postulate.....	2
1.3 Determination and Observation of Transient Intermediates in Crystals .....	5
1.4 Nanocrystalline Suspensions in Surfactant.....	7
1.5 Conclusion .....	9
1.6 References.....	11
<b>Chapter 2. Generation and Reactivity Studies of Diarylmethyl Radical Pairs in Crystalline Tetraarylacetones via Laser Flash Photolysis Using Nanocrystalline Suspensions.....</b>	<b>14</b>
2.1 Introduction .....	15
2.2 Results and Discussion.....	16
2.3 Conclusions.....	25
2.4 Experimental Section .....	26
2.5 Supplementary Information .....	28
2.6 References.....	95
<b>Chapter 3. Solid-State Photochemistry of Diphenylmethyl Radical Pairs in Nanocrystalline Suspensions Reveal a Correlation between Steric Bulk and Kinetics via Laser Flash Photolysis.....</b>	<b>99</b>
3.1 Introduction.....	100
3.2 Results and Discussion.....	101
3.3 Conclusions.....	107
3.4 Experimental Section.....	108

3.5	Supplementary Information.....	109
3.6	References .....	145
<b>Chapter 4. Transient Kinetics and Quantum Yield Studies of Nanocrystalline <math>\alpha</math>-Phenyl-</b>		
<b>Substituted Ketones: Sorting Out Reactions from Singlet and Triplet Excited States.....</b>		
4.1	Introduction.....	149
4.2	Results and Discussion.....	151
4.3	Conclusion.....	162
4.4	Experimental Section .....	163
4.5	Supplementary Information.....	165
4.6	References.....	205
<b>Chapter 5. Laser Flash Photolysis studies of a Photo-Induced Aryl-Acyl Radical Pair's</b>		
<b>Recombination Rates in Nanocrystalline Suspensions .....</b>		
5.1	Introduction.....	210
5.2	Results and Discussion.....	212
5.3	Conclusion.....	219
5.4	Supplementary Figures.....	221
5.5	References.....	274

## List of Schemes

1.2.1 .....	3
1.2.2 .....	4
1.3.1 .....	6
2.1.1 .....	15
2.2.1 .....	16
2.2.3 .....	18
3.1.1 .....	101
3.2.1 .....	102
4.1.1 .....	150
4.2.1 .....	151
4.2.3 .....	155
4.2.4 .....	160
5.1.1.....	211
5.1.2 .....	212

## List of Figures

<b>Figure 1.4.1</b> Dynamic light scattering spectrum of Tetraphenylacetone .....	8
<b>Figure 1.4.2</b> Dynamic light scattering spectrum of Tetraphenylacetone .....	9
<b>Figure 2.2.1</b> Powder X-ray diffraction of (A) recrystallized 1a in ethanol and (B) nanocrystals of 1a prepared by precipitation and collected by centrifugation, (C) product 4a obtained in situ by exposure of 1a to UV light of bulk solids, and (D) recrystallized samples of 4a in ethanol-.....	18
<b>Figure 2.2.2</b> Absorption spectra of 0.1 g/L tetraphenylacetone 1a in MeCN (red line) and an aqueous nanocrystalline suspension of 1a 0.025g/L in the presence of submicellar CTAB (green line). .....	19
<b>Figure 2.2.3</b> Time-dependent spectra of tetraphenylacetone 1a in MeCN collected between 0 and 16.1 $\mu$ s ( $\lambda_{\text{max}} = 330$ nm). Inset: Transient decay of 1a measured in MeCN at 298 K at $\lambda_{\text{max}} = 330$ nm.....	20
<b>Figure 2.2.4</b> Transient spectra of tetraphenylacetone 1a in the solid-state photoreaction with a $\lambda_{\text{max}}$ (apparent) $\approx 340$ nm. Inset: Decay of 1a in the nanocrystalline suspension detected at 340 nm. ....	22
<b>Figure 3.2.1.</b> Powder X-ray diffraction (PXRD) of 1c (A) bulk-powder, (B) nanocrystals, (C) as-formed photoproduct, (D) recrystallized photoproduct .....	103
<b>Figure 3.2.2.</b> Normalized UV spectra of 1c in solution (0.01 g/L) and, nanocrystalline suspension of 1c in cetyltrimethylammonium bromide (CTAB) surfactant (0.025 g/L). .....	104
<b>Figure 3.2.3.</b> Transient absorption spectra of 1c in MeCN ( $\lambda_{\text{max}} = 340$ nm). .....	105
<b>Figure 3.2.4.</b> Transient absorption spectra of 1c in MeCN ( $\lambda_{\text{max}} = 340$ nm). .....	105
<b>Figure 3.2.5.</b> Transient spectra of 1c in a nanocrystalline suspension ( $\lambda_{\text{max}} = 350$ nm). .....	106

<b>Figure 3.2.6.</b> Transient decay profile of <b>1c</b> in the solid-state via nanocrystalline suspensions ( $\lambda_{\text{max}} = 350 \text{ nm}$ ). .....	106
<b>Figure 4.2.1</b> Powder X-ray diffraction (PXRD) of <b>1b</b> (A) bulk-powder, (B) nanocrystals, (C) as-formed photoproduct, (D) recrystallized photoproduct. ....	153
<b>Figure 4.2.2</b> (Solid red line) Normalized UV spectra of <b>1b</b> in solution (0.01 g/L) and, (dashed blue line) nanocrystalline suspension of <b>1b</b> in cetyltrimethylammonium bromide (CTAB) surfactant (0.025 g/L). ....	153
<b>Figure 4.2.3</b> Transient absorption spectra of <b>1b</b> in MeCN ( $\lambda_{\text{max}} = 330 \text{ nm}$ ). ....	156
<b>Figure 4.2.4</b> Transient decay profile of <b>1b</b> in MeCN ( $\lambda_{\text{max}} = 330 \text{ nm}$ ). ....	157
<b>Figure 4.2.5</b> Transient spectra of <b>1b</b> in a nanocrystalline suspension ( $\lambda_{\text{max}} = 340 \text{ nm}$ ). ....	158
<b>Figure 4.2.6</b> Transient decay profile of <b>1b</b> in the solid-state via nanocrystalline suspensions at $\lambda_{\text{max}} = 340 \text{ nm}$ . ....	159
<b>Figure 5.2.1</b> Powdered X-Ray Diffractogram of 1,1,3-triphenylpropan-2-one in bulk solid (A) and Nanocrystalline suspensions (B) .....	214
<b>Figure 5.2.2</b> Photochemical Product Analysis of 1,1,3-triphenylpropan-2-one in Acetonitrile and in Bulk Solid .....	215
<b>Figure 5.2.3</b> UV-Vis of 1,1,3-triphenylpropan-2-one in MeCN solution (blue) and solid state (red) .. ..	215
<b>Figure 5.2.4</b> Time-dependent spectra of 1,1,3-triphenylpropan-2-one in MeCN solution collected 0 and 8.01 us ( $\lambda_{\text{max}} = 320 \text{ nm}$ ) .....	216
<b>Figure 5.2.4</b> Time-dependent spectra of 1,1,3-triphenylpropan-2-one in MeCN solution collected 0 and 8.01 us ( $\lambda_{\text{max}} = 320 \text{ nm}$ ) .. ..	217

<b>Figure 5.2.6</b> Time-dependent spectra of 1,1,3-triphenylpropan-2-one in nanocrystalline suspensions collected 0 and 2.8 us ( $\lambda_{\text{max}} = 320$ nm) .....	218
<b>Figure 5.2.7</b> Transient decay of 1,1,3-triphenylpropan-2-one in nanocrystalline suspensions at 330 nm .....	219

## List of Tables

<b>Table 2.2.1</b> Melting temperatures and crystallite size of 1,1,3,3-tetraaryl acetones suspended in water .....	17
<b>Table 2.2.2</b> Spectroscopic and kinetic data from solution and nanocrystalline photoreactions of 1a-1e in a single pass flow cell .....	21
<b>Table 3.2.1.</b> Characterizations and Lifetimes of 4-Substituted Tetraphenylacetones .....	102
<b>Table 4.2.1</b> Characterizations and lifetimes of $\alpha$ -phenyl-substituted acetones .....	151
<b>Table 5.2.1:</b> Solid State Characterization of Ketones for Pre-Decarbonylation Studies .....	213



## List of Abbreviations

Ar	aryl
ca	approximately
CDCl <sub>3</sub>	deuterated chloroform
d	doublet (NMR)
<i>d</i>	deuterium
dd	doublet of doublets (NMR)
dq	doublet of quartet
DSC	differential scanning calorimetry
eq.	equivalent
<i>et al.</i>	<i>et alia</i>
FTIR	Fourier transformed infrared spectroscopy
g	gram
Hz	hertz
hr	hour
ISC	intersystem crossing
K	Kelvin
kcal	kilocalories
m	multiplet
MHz	megahertz
min	minute
mL	milliliter

mol	mole
m.p.	melting point
m/z	mass to charge ratio
NMR	nuclear magnetic resonance
ns	nanosecond
Ph	phenyl
PXRD	powder X-ray diffraction
ppm	parts per million
R	general alkyl group substituent
rt	room temperature
s	singlet (NMR)
sec	second
T	temperature
THF	tetrahydrofuran
TLC	thin layer chromatography
t	triplet (NMR)
t	time
UV-Vis	ultraviolet-visible spectroscopy
Å	angstrom
μs	microsecond

## Acknowledgements

I would like to first thank Professor Miguel Garcia-Garibay for all of the mentorship and guidance that he has provided me throughout my graduate school years. Entering a doctoral program with minimal background in organic chemistry, the past five years at UCLA was one of the most challenging, humbling, and memorable experience. Throughout my life I would never have guessed that I would even meet an individual with such knowledge, charisma, passion, creativity, and generosity. Even after decades of toil, every day he still strives to push his limits to the test. His unwavering work-ethic commands so much respect that it is difficult to fail under his wing. This being said, without Miguel's patience and guidance, the very thought of an individual with my particular background to achieve this feat is simply ludicrous. Again, I am forever grateful for his mentorship and for molding me into the individual I am today. In addition, I would also like to thank my committee members: Professors Neil Garg, Yi Tang, and Nanthia Suthana for their support and advice throughout my graduate career. Additionally, I would like to thank my undergraduate Prof. Catharine Larsen at UCR for conceiving and implanting the idea of pursuing a path in organic chemistry.

I would also like to thank my parents, Chan and Bok Park for acting as beacon. I am also grateful to my sister, Su Park, for her endless sacrifices and acting as the pillars of my success and defining what it is to be an honest and well-rounded person. I would also like to thank my childhood friends Sean Hung, Allen V. Tran, Eddie Vasquez, Stanley Hua, Kenny Luk, John Au, and Scott Hwang for collectively supporting me since day one of my program. In addition, I would also like to thank the members of the Garcia-Garibay family and peers at UCLA: Dr. Jesse Ko, Dr. Braulio Molina, Dr. Salvador Perez, Dr. Donghyuk Kim, Dr. Hochul Lee, Dr. Ira Staehle, Dr. Geeta Vadehra, Dr. Pat Commins, Dr. Xing Jiang, Dr. Tim Wolfgang Chung, Prof.

Jean-Luc Ayitou, Dr. Jee Yeon Hwang, Dr. Yuri Noh, Edris Rivera, Vince Hipwell, Jordan Dotson, Marcus Jellen, Trevor Chang, Mingoo Jin, Vanessa Breslin, Morgan Howe, Leadra Forte, Iris Xue, Ieva Liepuoniute, Annabell Cantu, Jeong Hoon Ko, Junyoung Kim, and Ha Song Kim for the all their support during and company in the program. Lastly, I would like thank Julia Haeyun Park, for being an amazing individual who supported me through this time of endeavor.

## VITA

- 2008-2012** B.S. Biochemistry: Medical Science Emphasis  
University of California, Riverside (UCR)
- 2010-2012** Undergraduate Research Assistant  
Chemistry Department  
University of California, Riverside (UCR)  
Advisor: Professor Catharine Larsen
- 2013** Competitive Edge Program:  
Summer Transition Program to the Doctorate  
University of California, Los Angeles (UCLA)
- 2013-2016** Eugene V. Cota Robles Fellowship  
University of California, Los Angeles (UCLA)
- 2014-2018** Graduate Division Fellowship  
University of California, Los Angeles (UCLA)
- 2013-2015** M.S. Chemistry  
University of California, Los Angeles (UCLA)  
Advisor: Professor Miguel Garcia-Garibay
- 2013-2018** Teaching Assistant  
University of California, Los Angeles (UCLA)
- 2013-2018** Research Assistant  
University of California, Los Angeles (UCLA)

## Publications

- 1). Chung, T. S.; Ayitou, A. J.-L.; Park, J. H.; Breslin, V. M.; Garcia-Garibay, M.A. "Photochemistry and Transmission Pump-Probe Spectroscopy of 2-Azidobiphenyls in Aqueous Nanocrystalline Suspensions: Simplified Kinetics in Crystalline Solids" *J. Phys. Chem. Lett.*, **2017**, 8, 1845–1850.
- 2). Park, J. H.; Hughs, M.; Chung, T.S.; Ayitou, A. J.-L.; Breslin, V. M.; Garcia-Garibay, M.A. "Generation and Reactivity Studies of Diarylmethyl Radical Paris in Crystalline Tetraarylacetonones via Laser Flash Photolysis using Nanocrystalline Suspensions" *J. Am. Chem. Soc.*, **2017**, 139, 13312-13317.
- 3). Chung, T. S.; Park, J. H.; Garcia-Garibay, M.A. "Kinetics and Mechanism of the Photodenitrogenation of  $\Delta^2$ -1,2,3-Triazolines to form Aziridines in Solution and in Solid-

State: Observation of the Triplet 1,3-Alkyl-aminyl Biradical” *J. Org. Chem.*, **2017**, *82*, 12128-12133.

4). Park, J. H.; Chung, T. S.; Hipwell, V. M.; Rivera, E.; Garcia-Garibay, M. A. “Transient Kinetics and Quantum Yield Studies of Nanocrystalline  $\alpha$ -Phenyl-Substituted Ketones: Sorting Out Reactions from Singlet and Triplet Exited States” *J. Am. Chem. Soc.*, **2018**, *140*, 8192-8197.

## Presentations

1. Poster Presentation: “Kinetic Analysis of Substituted Tetraphenylacetones via Laser Flash Photolysis (LFP) in nanocrystalline suspensions”- Sessions: Sci mix, Paper ID: 2650933. Park, J. H.; Garcia-Garibay, M. A. 253<sup>th</sup> American Chemical Society National Meeting, San Francisco, CA, United States.
2. Poster Presentation: “Kinetic Analysis of Substituted Tetraphenylacetones via Laser Flash Photolysis (LFP) in nanocrystalline suspensions”- Sessions: 2017 ACS UCLA Research Showcase. Park, J. H.; Garcia-Garibay, M. A. 253<sup>th</sup> American Chemical Society National Meeting, San Francisco, CA, United States.
3. Poster Presentation: “Kinetic Analysis of Substituted Tetraphenylacetones via Laser Flash Photolysis (LFP) in nanocrystalline suspensions”- Sessions: Physical Organic Chemistry. Park, J. H.; Garcia-Garibay, M. A. 253<sup>th</sup> American Chemical Society National Meeting, San Francisco, CA, United States.
4. Oral Presentation: “Laser Flash Photolysis Studies of Radical Pairs in Nanocrystalline Suspensions of  $\alpha$ -Phenyl-Substituted Acetones” Park, J. H.; Garcia-Garibay, M. A. University of California Chemical Symposium (UCCS), Lake Arrowhead, CA, United States.

# **Chapter 1**

## **Solid-State Organic Photochemistry and Nanocrystalline Suspensions**

## **1.1 Overview and Background:**

This chapter will encompass background information regarding solid-state photochemistry and its history of development. Furthermore, it will also focus on the important milestones in the context of the available methods to analyze mechanistic avenues of solid-state photochemistry. This section will ease into the field of solid-state photochemistry by introducing early pioneering work and transitioning into the work of Cohen and Schmidt in regards to the development of the topochemical postulate. This will be followed by a brief discussion of the determination and observation of transient intermediates in the solid-state. Lastly, the chapter closes by elucidating the work of Kasai et al. on the development of nanocrystals suspended in water with the help of surfactants, and its importance to overcome the optical limitations that otherwise limit the utility of absorption methods to extract mechanistic and kinetic data from solid-state reactions.

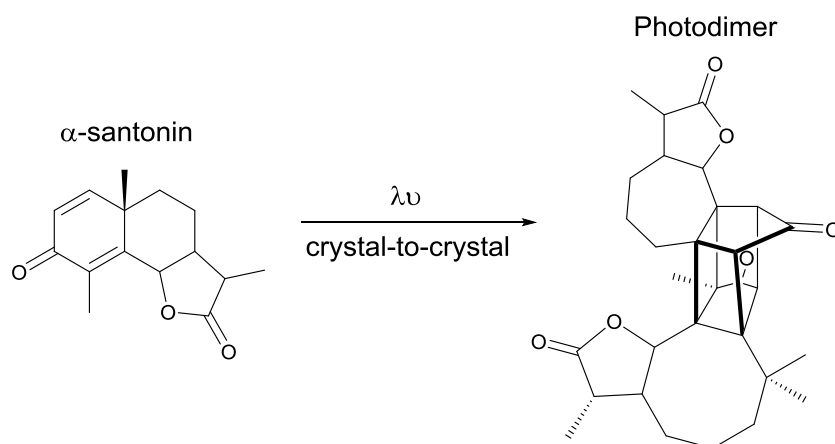
## **1.2 Solid-State Photochemistry and the Topochemical Postulate**

Solid-state photochemistry deals with the photochemical and photophysical transformation of molecules trapped in the solid state via irradiation with a light source. The first photochemical reaction in the solid-state was reported in 1834 by Trommsdorff, who made an unusual observation that took place when crystals of  $\alpha$ -santonin had been exposed to sunlight.<sup>1</sup> He described that sunlight would cause the  $\alpha$ -santonin crystals to undergo a color change and, more surprisingly, the crystals would burst into pieces. It was subsequently shown that Santonin reacts in solution to give Lumisantonin, a product that is different from than the one observed in the solid state. The solid state photoproduct was shown by Matsuura to be a cage dimer from a ring contracted product, as represented in Scheme 1.2.1, and later work by members from the Garcia-



Garibay group showed that the solid state reaction starts as a single-crystal to single crystal reaction with kinetics that are in agreement with Matsuura's proposal.<sup>2</sup> It was also suggested that the new crystal form of the photoproduct was responsible for the bursting effect. The reason behind this slow progress is that photochemical reactions in the solid-state demands more powerful analytical methods to study the photochemical intermediates in the solid-state. Therefore, the development of novel approaches to decipher photochemical reactions in the solid-state has been extensively studied through the help of technological improvements such as cryogenic technologies, and photocrystallographic techniques.<sup>3</sup> Furthermore, our group has also done extensive research to understand the reactivity of photochemical reactions in the solid.<sup>4</sup>

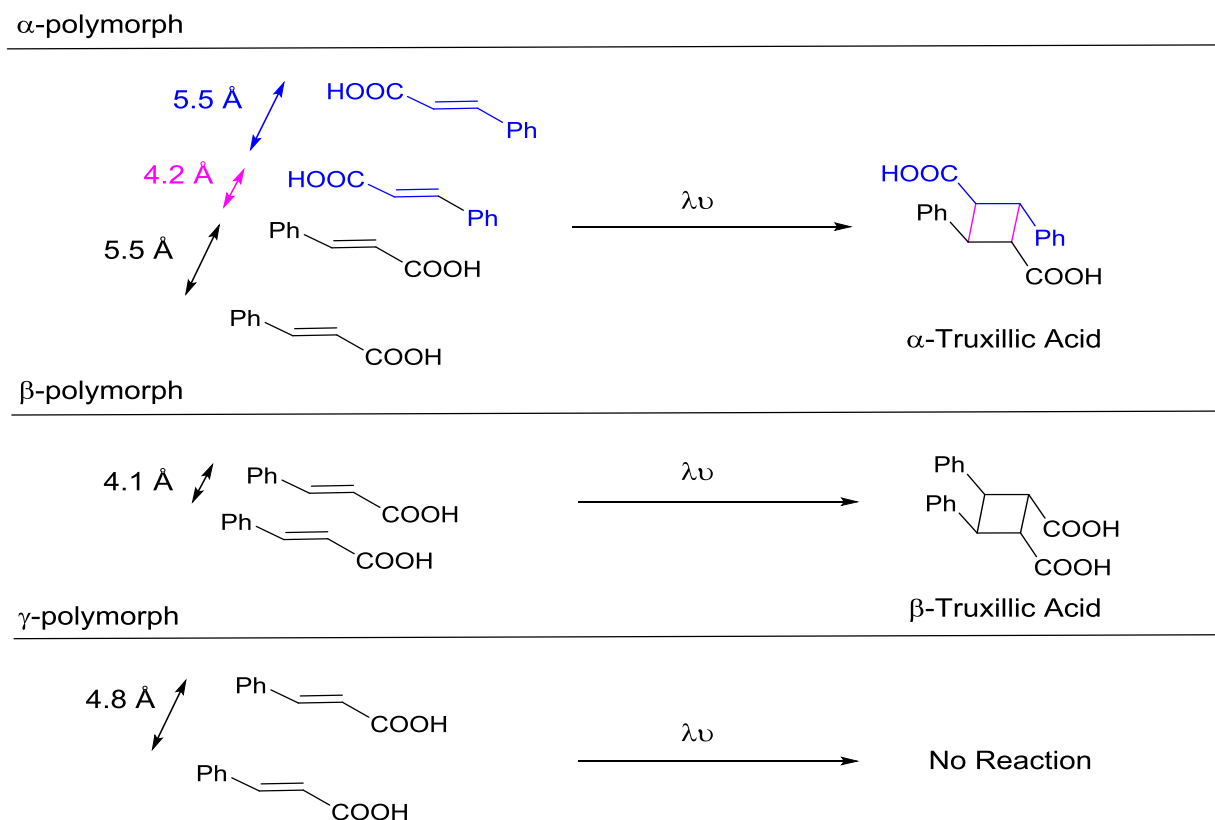
### Scheme 1.2.1



Nonetheless, much of the literature precedent indicates that most of the earlier solid-state photochemical studies were purely phenomenological and conducted through product analysis.<sup>5</sup> However, with the generalized access to X-ray crystallography in the 1960's, structural chemists were able to extract chemical information regarding the structure of the reactants, which could be correlated with the observed reactivity and the structure of the products in terms of their precise atomic and molecular positions in the crystalline lattice. Schmidt and Cohen are considered pioneers of solid-state photochemistry because of their contributions to the analysis of numerous

solid state reactions, including the photochemical reactivity of the different polymorphs of cinnamic acid (Scheme 1.2), which led to the structural formulation of the Topochemical postulate based on their analysis of reacting crystals with use of the X-ray crystallography.<sup>6</sup>

### Scheme 1.2.2



It had been reported that *trans*-cinnamic acid crystallizes in three different crystal polymorphs that are referred to as  $\alpha$ ,  $\beta$ , and  $\gamma$  forms of *trans*-cinnamic acid. Each of these polymorphs is different in terms of the orientation and intermolecular distance between the *trans*-cinnamic acid molecules. In the case of the  $\alpha$ -cinnamic acid, the intermolecular distance between molecules in the unit cell is measured to be 5.5 Å, whereas the distance between the molecules of adjacent unit cells are only 4.8 Å. Upon ultraviolet irradiation, instead of having reactions between molecules in the same unit cell, the reaction occurs between molecules that are in closer proximity, which

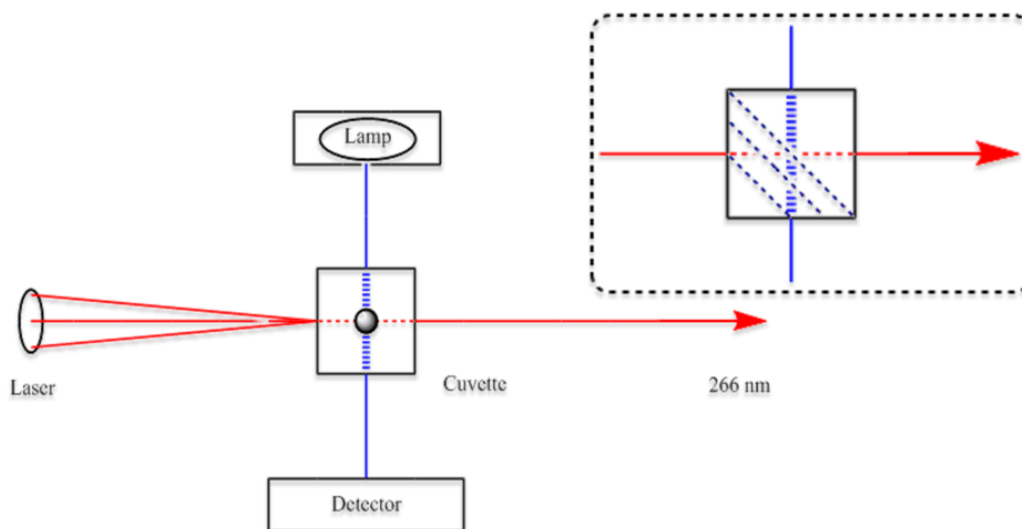
undergoes a [2+2] cycloaddition to yield the centrosymmetric  $\alpha$ -truxillic acid dimer. In the case of the  $\beta$ -trans-cinnamic acid, all the molecules in the crystal stack in a parallel orientation at only 4.1 Å away. Therefore, upon irradiation, the [2+2] photo-dimerization occurs to form the  $\beta$ -truxillic acid. In the final example, excitation of  $\gamma$ -trans-cinnamic acid results in no reaction and shows complete recovery of the starting material. This is because the intermolecular distance in this polymorph is too far apart, at 4.8 Å, making it impossible for the [2+2] photo-dimerization to proceed. With this analysis, Schmidt and Cohen confirm the Topochemical postulate by showing that solid-state reactivity occurs in a manner that is determined by the crystal packing with minimal motion of the molecules within their crystal cavity in a manner that crystal packing and geometry take precedence over the inherent photo reactivity of the molecule in solution.

### **1.3 Determination and Observation of Transient Intermediates in the Solid-State**

In order to have an in-depth knowledge on the reactivity of a chemical reaction, detection of an intermediate species of a reaction mechanism provides valuable data and is demonstrated by many of the chemists studying radicals and other transients in crystals.<sup>7</sup> In our group, we decided to take advantage of the Laser flash photolysis, a well-known analytical technique to measure absorption spectra of excited states and transient intermediates involved in photochemical reactions. Laser flash photolysis has been used extensively in the solution state. The method is also known as “pump-probe spectroscopy” because one uses a short laser pulse to create (pump) excited states and reactive intermediates, which are short-lived transients, and another laser pulse or a continuous light source to detect (probe) changes in absorption that occur upon formation of the transients. The experimental setup is depicted in figure 1.3.1 where a laser (pump) irradiates

the sample in the cuvette, thus electronically exciting the reactant molecules to induce a photochemical reaction, with a lamp and a detector that are used to detect it at right angles.

### Scheme 1.3.1



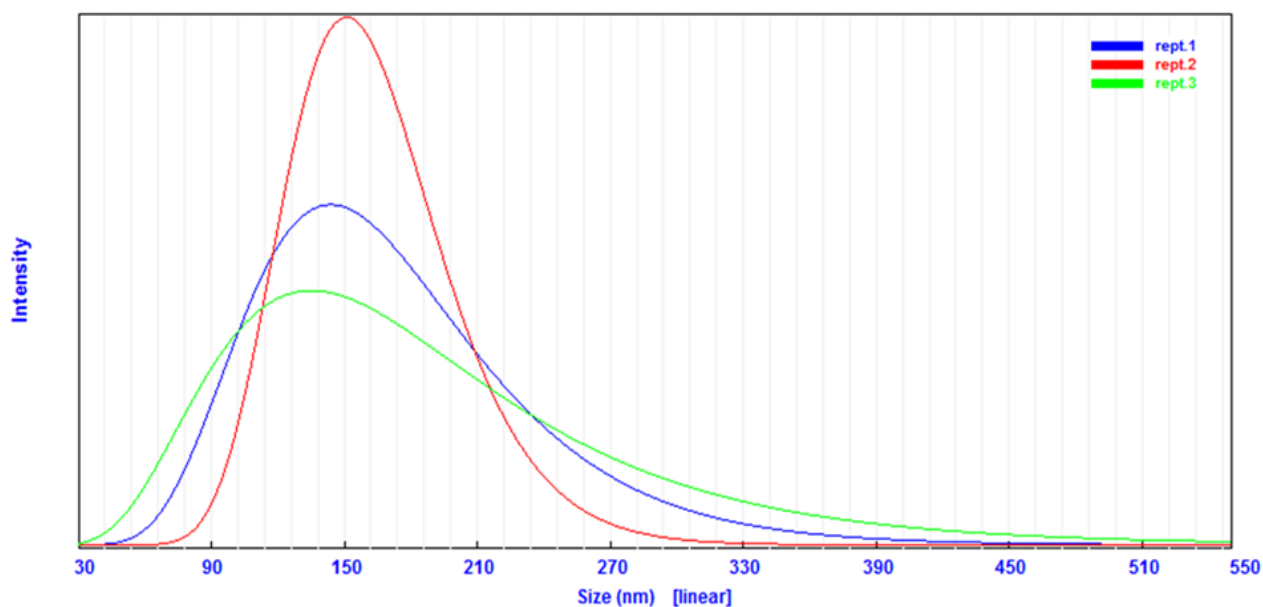
With this technique, there have been many multiple reports of photochemical transient studies that ultimately led to many of the kinetic analysis and deeper mechanistic understanding of numerous photochemical reaction pathways in solution.<sup>8</sup> When it comes to solid samples, a useful method to observe transient species is based on the use of diffuse reflectance transient absorption spectroscopy. This method has been widely utilized by Scaiano and others with the purpose of extracting kinetic information from the transients formed by observing changes in the light reflected by the crystals before and after excitation with a short laser pulse.<sup>9</sup> While diffuse reflectance is a useful method to study solids it has several drawbacks, which include the fact that bulk solids can undergo multiphotonic absorption under the conditions of high laser intensity required for the measurements. The formation of multiple excited states with a small volume leads to excited state interactions that are absent under low illumination conditions. Therefore, one of the objectives of this thesis will to establish the use of the laser flash photolysis for crystalline solids under conditions that are close to those generally used when studying

photochemical reactions in solution, in this case by taking advantage of nanocrystalline suspensions.

#### **1.4 Nanocrystalline Suspensions in Surfactant**

As mentioned above, one of the most efficient methods to extract kinetic information from photochemical reactions is by taking advantage of transmission pump-probe spectroscopy methods. However, the direct observation of these transients in bulk solids is impractical due to their high optical density, birefringence, and scattering, which makes the quantification of transmitted (or diffuse reflected) light difficult, whether in the form of single crystals or polycrystalline (powder) samples. In order to utilize the pump-probe spectroscopy for the study of photochemical reactions in crystalline solids, the Garcia-Garibay group has explored and optimized the use of nanocrystalline suspensions in water using a surfactant as a surface passivator. Dispersed nanocrystals have optical properties that approach those of solution samples and make it possible to diminish the above optical challenges.<sup>7</sup> The formation of nanocrystalline suspensions by the “reprecipitation” method was first reported by Kasai and co-workers.<sup>10</sup> For organic hydrophobic molecules, the method consists of mixing a small sample of the molecule dissolved in a polar, water-miscible organic solvent, into rapidly vortexing water with a sub-critical micelle concentration amount of a surfactant. These 50-500 nanometer sized crystals generally obtained in this manner retain most the physical characteristics of a macroscopic crystal but diminish the optical properties that scale inversely with crystal size. In general, Uv-Vis absorption measurements become possible when size of the crystals suspended in water is smaller than the wavelength of the incident irradiation. The surfactants used may include cetyltrimethylammonium bromide (CTAB), sodium dodecyl sulfate (SDS), or triton X-

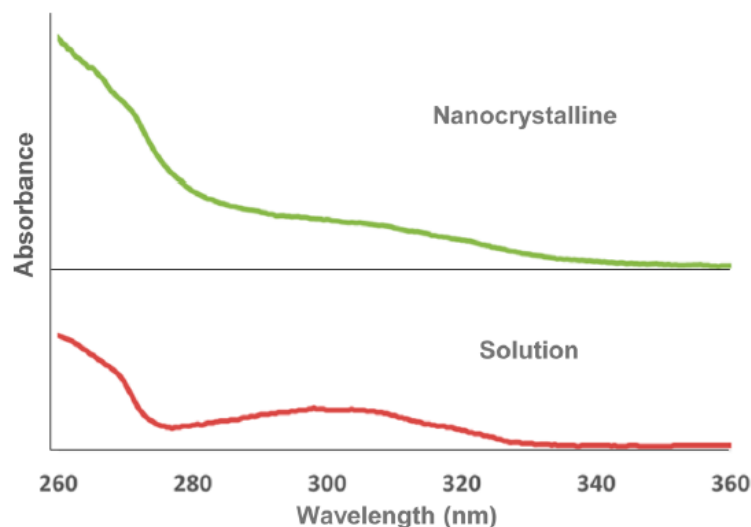
100, which as a surface passivators to slow down particle aggregation. Upon formation of nanocrystalline suspensions, the particle size can be measured through dynamic light scattering (DLS) or with scanning electron microscope (SEM). As depicted in Figure 1.4.1, the DLS data of tetraphenylacetone in CTAB reveals particle size in the range of  $140 \text{ nm} \pm 40 \text{ nm}$ .



**Figure 1.4.1** Dynamic light scattering spectrum of Tetraphenylacetone

In spite of the use of a surfactant to prevent particle aggregation, many nanocrystalline suspensions are often unstable and tend to aggregate and precipitate. For that reason, it is important to follow up changes as a function of time to make sure that laser flash measurements are carried out with suitable samples. To accomplish that one can take advantage of UV-Vis spectroscopy which reveals changes from an ideal suspension, which gives a spectrum that resembles the spectrum of the sample in solution, to a sample that has precipitated, where most of the solution features are lost and only scattering can be detected. Figure 1.5 represents almost identical spectra of tetraphenylacetone in the solution and solid-state indicating minimal scattering, which is indicative of minimal aggregation. Utilizing good quality nanocrystalline

suspensions and a single pass flow system to consistently offer new batches of sample in the irradiation volume of the laser flash photolysis instrument it is possible to measure the absorption spectra of various transients as well as their respective growths or decays.



**Figure 1.4.2** Ultraviolet-visible spectra of Tetraphenylacetone in solution and in solid-state

With this information at hand, it is possible to make a hypothesis about the photochemical mechanism in the solid-state. The following chapters of this thesis provide spectral data of solid-state reactions of various ketones, reinforcing the method of utilizing nanocrystalline suspensions with transmission spectroscopy to deduce photochemical mechanisms.

## 1.5 Conclusion

Solid-state photochemistry is useful in many aspects because the crystal rigidity forces reactive molecules to follow specific reaction pathways that can be rationalized or predicted by analysis of their X-ray crystal structures. This could make solid-state photochemistry a valuable tool to create molecules that are otherwise impractical targets. Unfortunately, our details understanding of photochemical reactions carried out in the solid state are limited because the tools needed to analyze their mechanism are relatively limited. However, the advent of nanocrystalline

suspensions in conjunction with laser flash photolysis offers a powerful method to measured transient spectra and kinetic data of short-lived excited state and photochemical intermediates. One of the goals of this thesis is to further enhance the field of solid-state photochemistry by exploring the kinetic analysis of various  $\alpha$ -substituted ketones in solution and solid-state via nanocrystalline suspensions.



## 1.6 References

- 1). (a) Trommsdorf, H. *Ann. Chem. Pharm.* **1834**, 11. (b) Garcia-Garibay, M. A. *Acc. Chem. Res.* **2003**, 36, 491.
- 2). (a) Kitabayashi, C.; Matsuura, Y.; Tanaka, N.; Katsube, Y. *Acta Cryst.* **1985**, 41, 1779-1781. (b) Cocker, W.; McMurry, T. B. H. *J. Chem. Soc.* **1955**, 0, 4430-4435. (c) Natarajan, A.; Tsai, C. K.; Khan, S. I.; McCarren, P.; Houk, K. N.; and Garcia-Garibay, M. A. *J. Am. Chem. Soc.* **2007**, 129 (32), 9846–9847.
- 3). (a) Goeta, A. E.; Howard, J. A. K. *Chem. Soc. Rev.* **2004**, 33, 490-500. (b) Johnson, D. A.; Pashman, K. A. *Inorg. Nuc. Chem. Lett.* **1975**, 11, 23-28. (c) Hatcher, L. E.; Raithby, P.R. *Acta Cryst.* **2013**, 69, 1448-1456.
- 4). (a) Garcia-Garibay, M. A.; Shin, S.; Sanrame, C. *Tetrahedron*, **2000**, 56, 6729-6737. (b) Yang, Z.; Garcia-Garibay, M.A. *Org. Lett.* **2000**, 2, 1963-1965. (c) Campos, L.M.; Dang, H.; Ng, D.; Yang, Z.; Martinez, H.L.; Garcia-Garibay, M. A. *J. Org. Chem.* **2002**, 67, 3749-3754. (d) Garcia-Garibay, M.A.; Houk, K.N.; Keating, A.E.; Cheer, C.J.; Leibovitch, M.; Scheffer, J.R.; Wu, L.-C. *Org. Lett.* **1999**, 8, 1279-1281. (e) Peterfy, K.; Garcia-Garibay, M.A. *J. Am. Chem. Soc.* **1998**, 120, 4540-4541.
- 5). (a) Campos, L. M.; Garcia-Garibay, M. A. Reactive Intermediates in Crystals: Form and Function. In *Reactive Intermediates*. (b) Platz, M. S., Jones, M., Moss, R., Eds.; John Wiley & Sons: Hoboken, NJ, **2007**. (c) Scheffer, J. R.; Scott, C. In *CRC Handbook of Organic Photochemistry and Photobiology*, 2nd ed.; Lenci, F., Horspool, W., Eds.; CRC Press: Boca Raton, FL, **2003**; Vols. 1 and 2, Chapter 54.

- 6). (a) Cohen, M. D.; Schmidt, G. M. J. *J. Am. Chem. Soc.* **1964**, *53*, 1996. (b) Cohen, M. D.; Schmidt, G. M. J.; Sonntag, F. I. *J. Am. Chem. Soc.* **1964**, *53*, 2000. (c) Schmidt, G. M. J. *J. Am. Chem. Soc.* **1964**, *53*, 2014.
- 7). (a) Bowers II, M.J., McBride, J.R., Garrett, M.D., Sammons, J.A., Dukes III, A.D., Schreuder, M.A., Watt, T.L., Lupini, A.R., Pennycook, S.J. and Rosenthal, S.J. *J. Am. Chem. Soc.* **2009**, *131(16)*, 5730-5731. (b) Tomioka: Kawano, M., Hirai, K., Tomioka, H. and Ohashi, Y. *J. Am. Chem. Soc.* **2001**, *123(28)*, 6904-6908. (c) Tomioka, H., Watanabe, T., Hirai, K., Furukawa, K., Takui, T. and Itoh, K. *J. Am. Chem. Soc.* **1995**, *117(23)*, 6376-6377. (d) Closs, F., Siemensmeyer, K., Frey, T. and Funhoff, D. *Liquid Cryst.*, **1993**, *14(3)*, 629-634. (e) Adam, D., Closs, F., Frey, T., Funhoff, D., Haarer, D., Schuhmacher, P. and Siemensmeyer, K. *Phys. Rev. Lett.*, **1993**, *70(4)*, 457.
- 8). Dimitrijevic, N. M.; Kamat, P. V. *J. Phys. Chem.* **1992**, *96*, 4811-4814. (b) Watanabe, A.; Ito, O. *J. Phys. Chem.* **1994**, *98*, 7736-7740. (c) Gritsan, N. P.; Gudmundsdóttir, A. D.; Tigelaar, D.; Platz, M. S. *J. Phys. Chem. A*, **1999**, *103* (18), 3458–3461. (d) Mandel, S. M.; Singh, P. N. D.; Muthukrishnan, S.; Chang, M.; Krause, J. A.; and Gudmundsdóttir, A. D. *Org. Lett.*, **2006**, *8* (19), 4207–4210.
- 9). Kelly, G.; Willsher, C. J.; Wilkinson, F.; Netto-Ferreira, J. C.; Olea, A.; Weir, D.; Johnston, L. J.; Scaiano, J. C. *Canadian Journal of Chemistry*, **1990**, *68*, (6): 812-819 (b) Barra, M.; Bohne, C.; Scaiano, J. C. *Photochem. and photobio.* **1991**, *vol 54*, 1-5. (c) Atienzar, P.; Corma, A.; García, H.; Scaiano, J. C. *Chem. Mater.*, **2004**, *16* (6), 982–987.
- 10). Chung, T.S.; Park, J.H.; Garcia-Garibay, M.A. *J. Org. Chem.*, **2017**, *82*, 12128–12133. (b) Park, J.H.; Hughs, M.; Chung, T.S.; Ayitou, A. J.-L.; Breslin, V.M.; Garcia-Garibay, M.A. *J. Am. Chem. Soc.* **2017**, *139*, 13312–13317. (c) Chung, T.S.; Ayitou, A. J.-L.; Park,

- J. H.; Breslin, V. M.; Garcia-Garibay, M. A. *Phys. Chem. Lett.*, **2017**, *8*, 1845–1850.
- (d) Anoklase J.-L. Ayitou, A. J.-L.; Flynn, K.; Jockusch, S.; Khan, S.I.; Garcia-Garibay, M.A. *J. Am. Chem. Soc.*, **2016**, *138*, 2644-2648.
- 11). Kasai, H.; Nalwa, H. S.; Oikawa, H.; Okada, S.; Matsuda, H.; Minami, N.; Kuakuta, A.; Ono, K.; Mukoh, A.; Nakanishi, H. *Jpn. J. Appl. Phys.*, **1992**, *31*, 1132-1134.

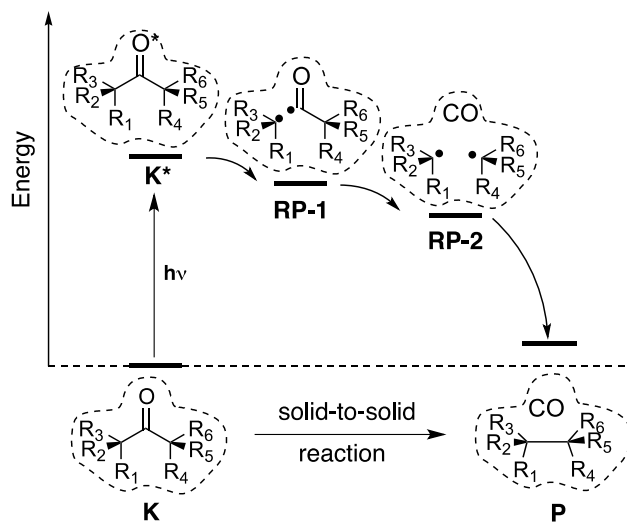
## **Chapter 2**

### **Generation and Reactivity Studies of Diarylmethyl Radical Pairs in Crystalline Tetraarylacetones via Laser Flash Photolysis Using Nanocrystalline Suspensions**

## 2.1 Introduction

Photochemical reactions in crystalline solids tend to display extraordinary levels of reaction control.<sup>1</sup> Although they are not as common and general as reactions in solution, we have suggested that they can be “engineered” in a reliable manner by selecting reactions that display a downward staircase energy profile.<sup>2</sup> As shown in Scheme 2.1.1 with the photodecarbonylation of ketones with radical-stabilizing substituents R1-R6, this strategy combines molecularly encoded energetics with the homogeneity and rigidity of the crystal lattice to obtain unprecedented levels of reaction control.<sup>3</sup> Substituents R1-R6 are selected to make the reaction intermediates increasingly stable, whereas the reaction cavity formed by close neighbors in the lattice (dotted line in Scheme 2.1.1) accounts for the high selectivity and specificity that generally characterize reactions in the crystalline state.

**Scheme 2.1.1**



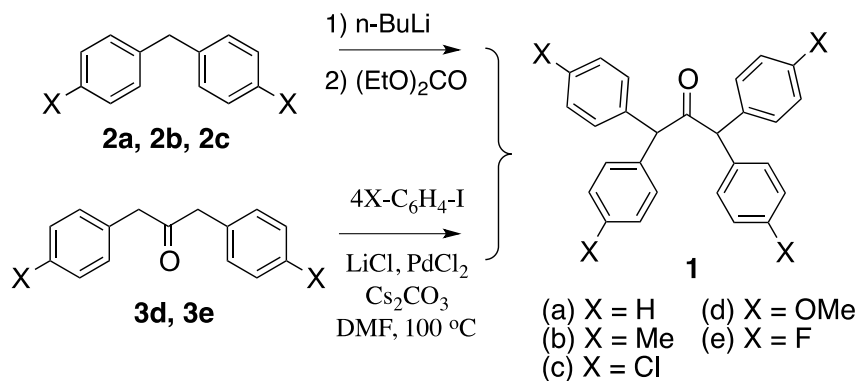
Although this general strategy has been developed and demonstrated with numerous examples using product analysis,<sup>2</sup> the optical (UV-vis) detection of the transient intermediates has not been previously possible. In fact, practical limitations arise from complications associated with spectroscopic measurements in the solid state due to their high absorbance and strong scattering,

as well as the kinetic complexities that arise from exciton delocalization and multiphotonic interactions, which are common in bulk powders and large crystals.<sup>4</sup> Fortunately, it has been shown that nanocrystals in the 50–200 nm range may be viewed as a state in transition between large supramolecular entities and bulk solids, such that it is possible to carry out spectroscopic measurements using conventional transmission methods.<sup>5,6</sup> With that in mind, we set out to explore the UV spectroscopy detection of the radical pairs involved in the solid state photodecarbonylation reaction (RP-1 and RP-2).

## 2.2 Results and Discussion

To have the greatest chance of success, we decided to investigate a set of symmetric 1,1,3,3-tetraarylacetonones **1** with substituents in the four para-phenyl positions (Scheme 2.2.1).

### Scheme 2.2.1



On the basis of the high energy of the excited ketone and the relatively high stability of the diphenylmethyl radicals in RP-1 and RP-2 (Scheme 2.2.1 with R<sub>2</sub>, R<sub>3</sub>, R<sub>5</sub>, R<sub>6</sub> = Ar and R<sub>1</sub>, R<sub>4</sub> = H), we expect the two bond-cleavage reactions to be highly exothermic and, according to the Hammond postulate, to have very low barriers, such that rapid formation of RP-2 may occur and the kinetics observed in our experiment can be related to the rate of bond formation leading to product P. We take advantage of the relatively well-known spectroscopic properties and

chemical behavior of benzylic<sup>7,8</sup> and diphenylmethyl<sup>9</sup> radicals with the expectation that their radical pairs should behave similarly.

To test our hypothesis, we prepared five 1,1,3,3-tetraarylacetones 1a–1e with either simple phenyl groups (1a), or with phenyl groups bearing substituents with varying electronic effects, including para-methyl (1b), para-chloro (1c), paramethoxy groups (1d), and para-fluoro-substituents (1e). Ketones 1a–1e were obtained in modest to good yields using the synthetic pathways shown in Scheme 2.2.1, which are described in detail in the supporting information section. Compounds 1a–1e were characterized by spectroscopic methods and were shown to be crystalline solids with relatively high melting points in the range of 86–171 °C (Table 2.2.1), which allowed for their solid-state photochemistry to be studied at room temperature.<sup>10</sup>

**Table 2.2.1** Melting temperatures and crystallite size of 1,1,3,3-tetraaryl acetones suspended in water.

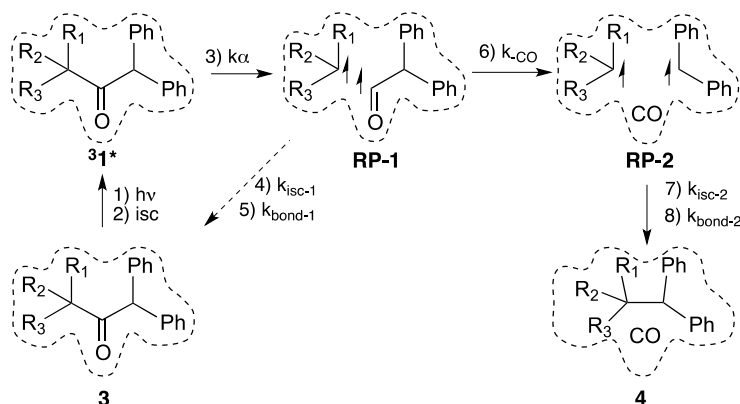
Ketone	Substituents	m.p. (°C)	Mean Nanocrystal size (nm) <sup>a</sup>
1a	H	134-135 <sup>18</sup>	140 ± 40
1b	4-Me	86-87	150 ± 60
1c	4-Cl	162-164	200 ± 70
1d	4-OMe	102-103	170 ± 50
1e	4-F	170-171	160 ± 50

<sup>a</sup>Mean crystal sizes and standard deviations measured by dynamic light scattering

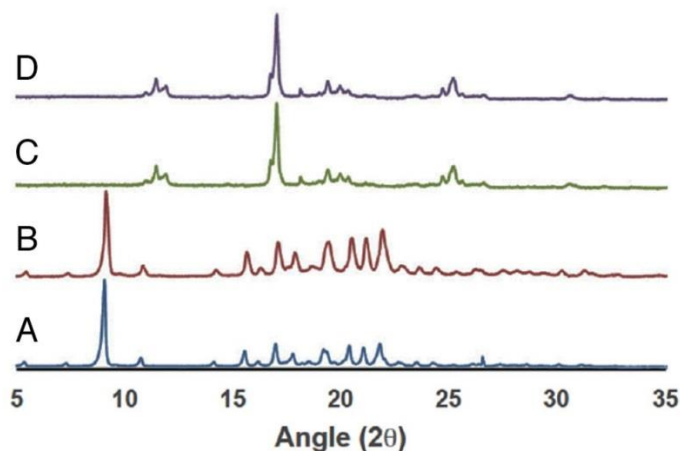
All nanocrystalline suspensions were prepared by the solvent shift, or reprecipitation method,<sup>11</sup> which resulted in sizes that range from ca. 140 to 200 nm as determined by dynamic light scattering (Table 2.2.1). We confirmed that when dry powders and nanocrystalline suspensions of ketones 1a-1e were exposed to UV light from a Hanovia photochemical reactor containing a

medium pressure Hg lamp with  $\lambda > 290$  nm using Pyrex filter, they all give tetraaryl-ethanes 4a–4e as the only photoproducts (Scheme 2.2.3).<sup>12</sup>

### Scheme 2.2.3



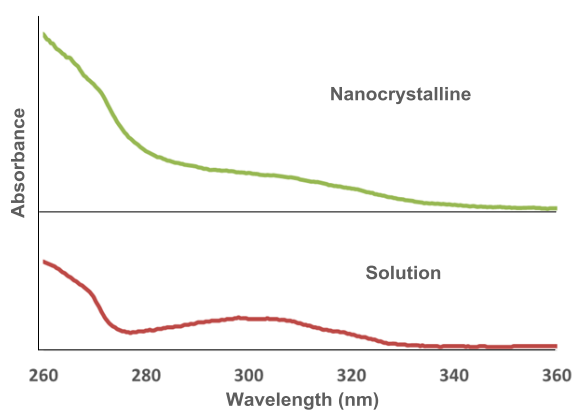
Furthermore, as illustrated in Figure 2.2.1 with data acquired using samples of ketone **1a**, powder X-ray diffraction analysis of the bulk solids (Figure 2.2.1, PXRD A) and the collected nanocrystals (Figure 2.2.1, PXRD B) were essentially identical, which helped establish the fact that they belong to same crystal form. It was also shown that the diffractogram of photoproduct **4a** formed in crystals, in situ (Figure 2.2.1, PXRD C), matches very well with the one obtained after recrystallization (Figure 2.2.1, PXRD D), indicating that the reaction proceeds by a reconstructive phase transition mechanism.<sup>13</sup>



**Figure 2.2.1** Powder X-ray diffraction of (A) recrystallized **1a** in ethanol and (B) nanocrystals of **1a** prepared by precipitation and collected by centrifugation, (C) product **4a** obtained in situ by exposure of **1a** to UV light of bulk solids, and (D) recrystallized samples of **4a** in ethanol

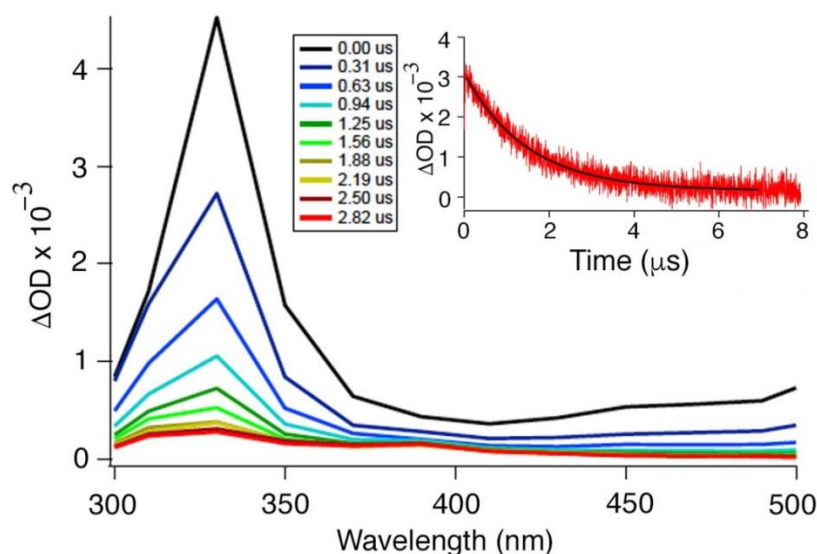


To carry out laser pump–probe spectroscopic and kinetics studies with nanocrystalline suspensions of 1a–1e we first analyzed their optical properties in the UV range. We found that the UV spectrum of the suspended nanocrystals varied over the first 10 min indicating some degree of aggregation, probably as a result of particle coalescence.<sup>14</sup> We also noticed that the amount of scattering in the absorbance spectrum seems to be greater for the less polar ketones 1a and 1b as compared to that observed for ketones 1c–1e. It was shown that all the spectral features of the former can be recovered by assuming that Rayleigh scattering is the main contributor to the apparent absorbance, such that it may be corrected by an inverse fourth power function,  $A_{\text{scatt}} = f(1/\lambda^4)$ .<sup>15</sup> As illustrated with the scattering-corrected absorbance spectrum of ketone 1a in Figure 2.2.2, there is a reasonable agreement between the features of the  $n,\pi^*$  transition at ca. 310 nm of the spectrum obtained in solution and those present in the solid state. We presume that the small differences recorded in the two media reflect a relatively weak coupling between close neighbors, which was also seen for the other four ketones. On the basis of these observations, we prepared nanocrystalline suspensions with optical densities at the laser excitation wavelength of  $\lambda = 266$  nm on the order of ca. 0.2–0.7, which we found was sufficient for the detection of the transients.



**Figure 2.2.2** Absorption spectra of 0.1 g/L tetraphenylacetone 1a in MeCN (red line) and an aqueous nanocrystalline suspension of 1a 0.025g/L in the presence of submicellar CTAB (green line).

To avoid the potential interference from transients originated by excitation of accumulating photoproducts, all pump–probe measurements were carried out in a single pass flow system that assures the presence of unreacted sample in the excitation volume with the laser operating at one pulse every 3s. Measurements carried out in MeCN solution helped us confirm the identity of the transient absorption obtained in the case of 1a, which as reported in the literature, occurs in the 320–350 nm region with a  $\lambda_{\text{max}} = 330$  nm and is assigned to free diphenylmethyl radicals (Figure 2.2.3).<sup>16</sup>



**Figure 2.2.3** Time-dependent spectra of tetraphenylacetone 1a in MeCN collected between 0 and 16.1  $\mu\text{s}$  ( $\lambda_{\text{max}} = 330$  nm). Inset: Transient decay of 1a measured in MeCN at 298 K at  $\lambda_{\text{max}} = 330$  nm.

Similar measurements carried out in solution with all other ketones revealed similar results with  $\lambda_{\text{max}}$  varying from 320 nm in the case of the fluoroderivative 1e to 350 nm in the case of the methoxy compound 1d (Table 2.2.2). A bathochromic shift of the respective  $\lambda_{\text{max}}$  of ketones 1a–1e that follows the order 1e (F) < 1a (H) < 1c (Cl) = 1b (Me) < 1d (OMe). Although the decay kinetics of the diphenylmethyl radicals in degassed solution displayed the expected second-order kinetics with decay times into the millisecond regime (Supporting information:

Figure 2.S73), removal of oxygen from the flow system was challenging. Traces acquired with air-saturated acetonitrile decayed within time windows of ca. 500 ns. Decay measurements carried out with argon-purged solutions extended into ca. 10  $\mu$ s windows, which are indicative of oxygen quenching, as shown for 1a in the inset of Figure 2.2.3. Oxygen-limited apparent first-order kinetics in the flow system ranged from 0.6 to 2.0  $\mu$ s, as indicated in Table 2.2.2.

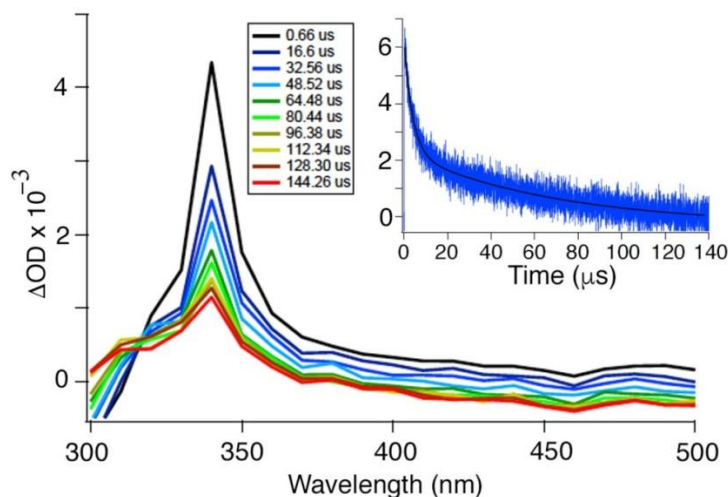
**Table 2.2** Spectroscopic and kinetic data from solution and nanocrystalline photoreactions of 1a–1e in a single pass flow cell

Ketone	Solution		Nanocrystals		
	$\lambda_{\max}$ , nm	$\tau^a$ , $\mu$ s	$\lambda_{\max}^b$ , nm	$\tau_1^a$ $\mu$ s (%) <sup>c</sup>	$\tau_2^d$ $\mu$ s (%) <sup>c</sup>
<b>1a</b>	330	1.5	340	2.4 (3%)	70 (97%)
<b>1b</b>	340	0.8	350	2.0 (5%)	50 (95%)
<b>1c</b>	340	0.9	350	1.9 (3%)	57 (97%)
<b>1d</b>	350	0.6	360	2.4 (8%)	40 (92%)
<b>1e</b>	320	2.0	330	2.8 (3%)	90 (97%)

<sup>a</sup>Solution time constant in the flow cell are limited by O<sub>2</sub> quenching. <sup>b</sup>Apparent value shifted to the red due to the interference from high light scattering. <sup>c</sup>Percentage weighted contribution from a double exponential decay (ref 20). <sup>d</sup>Estimated error,  $\pm 0.2$  to  $\pm 0.4$ .

Having determined the spectral properties and kinetics of the free radicals generated from 1a–1e in MeCN solution we turned our attention to measurements in nanocrystalline suspensions. Using similar experimental conditions with a flowing aqueous suspension of ketone 1a, we were able to record the transient spectrum shown in Figure 2.2.4. Although the time-dependent absorption spectrum appears to have a  $\lambda_{\max}$  of 340 nm, which would indicate a red shift as compared to the spectrum in solution ( $\lambda_{\max} = 330$  nm), the data obtained in suspension are relatively distorted by the greater scattering, and consequently lower transmission, that occurs toward the blue. An apparent red shift seems to be evident for all the derivatives 1a–1e as indicated in Table 2.2.2. A comparison of the spectral data shown in Figures 2.2.3 and 2.2.4 indicates that the absorption spectrum corresponding to  $\pi, \pi^*$  transitions in the UV region of

diphenylmethyl free radicals in solution is very similar to the absorption spectrum of the radical pair in the solid state. Decay experiments carried out with 50 laser pulses in argon- and air saturated standing suspensions of 1a were noisy, but gave identical results. We interpret the lack of quenching as an indication that there are no contributions from transients formed in solution, which would occur if a small amount of the ketone had remained in the aqueous medium. This was persuasively confirmed when no change in the decay profile was observed when suspensions were purged with oxygen. Decay measurements carried out with flowing nanocrystalline suspensions revealed clear contributions from short- and long-lived components, as shown in the inset of Figure 2.2.4 for ketone 1a, which has components of ca. 2.4 and 70  $\mu\text{s}$ , respectively. Additional experiments carried out as a function of laser intensity showed no changes in the observed kinetics, indicating that multiphotonic processes do not occur in the nanocrystalline samples under the conditions of our experiments.



**Figure 2.2.4** Transient spectra of tetraphenylacetone 1a in the solid-state photoreaction with a  $\lambda_{\text{max}}$  (apparent)  $\approx 340$  nm. Inset: Decay of 1a in the nanocrystalline suspension detected at 340 nm.

To interpret the observed kinetics we recall that the reaction is thought to begin by excitation of 1 followed by a rapid intersystem crossing to the triplet excited state  $^31^*$  (Scheme 2.2.3, steps 1

and 2).<sup>17</sup> The next step consists of an  $\alpha$ -cleavage reaction (step 3) that generates free radicals in solution (not shown) and a diphenylmethyl-diphenylmethylacyl radical pair (<sup>3</sup>RP-1) in the solid state. The latter can either undergo intersystem crossing to the singlet state (<sup>1</sup>RP-1) and go back to the starting material (steps 4 and 5), or it can lose a molecule of CO to generate the triplet bis(diphenylmethyl) radical pair <sup>3</sup>RP-2 (step 6). It is known that the loss of CO from the diphenylmethyl-acyl radical ( $k_{-CO}$ ) in solution occurs with a time constant of ca. 8 ns,<sup>18</sup> which is very close to the pulse width of the Nd:YAG laser used for our experiments. On the basis of the decay data shown in the inset of Figure 2.2.4, we propose that the solid-state decarbonylation step occurs within the same time frame as the reaction in solution, or faster. Indeed, if decarbonylation were slower in crystals, we would see a fraction of the signal showing a slow growth phase, as the amount of diphenylmethyl radical would double in going from <sup>3</sup>RP-1 to <sup>3</sup>RP-2. We propose that the time constant for the signal decay observed in the nanocrystals is associated with a rate-limiting intersystem crossing step from <sup>3</sup>RP-2 to <sup>1</sup>RP-2 ( $k_{isc-2}$ , step 7), with the latter singlet radical pair being able to go on to photoproduct 4 very rapidly and in quantitative yield ( $k_{bond-2}$ , step 8). This interpretation is consistent with previously reported chemically induced dynamic electron polarization (CIDEP) studies carried out with nanocrystalline suspension of analogous cumyl radical pairs, which also displayed a biradical lifetime in the microsecond time scale.<sup>19</sup>

The observation of short and long lifetimes for all ketones studied is indicative of two radical pair populations. The short lived component in the solid state has a small weighted contribution to the total decay, ranging from 3% in the case of 1a to only 8% for 1d (Table 2.2.2).<sup>20</sup> The range of time constants for the short-lived component is also narrow, varying from 1.9  $\mu$ s in the case of 1c to 2.8  $\mu$ s in the case of 1e (Table 2.2.2). The major component varies by a

factor of 2.25 from 40  $\mu\text{s}$  in crystals of 1d to 90  $\mu\text{s}$  in the case of 1e. It is significant that the observations determined for the entire set are all consistent, with relatively modest changes in the lifetimes despite variations in the nature of the aryl substituents,<sup>21</sup> physical properties, and crystal forms. The presence of short- and long- lived radical populations is interesting and significant. Although the small contribution of the short-lived components may represent a small fraction of radicals that form at defect sites where additional mobility may allow them to explore configurations with faster intersystem crossing, the two populations may reflect specific aspects of the ISC mechanism.<sup>22</sup> For tightly held, or “geminate” radicals that are in principle identical (have the same g-factor), ISC depends strongly on the magnitudes of: (1) the electron spin exchange interaction (J), (2) the spin-orbit coupling (SOC), and (3) the zero-field splitting parameters (ZFS) that determine the relative energies of the triplet sublevels ( $T_+$ ,  $T_0$ , and  $T_-$ ). It is interesting to note that all three quantities depend strongly on the distance and orientation between the two radical centers. Although the value of J determines the energy difference between the singlet and triplet states ( $\Delta_{\text{EST}} = 2J$ ), SOC provides a mechanism to switch spin states with conservation of angular momentum by taking advantage of orbital motion, and ZFS determines which of the triplet sublevels can interconvert with the singlet state. Interestingly, if structural factors were to be met where  $J \approx 0$ , SOC would also vanish and one would have to consider mechanisms where ISC could be influenced by external magnetic fields and hyperfine interactions between the electron and nuclear spins, which would result in the observation of magnetic isotope effects. While intersystem crossing in the case of RP-2 is likely to be determined by a SOC mechanism,<sup>23</sup> the possibility of triplet radical pairs with a relatively small singlet-triplet gap in slowly interconverting triplet sublevels undergoing ISC at different rates would be consistent with the available kinetic data. Then again, it might be the

case that a small fraction of the initial  $\alpha$ -cleavage reaction occurs in competition with the intersystem crossing step, going directly from  $1K^*$  to  $^1RP-1$ , such that a fraction of singlet state  $^1RP-1$  formed in this manner can undergo fast decarbonylation to  $^1RP-2$ , which goes on fast toward the final product. This interpretation would imply that the short-lived component represents the rate of bond-formation ( $k_{\text{bond-2}}$ ) from  $^1RP-2$  to product 4.

### 2.3. Conclusions

In conclusion, using a set of crystalline tetraarylacetones as a test system, we have been able to observe the UV spectra of a series of bis(diarylmethyl) radical pairs. Kinetic measurements at their wavelength of maximum absorption indicate that radical pair formation in crystals is just as fast, or perhaps faster than in solution, with kinetics that are largely determined by a slow component that accounts for 92–95% of the integrated decay signal. Time constants that range from 40 to 90  $\mu\text{s}$  are assigned to the rate limiting intersystem crossing of the triplet bis(diarylmethyl) radical pair to the singlet manifold followed by rapid bond formation to give the final product. Kinetic measurements carried out in the presence of external magnetic fields and with different isotopologues will be aimed at exploring the origin of the two components and the most likely mechanism for intersystem crossing. In a more general context, we expect that a robust strategy to engineer reaction in crystals and the ability to study their kinetics by pulsed laser methods will help the faster development of crystal-to-crystal photochemistry.

## 2.4. Experimental section

**Synthesis.** The synthesis of all tetraarylacetones used in this work was accomplished by conventional procedures as illustrated in Scheme 2.2.1 and as described in detail in the Supporting Information.

**Preparation of Nanocrystalline Suspensions.** A sample of 10  $\mu\text{L}$  of a stock solution of the tetraaryl ketone (5 mg/mL) in acetonitrile was injected dropwise via syringe into a 100 mL graduated cylinder containing 20 mL of rapidly stirring cetyltrimethylammonium bromide (CTAB) at 1/25th of its critical micelle concentration (CMC = 0.9 mM).<sup>24</sup> The stirring continued for ca. 15s after injection and then the suspension was transferred to a quartz cuvette via pipet. Dynamic Light Scattering (DLS) data were recorded using a Beckman- Coulter N4 Plus particle analyzer with a 10 mW helium–neon laser at 632.8 nm. The particle size was determined using the 62.6° detection angle, and was calculated using the size distribution processor (SDP) analysis package provided by the manufacturer.

**Laser Flash Photolysis Experiments.** Nanosecond transient absorption experiments were performed using Laser Flash Photolysis instrument from Edinburgh Instruments in conjunction with a Nd:YAG laser (Brilliant b, Quantel) with 266 nm output, 8 ns pulse width and 36–40 mJ pulse energy. The optical detection is based on a pulsed Xenon arc lamp (450 W), a monochromator (TMS300, Czerny-Turner), a photomultiplier detector (Hamamatsu R928) and a digital oscilloscope (TDS3012C, 100 MHz and 1.25 GS/s from Tektronix). The laser flash photolysis experiments were performed using a 1 cm quartz flow cell mounted on a home-built sample holder that is placed at the cross-section of the laser incident beam and the probe light.



Argon gas was continuously purged through acetonitrile solutions or nanocrystalline suspensions of ketones (0.0025g/L) while being flowed through the quartz cell using a peristaltic pump (Masterflex L/S) at a rate of 1.6–3.2 mL/min. To diminish the effect of aggregation fresh samples were made in batches of 20 mL for the nanocrystalline suspensions every 10 min. Time-resolved absorption maps were recorded with continuous flow of sample through the quartz cell. Lifetimes at  $\lambda_{\text{max}}$  for end-of-pulse spectra were reproducible and doubly verified/processed with Edinburgh Instruments L900 internal software and Igor Pro (version 6.34A, Wavemetrics) software. The parameters under the detector monochromator settings are as follows: the ketones were observed at the corresponding  $\lambda_{\text{max}}$  in solution (320–350 nm) and in nanocrystalline suspensions (330–360 nm), and the bandwidth (BW) was set between 1.00 to 3.00 nm. The flash lamp settings were set where the frequency was at 10 Hz, width at 40  $\mu\text{s}$ , and delay at 4000  $\mu\text{s}$ . The Q-switch settings were set where the frequency was at 1.0 Hz, width at 20  $\mu\text{s}$ , and delay between 270 and 310  $\mu\text{s}$ .

## **2.5 Supplementary Information for Chapter 2**

<b>Contents:</b>	<b>Page number</b>
<b>2.5.1</b> General Methods	29
<b>2.5.2</b> Synthesis	30
<b>2.5.3</b> Spectral characterization data, $^1\text{H}$ NMR and $^{13}\text{C}$ NMR, UV-VIS	36
<b>2.5.4</b> Solid-State Photochemistry of Dry Powder	69
<b>2.5.5</b> Power X-Ray Diffraction (PXRD) Analysis	75
<b>2.5.6</b> Laser Flash Photolysis	80
<b>2.5.7</b> Dynamic Light Scattering	92

**2.5.1 General Methods.** All commercially obtained reagents/solvents were used as received without further purification. Unless stated otherwise, reactions were conducted in oven-dried glassware under argon atmosphere. Proton magnetic resonance spectra were recorded at 500 MHz, and carbon-13 magnetic resonance spectra were recorded at 125 MHz, respectively. All chemical shifts are reported in ppm on the  $\delta$ -scale relative to TMS ( $\delta$  0.0) using residual solvent as reference ( $\text{CDCl}_3$   $\delta$  7.26 and  $\delta$  77.16 for proton and carbon, respectively,  $\text{CD}_3\text{CN}$   $\delta$  1.94 and 1.32, 118.26 for proton and carbon respectively). Standard abbreviations indicating multiplicity were used as follows: s (singlet), b (broad), d (doublet), t (triplet), q (quartet), and m (multiplet). Data for  $^{13}\text{C}$  NMR spectra are reported in terms of chemical shift ( $\delta$  ppm). High-resolution mass spectrum data were recorded on a DART spectrometer in positive (ESI+) ion mode. UV-Vis absorption and transmission spectra were recorded on Ocean Optics spectrometer (DT-MINI-2-GS UV-VIS-NIR LightSource and USB2000+ using SpectraSuite software package). Dynamic Light Scattering (DLS) data were recorded using a Beckman-Coulter N4 Plus particle analyzer with a 10 mW helium-neon laser at 632.8 nm. The particle size was determined using the  $62.6^\circ$  detection angle and was calculated using the size distribution processor (SDP) analysis package provided by the manufacturer. Melting point values were recorded on a Melt-Point II<sup>®</sup> apparatus. Infra-Red spectra were recorded on a PerkinElmer<sup>®</sup> Spectrum Two spectrometer equipped with a universal ATR sampling accessory. Nanosecond transient absorption experiments were performed using Laser Flash Photolysis instrument from Edinburgh Instruments in conjunction with a Nd:YAG laser (Brilliant b, Quantel<sup>®</sup>) with 266-nm output, 4-6 ns pulse width and 36-40 mJ pulse energy. The optical detection is based on a pulsed Xenon arc lamp (450 W), a monochromator (TMS300, Czerny-Turner), a photomultiplier detector (Hamamatsu R928) and a digital oscilloscope (TDS3012C, 100 MHz and 1.25 GS/s from Tektronix). The laser flash

photolysis experiments were performed with 1 cm quartz flow cell mounted on a home-built sample holder that is placed at the cross-section of the laser incident beam and the probe light. Continuously Argon gas purged acetonitrile solutions or crystalline suspensions of ketones (0.0025g/L) were flown through the quartz cell using a peristaltic pump (Masterflex L/S) at a rate of 1.6 – 3.2 mL/min. Due to aggregation fresh samples in batches of 20 mL were made for the crystalline suspensions every 10 minutes. Time-resolved absorption maps were recorded with continuous flow of samples through the quartz cell. Lifetimes at  $\lambda_{\text{max}}$  for end-of-pulse spectra were reproducible and doubly verified/processed with Edinburgh Instruments L900 internal software and Igor Pro (version 6.34A, Wavemetrics) software. The parameters under the detector monochromator settings are as follows: the ketones were observed at the corresponding  $\lambda_{\text{max}}$  in solution (320-350 nm) and in crystalline suspensions (330-360 nm), and the band width was set between 1.00 to 3.00 nm. The flash lamp settings were set where the frequency was at 10 Hz, width at 40  $\mu\text{s}$ , and delay at 4000  $\mu\text{s}$ . The Q-switch settings were set where the frequency was at 1.0 Hz, width at 20  $\mu\text{s}$ , and delay between 270-310  $\mu\text{s}$ .

### 2.5.2 Synthesis:

Unless reported, all of the tetraphenylacetones were synthesized using commercially available starting materials.

**General Synthesis of Di-p-tolylmethane (2b).** Following the well-known Wolff-Kishner reaction<sup>25a,25b</sup> in a flame-dried, three neck flask fitted with a reflux condenser, benzophenone (1 eq), sodium hydroxide (3 eq), hydrazine (2.5 eq), ethylene glycol (3.5 eq) are added. The reaction is then heated up to 180 °C and left to stir to completion (5 h). The reaction is allowed to cool the room temperature and is quenched with 0.5M HCl and the organic layer is extracted

with DCM (5 X 20 mL). The solvents are then removed under reduced pressure and the crude is subjected to column chromatography (1:19 ethyl acetate:hexane). This resulted in a crystalline solid in 80% yield. Compounds **2a**, **2c** are commercially available.

**General Synthesis of 1,3-Diarylacetonnes (compound 3d, 3e).** Following a procedure reported from our group,<sup>3a</sup> in two separate flame-dried, argon filled round-bottom flasks add dicyclohexylcarbodiimide (DCC) (1 eq) and 4-(dimethylamino) pyridine (0.25 eq) and stir with dry DCM (36 eq). In the second flask add the phenylacetic acid (1 eq) and dissolve in dry DCM (24 eq). Transfer the phenylacetic acid drop wise via cannula over 5 minutes. The reaction is stirred to completion (3 h). The reaction is quenched with 10 mL of 0.5M HCl and extracted with (5 X 20 mL). The solvents remaining are removed under reduced pressure and the crude is subjected to column chromatography (1:9 ethyl acetate:hexane). This resulted the crystalline solid of 60-71% yield.

**General Synthesis of Tetraphenylacetones (compound 1a, 1b, 1c).** Following a modified procedure by Rajca *et.al.*<sup>26</sup> in a flame-dried, argon filled round-bottom flask, diethyl carbonate (0.5 eq) in THF (15 eq) was added over 5 minutes to a 5:1 THF/hexane solution of (diphenylmethyl)lithium solution (5 eq) stirring at 0 °C. The reaction undergoes a color change from a light orange-red to a deep dark-red. After 1 h. the remaining diethyl carbonate (0.5 eq) in THF (15 eq) was added over 5 minutes. The reaction is warmed to room temperature and is stirred overnight. The reaction is quenched with 10 mL of 0.5M HCl and the extracted with diethyl ether (3 X 20mL) and dried over Na<sub>2</sub>SO<sub>4</sub>. The solvents were removed under reduced pressure and was subjected to column chromatography (1:4-9 acetone:hexane). The resulting crystalline solid (20-66% yield) was further recrystallized from ethanol.

**General Synthesis of Tetraphenylacetone (compound 1d, 1e).** Following a modified procedure from Satoh *et al.*,<sup>27</sup> cesium carbonate (2 eq), lithium chloride (0.2 eq), 1,3-dibenzylacetone (1 eq), and a stir bar is added into a flame-dried round-bottom flask under argon gas. The flask is then subjected to high vacuum pressure in order to rid of any oxygen. Palladium (II) chloride (0.05 eq) is added into the flask. Afterwards, anhydrous dimethylformamide (DMF) (64 eq) is added and the reaction is stirred until the mixture is homogenous. 4-iodoanisole (4 eq) is added dropwise and the reaction is heated to 100 °C and stirred to completion (5 h). The reaction is quenched with 10 mL of 0.5M HCl and the extracted with diethyl ether (3 X 20mL) and dried over Na<sub>2</sub>SO<sub>4</sub>. The solvents were removed under reduced pressure and was subjected to column chromatography (1:2.5-9 ether:hexane). The resulting solid (11-30%) was further recrystallized from ethanol.

**Solid-State Photochemistry Reaction:** Respective ketone (5-10 mg) is placed on a clean microscope slide. By using another microscope slide, the crystals are grinded down to a fine powder. Irradiate the samples via a medium-pressure Hg hanovia lamp with a pyrex filter with a cut off via medium-pressure Hg cutoff of  $\lambda \leq 270$  nm. After irradiating the sample for the allotted time, take the samples and analyze by <sup>1</sup>H NMR (500 MHz, CDCl<sub>3</sub>) for product formation.

**Di(p-tolyl)methane (compound 2b):**

80% yield. m.p. 28°C, (lit., m.p. 28°C); IR (neat)  $\nu_{\max}$  = 3049, 3019, 2915, 2855, 1510, 1438, 1107, 1021 cm<sup>-1</sup>. <sup>1</sup>H NMR (500 MHz, CDCl<sub>3</sub>)  $\delta$  7.08 (m, 8H), 3.91 (s, 2H), 2.32 (s, 6H); <sup>13</sup>C NMR (125 MHz, CDCl<sub>3</sub>)  $\delta$  138.37, 135.45, 129.13, 128.76, 41.09, 21.02. Compound spectra have been matched with reported literature values.<sup>25c</sup>

**1,3-bis(4-methoxyphenyl)propan-2-one (compound 3d):**

Yield 60%. m.p. 84-85°C, (lit., m.p. 84°C); IR(neat)  $\nu_{\max}$  = 3051, 2930, 2841, 1701, 1607, 1508, 1453, 1235, 1180, 1023  $\text{cm}^{-1}$ .  $^1\text{H}$  NMR (500 MHz,  $\text{CDCl}_3$ )  $\delta$  6.85-7.05 (AA'BB', 8H), 3.79 (s, 6H), 3.64 (s, 4H);  $^{13}\text{C}$  NMR (125 MHz,  $\text{CDCl}_3$ )  $\delta$  206.52, 158.66, 130.52, 126.11, 114.15, 55.28, 48.06. Compound spectra have been matched with reported literature values.<sup>3a</sup>

**1,3-bis(4-fluorophenyl)propan-2-one (compound 3e):**

71%. m.p. 61-63 °C, (lit., m.p. 62-64°C); IR (neat)  $\nu_{\max}$  = 3042, 2925, 2855, 1711, 1604, 1508, 1338, 1209, 1160, 1058  $\text{cm}^{-1}$ .  $^1\text{H}$  NMR (500 MHz,  $\text{CDCl}_3$ )  $\delta$  7.04 (m, 8H), 3.70 (s, 4H);  $^{13}\text{C}$  NMR (125 MHz,  $\text{CDCl}_3$ )  $\delta$  205.07, 163.01, 160.85, 131.03, 130.97, 129.47, 129.43, 115.72, 115.55, 48.18. Compound spectra have been matched with reported literature values.<sup>3a</sup>

**1,1,3,3-tetraphenylpropan-2-one (compound 1a):**

Yield 66%. m.p. 133-134°C, (lit., m.p. 134°C); Using ethyl acetate and hexanes (1:19) ( $R_f$  = 0.4); IR(neat)  $\nu_{\max}$  = 3054, 3022, 1706, 1597, 1493, 1451, 1058  $\text{cm}^{-1}$ .  $\lambda_{\max}$  = 227.13, 261.76, 302.81. DLS = 68 nm  $\pm$  23 nm.  $^1\text{H}$  NMR (500 MHz,  $\text{CDCl}_3$ )  $\delta$  7.24 (m, 20H), 7.25 (s, 2H);  $^{13}\text{C}$  NMR (125 MHz,  $\text{CDCl}_3$ )  $\delta$  205.51, 138.06, 129.12, 128.69, 127.28, 63.52. Compound spectra have been matched with reported literature values.<sup>26</sup>

**1,1,3,3-tetra-p-tolylpropan-2-one (compound 1b):**

Yield 51%. m.p. 85.5-86.8°C. Using ethyl acetate and hexanes (1:19) ( $R_f$  = 0.44); IR(neat)  $\nu_{\max}$  = 3091, 3024, 2923, 2863, 1704, 1510, 1307, 1066, 1026  $\text{cm}^{-1}$ .  $\lambda_{\max}$  = 234, 267.81, 275.75. DLS = 140 nm  $\pm$  60 nm.  $^1\text{H}$  NMR (500 MHz,  $\text{CDCl}_3$ )  $\delta$  7.01-7.09 (AA'BB', 16H), 5.17 (s, 2H), 2.31 (s, 12H).  $^{13}\text{C}$  NMR (125 MHz,  $\text{CDCl}_3$ )  $\delta$  205.92, 136.76, 135.46, 129.34, 128.93, 62.56, 21.06. HRMS (DART) calcd. for  $[\text{C}_{31}\text{H}_{30}\text{O}+\text{H}]^+$  419.23302, found 419.23326

**1,1,3,3-tetrakis(4-chlorophenyl)propan-2-one (compound 1c):**

Yield 20%. m.p. 162.1-163.4°C. Using ethyl acetate and hexanes (1:19) ( $R_f = 0.4$ ); IR(neat)  $\nu_{\max} = 3086, 2982, 2913, 2856, 1721, 1493, 1406, 1286, 1091, 1014 \text{ cm}^{-1}$ .  $\lambda_{\max} = 236.67, 269.33, 278.01$ . DLS = 200 nm  $\pm$  77nm.  $^1\text{H}$  NMR (500 MHz,  $\text{CDCl}_3$ )  $\delta$  7.03-7.26 (AA'BB', 16H), 5.13 (s, 2H).  $^{13}\text{C}$  NMR (125 MHz,  $\text{CDCl}_3$ )  $\delta$  204.36, 135.69, 133.83, 130.18, 129.15, 62.15. HRMS (DART) calcd. for  $[\text{C}_{27}\text{H}_{18}\text{Cl}_4\text{O}+\text{H}]^+$  499.01118, found 499.01110

**1,1,3,3-tetrakis(4-methoxyphenyl)propan-2-one (compound 1d):**

Yield 11%. m.p. 101.8-102.7°C. Using ethyl acetate and hexanes (1:19) ( $R_f = 0.05$ ); IR(neat)  $\nu_{\max} = 3064, 3002, 2935, 2836, 1716, 1607, 1505, 1297, 1247, 1172, 1031 \text{ cm}^{-1}$ .  $\lambda_{\max} = 241.63, 277.63$ . DLS = 160 nm  $\pm$  65nm.  $^1\text{H}$  NMR (500 MHz,  $\text{CDCl}_3$ )  $\delta$  6.82-7.04 (AA'BB', 16H), 5.14 (s, 2H), 3.78 (s, 12H).  $^{13}\text{C}$  NMR (125 MHz,  $\text{CDCl}_3$ )  $\delta$  206.60, 158.68, 130.66, 130.08, 114.06, 61.64, 55.26. HRMS (DART) calcd. for  $[\text{C}_{31}\text{H}_{30}\text{O}_5+\text{H}]^+$  483.21268, found 483.21658

**1,1,3,3-tetrakis(4-fluorophenyl)propan-2-one (compound 1e):**

Yield 30%. m.p. 169.3-171.1°C. Using ethyl acetate and hexanes (1:19) ( $R_f = 0.4$ ); IR(neat)  $\nu_{\max} = 3074, 2910, 1716, 1602, 1508, 1230, 1158 \text{ cm}^{-1}$ .  $\lambda_{\max} = 224.45, 266.3, 270.35$ . DLS = 160 nm  $\pm$  67 nm.  $^1\text{H}$  NMR (500 MHz,  $\text{CDCl}_3$ )  $\delta$  7.00-7.07 (m, 16H), 5.19 (s, 2H).  $^{13}\text{C}$  NMR (125 MHz,  $\text{CDCl}_3$ )  $\delta$  205.29, 163.16, 163.19, 133.38, 133.36, 130.52, 130.45, 115.91, 115.74, 61.85. HRMS (DART) calcd. for  $[\text{C}_{27}\text{H}_{18}\text{F}_4\text{O}+\text{H}]^+$  435.13273, found 435.12813

**1,1,2,2-tetraphenylethane (compound 4a):**

Yield <99%. m.p. 213 °C, (lit., m.p. 213°C); IR(neat)  $\nu_{\max} = 3024, 2890, 1597, 1495, 1448, 173, 1028 \text{ cm}^{-1}$ .  $\lambda_{\max} = 227.89, 263.27$ .  $^1\text{H}$  NMR (500 MHz,  $\text{CDCl}_3$ )  $\delta$  7.08 (m, 20H), 4.77 (s, 2H);  $^{13}\text{C}$  NMR (125 MHz,  $\text{CDCl}_3$ )  $\delta$  143.47, 128.52, 128.15, 125.85, 56.34. Compound spectra have been matched with reported literature values.<sup>12b</sup>



**1,1,2,2-tetra-p-tolylethane (compound 4b):**

Yield <99%. m.p. 278°C, (lit., m.p. 278-280°C); IR(neat)  $\nu_{\max}$  = 3096, 3019, 2920, 1510, 1190, 1019  $\text{cm}^{-1}$ .  $\lambda_{\max}$  = 235.91, 267.44.  $^1\text{H}$  NMR (500 MHz,  $\text{CDCl}_3$ )  $\delta$  7.01-7.09 (AA'BB', 16H), 5.17 (s, 2H), 2.31 (s, 12H).  $^{13}\text{C}$  NMR (125 MHz,  $\text{CDCl}_3$ )  $\delta$  205.92, 136.76, 135.46, 129.34, 128.93, 62.56, 21.06. Compound spectra have been matched with reported literature values.<sup>12b</sup>

**1,1,2,2-tetrakis(4-chlorophenyl)ethane (compound 4c):**

Yield <99%. m.p. 300°C, (lit., m.p. 300-325°C); IR(neat)  $\nu_{\max}$  = 3029, 2925, 1493, 1406, 1290, 1088, 1011  $\text{cm}^{-1}$ .  $\lambda_{\max}$  = 236.47, 258.73.  $^1\text{H}$  NMR (500 MHz,  $\text{CDCl}_3$ )  $\delta$  7.01-7.011 (AA'BB', 16H), 4.61 (s, 2H).  $^{13}\text{C}$  NMR (125 MHz,  $\text{CDCl}_3$ )  $\delta$  140.55, 132.03, 128.69, 129.57, 54.83. Compound spectra have been matched with reported literature values.<sup>12b</sup>

**1,1,2,2-tetrakis(4-methoxyphenyl)ethane (compound 4d):**

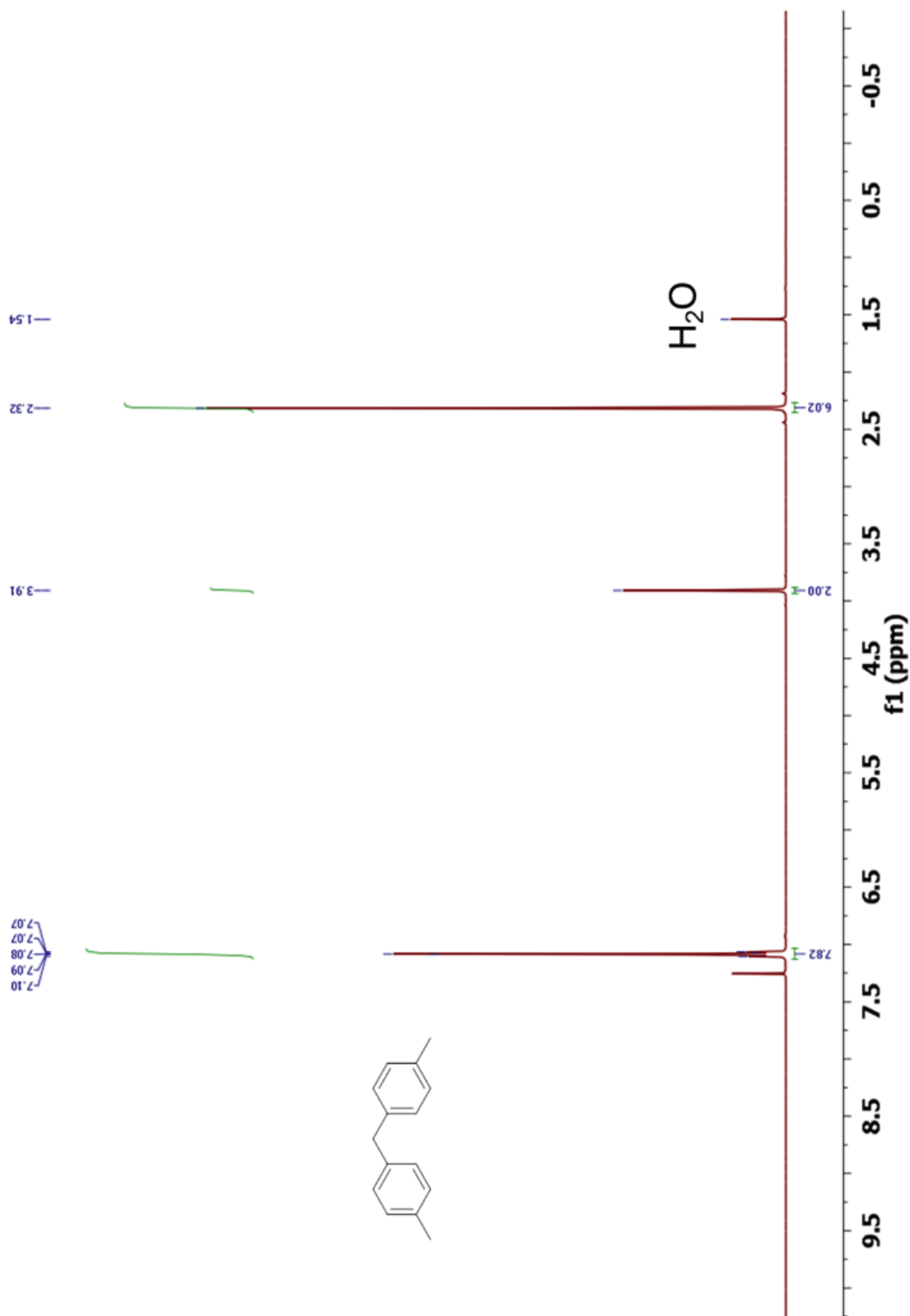
Yield <99%. m.p. 196°C, (lit., m.p. 198-199°C); IR(neat)  $\nu_{\max}$  = 3034, 2922, 2850, 1609, 1508, 1463, 1247, 1172, 1031.  $\lambda_{\max}$  = 246.2, 273.48.  $^1\text{H}$  NMR (500 MHz,  $\text{CDCl}_3$ )  $\delta$  6.65-7.00 (AA'BB', 16H), 4.55 (s, 2H), 3.68 (s, 12H).  $^{13}\text{C}$  NMR (125 MHz,  $\text{CDCl}_3$ )  $\delta$  157.65, 136.46, 129.30, 113.50, 55.07. Compound spectra have been matched with reported literature values.<sup>12b</sup>

**1,1,2,2-tetrakis(4-fluorophenyl)ethane (compound 4e):**

Yield <99%. m.p. 251°C, (lit., m.p. 254-256°C); IR(neat)  $\nu_{\max}$  = 3042, 1602, 1505, 1420 1304, 1217, 1157, 1016  $\text{cm}^{-1}$ .  $\lambda_{\max}$  = 232.48, 261, 270.84.  $^1\text{H}$  NMR (500 MHz,  $\text{CDCl}_3$ )  $\delta$  7.03-6.82 (m, 16H), 4.62 (s, 2H), 2.31 (s, 12H).  $^{13}\text{C}$  NMR (125 MHz,  $\text{CDCl}_3$ )  $\delta$  162.11, 160.17, 138.58, 138.54, 129.74, 129.68, 115.33, 115.16, 55.09. Compound spectra have been matched with reported literature values.<sup>12b</sup>

### 2.5.3 Spectral Characterization Data $^1\text{H}$ NMR and $^{13}\text{C}$ NMR, UV-VIS

Figure 2.S1.  $^1\text{H}$  NMR (500 MHz,  $\text{CDCl}_3$ ) of Di(p-tolyl)methane (2b)



**Figure 2.S2:**  $^{13}\text{C}$  NMR (125 MHz,  $\text{CDCl}_3$ ) of Di(p-tolyl)methane (**2b**)

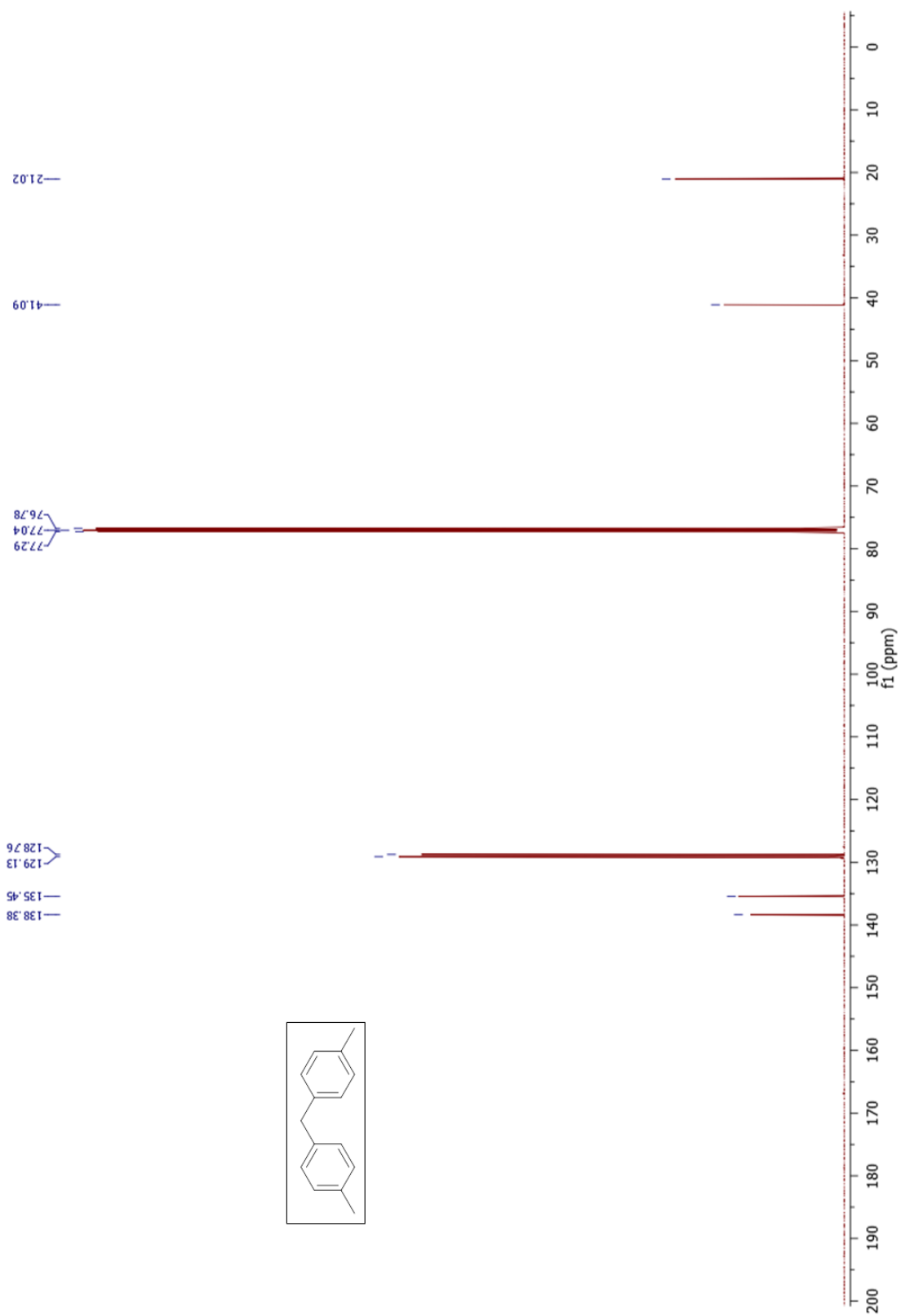
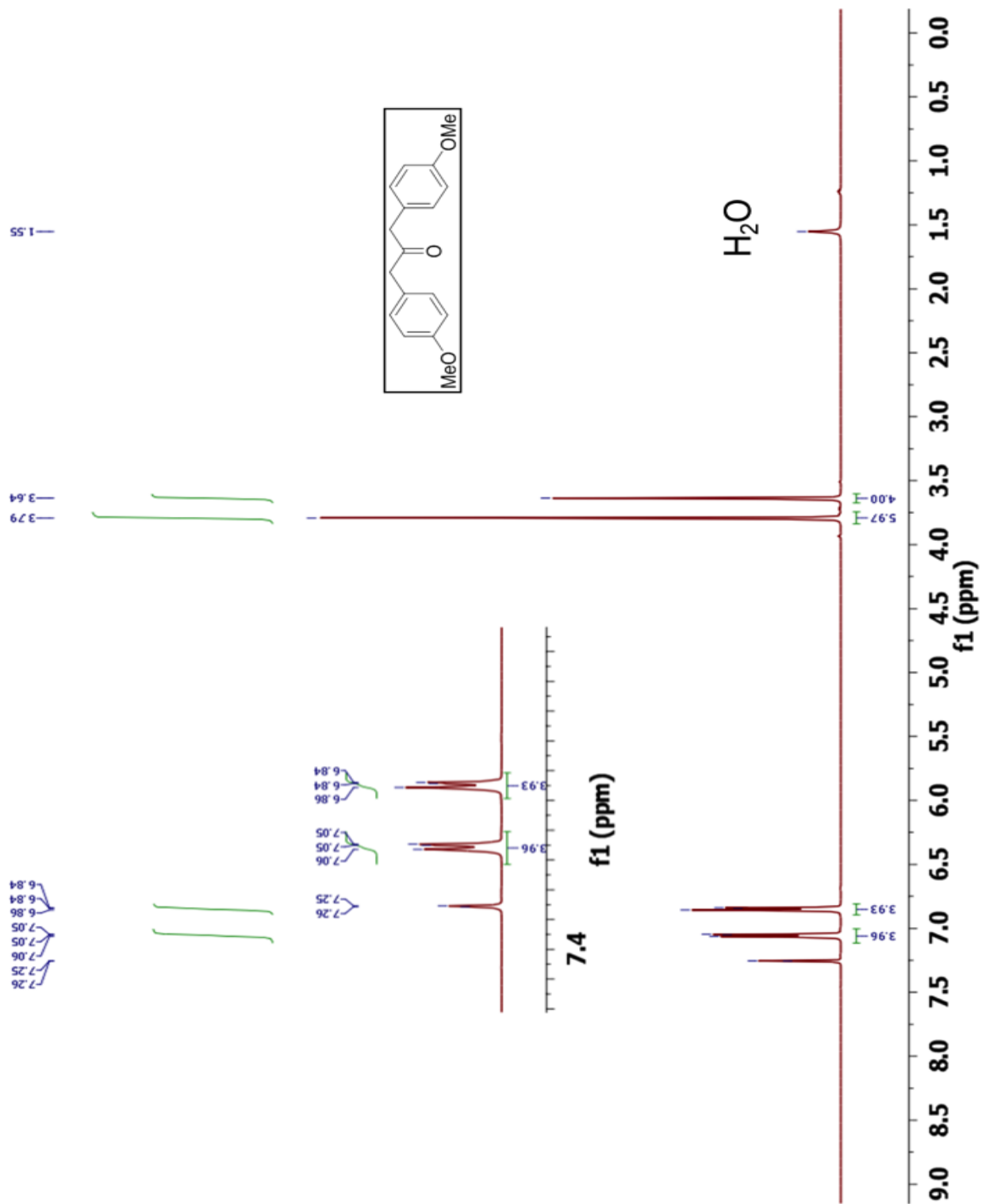


Figure 2.S3.  $^1\text{H}$  NMR (500 MHz,  $\text{CDCl}_3$ ) of 1,3-bis(4-methoxyphenyl)propan-2-one (**3d**)



**Figure 2.S4:**  $^{13}\text{C}$  NMR (125 MHz,  $\text{CDCl}_3$ ) of 1,3-bis(4-methoxyphenyl)propan-2-one (**3d**)

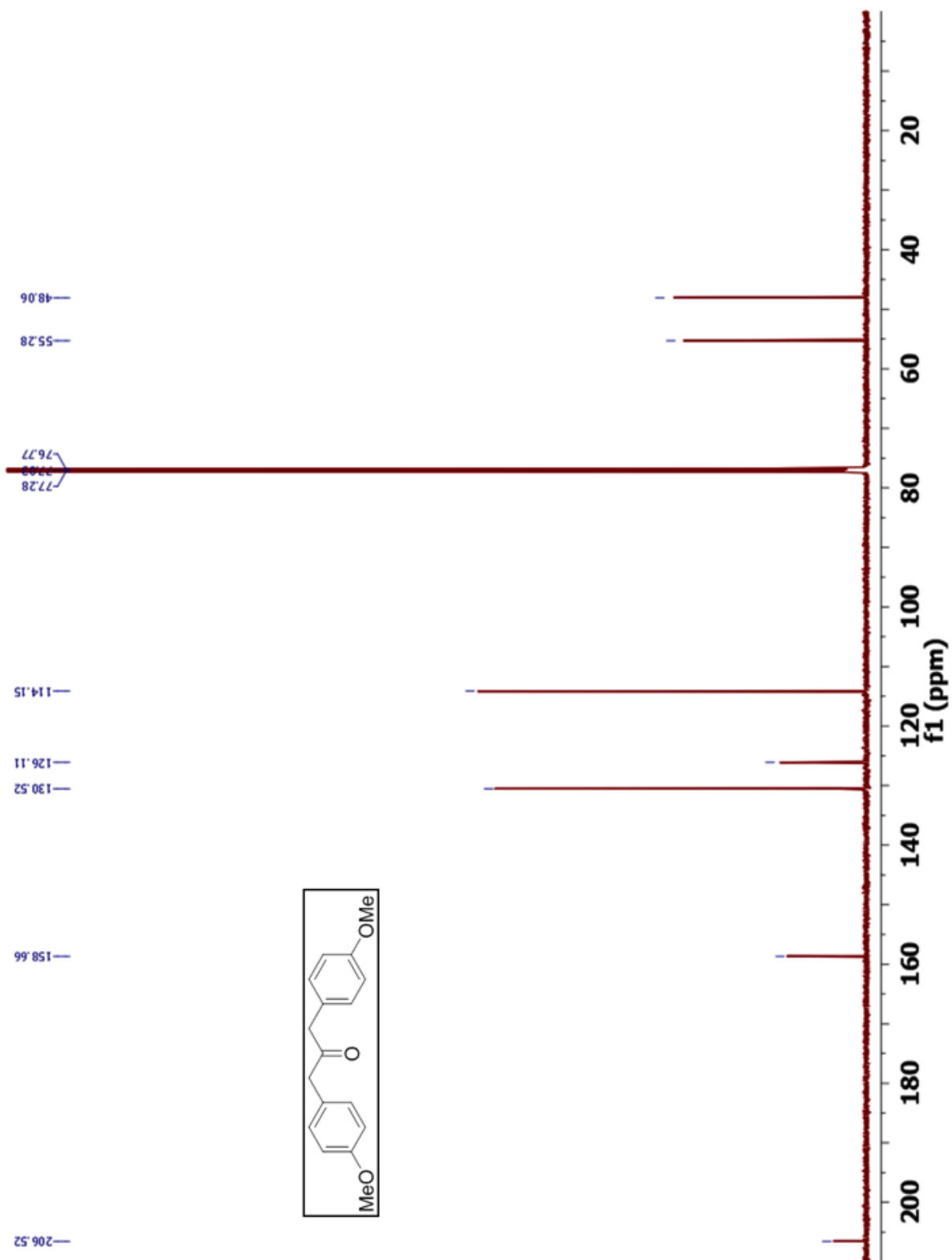


Figure 2.S5.  $^1\text{H}$  NMR (500 MHz,  $\text{CDCl}_3$ ) of 1,3-bis(4-fluorophenyl)propan-2-one (**3e**)

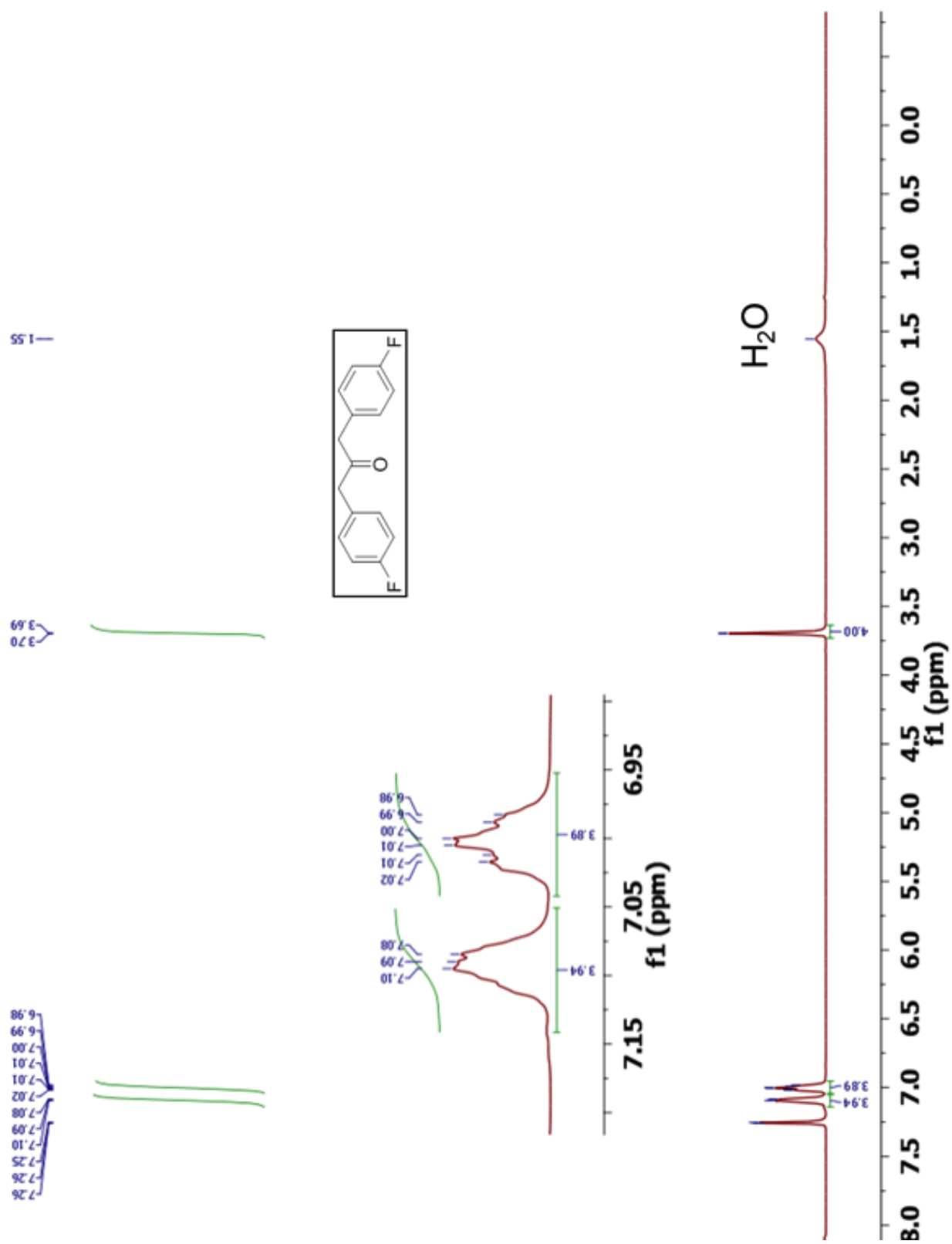


Figure 2.S6:  $^{13}\text{C}$  NMR (125 MHz,  $\text{CDCl}_3$ ) of 1,3-bis(4-fluorophenyl)propan-2-one (**3e**)

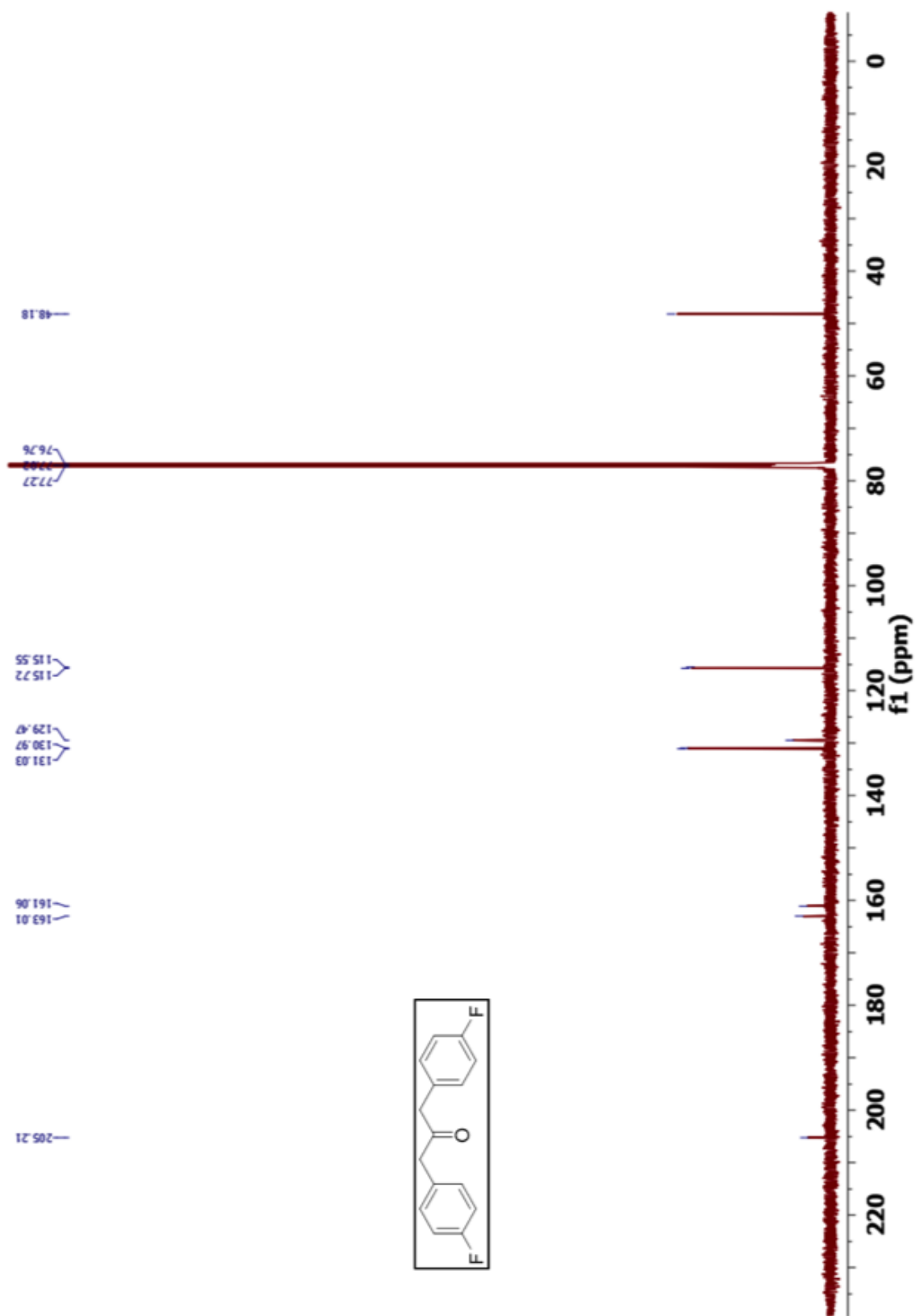
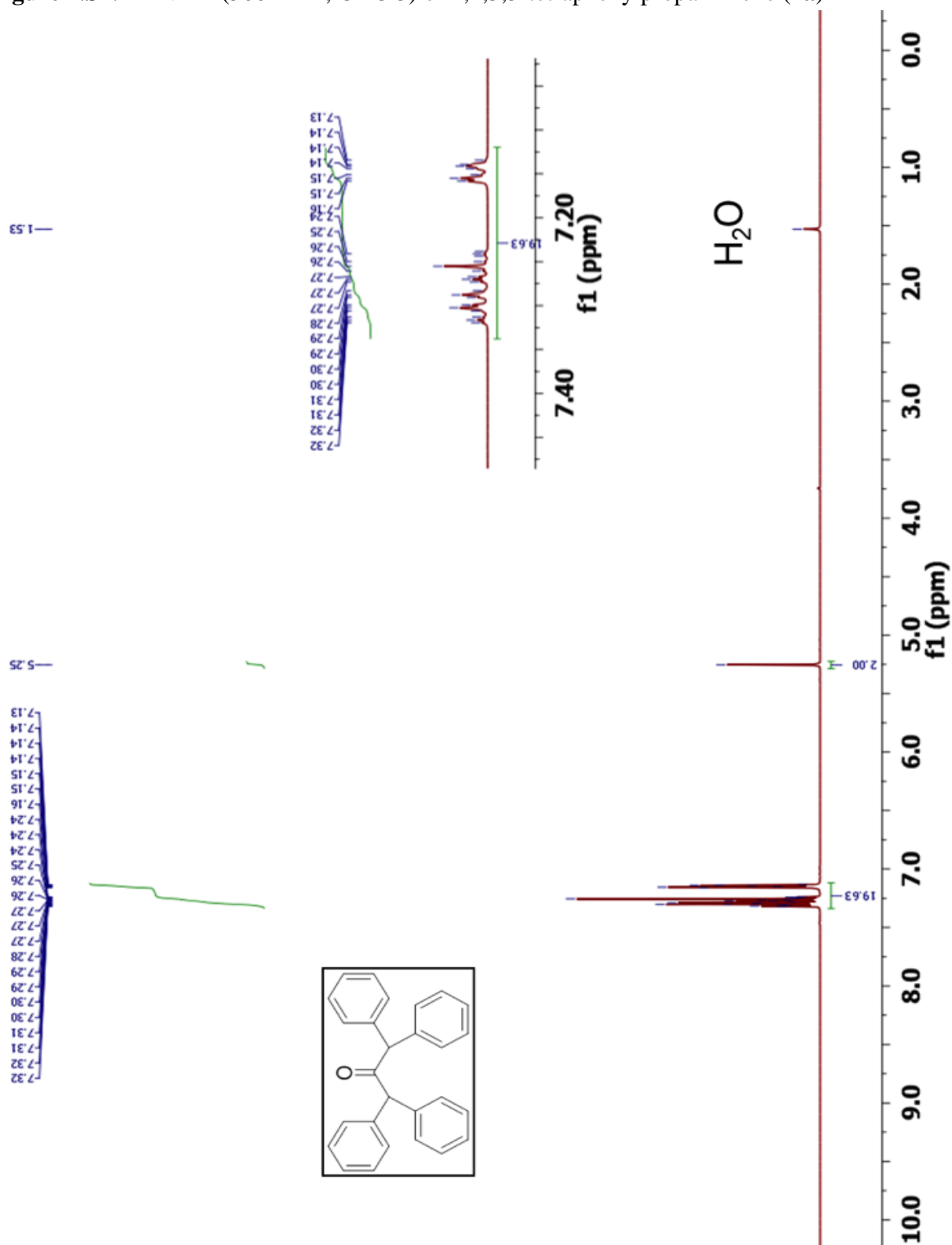
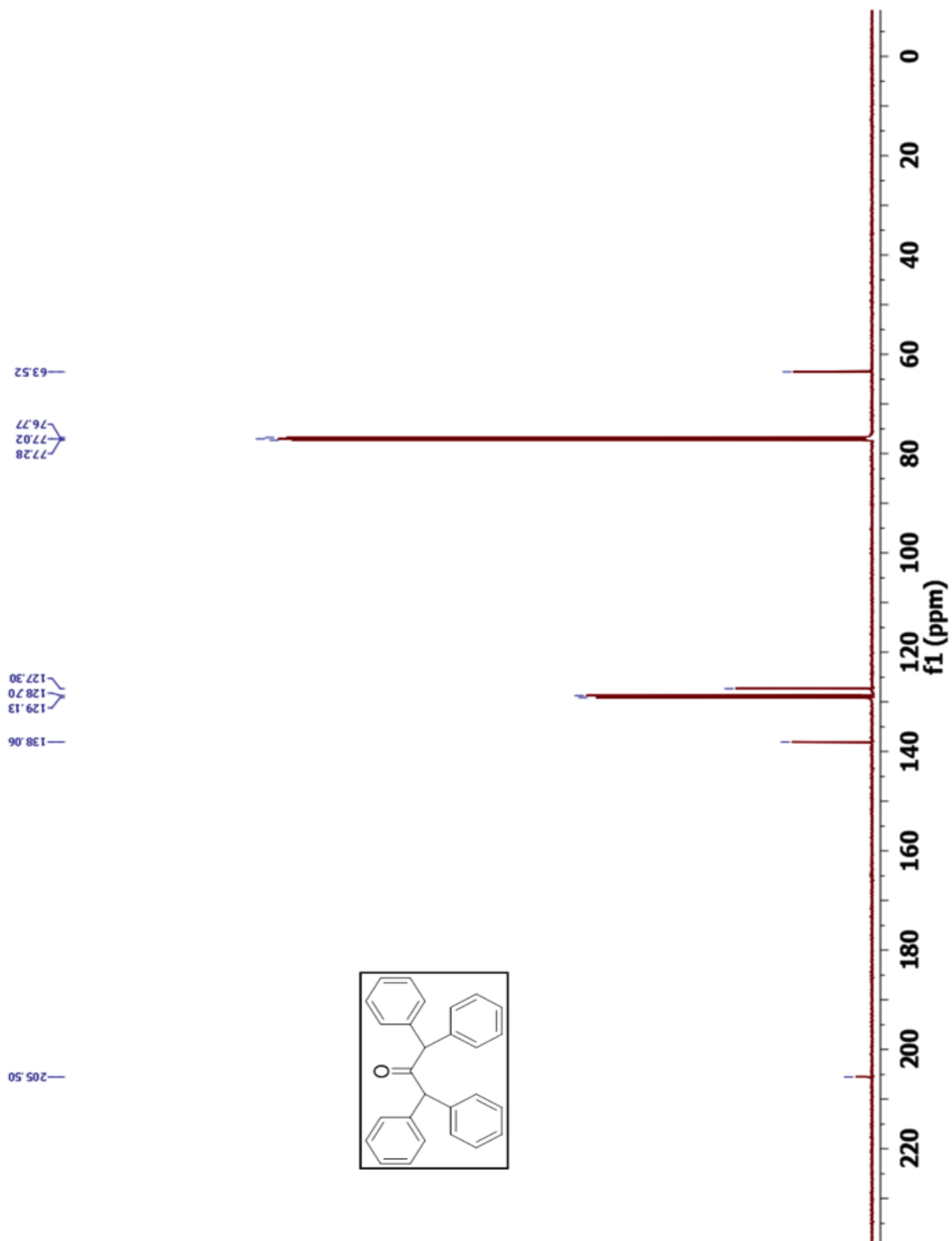


Figure 2.S7.  $^1\text{H}$  NMR (500 MHz,  $\text{CDCl}_3$ ) of 1,1,3,3-tetraphenylpropan-2-one (**1a**)





**Figure 2.S8.**  $^{13}\text{C}$  NMR (500 MHz,  $\text{CDCl}_3$ ) of 1,1,3,3-tetraphenylpropan-2-one (**1a**)



**Figure S9:**  $^1\text{H}$  NMR (125 MHz,  $\text{CDCl}_3$ ) of 1,1,3,3-tetra-*p*-tolylpropan-2-one (**1b**)

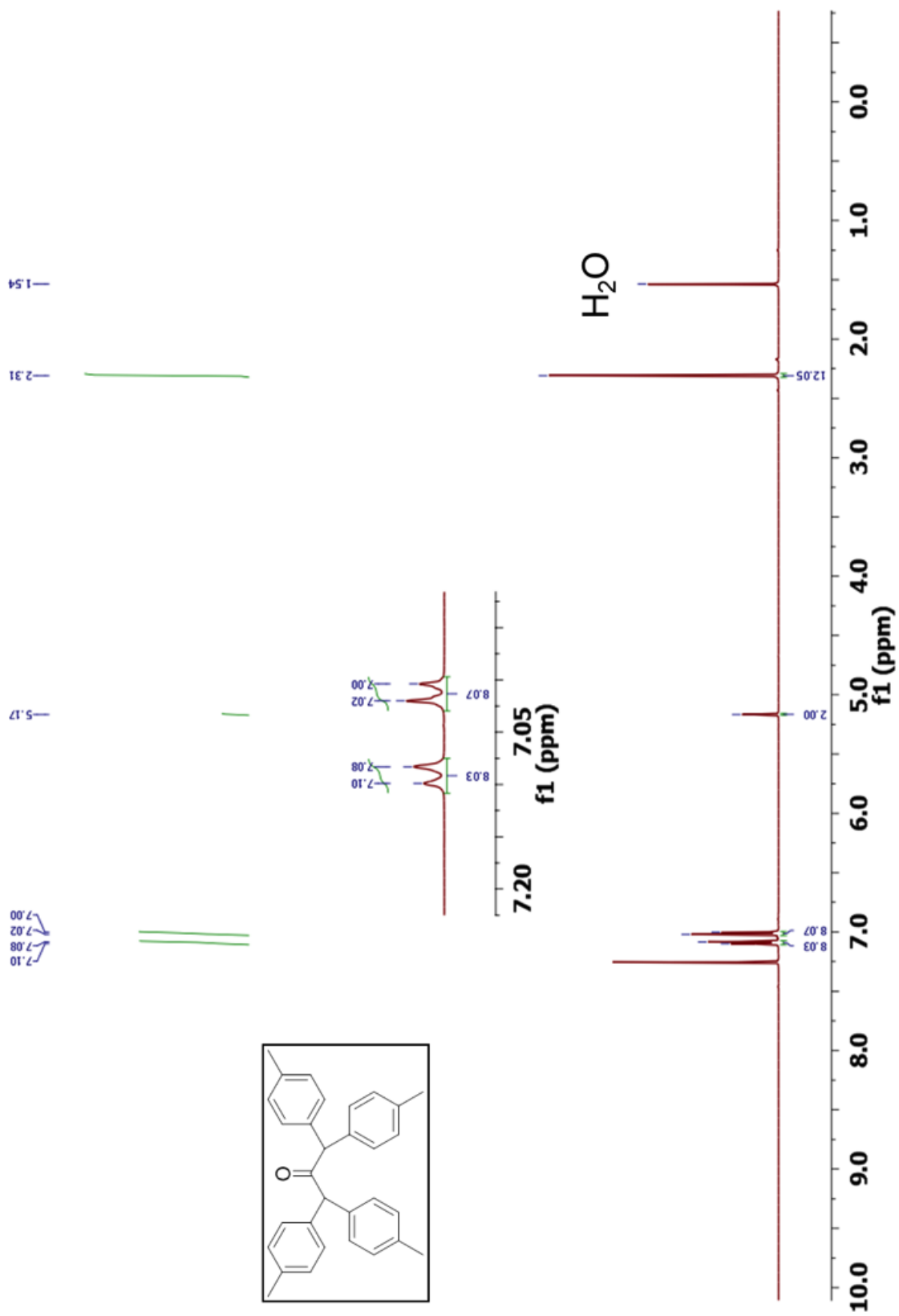
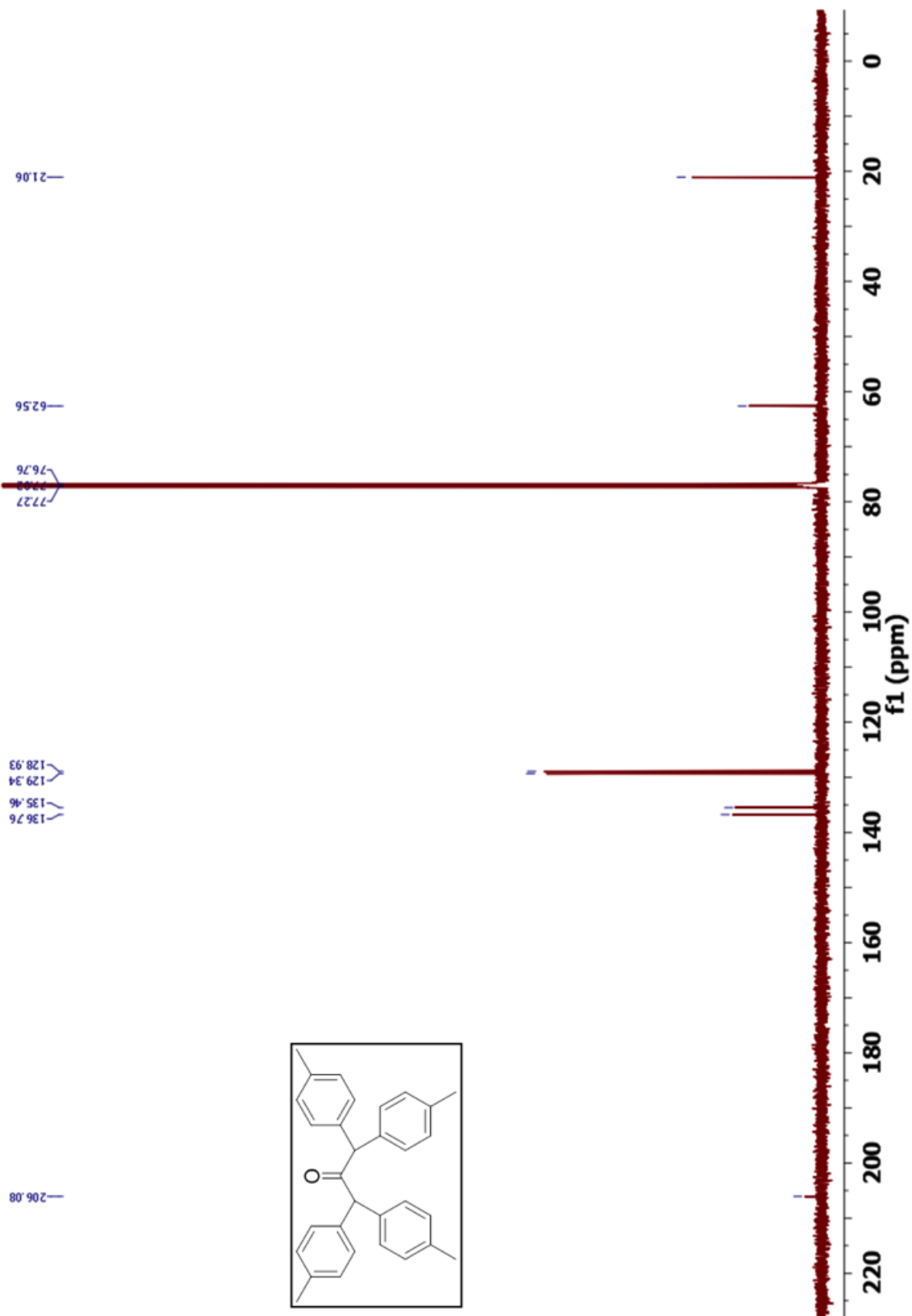
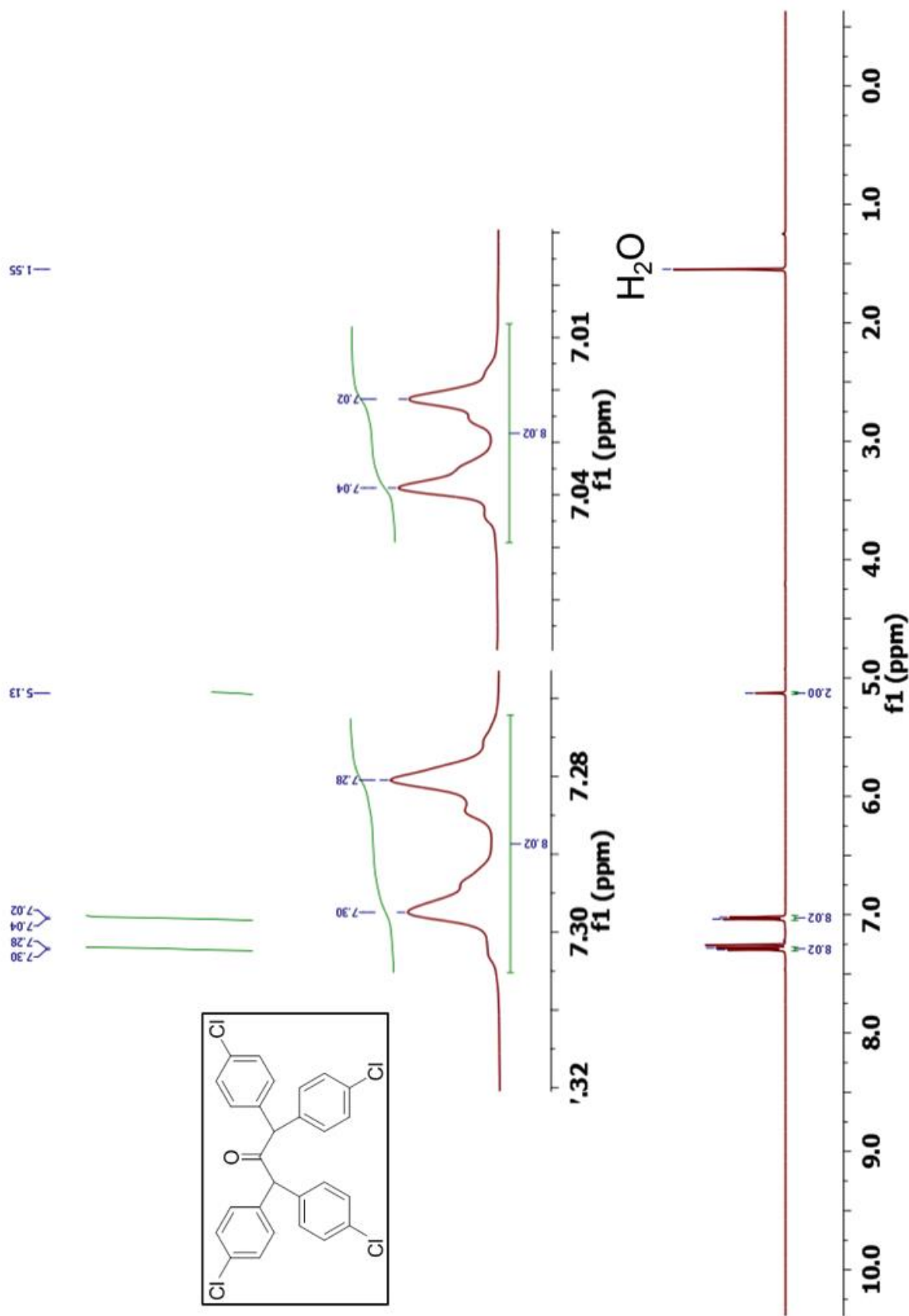


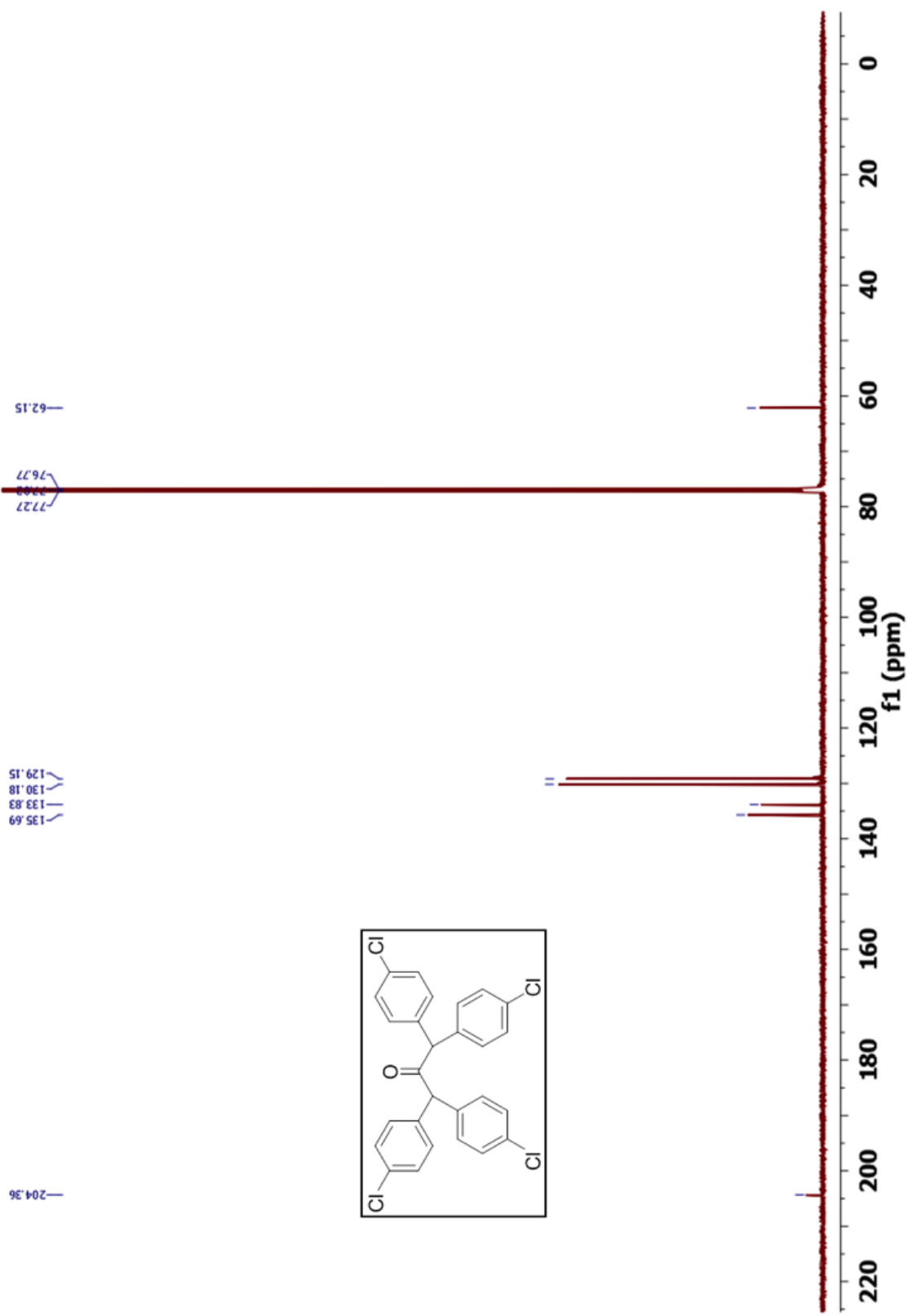
Figure 2.S10.  $^{13}\text{C}$  NMR (125 MHz,  $\text{CDCl}_3$ ) of 1,1,3,3-tetra-p-tolylpropan-2-one (**1b**)



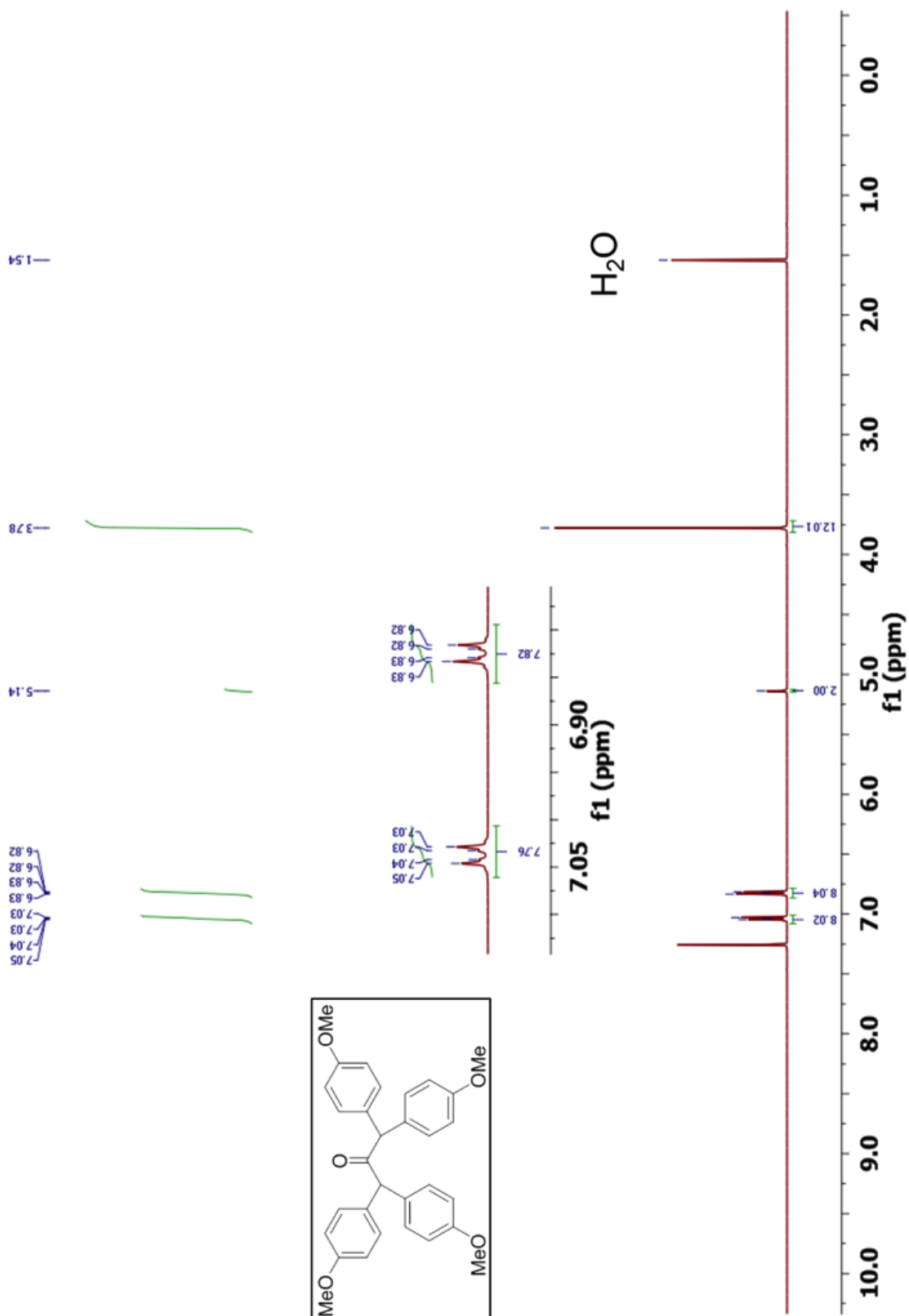
**Figure 2.S11:**  $^1\text{H}$  NMR (500 MHz,  $\text{CDCl}_3$ ) of 1,1,3,3-tetrakis(4-chlorophenyl)propan-2-one (**1c**)



**Figure 2.S12.**  $^{13}\text{C}$  NMR (125 MHz,  $\text{CDCl}_3$ ) of 1,1,3,3-tetrakis(4-chlorophenyl)propan-2-one (**1c**)



**Figure 2.S13:**  $^1\text{H}$  NMR (500 MHz,  $\text{CDCl}_3$ ) of 1,1,3,3-tetrakis(4-methoxyphenyl)propan-2-one (**1d**)



**Figure S14.**  $^{13}\text{C}$  NMR (125 MHz,  $\text{CDCl}_3$ ) of 1,1,3,3-tetrakis(4-methoxyphenyl)propan-2-one (**1d**)

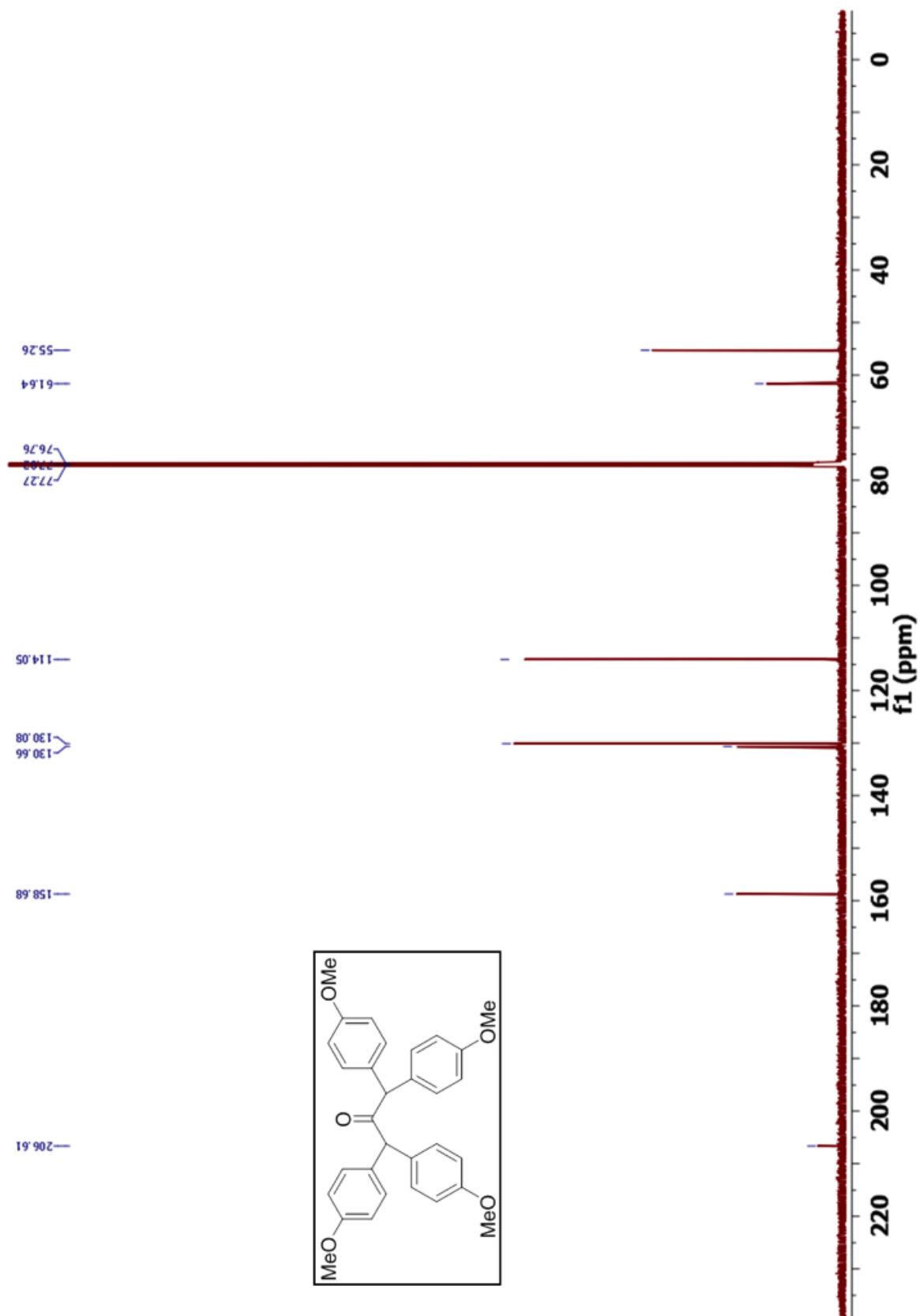
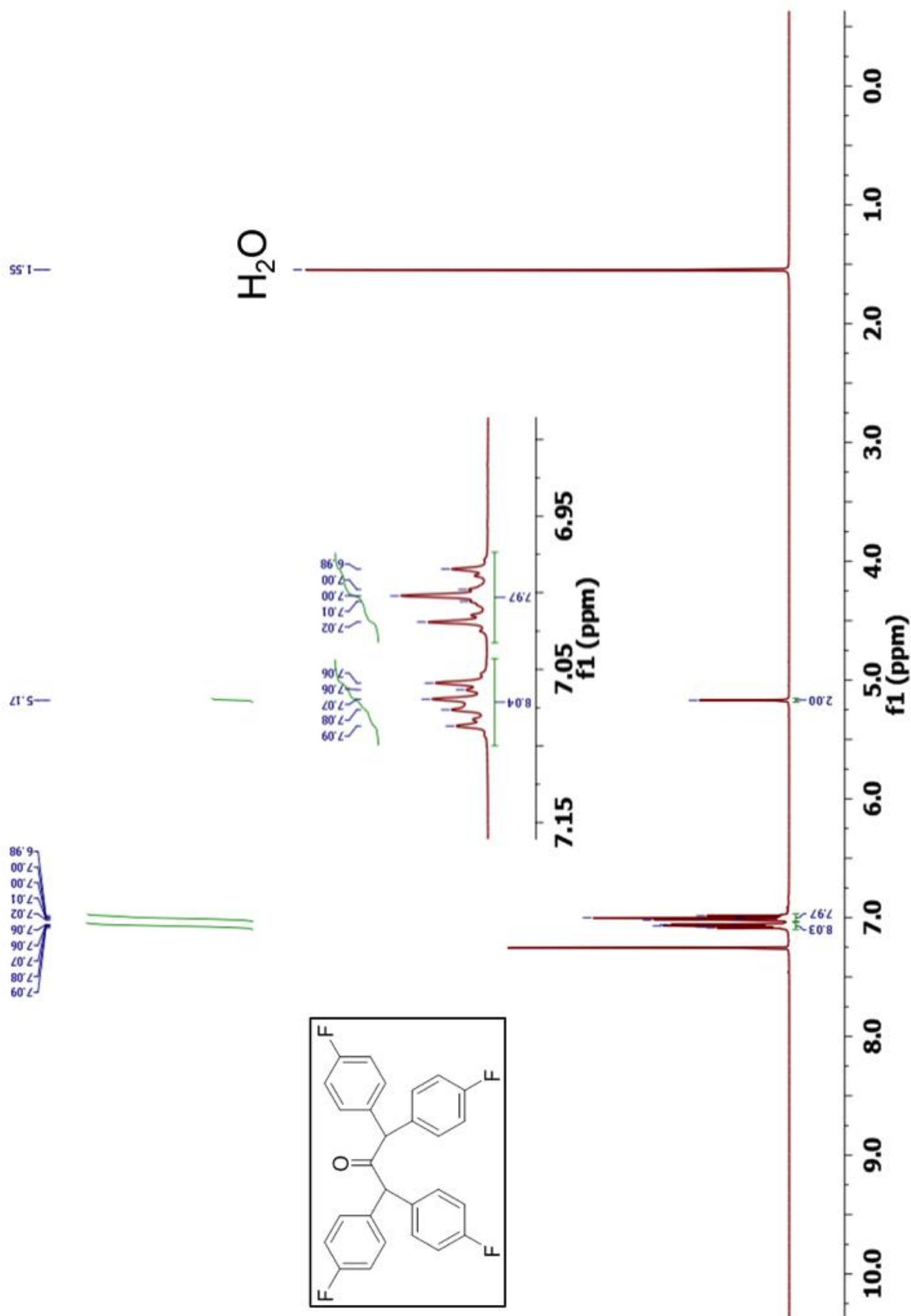


Figure 2.S15.  $^1\text{H}$  NMR (125 MHz,  $\text{CDCl}_3$ ) of 1,1,3,3-tetrakis(4-fluorophenyl)propan-2-one (**1e**)





**Figure 2.S16.**  $^{13}\text{C}$  NMR (125 MHz,  $\text{CDCl}_3$ ) of 1,1,3,3-tetrakis(4-fluorophenyl)propan-2-one (**1e**)

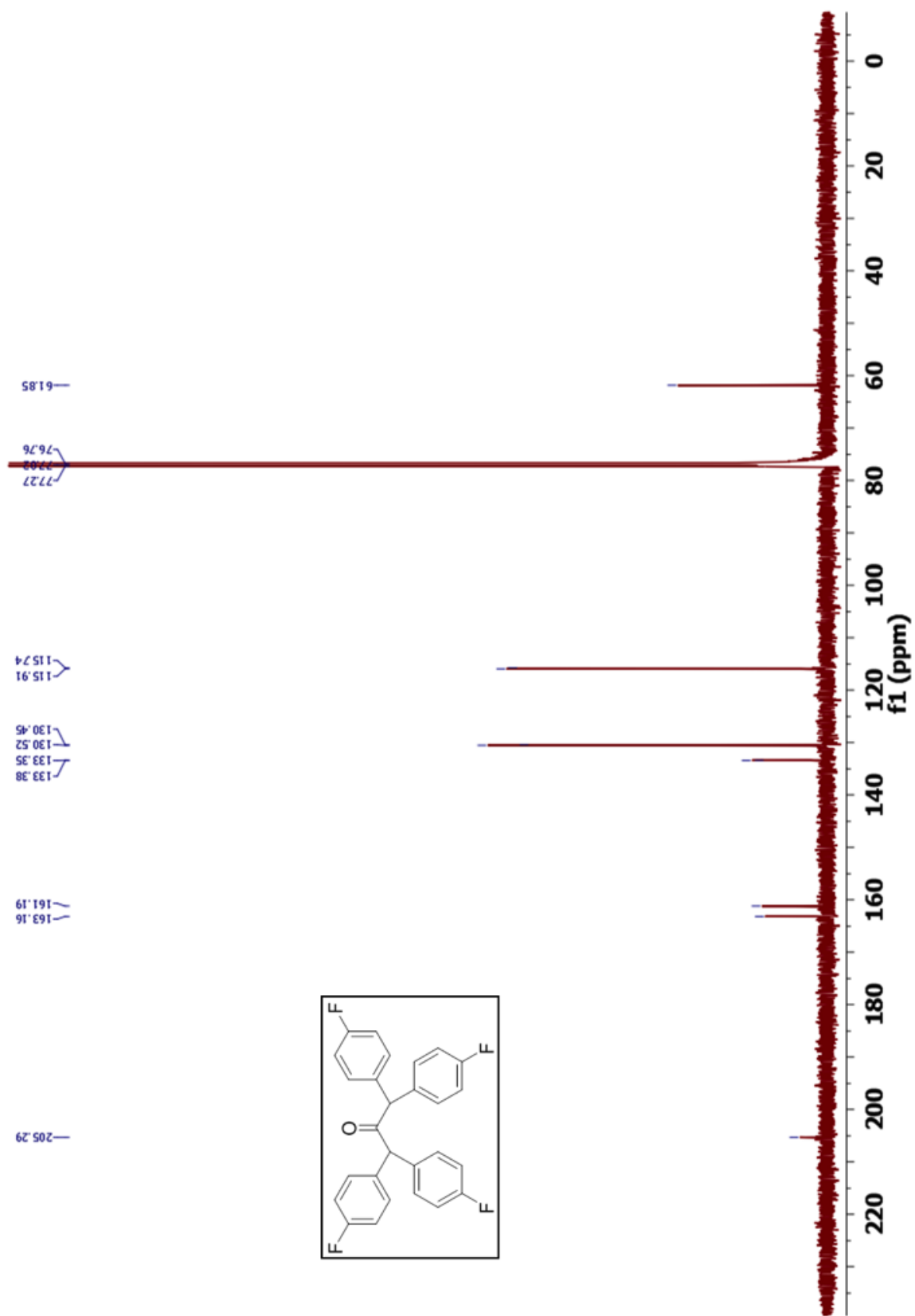
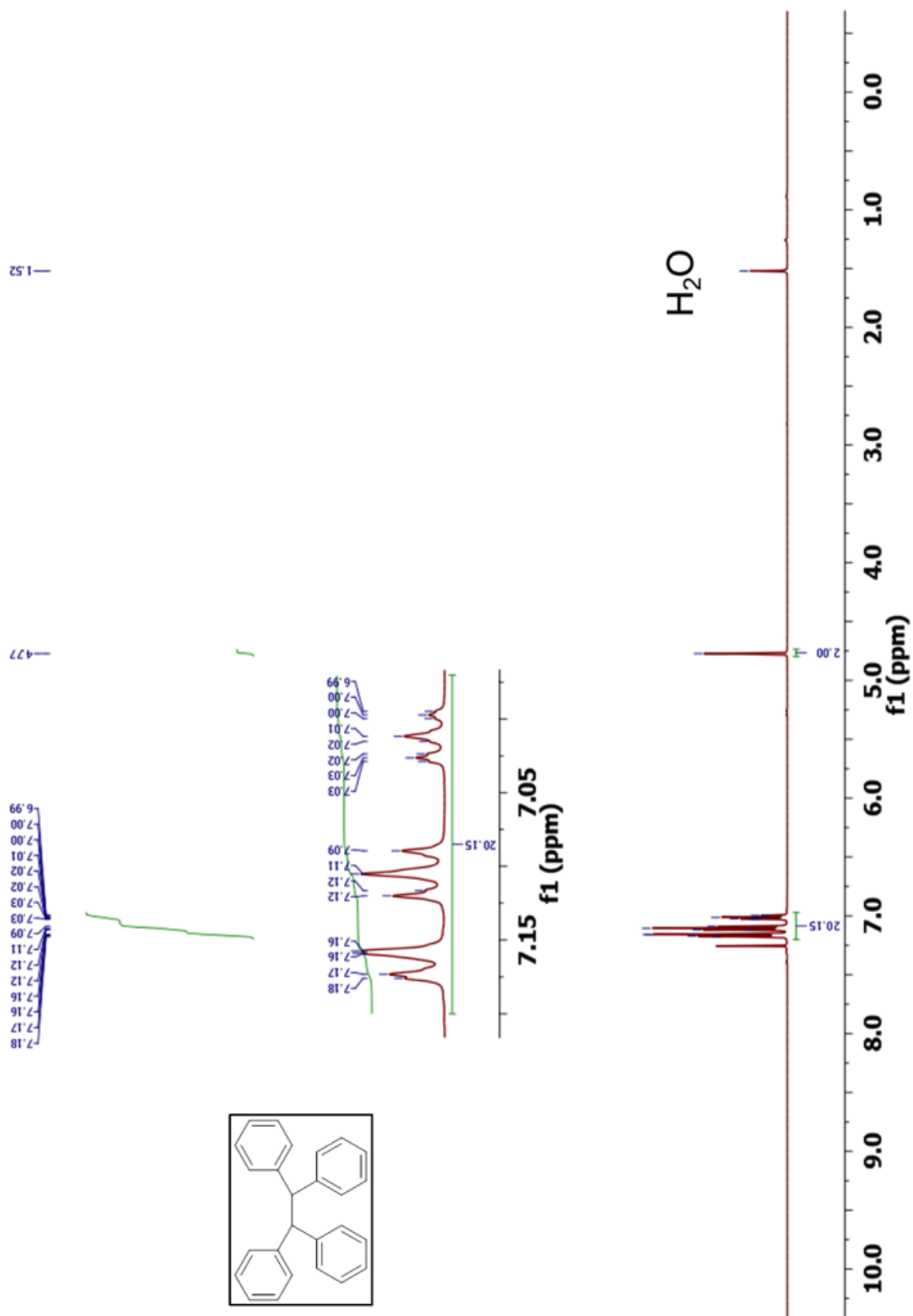


Figure 2.S17.  $^1\text{H}$  NMR (500 MHz,  $\text{CDCl}_3$ ) of 1,1,2,2-tetraphenylethane (**4a**)<sup>28</sup>



**Figure 2.S18:**  $^{13}\text{C}$  NMR (125 MHz,  $\text{CDCl}_3$ ) of 1,1,2,2-tetraphenylethane (**4a**)<sup>28</sup>

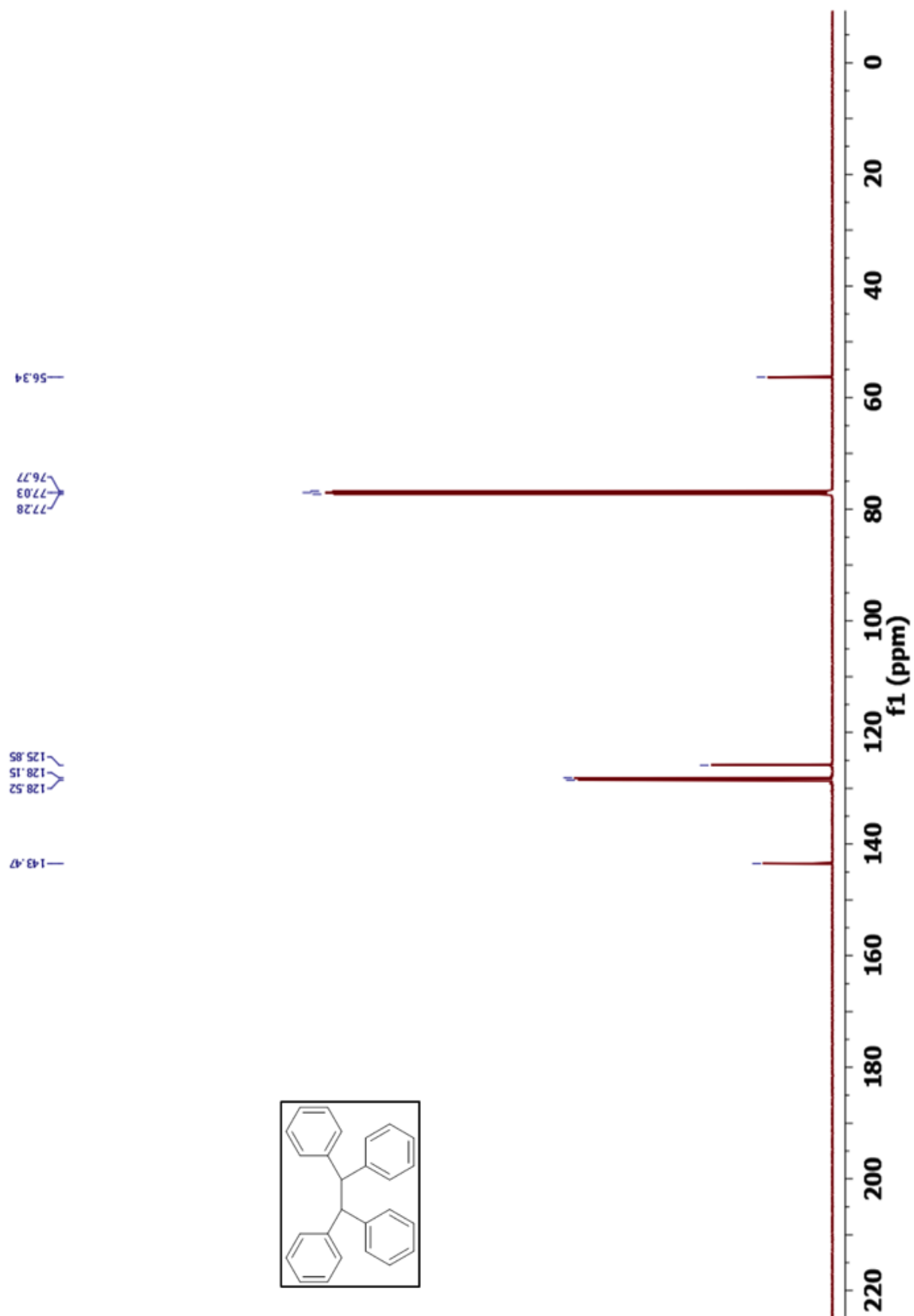


Figure 2.S19.  $^1\text{H}$  NMR (500 MHz,  $\text{CDCl}_3$ ) of 1,1,2,2-tetra-*p*-tolylethane (**4b**)<sup>12b</sup>

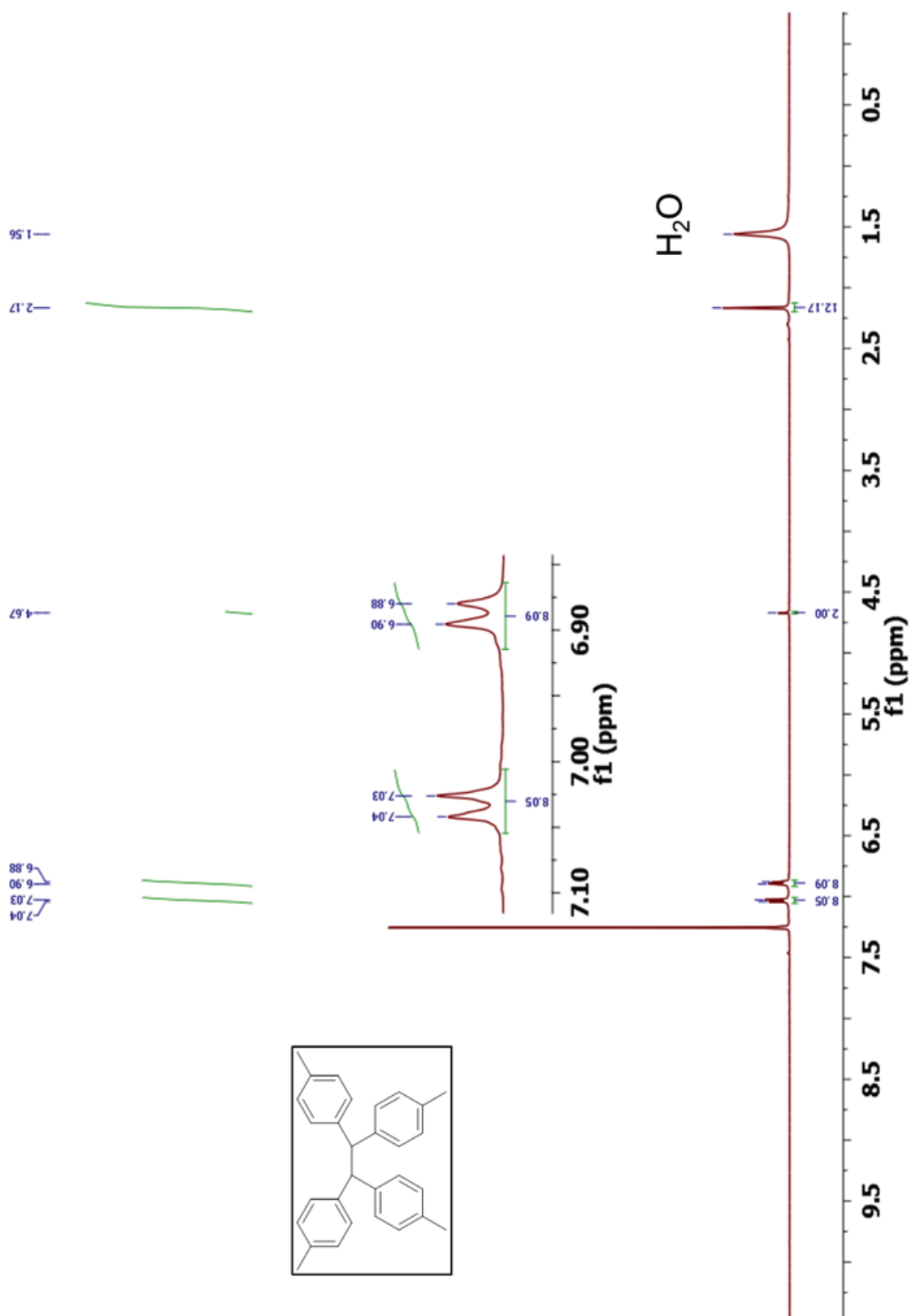
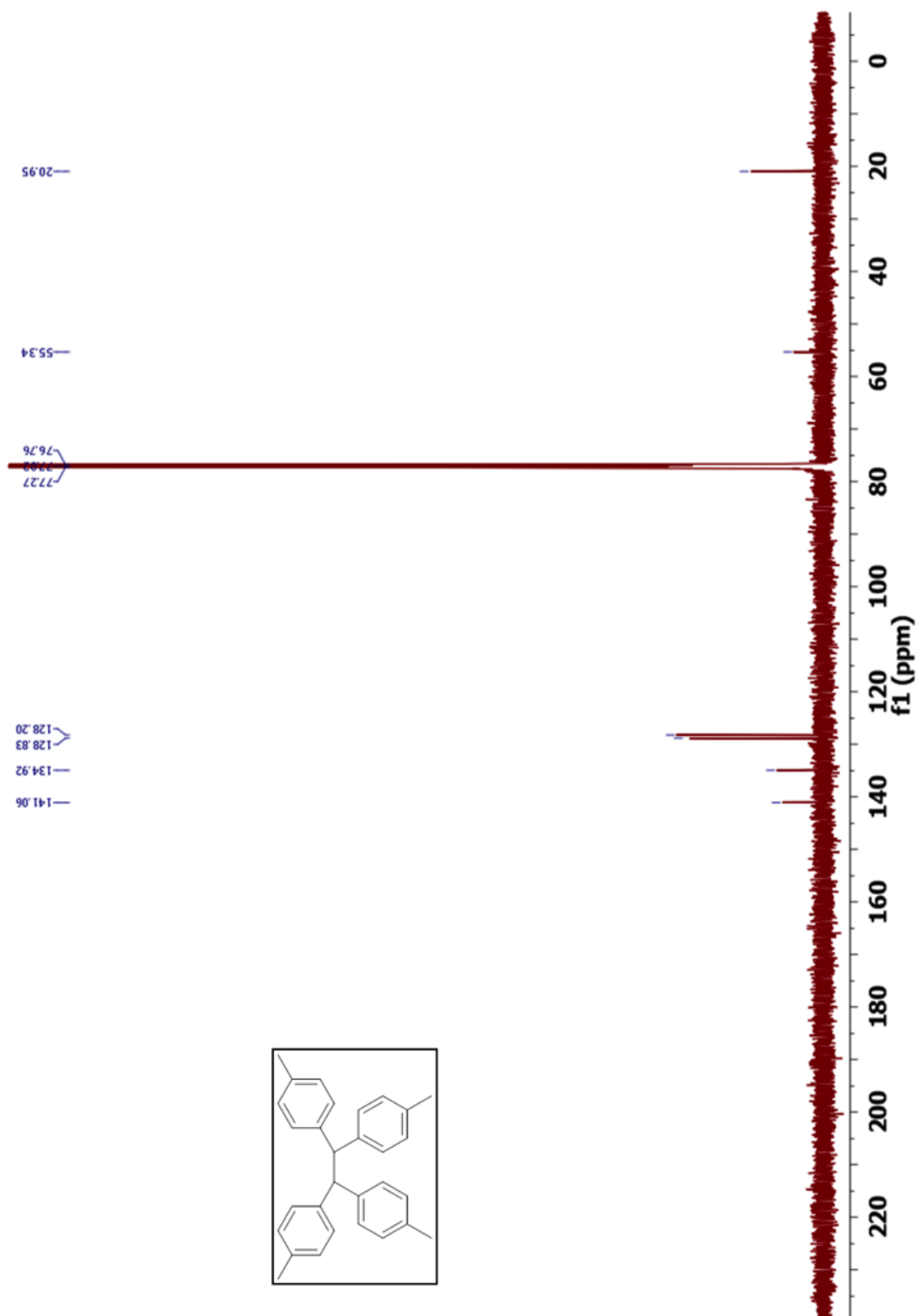


Figure 2.S20:  $^{13}\text{C}$  NMR (125 MHz,  $\text{CDCl}_3$ ) of 1,1,2,2-tetra-p-tolylolethane (**4b**)<sup>12b</sup>



**Figure 2.S21.**  $^1\text{H}$  NMR (500 MHz,  $\text{CDCl}_3$ ) of 1,1,2,2-tetrakis(4-chlorophenyl)ethane (**4c**)

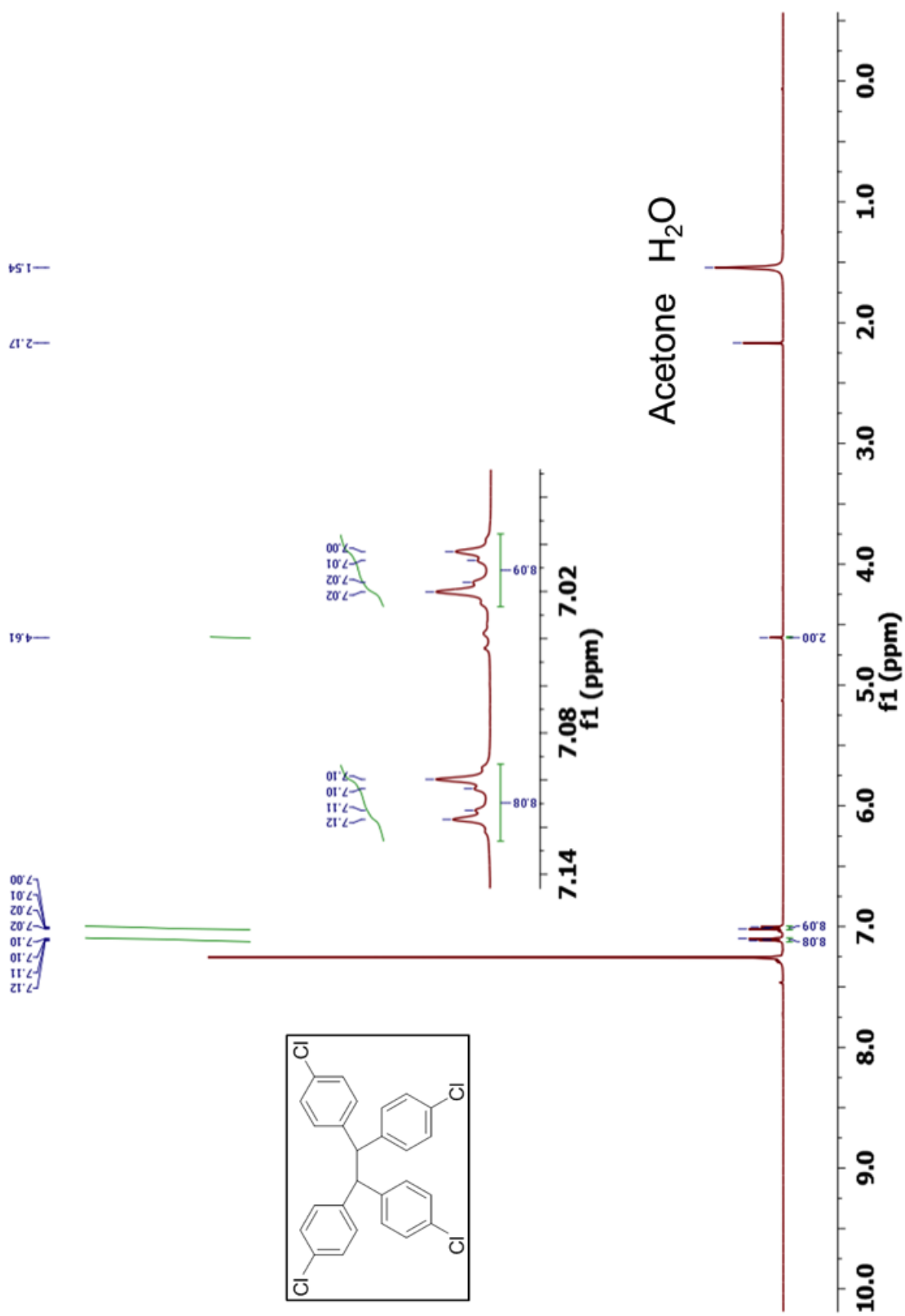


Figure 2.S22:  $^{13}\text{C}$  NMR (125 MHz,  $\text{CDCl}_3$ ) of 1,1,2,2-tetrakis(4-chlorophenyl)ethane (**4c**)

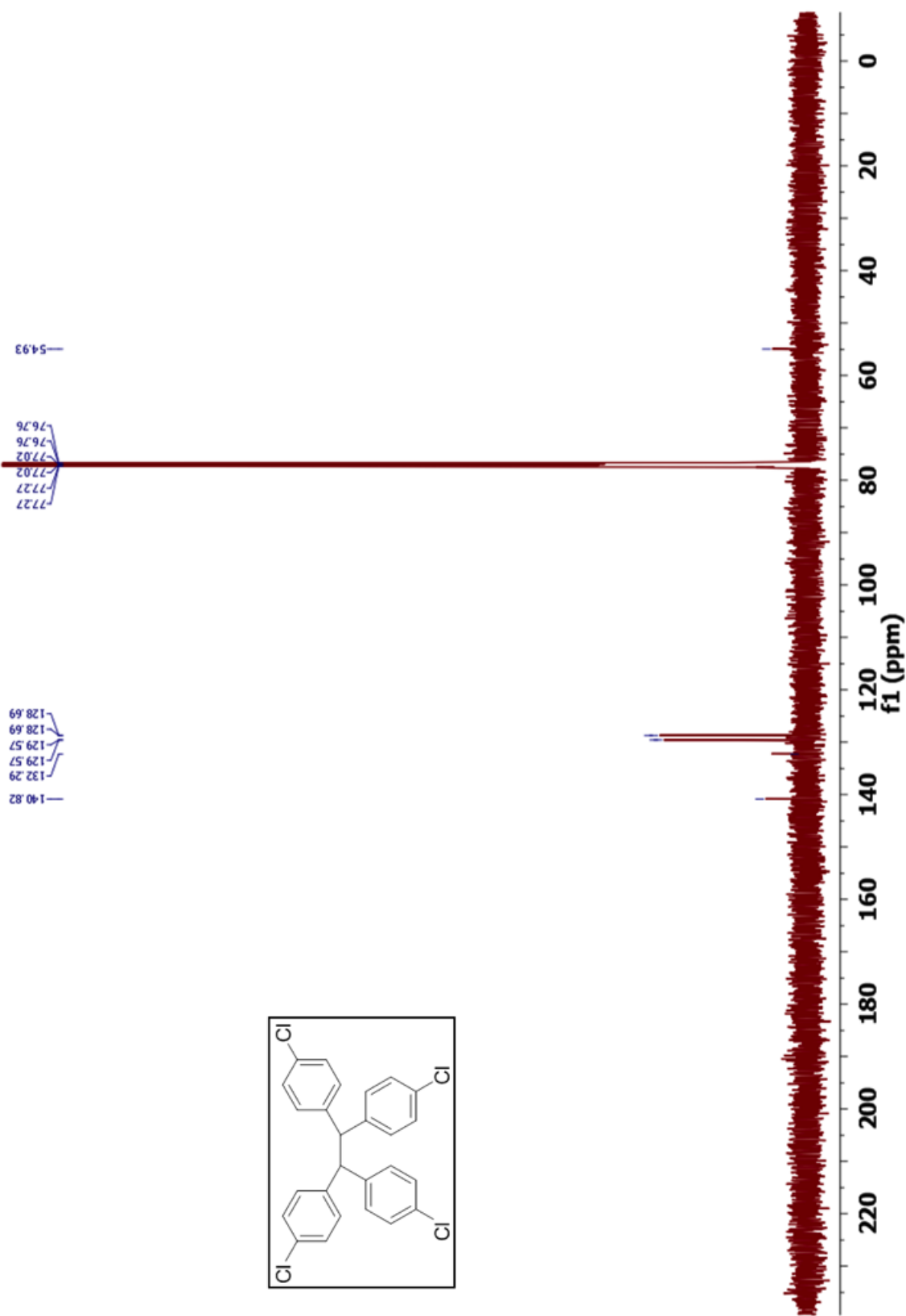
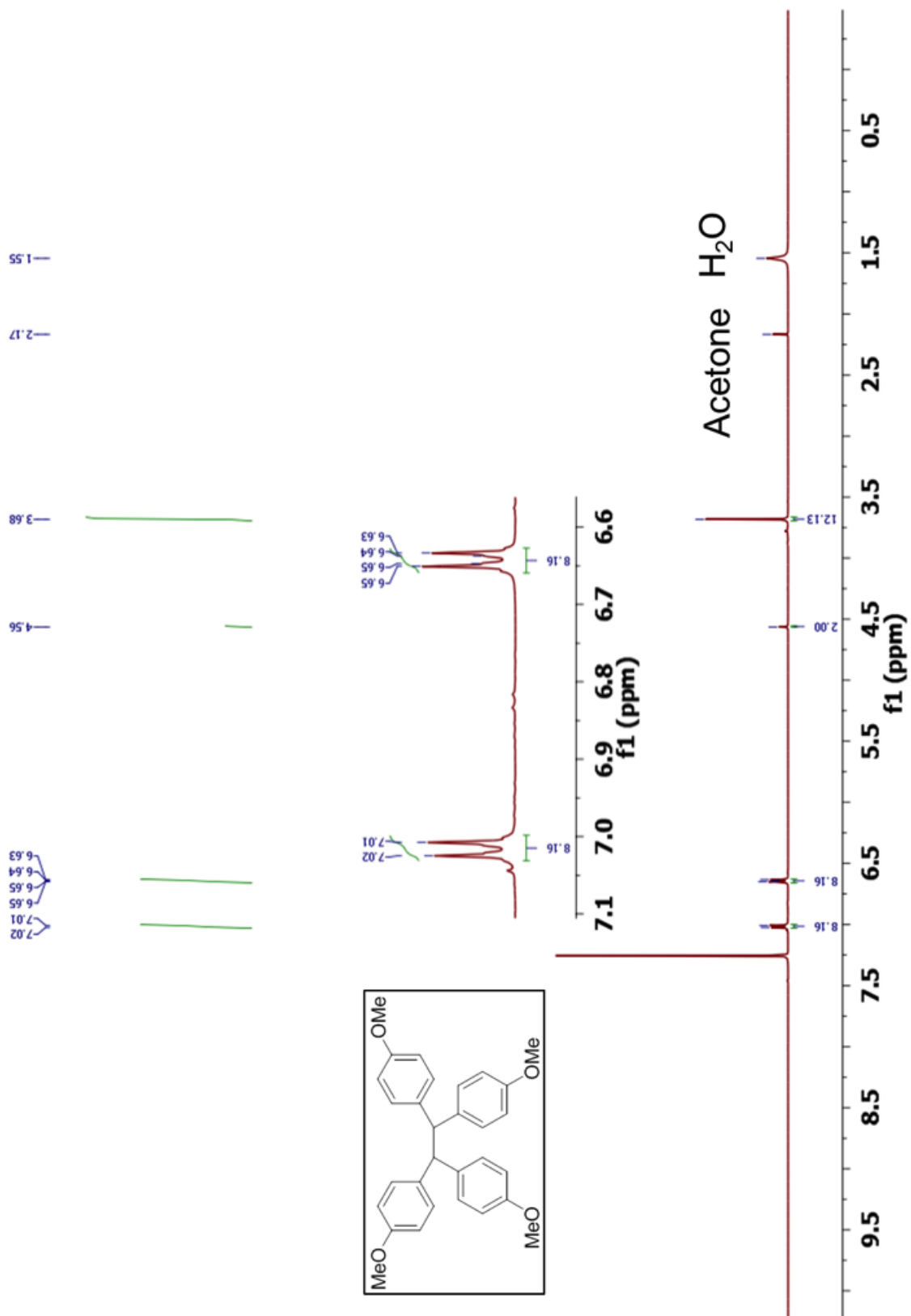


Figure 2.S23.  $^1\text{H}$  NMR (500 MHz,  $\text{CDCl}_3$ ) of 1,1,2,2-tetrakis(4-methoxyphenyl)ethane (**4d**)<sup>12b</sup>





**Figure 2.S24:**  $^{13}\text{C}$  NMR (125 MHz,  $\text{CDCl}_3$ ) of 1,1,2,2-tetrakis(4-methoxyphenyl)ethane (**4d**)<sup>12b</sup>

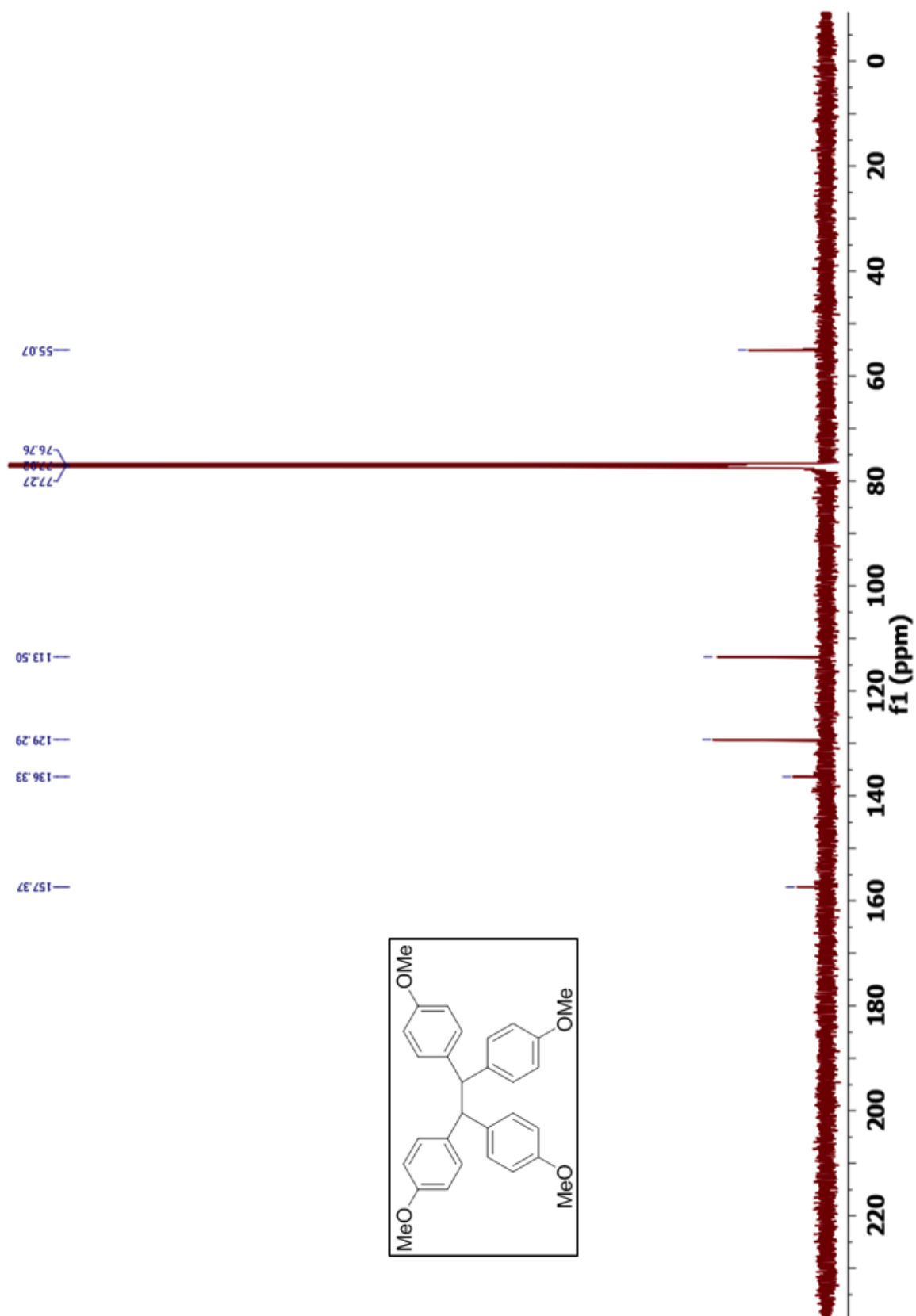


Figure 2.S25:  $^1\text{H}$  NMR (125 MHz,  $\text{CDCl}_3$ ) of 1,1,2,2-tetrakis(4-fluorophenyl)ethane (**4e**)<sup>12b</sup>

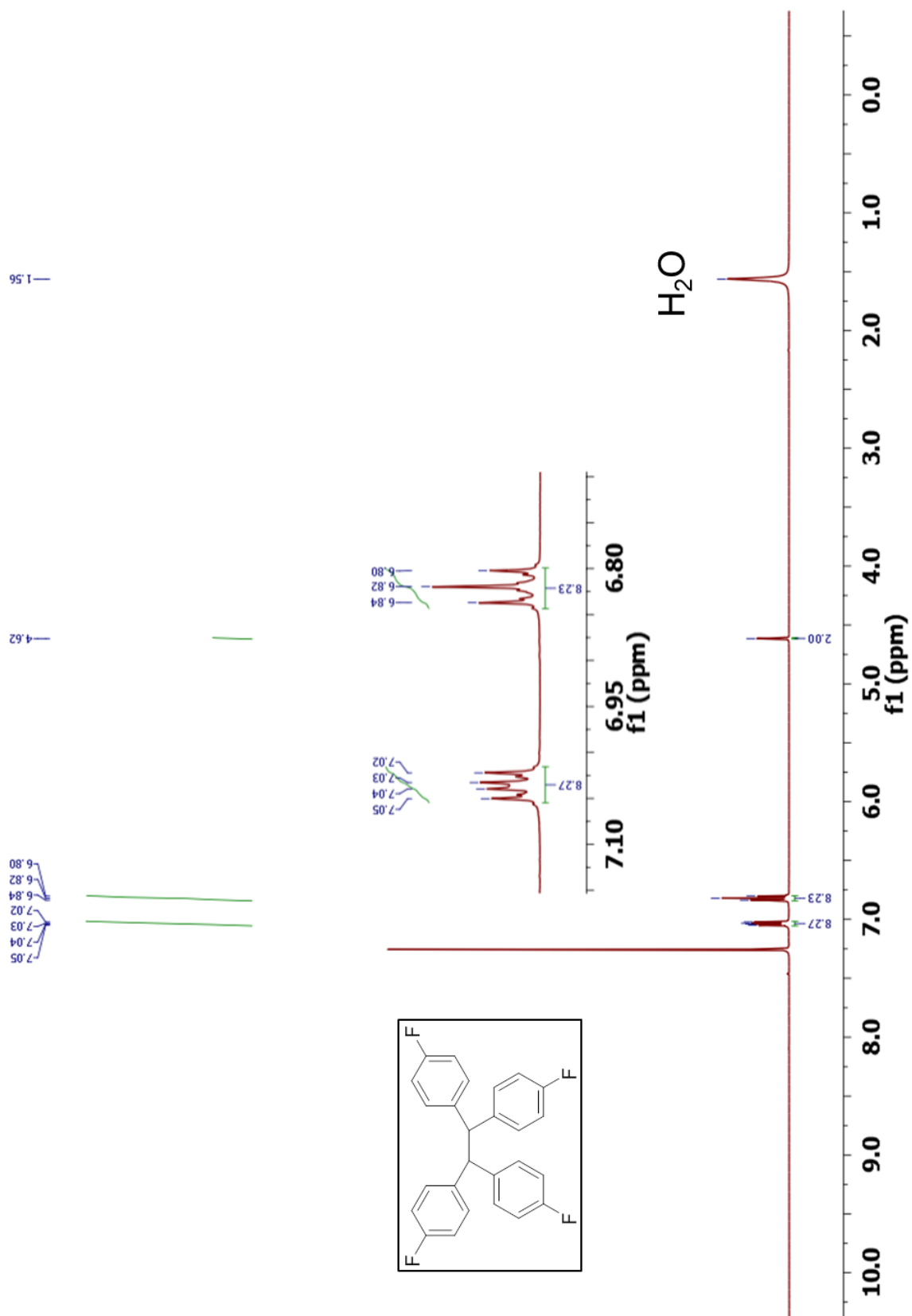
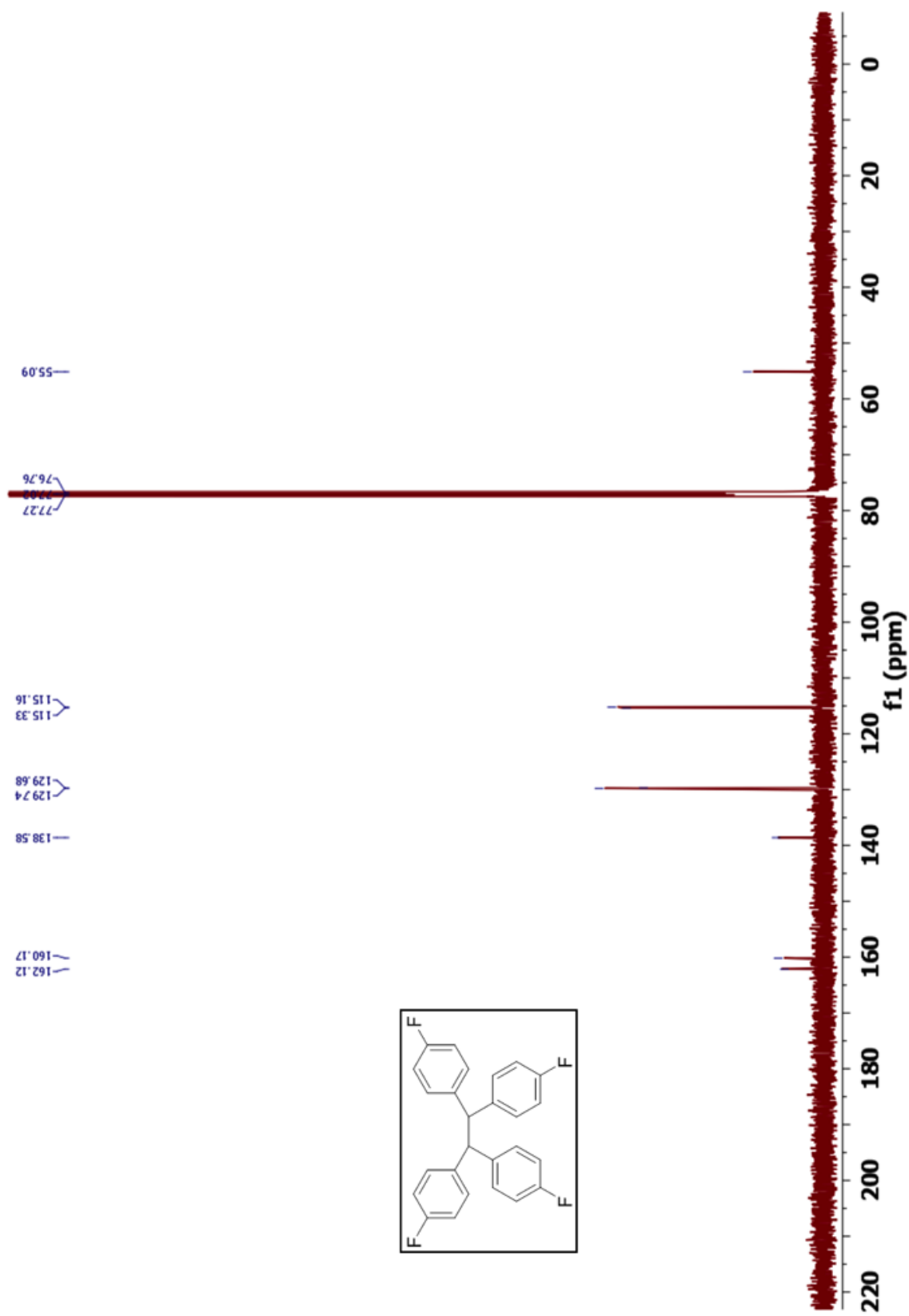
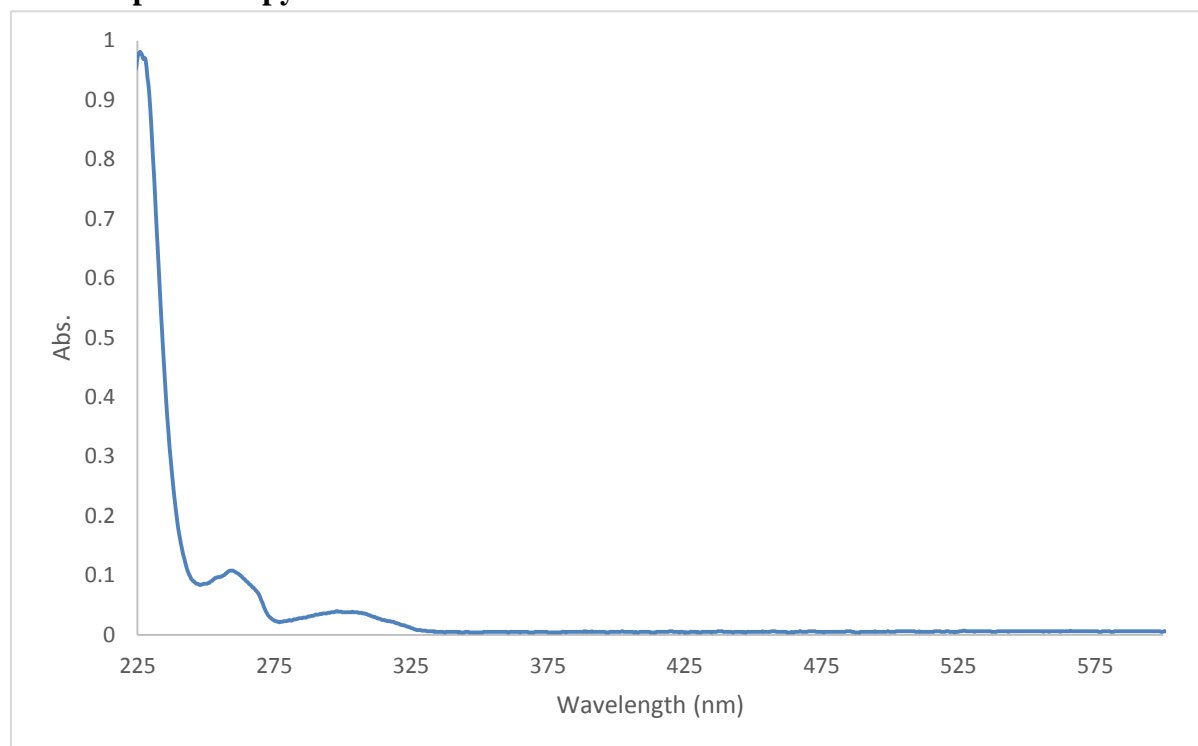


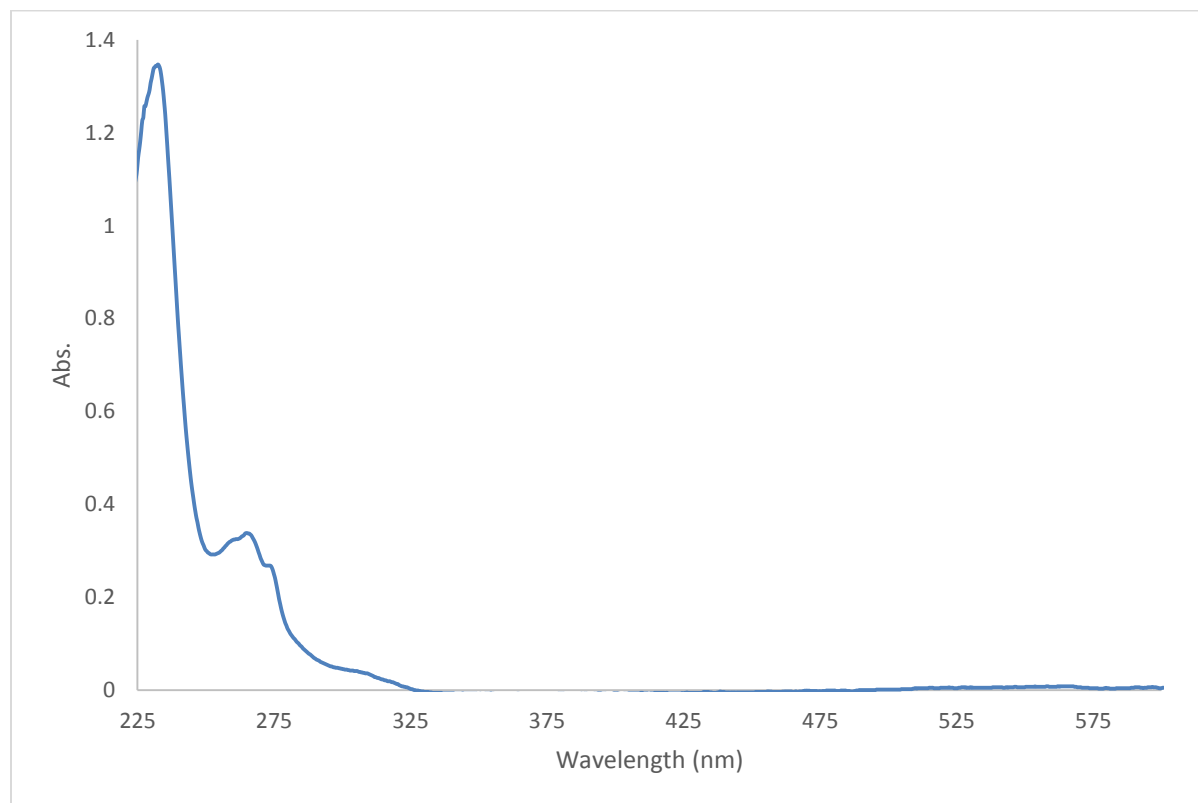
Figure 2.S26:  $^{13}\text{C}$  NMR (125 MHz,  $\text{CDCl}_3$ ) of 1,1,2,2-tetrakis(4-fluorophenyl)ethane (**4e**)<sup>12b</sup>



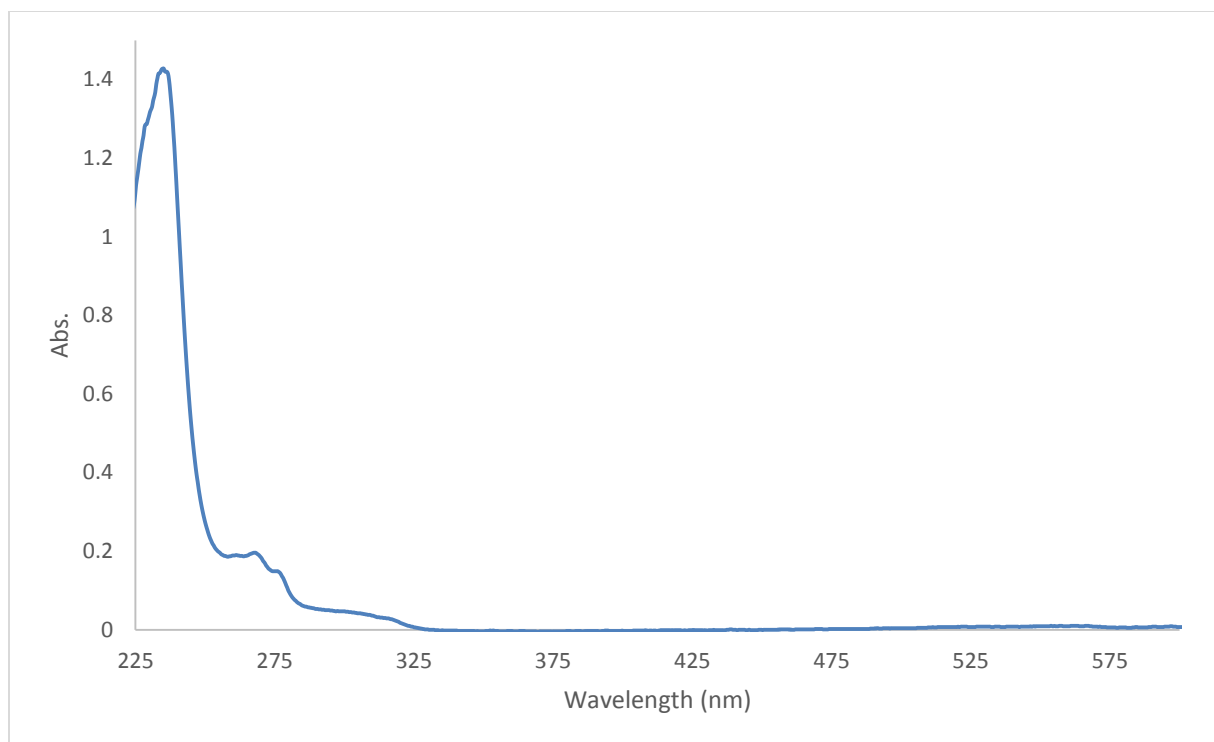
**UV-Vis spectroscopy:**



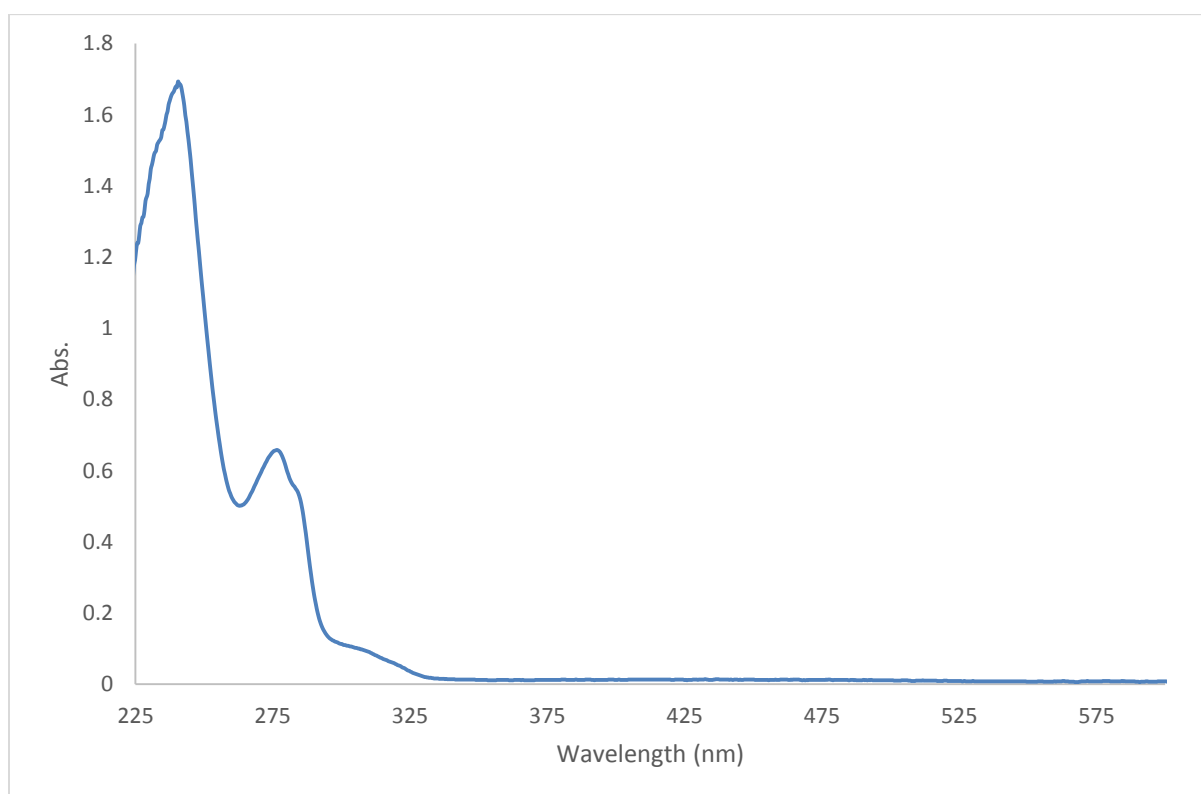
**Figure 2.S27:** UV-vis of 0.1 mg/mL 1,1,3,3-tetraphenylpropan-2-one (**1a**) in MeCN



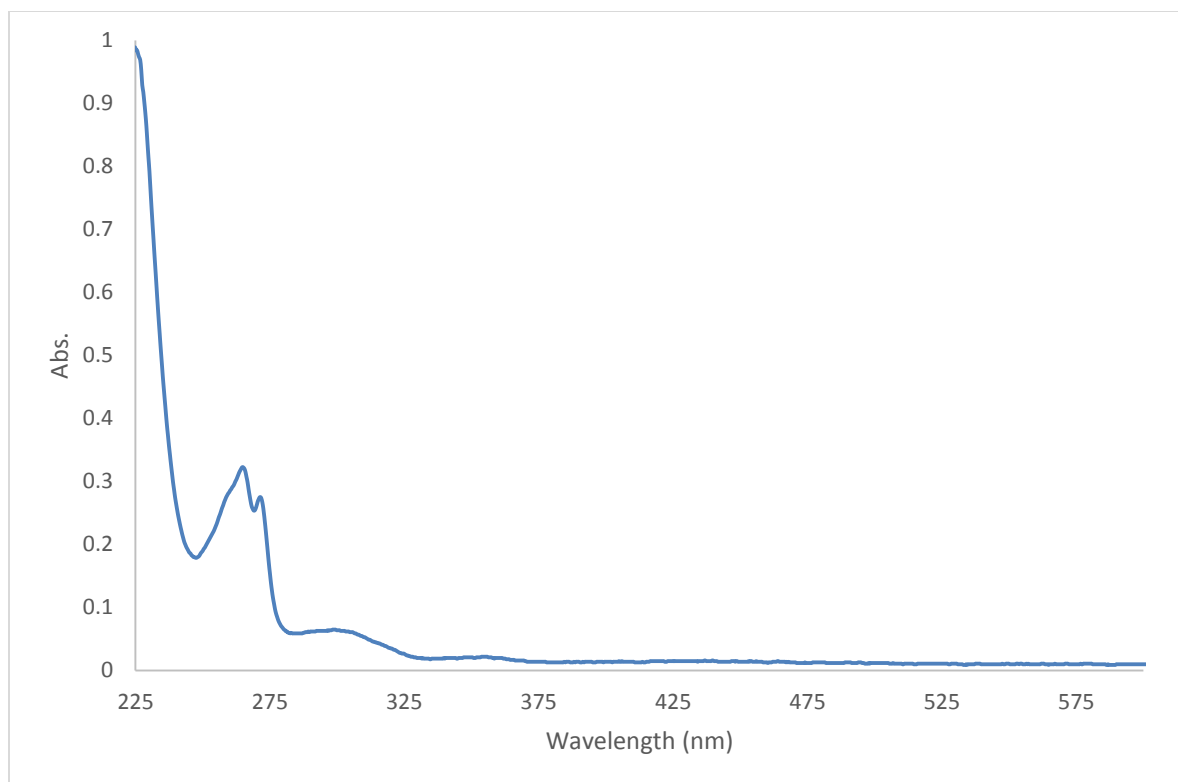
**Figure 2.S28:** UV-vis of 0.1 mg/mL 1,1,3,3-tetra-p-tolylpropan-2-one (**1b**) in MeCN



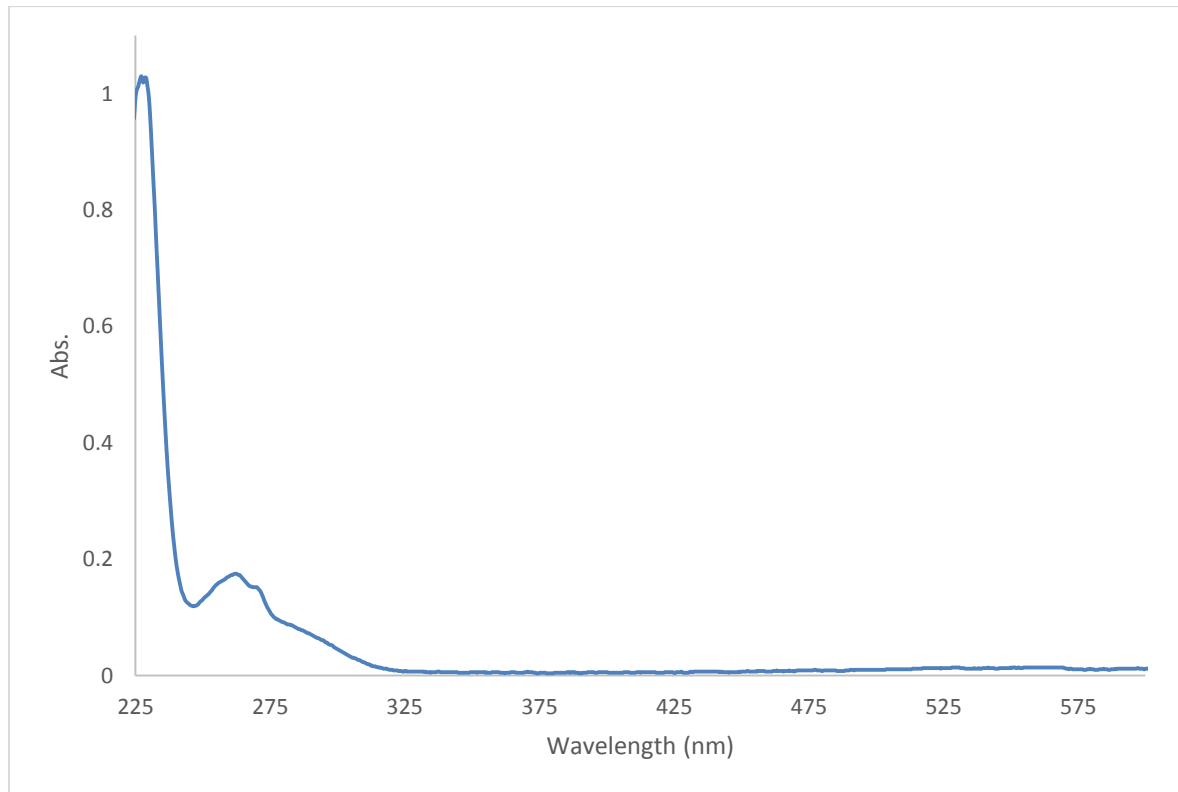
**Figure 2.S29:** UV-vis of 0.1 mg/mL 1,1,3,3-tetrakis(4-chlorophenyl)propan-2-one (**1c**) in MeCN



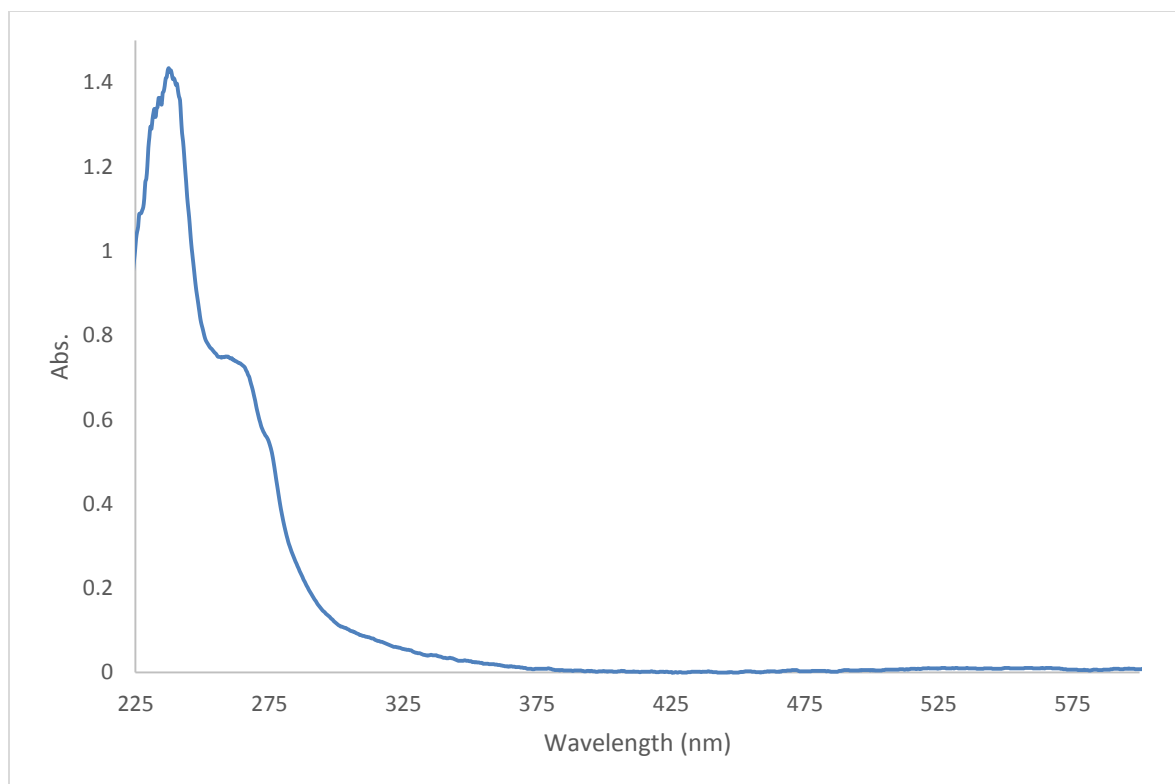
**Figure 2.S30:** UV-vis of 0.1 mg/mL 1,1,3,3-tetrakis(4-methoxyphenyl)propan-2-one (**1d**) in MeCN



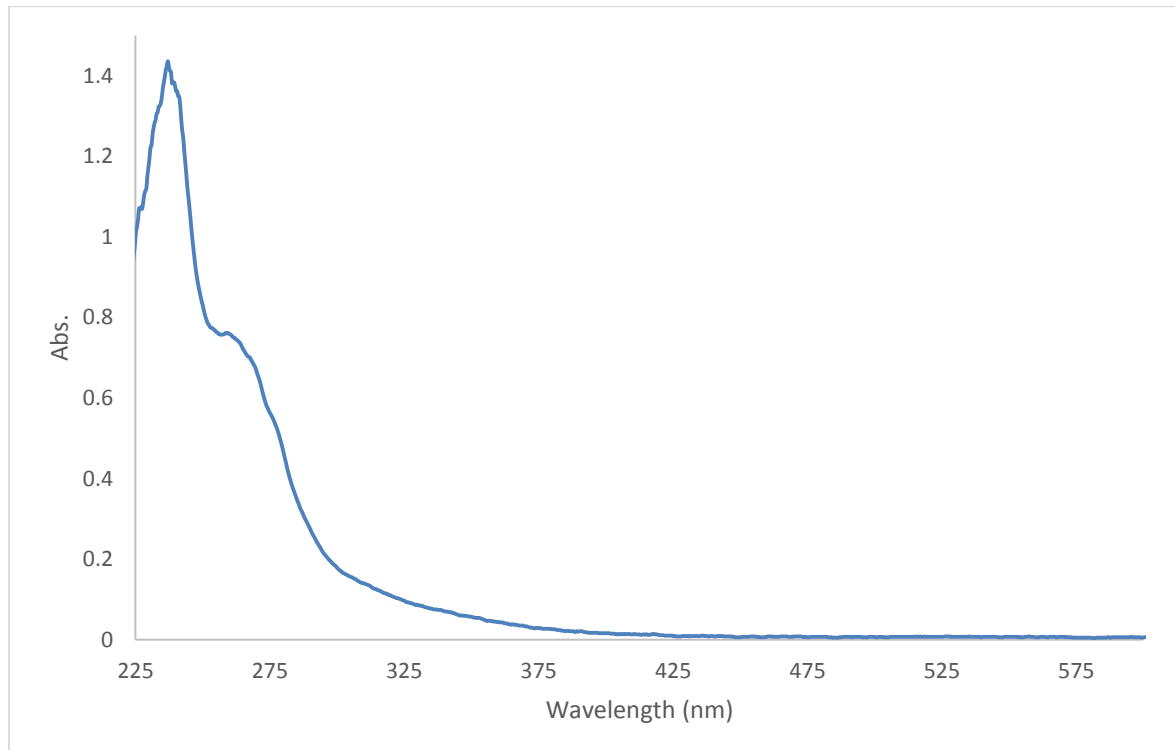
**Figure 2.S31:** UV-vis of 0.1 mg/mL 1,1,3,3-tetrakis(4-fluorophenyl)propan-2-one (**1e**) in MeCN



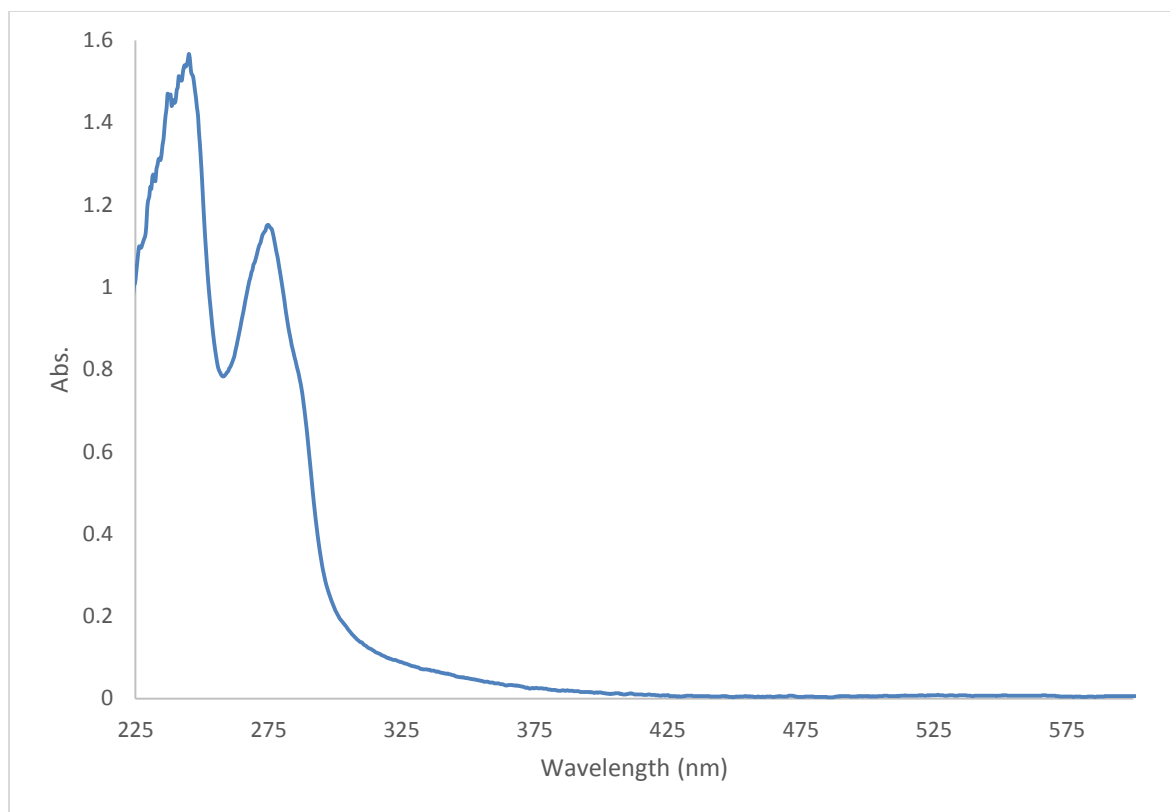
**Figure 2.S32:** UV-vis of 0.3 mg/mL 1,1,2,2-tetraphenylethane (**4a**) in MeCN



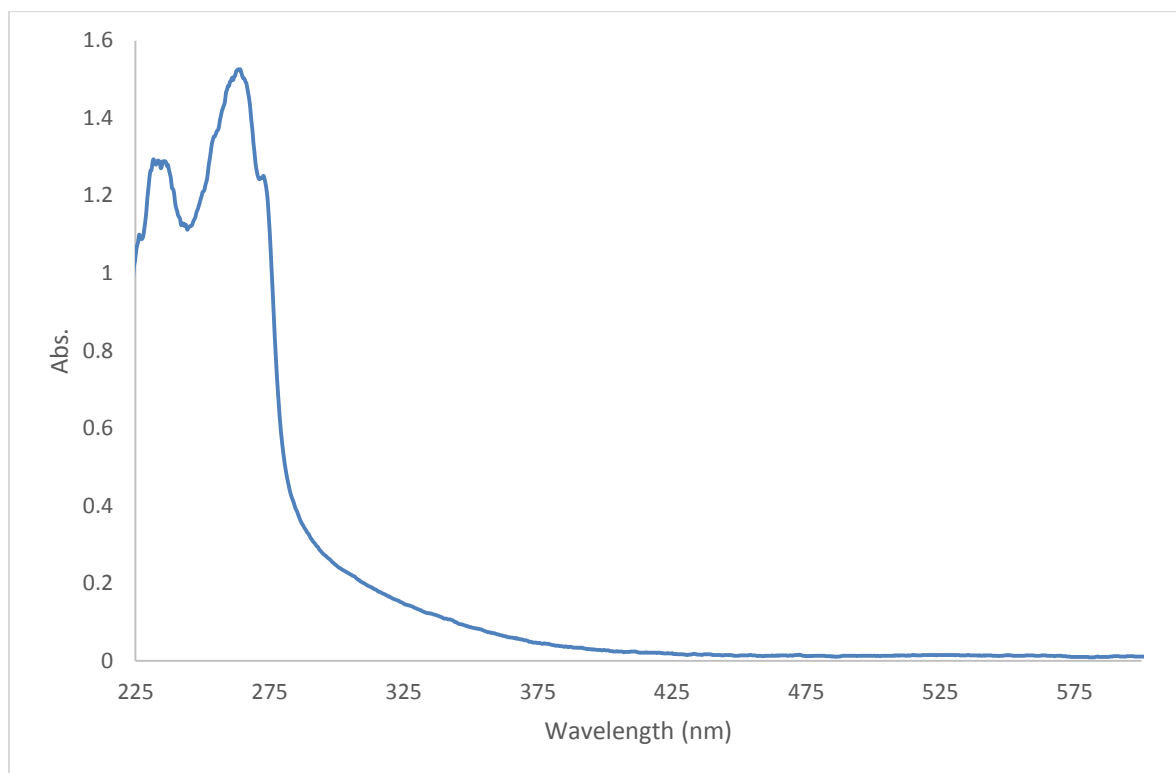
**Figure 2.S33:** UV-vis of 0.3 mg/mL 1,1,2,2-tetra-p-tolyethane (**4b**) in MeCN



**Figure 2.S34:** UV-vis of 0.3 mg/mL 1,1,2,2-tetrakis(4-chlorophenyl)ethane (**4c**) in MeCN



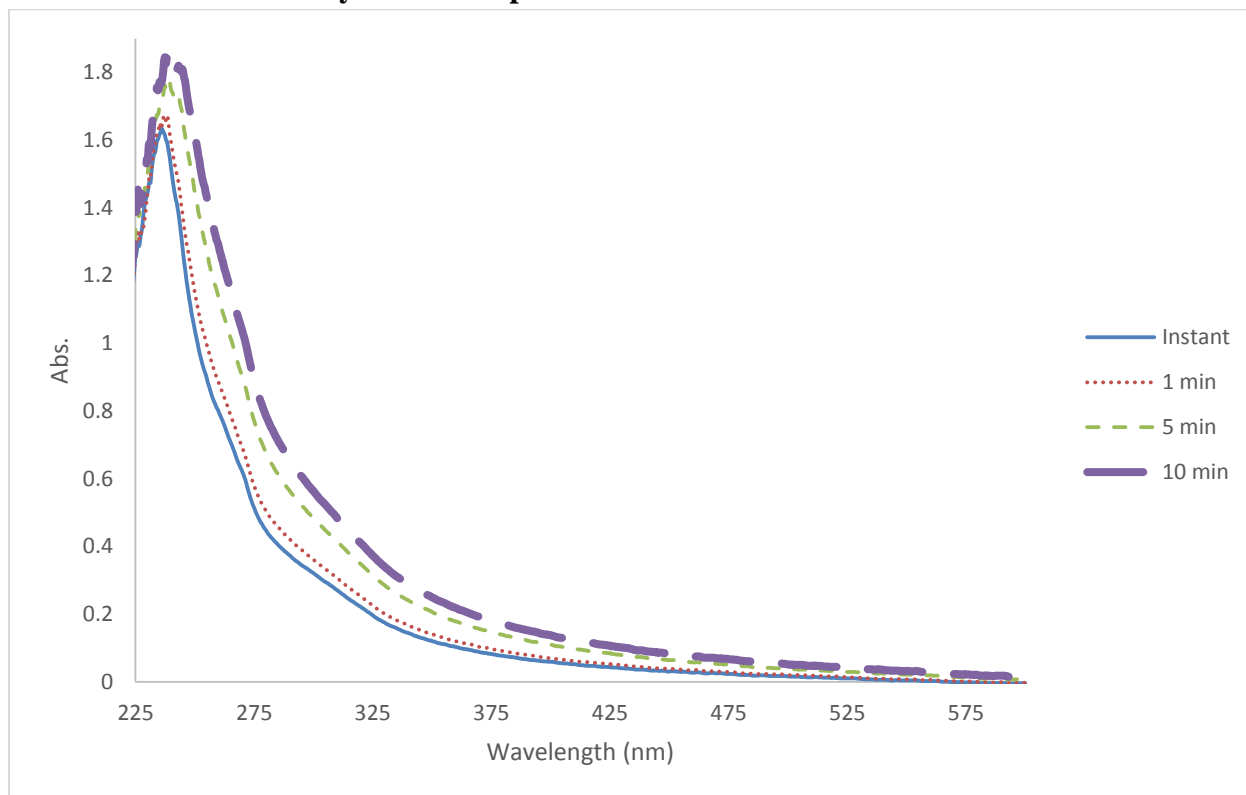
**Figure 2.S35:** UV-vis of 0.3 mg/mL 1,1,2,2-tetrakis(4-methoxyphenyl)ethane (**4d**) in MeCN



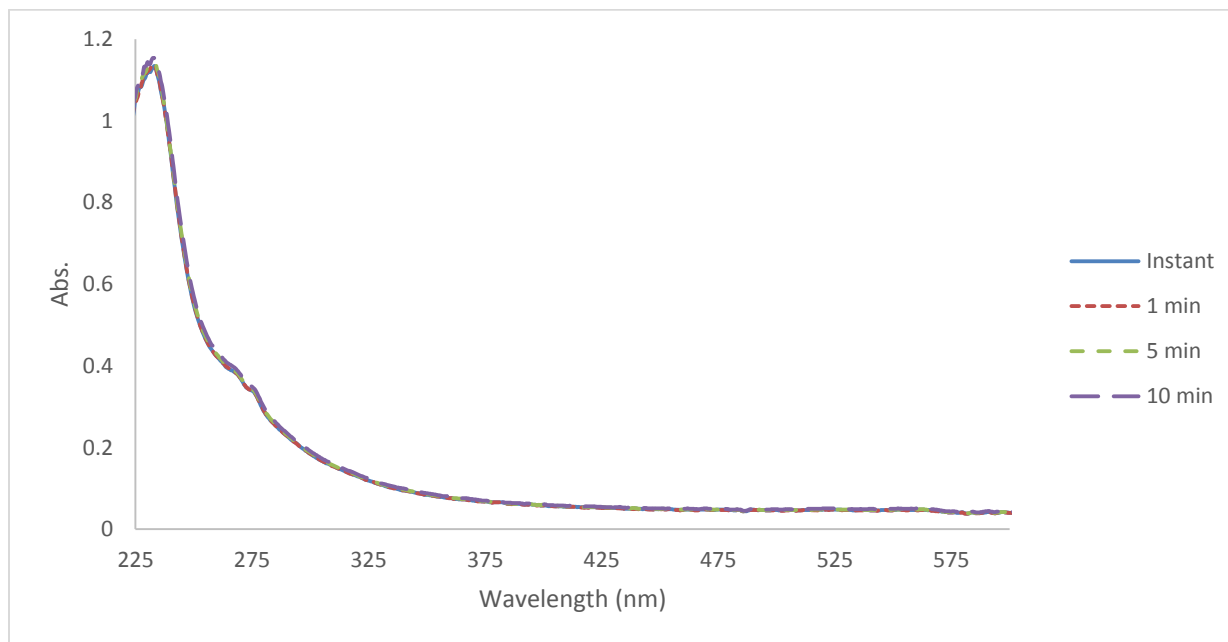
**Figure 2.S36:** UV-vis of 0.3 mg/mL 1,1,2,2-tetrakis(4-fluorophenyl)ethane (**4e**) in MeCN



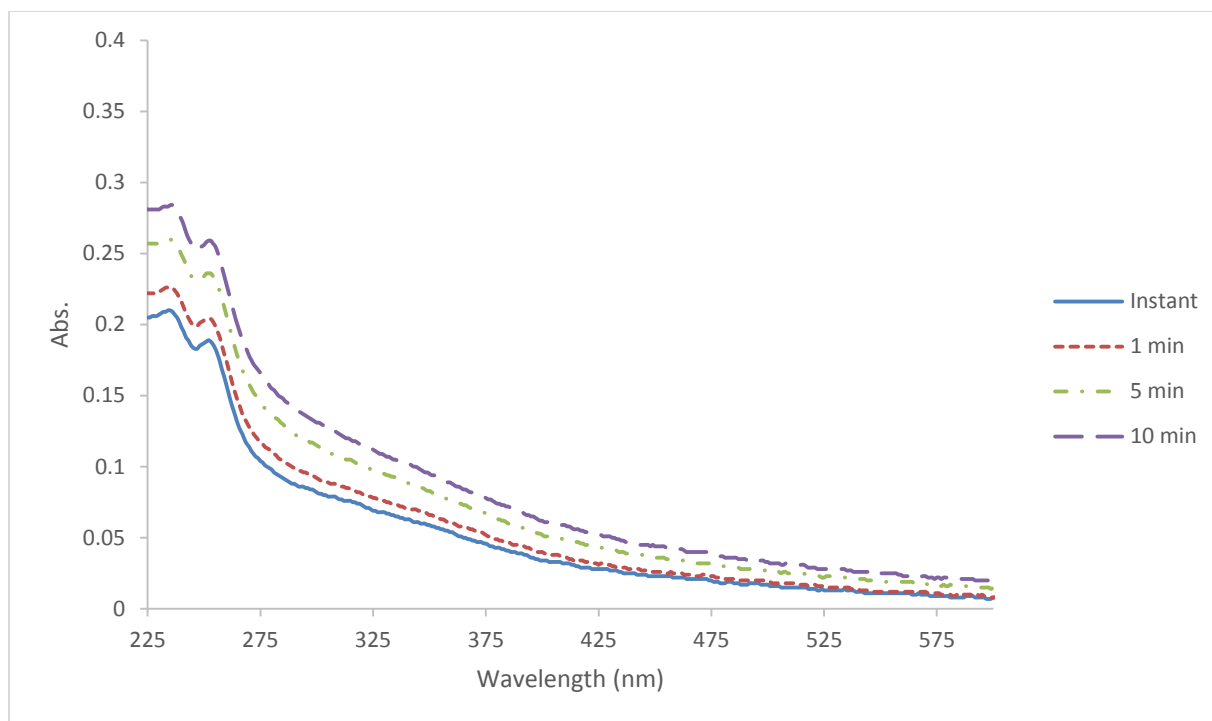
### UV Vis Data for Nanocrystalline Suspension:



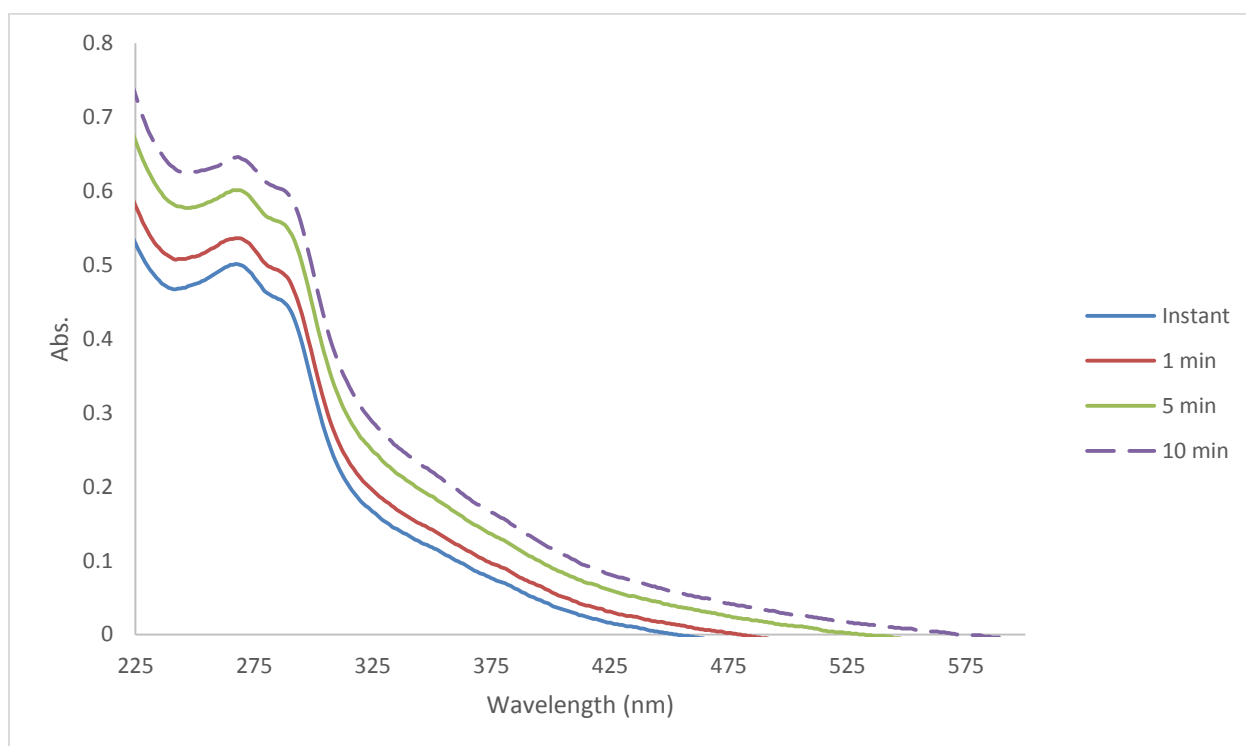
**Figure 2.S37:** UV-vis of 0.0025 g/L 1,1,3,3-tetraphenylpropan-2-one (**1a**) nanocrystalline suspension



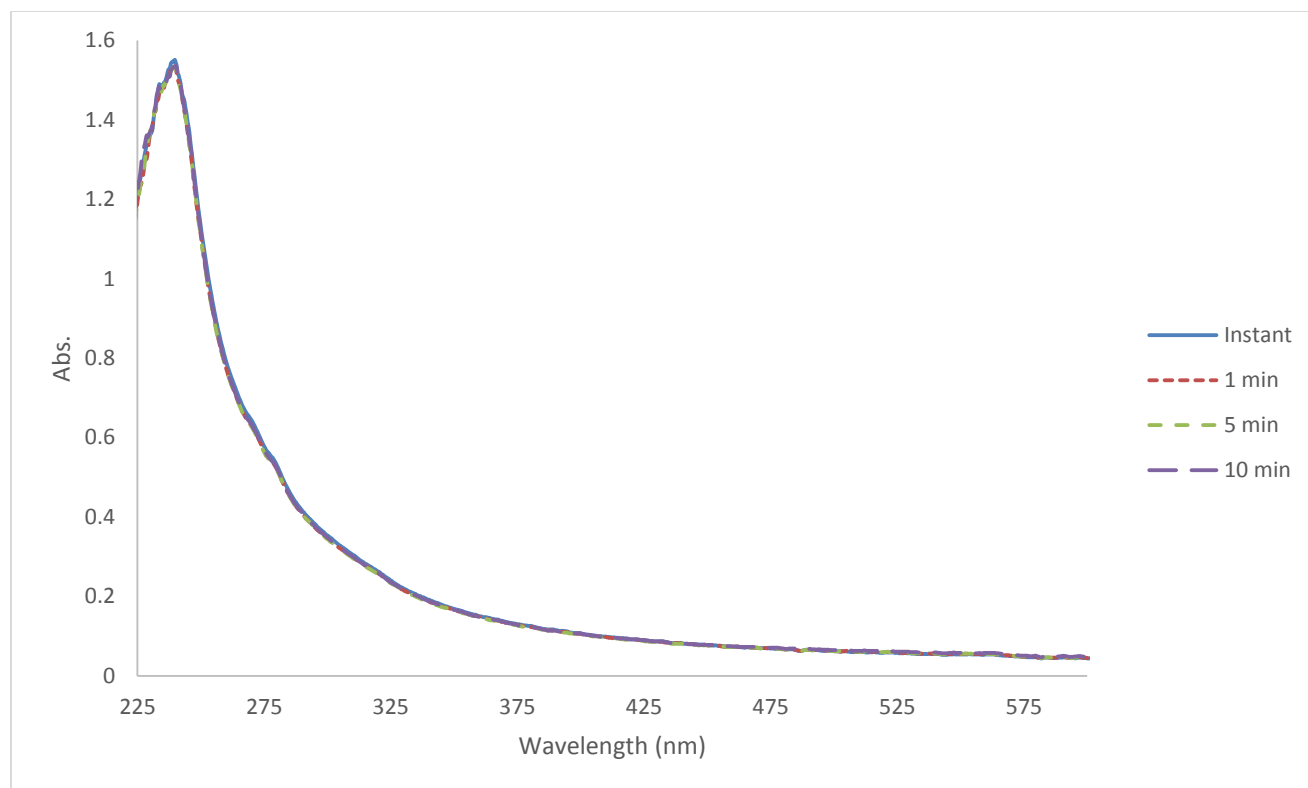
**Figure 2.S38:** UV-vis of 0.0025 g/L 1,1,3,3-tetra-p-tolylpropan-2-one (**1b**) nanocrystalline suspension



**Figure 2.S39:** UV-vis of 0.0025 g/L 1,1,3,3-tetrakis(4-chlorophenyl)propan-2-one (**1c**) nanocrystalline suspension



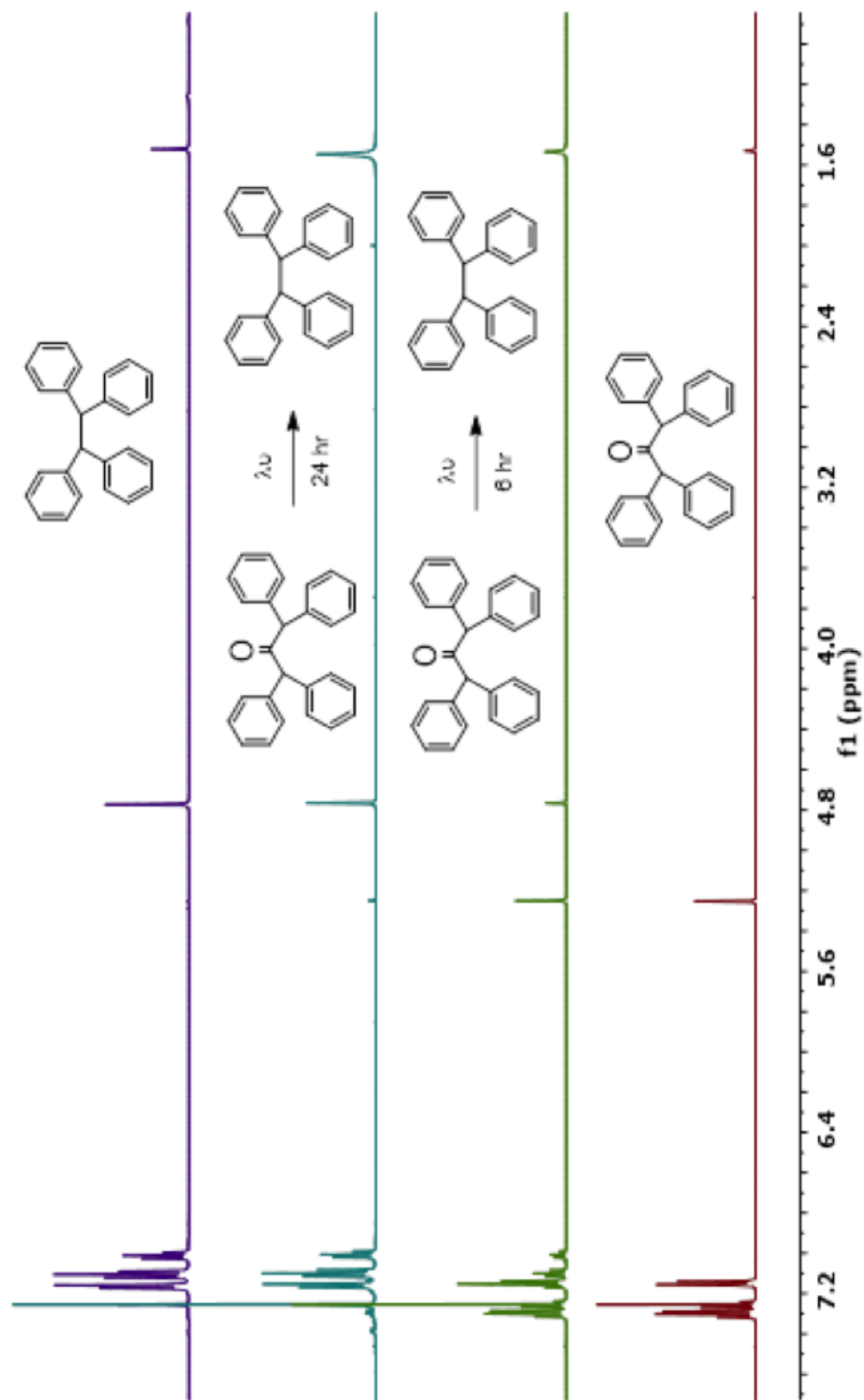
**Figure 2.S40:** UV-vis of 0.0025 g/L 1,1,3,3-tetrakis(4-methoxyphenyl)propan-2-one (**1d**) nanocrystalline suspension



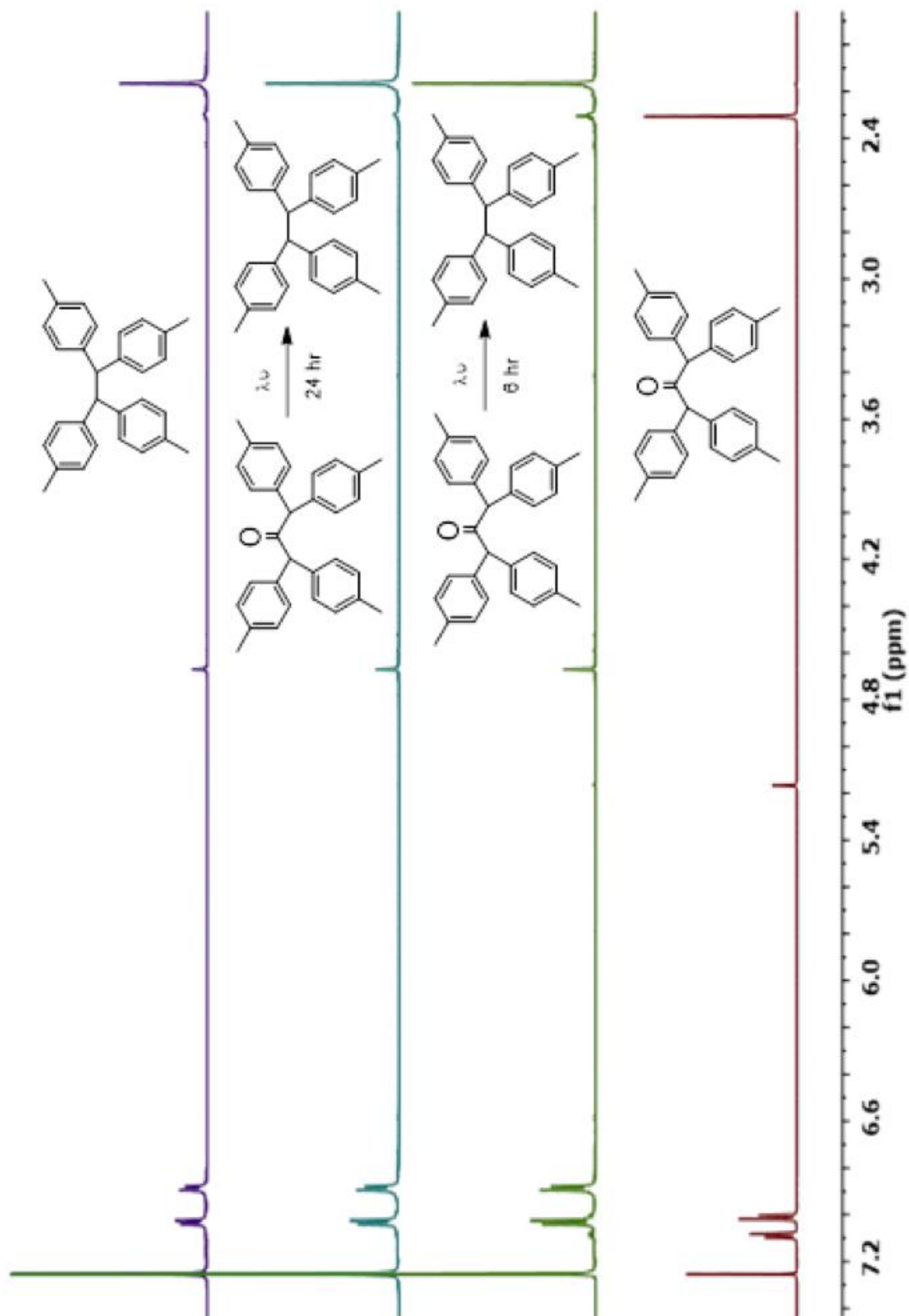
**Figure 2.S41:** UV-vis of 0.0025 mol/L 1,1,3,3-tetrakis(4-fluorophenyl)propan-2-one (**1e**) nanocrystalline suspension

#### 2.5.4 Solid-State Photochemistry of Dry Powder:

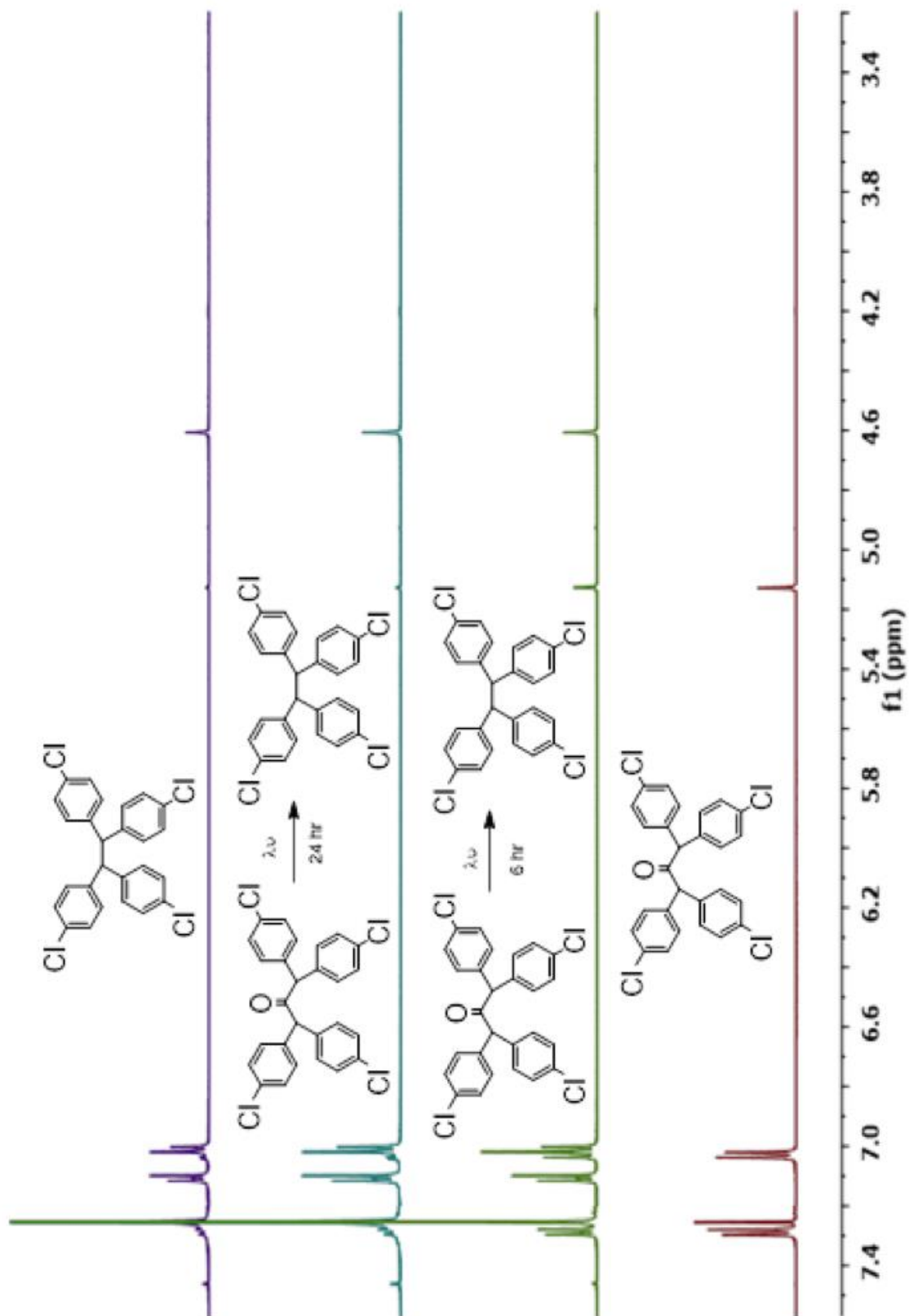
All Solid-State photochemistry product analysis were conducted via a medium-pressure Hg Hanovia lamp with a Pyrex immersion with a cutoff of  $\lambda \leq 275$  nm and analyzed by  $^1\text{H}$  NMR (500 MHz,  $\text{CDCl}_3$ ). Samples were ground between two microscope slides which were then subjected to UV light inside an irradiation chamber.



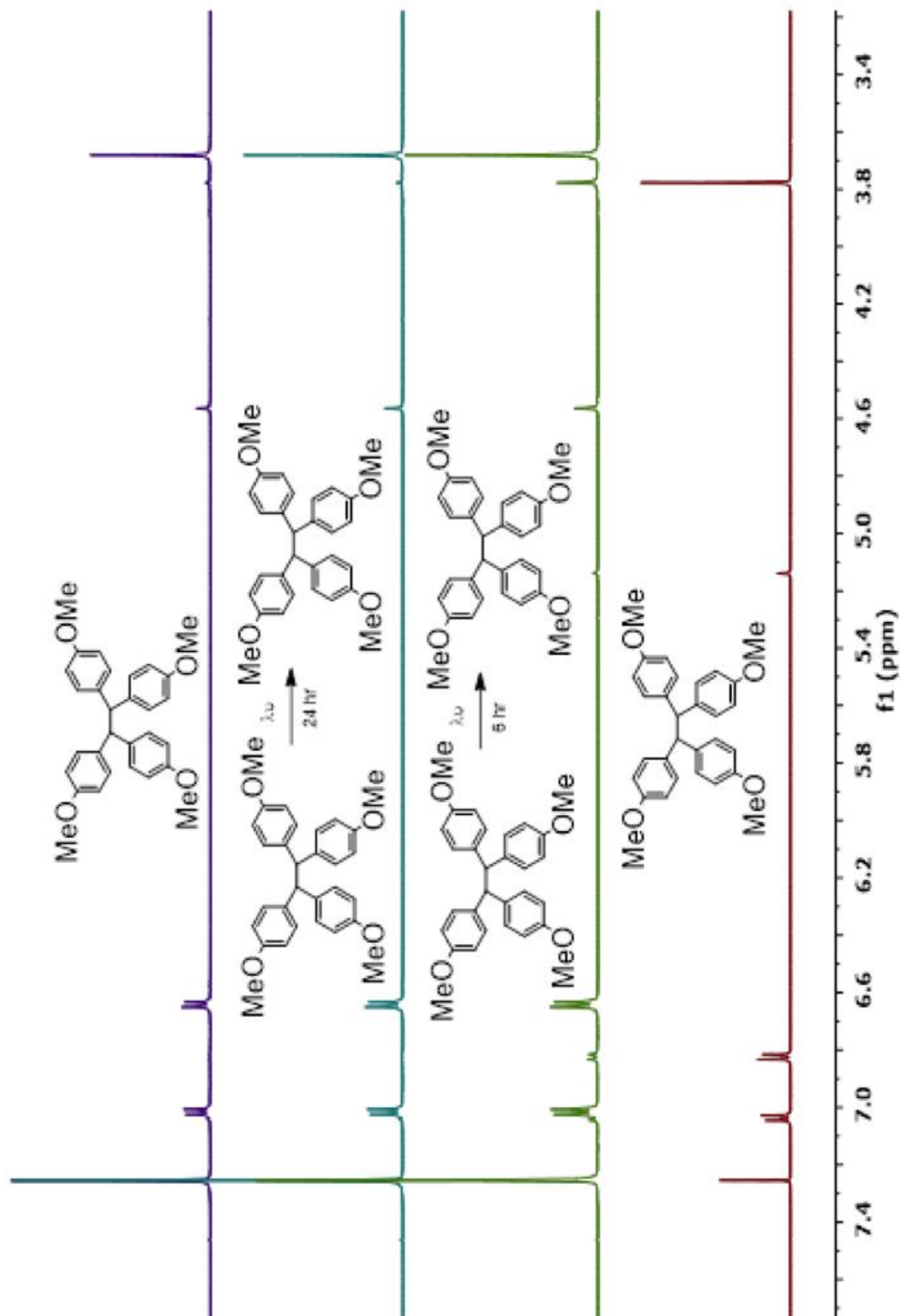
**Figure 2.S42:**  $^1\text{H}$  NMR (500 MHz,  $\text{CDCl}_3$ ) product analysis of 1,1,3,3-tetraphenylpropan-2-one (**1a**) to 1,1,2,2-tetraphenylethane (**4a**) in the solid-state



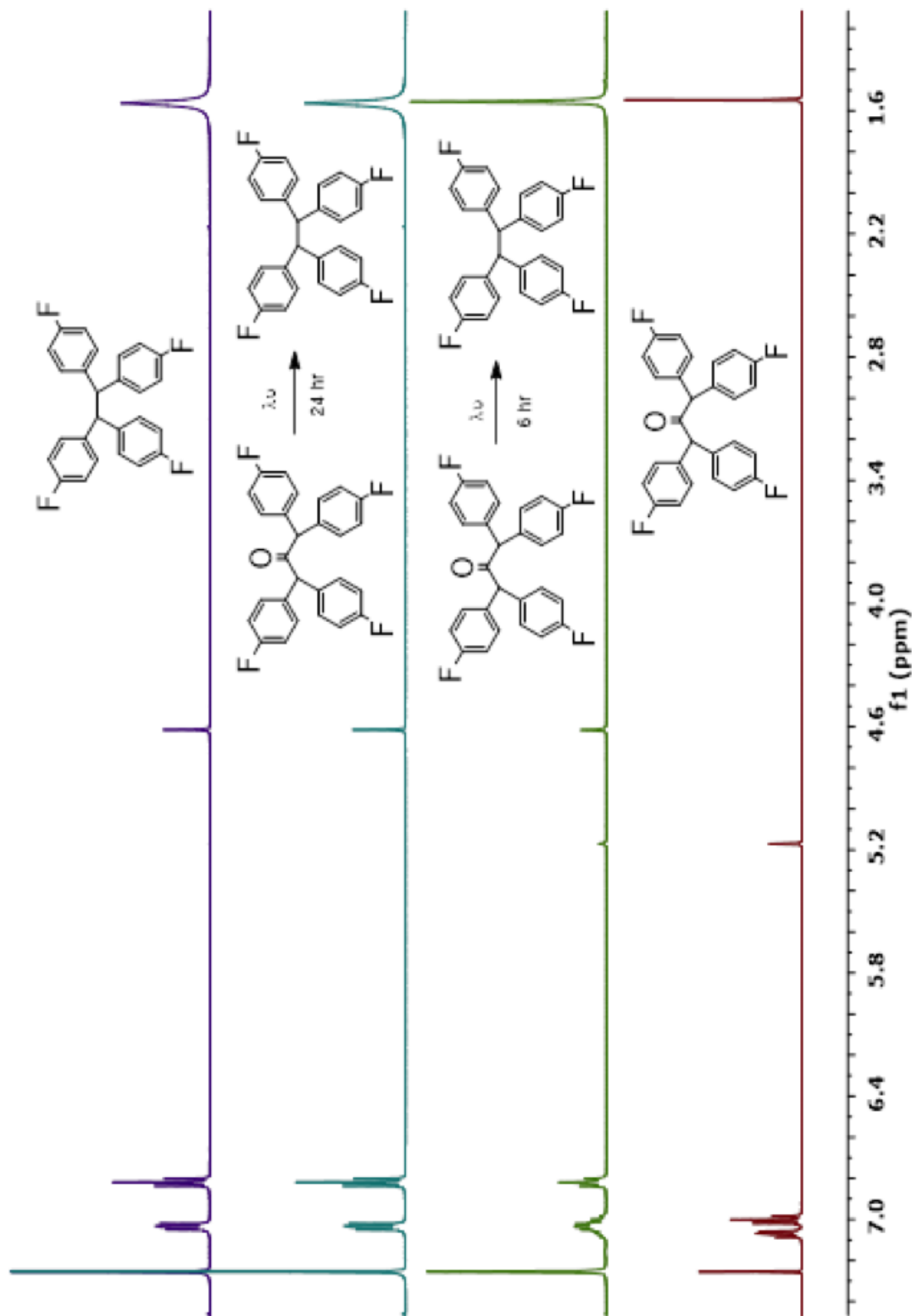
**Figure 2.S43:** <sup>1</sup>H NMR (500 MHz, CDCl<sub>3</sub>) product analysis of 1,1,3,3-tetra-p-tolylpropan-2-one (**1b**) to 1,1,2,2-tetra-p-tolyloethane (**4b**) in the solid-state



**Figure 2.S44:** <sup>1</sup>H NMR (500 MHz, CDCl<sub>3</sub>) product analysis of 1,1,3,3-tetrakis(4-chlorophenyl)propan-2-one (**1c**) to 1,1,2,2-tetrakis(4-chlorophenyl)ethane (**4c**) in the solid-state



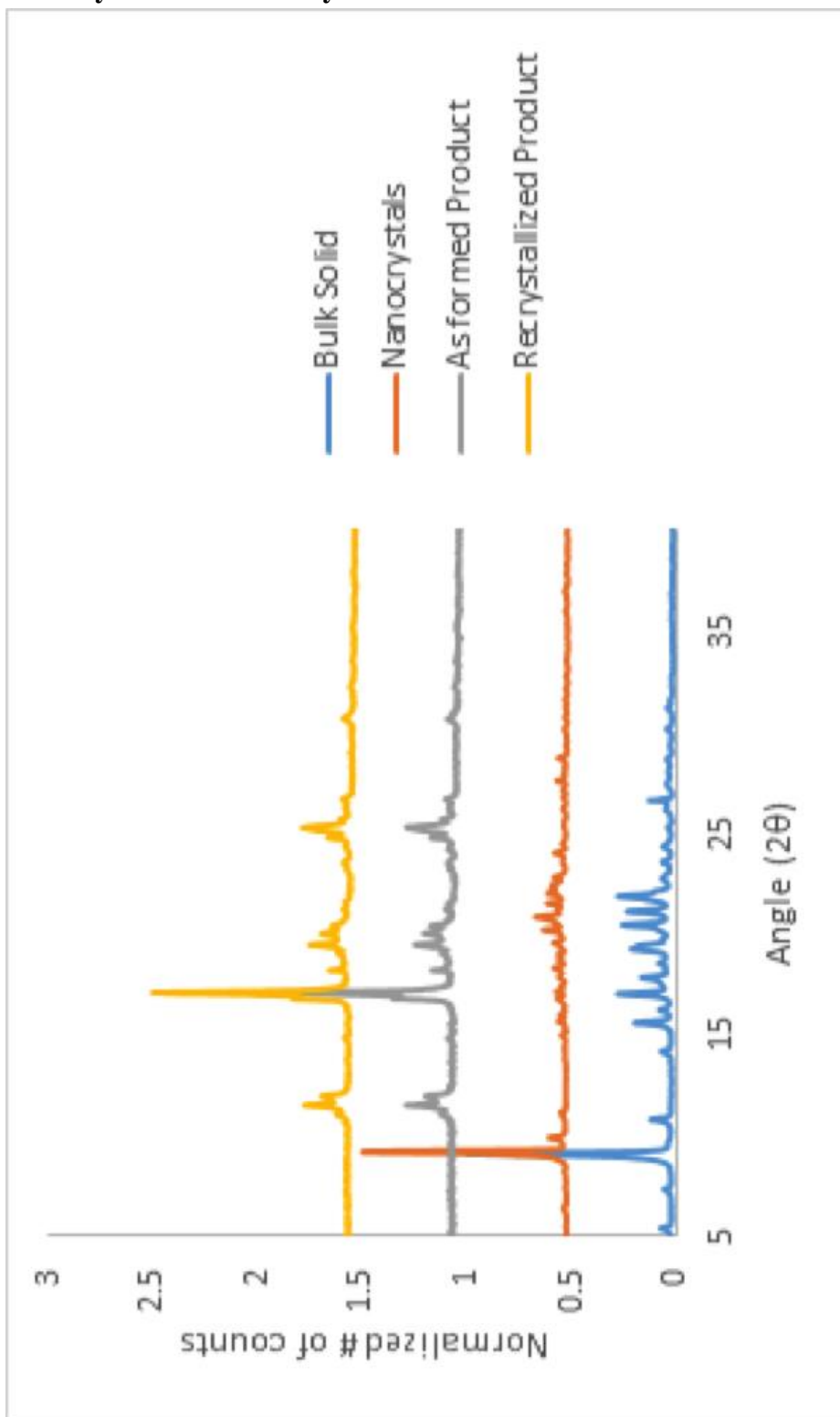
**Figure 2.S45:**  $^1\text{H}$  NMR (500 MHz,  $\text{CDCl}_3$ ) product analysis of 1,1,3,3-tetrakis(4-methoxyphenyl)propan-2-one (**1d**) to 1,1,2,2-tetrakis(4-methoxyphenyl)ethane (**4d**) in the solid-state



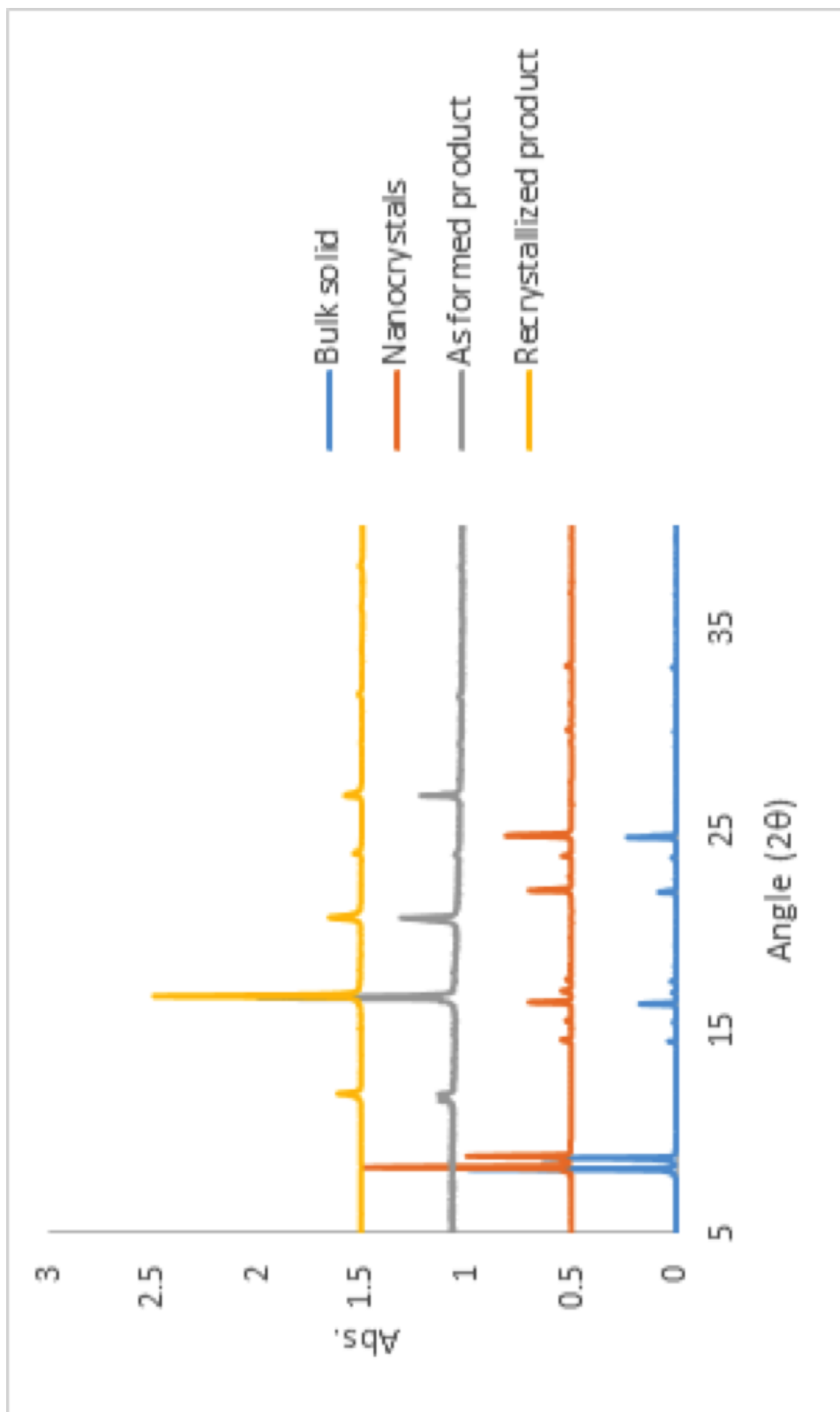
**Figure 2.S46:**  $^1\text{H}$  NMR (500 MHz,  $\text{CDCl}_3$ ) product analysis of 1,1,3,3-tetrakis(4-fluorophenyl)propan-2-one (**1e**) to 1,1,2,2-tetrakis(4-fluorophenyl)ethane (**4e**) in the solid-state



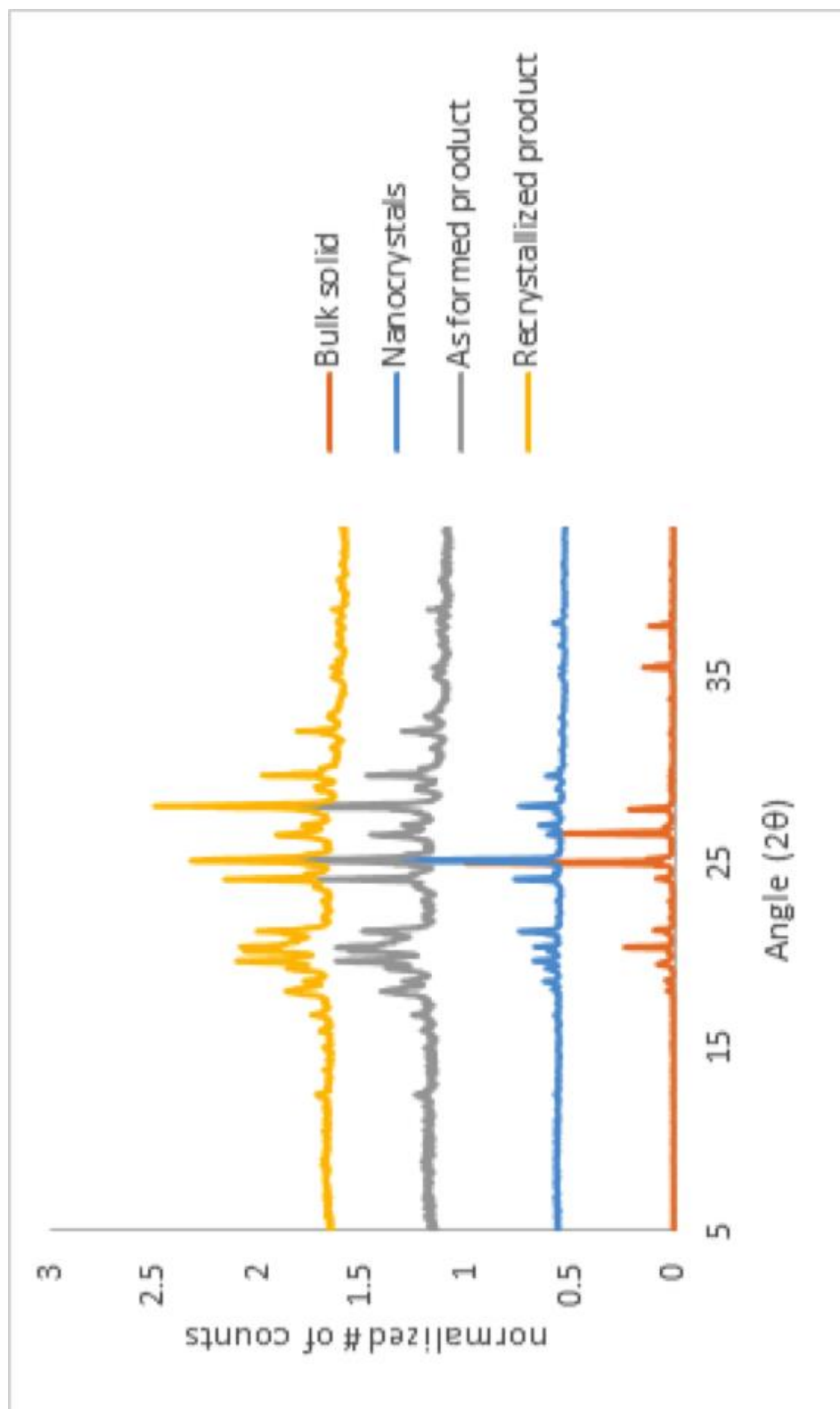
### 2.5.5 Powder X-Ray Diffraction Analysis:



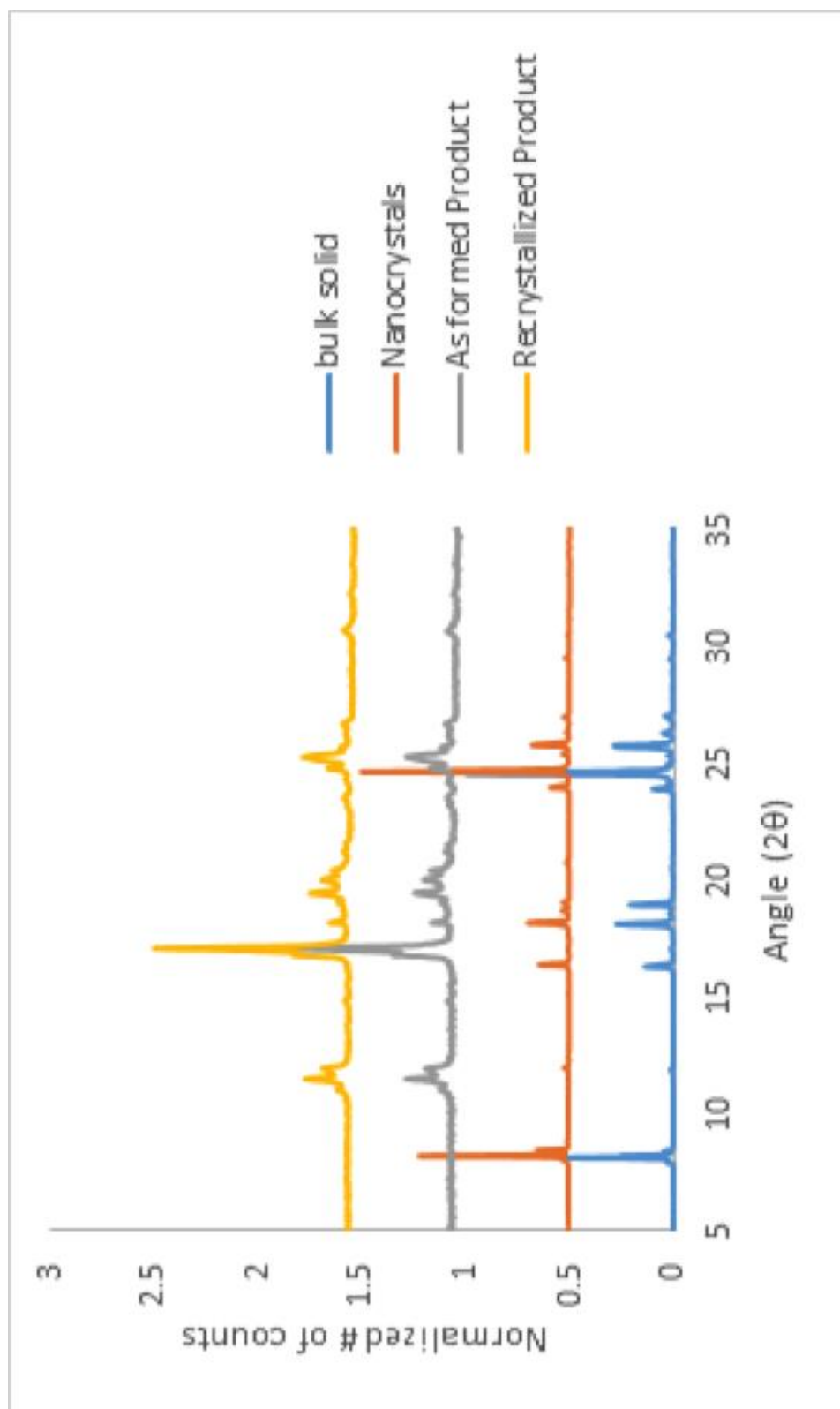
**Figure 2.S47:** PXRD of 1,1,3,3-tetra-p-tolylpropan-2-one (**1a**) in the bulk solid and nanocrystalline suspensions; 1,1,2,2-tetraphenylethane (**4a**) As formed and recrystallized in ethanol.



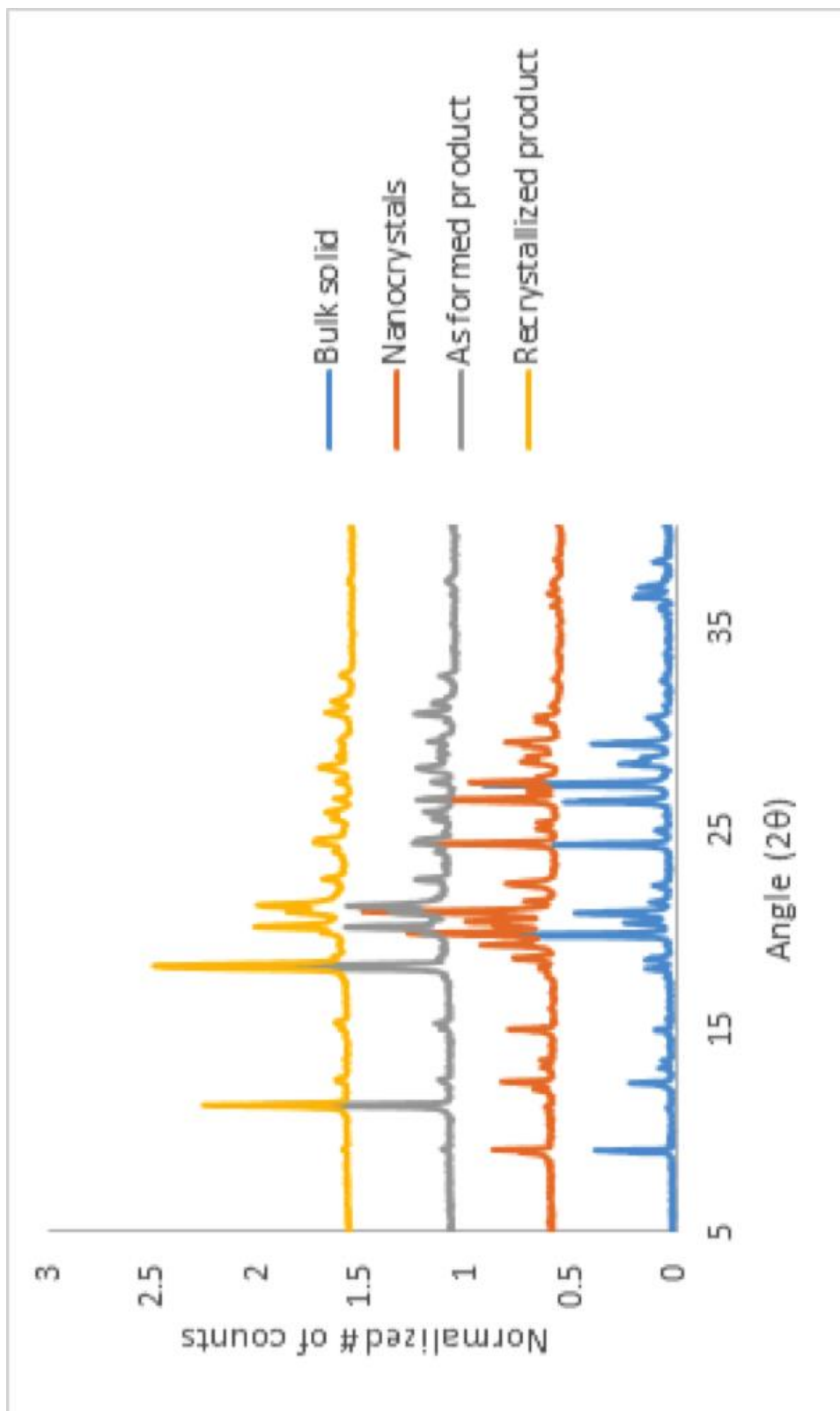
**Figure 2.S48:** PXRD of 1,1,3,3-tetra-p-tolylpropan-2-one (**1b**) in the bulk solid and nanocrystalline suspensions; 1,1,2,2-tetra-p-tolyethane (**4b**) As formed and recrystallized in ethanol.



**Figure 2.S49:** PXRD of 1,1,3,3-tetrakis(4-chlorophenyl)propan-2-one (**1c**) in the bulk solid and nanocrystalline suspensions; 1,1,2,2-tetrakis(4-chlorophenyl)ethane (**4c**) as formed and recrystallized in ethanol.



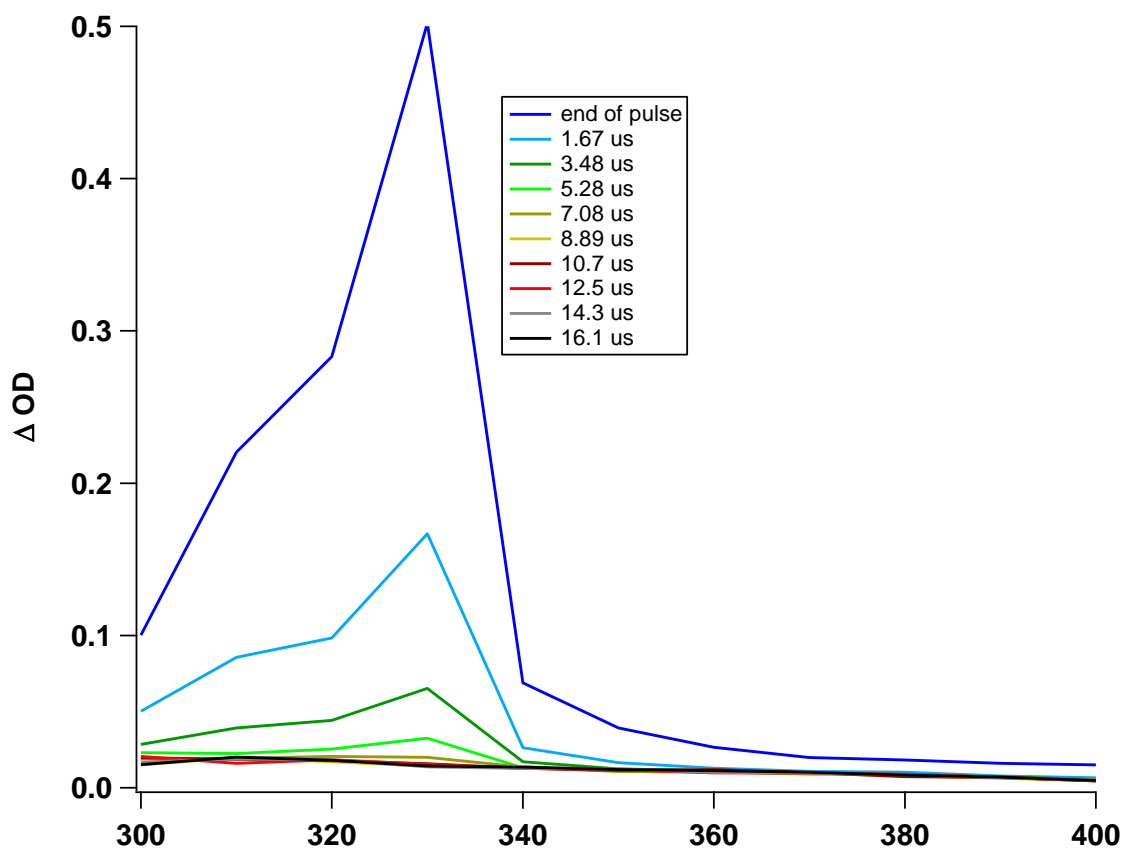
**Figure 2.S50:** PXRD of 1,1,3,3-tetrakis(4-methoxyphenyl)propan-2-one (**1d**) in the bulk solid and nanocrystalline suspensions; 1,1,2,2-tetrakis(4-methoxyphenyl)ethane (**4d**) as formed and recrystallized in ethanol.



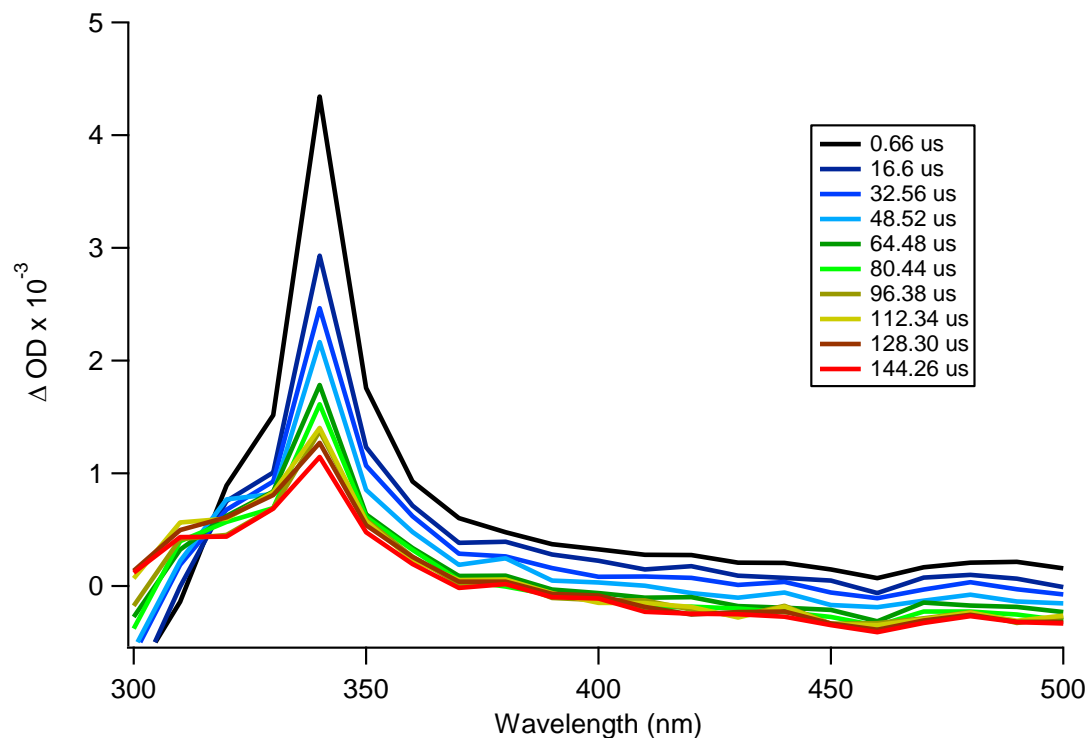
**Figure 2.S51:** PXRD of 1,1,3,3-tetrakis(4-fluorophenyl)propan-2-one (**1e**) in the bulk solid and nanocrystalline suspensions; 1,1,2,2-tetrakis(4-fluorophenyl)ethane (**4e**) as formed and recrystallized in ethanol.

### 2.5.6 Laser Flash Photolysis:

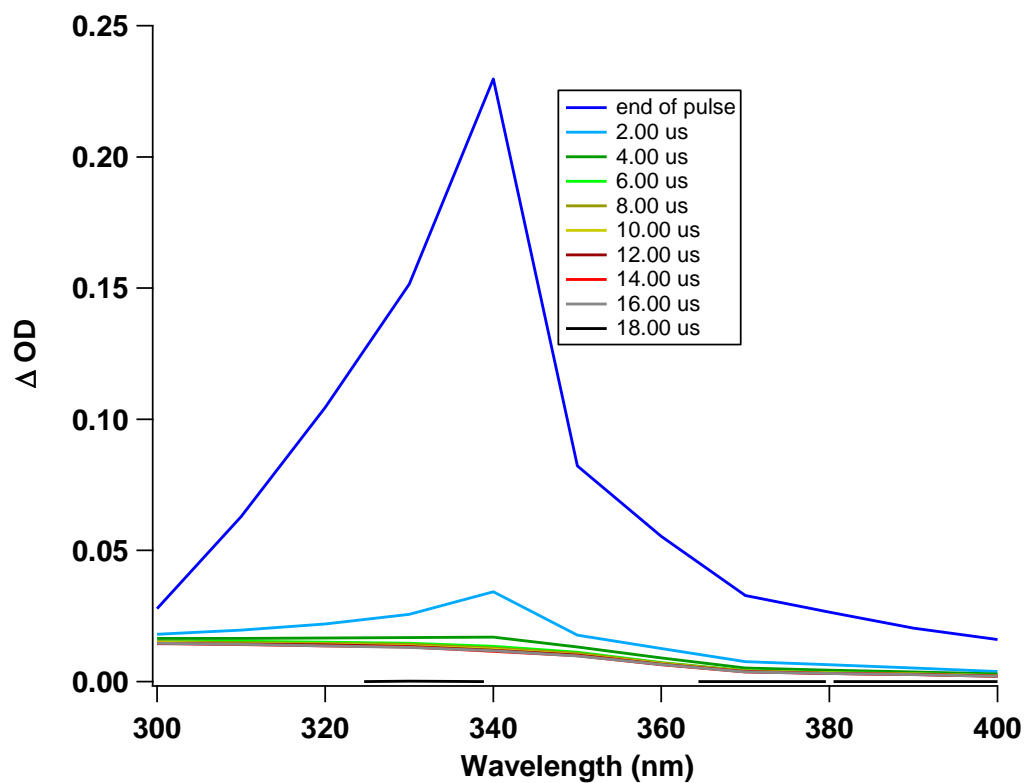
The laser flash photolysis experiments were performed with 1 cm quartz flow cell mounted on a home-built sample holder that is placed at the cross-section of the laser incident beam and the probe light. Continuously Argon gas purged acetonitrile solutions or crystalline suspensions of ketones were flown through the quartz cell using a peristaltic pump (Masterflex L/S) at a rate of 2.5–4 mL/min. Lifetimes at  $\lambda_{\max}$  for end-of-pulse spectra were reproducible and doubly verified/processed with Edinburgh Instruments L900 and lifetimes were plotted on Igor Pro (version 6.34A, Wavemetrics) software. All measurements were performed on sample concentrations of ketones having an O.D. of ca. < 1.0 at 266 nm.



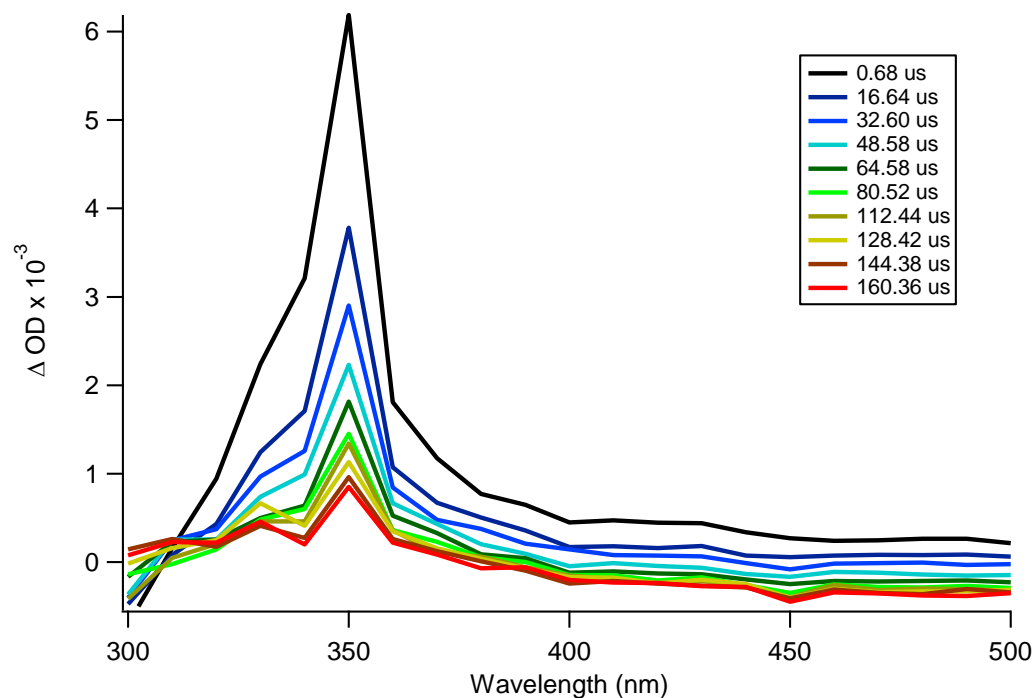
**Figure 2.S52:** Transient Spectroscopy of 1,1,3,3-tetraphenylpropan-2-one (**1a**) in solution state ( $\lambda_{\max} = 330$  nm)



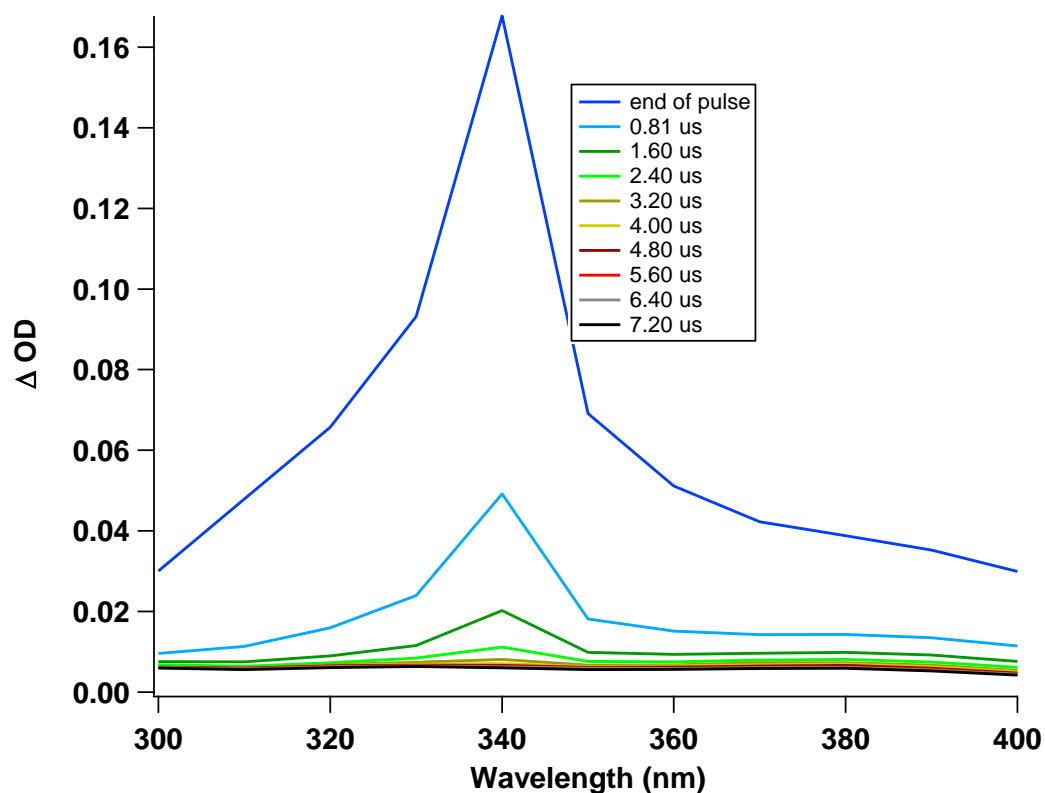
**Figure 2.S53:** Transient Spectroscopy of 1,1,3,3-tetraphenylpropan-2-one (**1a**) in nanocrystalline suspension ( $\lambda_{max} = 340$  nm)



**Figure 2.S54:** Transient Spectroscopy of 1,1,3,3-tetra-p-tolylpropan-2-one (**1b**) in solution-state ( $\lambda_{max} = 340$  nm)

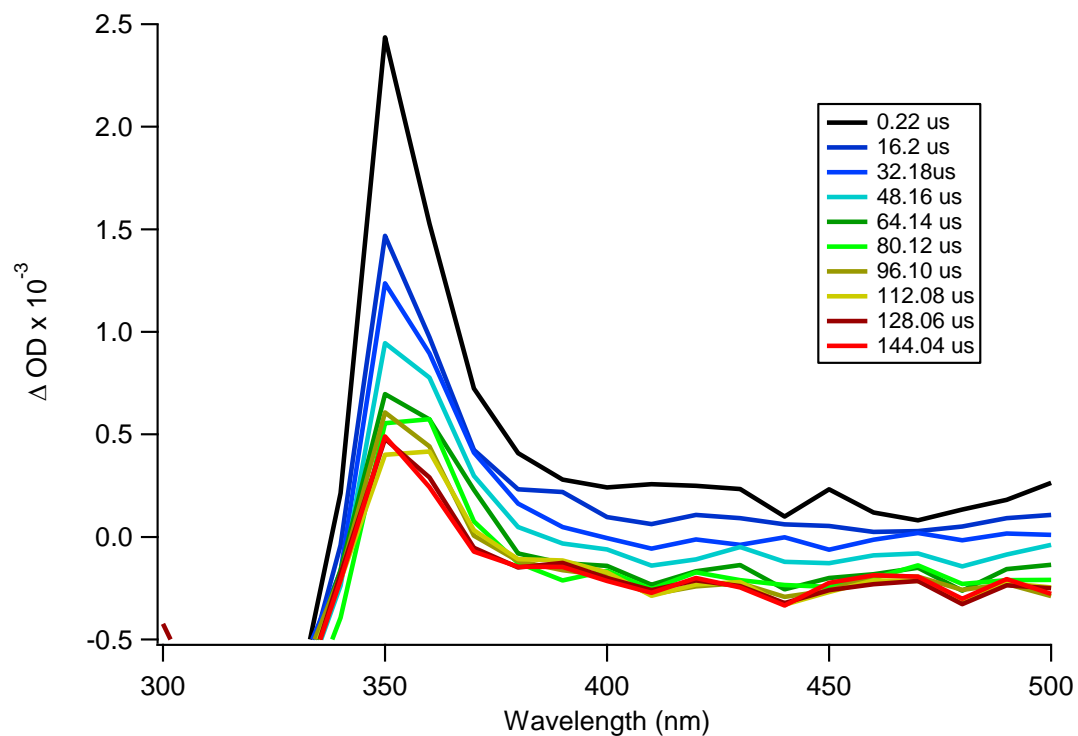


**Figure 2.S55:** Transient Spectroscopy of 1,1,3,3-tetra-p-tolylpropan-2-one (**1b**) in nanocrystalline suspension ( $\lambda_{max} = 350$  nm)

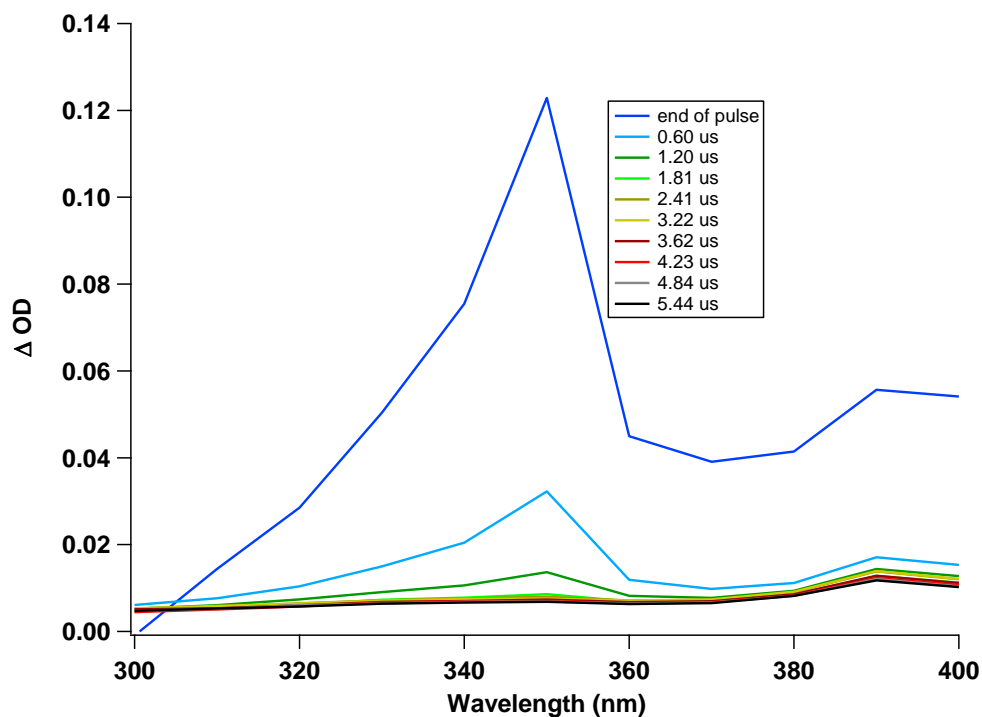


**Figure 2.S56:** Transient Spectroscopy of 1,1,3,3-tetrakis(4-chlorophenyl)propan-2-one (**1c**) in solution-state ( $\lambda_{max} = 340$  nm)

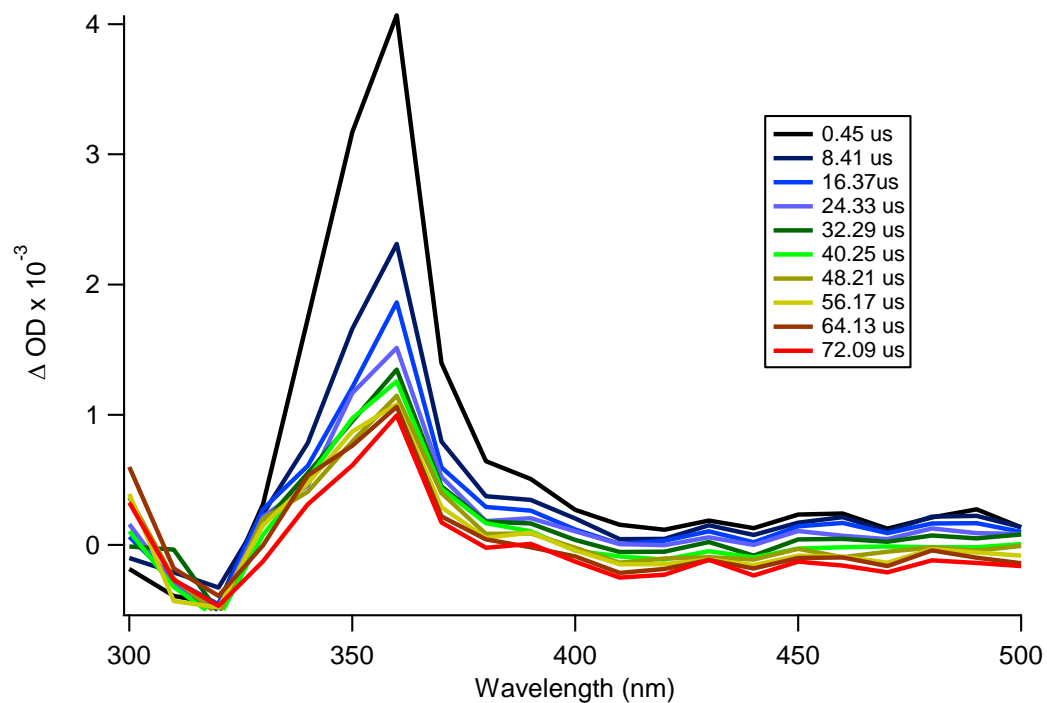




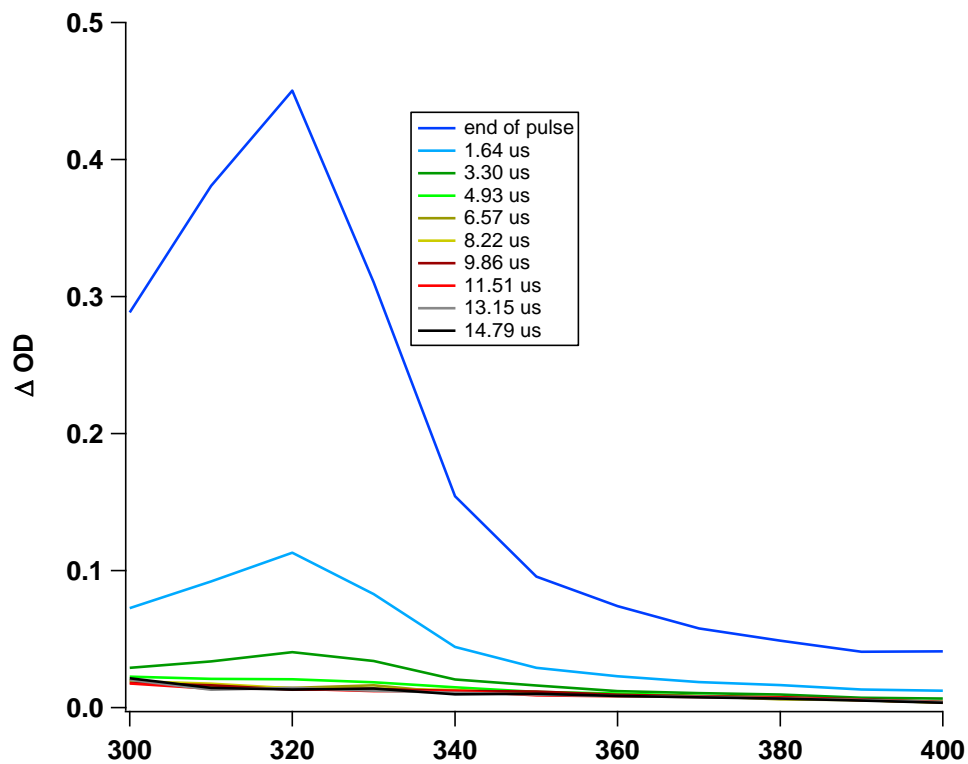
**Figure 2.S57:** Transient Spectroscopy of 1,1,3,3-tetrakis(4-chlorophenyl)propan-2-one (**1c**) in nanocrystalline suspension ( $\lambda_{\text{max}} = 350 \text{ nm}$ )



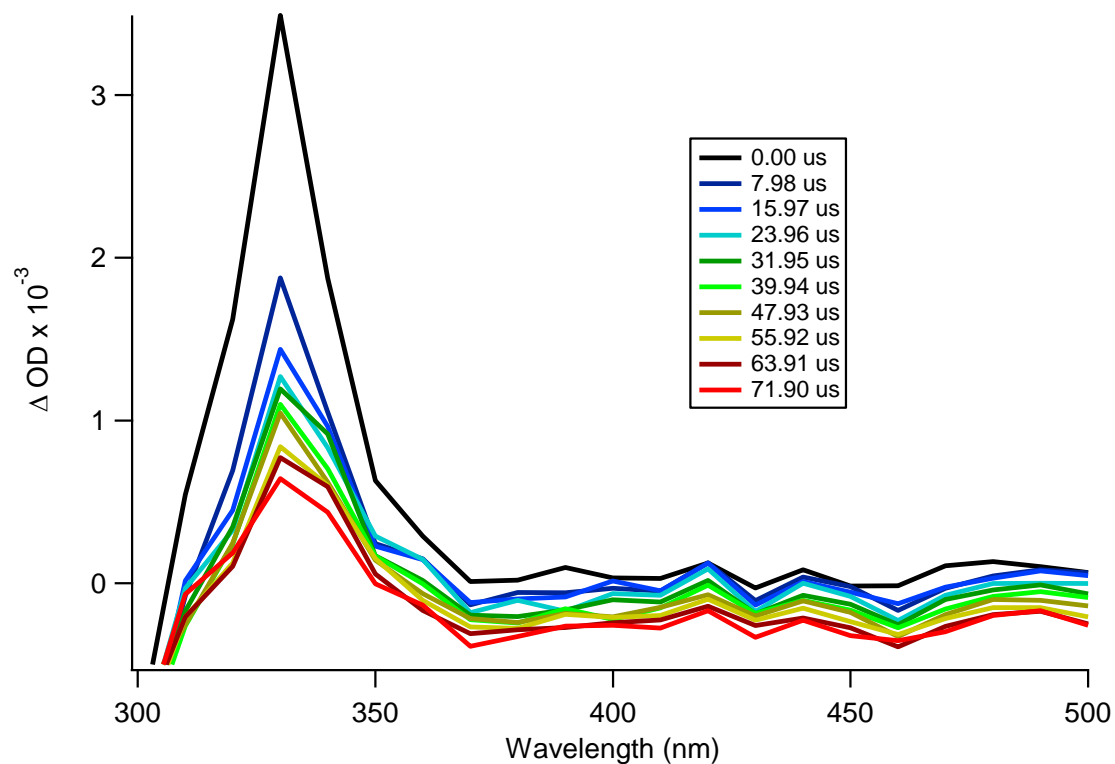
**Figure 2.S58:** Transient Spectroscopy of 1,1,3,3-tetrakis(4-methoxyphenyl)propan-2-one (**1d**) in solution-state ( $\lambda_{\text{max}} = 350 \text{ nm}$ )



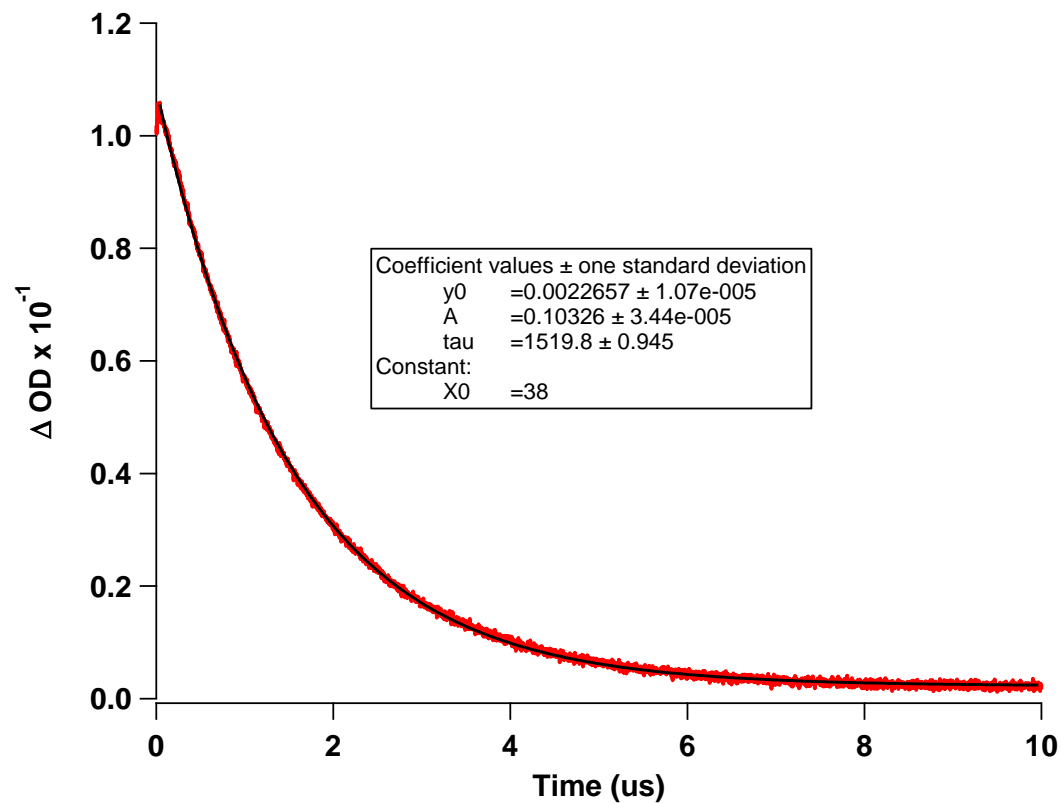
**Figure 2.S59:** Transient Spectroscopy of 1,1,3,3-tetrakis(4-methoxyphenyl)propan-2-one (**1d**) in nanocrystalline suspension ( $\lambda_{\text{max}} = 360 \text{ nm}$ )



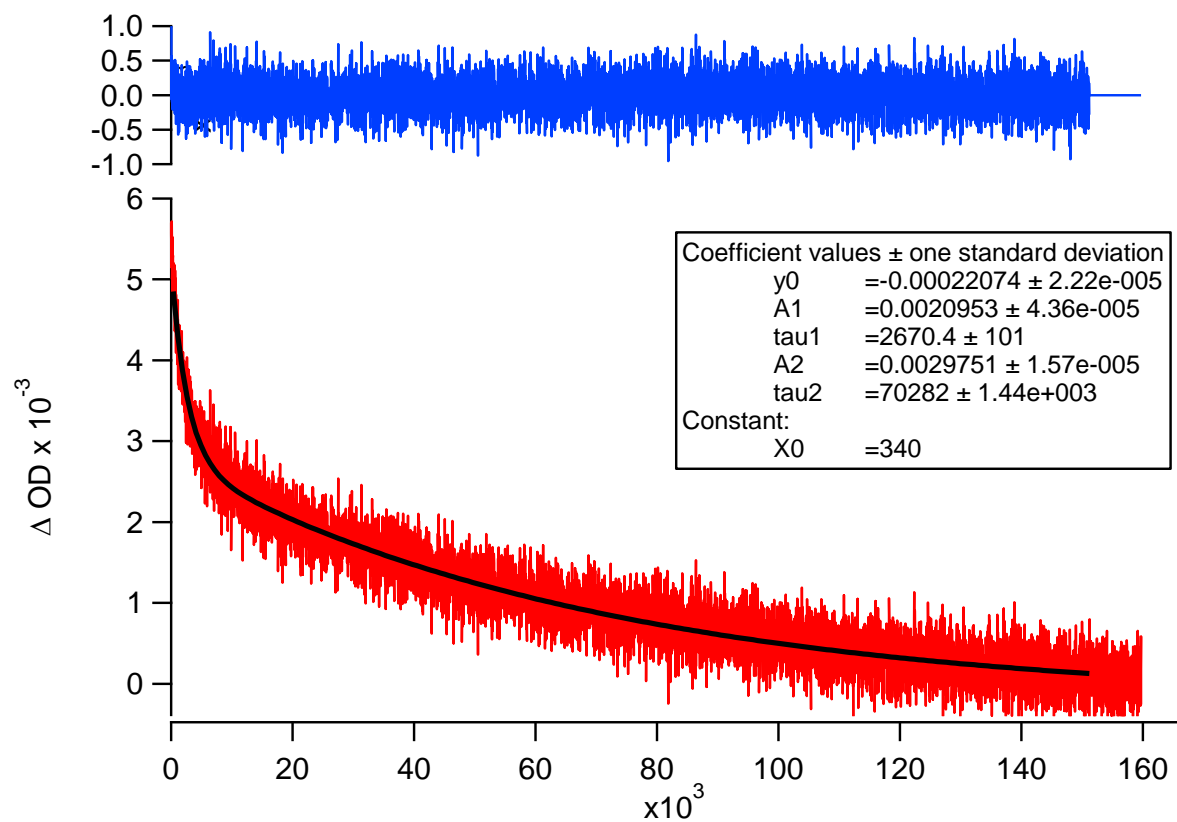
**Figure 2.S60:** Transient Spectroscopy of 1,1,3,3-tetrakis(4-fluorophenyl)propan-2-one (**1e**) in solution-state ( $\lambda_{\text{max}} = 320 \text{ nm}$ )



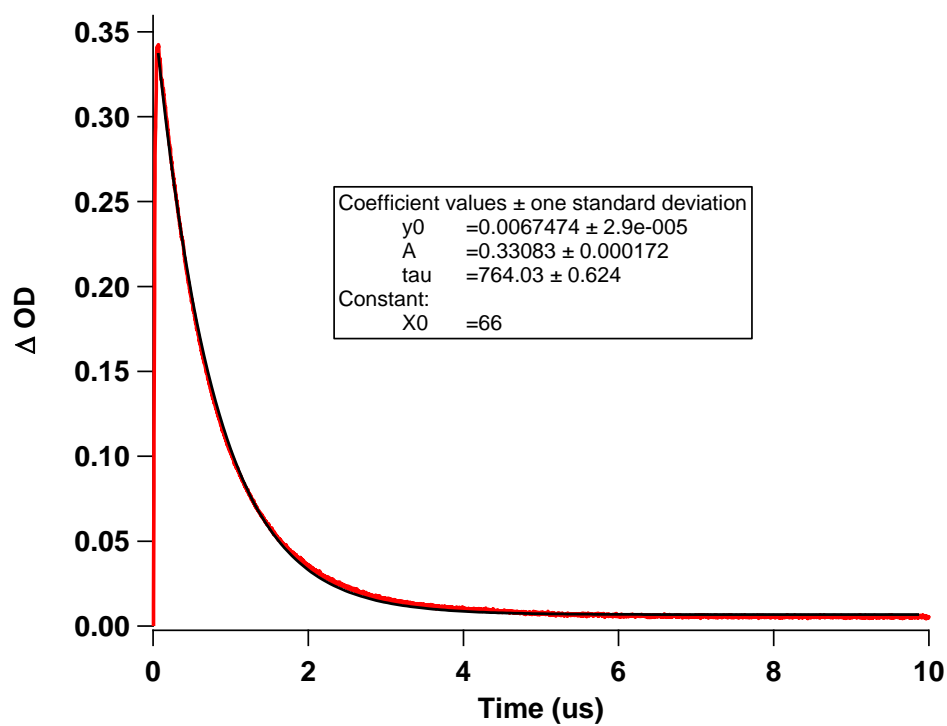
**Figure 2.S61:** Transient Spectroscopy of 1,1,3,3-tetrakis(4-fluorophenyl)propan-2-one (**1e**) in nanocrystalline suspension ( $\lambda_{\text{max}} = 330 \text{ nm}$ )



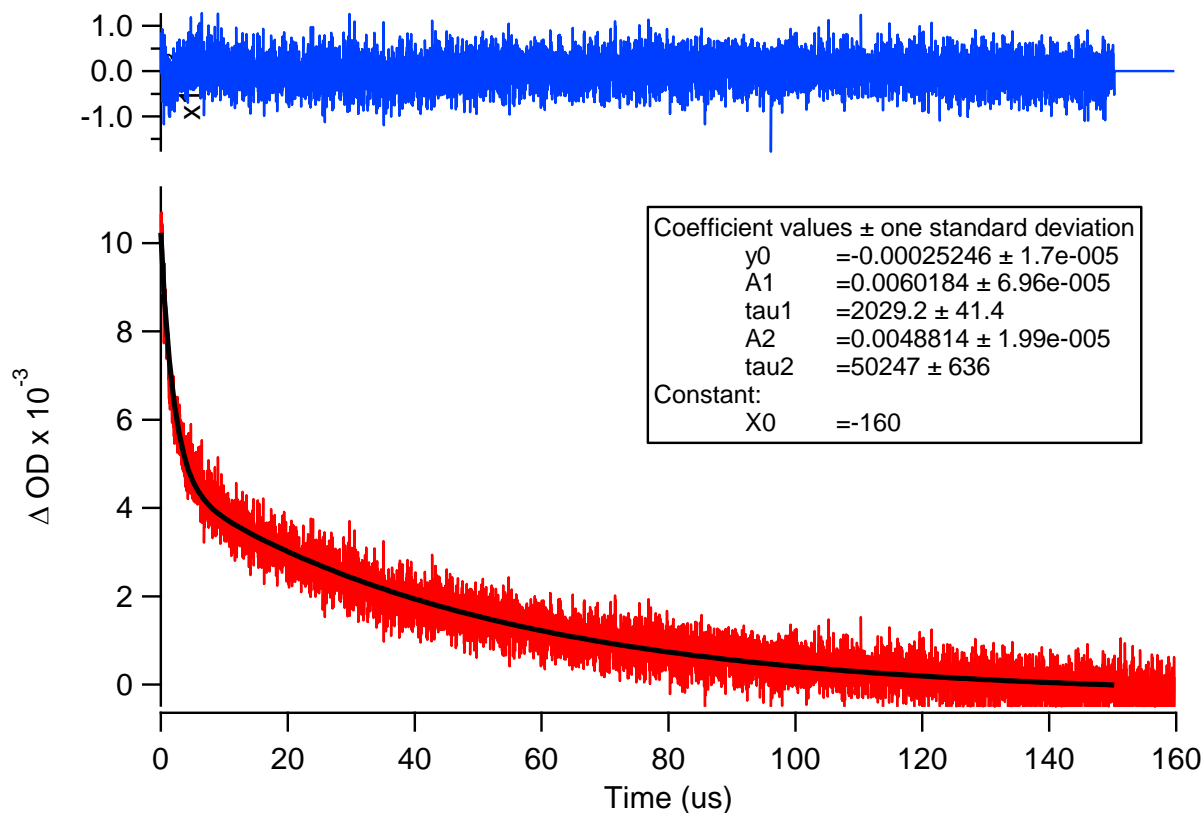
**Figure 2.S62:** Transient decay of 1,1,3,3-tetraphenylpropan-2-one (**1a**) in solution



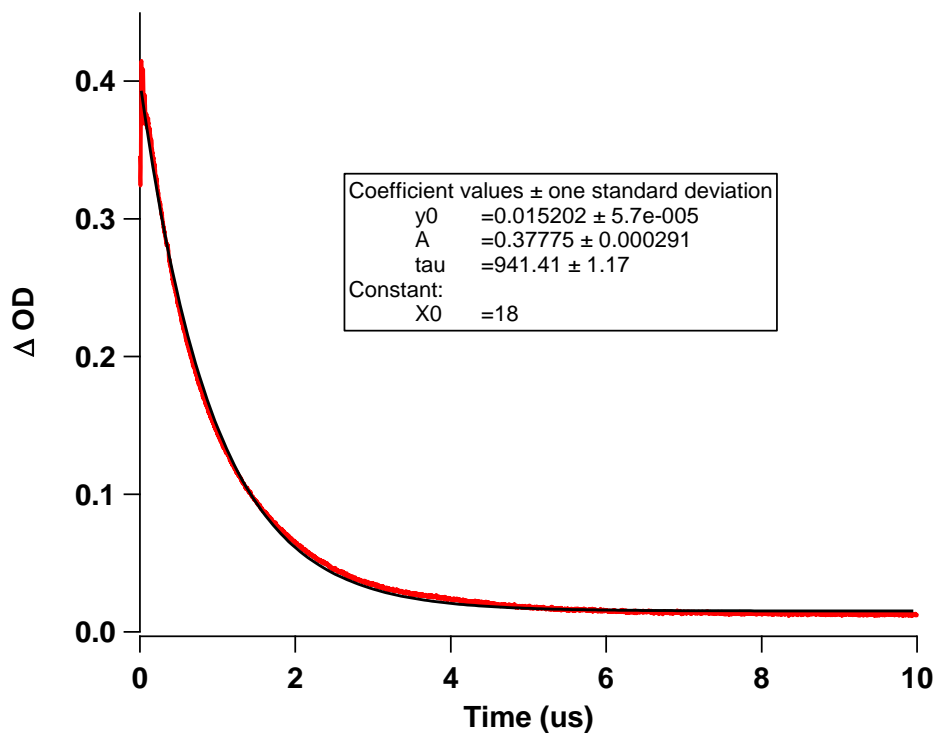
**Figure 2.S63:** Transient decay of 1,1,3,3-tetraphenylpropan-2-one (**1a**) in nanocrystalline suspension.



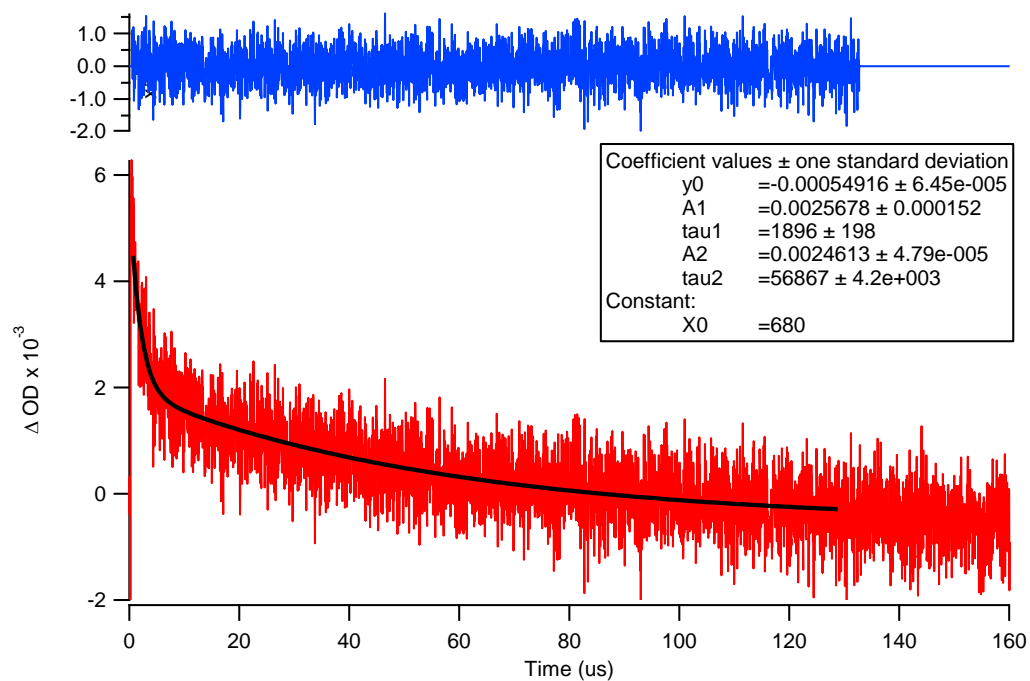
**Figure 2.S64:** Transient decay of 1,1,3,3-tetra-p-tolylpropan-2-one (**1b**) in solution.



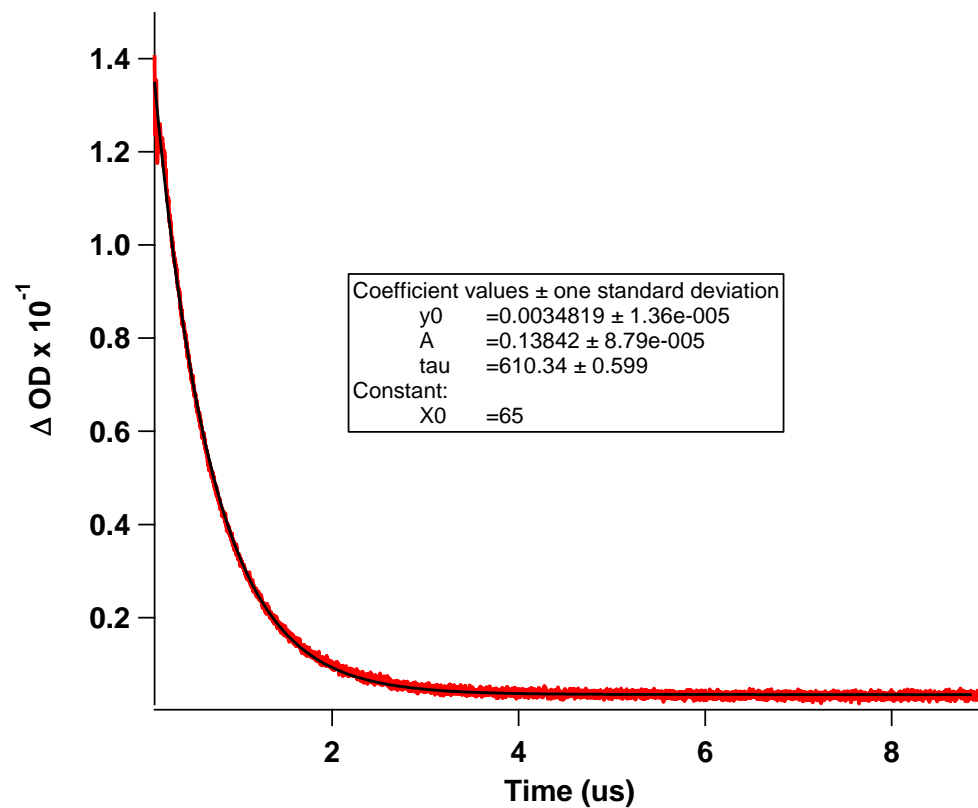
**Figure 2.S65:** Transient decay of 1,1,3,3-tetra-p-tolylpropan-2-one (**1b**) in nanocrystalline suspension.



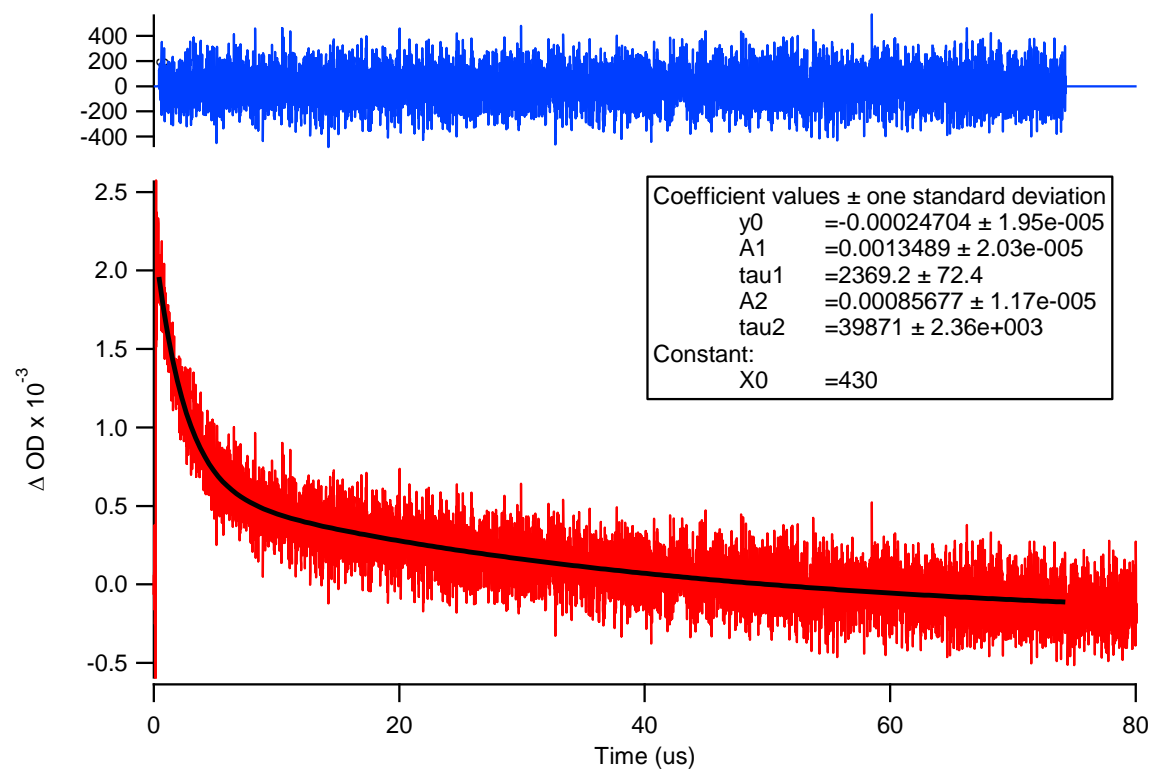
**Figure 2.S66:** Transient decay of 1,1,3,3-tetrakis(4-chlorophenyl)propan-2-one (**1c**) in solution.



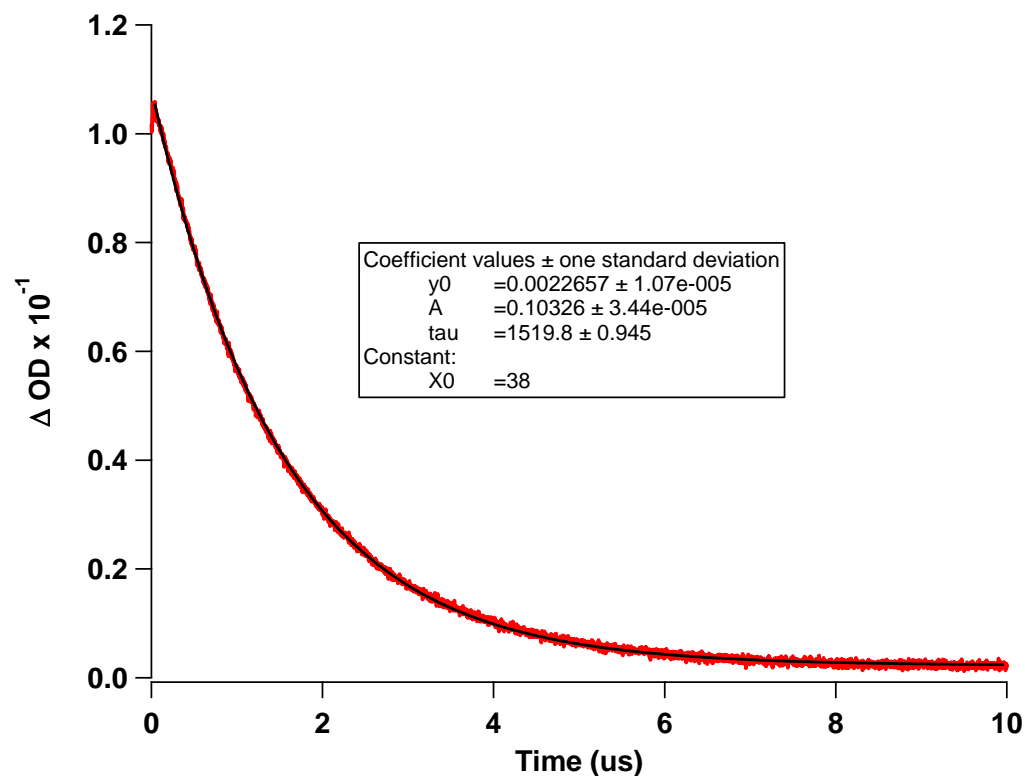
**Figure 2.S67:** Transient decay of 1,1,3,3-tetrakis(4-chlorophenyl)propan-2-one (**1c**) in nanocrystalline suspension.



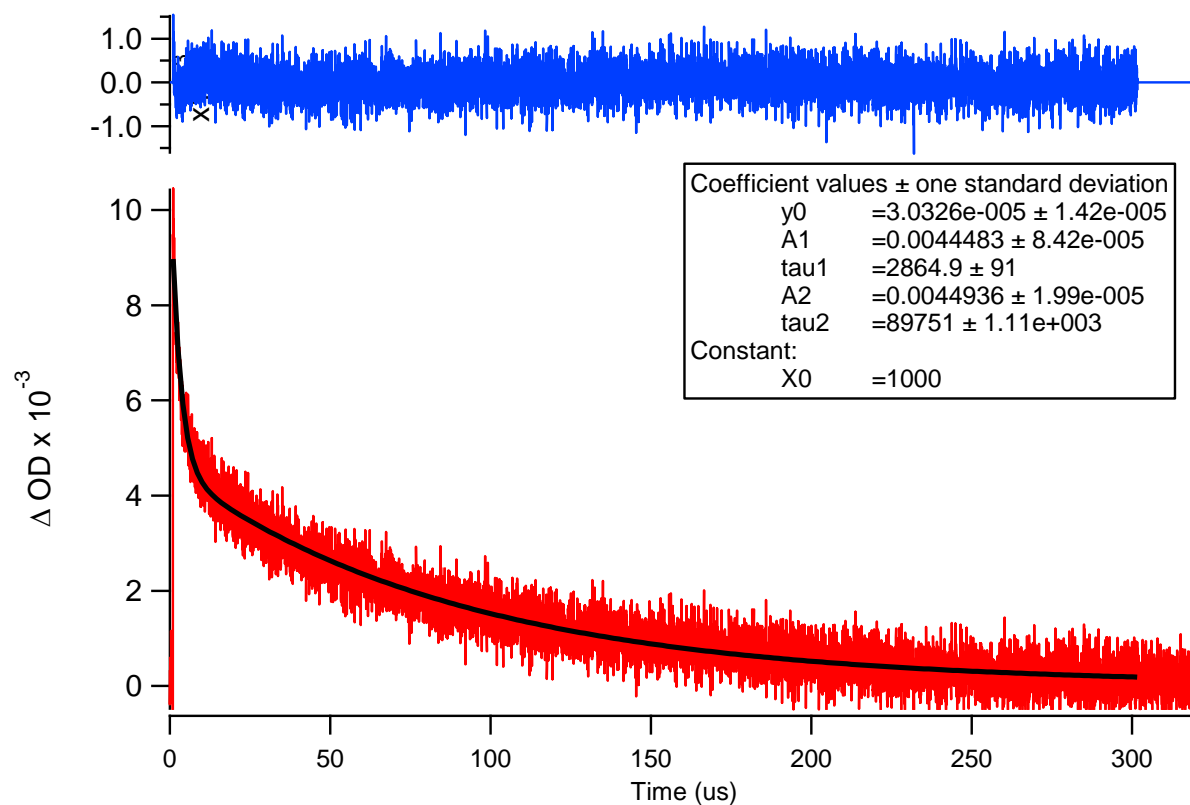
**Figure 2.S68:** Transient decay of 1,1,3,3-tetrakis(4-methoxyphenyl)propan-2-one (**1d**) in solution.



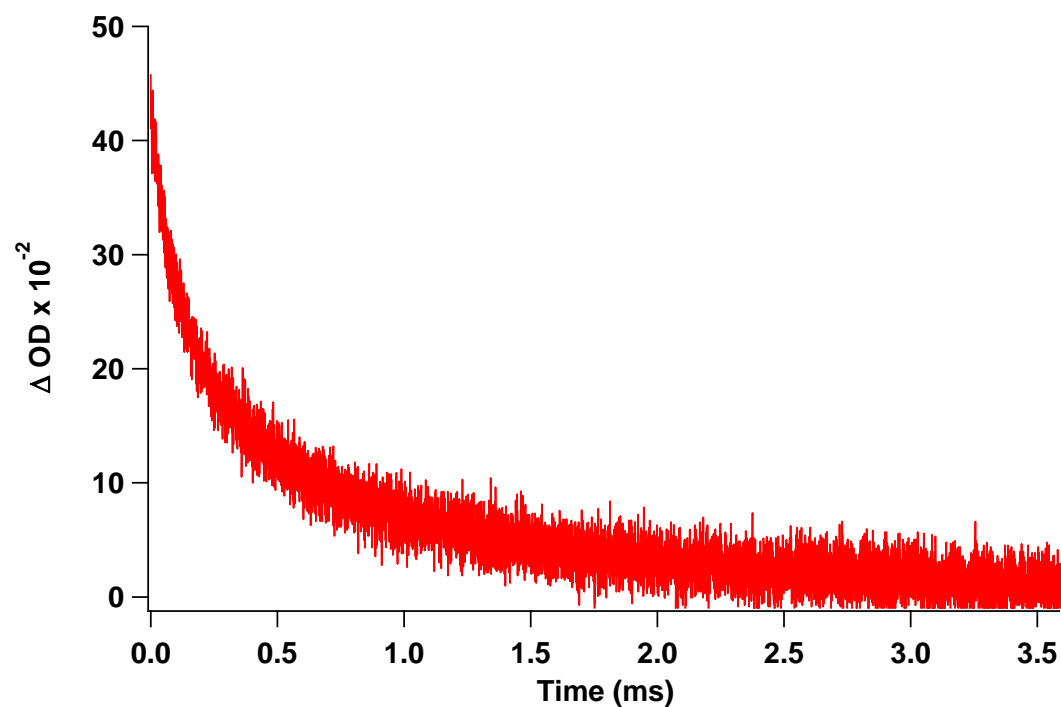
**Figure 2.S69:** Transient decay of 1,1,3,3-tetrakis(4-methoxyphenyl)propan-2-one (**1d**) in nanocrystalline suspension.



**Figure 2.S70:** Transient decay of 1,1,3,3-tetrakis(4-fluorophenyl)propan-2-one (**1e**) in solution.

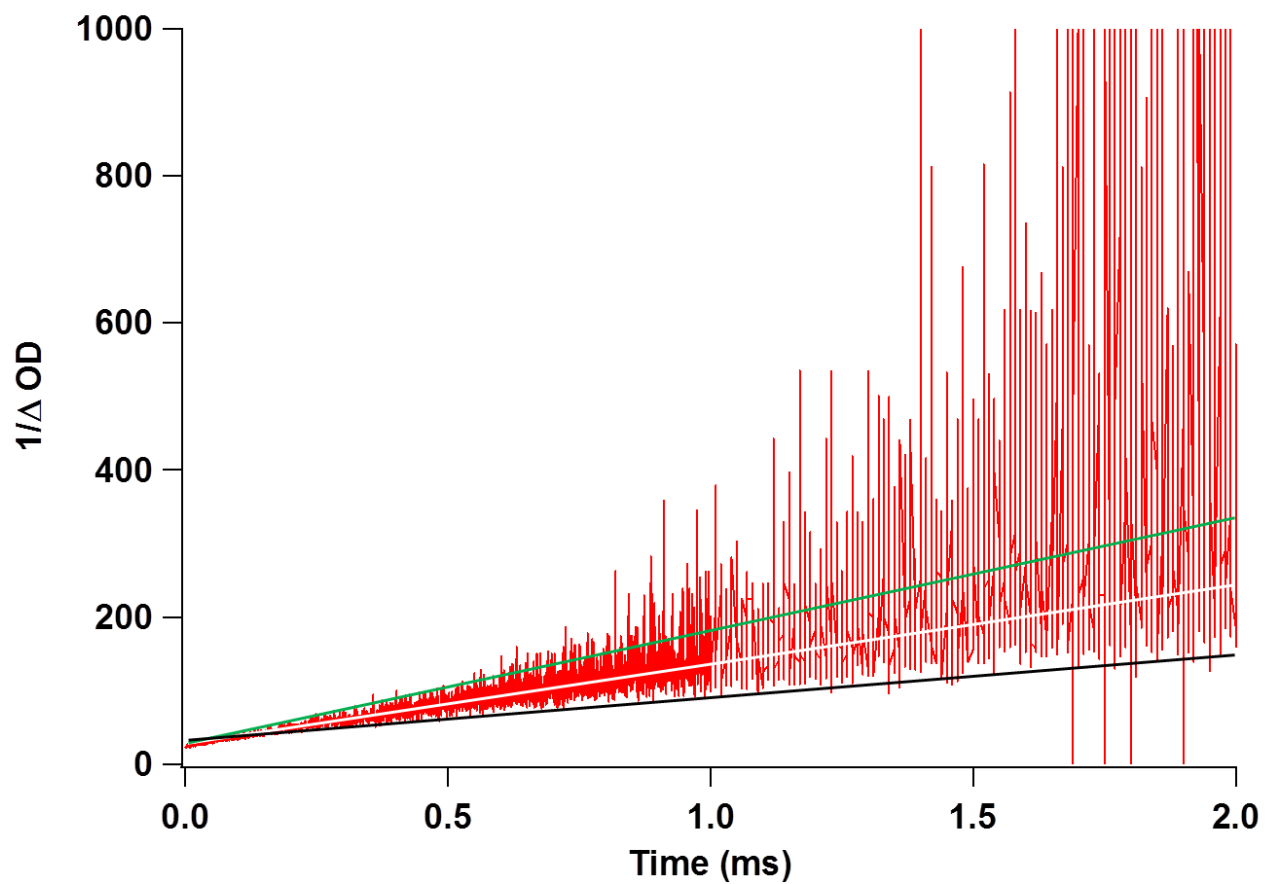


**Figure 2.S71:** Transient decay of 1,1,3,3-tetrakis(4-fluorophenyl)propan-2-one (**1e**) in nanocrystalline suspension



**Figure 2.S73:** Transient decay of 1,1,3,3-tetraphenylpropan-2-one (**1a**) in solution degassed in a cuvette for two hours





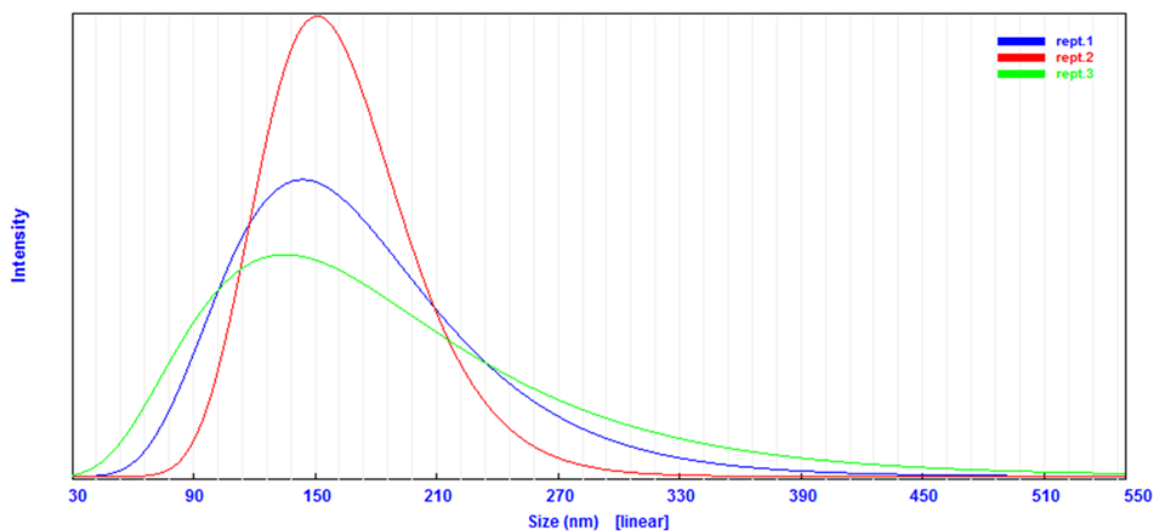
**Figure 2.S74:** Second order kinetics of 1,1,3,3-tetraphenylpropan-2-one (**1a**) in solution degassed in a cuvette for two hours. Green line  $k = 8.1\text{E-}5$  ( $1/[\text{OD}][\text{ms}]$ ); white line  $k = 1.45\text{E-}4$  ( $1/[\text{OD}][\text{ms}]$ ); black line  $k = 1.07\text{E-}4$  ( $1/[\text{OD}][\text{ms}]$ ); average  $k = 1.11\text{E-}4$  ( $1/[\text{OD}][\text{ms}]$ )

## 2.5.7 Dynamic Light Scattering:

### General preparation of nanocrystalline suspensions:

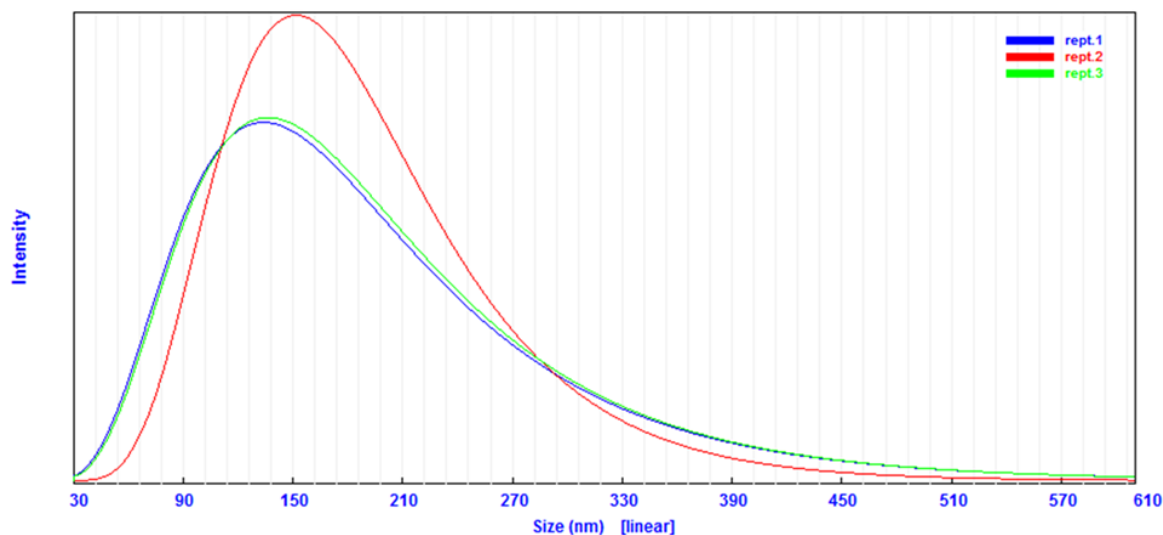
10  $\mu\text{L}$  of stock solution (5mg/mL) in acetonitrile is injected drop wise via syringe into a 100 mL graduated cylinder containing a 20 mL of a cationic detergent made of cetrimonium bromide (CTAB) surfactant dissolved in deionized water so that the critical micelle concentration of CTAB (0.9 mM)<sup>28</sup> is 1/25 or 1.25 mg of CTAB in 1L of deionized water. Prior to the injection of the stock solution, it is important to take note that the vortex is generated from a conventional stir plate and stir bar. After the stock solution is added the stirring continues for 15 seconds before it is carefully transferred so that bubbles are not generated during the transfer of liquid.

Rept#.	Mean (nm)	Std.Dev (nm)	Baseline Error	P.I.	Counts/s	Diff.Coeff (m <sup>2</sup> /s)	Overflow
Rept.1	143.4	40.7	0.01%	-0.059	4.13e+05	3.16e-12	0
Rept.2	146.5	25.8	0.01%	0.018	4.08e+05	3.09e-12	0
Rept.3	142.8	57.1	0.02%	0.222	4.07e+05	3.17e-12	0
Average	144.3	41.21		0.060			



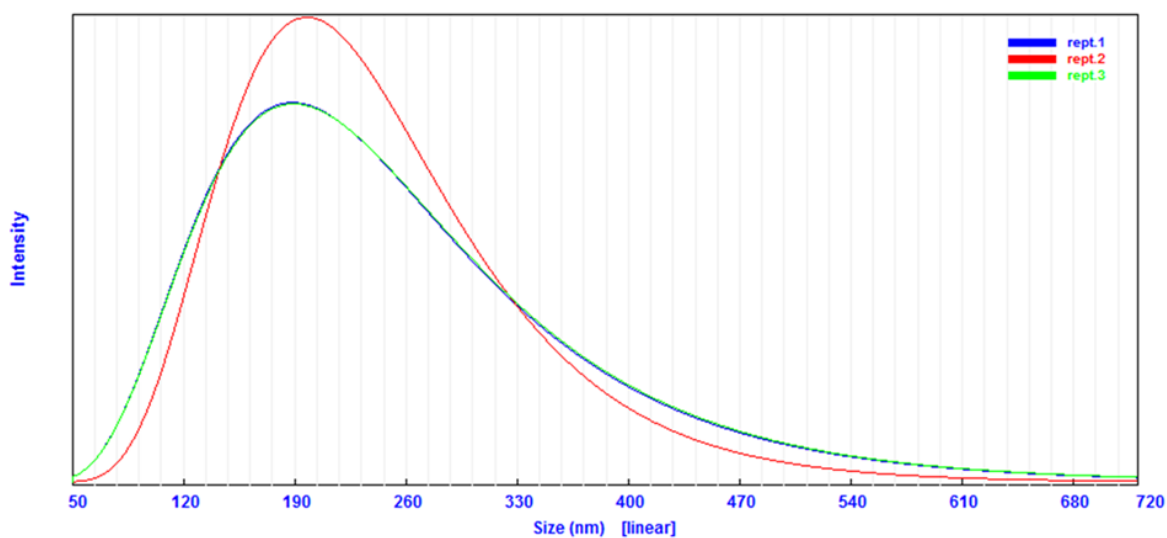
**Figure 2.S75:** Dynamic light scattering results of 1,1,3,3-tetraphenylpropan-2-one (**1a**) in nanocrystalline suspension with an average value of 140 nm.

Rept#.	Mean (nm)	Std.Dev (nm)	Baseline Error	P.I.	Counts/s	Diff.Coeff (m <sup>2</sup> /s)	Overflow
Rept.1	144.1	61.8	0.00%	0.348	2.74e+05	2.98e-12	0
Rept.2	153.2	47.8	-0.00%	-0.080	2.77e+05	2.80e-12	0
Rept.3	146.1	61.6	0.00%	0.308	2.81e+05	2.94e-12	0
Average	147.8	57.08		0.192			



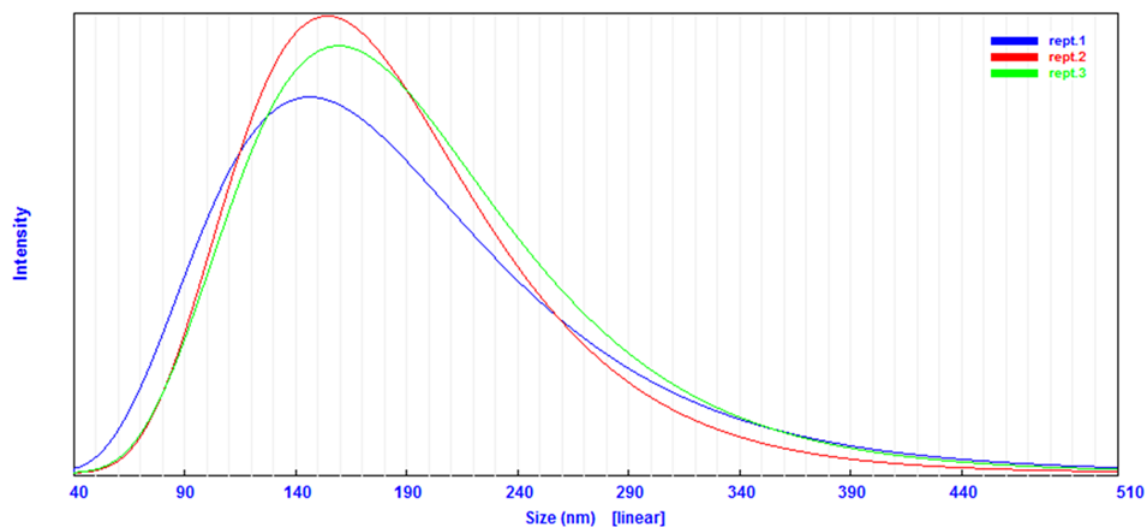
**Figure 2.S76:** Dynamic light scattering results of 1,1,3,3-tetra-p-tolylpropan-2-one (**1b**) in nanocrystalline suspension with an average value of 150 nm

Rept#.	Mean (nm)	Std.Dev (nm)	Baseline Error	P.I.	Counts/s	Diff.Coeff (m <sup>2</sup> /s)	Overflow
Rept.1	196.8	74.3	-0.00%	0.166	5.90e+05	2.18e-12	0
Rept.2	198.3	59.0	0.01%	0.068	5.89e+05	2.16e-12	0
Rept.3	197.7	75.0	0.01%	0.169	5.89e+05	2.17e-12	0
Average	197.6	69.44		0.135			



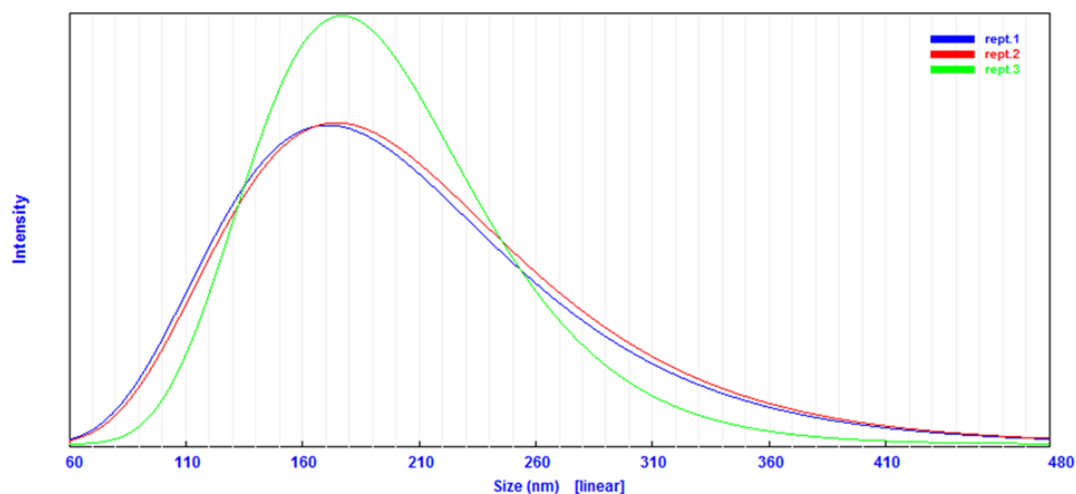
**Figure 2.S77:** Dynamic light scattering results of 1,1,3,3-tetrakis(4-chlorophenyl)propan-2-one (**1c**) in nanocrystalline suspension with an average value of 200 nm

Rept.#.	Mean (nm)	Std.Dev (nm)	Baseline Error	P.I.	Counts/s	Diff.Coeff (m <sup>2</sup> /s)	Overflow
Rept.1	150.8	53.3	0.01%	-0.125	7.98e+05	3.00e-12	0
Rept.2	153.9	43.3	0.00%	0.058	8.02e+05	2.94e-12	0
Rept.3	160.5	48.8	-0.00%	-0.073	7.98e+05	2.82e-12	0
Average	155.1	48.47		-0.047			



**Figure 2.S78:** Dynamic light scattering results of 1,1,3,3-tetrakis(4-methoxyphenyl)propan-2-one (**1d**) in nanocrystalline suspension with an average value of 160 nm

Rept.#.	Mean (nm)	Std.Dev (nm)	Baseline Error	P.I.	Counts/s	Diff.Coeff (m <sup>2</sup> /s)	Overflow
Rept.1	170.9	49.5	0.01%	0.063	2.89e+05	2.65e-12	0
Rept.2	174.4	50.1	0.01%	-0.061	2.77e+05	2.60e-12	0
Rept.3	172.7	36.1	0.00%	0.027	2.71e+05	2.62e-12	0
Average	172.6	45.22		0.009			



**Figure S79:** Dynamic light scattering results of 1,1,3,3-tetrakis(4-fluorophenyl)propan-2-one (**1e**) in nanocrystalline suspension with an average value of 170 nm

## 2.6 References

- 1). (a) Ramamurthy, V.; Venkatesan, K. *Chem. Rev.* **1987**, *87*, 433. (b) Gamlin, J. N.; Jones, R.; Leibovitch, M.; Patrick, B.; Scheffer, J. R.; Trotter, J. *Acc. Chem. Res.* **1996**, *29*, 203. (c) Zimmerman, H. E.; Nesterov, E. E. *Acc. Chem. Res.* **2002**, *35*, 77. (d) Friscic, T.; MacGillivray, L. R. In *Frontiers in Crystal Engineering*; Vittal, J. J. Tiekink, E. R. T., Eds.; Wiley-VCH: Weinheim, Germany, **2005**; pp 53–68. (e) MacGillivray, L. R.; Papaefstathiou, G. S.; Frišćić, T.; Hamilton, T. D.; Bučar, D.-K.; Chu, Q.; Varshney, D. V.; Georgiev, I. G. *Acc. Chem. Res.* **2008**, *41*, 280. (f) Chung, T. S.; Ayitou, A. J.; Park, J. H.; Breslin, V. M.; Garcia-Garibay, M. A. *J. Phys. Chem. Lett.* **2017**, *8*, 1845–1850. (g) Cole, J. M.; Irie, M. *CrystEngComm* **2016**, *18*, 7175–7179.
- 2). (a) Campos, L. M.; Garcia-Garibay, M. A. In *Reviews of Reactive Intermediate Chemistry*; Platz, M. S., Jones, M., Moss, R., Eds.; Wiley: Hoboken, NJ, 2007. (b) Garcia-Garibay, M. A. *Acc. Chem. Res.* **2003**, *36*, 491–498. (c) Garcia-Garibay, M. A.; Shin, S.; Sanrame, C. *Tetrahedron* **2000**, *56*, 6729–6737.
- 3). (a) Campos, L. M.; Ng, D.; Yang, Z.; Dang, H.; Martinez, H. L.; Garcia-Garibay, M. A. *J. Org. Chem.* **2002**, *67*, 3749. (b) Resendiz, M. J. E.; Garcia-Garibay, M. A. *Org. Lett.* **2005**, *7*, 371. (c) Mortko, C. J.; Garcia-Garibay, M. A. *Top Stereochem.* **2006**, *25*, 205.
- 4). (a) Wilkinson, F.; Kelly, G. Diffuse reflectance flash photolysis. In *Handbook of Organic Photochemistry*; Scaiano, J. C., Ed.; CRC Press: Boca Raton, FL, 1989; Vol. 1, Chapter 12, pp 293–314. (b) Kessler, R. W.; Krabichler, G.; Uhl, S.; Oelkrug, D.; Hagan, W. P.; Hyslop, J.; Wilkinson, F. *Opt. Acta* **1983**, *30*, 1099.
- 5). Simoncelli, S.; Kuzmanich, G.; Gard, M. N.; Garcia-Garibay, M. A. *J. Phys. Org. Chem.* **2010**, *23*, 376. (6) (a) Veerman, M.; Resendiz, M. J. E.; Garcia-Garibay, M. A. *Org. Lett.*

- 2006, 8, 2615. (b) Hernández-Linares, M. G.; Guerrero-Luna, G.; Pérez-Estrada, S.; Ellison, M.; Ortin, M.; Garcia-Garibay, M. A. *J. Am. Chem. Soc.* **2015**, *137*, 1679.
- 7). Jockusch, S.; Hirano, T.; Liu, Z.; Turro, N. J. *J. Phys. Chem. B* **2000**, *104*, 1212.
- 8). (a) Bromberg, A.; Schmidt, K. H.; Meisel, D. J. *J. Am. Chem. Soc.* **1984**, *106*, 3056. (b) Bromberg, A.; Schmidt, K. H.; Meisel, D. J. *J. Am. Chem. Soc.* **1985**, *107*, 83. (c) Scaiano, J. C.; Tanner, M.; Weir, D. J. *J. Am. Chem. Soc.* **1985**, *107*, 4396.
- 9). (a) Kelly, G.; Willsher, C. J.; Wilkinson, F.; Netto-Ferreira, J. C.; Olea, A.; Weir, D.; Johnston, L. J.; Scaiano, J. C. *Can. J. Chem.* **1990**, *68*, 812. (b) Gould, I. R.; Zimmt, M. B.; Turro, N. J.; Baretz, B. H.; Lehr, G. F. *J. Am. Chem. Soc.* **1985**, *107*, 4607.
- 10). Keating, A. E.; Garcia-Garibay, M. A. *Molecular and Supramolecular Photochemistry*; Ramamurthy, V. K., Ed.; Marcel Dekker: New York, 1998; Vol. 2, pp 195–248.
- 11). Kasai, H.; Nalwa, H. S.; Oikawa, H.; Okada, S.; Matsuda, H.; Minami, N.; Kakuta, A.; Ono, K.; Mukoh, A.; Nakanishi, H. *Jpn. J. Appl. Phys.* **1992**, *31*, 1132.
- 12). (a) Barton, D. H. R.; Finet, J.; Giannotti, C.; Halley, F. *J. Chem. Soc., Perkin Trans. 1* **1987**, *1*, 241. (b) Wakui, H.; Kawasaki, S.; Satoh, T.; Miura, M.; Nomura, M. *J. Am. Chem. Soc.* **2004**, *126* (28), 8658–8659. (c) Grummitt, O.; Arters, A. A.; Stearns, J. A. *J. Am. Chem. Soc.* **1951**, *73* (4), 1856–1857.
- 13). (a) Dauber, P.; Hagler, A. *Acc. Chem. Res.* **1980**, *13*, 105–112. (b) He, X.; Benniston, A. C.; Saarenpää, H.; Lemmetyinen, H.; Tkachenko, N. V.; Baisch, U. *Chem. Sci.* **2015**, *6*, 3525–3532. (c) Moulton, B.; Zaworotko, M. J. *Chem. Rev.* **2001**, *101*, 1629–1658.
- 14). (a) Boistelle, R.; Astier, J. P. *J. Cryst. Growth* **1988**, *90*, 14. (b) Lifshitz, I. M.; Slyozov, R. *J. Phys. Chem. Solids* **1961**, *19*, 35.

- 15). Owen, T. *Fundamentals of UV–Visible Spectroscopy, A Primer*. Hewlett-Packard Company, Böblingen, Germany, 1996.
- 16). (a) Bartl, J.; Steenken, S.; Mayr, H.; McClelland, R. A. *J. Am. Chem. Soc.* **1990**, *112*, 6918. (b) Cyr, D.; Das, P. *J. Phys. Chem. A* **2014**, *118*, 11155.
- 17). (a) Engel, P. S. *J. Am. Chem. Soc.* **1970**, *92*, 6074. (b) Baretz, B.; Turro, N. J. *J. Am. Chem. Soc.* **1983**, *105*, 1309. (c) Turro, N. J.; Cherry, W. R. *J. Am. Chem. Soc.* **1978**, *100*, 7431.
- 18). Gould, I. R.; Baretz, B. H.; Turro, N. J. *J. Phys. Chem.* **1987**, *91*, 925.
- 19). Lebedeva, N. V.; Tarasov, V. F.; Resendiz, M. J. E.; GarciaGaribay, M. A.; White, R. C.; Forbes, M. D. E. *J. Am. Chem. Soc.* **2010**, *132*, 82.
- 20). (a) Garcia-Garibay, M. A.; Gamarnik, A.; Pang, L.; Jenks, W. *J. Am. Chem. Soc.* **1994**, *116*, 12095. (b) Intensity data were fit to the function  $I(t) = a \exp(-bt) + c \exp(-dt)$ . The weighted contribution from each component was calculated from the ratios  $a/b$  and  $c/d$ .
- 21). (a) Johnston, L. J.; de Mayo, P.; Wong, S. K. *J. Am. Chem. Soc.* **1982**, *104*, 307. (b) Brown, H. C.; Okamoto, Y. *J. Am. Chem. Soc.* **1958**, *80*, 4979. (c) Zhang, X.; Nau, W. M. *J. Phys. Org. Chem.* **2000**, *13*, 634.
- 22). Turro, N. J.; Ramamurthy, V.; Scaiano, J. C. *Modern Molecular Photochemistry of Organic Molecules*; University Science Books: Sausalito, CA. 2010.
- 23). Doubleday, C., Jr.; Turro, N. J.; Wang, J.-F. *Acc. Chem. Res.* **1989**, *22*, 199.
- 24). Razavizadeh, B. M.; Mousavi-Khoshdel, M.; Gharibi, H.; Behjatmanesh-Ardakani, R.; Javadian, S.; Sohrabi, B. *J. Colloid Interface Sci.* **2004**, *276*, 197.

- 25). (a) Kishner, N. *J. Russ. Phys. Chem. Soc.* **1911**, *43*, 582; (b) Wolff, L. *Justus Liebig's Annalen der Chemie*, **1912**, *394*, 86-108; (c) Tashiro, M.; Yamato, T.; Fukata, G.; Fukuda, Y., *J. Org. Chem.*, **1981**, *11*, 2376-2379
- 26). Rajca, A.; Tolbert, L. M. *J. Am. Chem. Soc.*, **1988**, *110*, 871-876
- 27). Satoh, T.; Kawamura, Y.; Miura, M.; Nomura, M., *Angew. Chem. Int. Ed. Engl.*, **1997**, *36*, 1740-1742
- 28). Grummitt, O.; Arters, A. A.; Stearns, J. A., *J. Am. Chem. Soc.*, 1951, *73* (4), 1856-1857



## **Chapter 3**

### **Solid-State Photochemistry of Diphenylmethyl Radical Pairs in Nanocrystalline Suspensions Reveal a Correlation between Steric Bulk and Kinetics via Laser Flash Photolysis**

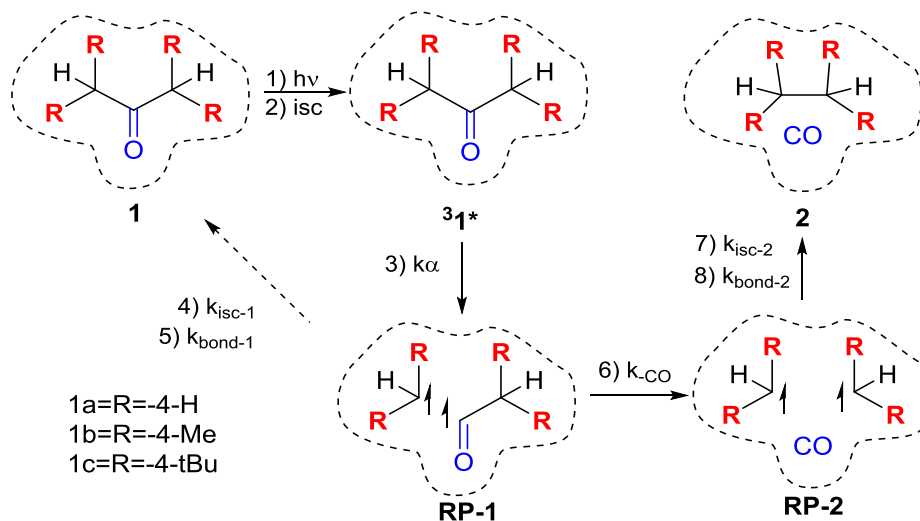
### 3.1 Introduction

It is widely known that chemical behavior and reactivity of molecules are directly correlated to the phase of matter.<sup>1</sup> Photochemistry of crystalline compounds has been receiving attention partly due to its attractive ability to stabilize the intermediate species that are generated upon irradiation.<sup>2</sup> In 1834 Tromsdorff reported the first photochemical reaction in the solid state<sup>3</sup> and since its remarkable discovery, chemists have developed the field of solid-state chemistry in conjunction with photochemistry.<sup>4</sup> However, much of solid-state photochemical reactions are underutilized because the scope of knowledge in determining the intermediates of photochemical reactions in the solid is still limited.<sup>5</sup> Transmission absorption measurements are widely used to determine mechanistic information from solution photochemistry, but this method was not ideal for retrieving mechanistic information for solid state reactions.<sup>6</sup> Upon irradiation, large crystals or bulk solids exhibit intense light scattering and, with an intrinsically high optical density, observing these solid compounds via transmission absorption measurements is impractical.<sup>7</sup> However, by adopting and further optimizing the reprecipitation method of Kasai et al.<sup>8</sup> to generate nanocrystalline (NC) suspensions, it is now possible to mirror with solids the transmission absorption spectroscopy measurements for photochemical reactions in the solid state.<sup>9</sup> In this chapter, we explore the ability of three crystalline ketones 1a-1c engineered with substituents that have different steric bulk to determine whether changes in the crystal packing may affect some aspect of the kinetics of the photodecarbonylation reaction in the solid state.

Ketones 1a-1c undergo a photo-induced decarbonylation process (Scheme 3.1.1) caused by promotion of the ground state ketone 1 to the first singlet excited state, which is expected to undergo a rapid intersystem crossing to yields the triplet ketone  $^31^*$ . In the triplet state, the  $\alpha$ -

positions undergo an initial bond cleavage to generate  $^3\text{RP-1}$  and the sequential reaction-limiting  $\alpha$ -cleavage expels carbon monoxide to yield the triplet radical pair  $^3\text{RP-2}$ . At this stage, one of the radicals undergoes a spin flip to form the singlet radical pair allowing a rapid bond formation to yield the respective aryl-ethane **2**.

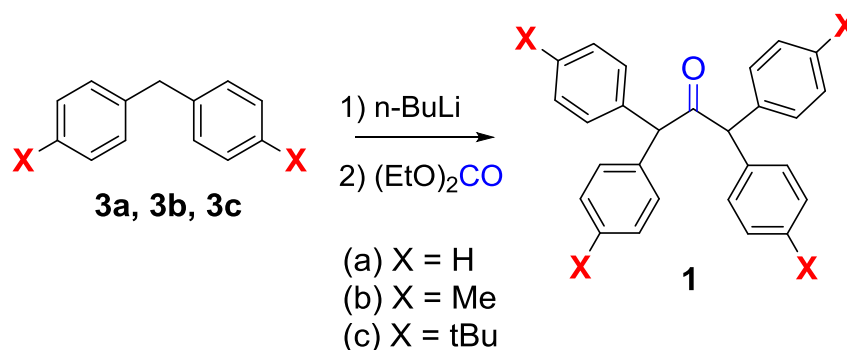
### Scheme 3.1.1



### 3.2 Results and Discussion

In order to elucidate the detailed kinetic of above reaction scheme, we selected three ketones with a common tetraphenylacetone moiety but with significantly different bulky groups at the para position: unsubstituted -H (1a), methyl substituted -4-Me (1b), tert-butyl substituted -4-tBu (1c). To reiterate, the objective of this study was to determine whether changes in steric bulk and crystal packing would alter the kinetics of the recombination of radical pair RP-2.

### Scheme 3.2.1



As represented in Scheme 3.2.1, these ketones were obtained via an initial activation of the diphenylmethane to a nucleophile with the addition of *n*-butyl-lithium. Afterwards, the diethylcarbonate is introduced drop wise and a double elimination via the diphenylmethyl nucleophile yields the product.<sup>10</sup> After the completion of synthesis, a detailed analysis of the ketones **1a-1c** showed that all ketones exhibited high melting points as well as high crystallinity, which are both desirable characteristics for room temperature solid state photochemistry (Table 3.2.1). Further details on synthesis and characterizations are listed in the SI section.

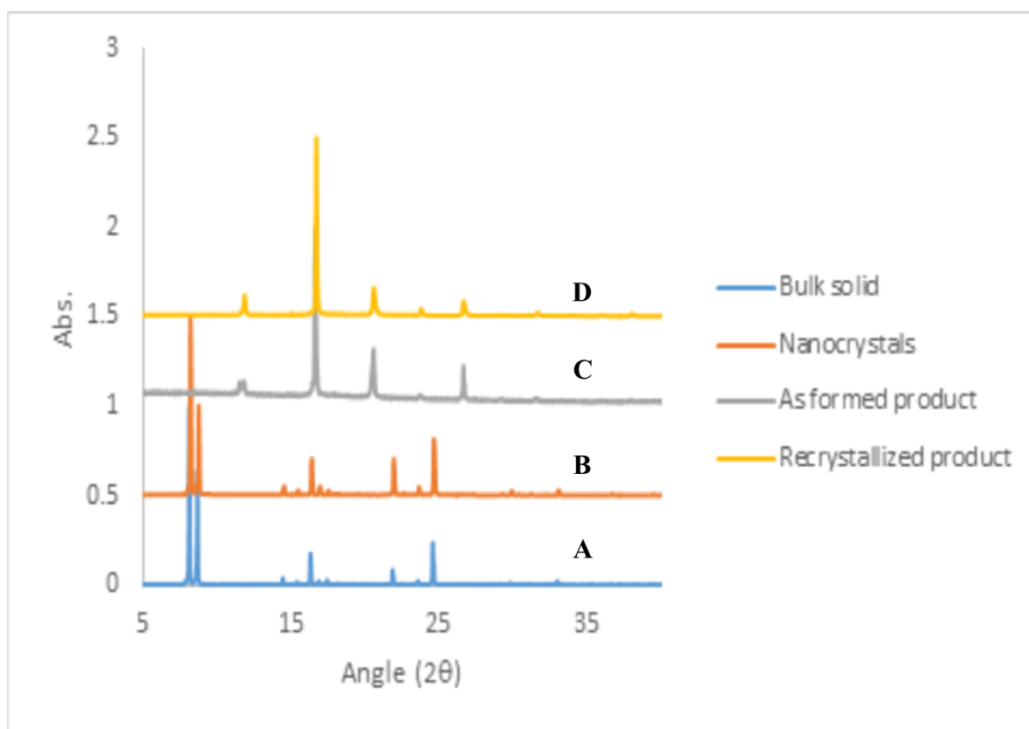
Table 3.2.1. Characterizations and Lifetimes of 4-Substituted Tetraphenylacetones

Ketone	R	m.p. (°C)	Crystal size (nm) <sup>a</sup>	Biradical Lifetimes, $\mu\text{s}$ <sup>b</sup>
1a	H	134-135 <sup>II</sup>	140 ± 40	1.5 (MeCN) 2.4, 70 (97) <sup>b</sup>
1b	Me	86-87 <sup>II</sup>	150 ± 60	0.5 (MeCN) 2.0, 50 (95) <sup>b</sup>
1c	tBu	228-229	190 ± 60	3.2 (MeCN) 1.7, 32 (87) <sup>b</sup>

<sup>a</sup>Measured by dynamic light scattering (DLS). <sup>b</sup>Short and long-lived components were observed in the solid state. The number in parenthesis indicates the contribution of the long-lived component to the total decay

One of the most crucial points of this study is the ability to form stable nanocrystalline suspensions. Upon further modification of the re-precipitation method<sup>8</sup>, we are able to effectively generate nanocrystalline suspensions of ketones **1a-1c**. In order to justify the crystallinity of the

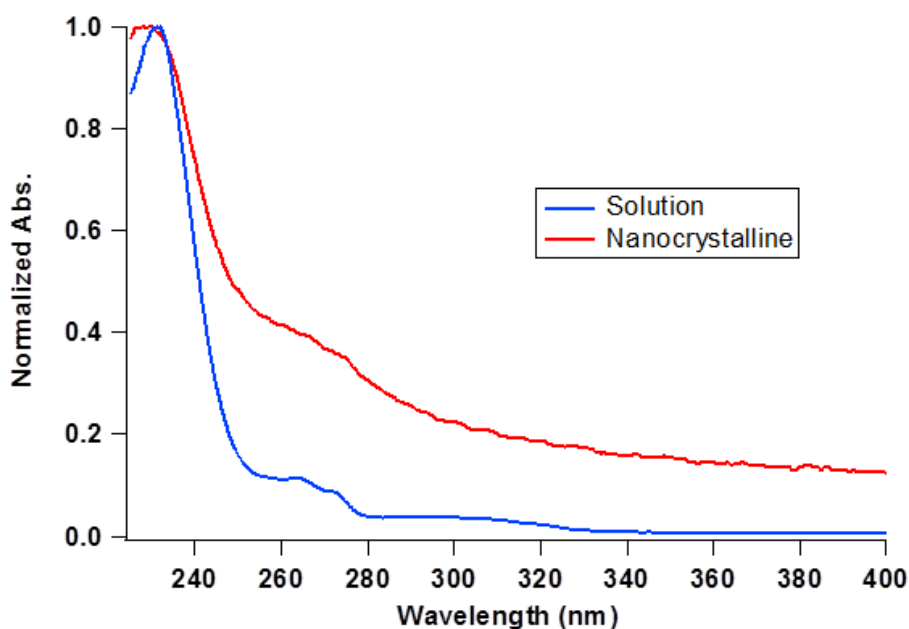
compounds, the powder X-ray diffractogram (PXRD) is shown for sample 1b (Figure 3.2.1). The sharp peaks and similarity of the bulk powder and the nanocrystals of the starting material demonstrate that the ketones are highly crystalline and that they share the same polymorph.



**Figure 3.2.1.** Powder X-ray diffraction (PXRD) of *tert*-butyl substituted ketone 1c (A) bulk-powder, (B) nanocrystals, (C) as-formed photoproduct, (D) recrystallized photoproduct

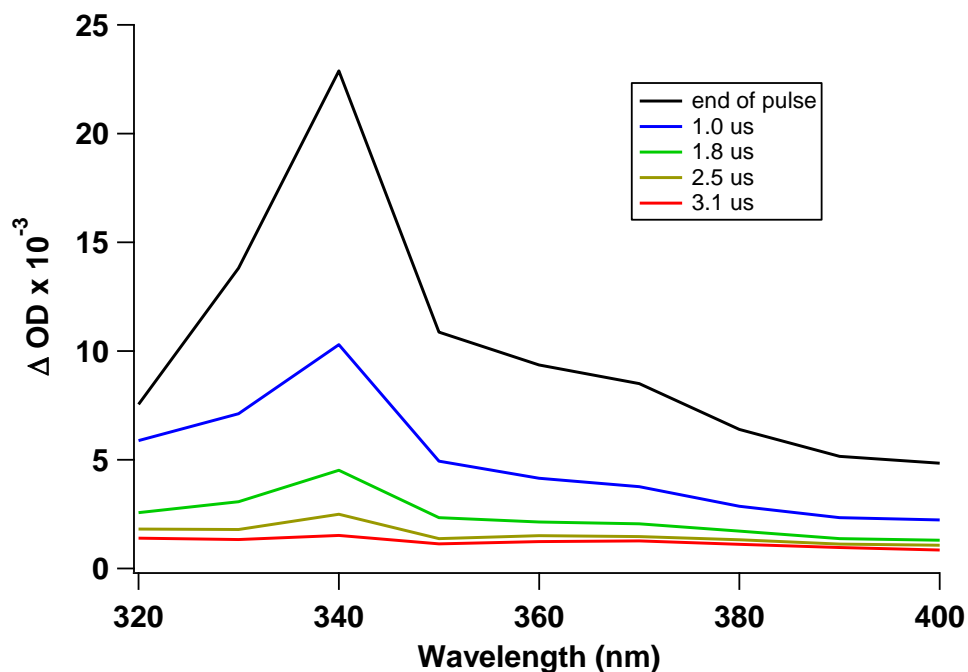
After establishing the ketone's crystallinity, the next natural step was to form stable nanocrystals with sizes that are suitable for kinetic studies via the laser flash photolysis instrument. Confirmation of this characterization is derived from a combination of UV-Vis and dynamic light scattering (DLS) studies in solution and in solid state. The UV spectra of the representative ketone 1c (Figure 3.2.2) verifies similar UV features between the solution and solid state. The quality of the nanocrystal spectra is less defined due to scattering that may occur

from aggregation. However, absorption at 266 nm is evident and transmission absorption spectra supports the nanocrystalline suspensions are sufficient to yield healthy decays.

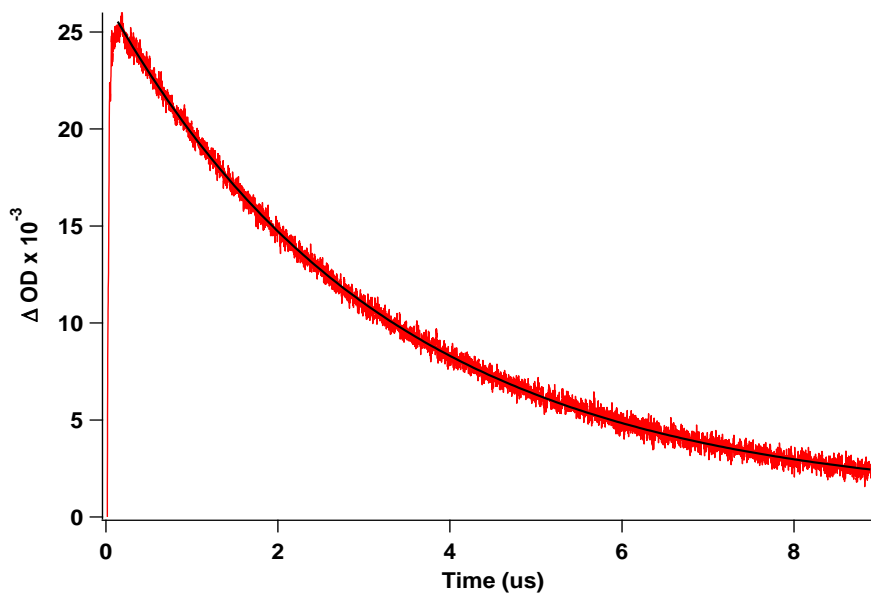


**Figure 3.2.2.** Normalized UV spectra of 1c in solution (0.01 g/L) and nanocrystalline suspension of 1c in cetyltrimethylammonium bromide (CTAB) surfactant (0.025 g/L).

Transient absorption experiments were carried out with the fourth Harmonic on a Nd-YAG laser at  $\lambda_{\text{ex}}=266$  nm with a pulse width of ca. 8 ns. In order to record transient lifetimes not contaminated with photoproducts, the laser was also set up with a single pass flow system where a pump introduced a fresh sample pushing a fresh sample of nanocrystalline suspensions at a rate of 2 mL/min. Realizing that these nanocrystals are stable for at least 10 minutes (**SI**) we deem a rate of 2 mL/min for a 3 mL cell to be sufficient.



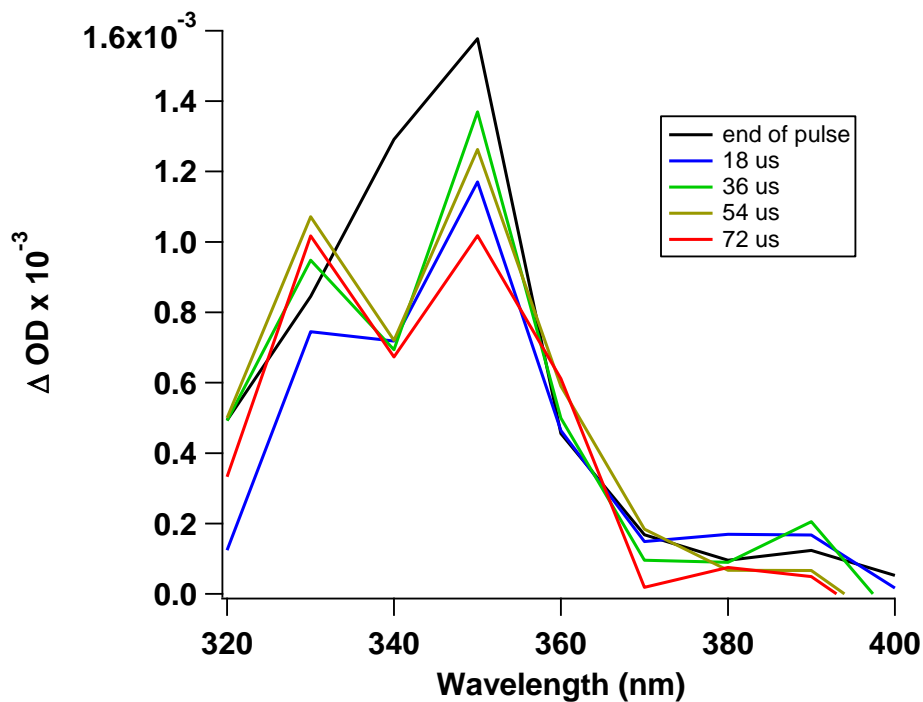
**Figure 3.2.3.** Transient absorption spectra of 1c in MeCN ( $\lambda_{\text{max}} = 340 \text{ nm}$ ).



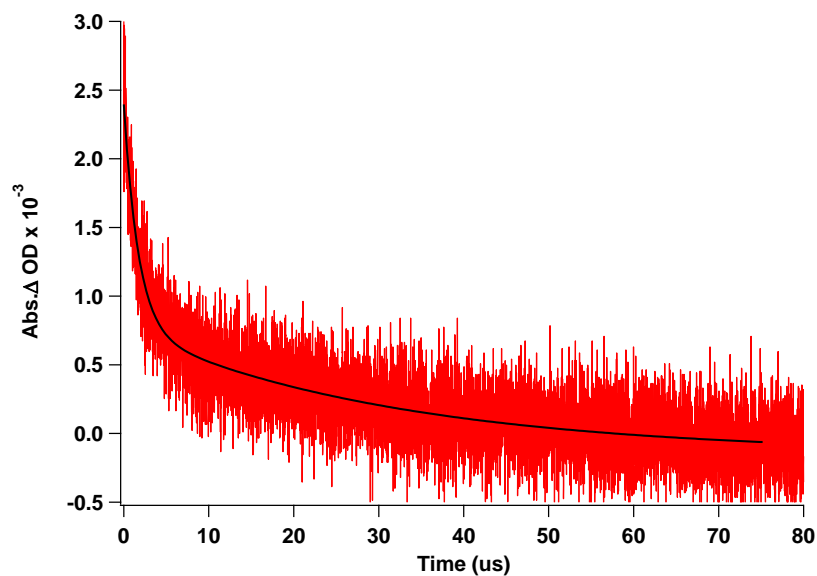
**Figure 3.2.4.** Transient absorption spectra of 1c in MeCN ( $\lambda_{\text{max}} = 340 \text{ nm}$ ).

All samples observed in the solution and solid-state had an  $\text{OD} < 1.0$  in MeCN and the analogous transient absorption spectra represent maximums at  $\lambda \approx 330\text{-}340 \text{ nm}$ . The radical pair of the represented 1c has red-shifted maxima at 340 nm (Figure 3.2.3) due to the electronic

donating ability of the methyl group. After probing the  $\lambda_{\max}$ , we obtain the lifetime by plotting a decay profile (Figure 3.2.4).



**Figure 3.2.5.** Transient spectra of 1c in a nanocrystalline suspension ( $\lambda_{\max} = 350$  nm).



**Figure 3.2.6.** Transient decay profile of 1c in the solid-state via nanocrystalline suspensions ( $\lambda_{\max} = 350$  nm).



### 3.3 Conclusion

It is evident that kinetic data of solution state reactions can be effectively extracted via optical measurements. Therefore we challenge these parameters to the solid state studies via nanocrystalline suspensions. Figure 3.2.5 is the transmission absorption spectra of the nanocrystalline suspension of 1c. The key difference that we observe from the solid state is the red shift in the  $\lambda_{\text{max}}$  wavelength from 340 to 350 nm which we believe is due to scattering induced by the nanocrystalline suspensions which would lower transmission of light. With this data in hand, we plot the decay at 350 nm and recover a decay profile Figure 3.2.6. In comparison to the solution state 8  $\mu\text{s}$  lifetime window, the solid state data requires a significantly longer lifetime window of 80  $\mu\text{s}$ . Also, the solid-state decay for all of the ketones requires a double exponential function that represents a fast and a slow component. We are unable to specifically state what the reason is for this phenomenon, but it seems that the contribution of the fast component increases as the steric bulk increases 3% to 12%. One hypothesis for this data is the fact that an increase in steric bulk is going to increase the space within the crystal cavity. This would allow a higher degree of freedom which would destabilize the radicals and thus increasing the spin of the radical pairs to obtain the correct orientation to form the photoproduct. The trend for the long lived lifetimes in the solid state seems to decrease as the steric bulk increases. This is probably explained by the fact that as the bulkiness of the substituent increases it creates spaces that allow greater freedom of rotation. This allows the radicals to spin into the correct orientation much easier which would explain why the lifetimes would be decreasing. In order to increase the validity of this study we believe that there should be a larger scope of compounds and therefore devising the synthesis of tetraphenylacetones with bulkier substituents such as a trityl or an

adamantyl group. We are also interested in presenting the crystal structures of these derivatives to verify any possible correlation between crystal packing and kinetics.

### **3.4 Experimental Section:**

Nanocrystalline Suspensions: Dissolve 50 mg of tetraphenylacetone in 10 mL of acetonitrile to generate a stock solution (5mg/mL) and sonicate the solution for 5 minutes to completely dissolve the solid. Then prepare a  $1/25^{\text{th}}$  critical micelle concentration solution of cetyltrimethylammonium bromide (CTAB) by dissolving 12 mg of CTAB into 2 L of Millipore water. Stir 20 mL of CTAB solution in a 100 mL graduated cylinder and inject 10-15uL of stock solution drop wise. Vigorously stir for approximately 15 seconds after the injection. Transfer nanocrystalline suspension in CTAB into a quartz cuvette for ultraviolet-visible light spectroscopy or into a 150 mL volumetric flask for laser flash photolysis studies. In the case for transient absorption kinetics, a fresh batch of nanocrystalline suspensions are made in 20 mL batches every 10 minutes to ensure minimal aggregation. All Dynamic Light Scattering (DLS) studies were measured using a Beckman-Coulter N4 Plus particle analyzer with a 10mW helium-neon laser at 632.8 nm. The particle size was determined using the 62.6 detection angle, and was calculated using the size distribution processor (SDP) analysis.

### 3.5 Supplementary Information for Chapter 3

Contents:	Page number
3.5.1). General Methods	110
3.5.2). Spectral data ( $^1\text{H}$ NMR, $^{13}\text{C}$ NMR, UV-VIS)	114
3.5.3). Solid-State Photochemistry of Dry Powder	134
3.5.4). Power X-Ray Diffraction (PXRD) Analysis	138
3.5.5). Laser Flash Photolysis	140

**3.5.1 General Methods.** All commercially obtained reagents/solvents were used as received without further purification. Unless stated otherwise, reactions were conducted in oven-dried glassware under argon atmosphere. Proton magnetic resonance spectra were recorded at 500 MHz, and carbon-13 magnetic resonance spectra were recorded at 125 MHz, respectively. All chemical shifts are reported in ppm on the  $\delta$ -scale relative to TMS ( $\delta$  0.0) using residual solvent as reference ( $\text{CDCl}_3$   $\delta$  7.26 and  $\delta$  77.16 for proton and carbon, respectively,  $\text{CD}_3\text{CN}$   $\delta$  1.94 and 1.32, 118.26 for proton and carbon respectively). Standard abbreviations indicating multiplicity were used as follows: s (singlet), b (broad), d (doublet), t (triplet), q (quartet), and m (multiplet). Data for  $^{13}\text{C}$  NMR spectra are reported in terms of chemical shift ( $\delta$  ppm). High-resolution mass spectrum data were recorded on a DART spectrometer in positive (ESI+) ion mode. UV-Vis absorption and transmission spectra were recorded on Ocean Optics spectrometer (DT-MINI-2-GS UV-VIS-NIR LightSource and USB2000+ using SpectraSuite software package). Dynamic Light Scattering (DLS) data were recorded using a Beckman-Coulter N4 Plus particle analyzer with a 10 mW helium-neon laser at 632.8 nm. The particle size was determined using the  $62.6^\circ$  detection angle and was calculated using the size distribution processor (SDP) analysis package provided by the manufacturer. Melting point values were recorded on a Melt-Point II<sup>®</sup> apparatus. Infra-Red spectra were recorded on a PerkinElmer<sup>®</sup> Spectrum Two spectrometer equipped with a universal ATR sampling accessory. Nanosecond transient absorption experiments were performed using Laser Flash Photolysis instrument from Edinburgh Instruments in conjunction with a Nd:YAG laser (Brilliant b, Quantel<sup>®</sup>) with 266-nm output, 4-6 ns pulse width and 36-40 mJ pulse energy. The optical detection is based on a pulsed Xenon arc lamp (450 W), a monochromator (TMS300, Czerny-Turner), a photomultiplier detector (Hamamatsu R928) and a digital oscilloscope (TDS3012C, 100 MHz and 1.25 GS/s from Tektronix). The laser flash

photolysis experiments were performed with 1 cm quartz flow cell mounted on a home-built sample holder that is placed at the cross-section of the laser incident beam and the probe light. Continuously Argon gas purged acetonitrile solutions or crystalline suspensions of ketones (0.0025g/L) were flown through the quartz cell using a peristaltic pump (Masterflex L/S) at a rate of 1.6 – 3.2 mL/min. Due to aggregation fresh samples in batches of 20 mL were made for the crystalline suspensions every 10 minutes. Time-resolved absorption maps were recorded with continuous flow of samples through the quartz cell. Lifetimes at  $\lambda_{\max}$  for end-of-pulse spectra were reproducible and doubly verified/processed with Edinburgh Instruments L900 internal software and Igor Pro (version 6.34A, Wavemetrics) software. The parameters under the detector monochromator settings are as follows: the ketones were observed at the corresponding  $\lambda_{\max}$  in solution (320-350 nm) and in crystalline suspensions (330-360 nm), and the band width was set between 1.00 to 3.00 nm. The flash lamp settings were set where the frequency was at 10 Hz, width at 40  $\mu$ s, and delay at 4000  $\mu$ s. The Q-switch settings were set where the frequency was at 1.0 Hz, width at 20  $\mu$ s, and delay between 270-310  $\mu$ s.

**General Synthesis of Tetraphenylacetones** Following a modified procedure by Rajca *et al.*,<sup>3</sup> in a flame-dried, argon filled round-bottom flask, diethyl carbonate (0.5 eq) in THF (15 eq) was added over 5 minutes to a 5:1 THF/hexane solution of (diphenylmethyl)lithium solution (5 eq) stirring at 0 °C. The reaction. The reaction undergoes a color change from a light orange-red to a deep dark-red. After 1 h. the remaining diethyl carbonate (0.5 eq) in THF (15 eq) was added over 5 minutes. The reaction is warmed to room temperature and is stirred overnight. The reaction is quenched with 0.5M HCl and the extracted with diethyl ether (3 X 20 mL) and dried over Na<sub>2</sub>SO<sub>4</sub>. The solvents were removed under reduced pressure and was subjected to column chromatography (1:4-9 acetone:hexane). The resulting crystalline solid (20-66% yield) was further recrystallized from ethanol.

**Solid-State Photochemistry Reaction:** Respective ketone (10 mg) is placed on a clean microscope slide. By using another microscope slide, the crystals are grinded down to a fine powder.

Irradiate the samples via a medium-pressure Hg hanovia lamp with a pyrex filter with a cut off via medium-pressure Hg cutoff of  $\lambda \leq 275$  nm. After irradiating the sample for the allotted time, take the samples and analyze by  $^1\text{H}$  NMR (500 MHz,  $\text{CDCl}_3$ ) for product formation.

**Tetraphenylacetone:** Yield 66%. m.p. 133-134°C, (lit., m.p. 134°C); IR(neat)  $\nu_{\text{max}} = 3054, 3022, 1706, 1597, 1493, 1451, 1058$   $\text{cm}^{-1}$ .  $\lambda_{\text{max}} = 227.13, 261.76, 302.81$ . DLS = 68 nm  $\pm$  23 nm.  $^1\text{H}$  NMR (500 MHz,  $\text{CDCl}_3$ )  $\delta$  7.24 (m, 20H), 7.25 (s, 2H);  $^{13}\text{C}$  NMR (125 MHz,  $\text{CDCl}_3$ )  $\delta$  205.51, 138.06, 129.12, 128.69, 127.28, 63.52.

**4,4',4'',4'''(tetramethyl)tetraphenylacetone:** Yield 51%. m.p. 85.5-86.8°C. IR(neat)  $\nu_{\text{max}} = 3091, 3024, 2923, 2863, 1704, 1510, 1307, 1066, 1026$   $\text{cm}^{-1}$ .  $\lambda_{\text{max}} = 234, 267.81, 275.75$ . DLS = 140 nm  $\pm$  60 nm.  $^1\text{H}$  NMR (500 MHz,  $\text{CDCl}_3$ )  $\delta$  7.01-7.09 (AA'BB', 16H), 5.17 (s, 2H), 2.31 (s, 12H).  $^{13}\text{C}$  NMR (125 MHz,  $\text{CDCl}_3$ )  $\delta$  205.92, 136.76, 135.46, 129.34, 128.93, 62.56, 21.06.

**4,4',4'',4'''(tetra-tertbutyl)tetraphenylacetone:** Yield 75%. m.p. 228°C. IR(neat)  $\nu_{\text{max}} = 3054, 2963, 2903, 2866, 1708, 1509, 1361, 1270, 1056$   $\text{cm}^{-1}$ .  $\lambda_{\text{max}} = 263, 301$ . DLS = 123 nm  $\pm$  61 nm.  $^1\text{H}$  NMR (500 MHz,  $\text{CDCl}_3$ )  $\delta$  7.28-7.06 (AA'BB', 16H), 5.18 (S, 2H), 1.29 (S, 36H).  $^{13}\text{C}$  NMR (125 MHz,  $\text{CDCl}_3$ )  $\delta$  206.18, 149.82, 135.38, 128.75, 125.47.

**Tetraphenylethane:** Yield <99%. m.p. 213 °C, (lit., m.p. 213°C); IR(neat)  $\nu_{\text{max}} = 3024, 2890, 1597, 1495, 1448, 173, 1028$   $\text{cm}^{-1}$ .  $\lambda_{\text{max}} = 227.89, 263.27$ .  $^1\text{H}$  NMR (500 MHz,  $\text{CDCl}_3$ )  $\delta$  7.08 (m, 20H), 4.77 (s, 2H);  $^{13}\text{C}$  NMR (125 MHz,  $\text{CDCl}_3$ )  $\delta$  143.47, 128.52, 128.15, 125.85, 56.34.

**4,4',4'',4'''(tetramethyl)tetraphenylethane:** Yield <99%. m.p. 278°C, (lit., m.p. 278-280°C); IR(neat)  $\nu_{\text{max}} = 3096, 3019, 2920, 1510, 1190, 1019$   $\text{cm}^{-1}$ .  $\lambda_{\text{max}} = 235.91, 267.44$ .  $^1\text{H}$  NMR (500

MHz, CDCl<sub>3</sub>) δ 7.01-7.09 (AA'BB', 16H), 5.17 (s, 2H), 2.31 (s, 12H). <sup>13</sup>C NMR (125 MHz, CDCl<sub>3</sub>) δ 205.92, 136.76, 135.46, 129.34, 128.93, 62.56, 21.06.

3.5.2). Spectral data ( $^1\text{H}$  NMR,  $^{13}\text{C}$  NMR, UV-VIS)

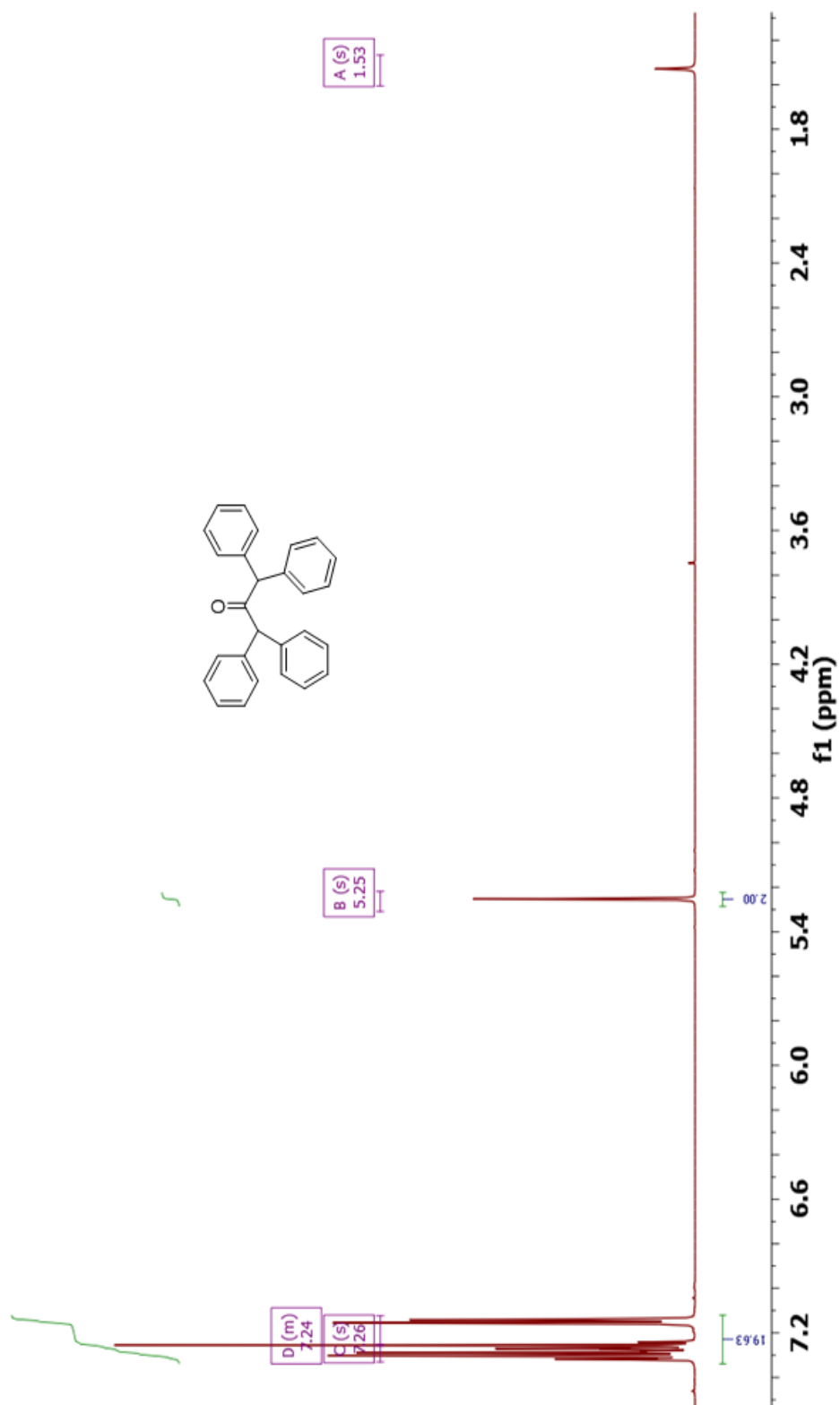




Figure 4.S1  $^{13}\text{C}$  NMR (125 MHz,  $\text{CDCl}_3$ ) of Tetraphenylacetone

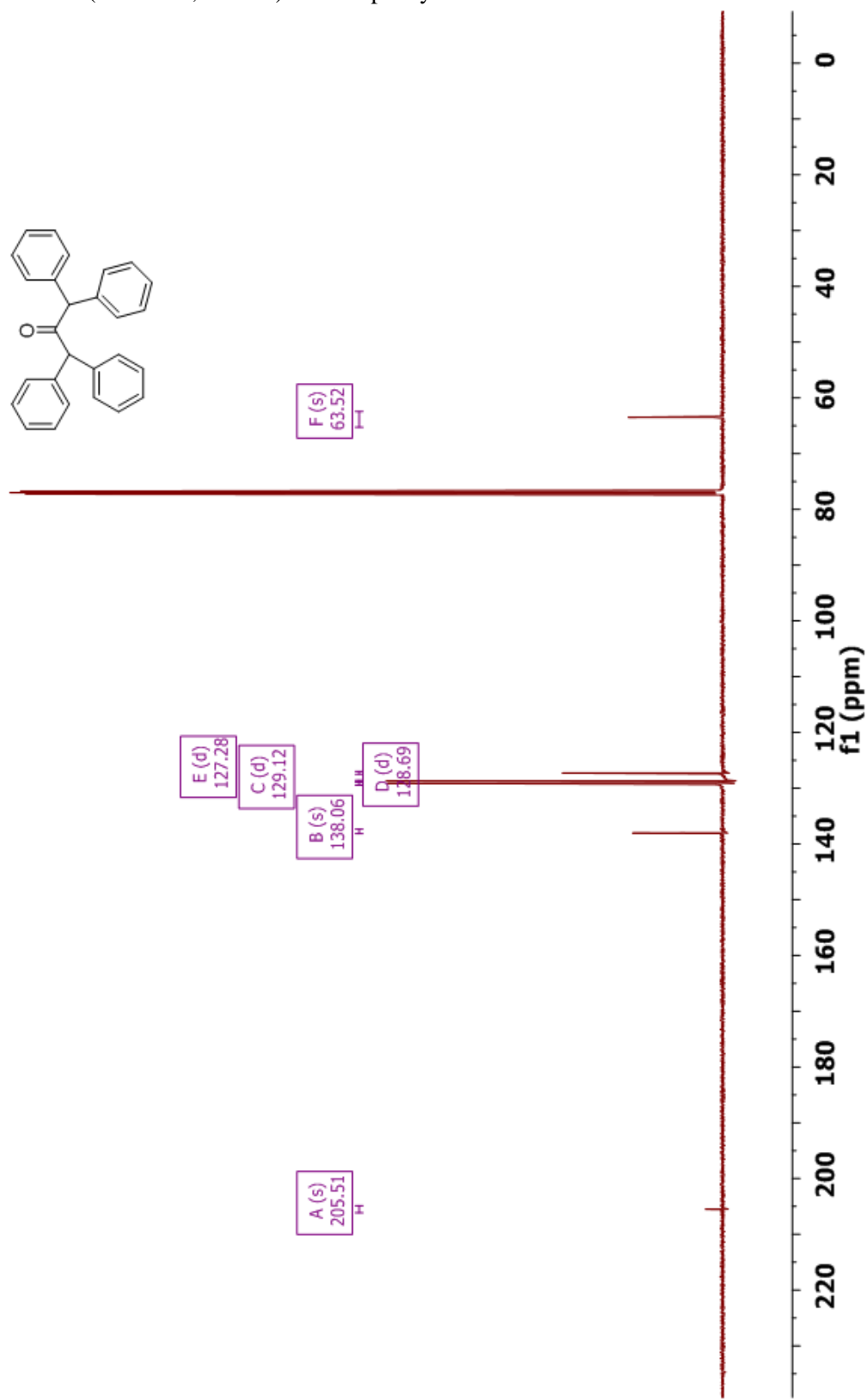


Figure 4.S2  $^1\text{H}$  NMR (500 MHz,  $\text{CDCl}_3$ ) of Tetraphenylacetone

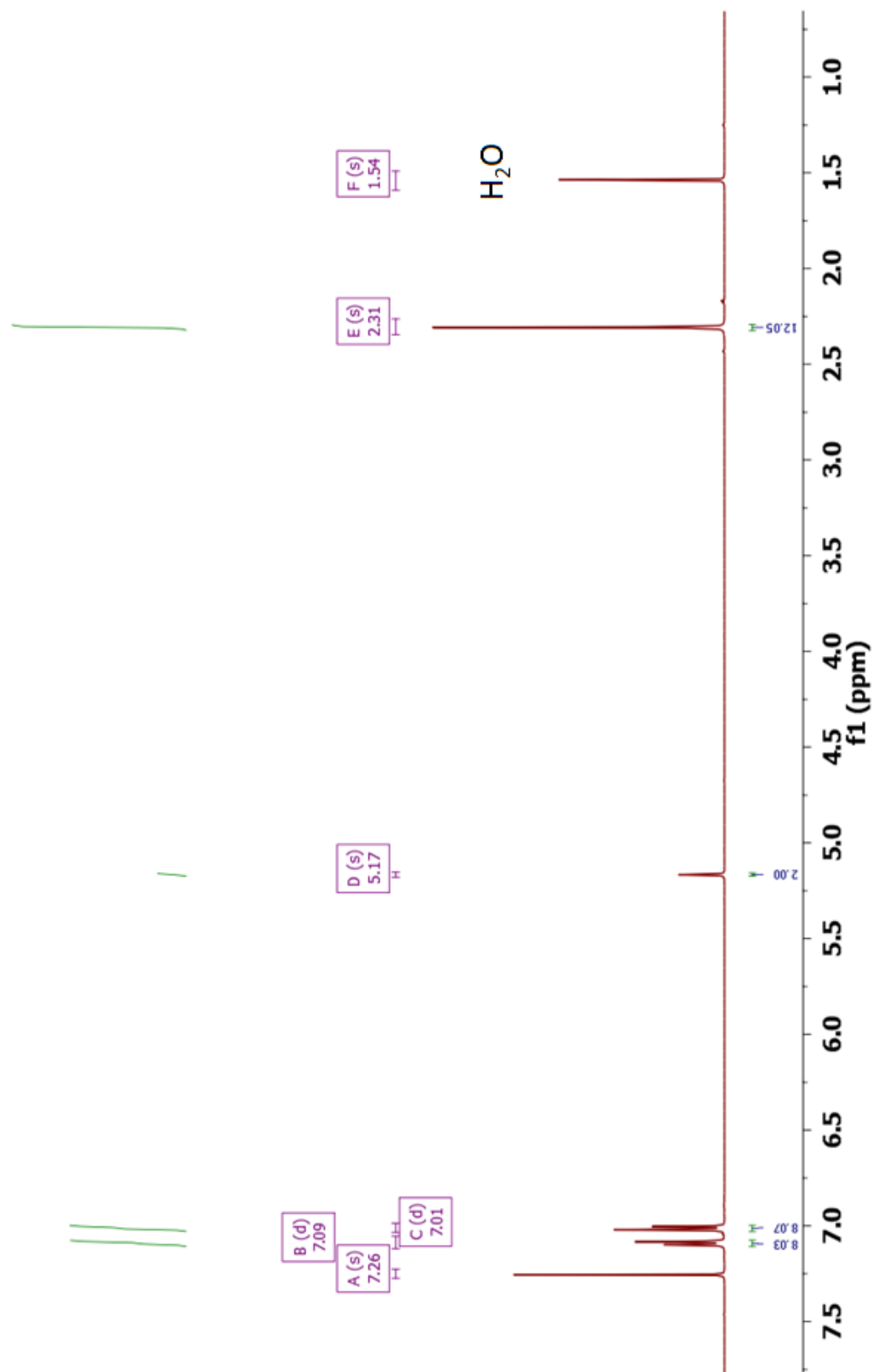
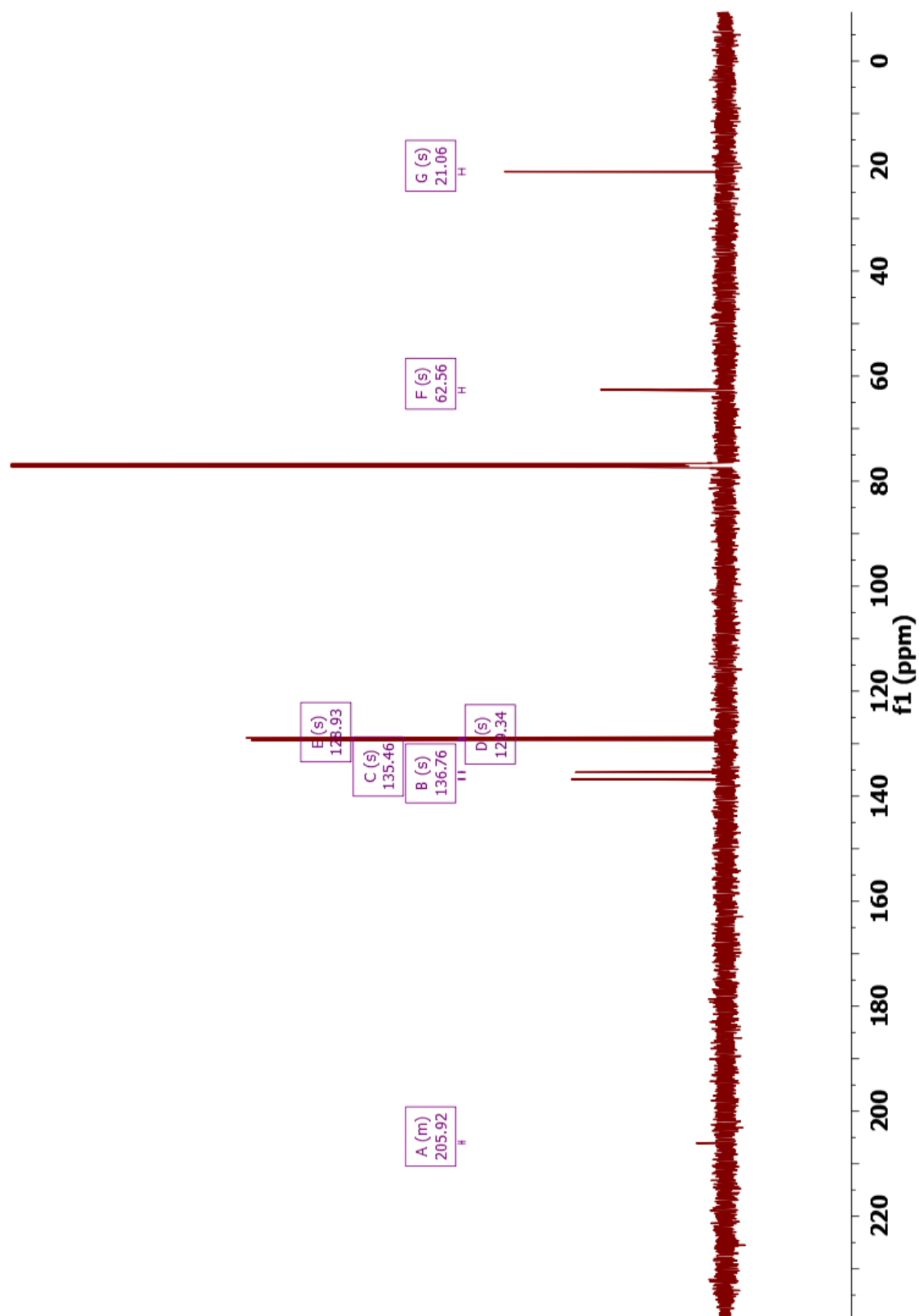


Figure 4.S3  $^1\text{H}$  NMR (500 MHz,  $\text{CDCl}_3$ ) of 4,4',4'',4'''(tetramethyl)tetraphenylacetone



**Figure 4.S4:**  $^{13}\text{C}$  NMR (125 MHz,  $\text{CDCl}_3$ ) of 4,4',4'',4'''(tetramethyl)tetraphenylacetone

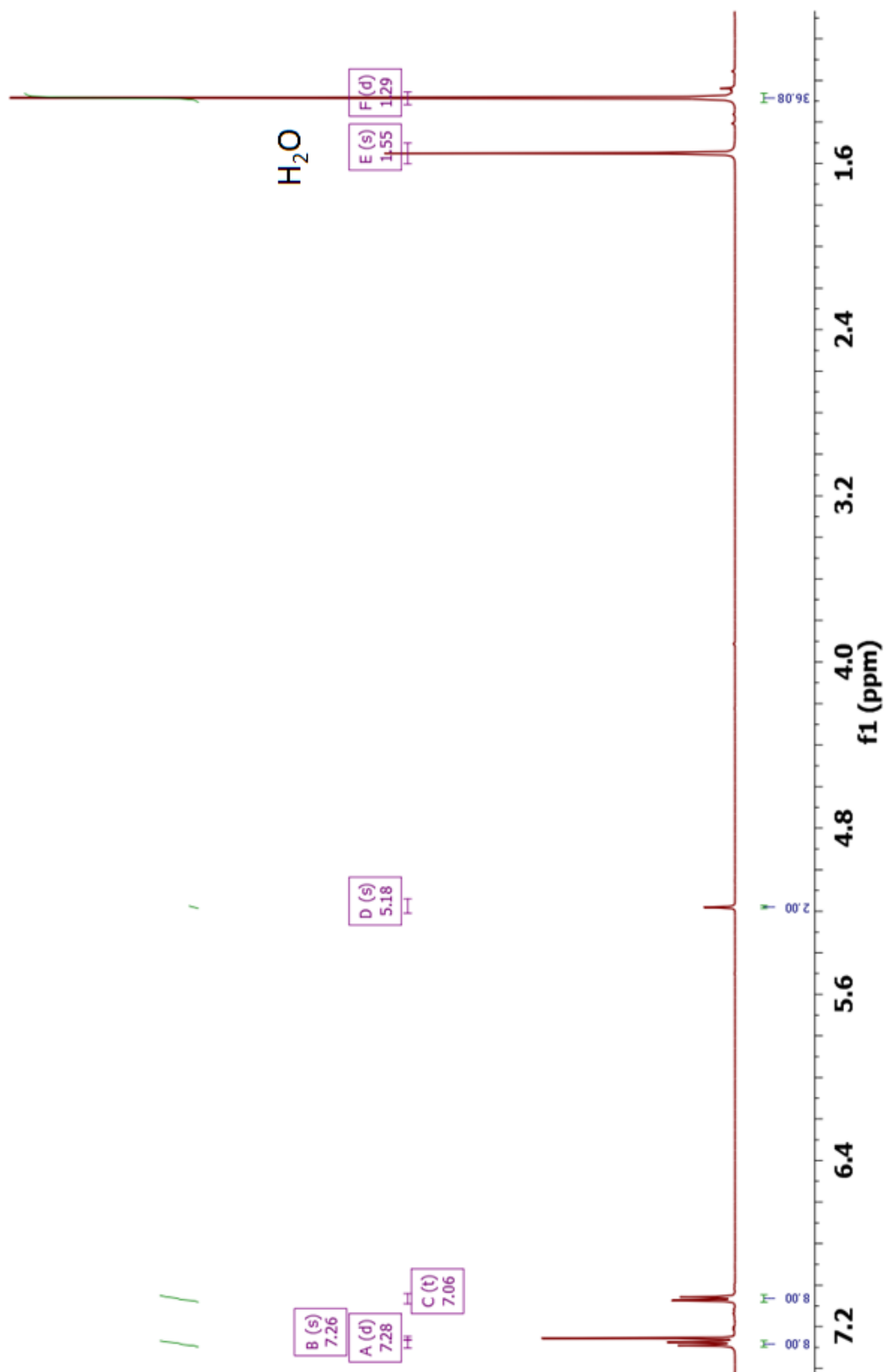


Figure 4.S5  $^1\text{H}$  NMR (500 MHz,  $\text{CDCl}_3$ ) of 4,4',4'',4'''(tetratertbutyl)tetraphenylacetone

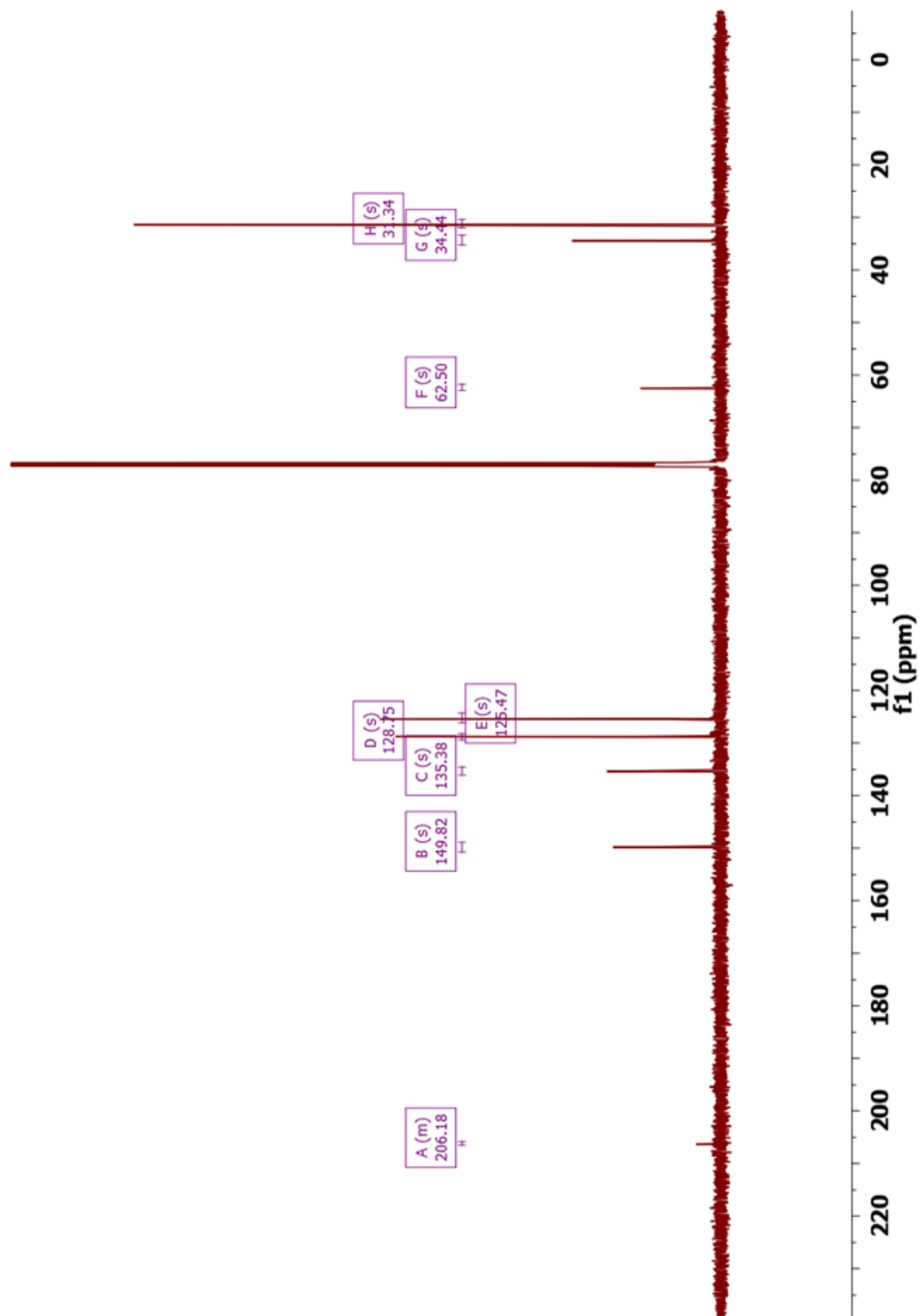


Figure 4.S6  $^{13}\text{C}$  NMR (125 MHz,  $\text{CDCl}_3$ ) of 4,4',4'',4'''(tetraterbutyl)tetraphenylacetone

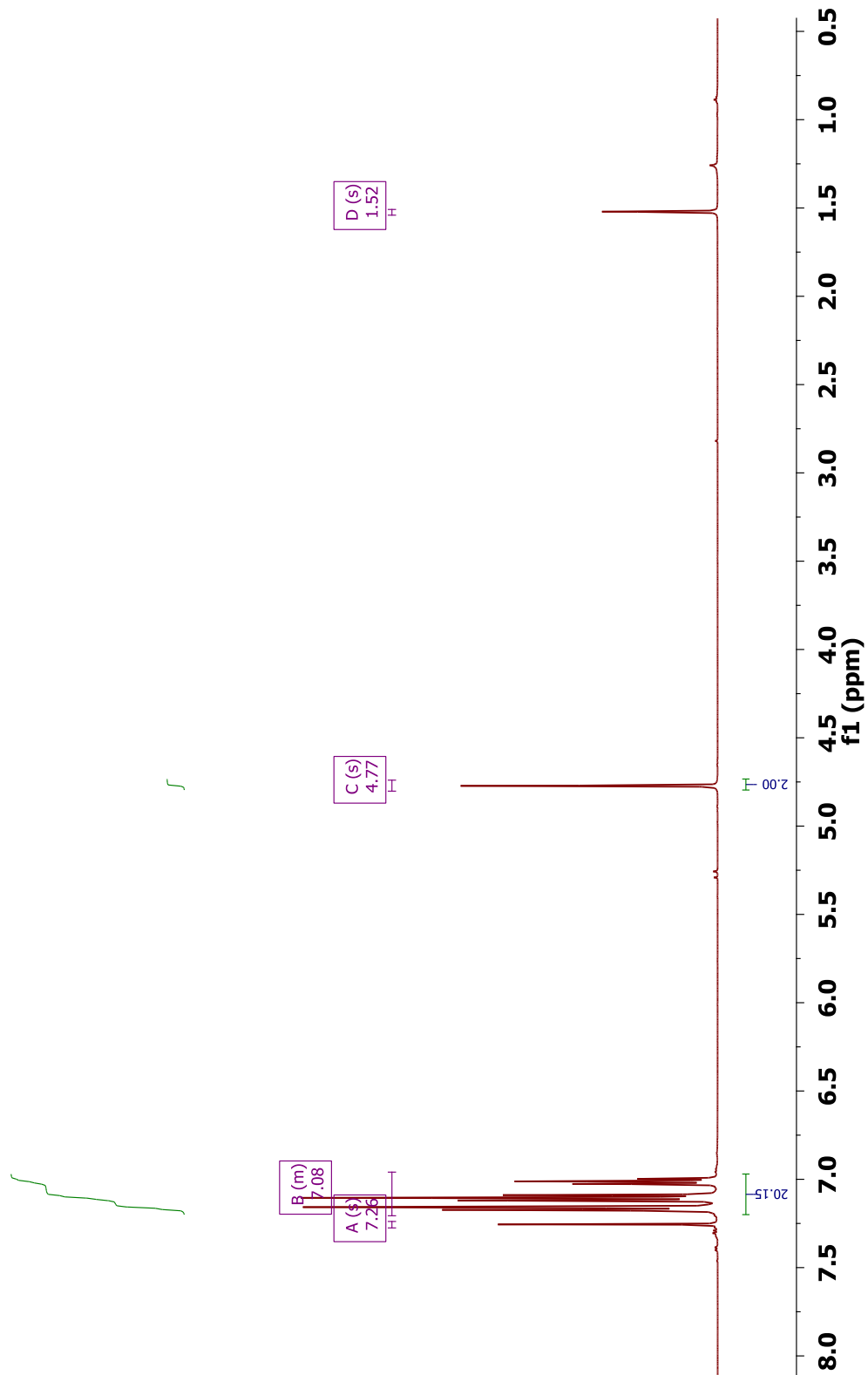


Figure 4.S7  $^1\text{H}$  NMR (500 MHz,  $\text{CDCl}_3$ ) of Tetraphenylethane

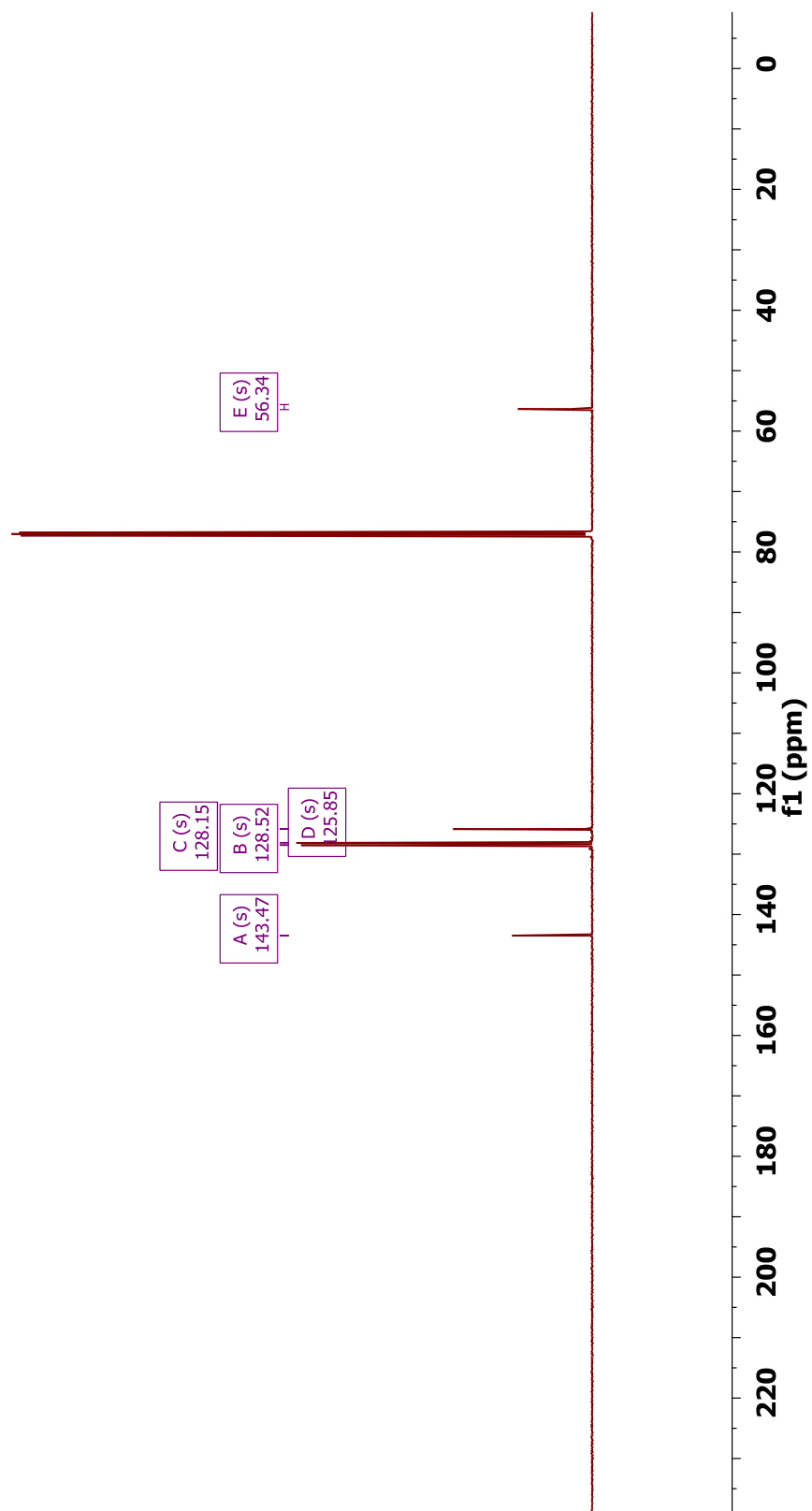


Figure 4.S8  $^{13}\text{C}$  NMR (125 MHz,  $\text{CDCl}_3$ ) of Tetraphenylethane

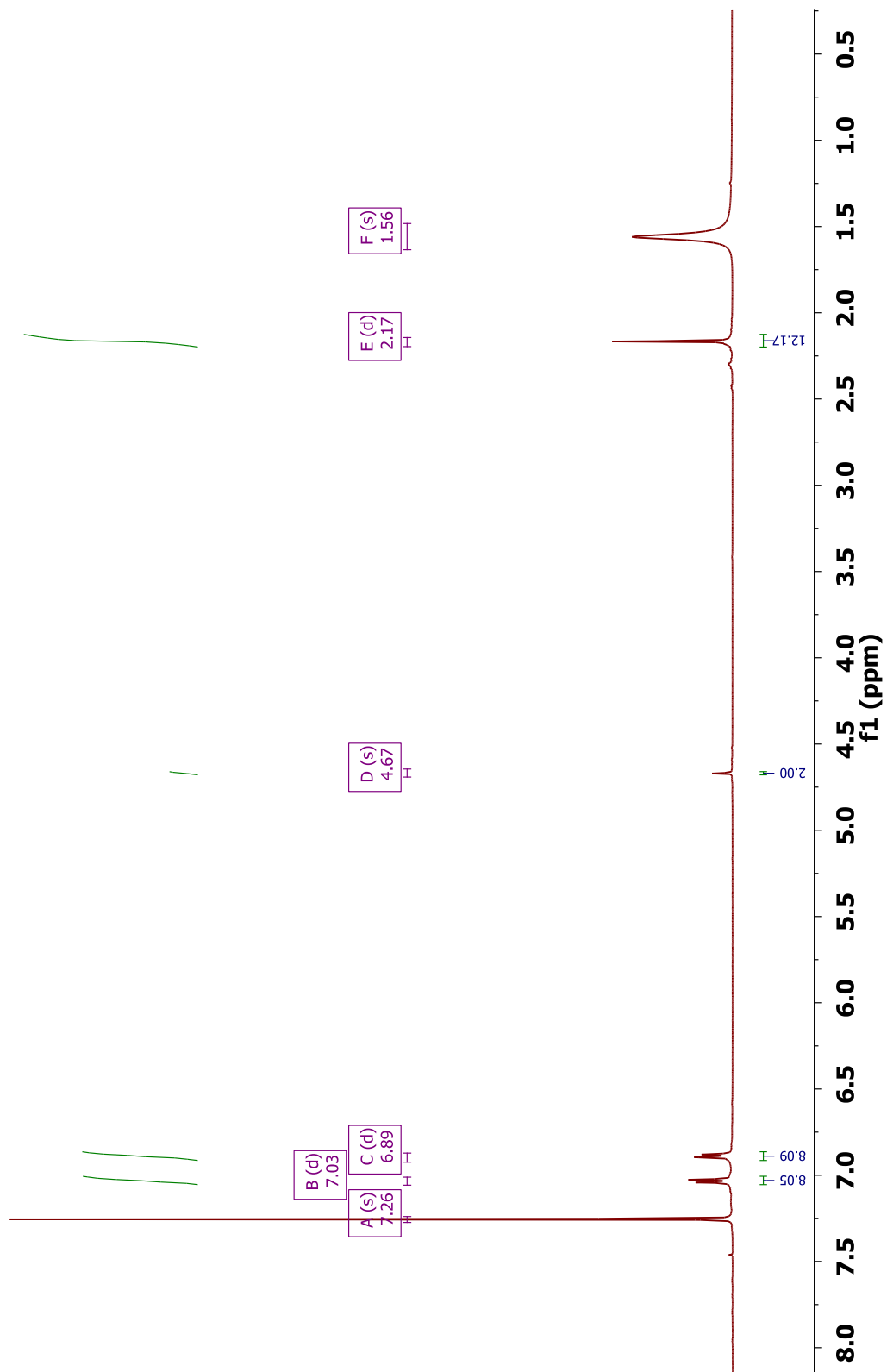




Figure 4.S9  $^1\text{H}$  NMR (500 MHz,  $\text{CDCl}_3$ ) of 4,4',4'',4'''(tetramethyl)tetraphenylethane

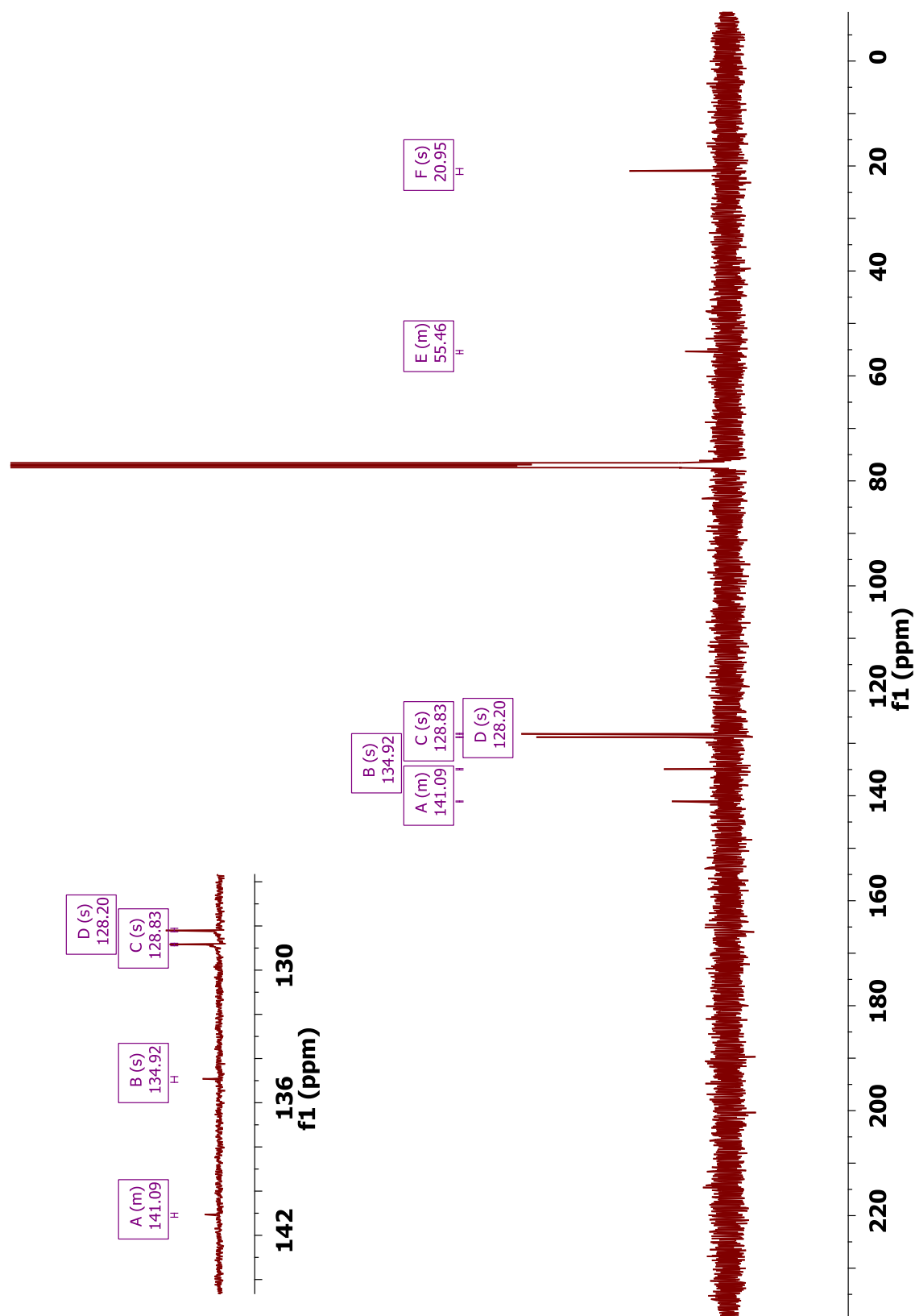


Figure 4.S10:  $^{13}\text{C}$  NMR (125 MHz,  $\text{CDCl}_3$ ) of 4,4',4'',4'''(tetramethyl)tetraphenylethane

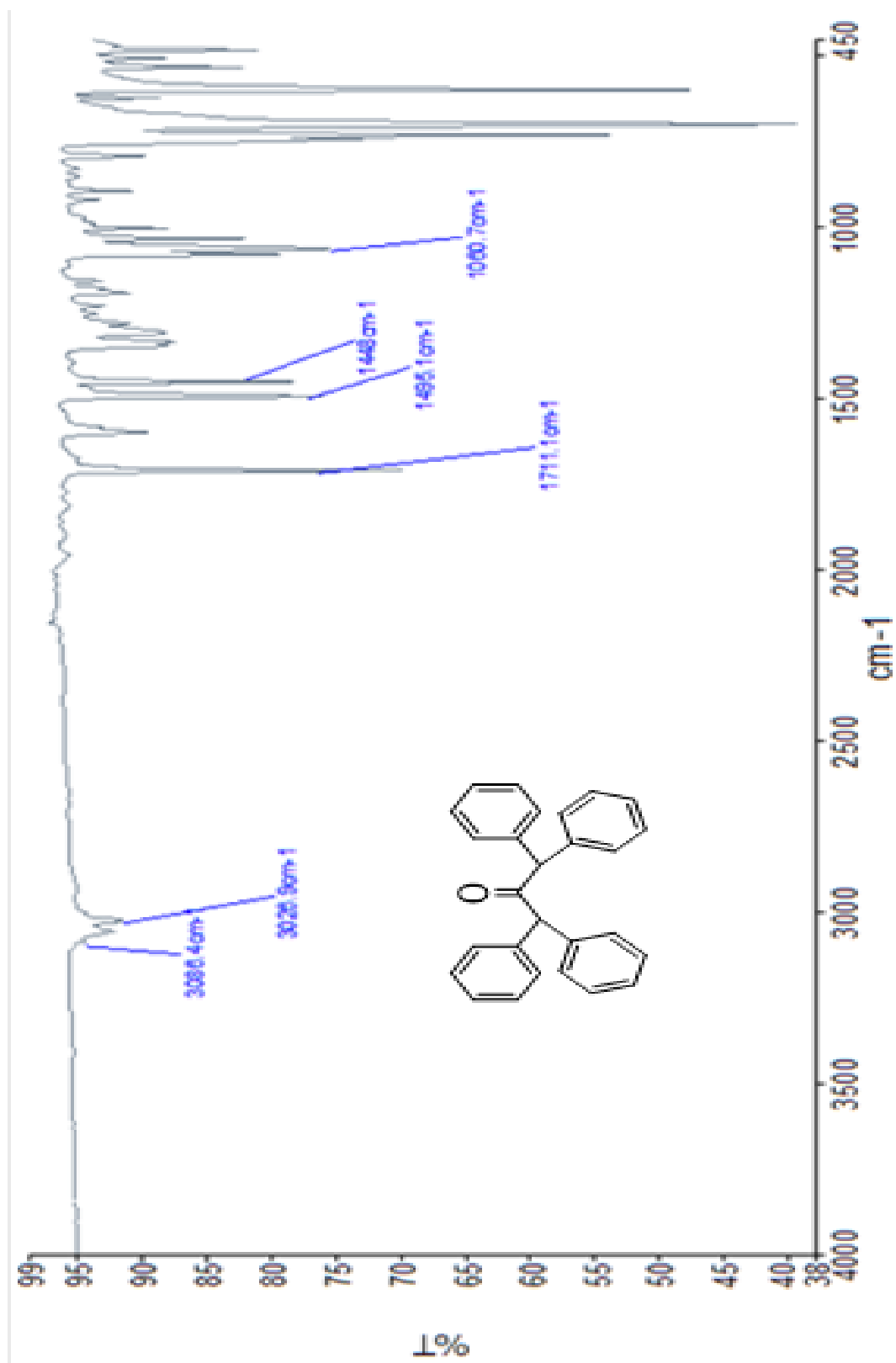


Figure 4.S11: IR(neat)  $\nu_{\max}$  of Tetraphenylacetone

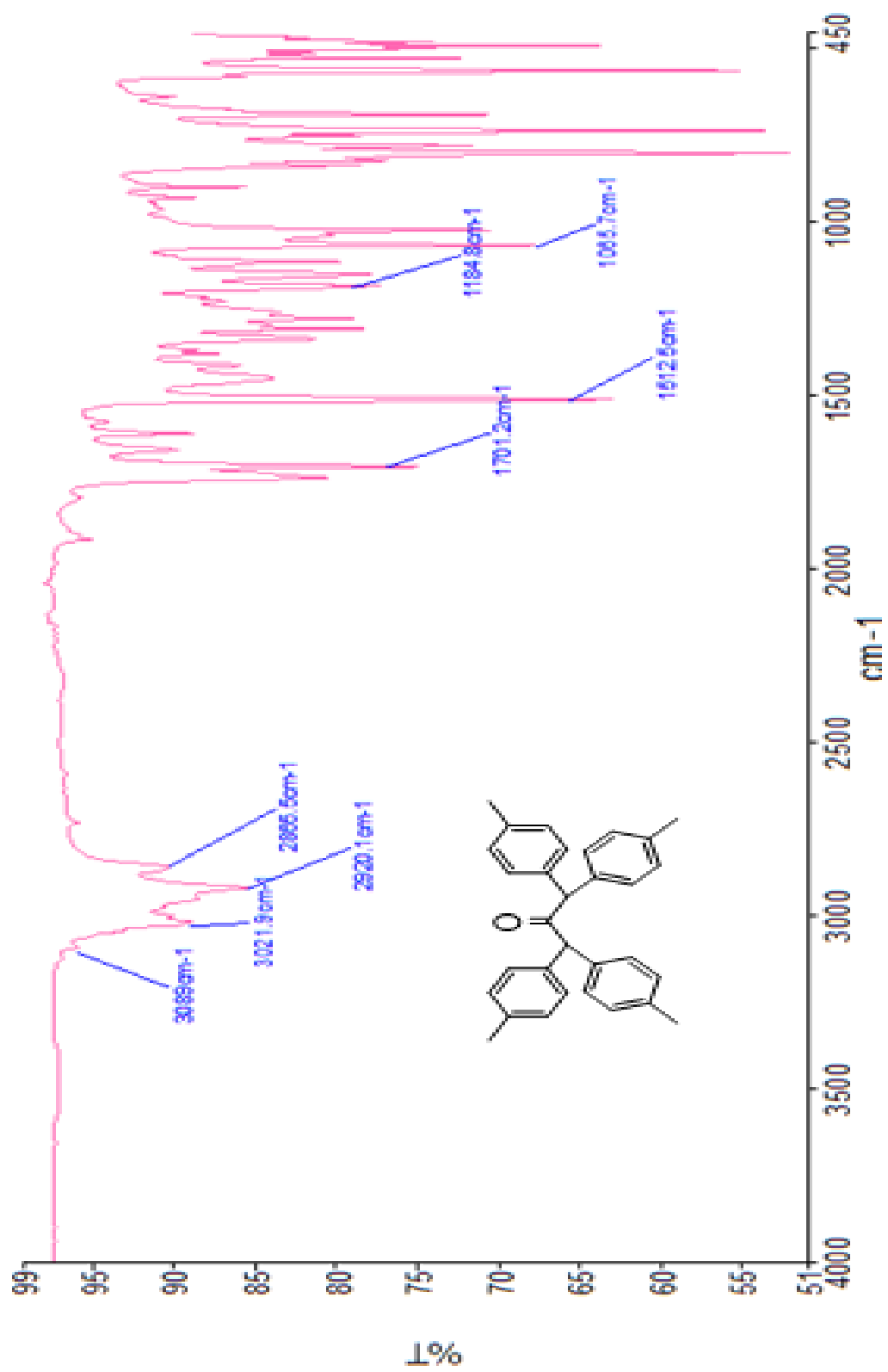


Figure 4.S12: IR(neat)  $\nu_{\max}$  of 4,4',4'',4'''(tetramethyl)tetraphenylacetone

PerkinElmer Spectrum Version 10.4.4  
Wednesday, October 19, 2016 5:10 PM

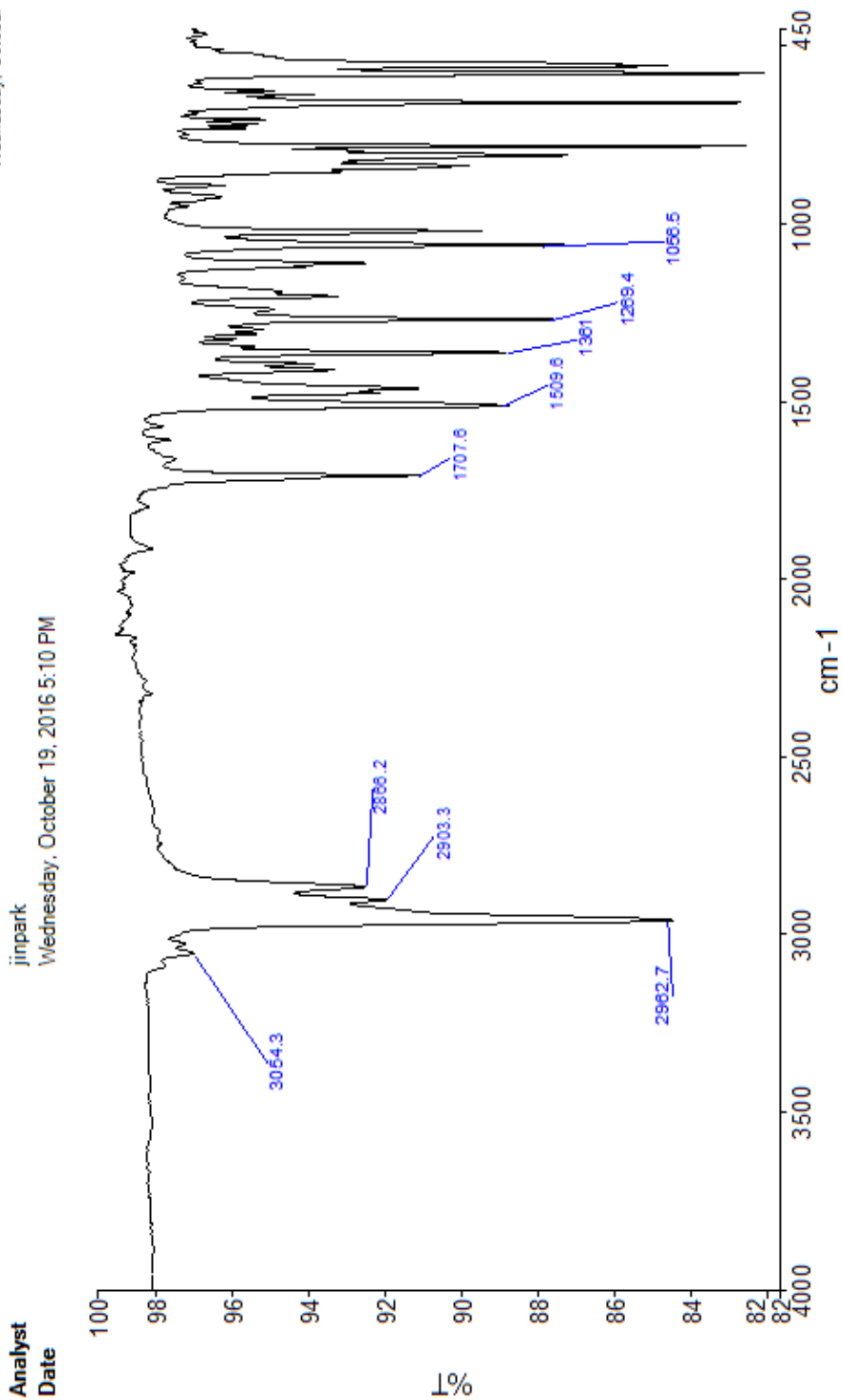


Figure 4.S13: IR(neat)  $\nu_{\max}$  of 4,4',4'',4'''(tetra-tertbutyl)tetraphenylacetone

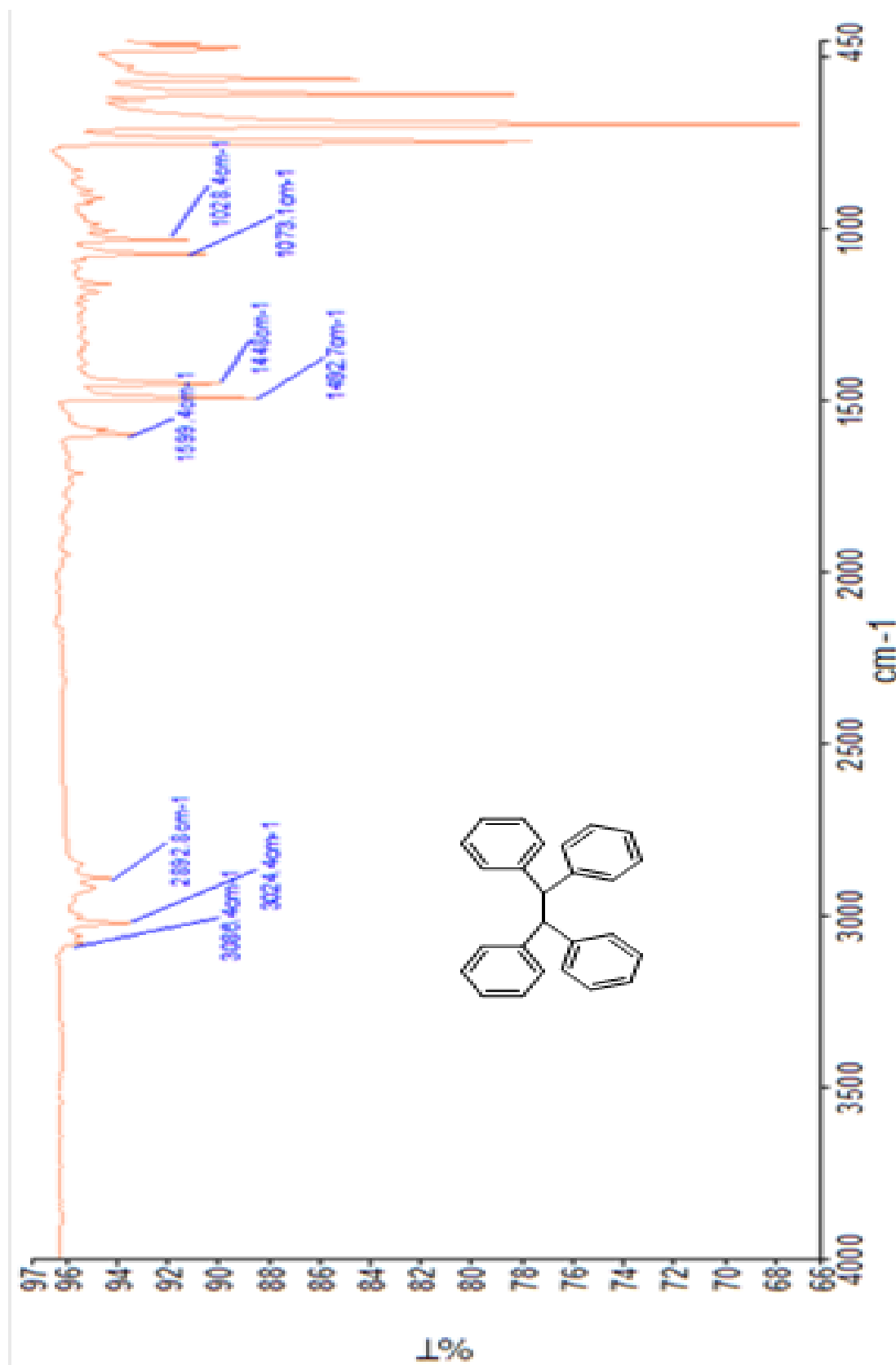
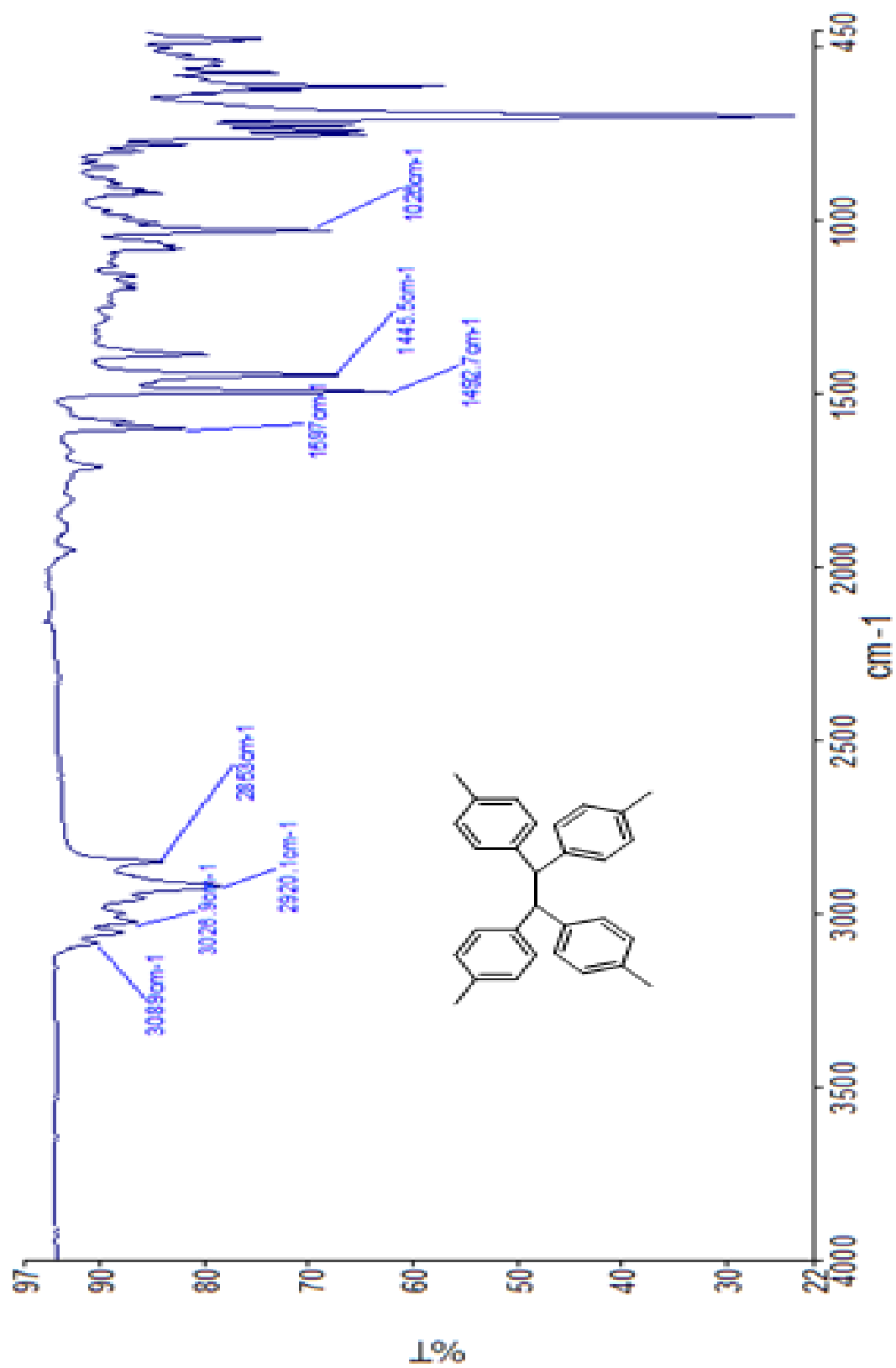
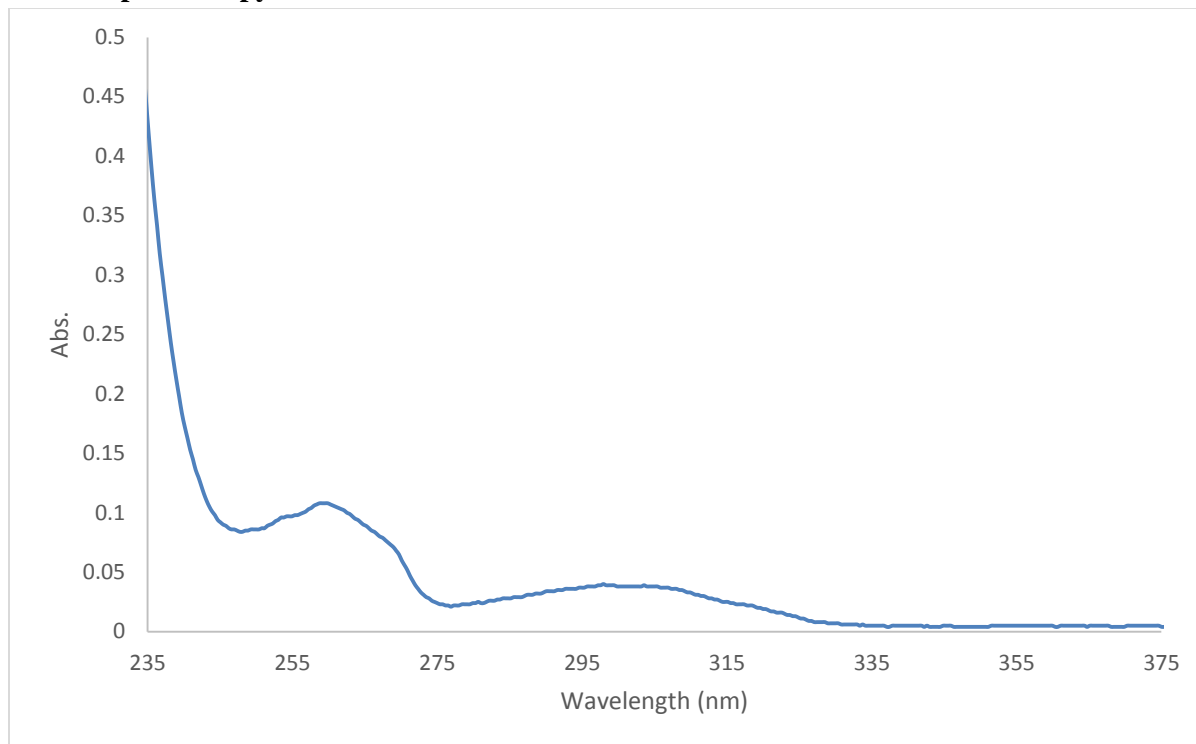


Figure 4.S14: IR(neat)  $\nu_{\max}$  of Tetraphenylethane



**Figure 4.S15:** IR(neat)  $\nu_{\max}$  of 4,4',4'',4'''(tetramethyl)tetraphenylethane

**UV-Vis spectroscopy:**



**Figure 4.S16:** UV-vis of 0.01 (mol/L) Tetraphenylacetone in MeCN

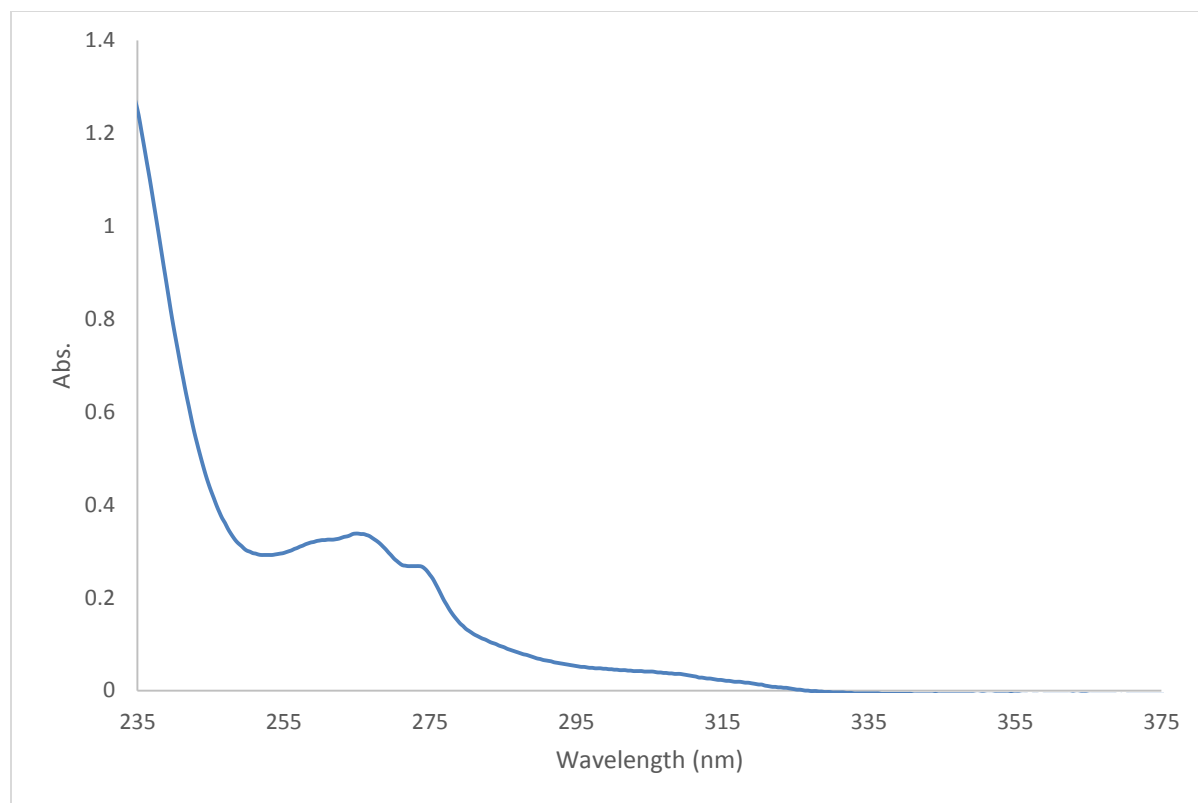


Figure 4.S17: UV-vis of 0.01 (mol/L) 4,4,4',4''-(tetramethyl) tetraphenylacetone in MeCN

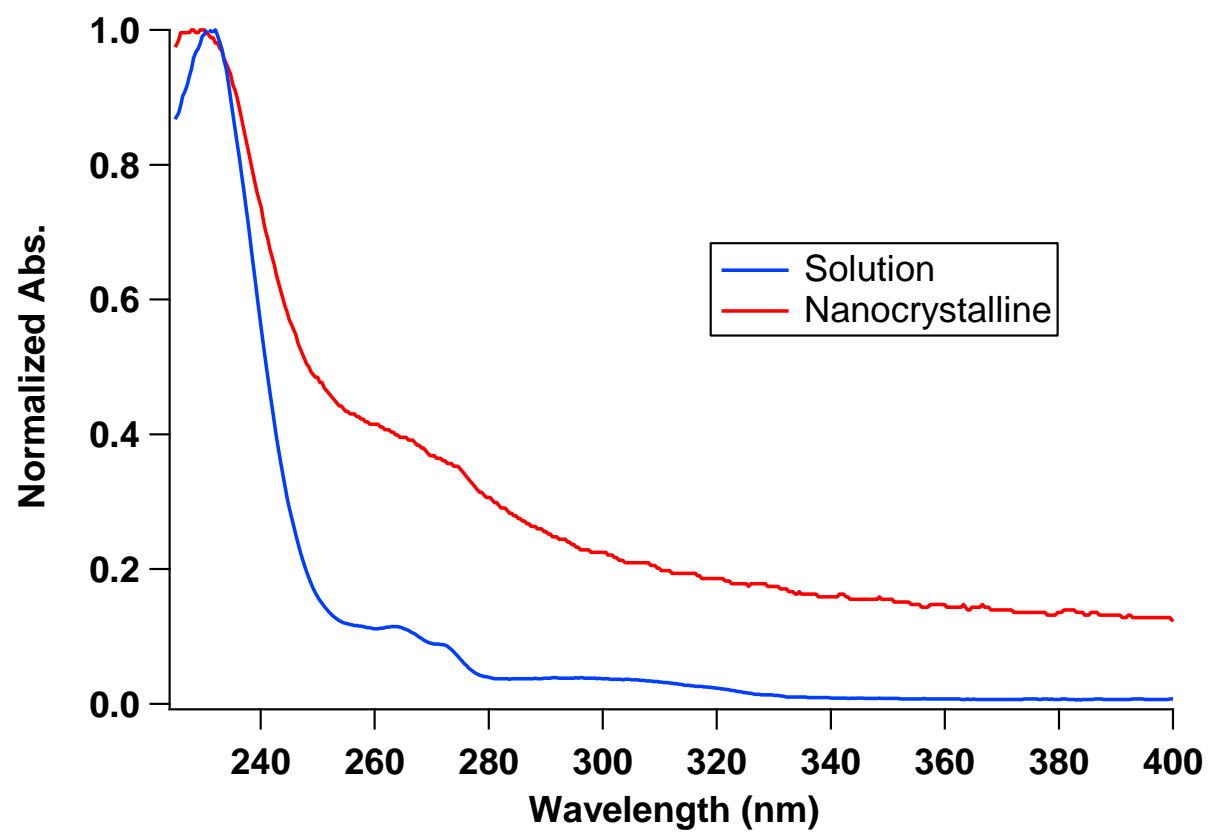
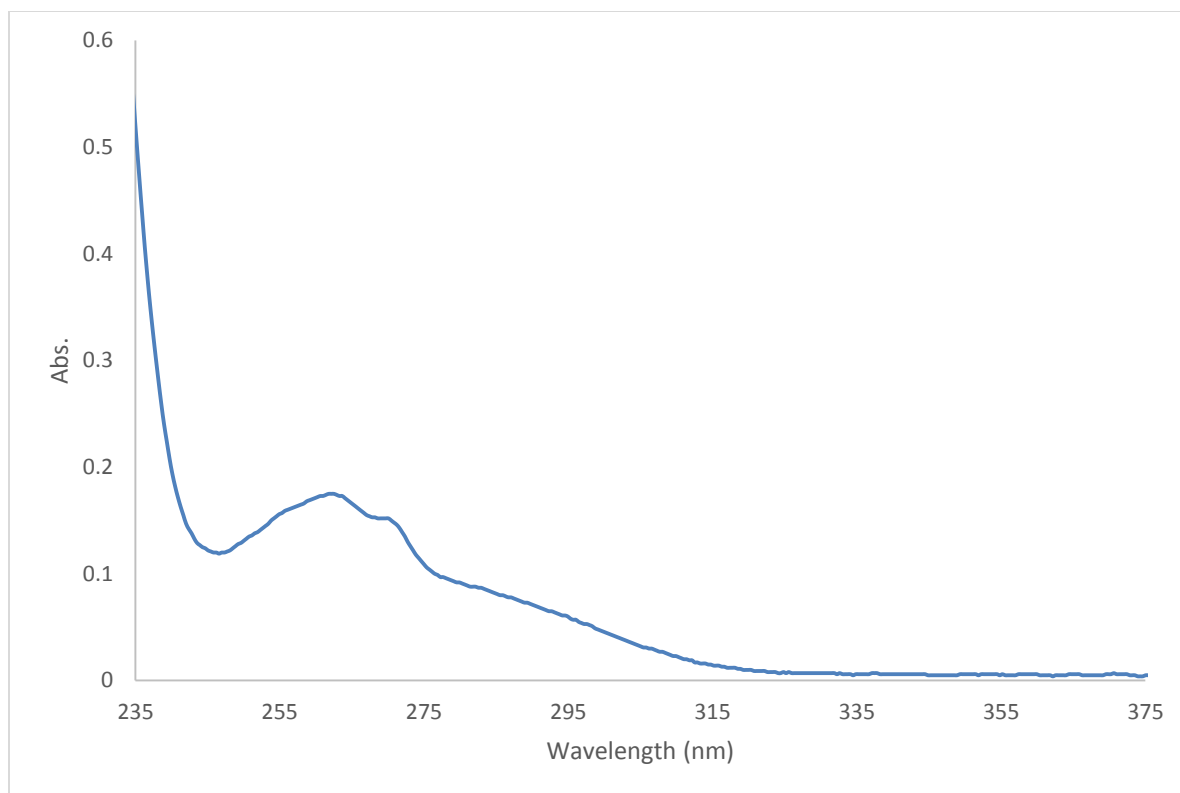
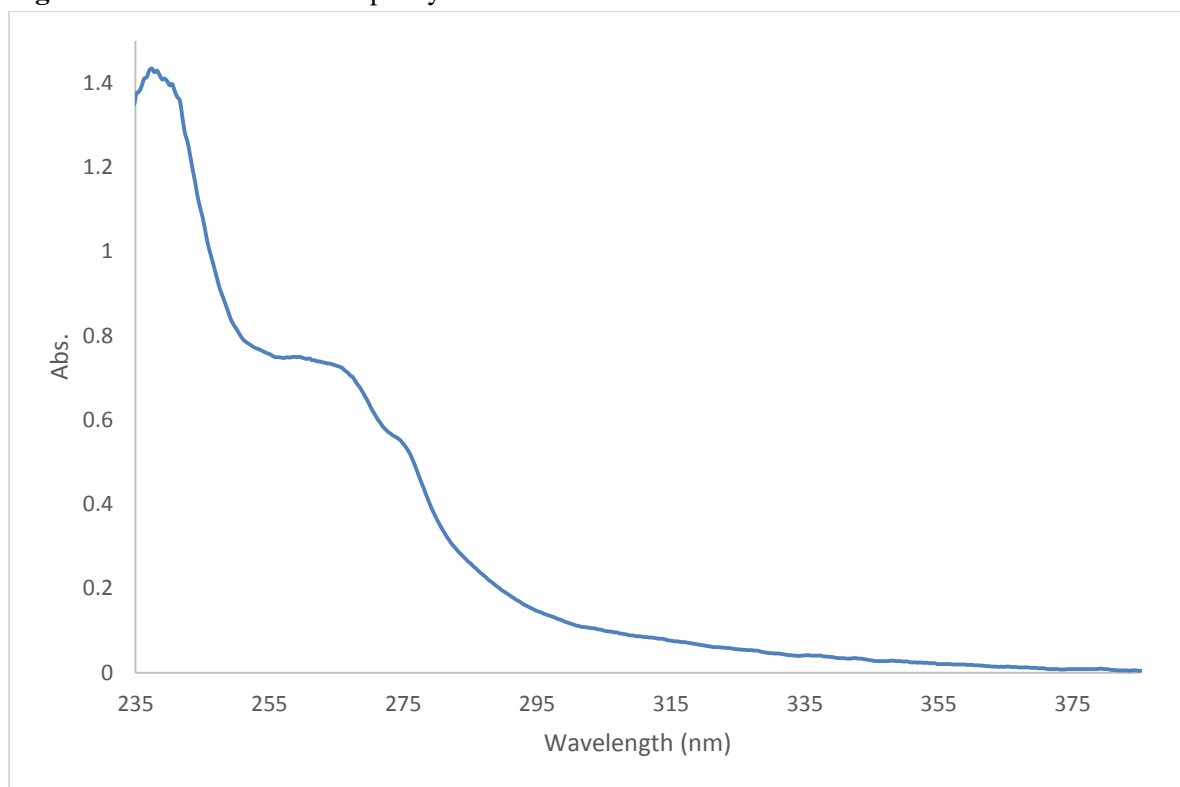


Figure 4.S18: UV-vis of 0.01 (mol/L) 4,4,4',4''-(tetra-tertbutyl) tetraphenylacetone in MeCN



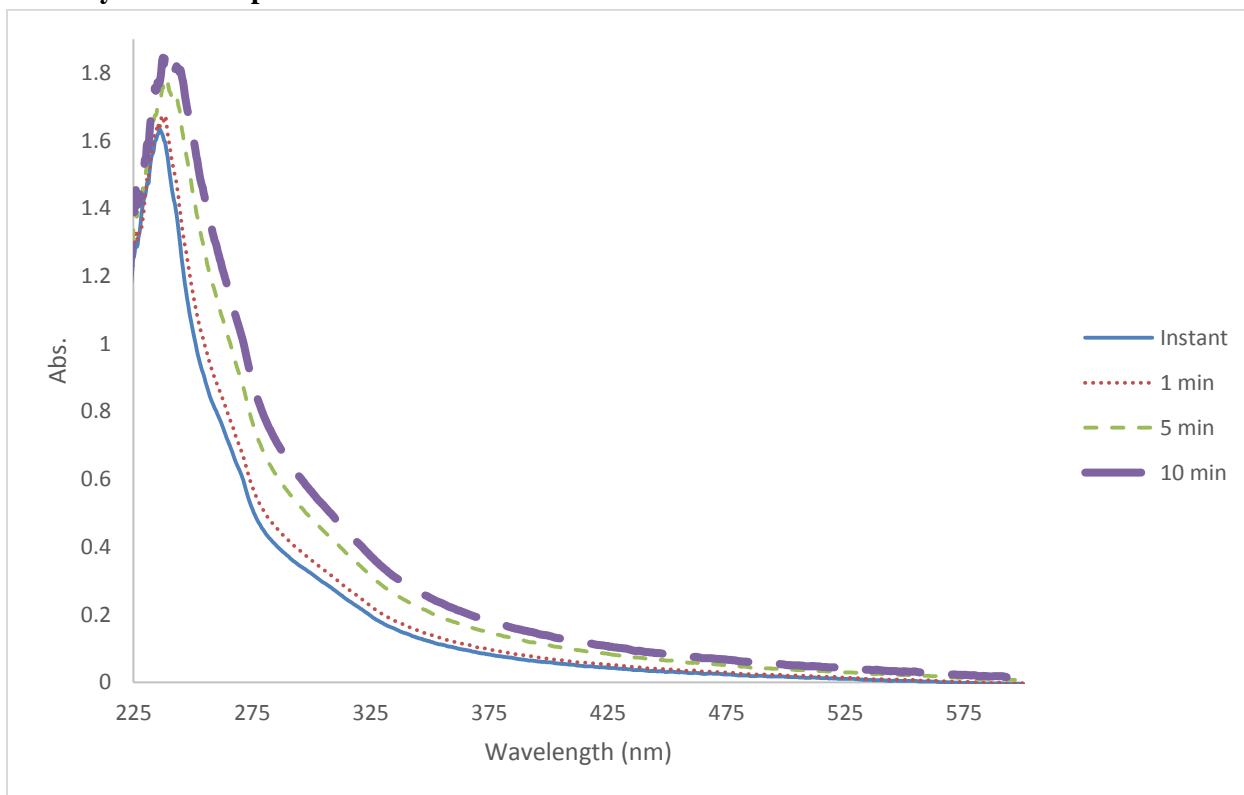


**Figure 4.S19:** UV-vis of Tetraphenylethane

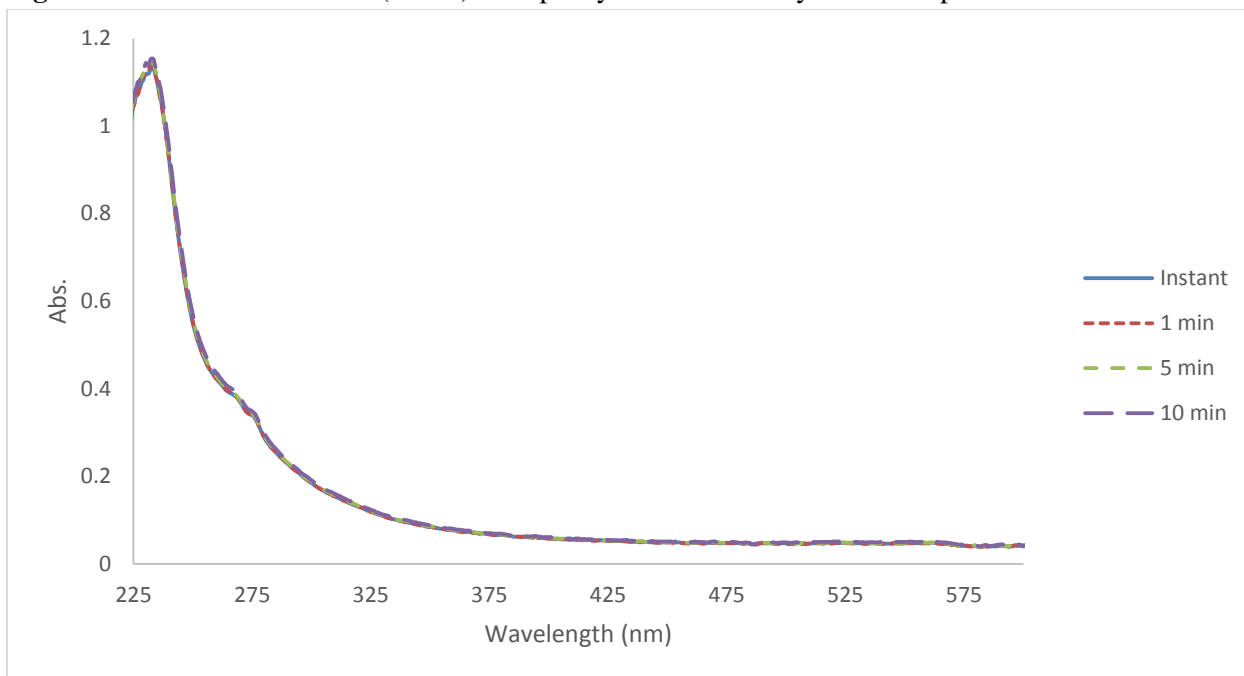


**Figure 4.S20:** UV-vis of 4,4',4'',4'''-(tetramethyl)tetraphenylethane in MeCN

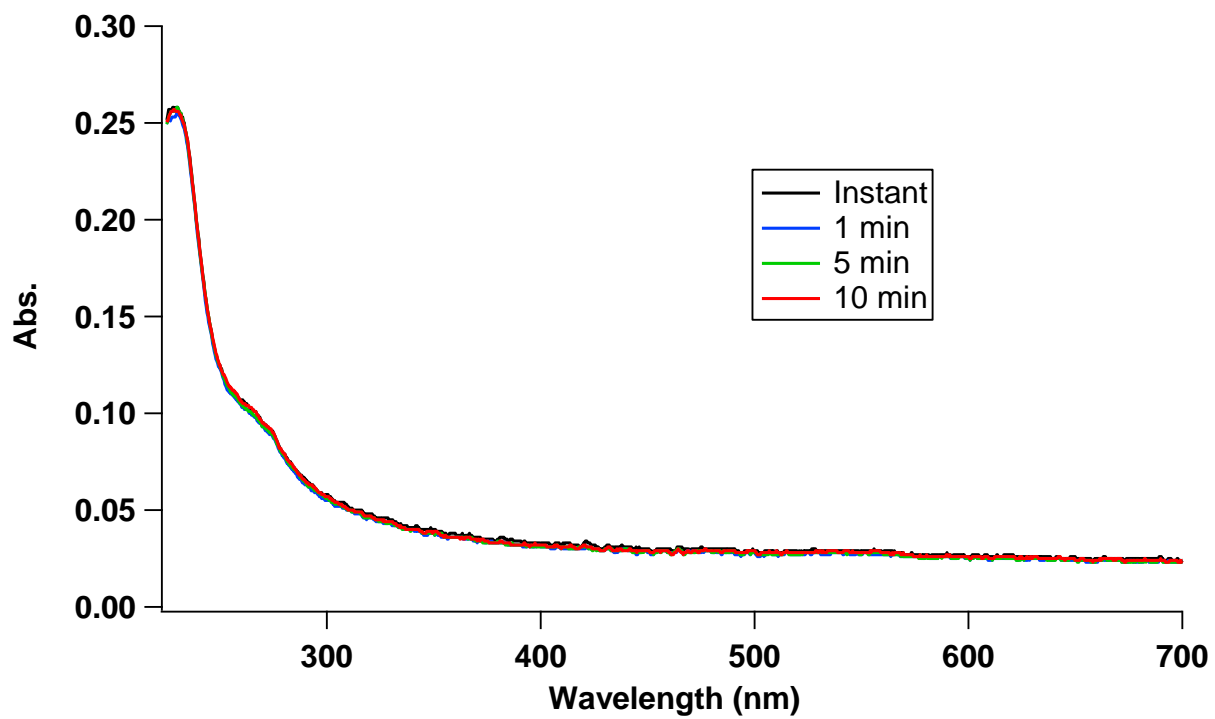
**Nanocrystalline suspension:**



**Figure 4.S21:** UV-vis of 0.005 (mol/L) Tetraphenylacetone nanocrystalline suspension



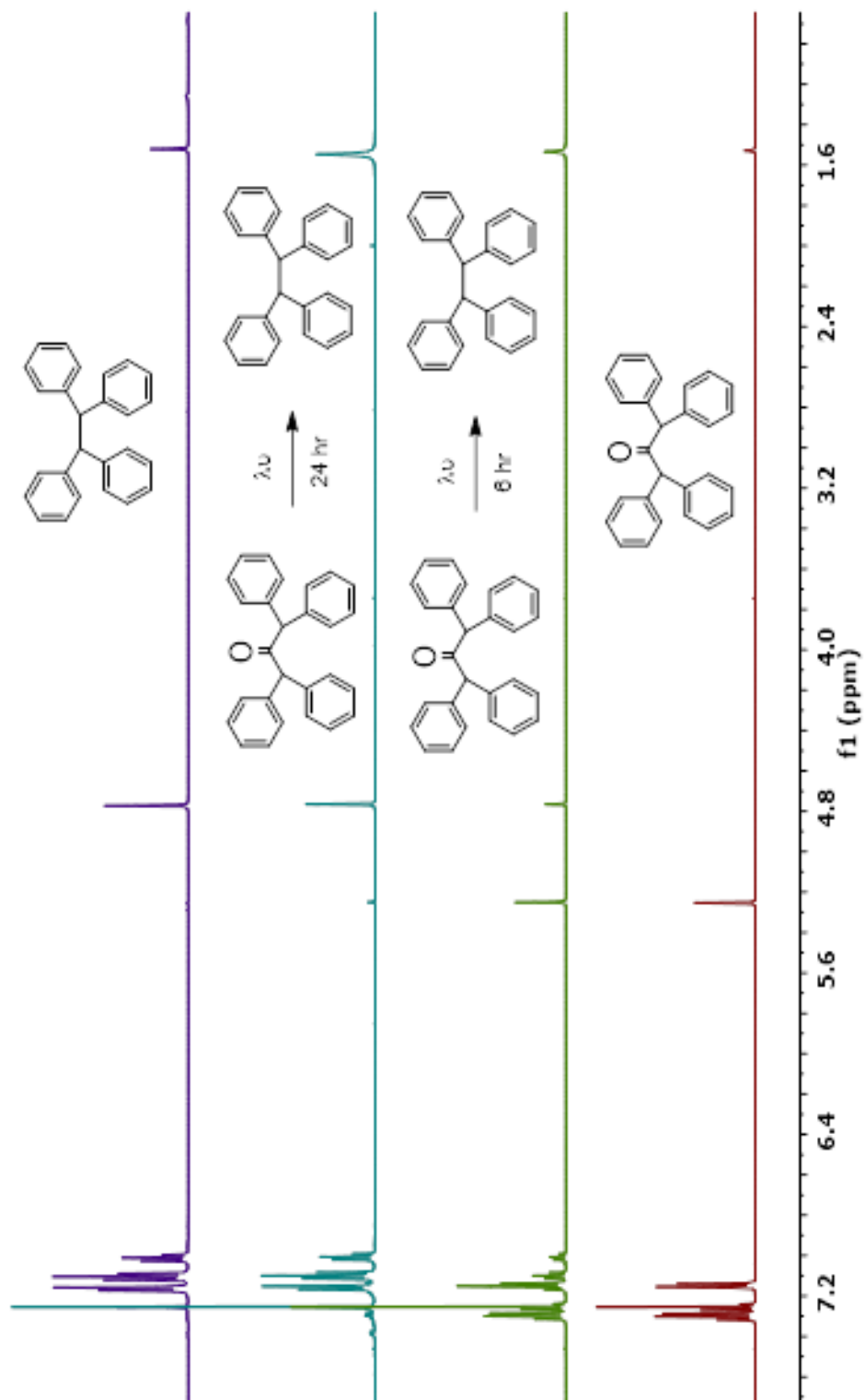
**Figure 4.S22:** UV-vis of 0.005 (mol/L) 4,4',4'',4'''-(tetramethyl) tetraphenylacetone nanocrystalline suspension



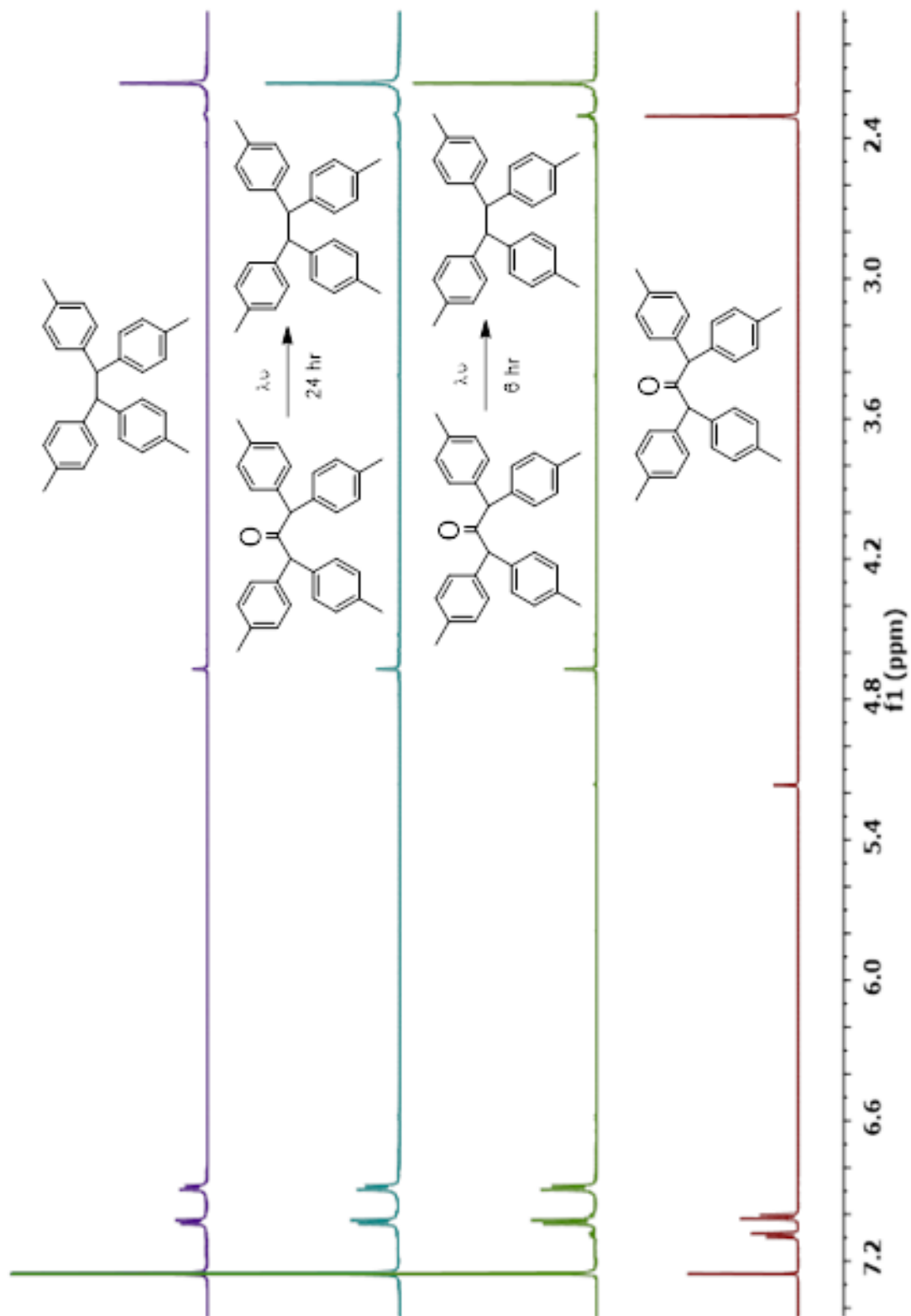
**Figure 4.S23:** UV-vis of 0.005 (mol/L) 4,4',4'',4'''-(tetra-tertbutyl) tetraphenylacetone nanocrystalline suspension

### 3.5.3). Solid-State Photochemistry of Dry Powder:<sup>12</sup>

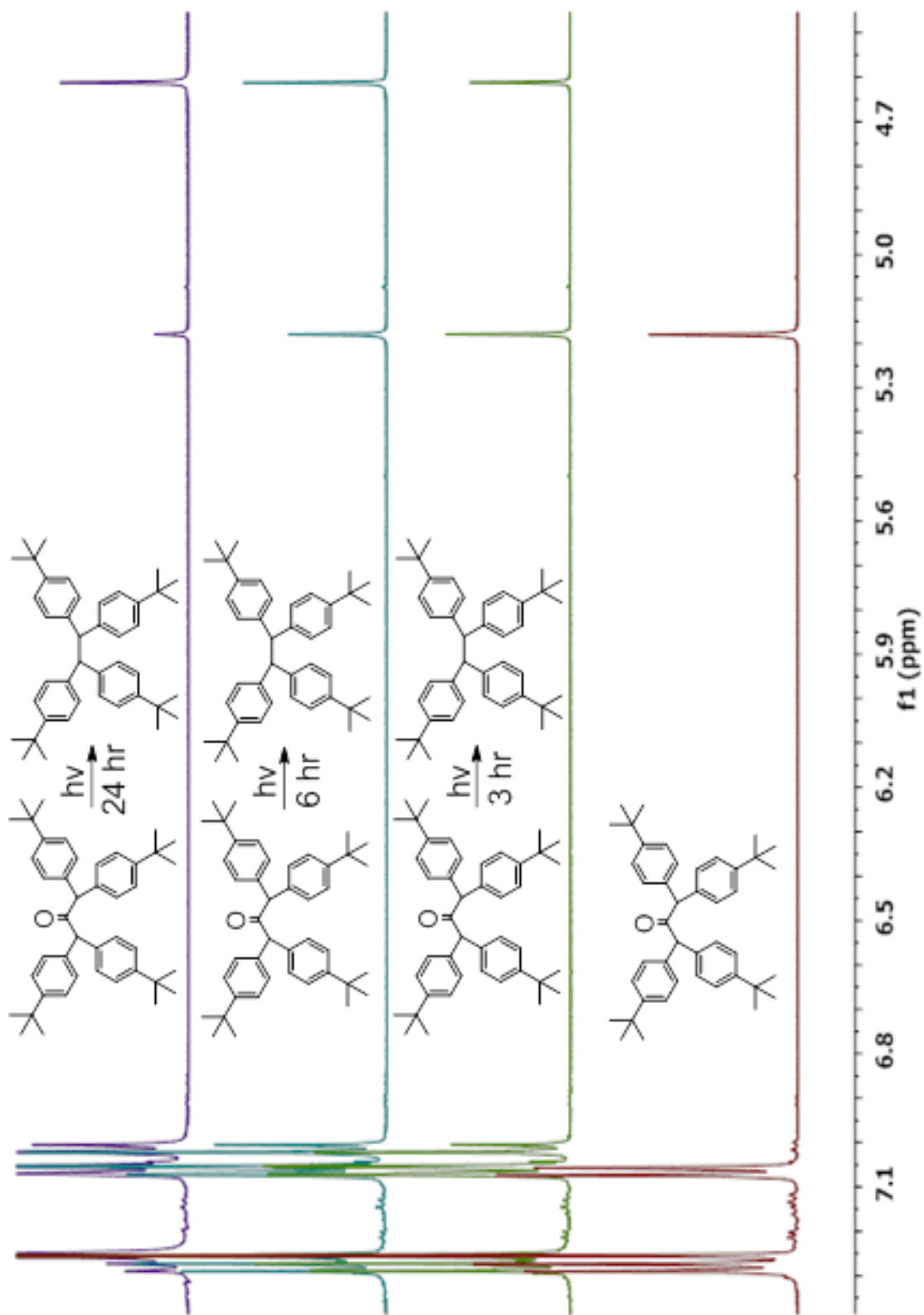
All solid state photochemistry product analysis was conducted via a medium-pressure Hg Hanovia lamp with a pyrex emersion well filter with a cutoff of  $\lambda \leq 275$  nm and analyzed by <sup>1</sup>H NMR (500 MHz, CDCl<sub>3</sub>). Samples are grinded between two microscope slides which are then subjected to UV light irradiation inside a chamber.



**Figure 4.S24:** <sup>1</sup>H NMR (500 MHz, CDCl<sub>3</sub>) product analysis of Tetraphenylacetone to tetraphenylethane in the solid state

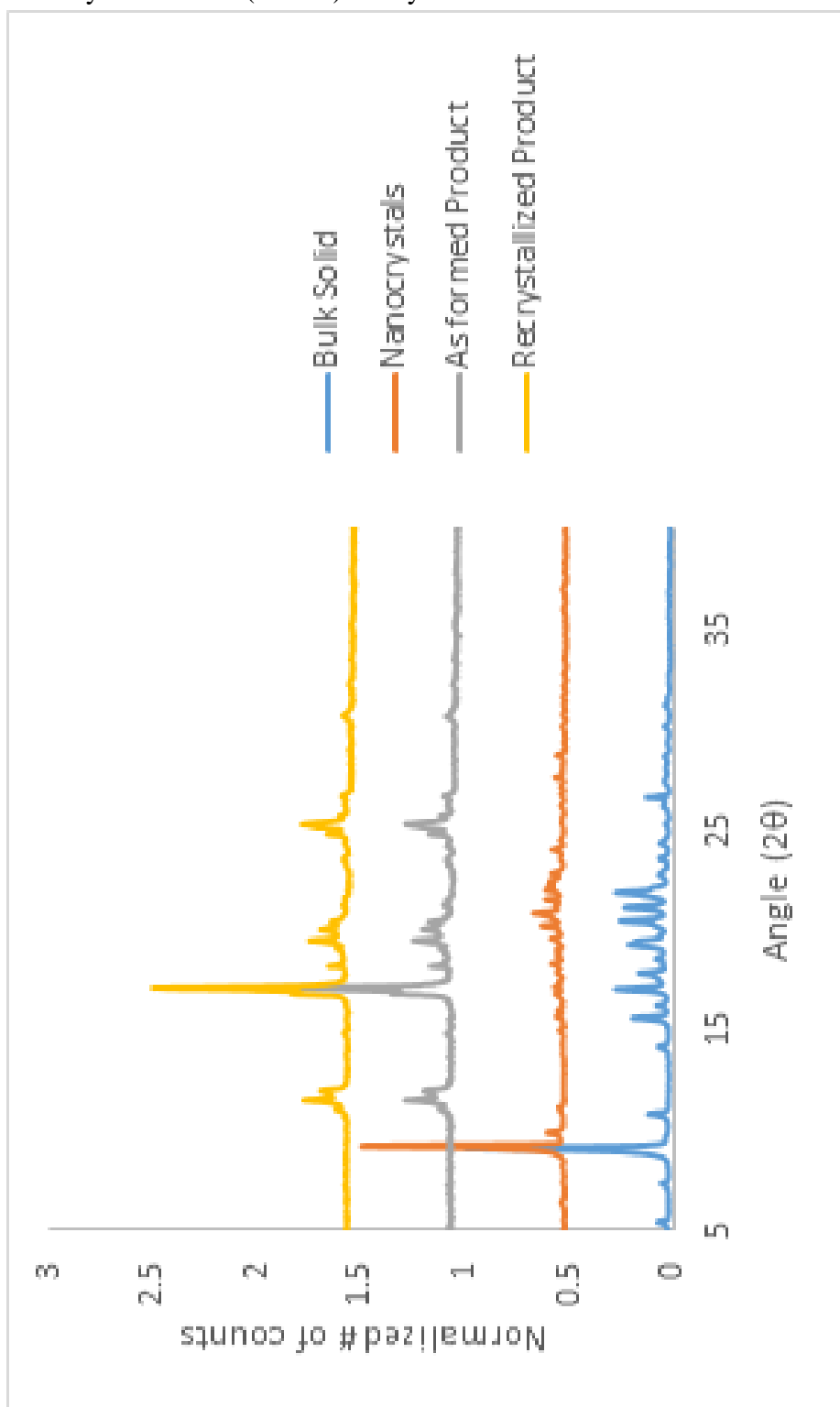


**Figure 4.S25:** <sup>1</sup>H NMR (500 MHz, CDCl<sub>3</sub>) product analysis of 4,4',4'',4'''-(tetramethyl) tetraphenylacetone to 4,4',4'',4'''-(tetramethyl) tetraphenylethane in the solid state



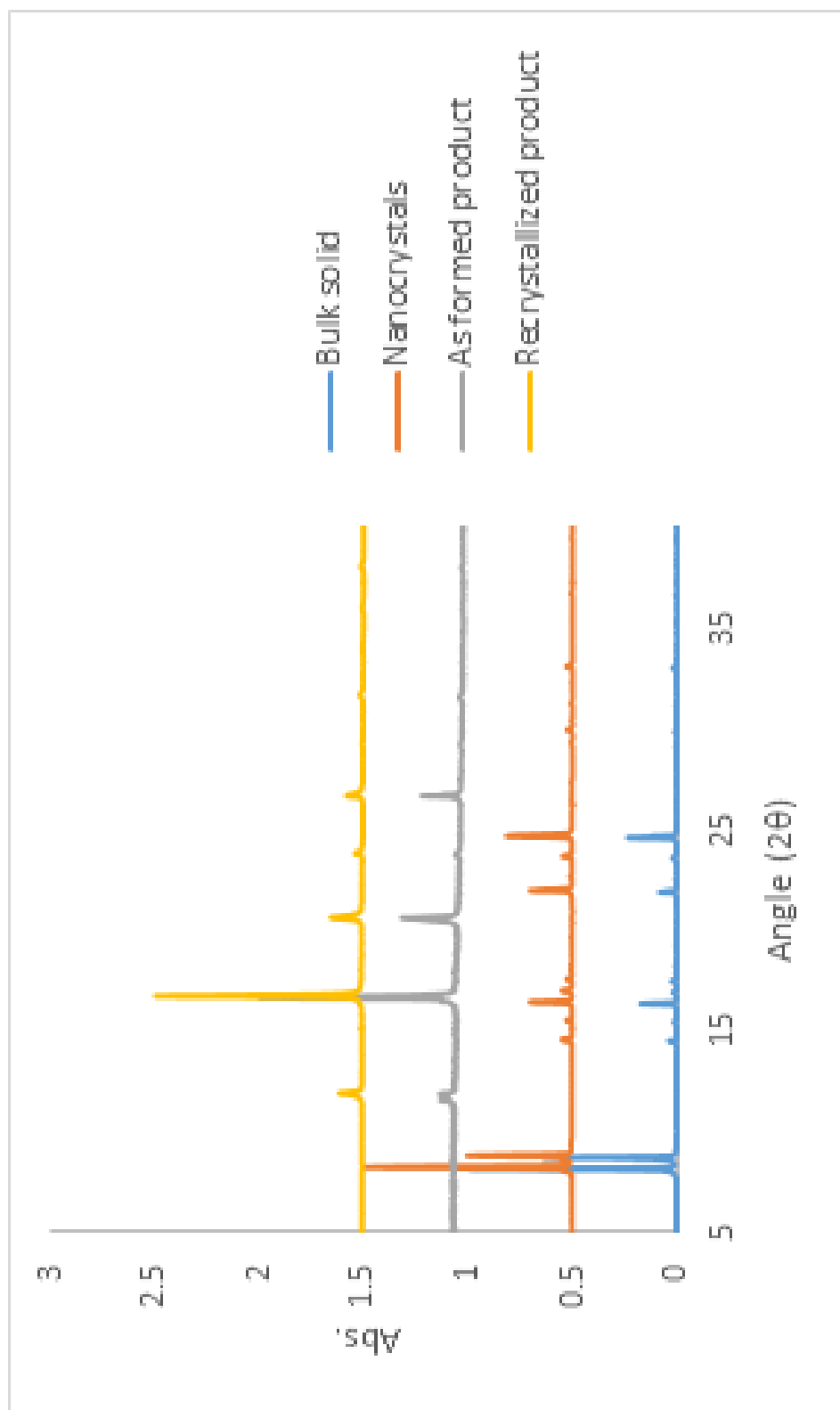
**Figure 4.S26:**  $^1\text{H}$  NMR (500 MHz,  $\text{CDCl}_3$ ) product analysis of 4,4',4'',4'''-(tetra-tertbutyl) tetraphenylacetone to 4,4',4'',4'''-(tetra-tertbutyl) tetraphenylethane in the solid state

3.5.4). Power X-Ray Diffraction (PXRD) Analysis:



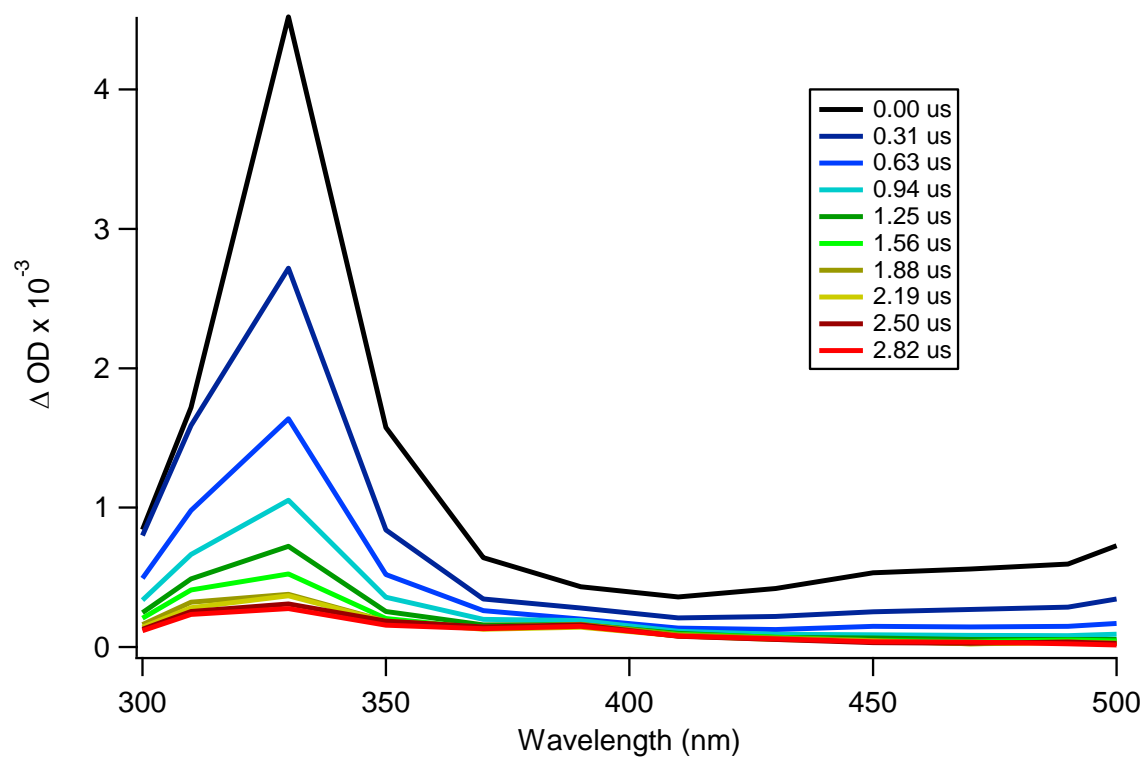
**Figure 4.S27:** PXRD of Tetraphenylacetone in the bulk solid and nanocrystalline suspensions; Tetraphenylethane As formed and recrystallized in ethanol.



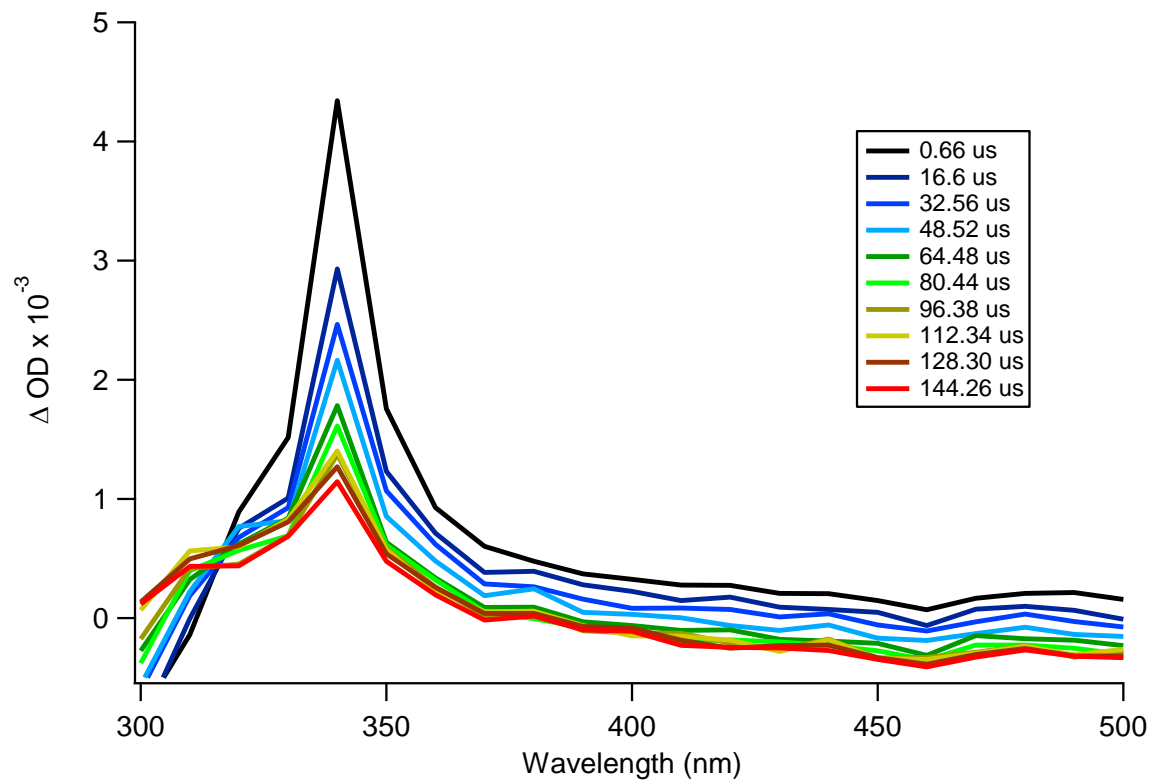


**Figure 4.S28:** PXRD of 4,4',4'',4'''-(tetramethyl) tetraphenylacetone in the bulk solid and nanocrystalline suspensions; 4,4',4'',4'''-(tetramethyl) tetraphenylethane As formed and recrystallized in ethanol.

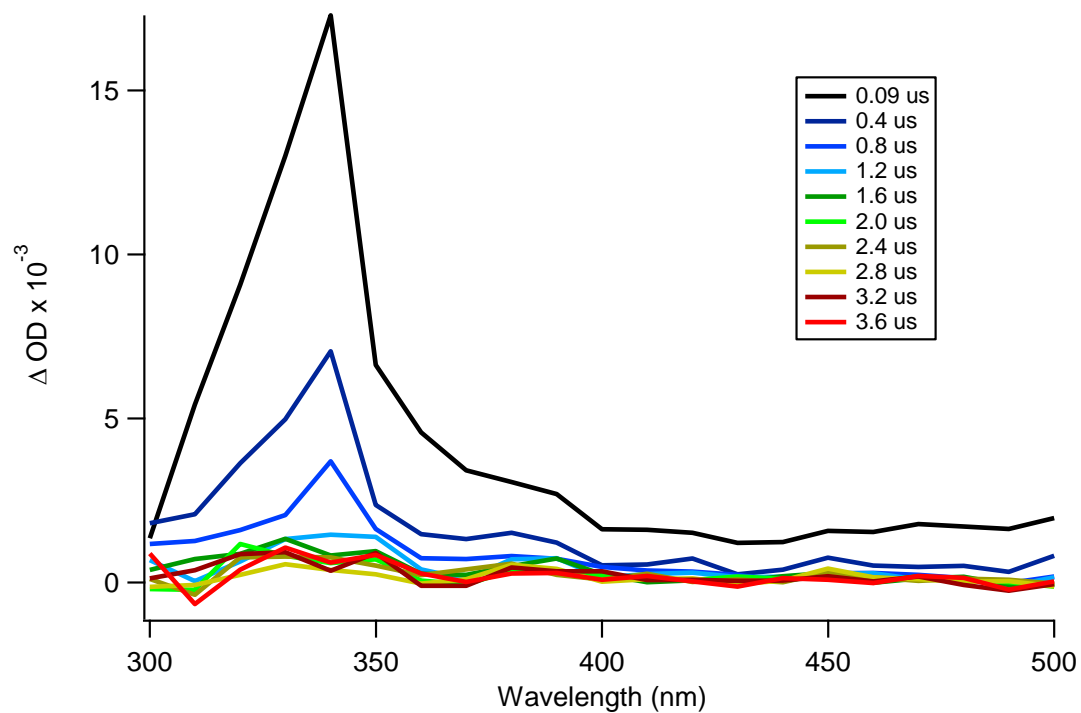
### 3.5.5). Laser Flash Photolysis



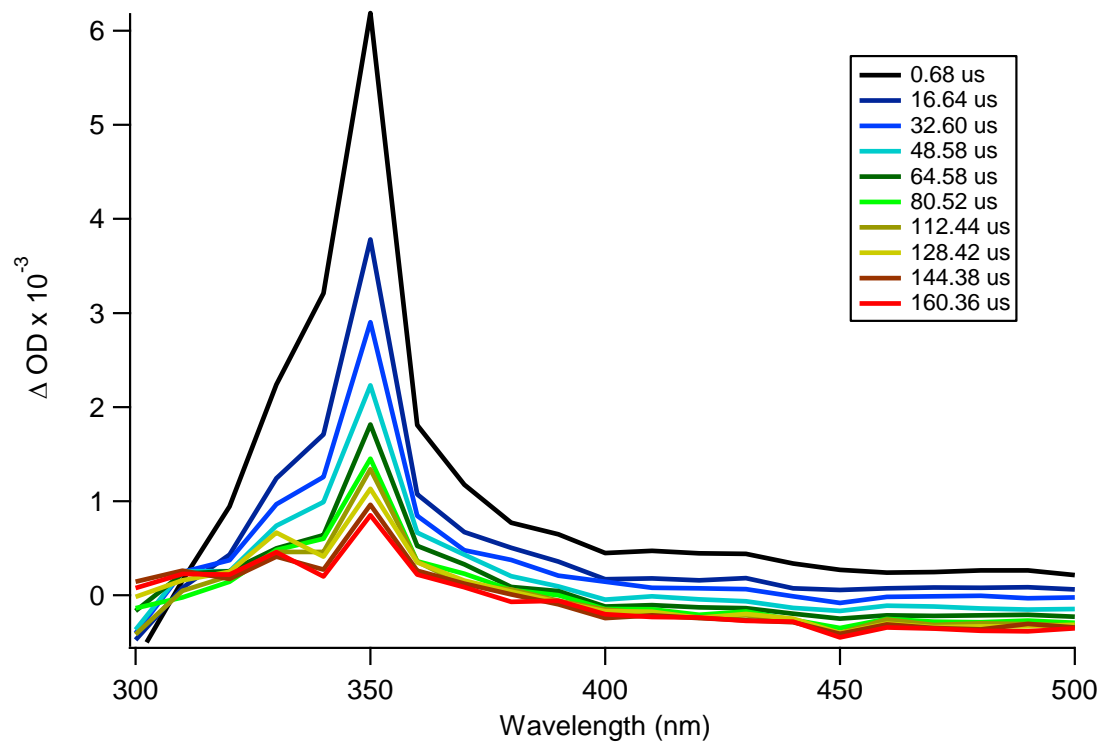
**Figure 4.S29:** Transient Spectroscopy of Tetraphenylacetone in solution state ( $\lambda_{\text{max}} = 330 \text{ nm}$ )



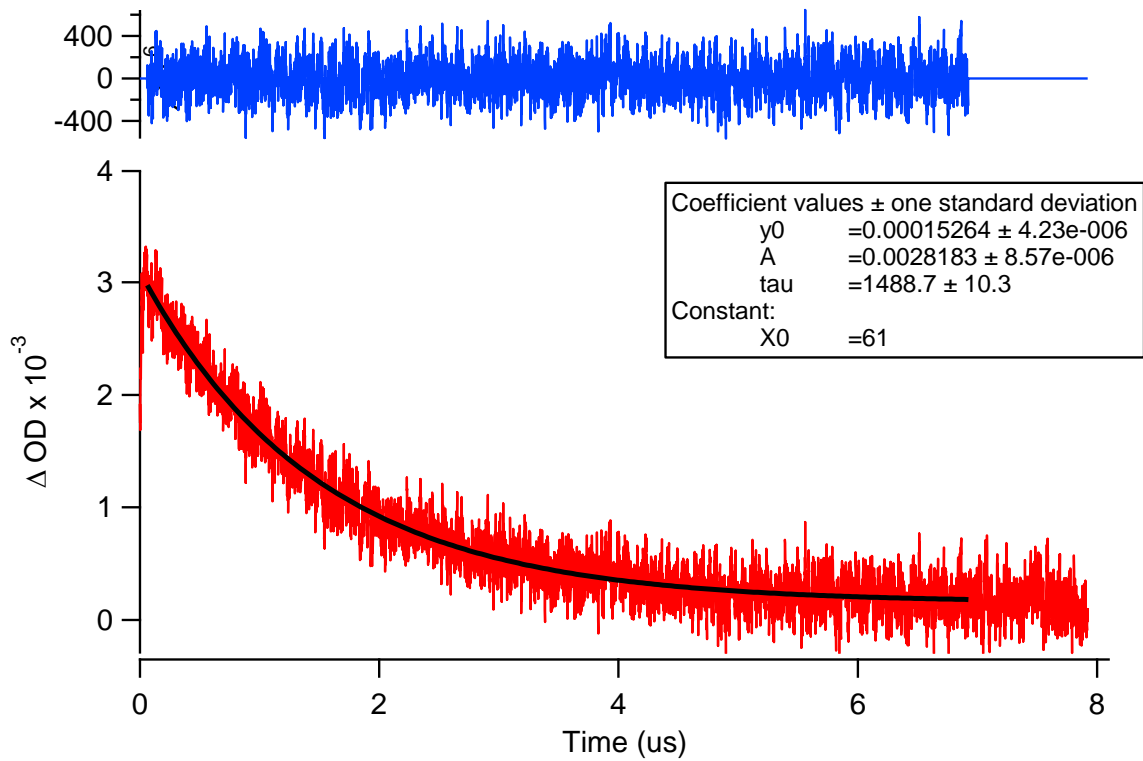
**Figure 4.S30:** Transient Spectroscopy of Tetraphenylacetone in nanocrystalline suspension ( $\lambda_{\text{max}} = 340 \text{ nm}$ )



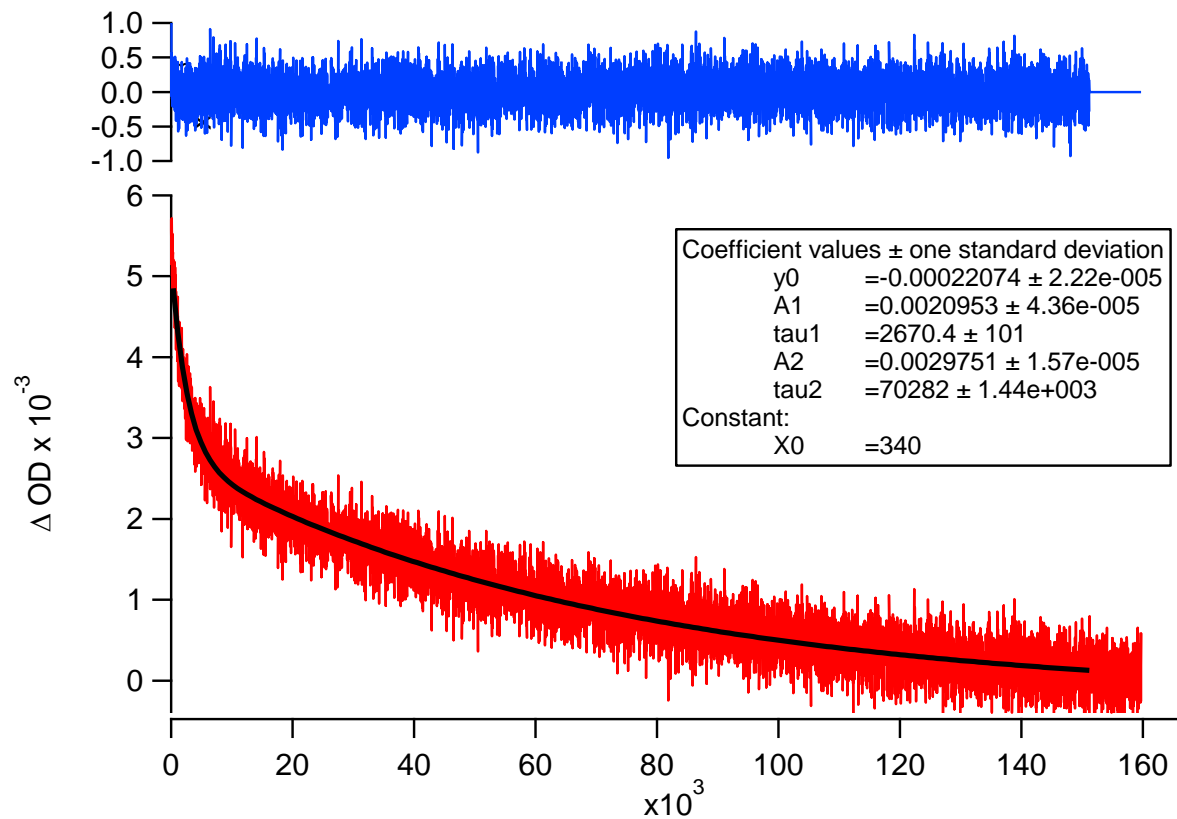
**Figure 4.S31:** Transient Spectroscopy of 4,4',4'',4'''-(tetramethyl) tetraphenylacetone in solution-state ( $\lambda_{\text{max}} = 340 \text{ nm}$ )



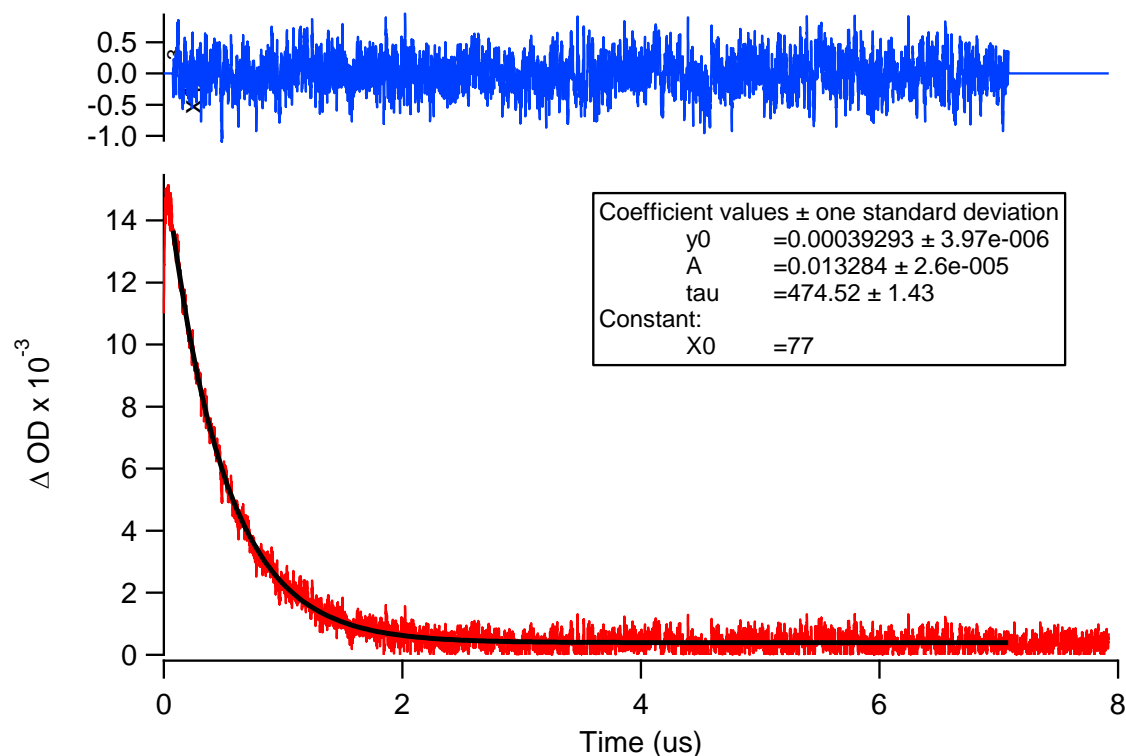
**Figure 4.S32:** Transient Spectroscopy of 4,4',4'',4'''-(tetramethyl) tetraphenylacetone in nanocrystalline suspension ( $\lambda_{\text{max}} = 350 \text{ nm}$ )



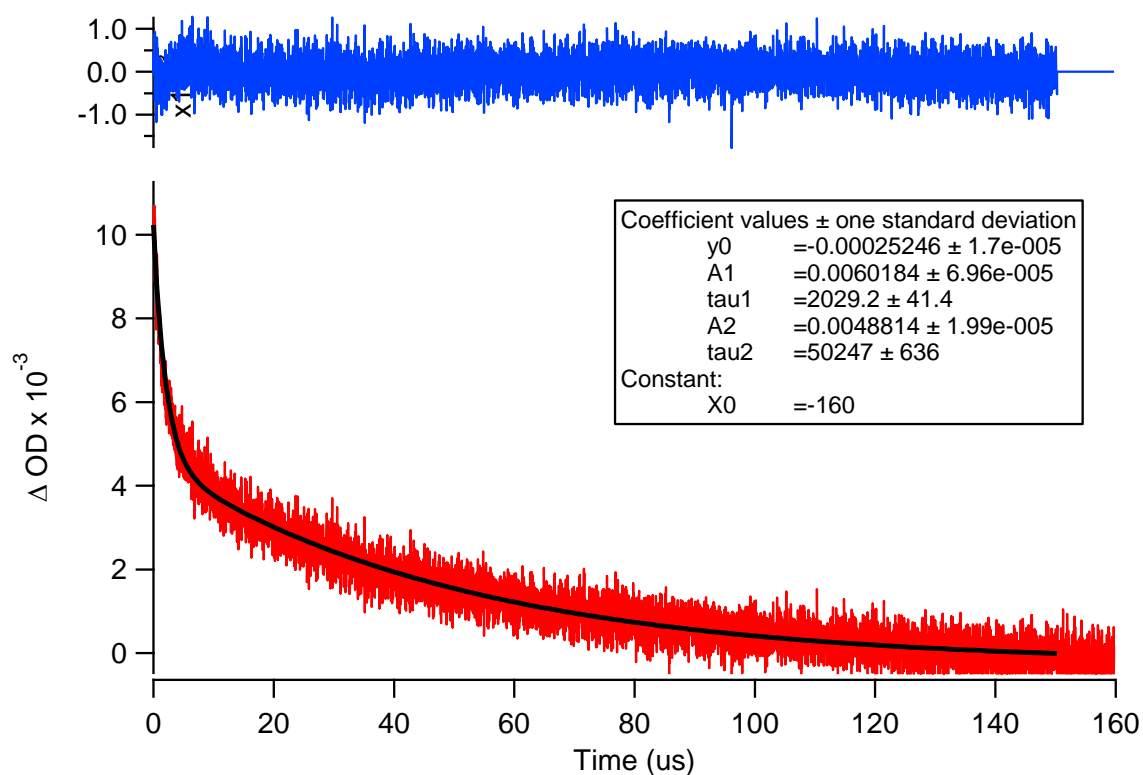
**Figure 4.S33:** Transient decay of tetraphenylacetone in solution



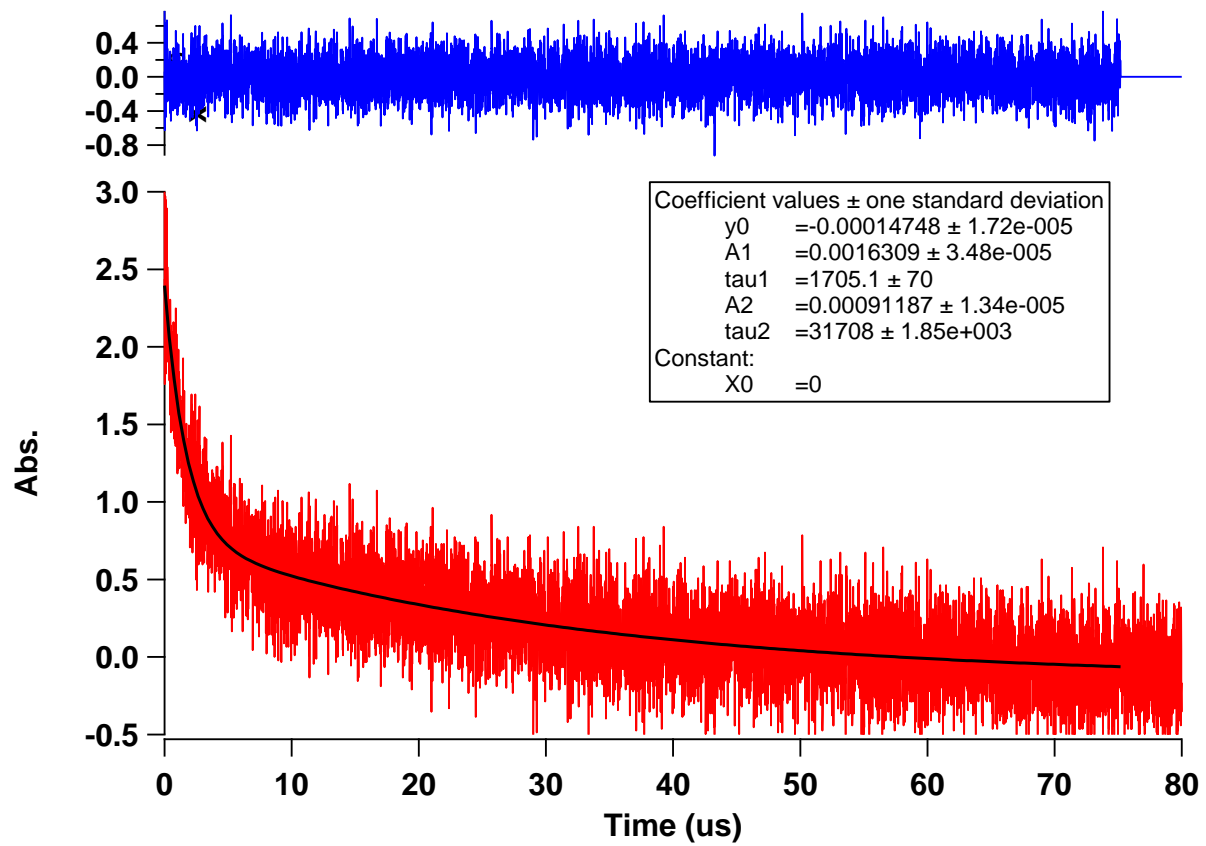
**Figure 4.S34:** Transient decay of tetraphenylacetone in nanocrystalline suspension.



**Figure 4.S35:** Transient decay of 4,4',4'',4'''-(tetramethyl) tetraphenylacetone in solution.



**Figure 4.S36:** Transient decay of 4,4',4'',4'''-(tetramethyl) tetraphenylacetone in nanocrystalline suspension.



**Figure 4.S37:** Transient decay of 4,4',4'',4'''-(tetra-tertbutyl) tetraphenylacetone in nanocrystalline suspension.

### 3.6 References

- 1). (a) Kopelman, R. *Science*, **1988**, *241*, 1620-1626. (b) Caronna, T.; Liantonjo, R.; Logothetis, T. A.; Metragolo, P.; Pilati, T.; Resnati, G. *J. Am. Chem. Soc.*, **2004**, *126* (14), pp 4500–4501. (c) Marafie, J. A.; Bradley, D. D. C.; Williams C. K. *Inorg. Chem.*, **2017**, *56* (10), pp 5688–5695. (d) Maliakal, A.; Raghavachari, K.; Katz, H.; Chandross, E.; Siegrist, T. *Chem. Mater.*, **2004**, *16* (24), pp 4980–4986. (e) Vittal, J. J.; Quah, H. S. *Dalton Trans.*, **2017**, *46*, 7120-7140. (f) Zhu, L.; Agarwal, A.; Lai, J.; Al-Kaysi, R. O.; Tham, F. S.; Tarek, G.; Mueller, L.; Bardeen, C. J. *J. Mater. Chem.*, **2011**, *21*, 6258-6268. (g) Barra, M.; Scaiano, J. C. *Photochem. and Photobiol.*, **1995**, *62*, 60-64.
- 2). (a) Sakamoto, M.; Takahashi, M.; Kamiya, K.; Yamaguchi, K.; Fujita, T.; Shoji, W. *J. Am. Chem. Soc.*, **1996**, *118* (43), 10664–10665. (b) Evans, S. V.; Garcia-Garibay, M.; Omkaram, N.; Scheffer, J. R.; Trotter, J.; Wireko, F. *J. Am. Chem. Soc.* **1986**, *108*, 5648–5649. (c) Roughton, A. L.; Muneer, M.; Demuth, M. *J. Am. Chem. Soc.* **1993**, *115*, 2085–2086. (d) Garcia-Garibay, M.; Scheffer, J. R.; Trotter, J.; Wireko, F. *J. Am. Chem. Soc.*, **1989**, *111*, 4985–4986. (e) Chung, C.-H.; Roh, Y.-S.; Cho, S.-Y.; Kim, J.-G. *Chem. Mater.*, **2004**, *16* (21), 3982–3984. (f) Renata, H.; Zhou, Q.; Baran, P. S. *Science*, **2013**, *339* (6115), 59-63. (g) Sekine, A.; Hori, K.; Ohashi, Y.; Yagi, M.; Toda, F. *J. Am. Chem. Soc.*, **1989**, *111*, 697–680.
- 3). Trommsdorf, H. *Ann. Chem. Pharm.*, **1834**, *11*. (b) Garcia-Garibay, M. A. *Acc. Chem. Res.*, **2003**, *36*, 491.
- 4). (a) Asher, S. A.; Tushcel, D. D.; Vargson, T. A.; Wang, L.; Geib, S. J. *J. Phys. Chem. A*, **2011**, *115* (17), 4279–4287. (b) Schmidt, G. M. J. *Pure Appl. Chem.* **1971**, *27*, 647. (c) M. A. Garcia-Garibay, *Acc. Chem. Res.*, **2003**, *36*, 491–498.

- 5). (a) McBride, J. M.; Vary, M. W.; Whitsel, B. L. *ACS Symp. Ser.*, **1978**, *69*, 208–223. (b) Zimmerman, H. E.; Zuraw, M. J. *J. Am. Chem. Soc.*, **1989**, *111*, 2358–2361. (c) Keating, A. E.; Houk, K. N.; Garcia-Garibay, M. A. *J. Am. Chem. Soc.*, **1997**, *119*, 1474–1475. (d) Novak, K.; Enkelmann, V.; Wegner, G.; Wagener, K. B. *Angew. Chem.*, **1993**, *32*, 16114–16116. (d) Rothenberg, G.; Downie, A. P.; Raston, C. L.; Scott, J. L. *J. Am. Chem. Soc.*, **2001**, *123* (36), 8701–8708.
- 6). (a) Antill, L. M.; Beardmore, J. P.; Woodward, J. R. *Rev. Sci. Inst.*, **2018**, *89*, 23707. (b) Jiang, J.; Zhao, H.; Liu, S. Chen, X.; Jiang, X.; Chen, J.; Quan, X. *Photochem. Photobiol. Sci.*, **2017**, *1*, 63-68. (c) Schneider, J.; Nikitin, K.; Dillert, R.; Bahnemann, D. W. *Faraday Discuss.*, **2017**, *197*, 505-516. (d) Fujitsuka, M.; Majima, T. *Photochem. Photobiol. Sci.*, **2018**, *35*, 25-37. (e) Shinozaki, Y.; Yamaji, M.; Arai, T.; *Chem. Phys.*, **2018**, *500*, 15-18. (f) Ren, Y.; Sun, D.; Cao, Y.; Tsao, H. K.; Yuan, Y.; Zakeeruddin, S. M.; Wang, P.; Gratzel, M. *J. Am. Chem. Soc.*, **2018**, *140* (7), 2405–2408
- 7). (a) Kaminsky, W.; Claborn, K.; Kahr, B. *Chem. Soc. Rev.*, **2004**, *33*, 514–525. (b) J. F. Nye, *Physical Properties of Crystals*, Oxford University Press, Oxford, **1985**, 235–273. (c) Wilkinson, F.; Kelly, G. Diffuse reflectance flash photolysis. In *Handbook of Organic Photochemistry*; Scaiano, J. C., Ed.; CRC Press: Boca Raton, FL, **1989**; Vol. 1, Chapter 12, 293–314.
- 8). H. Kasai, H. S. Nalwa, H. Oikawa, S. Okada, H. Matsuda, N. Minami, A. Kakuta, K. Ono, A. Mukoh and H. Nakanishi, A novel preparation method of organic microcrystals, *Jpn. J. Appl. Phys., Part 2*, **1992**, *31*, L1132–L1134
- 9). (a) Leyrer, R. J.; Wegner, G. *Berichte der Bunsengesellschaft für Physikalische Chemie.*, **1979**, *83*, 461-578. (b) Sarkar, S. K.; Gatlin, D. M.; Das, A.; Loftin, B.; Krause, J. K.; Abe,



- M.; Gudmundsdottir, A. D. *Org. Biomol. Chem.*, **2017**, *15*, 7380-7386. (c) Chin, K. K.; Natarajan, A.; Gard, M. N.; Campos, L. M. Shepherd, H.; Johansson, E.; Garcia-Garibay, M. *A. Chem. Commun.*, **2007**, 4266-4268.
- 10). Rajca, A.; Tolbert, L. M. *J. Am. Chem. Soc.*, **1988**, *110*, 871-876
- 11). Park, J. H.; Hughs, M.; Chung, T. S.; Ayitou, A. J.-L.; Breslin, V. M.; Garcia-Garibay, M. A. *J. Am. Chem. Soc.*, **2017**, *139*, 13312–13317.
- 12). (a) Chung, T. S.; Park, J. H. Garcia-Garibay, M. A. *J. Org. Chem.* **2017**, *82*, 12128–12133. (b) Chung, T. S.; Ayitou, A. J.-L.; Park, J. H.; Breslin, V. M.; Garcia-Garibay, M. A. *J. Phys. Chem. Lett.* **2017**, *8*, 1845–1850.

## **Chapter 4**

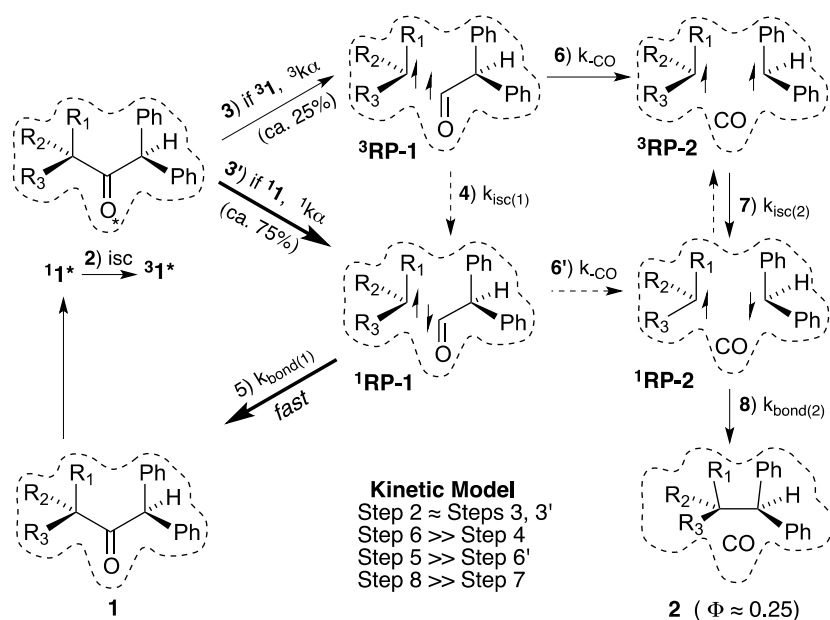
**Laser Flash Photolysis and Quantum Yield Studies of Radical Pairs in Nanocrystalline Suspensions of  $\alpha$ -Phenyl-Substituted Ketones: Sorting Out the Contributions from Singlet and Triplet States**

## 4.1 Introduction

Solid-state photochemical reactions have some attractive features, which often include high chemical yields, selectivity and specificity, and the opportunity to reduce the amount of volatile organic compounds in the production of complex chemicals.<sup>1</sup> However, the implementation of solid-state photochemical methods by the synthetic community is limited,<sup>2</sup> partly due to challenges in their experimental execution and scale up, and due to limitations in mechanistic knowledge that make it challenging to generalize reactions in crystals. Fortunately, advances in this area is made possible by the use of aqueous nanocrystalline suspensions.<sup>3,4</sup> On one hand, nanocrystals suspended in water can be exposed to UV light in a step-flow reactor such that solid-state photoreactions can be easily carried to completion at multi-gram scales. On the other hand, nanocrystals with sizes smaller than the wavelength of light can be seen as a state in transition between supramolecular entities and bulk crystals,<sup>5</sup> with strongly reduced scattering, dichroism and birefringence that enables their measurement by transmission spectroscopy methods, including laser flash photolysis.<sup>5</sup> With that in mind, it is now possible to address subtle mechanistic aspects of several solid-state photoreactions, including the photo-induced decarbonylation of crystalline ketones with radical stabilizing substituents at the two  $\alpha$ -positions, such as aryl-substituted ketones 1a-1c in Scheme 4.1.1.<sup>6,7</sup> The reaction results in the formation of product 2, which maintains the stereochemical information of the reactant by the stereospecific formation of a sterically congested C-C bond.<sup>6,7</sup> As indicated in Scheme 1 the reaction starts by electronic excitation (step 1),<sup>8</sup> which results in the sequential cleavage of the two  $\alpha$ -bonds (steps 3 and 6) to generate, respectively, radical pairs RP-1 and RP-2, which can exist either in a singlet or a triple state.<sup>8</sup> It has been reported that reactions in crystals require the

two bond-cleavage steps to be exothermic and with  $\alpha$ -substituents that provide radical stabilization energies (RSE) greater than 11 kcal/mol, a requirement that is easily met in ketones with aryl groups on both  $\alpha$ -carbons (the RSE of an  $\alpha$ -phenyl group is 16.5 kcal/mol).<sup>9</sup> In this study, we take advantage of asymmetric ketones that form diphenyl-methyl radicals to determine the generation and lifetimes of the radical pairs using transmission laser flash photolysis.<sup>9</sup> Additionally, we measure the quantum yield of the reaction to determine the efficiency of product formation. With that information, we can estimate the extent of  $\alpha$ -cleavage taking place from the triplet (step 3) and singlet (step 3') excited states to form  $^3\text{RP-1}$  and  $^1\text{RP-1}$ , respectively. The contribution from each multiplicity is determined by assuming that the long-lived triplet undergoes decarbonylation (step 6), while the singlet  $^1\text{RP-1}$  quickly undergoes recombination to the starting ketone (step 5). As in our previous study,<sup>10</sup> assign the transient detected as  $^3\text{RP-2}$ , and we propose that its lifetime is determined by the rate of intersystem crossing from  $^3\text{RP-2}$  to  $^1\text{RP-2}$  (step 7), which goes on to form product 2 very rapidly.

#### Scheme 4.1.1



## 4.2 Results and Discussion

To carry out and document the kinetic scheme above, we selected three ketones that would generate a common diphenylmethyl group in one  $\alpha$ -carbon, and either a diphenylmethyl (1a), 1,1-diphenylethyl (2b) or triphenylmethyl (3c) group on the other. (Scheme 4.2.1) Ketones 1a-1c were obtained in reasonable yields by simple substitution reactions with a suitable acyl chloride and lithium carbanion couple, as illustrated in Scheme 4.2.1. All three ketones are crystalline solids with reasonably high melting points (Table 4.2.1). A detailed description of the corresponding synthetic procedures, characterization and analytical results are included in the supplemental information section.

### Scheme 4.2.1

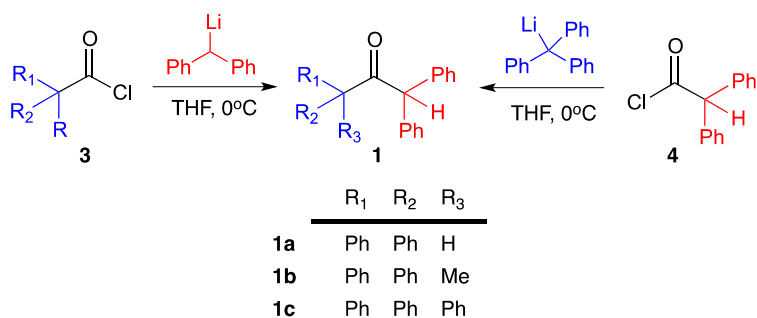


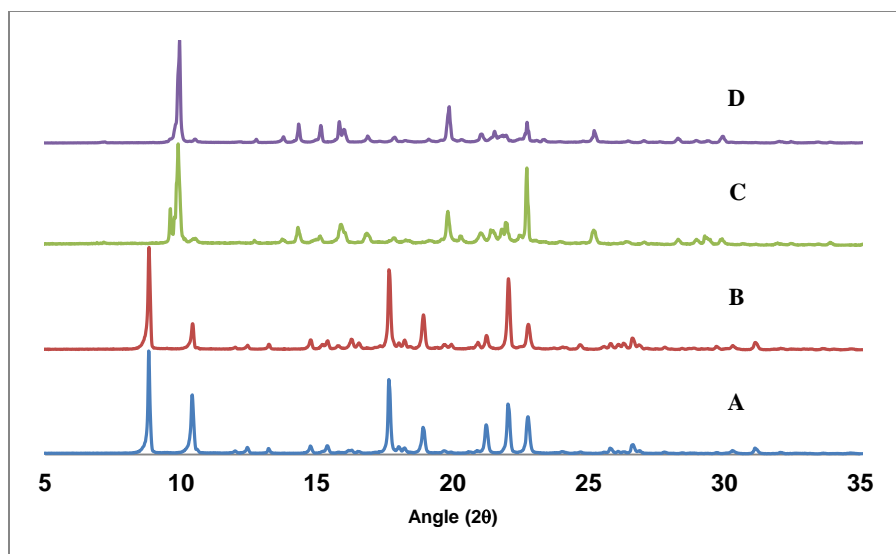
Table 4.2.1 Characterizations and lifetimes of  $\alpha$ -phenyl-substituted acetones

Ketone	R <sub>1</sub> ; R <sub>2</sub> ; R <sub>3</sub>	m.p. (°C)	Crystal size (nm) <sup>a</sup>	Biadical Lifetimes, $\mu$ s <sup>b</sup>	Quantum Yield of NC <sup>c</sup>
1a	Ph; Ph; H	133-134	140 $\pm$ 40	1.5 (MeCN) 2.4, 70 (97%) <sup>b</sup>	0.23 (0.06) <sup>d</sup>
1b	Ph; Ph; Me	101-102	150 $\pm$ 60	1.5 (MeCN) 3.9, 70 (92%) <sup>b</sup>	0.25 (0.06) <sup>d</sup>
1c	Ph; Ph; Ph	180-181	180 $\pm$ 60	1.3 (MeCN) 5.4, 70 (87%) <sup>b</sup>	0.28 (0.04) <sup>d</sup>

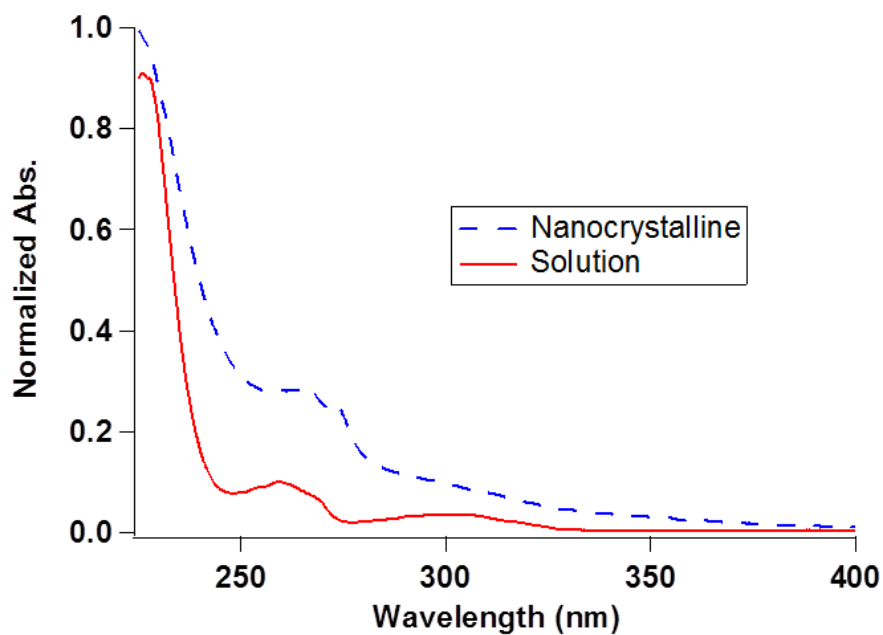
<sup>a</sup>Measured by dynamic light scattering (DLS). <sup>b</sup>Short and long-lived components were observed in the solid state. The number in parenthesis indicates the percentage contribution of the long-lived component to the total decay. <sup>c</sup>Quantum yields of product formation measured with optically dense suspensions at 302 nm using dicumyl ketone as a chemical actinometer.

<sup>d</sup>Standard deviation from six independent measurements with samples from two independent nanocrystal preparations.

The formation of nanocrystalline suspensions was accomplished by the re-precipitation, or solvent-shift method, originally reported by Kasai *et al.*<sup>11</sup> (supplementary information section). The crystalline nature of the suspended solids was confirmed by powder X-ray diffraction (PXRD) analysis of nanocrystals collected by centrifugation, as shown in Figure 1B for samples of 1b. One can see that filtered nanocrystals have a PXRD that is nearly identical to those recorded with samples obtained by grinding large single crystals (Figure 4.2.1A), indicating that the crystal packing of the bulk powder and the nanocrystals of 1b correspond to the same polymorph.<sup>12</sup> It was expected that nanocrystals of ketones 1a-1c with an average size < 200 nm (table 4.2.1), which is smaller than the wavelength of light used for their excitation and detection, would be suitable for transmission spectroscopy measurements. This was confirmed by measuring the UV-Vis absorption spectra for all three samples, as shown for 1b in Figure 4.2.2. The spectral features of the nanocrystalline suspension are a close match to those observed in solution with an underlying scattering contribution that increases exponentially as the wavelength gets shorter. Relatively weak benzenoid transitions in the neighborhood of 275 nm are accompanied by the carbonyl n- $\pi^*$  transition with a  $\lambda_{\text{max}} \approx 300$  nm. The stability of suspended nanocrystals was ascertained by following changes in the UV-Vis absorption as a function of time. Over the course of time, an increase in baseline accompanied with a decrease in absorption was often observed as the result of aggregation. Therefore, measurement had to be carried out with freshly prepared samples in increments of 20mL batches.



**Figure 4.2.1** Powder X-ray diffraction (PXRD) of 1b (A) bulk-powder, (B) nanocrystals, (C) as-formed photoproduct, (D) recrystallized photoproduct.

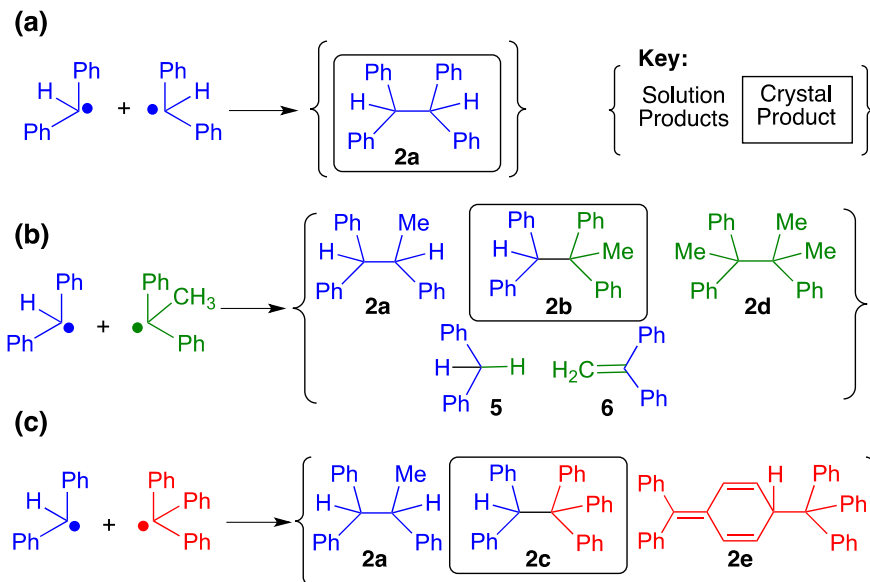


**Figure 4.2.2** (Solid red line) Normalized UV spectra of 1b in solution (0.01 g/L) and, (dashed blue line) nanocrystalline suspension of 1b in cetyltrimethylammonium bromide (CTAB) surfactant (0.025 g/L).

Steady state photochemical experiments were carried out in MeCN solutions with samples of 1a, 1b and 1c using a medium pressure Hg arc lamp equipped with a Pyrex filter ( $\lambda \leq 290$  nm). Product formation was established by  $^1\text{H}$  NMR analysis. While symmetric ketone 1a gave signals corresponding to photoproduct 2a, consistent with the combination of two identical free radicals (shown in blue in Scheme 4.2.3), ketone 1b gave three radical-radical combination products 2a, 2b and 2d, as expected from the three different radical combination possibilities. An additional bis-benzylic singlet in the  $^1\text{H}$  NMR spectrum observed in the reaction of 1b corresponds to the formation of diphenylmethane 5, which is accompanied by formation of 1,1,-diphenyl ethylene 6 by the transfer of a hydrogen atom from the methyl group of 1,1,-diphenylethyl radical (shown in green) to the diphenylmethyl radical (in blue). Irradiation of ketone 1c generates the relatively persistent trityl radical (shown in red), which is able to form stable pentaphenylethane 2c by combination with diphenyl methyl radicals (in blue). Interestingly, self-combination of trityl radicals is known to generate the Gomberg hydrocarbon 7, in a reversible process, which is observed in the  $^1\text{H}$  NMR in the form of several vinylic hydrogens. As expected, reactions carried out in the crystalline state result in the formation of a single product from the combination of the corresponding “geminate” radical pairs.<sup>13</sup> Crystals of ketones 1a, 1b and 1c, give rise, respectively, to products 2a, 2b and 2c, (Scheme 4.2.3). It was shown that these reactions occur from solid reactant to solid photoproduct by comparing the PXRD of the “as formed” products collected after the reaction with the ones from samples of the recrystallized photoproducts. This is shown in Figure 4.2.1, in the case of 1b with the PXRD of a solid sample exposed to UV light (Figure 4.2.1C), which gave the same pattern as the one obtained by recrystallization of pure 2b (Figure 4.2.1D), indicating that the solid-state photoreaction occurs by a reconstructive phase transition.<sup>14</sup>



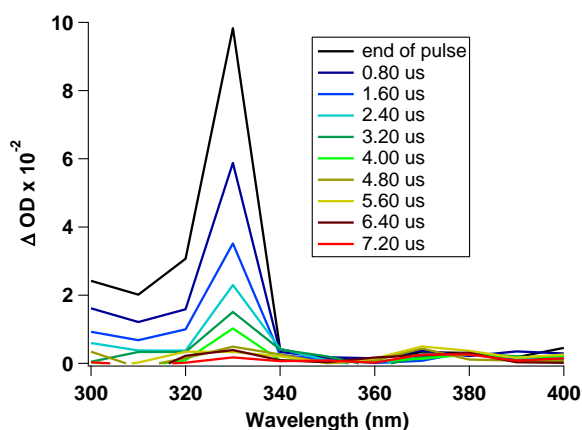
### Scheme 4.2.3



Transient absorption experiments were carried out with the fourth harmonic of a Nd-YAG laser at  $\lambda_{\text{ex}}=266$  nm with a pulse width of ca. 8 ns. Considering that the buildup of photoproducts can interfere with the observation of transient species, we use a single pass flow system to make sure that fresh sample is always available in the laser path. The need to maintain suspended crystals in a reservoir before they are flown into the cell requires suspensions to be stable for no less than ca. 10 min, which is approximately the length of time that it takes to reach the cell. Prior to the laser flash photolysis experiments we established the stability of our suspensions by measuring their UV spectra as a function of time. Fortunately all three ketones 1a-1c exhibit a modest level of scattering that does not interfere with kinetics measurements and displayed the required nanocrystalline stability.

As illustrated in Figure 4.2.3 with data obtained from a sample of ketone 1b with an OD < 1.0 in MeCN, the transient absorption spectrum of diphenylmethyl free radicals in solution displays a maximum at  $\lambda \approx 330$  nm. This result is in excellent agreement with data reported in the literature,

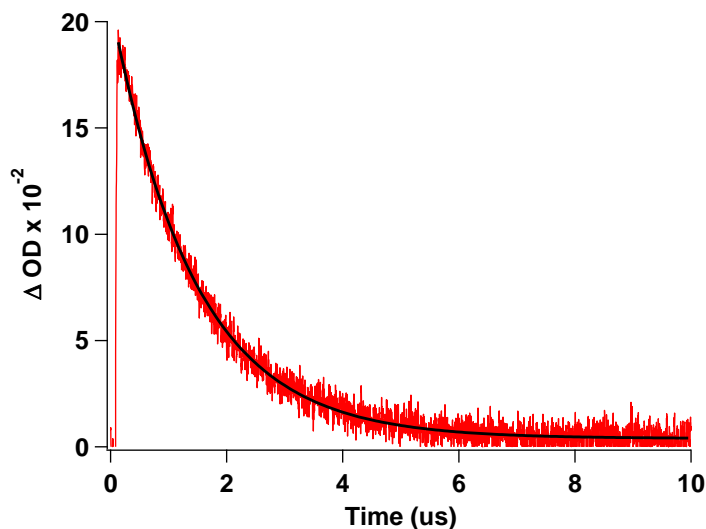
including a relatively recent study from our group that included samples of 1a. Similar observations recorded for ketone 1c are included in the supplemental figures section. An absorption decay measurement monitored at the  $\lambda_{\text{max}}$  over a 10  $\mu\text{s}$  window revealed a single exponential process with a lifetime of 1.5  $\mu\text{s}$  (Figure 4.2.4 and Table 4.2.1). The results observed with samples of 1a - 1c were virtually indistinguishable, as expected from the high similarity of the phenyl-substituted radicals (SI and Table 4.2.1). The fact that the growth of all observed radical absorption occurs within the laser pulse indicates that the  $\alpha$ -cleavage and decarbonylation steps 3 and 6 (Scheme 4.2.1) in solution are completed within the 8 ns laser pulse. This implies that we can only measure the kinetics of the product-forming radical-radical reactions in solution.



**Figure 4.2.3** Transient absorption spectra of 1b in MeCN ( $\lambda_{\text{max}} = 330$  nm).

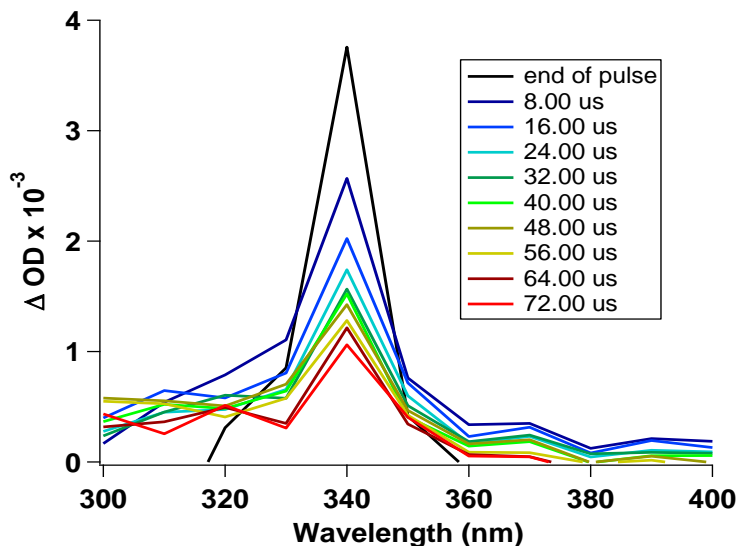
The results from transient absorption experiments carried out in the solid state with nanocrystalline suspensions of 1a-1c reveal some similarities to the ones carried out in solution, with spectra that seem sharper and with a  $\lambda_{\text{max}} \approx 340$  nm (Figure 4.2.5). As shown in Figure 4.2.6 with a sample of 1b, the lifetimes of the transient detected in nanocrystalline suspensions

were monitored at their respective maxima over a time window of 160  $\mu\text{s}$ , which is an order of magnitude larger than the window needed to record the corresponding decay in solution. Unlike solution, where a single exponential was observed, the decay of the radical pair in the solid state consisted of a very rapid component followed by a slower one. Fitting with a double exponential function showed that the integrated contribution of the fast components, with lifetimes between 2.5 and 5.5  $\mu\text{s}$ , is relatively small (ca. 3-13%, Table 1) compared to that of the long-lived components, all of which have a lifetime of 70  $\mu\text{s}$ .



**Figure 4.2.4** Transient decay profile of 1b in MeCN ( $\lambda_{\text{max}} = 330 \text{ nm}$ ).

Considering that the radical stabilizing energy that results from two  $\alpha$ -phenyl groups ( $\text{RSE} \geq 20.5 \text{ kcal/mol}$ )<sup>9</sup> is significantly larger than the values known to enable the reaction<sup>8</sup> ( $\text{RSE} \geq 11 \text{ kcal/mol}$ ), one may expect the  $\alpha$ -cleavage reaction in ketones 1a-1c to be very fast, and quantum efficiency for the solid state reactions to be high, especially if the reaction were to proceed exclusively from the triplet excited state. However, an increase in the radical stabilization of the  $\alpha$ -substituents also increases the rate of  $\alpha$ -cleavage from the singlet excited state,<sup>15</sup> so that formation of <sup>1</sup>RP-1 (Step 3' in Scheme 4.1.1) may compete with intersystem crossing (Step 2).



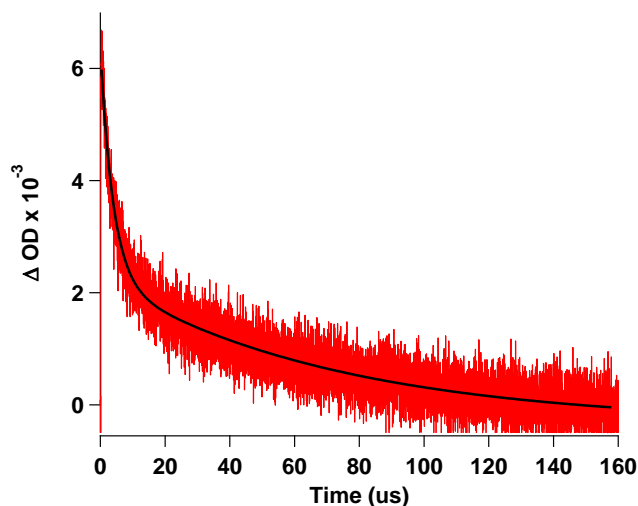
**Figure 4.2.5** Transient spectra of 1b in a nanocrystalline suspension ( $\lambda_{\max} = 340$  nm).

Also indicated in Scheme 4.1.1, one may expect that formation of singlet state  $^1\text{RP-1}$  would result in very rapid return to the ground state ketone (Step 5), so that very little, if any, singlet state decarbonylation (Step 6') should be observed. Effectively, singlet state  $\alpha$ -cleavage would constitute an energy-wasting step that would reduce the quantum yield of reaction. The quantum yield of product formation  $\Phi_p$  is defined as the number of moles of product molecules formed, i.e., Mol-2, in relation to the number of moles, or Einstein of photons absorbed by the reactant, Mol-hv,

$$\Phi_p = \text{Mol-2} / \text{Mol-hv} \quad \text{Eq. 1}$$

Measuring quantum yields in the solid state is complicated by the fact that it is not easy to determine the number of photons absorbed by bulk solids. Incident photons can be easily lost through reflection and scattering, which depend on geometric and optical variables. To address this challenge, we have implemented the use of nanocrystalline suspensions and submersible light sources. Using relatively high sample loadings (which tend to have a milky appearance) one can assure that most photon emitted by the immersed light source is absorbed by the

crystalline suspension (Scheme 4.2.4). Furthermore, one can take advantage of a mixed suspension with measured optical densities, where one of the components is a chemical actinometer with a reference quantum yield. A very convenient reference for the purpose of our study is nanocrystalline dicumyl ketone (DCK), which is known to form dicumene (DC) with a quantum yield of  $\Phi_{\text{DCK}} = 0.2$  (Scheme 4.2.4).<sup>3b</sup>



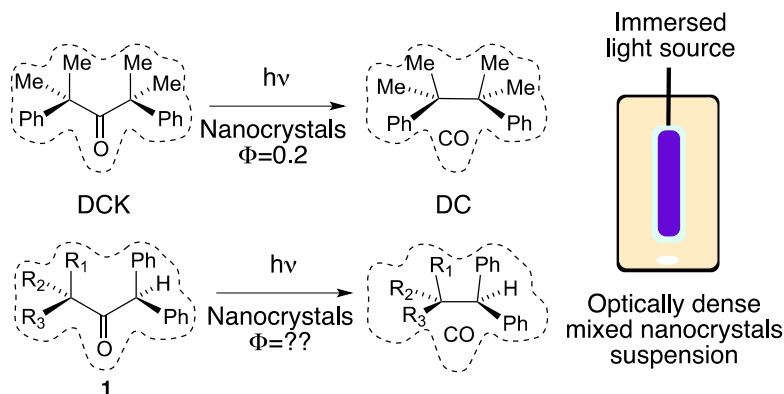
**Figure 4.2.6** Transient decay profile of 1b in the solid-state via nanocrystalline suspensions at  $\lambda_{\text{max}} = 340 \text{ nm}$ .

Thus, knowing the quantum yield of reaction for DCK,  $\Phi_{\text{DCK}}$  and measuring the moles of product formed (Mol-2) the number of Einstein (Mol-hv) coming from the light source can be measured. One can use optically matched suspensions of DCK and 1, or consider that the number of photons absorbed by DCK and 1 are proportional to their optical densities,  $\text{OD}_{\text{DCK}}$  and  $\text{OD}_1$ . Under those conditions, the number of product molecules Mol-2 formed from ketone 1, and the number of dicumene molecules Mol-DC formed from DCK. From the ratio of quantum yields for 1 and DCK (Eq. 2) one can reorganize to obtain Eq. 3, where optical densities and the amounts of product formed can be easily measured.

$$\Phi_1 / \Phi_{\text{DCK}} = (\text{Mol-2}/\text{OD}_1) / (\text{Mol-DC}/\text{OD}_{\text{DCK}}) \quad \text{Eq. 2}$$

$$\Phi_1 = (\Phi_{\text{DCK}}) (\text{Mol-2}) (\text{OD}_{\text{DCK}}) / (\text{OD}_1) (\text{Mol-DC}) \quad \text{Eq. 3}$$

#### Scheme 4.2.4



As a convenient source for these experiments we use a pen light with a 2.9 W output at  $\lambda=302$  nm that can be easily immersed in a test tube with a 2.54 cm diameter and 10.5 cm length. Separate optically dense suspensions of DCK and 1 with initial loading values on the order of 0.05-0.1 mg/ml were prepared, and their relative optical densities values measured with a UV-Vis immersion probe. Optical density values were adjusted by adding some of the surfactant solution that was originally used for suspension preparation. After reading final OD values in the range of  $A \approx 0.5-1.0$  at  $\lambda = 302$  nm, the two suspensions were mixed together, one half was left unreacted and the other half exposed to the immersed UV pen light under continued stirring. Mixed suspensions were prepared in duplicate for each of the three ketones, and up to three independent photochemical experiments were carried out with variable exposure times and conversion values. Quantum yield values close to 0.25 in Table 1 represent an average of six independent experiments with standard deviations suggesting that the small differences measured are probably not significant. A more detailed description of the sample preparation and data analysis is included in the experimental section.

Based on the quantum yield and transient decay values obtained in our experiments, we propose the kinetic relations indicated in Scheme 4.2.1. We propose that the relatively low quantum yields of reaction are the result of a considerable contribution of unproductive singlet state  $\alpha$ -cleavage. This implies that tetraphenyl substitution accelerates the singlet state bond-cleavage reaction such that it competes with intersystem crossing from the singlet to the triplet excited state. In Scheme 1, this implies that step 2 (isc) is of the same order of magnitude as the  $\alpha$ -cleavage steps 3 and 3'. It is reasonable to expect that  $^1\text{RP-1}$  should have no barrier for the two radicals to make a sigma bond, such that step 6 should be faster than cleavage of the CO group (step 6'). Barring a self-quenching process in the excited state, which is unlikely considering that our results represent three different crystal structures, we propose that the sequence,

**step 1  $\longrightarrow$  step 3'  $\longrightarrow$  step 5**

accounts for 75% of the total number of photons absorbed. This suggests that the remaining 25% of the total excitation starts with intersystem crossing to the triplet excited state (step 2) and is followed by a very efficient  $\alpha$ -cleavage reaction (step 3). The lack of a two-phase growth in the transient signal suggest that the loss of CO from  $^3\text{RP-1}$  (step 6) occurs within the ca. 8 ns of the laser pulse, which gives  $^3\text{RP-2}$  as the only observable transient within the observable time frame of our instrument. As previously noted with aryl-substituted analogs of 1a, it is interesting that all three ketones 1a, 1b and 1c, have a major component with a lifetime of ca. 70 ns that accounts for 97%, 92% and 87% of the total, respectively. The relative consistency of this kinetic behavior supports our suggestion that it represents the rate of intersystem crossing from  $^3\text{RP-2}$  to  $^1\text{RP-2}$ , with the latter going on to product 2 with little or no barrier. We tentatively interpret the presence of short and long-lived components as the result of distinct triplet sublevel populations in  $^3\text{RP-2}$  with different intersystem crossing rates. It is known that intersystem crossing in

excited ketones from  $^11^*$  to  $^31^*$  results in a spin-polarized triplet excited states that can carry their polarization into the triplet radical pair.<sup>16</sup> In addition to starting with different triplet sublevel ( $T_+$ ,  $T_0$ , and  $T_-$ ) populations, those sublevels are expected to have intersystem crossing rates that depend on their energetic proximity to the singlet pair (S) with mechanisms that may involve differences in g-factors, electron-nuclear hyperfine coupling (HFC), or spin-orbit coupling (SOC). Studies in progress addressing the effects of different magnetic nuclear isotopes and magnetic field effects may elucidate the mechanisms that account for a small fraction (3-13%) of the triplet biradical to intersystem crossing with rate constants that are up to 30 times faster than the rest of the triplet population.

#### 4.3 Conclusions

Using three crystalline  $\alpha$ -polyaryl substituted acetones we have taken advantage of aqueous nanocrystalline suspensions to measure their quantum yields of reaction and the kinetics of decay of their triplet dialkyl radical pairs. As with most previous examples, product analysis revealed reactions in crystals to be highly selective and easily carried out to completion. Quantum yields of reaction of the order of 0.25 are interpreted as the result of having most (ca. 75%) of the original  $\alpha$ -cleavage reaction taking place from the singlet excited state, which results in singlet acyl-alkyl radical pairs ( $^1RP-1$ ) that undergo recombination to reform the starting material. Transient species detected by laser flash photolysis experiments had spectra consistent with the well-known diphenylmethyl radical, suggesting that spin-spin interactions in the radical pair do not perturb in a drastic manner the absorption spectrum of the monoradical. We propose that the lifetime of the radical is determined by intersystem crossing, which acts as the rate-limiting step for product formation. The consistent observation of fast and slow components suggests that



reaction and intersystem crossing in the radical pair are likely to be triplet spin-sublevel specific. Studies addressing this mechanistic hypothesis are now in progress.

#### 4.4 Experimental Section

**Synthesis:** Ketones 1a-1c were prepared as shown in Scheme 4.2.1 by formation of a lithiated diphenylmethane species followed by an addition-elimination onto the required acyl chloride at 0°C in THF. Experimental details and analytical data are reported in the experimental section.

**Laser Flash Photolysis (LFP):** Measurements were carried out with an Edinburgh Laser Flash Photolysis (LFP) system using the 4<sup>th</sup> harmonic of a brilliant B Nd:YAG laser from Quantel® generating 8 ns pulses with 36-40 mJ of energy at 266 nm. Samples were introduced via a single-pass 1 cm quartz flow cell placed on the cross-section of the laser and a pulsed Xenon arc lamp (450W) that was used as the probe. A detailed description of the experimental setup has been described in detail in reference 11.

**Quantum Yield Determination:** Separate nanocrystalline suspensions of dicumyl ketones (DCK) and ketones 1a-1c were prepared, respectively, by injecting 0.1 mL of 17 mg/mL MeCN solution of DCK, and 0.2 mL of a 20 mg/mL MeCN solution of ketone 1a-1c into test tubes each containing 6 mL of a CTAB solution (164 mg/L) that was subject to a vortex. The transmittance (%T) of each resulting suspension (DCK and ketones 1a-1c) was measured via an Ocean Optics spectrometer (DT-MINI-2-GS UV-VIS-NIR LightSource and USB2000+ using the SpectraSuite software package). Mixed suspensions were prepared by adding 5.6 mL of the DCK suspension to a 5.6 mL suspension of each of the three ketones, 1a-1c, each in a separate container. Two

aliquots of 5 mL were drawn and one was set aside as a control and the other was irradiated by immersing a 2.9 W pen light at 302 nm in a glass tube with a 2.54 cm diameter and 10.5 cm height containing a magnetic bar. This procedure was repeated twice for irradiations performed for 3, 5, and 7 min. The irradiated and non-irradiated suspensions were analyzed by  $^1\text{H}$  NMR measurements. To that end, samples were diluted with 10 mL of D.I. water and extracted with (2 x 12 mL) diethyl ether. The ether phase was dried over  $\text{MgSO}_4$  and the solvent was removed via rotary evaporation. The dry samples were treated with 0.2 mL of a 2.7 mg/mL solution of 2-methoxy-benzophenone in  $\text{CDCl}_3$  and then sufficiently filled with  $\text{CDCl}_3$  for  $^1\text{H}$  NMR at 500 MHz. The (OMe) singlet at  $\delta = 3.73$  ppm from the 2-methoxy-benzophenone was normalized to 1.00 and the methine protons of ketones 1a-1c and the methyl groups ( $\delta = 1.28$  ppm) of DCK were integrated relative to the (OMe) signal. The quantum yields ( $\Phi_{1a-1c}$ ) were calculated using Eq. 3 where Mol-2a-2c and Mol-DC are the relative integrations of 2a-2c and dicumene (DC 2), respectively. The values  $\text{OD}_{1a-1c}$  and  $\text{OD}_{\text{DCK}}$  are the optical densities of 1a-1c and DCK, respectively and  $\theta_{\text{DC}} = 0.2$ . In addition to a summary included in Table 1 we have included all the tabulated data in the supplementary figures section.

## 4.5 Supplementary Figures for Chapter 4

Contents:	Page number
4.5.1). Experimental Section	166
4.5.2). Spectral data ( $^1\text{H}$ NMR, $^{13}\text{C}$ NMR, UV-VIS)	171
4.5.3). Solid-State Photochemistry of Dry Powder	189
4.5.4). Power X-Ray Diffraction (PXRD) Analysis	192
4.5.5). Laser Flash Photolysis	195
4.5.6). Dynamic Light Scattering (DLS)	201
4.5.7). Quantum Yield	203

#### 4.5.1 Experimental Section:

Unless reported, all of the substituted ketones were synthesized using commercially available starting materials.

**General Methods.** All commercial reagents and solvents were used as received without further purification. Unless stated otherwise, reactions were conducted in oven-dried glassware under argon atmosphere. Hydrogen magnetic resonance spectra were recorded at 500 MHz, and carbon-13 magnetic resonance spectra were recorded at 125 MHz, respectively. All chemical shifts are reported in ppm on the  $\delta$ -scale relative to TMS ( $\delta$  0.0) using residual solvent as reference (CDCl<sub>3</sub>  $\delta$  7.26 and  $\delta$  77.16 for <sup>1</sup>H and <sup>13</sup>C NMR measurements, respectively, and CD<sub>3</sub>CN  $\delta$  1.94 and 1.32, 118.26 for <sup>1</sup>H and <sup>13</sup>C NMR respectively). Standard abbreviations indicating multiplicity were used as follows: s (singlet), b (broad), d (doublet), t (triplet), q (quartet), and m (multiplet). High-resolution mass spectral data were recorded on a DART spectrometer in positive (ESI+) ion mode. UV-Vis absorption and transmission spectra were recorded on Ocean Optics spectrometer (DT-MINI-2-GS UV-VIS-NIR LightSource and USB2000+ using SpectraSuite software package). Dynamic Light Scattering (DLS) data were recorded using a Beckman-Coulter N4 Plus particle analyzer with a 10 mW helium-neon laser at 632.8 nm. The particle size was determined using the 62.6° detection angle and was calculated using the size distribution processor (SDP) analysis package provided by the manufacturer. Melting point values were recorded on a Melt-Point II® apparatus. Infra-Red spectra were recorded on a PerkinElmer® Spectrum Two spectrometer equipped with a universal ATR sampling accessory. Nanosecond transient absorption experiments were performed using Laser Flash Photolysis instrument from Edinburgh Instruments in conjunction with a Nd:YAG laser (Brilliant b, Quantel®) with 266-nm output, ca. 8 ns pulse width and 36-40 mJ pulse energy. The

optical detection is based on a pulsed Xenon arc lamp (450 W), a monochromator (TMS300, Czerny-Turner), a photomultiplier detector (Hamamatsu R928) and a digital oscilloscope (TDS3012C, 100 MHz and 1.25 GS/s from Tektronix). The laser flash photolysis experiments were performed with 1 cm quartz flow cell mounted on a home-built sample holder that is placed at the cross-section of the laser incident beam and the probe light. Continuously Argon gas purged acetonitrile solutions or crystalline suspensions of ketones (0.0025g/L) were flown through the quartz cell using a peristaltic pump (Masterflex L/S) at a rate of 1.6 – 3.2 mL/min. Due to aggregation fresh samples in batches of 20 mL were made for the crystalline suspensions every 10 minutes. Time-resolved absorption maps were recorded with continuous flow of samples through the quartz cell. Lifetimes measured at  $\lambda_{\text{max}}$  were reproducible and doubly verified/processed with Edinburgh Instruments L900 internal software and Igor Pro (version 6.34A, Wavemetrics) software. The parameters under the detector monochromator settings are as follows: the ketones were observed at the corresponding  $\lambda_{\text{max}}$  in solution (320-350 nm) and in crystalline suspensions (330-360 nm), and the band width was set between 1.00 to 3.00 nm. The flash lamp settings were set where the frequency was at 10 Hz, width at 40  $\mu\text{s}$ , and delay at 4000  $\mu\text{s}$ . The Q-switch settings were set where the frequency was at 1.0 Hz, width at 20  $\mu\text{s}$ , and delay between 270-310  $\mu\text{s}$ .

**General Synthesis of Acid Chlorides (3b, 4a):**<sup>17</sup> In an oven and flame-dried, argon filled round-bottom flask, carboxylic acid (1 eq) was stirred under dry DCM (15 eq) and was treated with oxalyl chloride (1.1 eq). The reaction was then allowed to stir for 20 minutes and was then treated with dry dimethylformamide (1 eq). After the formation of gas ceased the reaction was further allowed to react for 2 hours. The reaction was quenched with 0.5M HCl extracted with

DCM (3 X 20mL) and dried over Na<sub>2</sub>SO<sub>4</sub>. The solvents were removed under reduced pressure. The resulting liquid (<95% yield) was then stored in a vial for the proceeding steps.

**General Synthesis of ketones:** Following a modified procedure by Rajca *et al.*,<sup>18</sup> in a flame-dried, argon filled round-bottom flask, acid chloride (0.5 eq) in THF (15 eq) was added over 5 minutes to a 5:1 THF/hexane solution of (diphenylmethyl)lithium solution (2.5 eq) stirring at 0 °C. The reaction undergoes a color change from a light orange-red to a deep dark-red. After 1 hour, the remaining acid chloride (0.5 eq) in THF (15 eq) was added over 5 minutes. The reaction was warmed to room temperature and was stirred overnight. The reaction was quenched with 0.5M HCl extracted with diethyl ether (3 X 20 mL) and dried over Na<sub>2</sub>SO<sub>4</sub>. The solvents were removed under reduced pressure and the residue was subjected to column chromatography (1:4-9 acetone:hexane). The resulting crystalline solids were further recrystallized from ethanol (11-95% yield).

#### **Photochemistry of Dry Powders and MeCN Solutions:**

Photochemical experiments for product analysis were conducted with a medium-pressure Hg Hanovia lamp using a Pyrex glass immersion well with a cutoff of  $\lambda \leq 290$  nm. Solid samples were ground between two microscope slides, subject to UV light irradiation in a closed chamber, and analyzed after dissolution in CDCl<sub>3</sub> using <sup>1</sup>H NMR (500 MHz). Product analysis for experiments carried out in ca. 0.1 M MeCN solution were conducted in a similar manner after the irradiated solutions were evaporated and dissolved in the deuterated solvent.

**2,2-Diphenylpropanoyl chloride (compound 3b):** <95% Yield. <sup>1</sup>H NMR (500 MHz, CDCl<sub>3</sub>)  $\delta$  7.34 (m, 10H), 2.11 (s, 3H); <sup>13</sup>C NMR (125 MHz, CDCl<sub>3</sub>)  $\delta$  177.53, 141.41, 128.521, 128.32, 127.80, 65.97, 27.94 (commercially available)

**2,2-Diphenylacetyl chloride (compound 4a):** <95% Yield.  $^1\text{H}$  NMR (500 MHz,  $\text{CDCl}_3$ )  $\delta$  7.29 (m, 10H), 5.45 (s, 1H);  $^{13}\text{C}$  NMR (125 MHz,  $\text{CDCl}_3$ )  $\delta$  173.53, 136.22, 129.03, 128.74, 128.20, 68.67 (commercially available)

**1,1,3,3-Tetraphenylpropan-2-one (compound 1a):** Yield 66%. m.p. 133-134°C, (lit.<sup>17</sup>, m.p. 134°C); Using ethyl acetate and hexanes (1:19) ( $R_f = 0.4$ ); IR(neat)  $\nu_{\text{max}} = 3054, 3022, 1706, 1597, 1493, 1451, 1058 \text{ cm}^{-1}$ .  $\lambda_{\text{max}} = 227.13, 261.76, 302.81$ .  $^1\text{H}$  NMR (500 MHz,  $\text{CDCl}_3$ )  $\delta$  7.24 (m, 20H), 7.25 (s, 2H);  $^{13}\text{C}$  NMR (125 MHz,  $\text{CDCl}_3$ )  $\delta$  205.51, 138.06, 129.12, 128.69, 127.28, 63.52.

**1,1,3,3-Tetraphenylbutan-2-one (compound 1b):** 87% Yield. m.p. 101.5-101.9 °C; Using ethyl acetate and hexanes (1:19) ( $R_f = 0.42$ ); IR(neat)  $\nu_{\text{max}} = 3082, 3027, 2950, 1699, 1490, 1440, 1019 \text{ cm}^{-1}$ .  $\lambda_{\text{max}} = 261.76, 305.8$ .  $^1\text{H}$  NMR (500 MHz,  $\text{CDCl}_3$ )  $\delta$  7.18 (m, 20H), 5.28 (s, 1H), 1.83 (s, 3H);  $^{13}\text{C}$  NMR (125 MHz,  $\text{CDCl}_3$ )  $\delta$  208.09, 142.45, 139.75, 129.00, 128.40, 128.36, 128.18, 127.02, 126.74, 63.56, 60.07, 26.27. HRMS (DART) calcd. for  $[\text{C}_{28}\text{H}_{24}\text{O}+\text{H}]^+$  377.18607, found 377.18865

**1,1,1,3,3-Pentaphenylpropan-2-one (compound 1c):** 11% Yield. m.p. 180°C, (lit.<sup>19</sup>, m.p. 180-181°C). Using ethyl acetate and hexanes (1:19) ( $R_f = 0.44$ ); IR(neat)  $\nu_{\text{max}} = 3086, 3059, 3019, 2940, 1721, 1493, 1446, 1058 \text{ cm}^{-1}$ .  $\lambda_{\text{max}} = 240.87, 262.52, 312.9$ .  $^1\text{H}$  NMR (500 MHz,  $\text{CDCl}_3$ )  $\delta$  7.13 (m, 25H), 5.17 (s, 1H);  $^{13}\text{C}$  NMR (125 MHz,  $\text{CDCl}_3$ )  $\delta$  206.10, 141.08, 141.01, 130.89, 128.15, 127.90, 127.66, 126.83, 126.40, 74.61, 61.78. HRMS (DART) calcd. for  $[\text{C}_{33}\text{H}_{26}\text{O}+\text{H}]^+$  439.20172, found 439.20444

**1,1,2,2-Tetraphenylethane (compound 2a):** Yield <99%. m.p. 213 °C, (lit.<sup>20</sup>, m.p. 213°C); IR(neat)  $\nu_{\text{max}} = 3024, 2890, 1597, 1495, 1448, 173, 1028 \text{ cm}^{-1}$ .  $\lambda_{\text{max}} = 227.89, 263.27$ .  $^1\text{H}$  NMR

(500 MHz, CDCl<sub>3</sub>)  $\delta$  7.08 (m, 20H), 4.77 (s, 2H); <sup>13</sup>C NMR (125 MHz, CDCl<sub>3</sub>)  $\delta$  143.47, 128.52, 128.15, 125.85, 56.34<sup>20</sup>

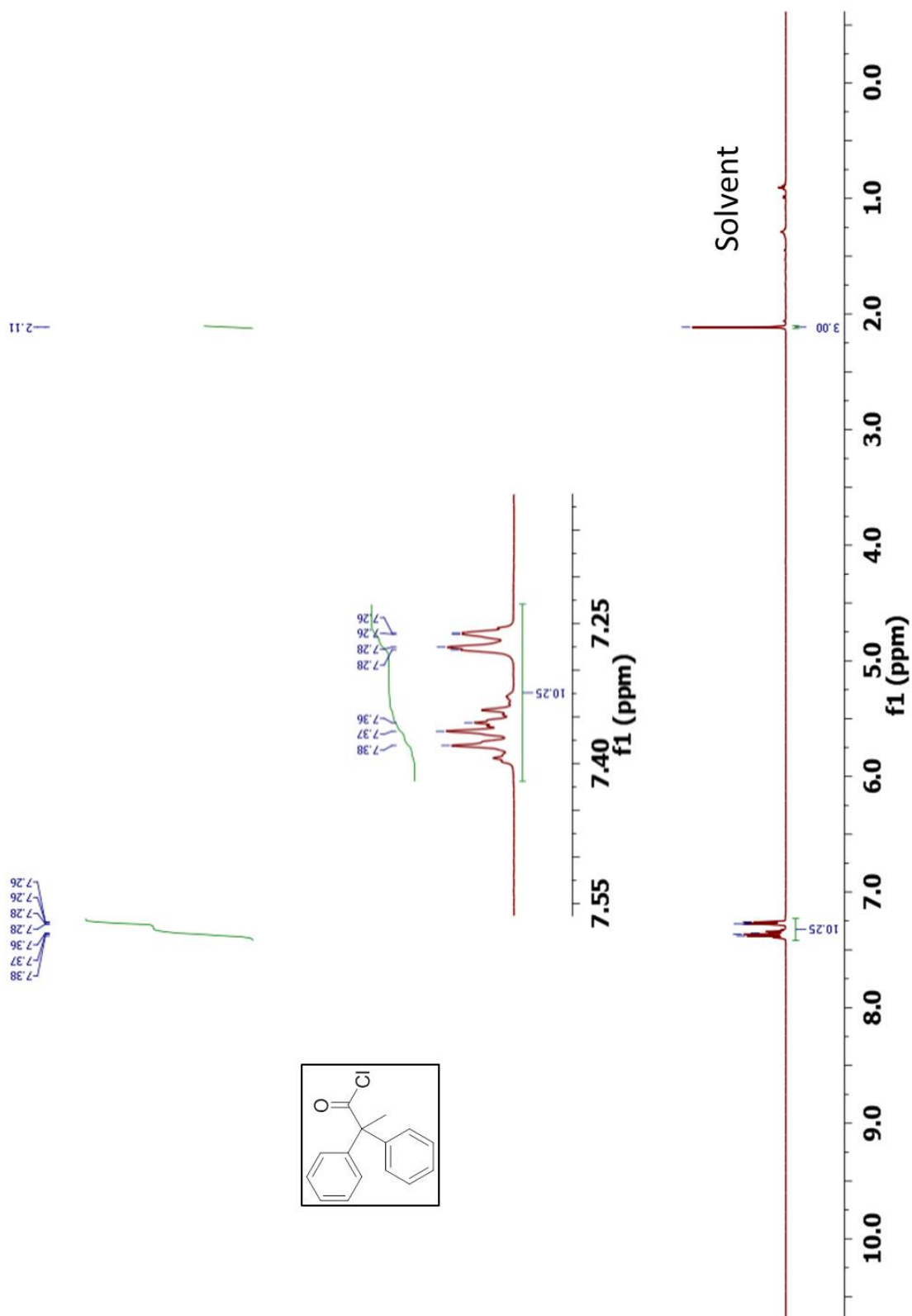
**Propane-1,1,2,2-tetrayltetrabenzene (compound 2b):** Yield <99%. m.p. 68 °C, (lit.<sup>21</sup>, m.p. 68.5-69.5 °C); IR(neat)  $\nu_{\max}$  = 3049, 2018, 1594, 1493, 1443, 1033.  $\lambda_{\max}$  = 227.89, 265.55. <sup>1</sup>H NMR (500 MHz, CDCl<sub>3</sub>)  $\delta$  7.08 (m, 20H), 5.08 (s, 1H), 2.01 (s, 3H); <sup>13</sup>C NMR (125 MHz, CDCl<sub>3</sub>)  $\delta$  148.11, 142.85, 131.01, 128.72, 127.50, 127.39, 125.72, 125.69, 60.75, 50.36, 24.40<sup>21</sup>

**Ethane-1,1,1,2,2-pentaylpentabenzene (compound 2c):** Yield <99%. m.p. 180 °C, (lit.<sup>21</sup>, m.p. 182 °C); IR(neat)  $\nu_{\max}$  = 3057, 2920, 2851, 1597, 1495, 1448, 1031 cm<sup>-1</sup>.  $\lambda_{\max}$  = 219.85, 265.17. <sup>1</sup>H NMR (500 MHz, CDCl<sub>3</sub>)  $\delta$  7.08 (m, 25H), 5.84 (s, 1H); <sup>13</sup>C NMR (125 MHz, CDCl<sub>3</sub>)  $\delta$  145.73, 143.02, 131.74, 131.45, 127.42, 126.99, 125.91, 125.88, 62.68, 59.31<sup>21</sup>

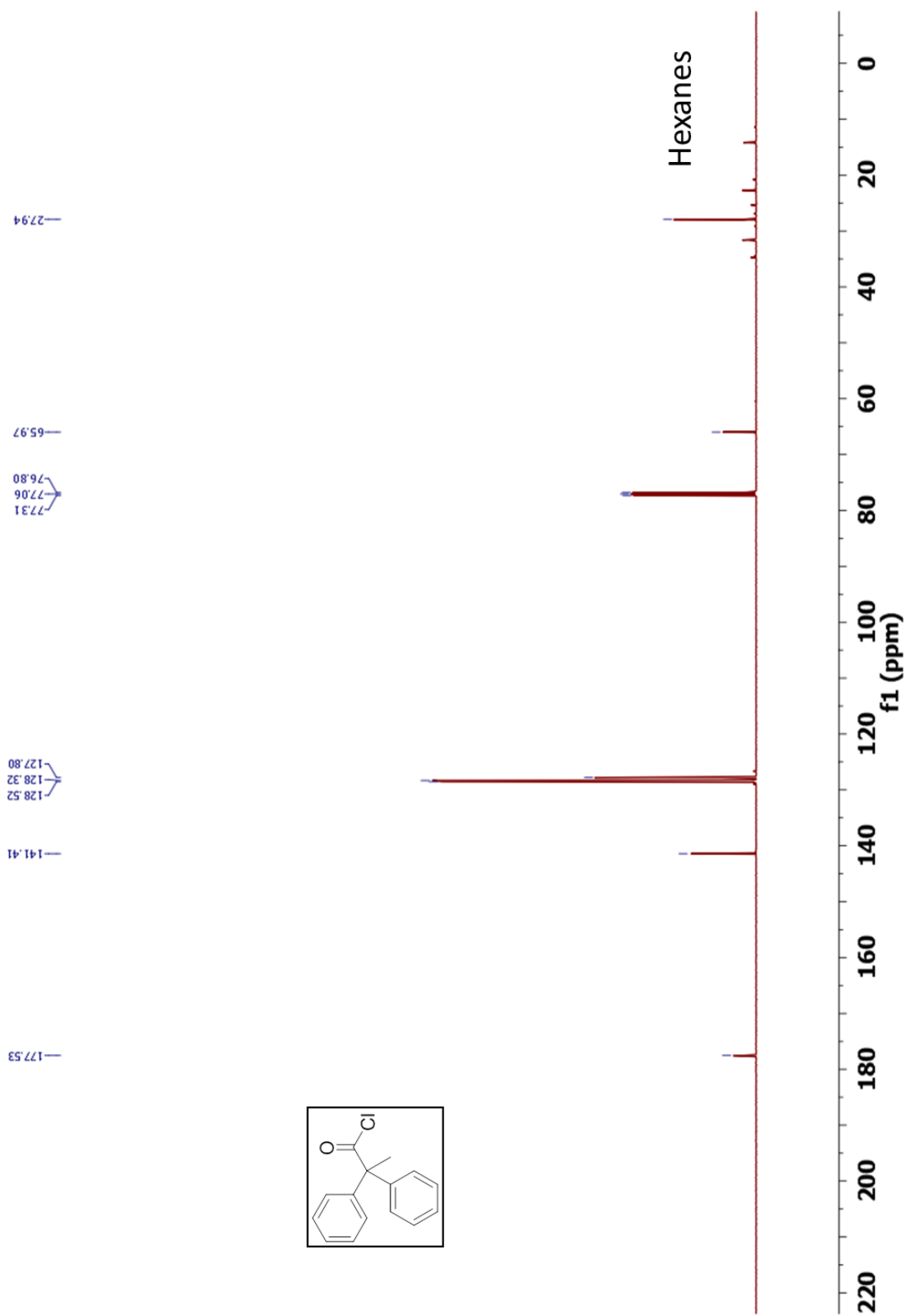


#### 4.5.2). Spectral data ( $^1\text{H}$ NMR, $^{13}\text{C}$ NMR, UV-VIS)

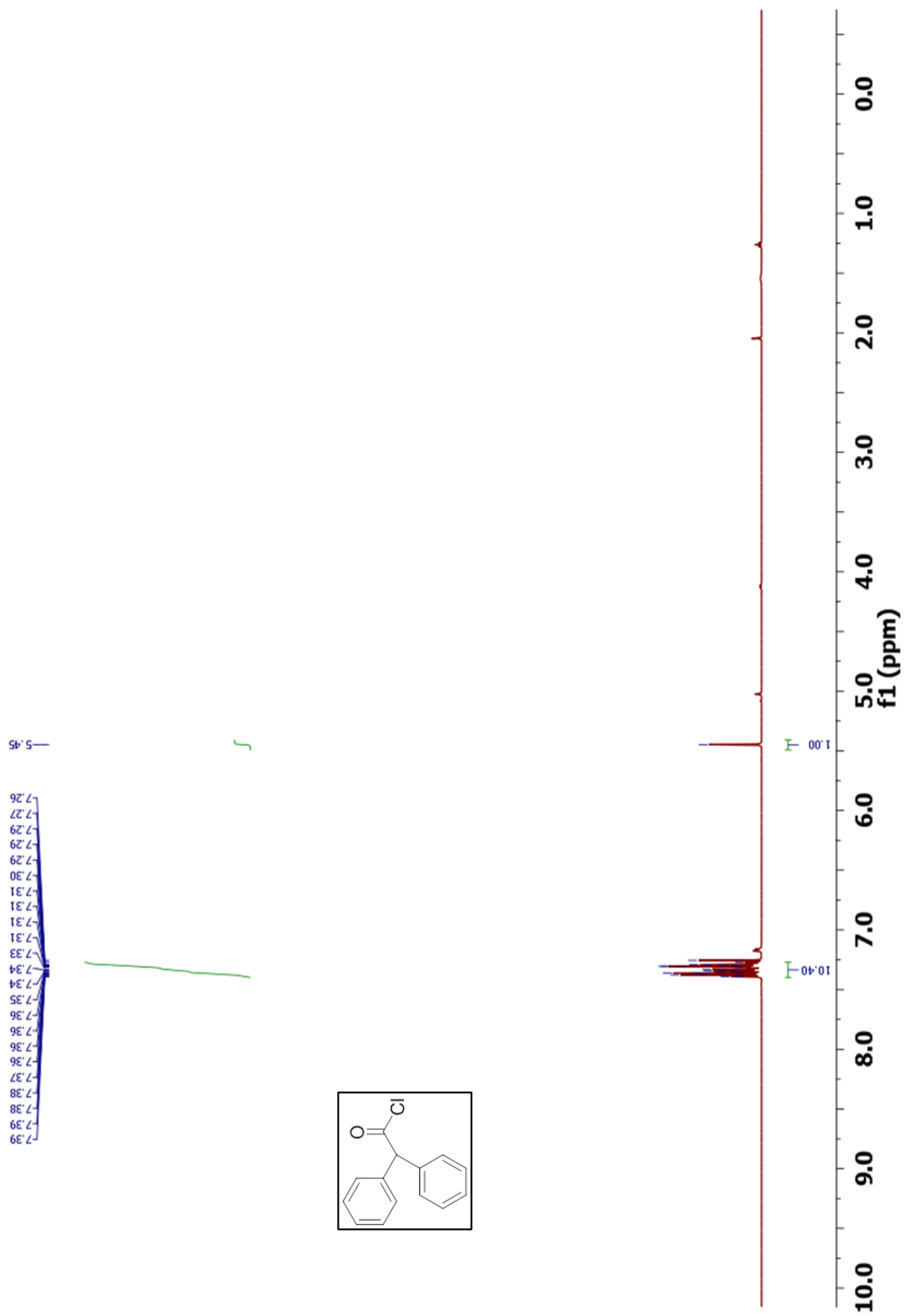
Figure 4.S1.  $^1\text{H}$  NMR (500 MHz,  $\text{CDCl}_3$ ) of 2,2-diphenylpropanoyl chloride



**Figure 4.S2.**  $^{13}\text{C}$  NMR (125 MHz,  $\text{CDCl}_3$ ) of 2,2-diphenylpropanoyl chloride



**Figure 4.S3.**  $^1\text{H}$  NMR (500 MHz,  $\text{CDCl}_3$ ) of 2,2-diphenylacetyl chloride



**Figure 4.S4.**  $^{13}\text{C}$  NMR (125 MHz,  $\text{CDCl}_3$ ) of 2,2-diphenylacetyl chloride

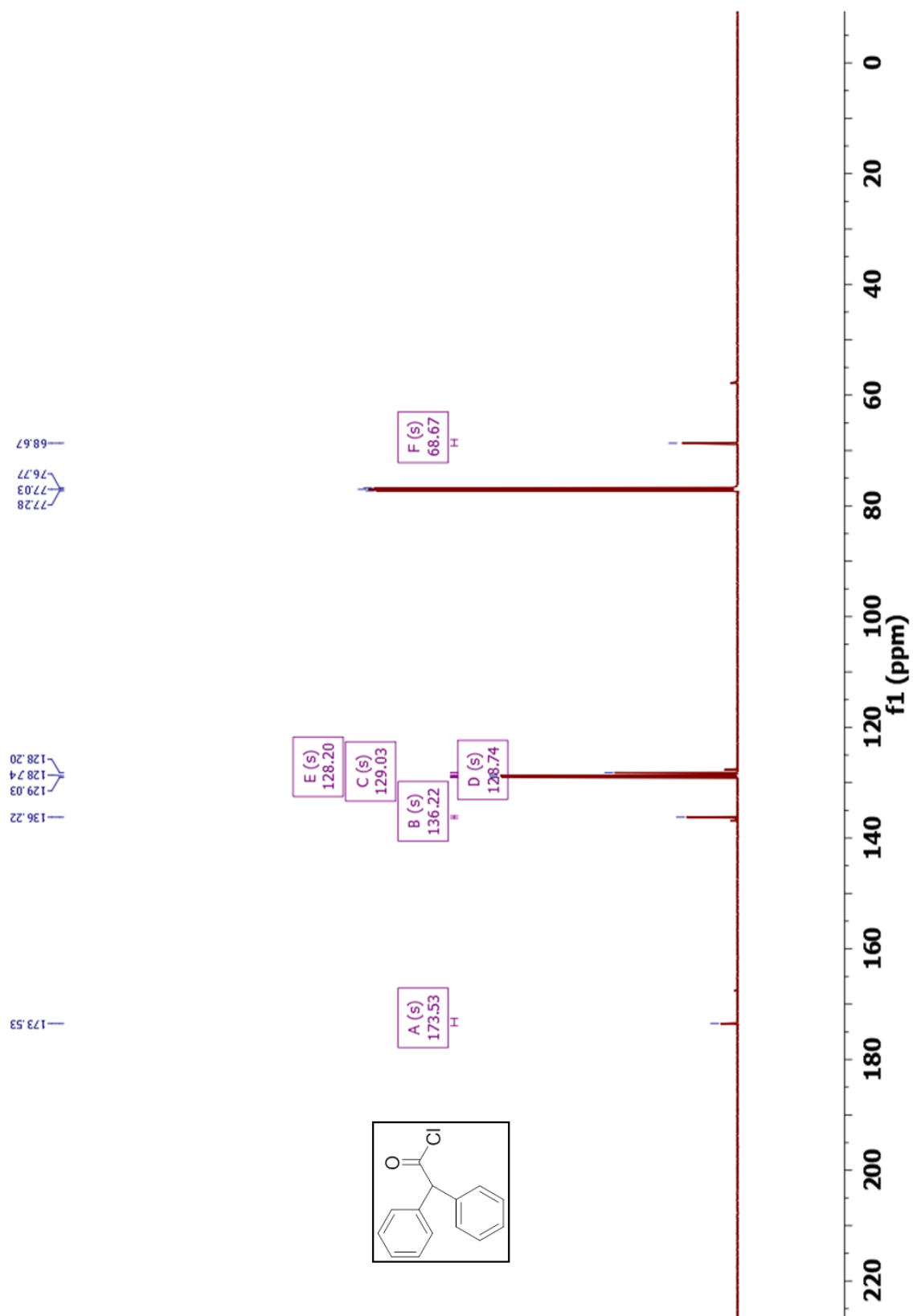
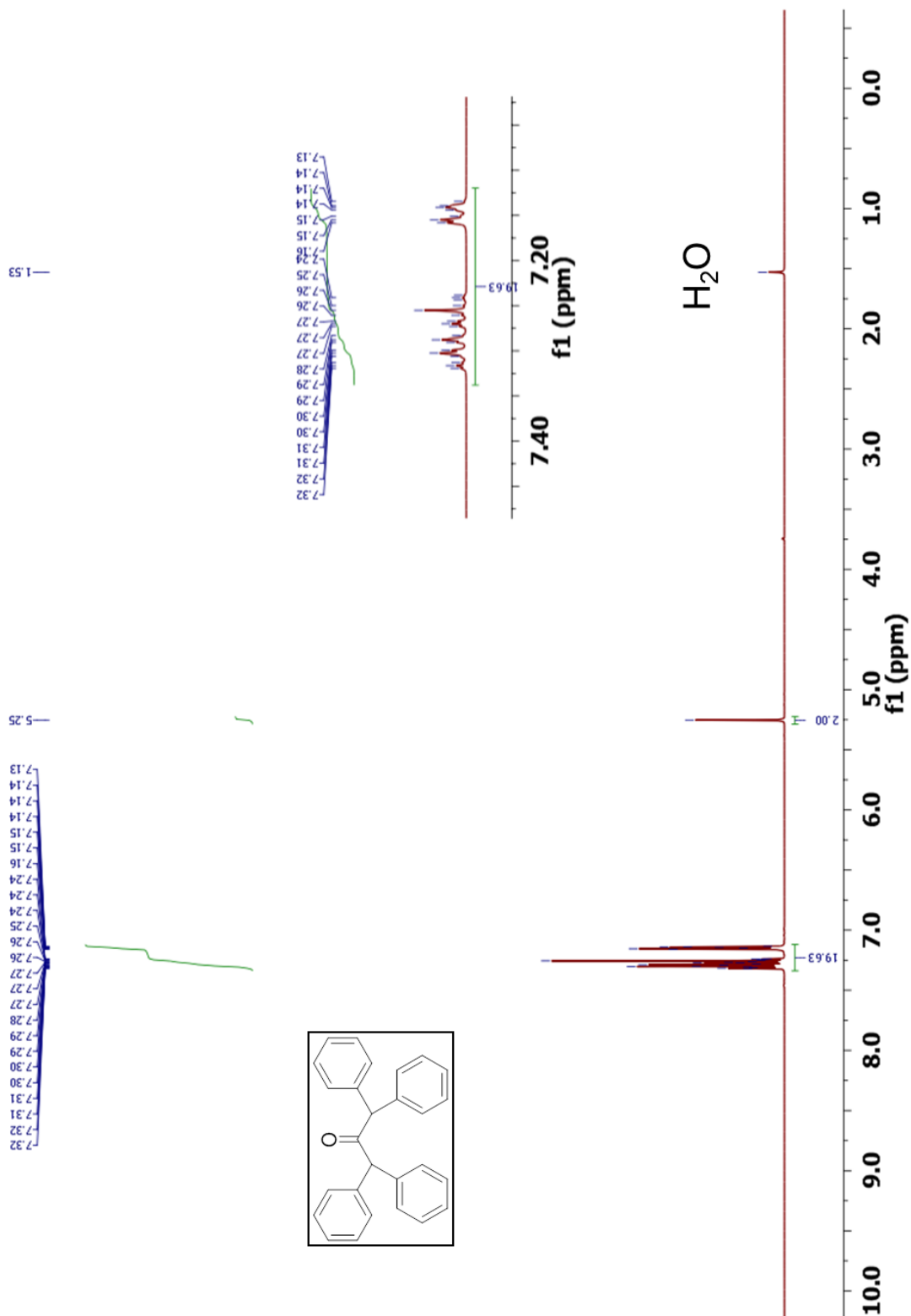


Figure 4.S5.  $^1\text{H}$  NMR (500 MHz,  $\text{CDCl}_3$ ) of 1,1,3,3-tetraphenylpropan-2-one



**Figure 4.S6.**  $^{13}\text{C}$  NMR (125 MHz,  $\text{CDCl}_3$ ) of 1,1,3,3-tetraphenylpropan-2-one

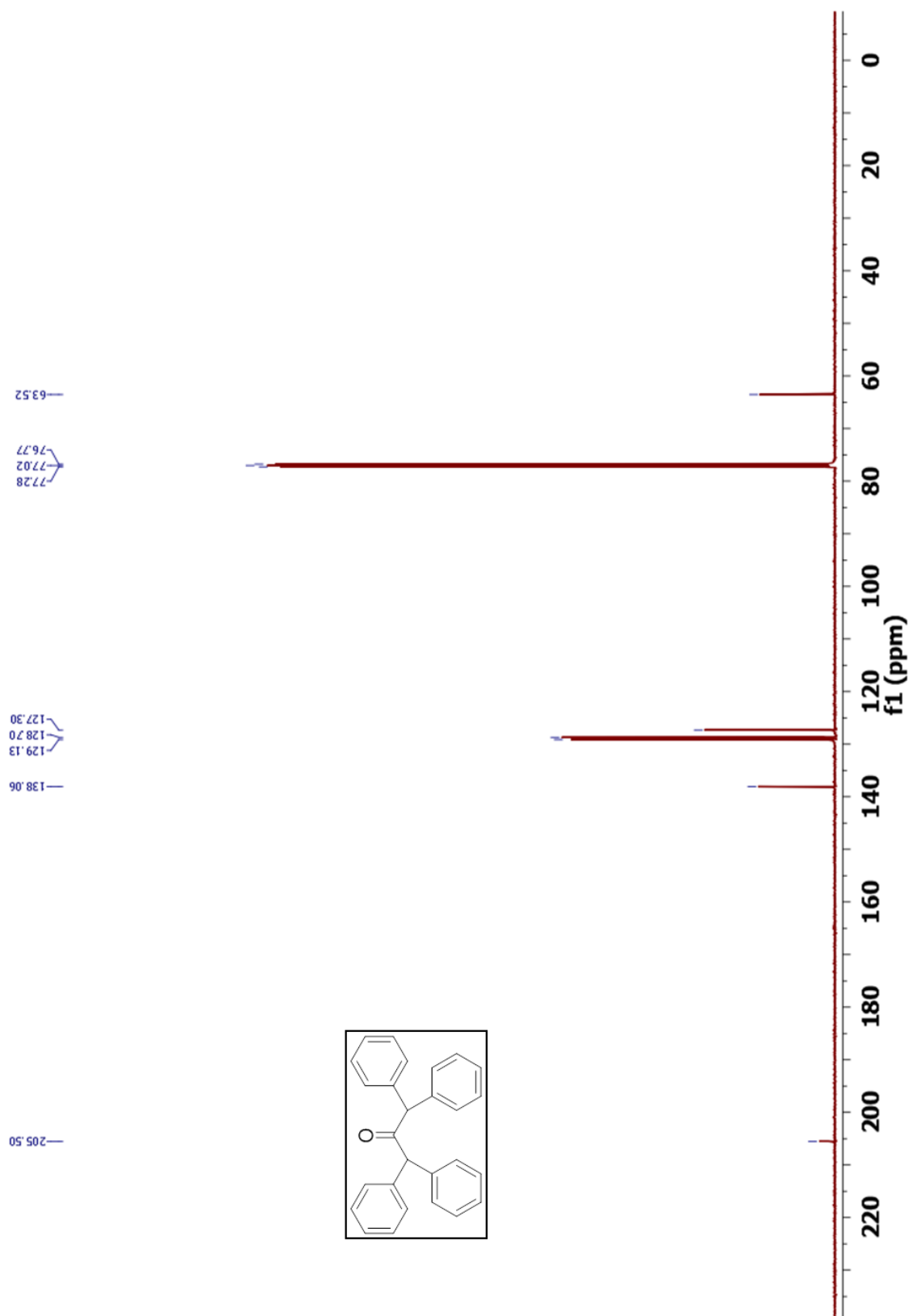
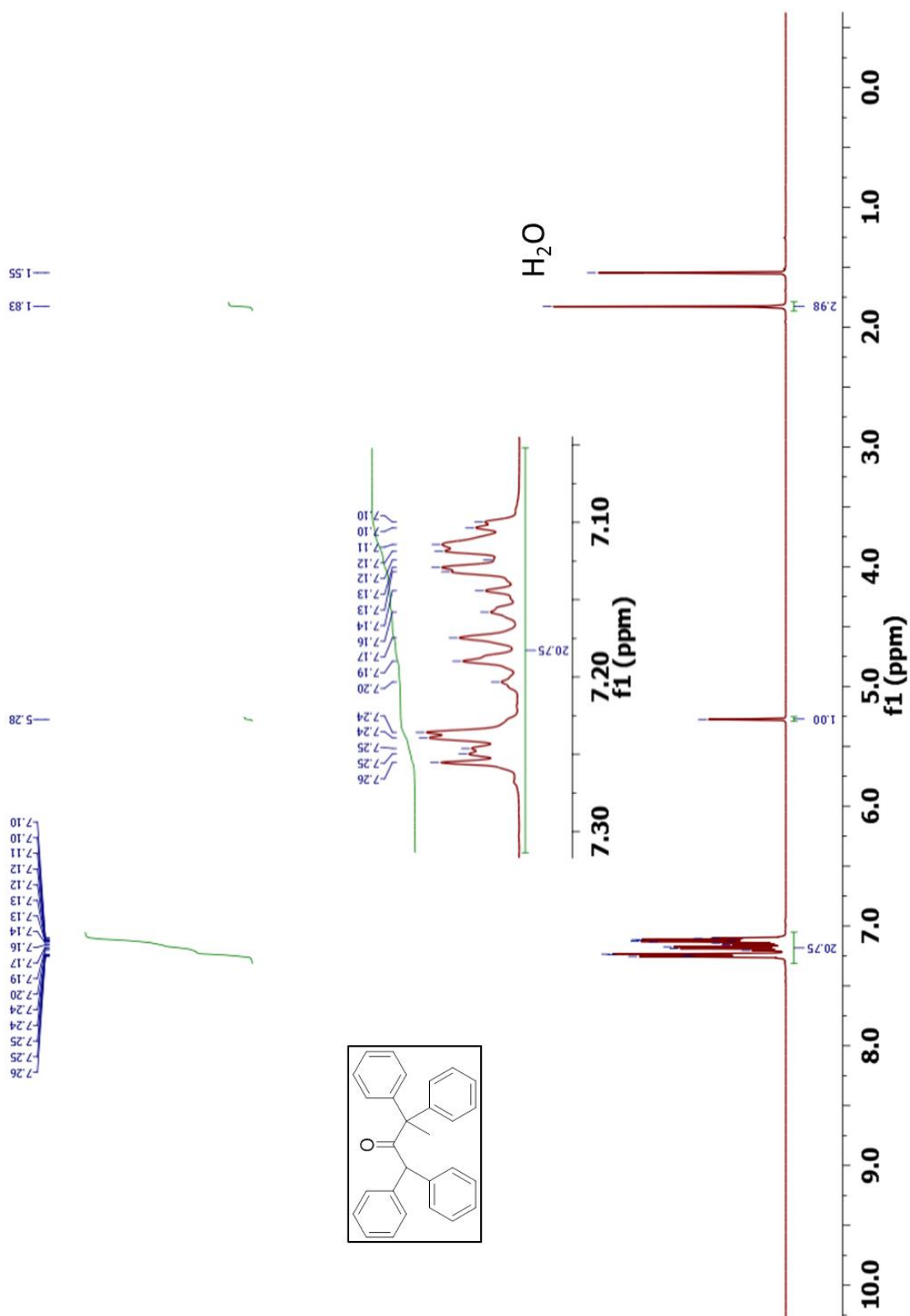
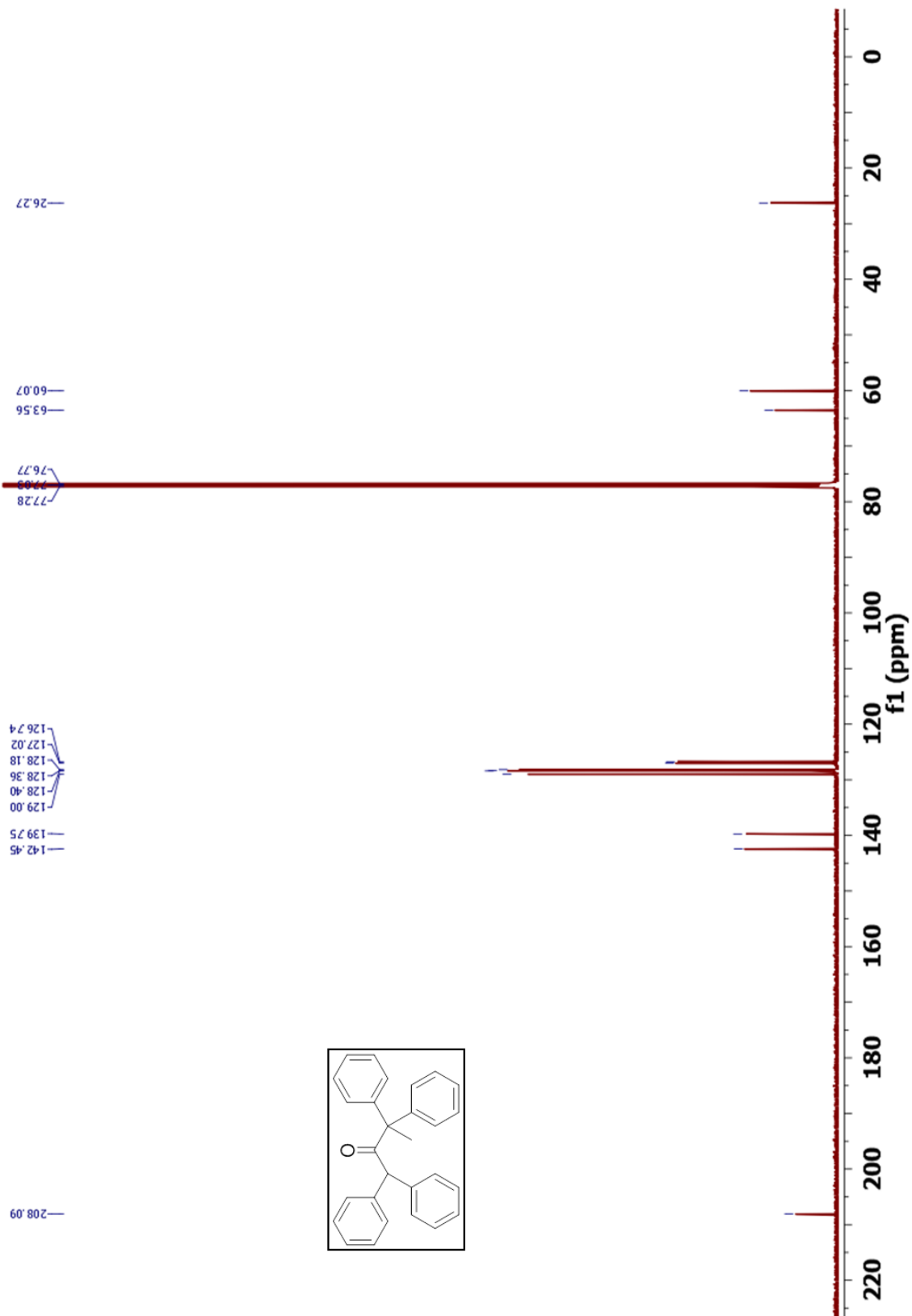


Figure 4.S7.  $^1\text{H}$  NMR (500 MHz,  $\text{CDCl}_3$ ) of 1,1,3,3-tetraphenylbutan-2-one

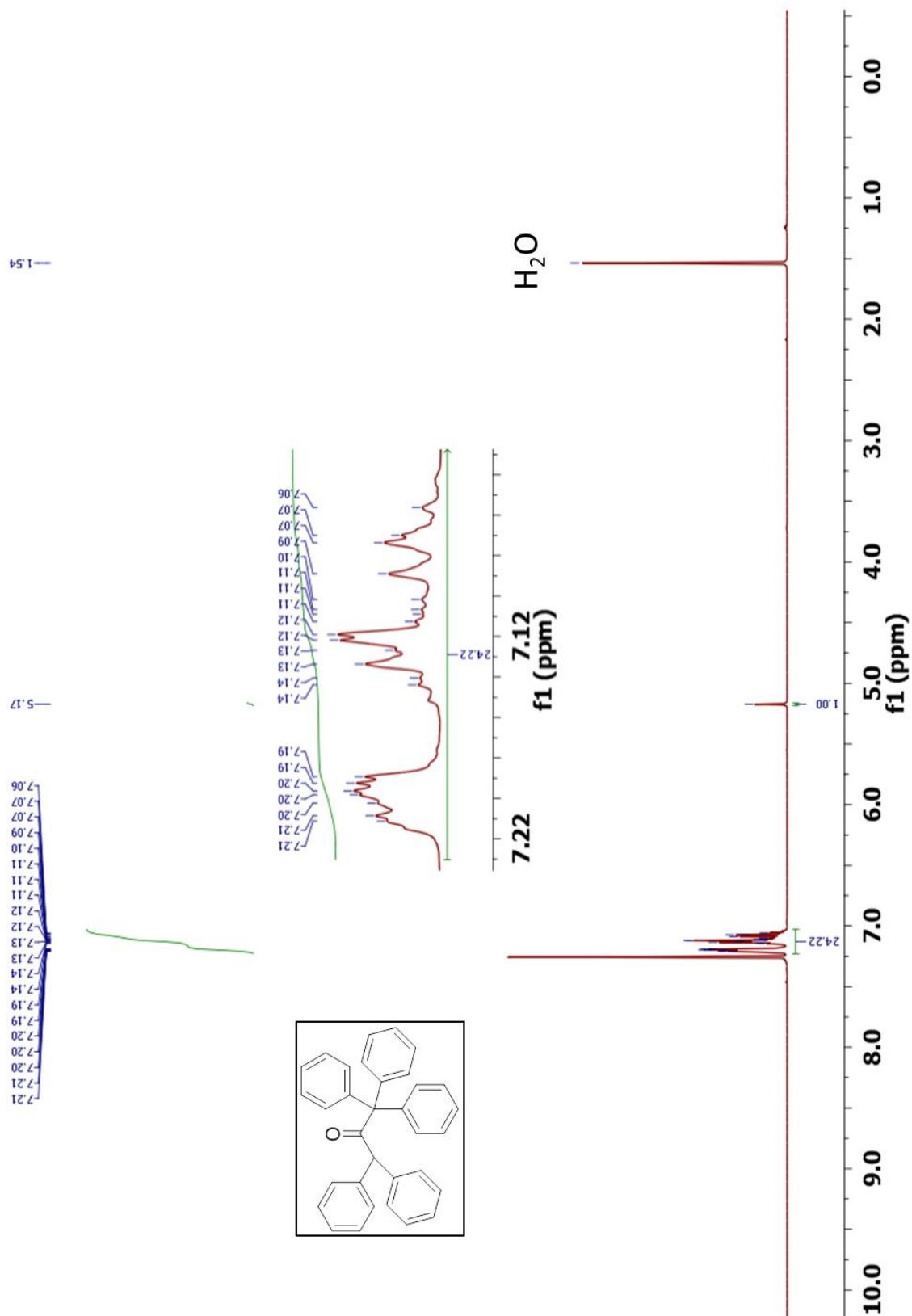


**Figure 4.S8.**  $^{13}\text{C}$  NMR (125 MHz,  $\text{CDCl}_3$ ) of 1,1,3,3-tetraphenylbutan-2-one





**Figure 4.S9.**  $^1\text{H}$  NMR (500 MHz,  $\text{CDCl}_3$ ) of 1,1,1,3,3-pentaphenylpropan-2-one



**Figure 4.S10.**  $^{12}\text{C}$  NMR (125 MHz,  $\text{CDCl}_3$ ) of 1,1,1,3,3-pentaphenylpropan-2-one

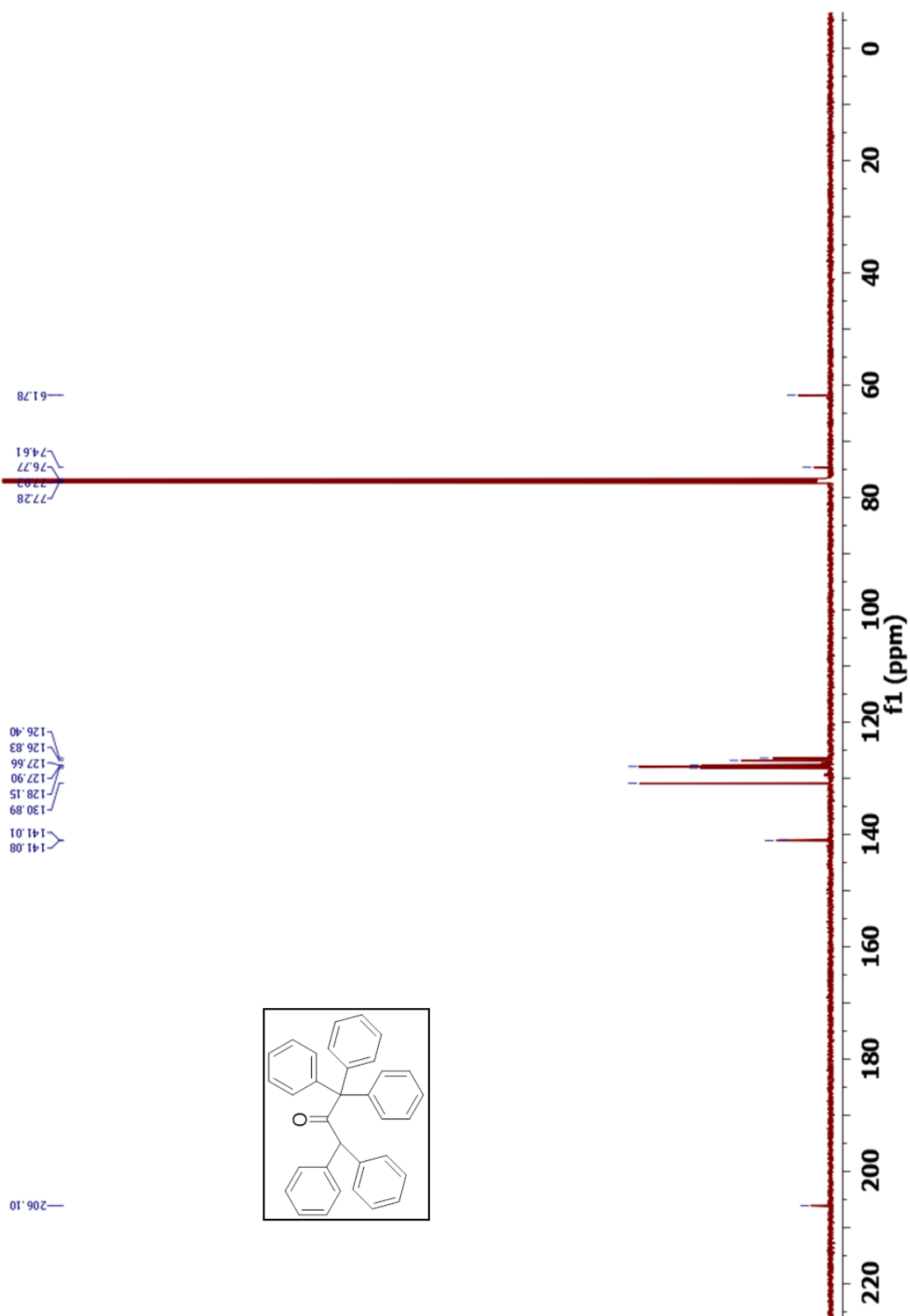


Figure 4.S11.  $^1\text{H}$  NMR (500 MHz,  $\text{CDCl}_3$ ) of 1,1,2,2-tetraphenylethane<sup>5a</sup>

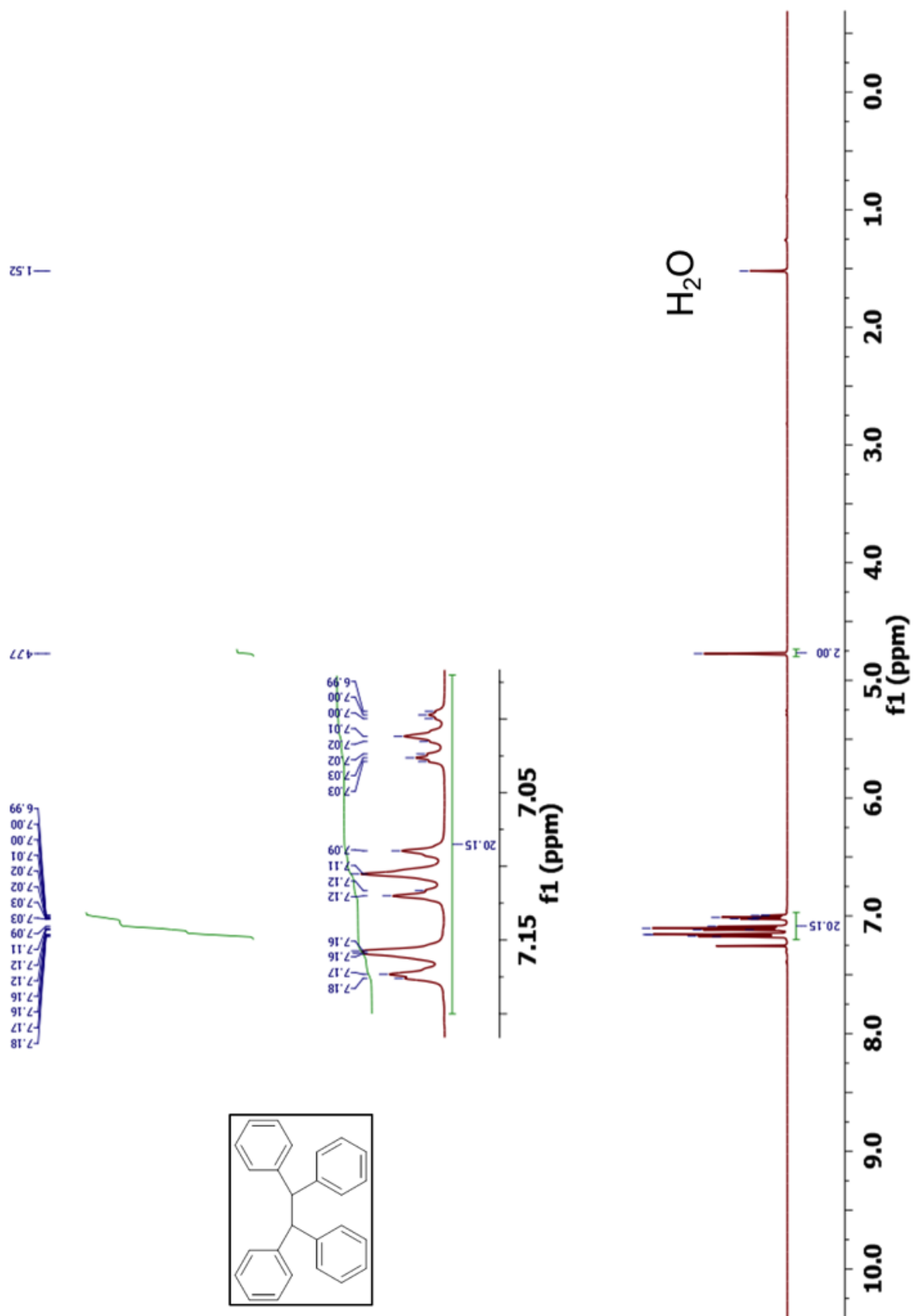
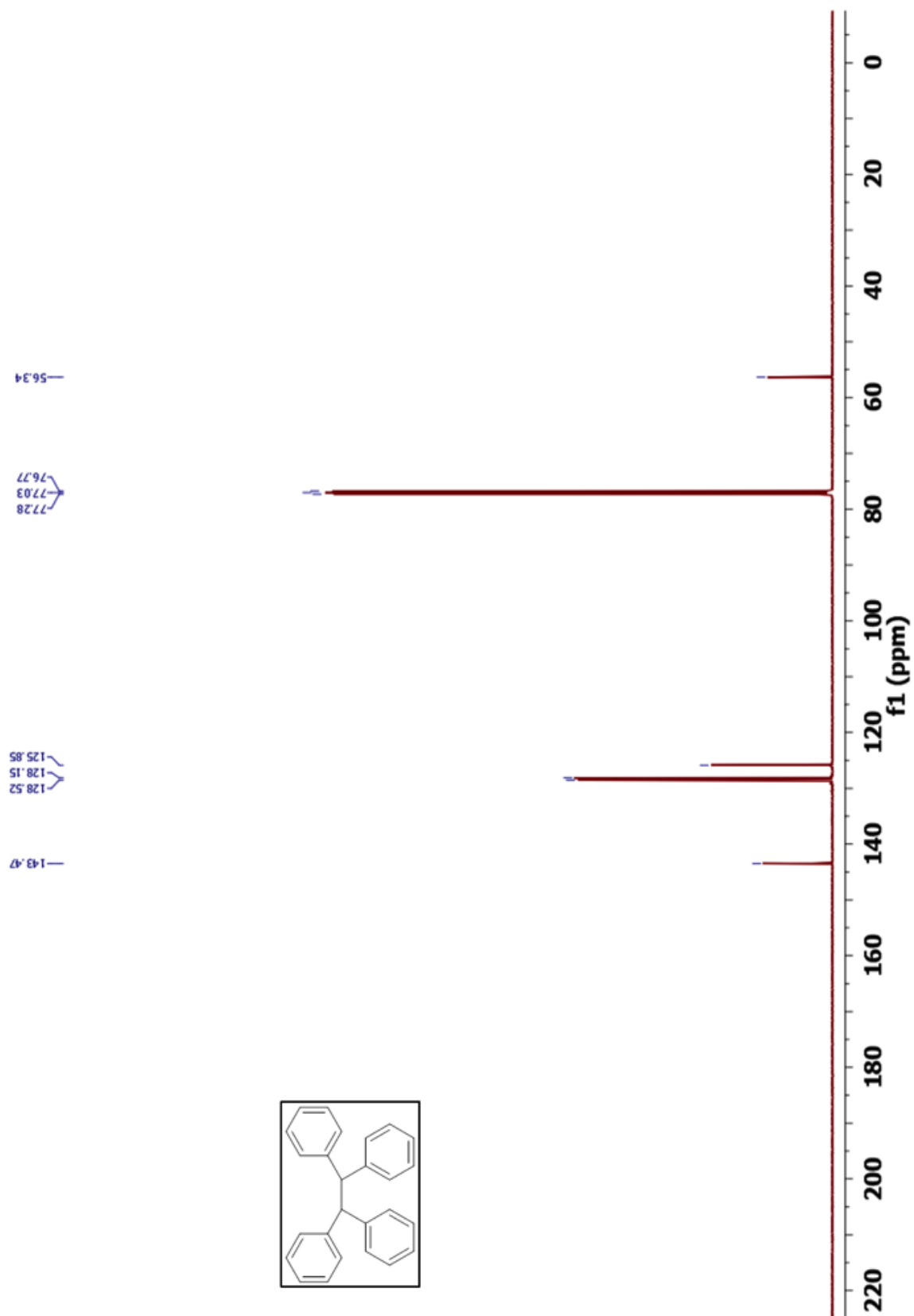


Figure 4.S12:  $^{13}\text{C}$  NMR (125 MHz,  $\text{CDCl}_3$ ) of 1,1,2,2-tetraphenylethane<sup>21a</sup>



**Figure 4.S13.**  $^1\text{H}$  NMR (500 MHz,  $\text{CDCl}_3$ ) of propane-1,1,2,2-tetrayltetrabenzene

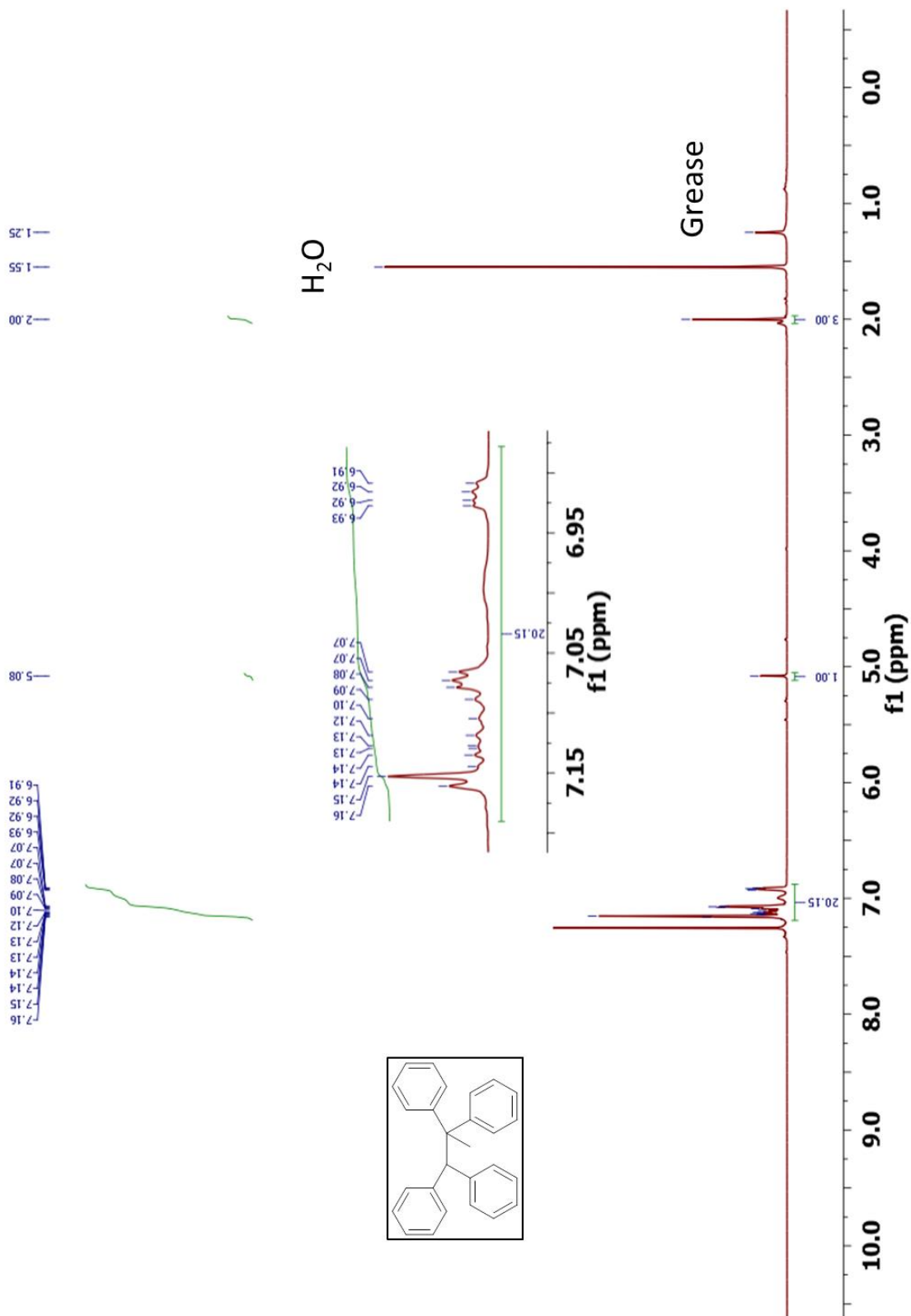
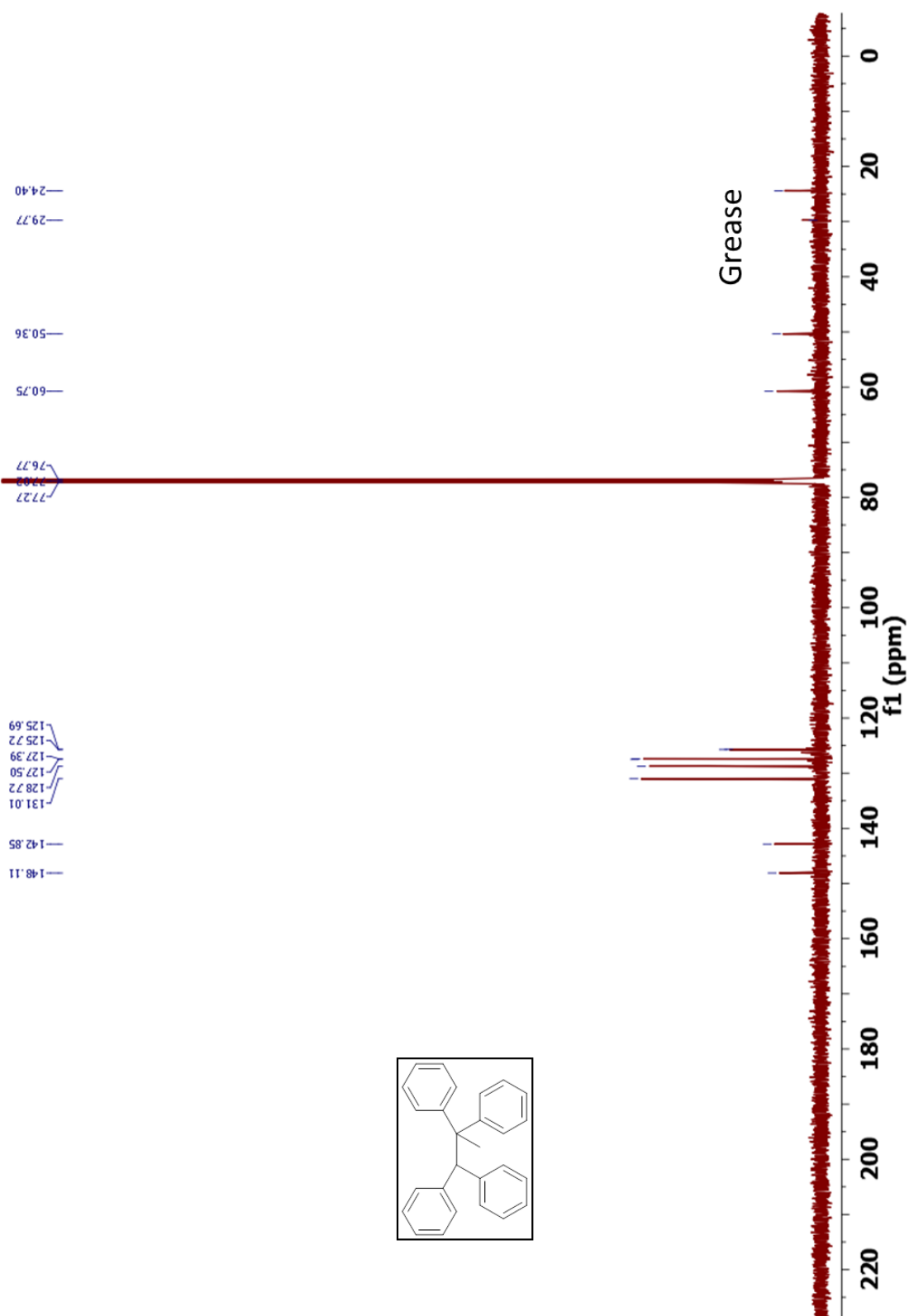
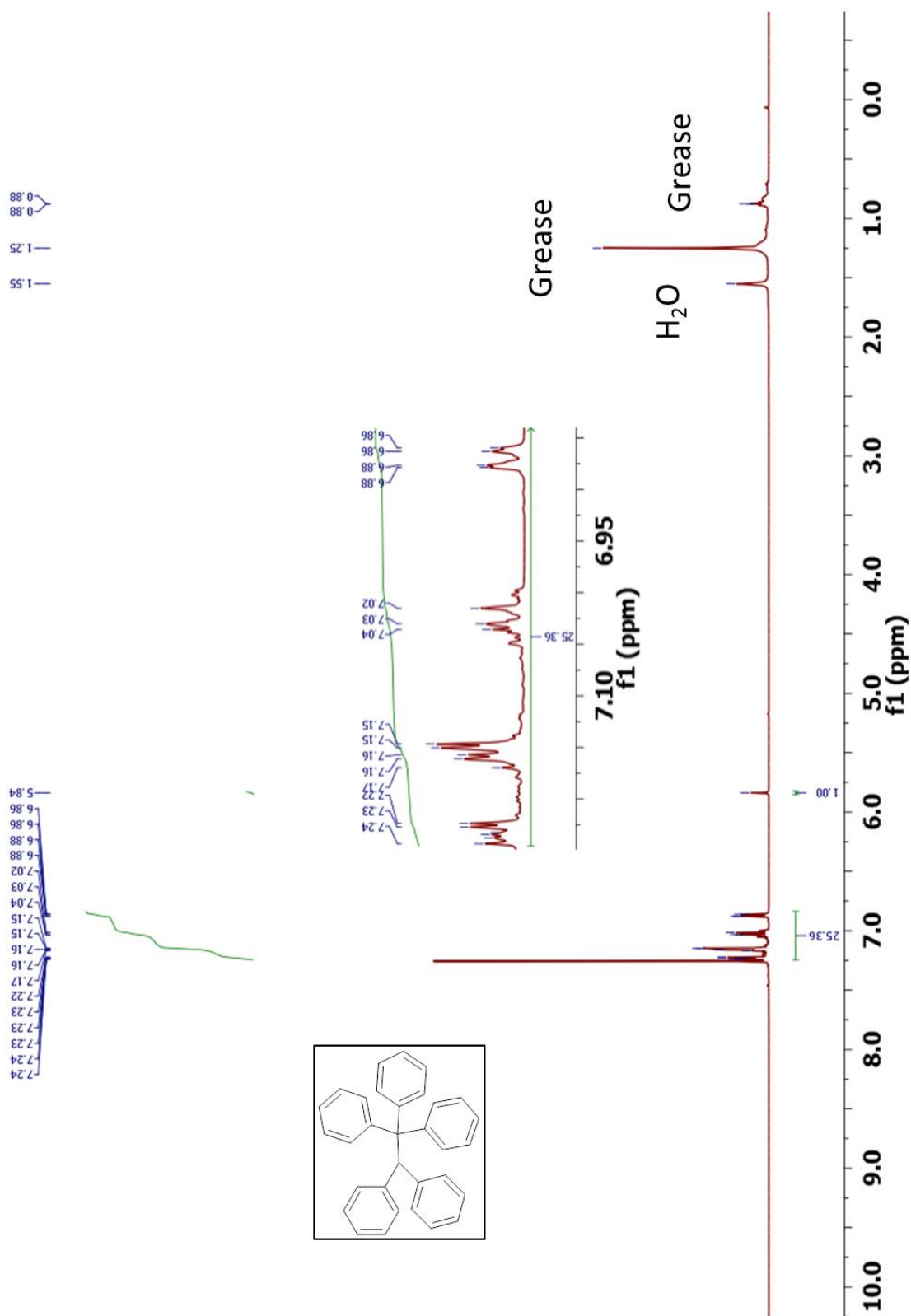


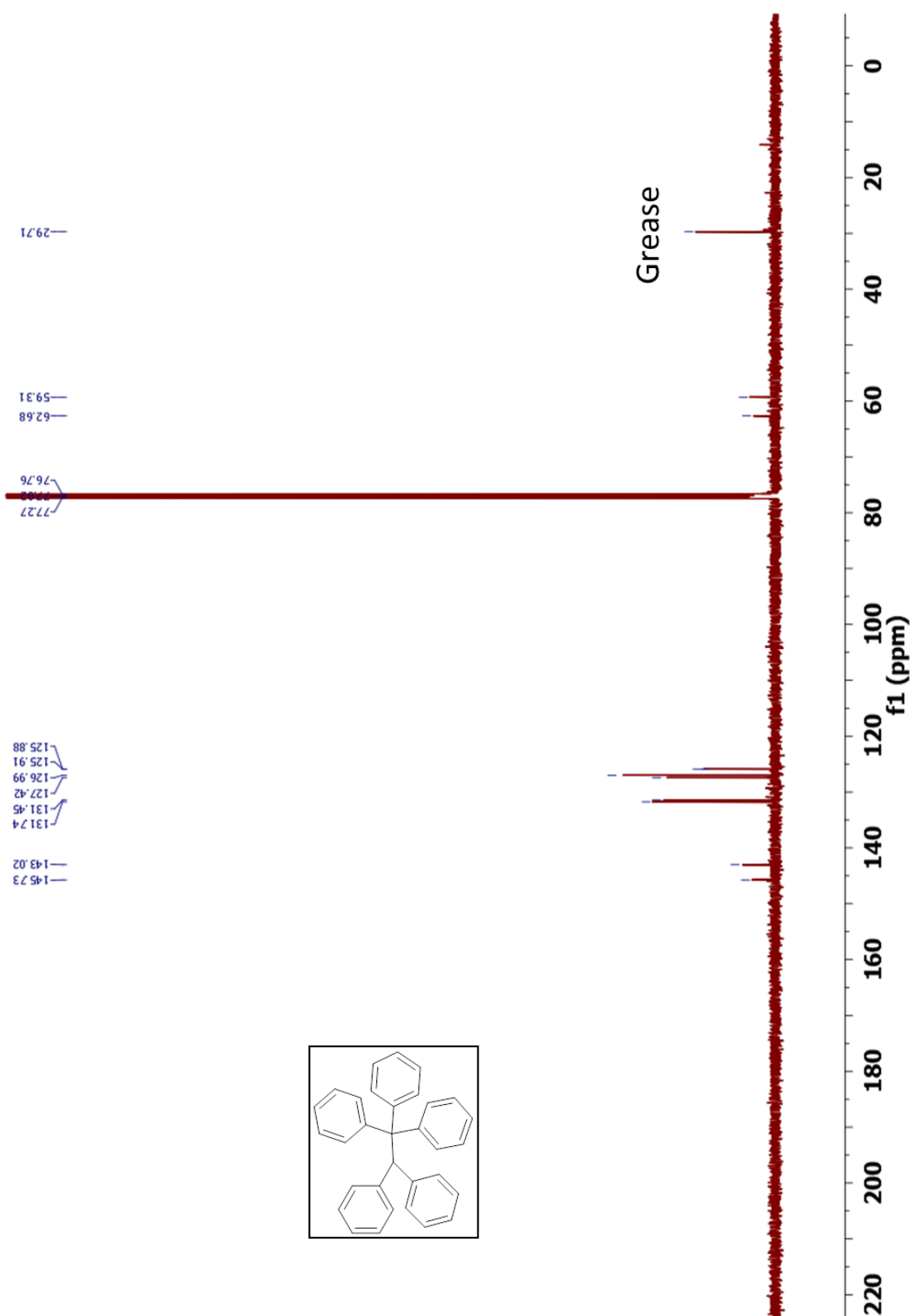
Figure 4.S14.  $^{13}\text{C}$  NMR (125 MHz,  $\text{CDCl}_3$ ) of propane-1,1,2,2-tetrayltetrabenzene



**Figure 4.S15.**  $^1\text{H}$  NMR (500 MHz,  $\text{CDCl}_3$ ) of ethane-1,1,1,2,2-pentaylpentabenzene

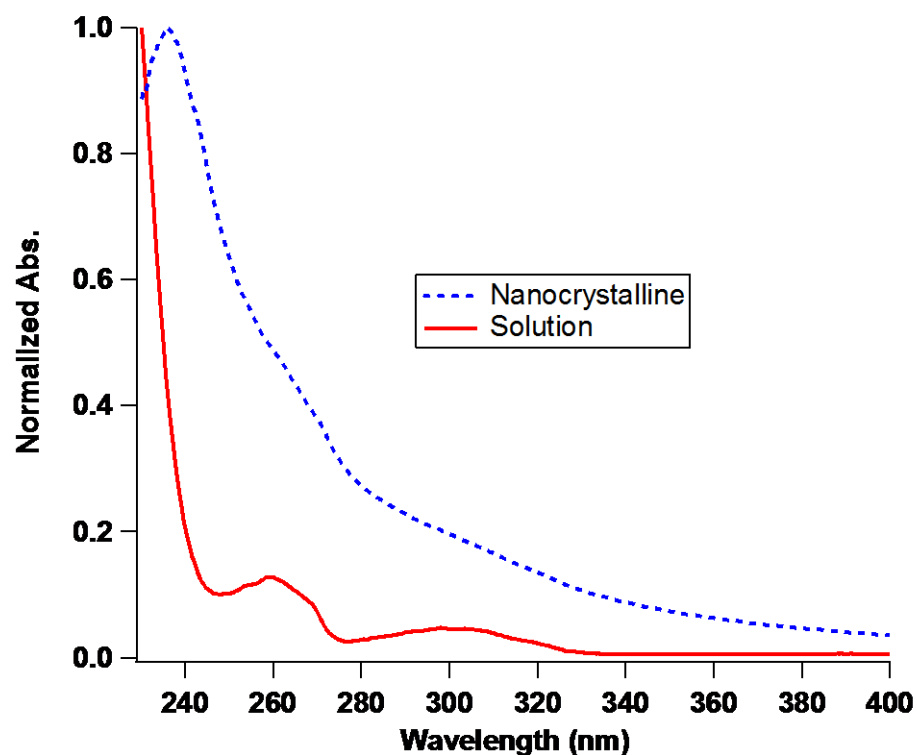


**Figure 4.S16.**  $^{13}\text{C}$  NMR (125 MHz,  $\text{CDCl}_3$ ) of ethane-1,1,1,2,2-pentaylpentabenzene

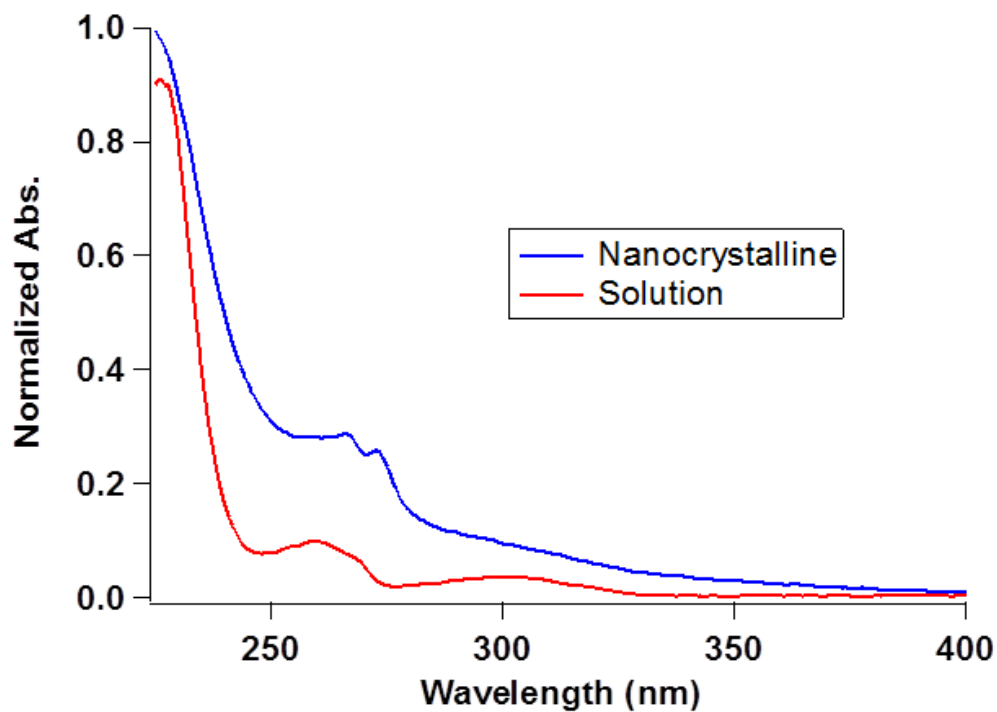




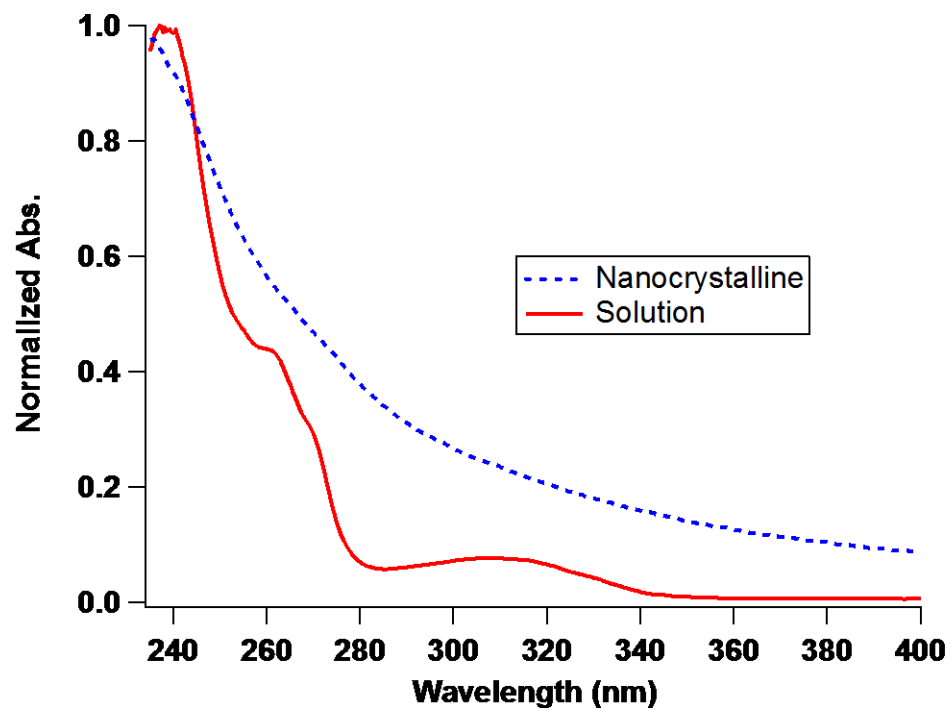
### UV Spectra



**Figure 4.S17:** UV-vis of 1,1,3,3-tetraphenylpropan-2-one in MeCN (0.1 g/L) and in nano crystalline suspensions (0.0025 g/L)

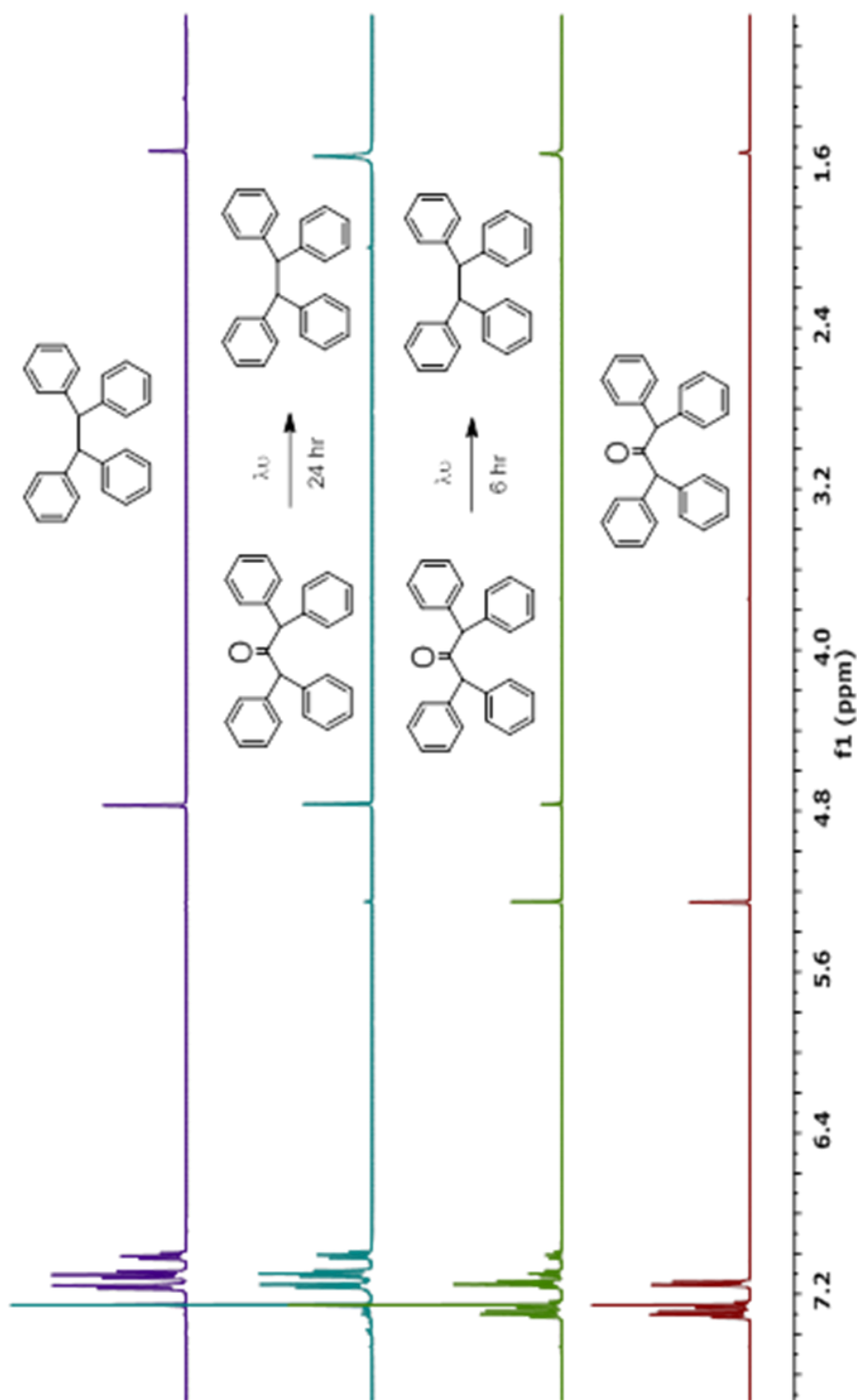


**Figure 4.S18:** UV-vis of 1,1,3,3-tetraphenylbutan-2-one in MeCN (0.1 g/L) and in nano crystalline suspensions (0.0025 g/L)

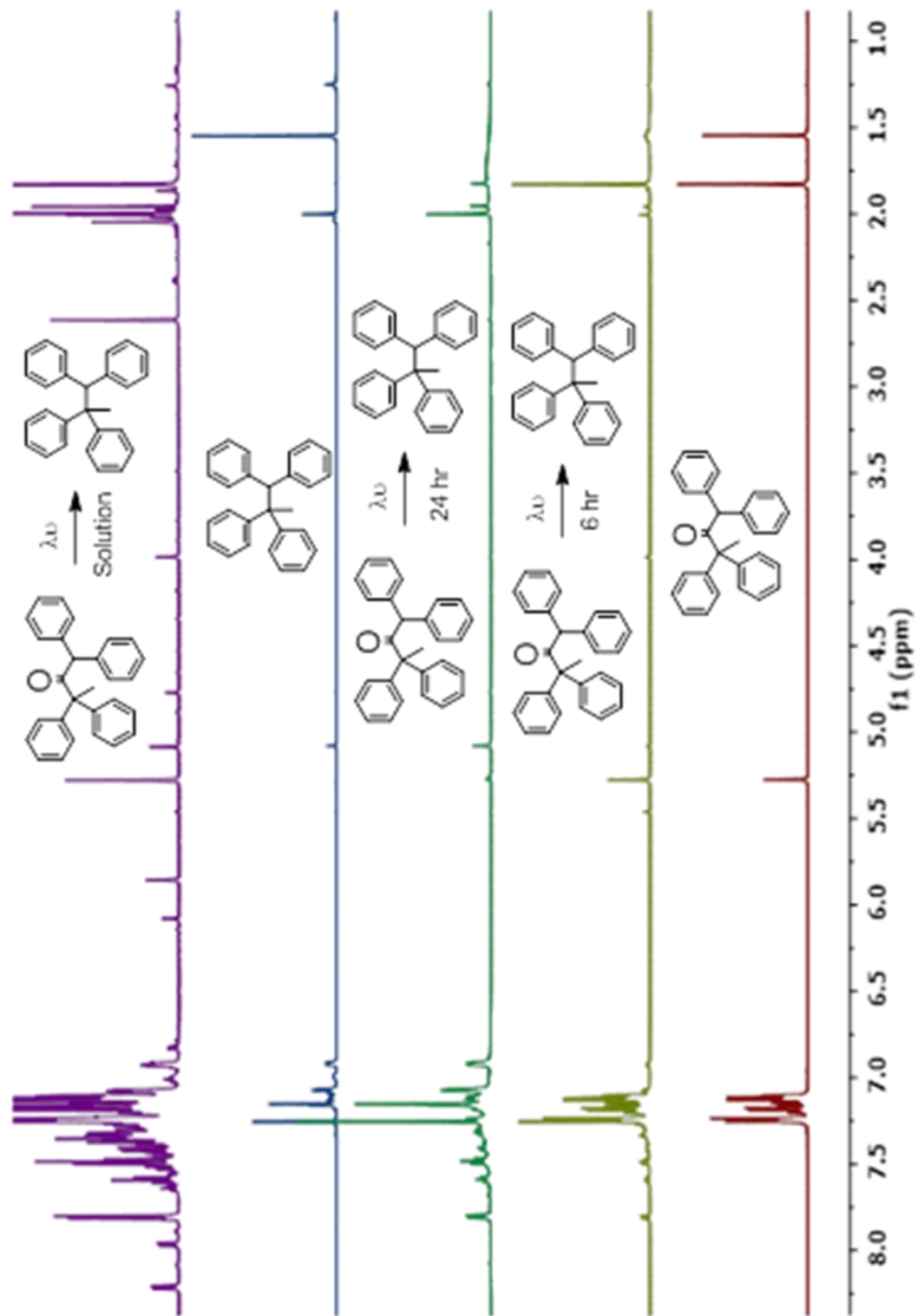


**Figure 4.S19:** UV-vis of 1,1,1,3,3-pentaphenylpropan-2-one in MeCN (0.1 g/L) and in nano crystalline suspensions (0.0025 g/L)

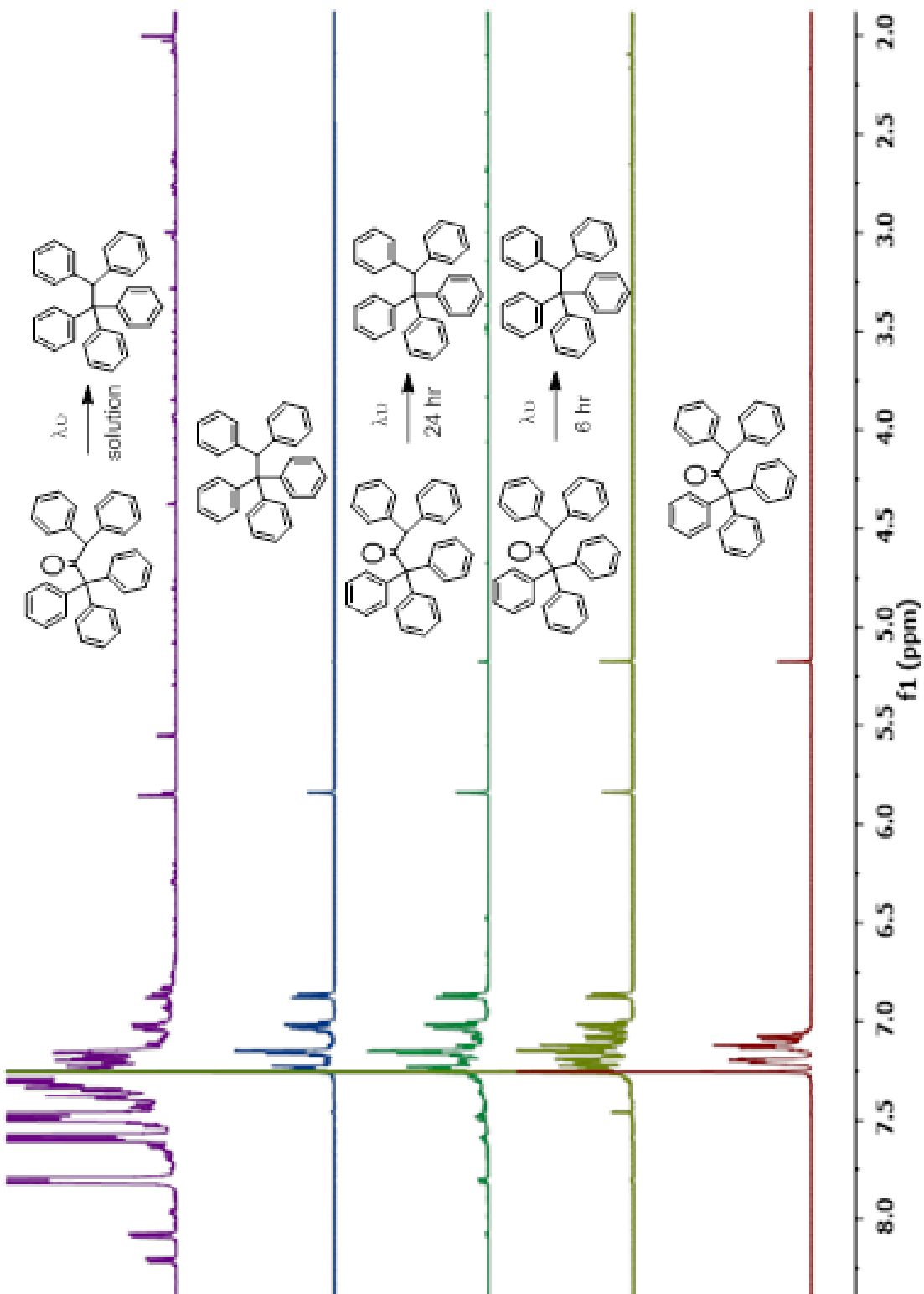
### 4.5.3). Solid-State Photochemistry of Dry Powder



**Figure 4.S20:** <sup>1</sup>H NMR (500 MHz, CDCl<sub>3</sub>) product analysis of 1,1,3,3-tetraphenylpropan-2-one to 1,1,2,2-tetraphenylethane in the solid state

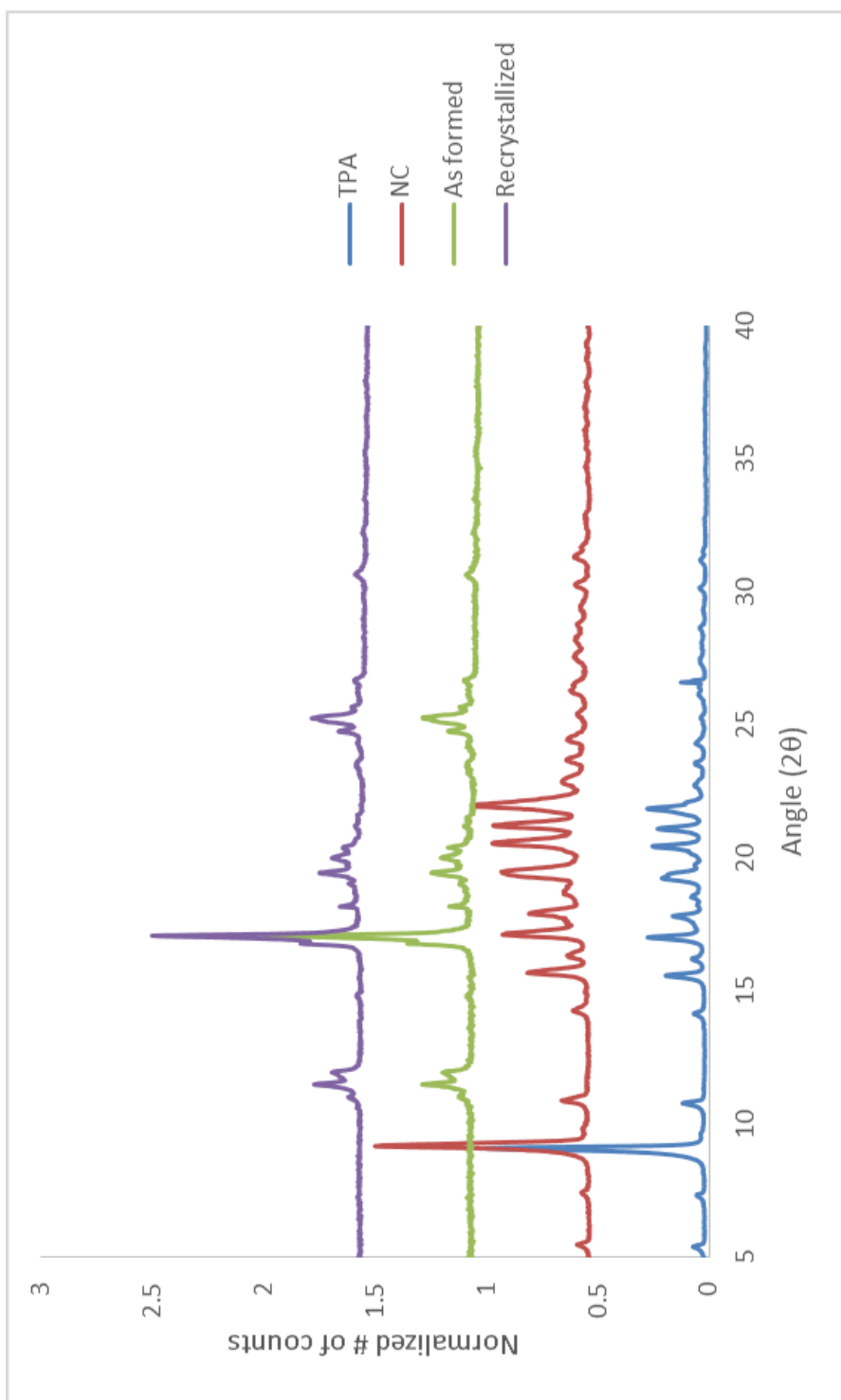


**Figure 4.S21:**  $^1\text{H}$  NMR (500 MHz,  $\text{CDCl}_3$ ) product analysis of 1,1,3,3-tetraphenylbutan-2-one to propane-1,1,2,2-tetra(phenyl)tetra(phenyl) in the solid and solution state

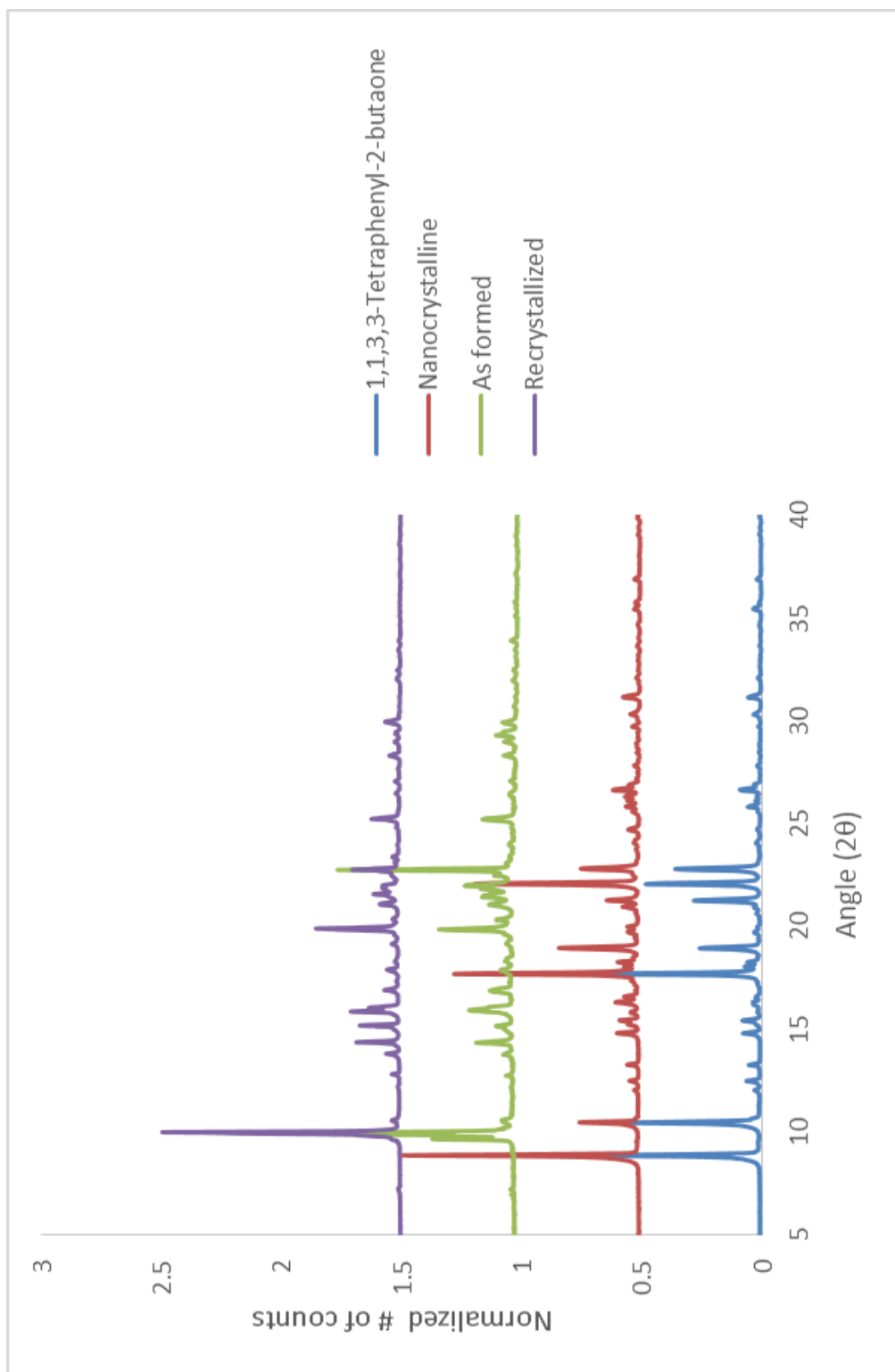


**Figure 4.S22:** <sup>1</sup>H NMR (500 MHz, CDCl<sub>3</sub>) product analysis of 1,1,1,3,3-pentaphenylpropan-2-one to ethane-1,1,1,2,2-pentaylpentabenzene in the solid and solution state

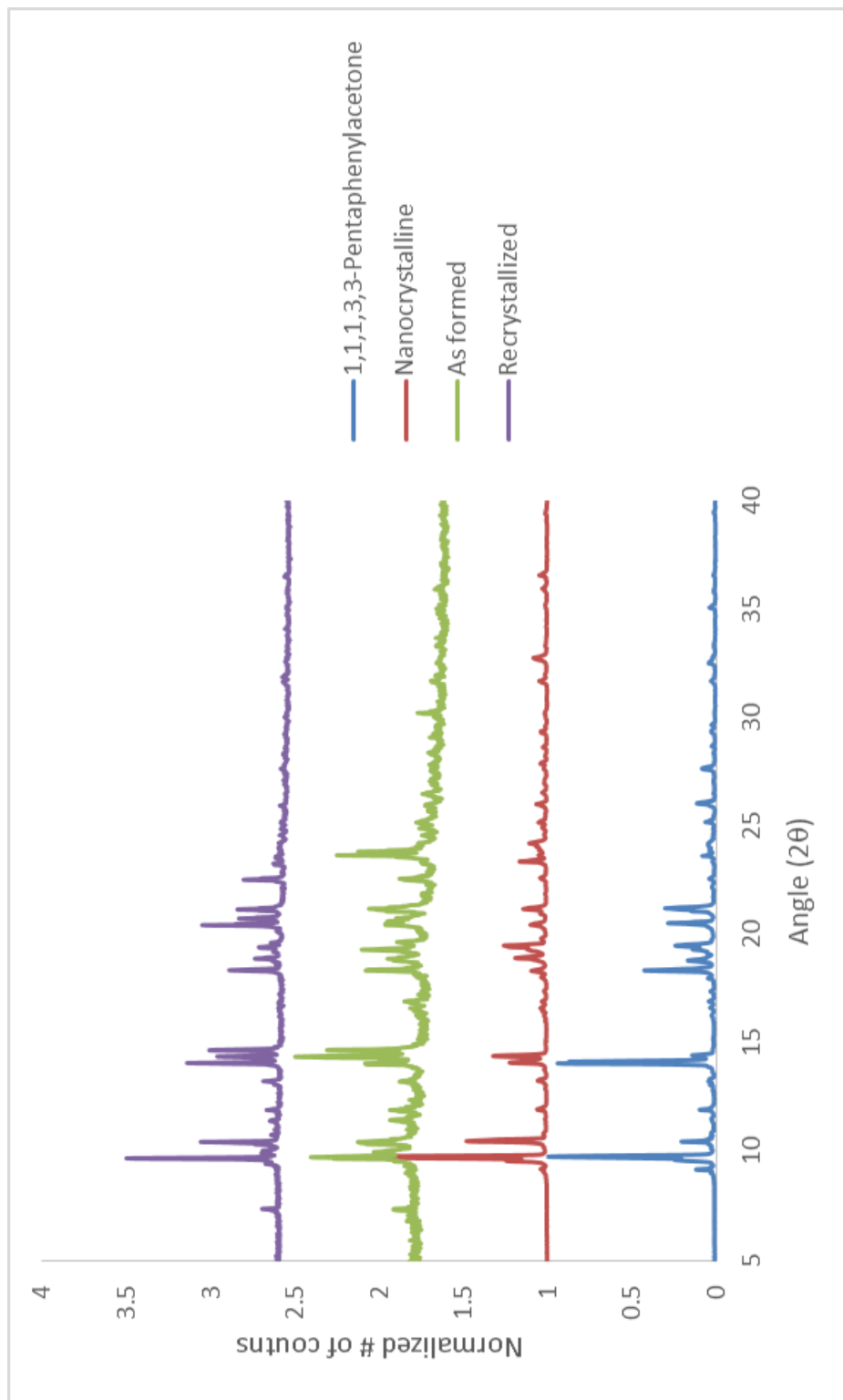
#### 4.5.4). Power X-Ray Diffraction (PXRD) Analysis



**Figure 4.S23:** Powder X-Ray Diffraction (PXRD) of 1,1,3,3-tetraphenylpropan-2-one in the bulk solid and nanocrystalline suspensions; 1,1,2,2-Tetraphenylethane as formed and recrystallized in ethanol.



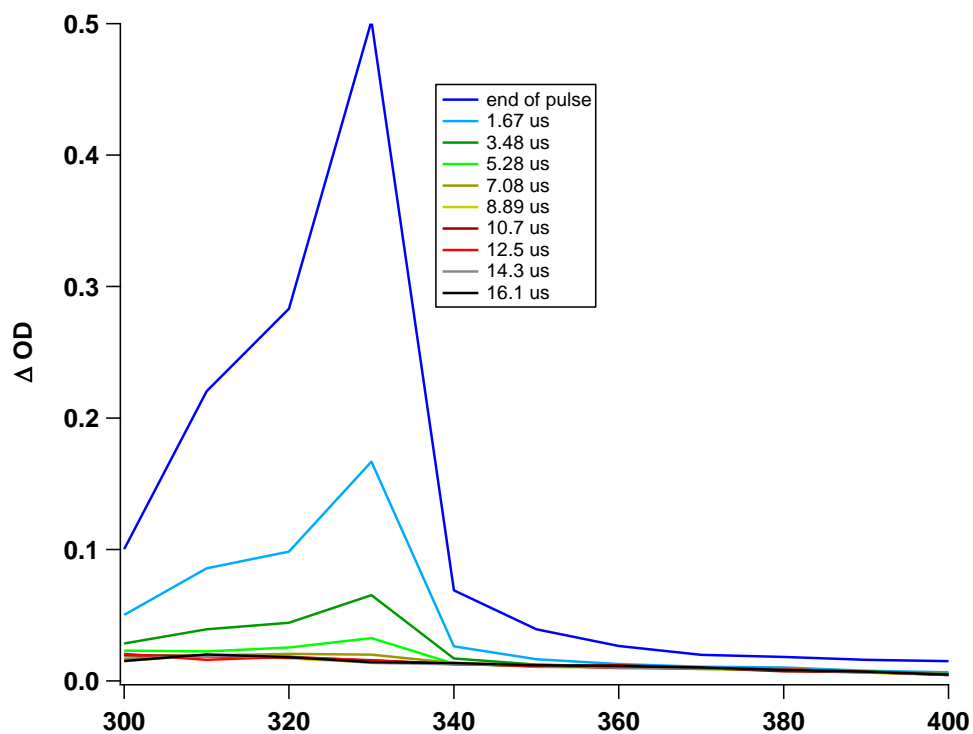
**Figure 4.S24:** Powder X-Ray Diffraction (PXRD) of 1,1,3,3-tetraphenylbutan-2-one in the bulk solid and nanocrystalline suspensions; Propane-1,1,2,2-tetrahydrobenzene as formed and recrystallized in ethanol.



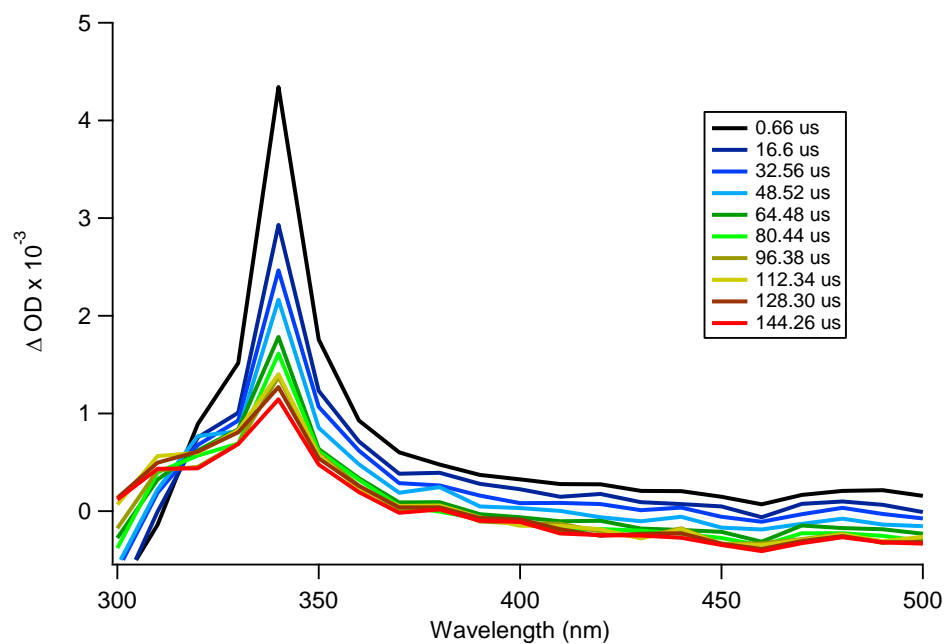
**Figure 4.S25:** Powder X-Ray Diffraction (PXRD) of 1,1,1,3,3-pentaphenylpropan-2-one in the bulk solid and nanocrystalline suspensions; ethane-1,1,1,2,2-pentaylpentabenzene as formed and recrystallized in ethanol.



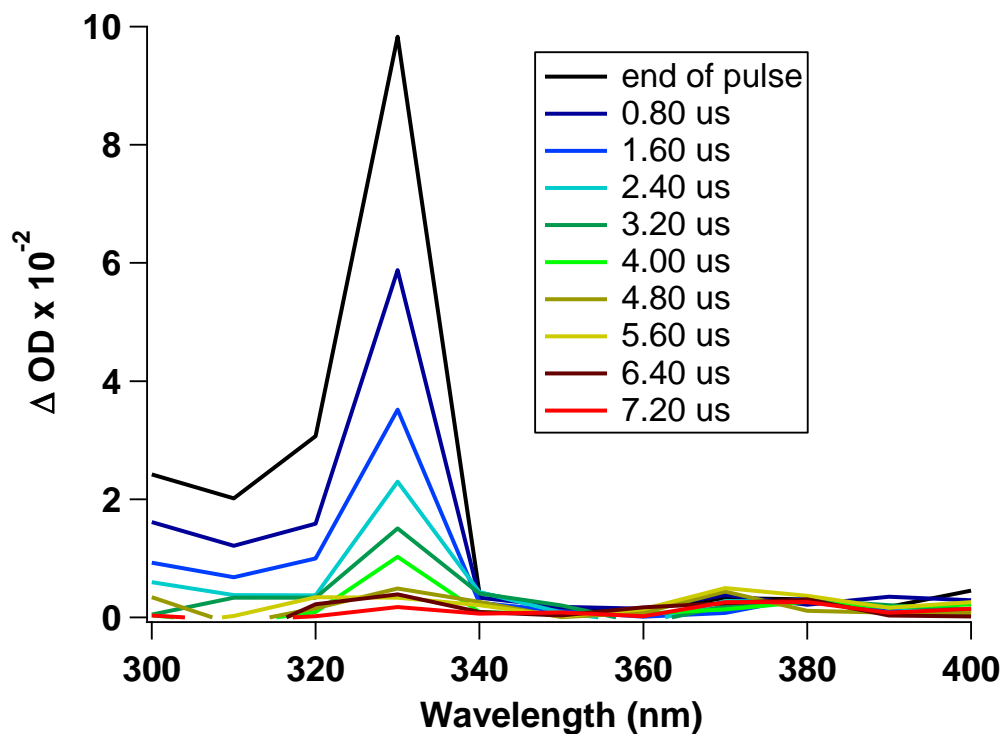
#### 4.5.5). Laser Flash Photolysis



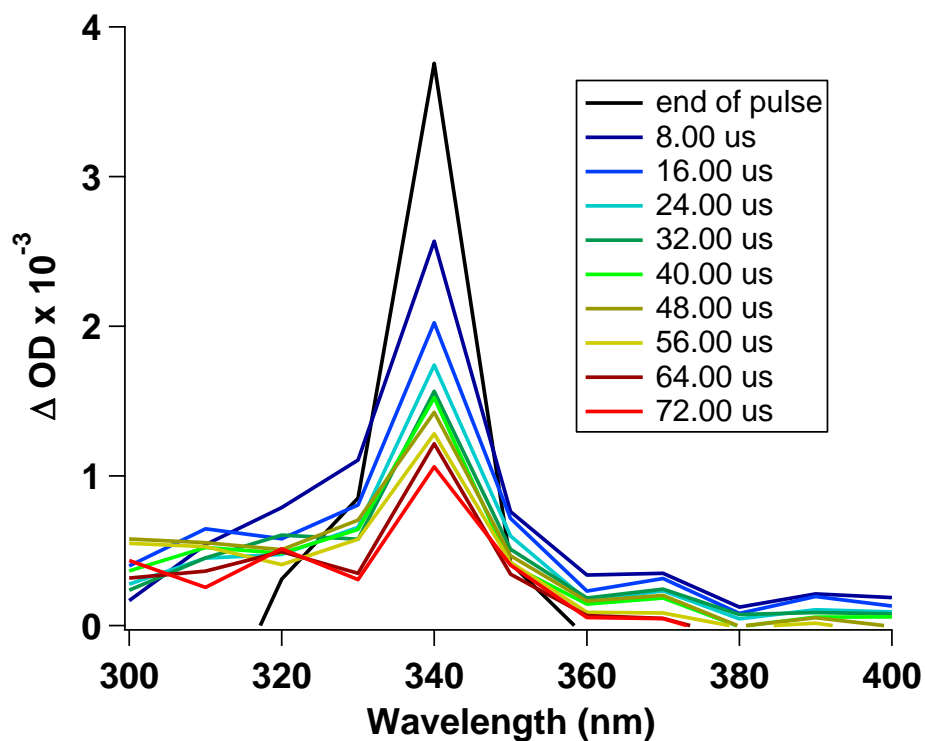
**Figure 4.S26:** Transient Spectroscopy of 1,1,3,3-tetraphenylpropan-2-one in solution state ( $\lambda_{\max} = 330$  nm)



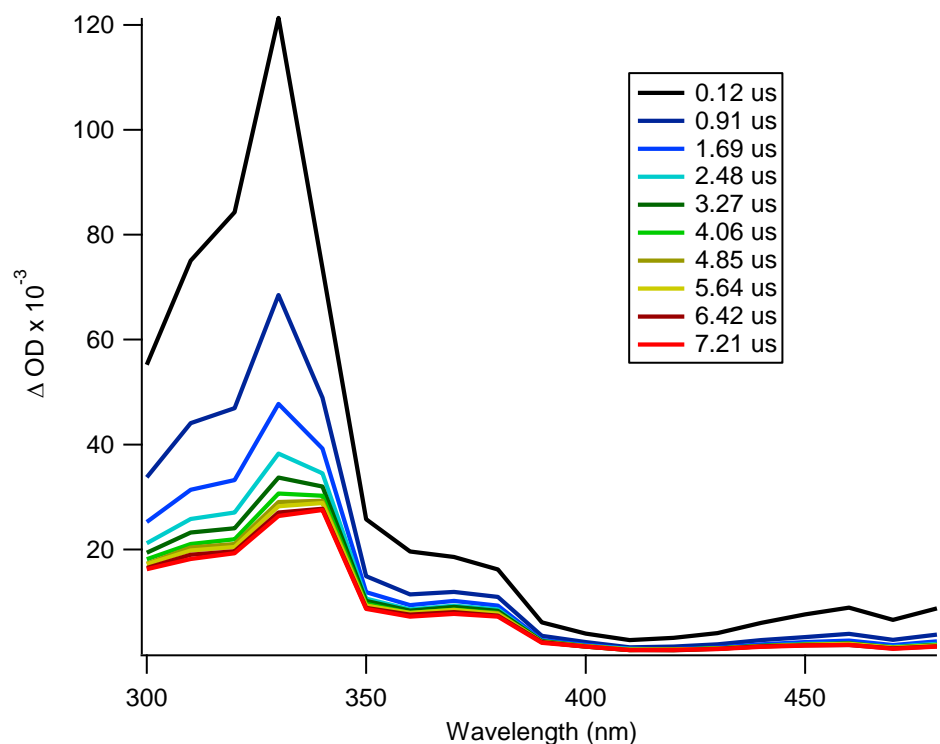
**Figure 4.S27:** Transient Spectroscopy of 1,1,3,3-tetraphenylpropan-2-one in nanocrystalline suspension ( $\lambda_{\max} = 340$  nm)



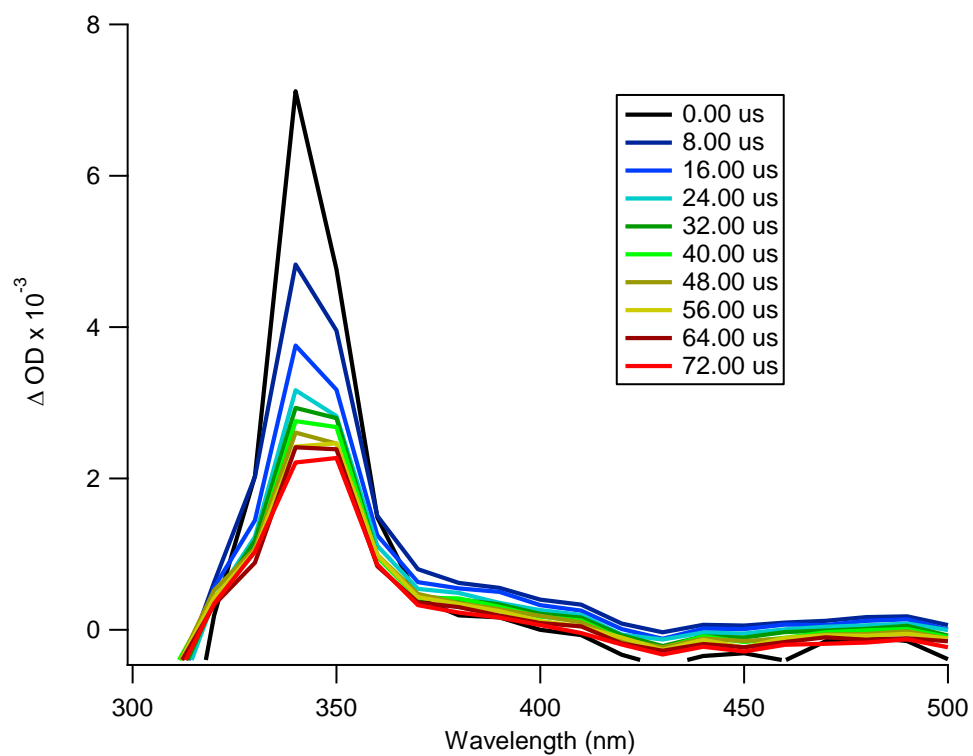
**Figure 4.S28:** Transient Spectroscopy of 1,1,3,3-tetraphenylbutan-2-one in solution state ( $\lambda_{\max} = 330$  nm)



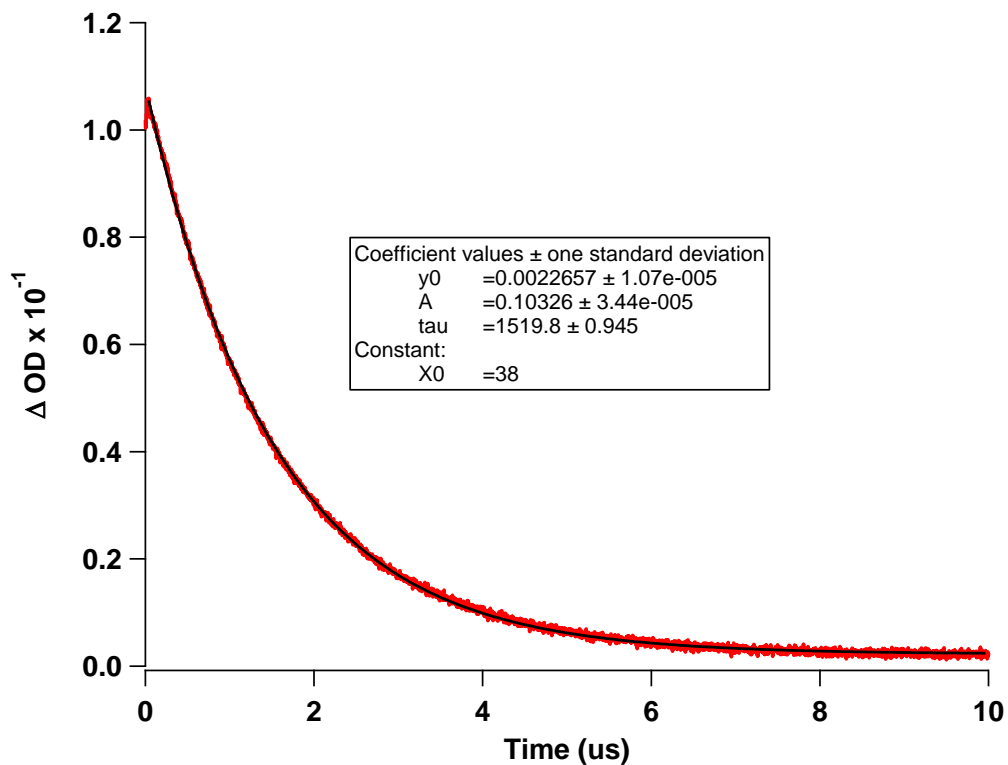
**Figure 4.S29:** Transient Spectroscopy of 1,1,3,3-tetraphenylbutan-2-one in nanocrystalline suspension ( $\lambda_{\max} = 340$  nm)



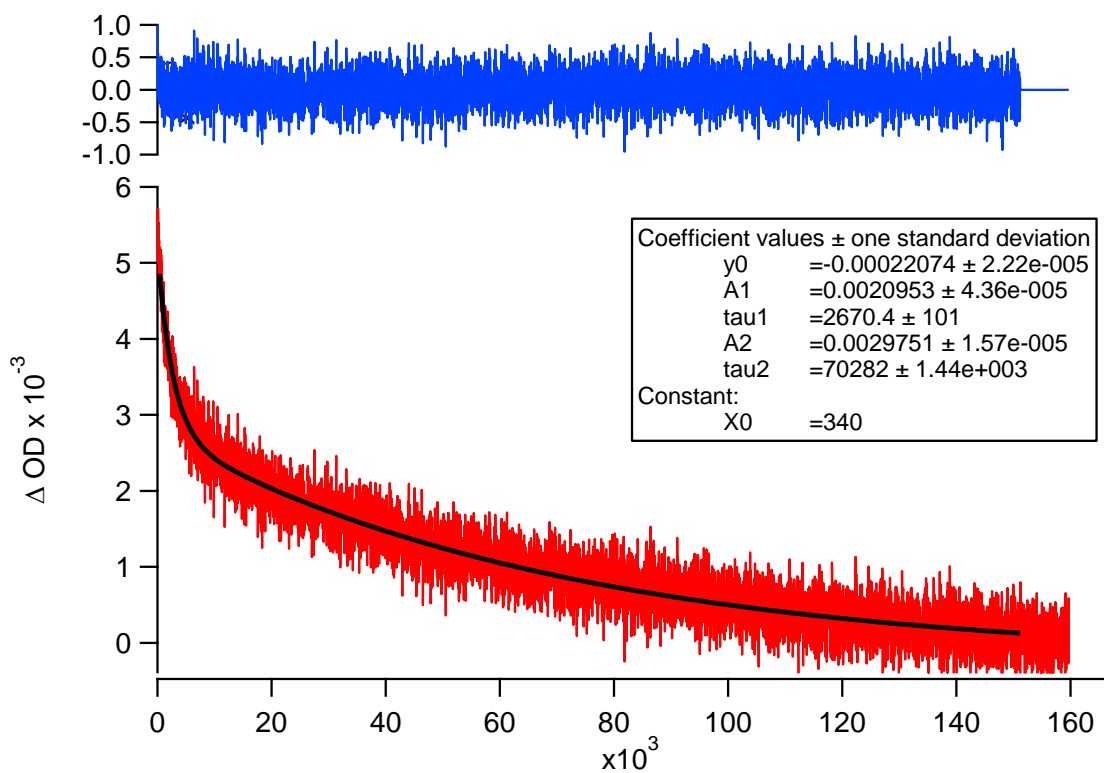
**Figure 4.S30:** Transient Spectroscopy of 1,1,1,3,3-pentaphenylpropan-2-one in solution state ( $\lambda_{\text{max}} = 330 \text{ nm}$ )



**Figure 4.S31:** Transient Spectroscopy of 1,1,1,3,3-pentaphenylpropan-2-one in nanocrystalline suspension ( $\lambda_{\text{max}} = 340 \text{ nm}$ )



**Figure 4.S32:** Transient decay of 1,1,3,3-tetraphenylpropan-2-one in MeCN solution



**Figure 4.S33:** Transient decay of 1,1,3,3-tetraphenylpropan-2-one in nanocrystalline suspension.

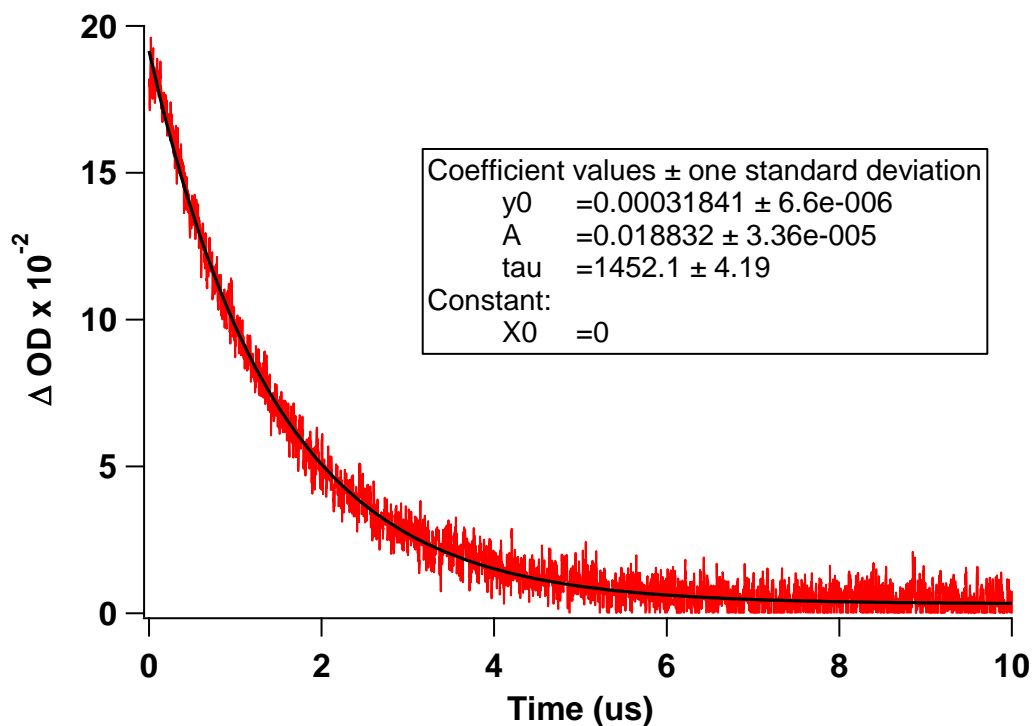


Figure 4.S34: Transient decay of 1,1,3,3-tetraphenylbutan-2-one in MeCN solution

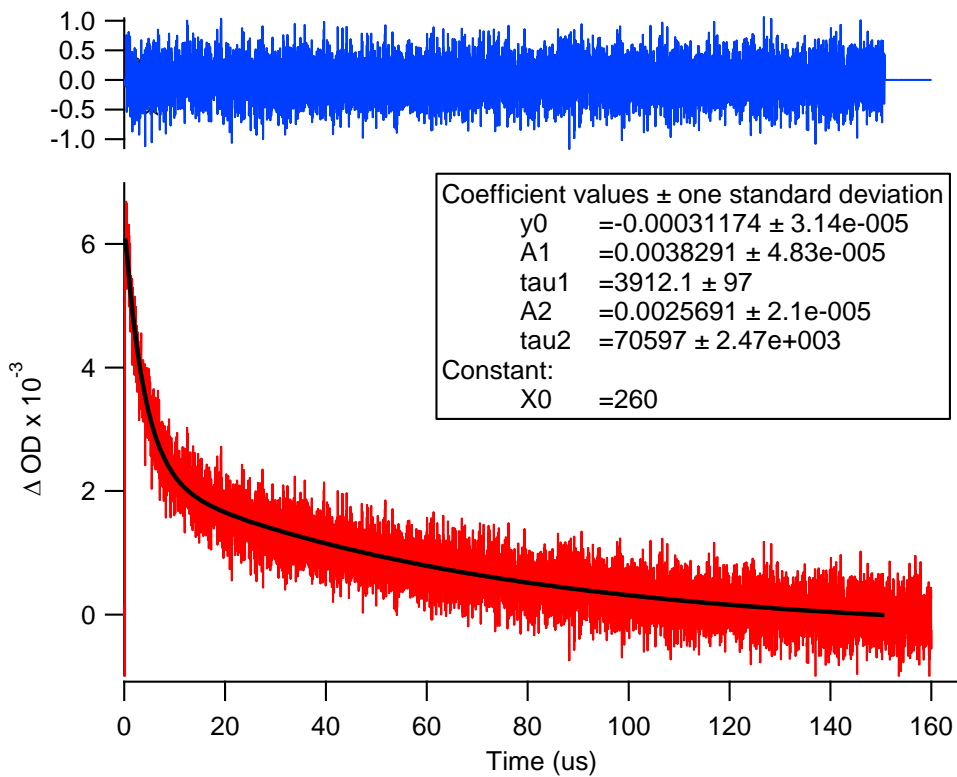
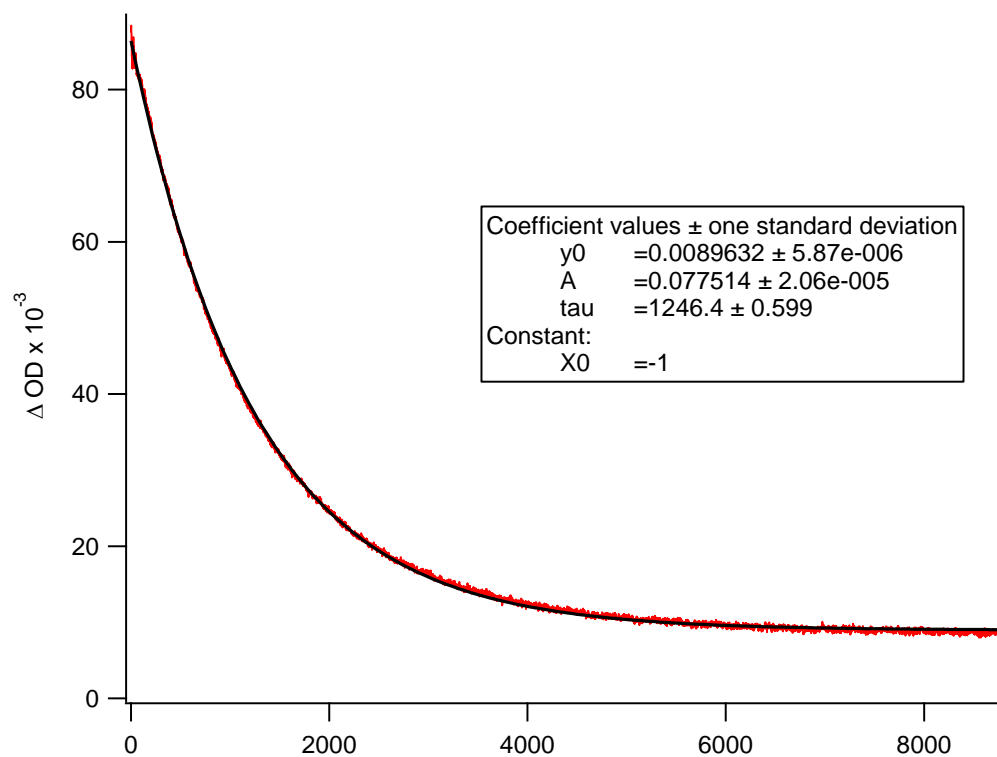
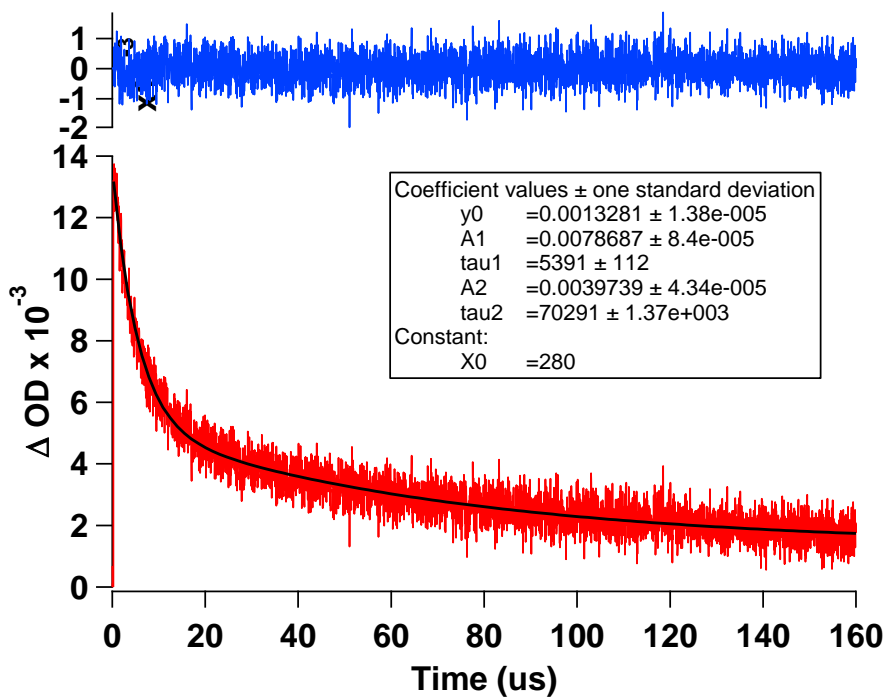


Figure 4.S35: Transient decay of 1,1,3,3-tetraphenylbutan-2-one in nanocrystalline suspension



**Figure 4.S36:** Transient decay of 1,1,1,3,3-pentaphenylpropan-2-one in MeCN solution

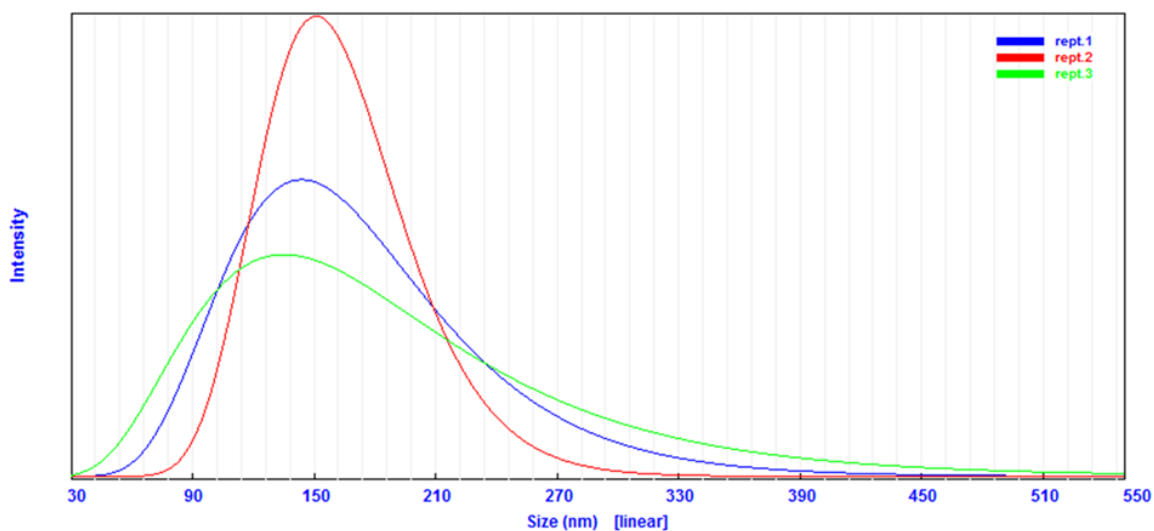


**Figure 4.S37:** Transient decay of 1,1,1,3,3-pentaphenylpropan-2-one in nanocrystalline suspension.

#### 4.5.6). Dynamic Light Scattering (DLS)

10  $\mu\text{L}$  of stock solution (5mg/mL) in acetonitrile is injected drop wise via syringe into a 100 mL graduated cylinder containing a 20 mL of a cationic detergent made of cetyltrimethylammonium bromide (CTAB) surfactant dissolved in deionized water so that the critical micelle concentration of CTAB  $(0.9 \text{ mM})^3$  is 1/25 or 1.25 mg of CTAB in 1L of deionized water. Prior to the injection of the stock solution, it is important to take note that the vortex is generated from a conventional stir plate and stir bar. After the stock solution is added the stirring continues for 15 seconds before it is carefully transferred so that bubbles are not generated during the transfer of liquid.

Rept#.	Mean (nm)	Std.Dev (nm)	Baseline Error	P.I.	Counts/s	Diff.Coeff ( $\text{m}^2/\text{s}$ )	Overflow
Rept.1	143.4	40.7	0.01%	-0.059	4.13e+05	3.16e-12	0
Rept.2	146.5	25.8	0.01%	0.018	4.08e+05	3.09e-12	0
Rept.3	142.8	57.1	0.02%	0.222	4.07e+05	3.17e-12	0
Average	144.3	41.21		0.060			



**Figure 4.S38:** Dynamic light scattering results of 1,1,3,3-tetraphenylpropan-2-one in nanocrystalline suspension with an average value of 140 nm.

Unimodal Results Summary

Rept.#	Mean (nm)	Std.Dev (nm)	Baseline Error	P.I.	Counts/s	Diff.Coeff (m <sup>2</sup> /s)	Overflow
Rept.1	134.4	54.1	0.05%	0.230	2.58e+05	3.37e-12	0
Rept.2	147.6	59.0	0.04%	-0.220	2.85e+05	3.07e-12	0
Rept.3	147.1	52.9	0.04%	0.134	3.09e+05	3.08e-12	0
Average	143.0	55.31		0.048			

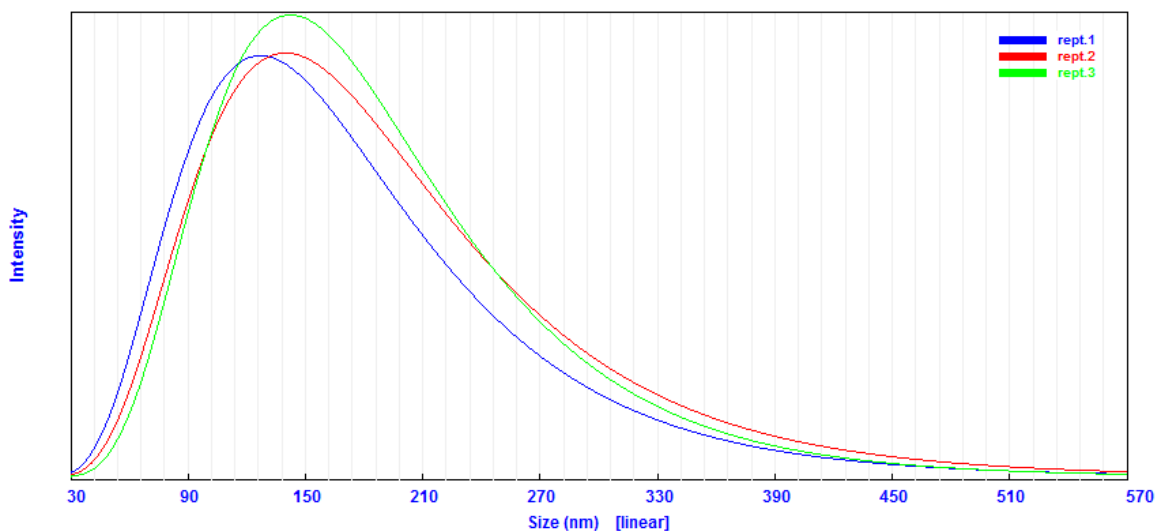


Figure 4.S39: Dynamic light scattering results 1,1,3,3-tetraphenylbutan-2-one in nanocrystalline suspension with an average value of 140 nm.

Unimodal Results Summary

Rept.#	Mean (nm)	Std.Dev (nm)	Baseline Error	P.I.	Counts/s	Diff.Coeff (m <sup>2</sup> /s)	Overflow
Rept.1	180.8	36.5	0.00%	0.024	7.59e+05	2.50e-12	0
Rept.2	180.8	70.5	0.01%	0.195	7.72e+05	2.50e-12	0
Rept.3	181.6	73.0	-0.01%	0.228	7.70e+05	2.49e-12	0
Average	181.1	60.02		0.149			

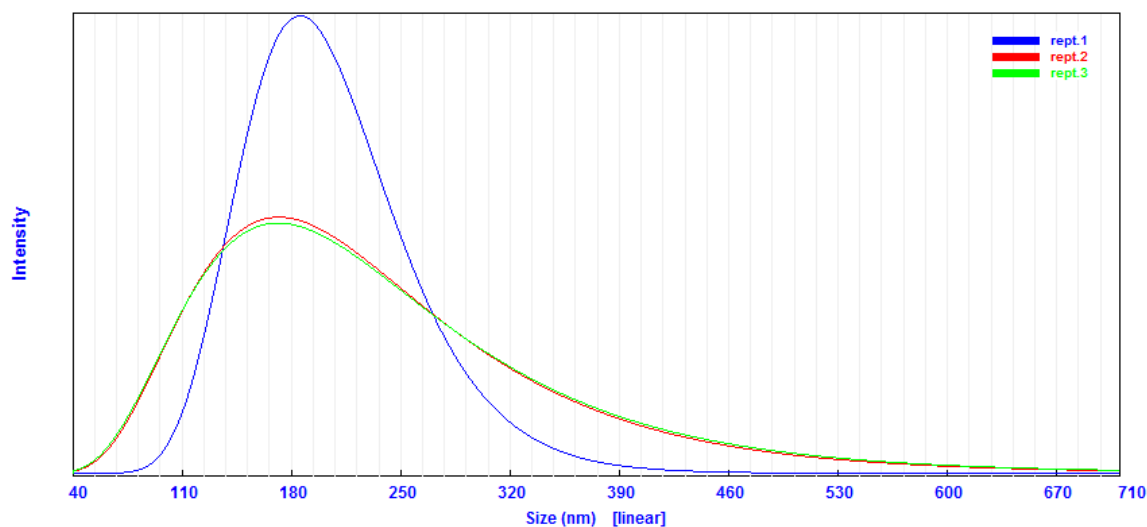


Figure S40: Dynamic light scattering results of 1,1,1,3,3-pentaphenylpropan-2-one in nanocrystalline suspension with an average value of 180 nm.



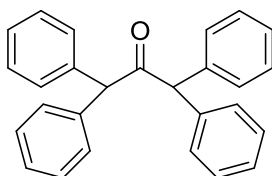
#### 4.5.7). Quantum Yield <sup>3</sup>

Optically dense nanocrystalline suspensions of dicumyl ketone (DCK) and ketones **1a-1c** were prepared by injecting a solution of the corresponding ketone in acetone into a vortexing solution of 3 mL of water and 1 mL of CTAB (164 mg/L). While still stirring, the suspension was diluted with 2 mL of CTAB solution (164 mg/L) and the resulting suspension was sonicated for 5 min. The suspension of dicumyl ketone was prepared using 0.1 mL of a 17 mg/mL solution of dicumyl ketone in acetone, whereas the suspensions of compounds **1a-1c** were made by using 0.2 mL of a 20 mg/mL solution in acetonitrile. Thereafter the transmittance as %T was measured with an immersion probe at  $\lambda = 300$  nm. Then 5.6 mL of each suspension were combined and from the resulting mixed suspension two aliquots of 5 mL were taken, the first aliquot was set aside as a standard and the second one was irradiated with an immersed 2.9 W pen light source emitting at a wavelength of 302 nm. The same procedure was repeated twice for irradiations performed at 3, 5 and 7 min. Afterwards the irradiated and non-irradiated suspensions were diluted with 10 mL of water, treated with 600 mg of calcium chloride and extracted with diethyl ether (2 x 12 mL). The ether phases were added 5 mL of hexanes and dried over MgSO<sub>4</sub>. The solvent was removed under vacuum and the residue was transferred to a 1.0 mL volumetric flask containing 0.2 mL of a 13.5 mg/5.0 mL solution of 2-methoxy-benzophenone as an external standard in CDCl<sub>3</sub> and then filled up to the graduation mark with CDCl<sub>3</sub>. <sup>1</sup>H NMR at 500 MHz of the irradiated and non-irradiated solutions in CDCl<sub>3</sub> were recorded, the singlet at 3.73 ppm of the methoxy group (OMe) of the 2 methoxybenzophenone was normalized to 1.00 and the methyne proton of ketones **1a-1c** and the four methyl groups ( $\delta = 1.28$  ppm) of the dicumyl ketone were integrated relative to this group. Under this conditions the quantum yield ( $\Phi_{1a-1c}$ ) is given by,

$$\Phi = (N_1)(\Phi_{DCK})(OD_{DCK})/(N_{DCK})(OD_1)$$

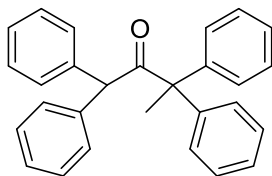
$$\Phi_1 = (\Phi_{DCK}) (\text{Mol-2}) (OD_{DCK}) / (OD_1) (\text{Mol-DC})$$

Where  $N_1$  and  $N_{DCK}$  are the relative integrations of **1a-1c** and **DCK**, respectively; in the case of **DCK** the  $N_{DCK} = \text{rel. integration}_{DCK}/n$ .  $OD_{1a-1c}$  and  $OD_{DCK}$  are the optical densities of **1a-1c** and **DCK** measured with the immersion probe, respectively, and  $\Phi_{DCK} = 0.2$ .



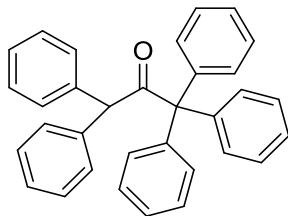
Entry	Time (min)	$T_{DCK}(\%)^a$	$A_{DCK}^b$	$T_{TPA}(\%)^a$	$A_{TPA}^b$	$N_{DCK(I)}^c$	$N_{DCK(II)}^d$	$N_{DCK}^e$	$N_{TPA(I)}^c$	$N_{TPA(II)}^d$	$N_{TPA}^e$	$\Phi_1(\%)$
1	3	17.65	0.753	26.00	0.585	0.830	0.265	0.565	1.020	0.69	0.33	15.0
2	3	15.65	0.805	21.64	0.665	0.880	0.233	0.647	1.070	0.54	0.53	19.8
3	5	16.29	0.788	27.19	0.566	0.575	0.140	0.435	0.930	0.42	0.51	32.6
4	5	15.21	0.818	28.89	0.539	0.368	0.035	0.333	0.735	0.44	0.295	26.9
5	7	15.64	0.806	29.48	0.530	0.765	0.123	0.642	0.830	0.255	0.575	27.2
6	7	12.14	0.916	15.59	0.807	0.648	0.115	0.533	0.945	0.285	0.660	28.1
Averaged Quantum Yield												25.0

**Figure 4.S41:** Quantum yield calculations of 1,1,3,3-tetraphenylpropan-2-one. <sup>a</sup>T: transmittance in %, <sup>b</sup>A: absorbance, <sup>c</sup>N(I): relative integration of the non-irradiated suspension, <sup>d</sup>N(II): relative integration of the irradiated suspension, <sup>e</sup>N = N(I) – N(II)



Entry	Time (min)	$T_{TPA}(\%)^a$	$A_{TPA}^b$	$T_{TPMA}(\%)^a$	$A_{TPMA}^b$	$N_{TPA(I)}^c$	$N_{TPA(II)}^d$	$N_{TPA}^e$	$N_{TPMA(I)}^c$	$N_{TPMA(II)}^d$	$N_{TPMA}^e$	$\Phi_1(\%)$
1	3	15.00	0.824	12.57	0.901	0.770	0.391	0.379	0.833	0.45	0.383	23.1
2	3	12.10	0.917	13.54	0.868	0.791	0.333	0.458	0.912	0.59	0.322	18.6
3	5	9.824	1.008	11.39	0.943	0.893	0.574	0.319	0.735	0.38	0.355	29.7
4	5	13.35	0.875	17.03	0.769	0.886	0.395	0.491	0.788	0.43	0.358	20.7
5	7	10.77	0.968	15.52	0.809	0.805	0.411	0.394	0.801	0.39	0.411	31.2
6	7	19.20	0.712	14.18	0.848	0.673	0.357	0.316	0.708	0.51	0.198	13.5
Averaged Quantum Yield												22.8

**Figure 4.S42:** Quantum yield calculations of 1,1,3,3-tetraphenylbutan-2-one. <sup>a</sup>T: transmittance in %, <sup>b</sup>A: absorbance, <sup>c</sup>N(I): relative integration of the non-irradiated suspension, <sup>d</sup>N(II): relative integration of the irradiated suspension, <sup>e</sup>N = N(I) – N(II)



Entry	Time (min)	T <sub>DCK</sub> (%) <sup>a</sup>	A <sub>DCK</sub> <sup>b</sup>	T <sub>PPA</sub> (%) <sup>a</sup>	A <sub>PPA</sub> <sup>b</sup>	N <sub>DCK(I)</sub> <sup>c</sup>	N <sub>DCK(II)</sub> <sup>d</sup>	N <sub>DCK</sub> <sup>e</sup>	N <sub>PPA(I)</sub> <sup>c</sup>	N <sub>PPA(II)</sub> <sup>d</sup>	N <sub>PPA</sub> <sup>e</sup>	Φ <sub>1</sub> (%)
1	3	11.59	0.936	10.68	0.971	0.623	0.315	0.308	1.02	0.57	0.45	28.2
2	3	8.575	1.067	8.465	1.072	0.598	0.293	0.305	1.05	0.63	0.42	27.4
3	5	15.00	0.824	8.250	1.084	0.435	0.133	0.302	1.02	0.42	0.60	30.2
4	5	8.091	1.092	6.732	1.172	0.588	0.120	0.468	1.05	0.48	0.57	22.7
5	7	11.58	0.936	6.176	1.209	0.340	0.078	0.262	0.87	0.27	0.60	35.5
6	7	15.53	0.809	4.868	1.313	0.410	0.091	0.319	0.89	0.27	0.62	23.9
Averaged Quantum Yield												28.0

**Figure 4.S43:** Quantum yield calculations of 1,1,1,3,3-pentaphenylpropan-2-one. <sup>a</sup>T: transmittance in %, <sup>b</sup>A: absorbance, <sup>c</sup>N(I): relative integration of the non-irradiated suspension, <sup>d</sup>N(II): relative integration of the irradiated suspension, <sup>e</sup>N = N(I) – N(II)

Reference:

- 1). (a) Cole, J. M.; Irie, M. *CrystEngComm.*, **2016**, *18*, 7175; (b) Cohen, M. D. *Tetrahedron*, **1987**, *43*, 1211-1224; (c) Ramamurthy, V.; Venkatesan, K., *Chem. Rev.*, **1987**, *87*, 433-481; (d) Hadjoudis, E.; Mavridis, I. M. *Chem. Soc. Rev.*, **2004**, *33*, 579-588; (e) Ramamurthy, V.; Sivaguru, J. *Chem. Rev.*, **2016**, *116*, 645-647.
- 2). (a) Atkinson, M. B. J.; Mariappan, S. V. S.; Bucar, D. K.; Baltrusaitis, J.; Friscic, T.; Sinada, N. G.; MacGillivray, L. R., *Proc. Nat. Acad. Sci. (USA)*. **2011**, *108*, 10974-10979. (b) Natarajan, A.; Ng, D.; Yang, Z.; Garcia-Garibay, M.A. *Angew Chem. Int. Ed.* **2007**, *46*, 6485-6487; (c) Ng, D.; Yang, Z.; Garcia-Garibay, M.A. *Org. Lett.* **2004**, *6*, 645-647. (d) Ellison, M.E.; Ng, D.; Dang, H.; Garcia-Garibay, M.A. *Org. Lett.* **2003**, *5*, 2531-2534.
- 3). (a) Hernandez-Linares, M. G.; Guerrero-Luna, G.; Perez-Estrada, S.; Ellison, M.; Ortin, M.; Garcia-Garibay, M. A., *J. Am. Chem. Soc.*, **2015**, *137*, 1679-1684; (b) Veerman, M.; Resendiz, M. J. E.; Garcia-Garibay, M. A. *Org. Lett.*, **2006**, *8*, 2615-2617
- 4). (a) Leonard R. MacGillivray, L. R., *J. Org. Chem.*, **2008**, *73* (9), 3311-3317; (b) Khan, M.; Enkelmann, V.; Brunklaus, G., *J. Org. Chem.*, **2009**, *74* (6), 2261-2270; (c) Chaudhary, A; Mohammad, A., *Crystal Growth & Design*, **2017**, *17* (5), 2893-2910.
- 5). (a) Chung, T. S.; Ayitou, A. J.-L.; Park, J. H.; Breslin, V. M.; Garcia-Garibay, M. A. *Phys. Chem. Lett.*, **2017**, *8*, 1845-1850. (b) Breslin, V. M.; Garcia-Garibay, M. A. *Crystal Growth and Design*, **2017**, *7*, 637-642. (c) Anoklase J.-L. Ayitou, A. J.-L.; Flynn, K.; Jockusch, S.; Khan, S. I.; Garcia-Garibay, M. A. *J. Am. Chem. Soc.*, **2016**, *138*, 2644-2648.
- 6). (a) Kuzmanich, G.; Garcia-Garibay, M. A. *J. Phys. Org. Chem.*, **2011**, *23*, 376-381; (b) Shiraki, S.; Natarajan, A.; Garcia-Garibay, M. A. *Photochem. Photobiol. Sci.*, **2011**, *10*,

- 1480-1487. (c) Resendiz, M. J. E.; Family, F.; Fuller, K.; Campos, L.M.; Khan, S.I.; Lebedeva, N.V.; Forbes, M. D. E.; Garcia-Garibay, M. A. *J. Am. Chem. Soc.* **2009**, *131*, 8425-8433. (e) Family, F.; Garcia-Garibay, M. A. *J. Org. Chem.* **2009**, *74*, 2476-2480; (f) Resendiz, M. J. E.; Taing, J.; Garcia-Garibay, M. A. *Org. Lett.* **2007**, *9*, 4351-4354.
- 7). (a) Mondal, R.; Okhrimenko, A. N.; Shah, B. K.; Neckers, D. C., *J. Phys. Chem. B*, **2008**, *112* (1), 11–15. (b) Poloukhine, A.; Popik, V. V., *J. Org. Chem.*, **2003**, *68* (20), 7833–7840. (c) Mondal, R.; Shah, B. K.; Neckers, D. C., *J. Am. Chem. Soc.*, **2006**, *128* (30), 9612–9613.
- 8). (a) Campos, L. M.; Dang, H.; Ng, D.; Yang, Z.; Martinez, H. L.; Garcia-Garibay M. A. *J. Org. Chem.* **2002**, *67*, 3749-3754. (b) Garcia-Garibay, M. A.; Campos, L. in *The Handbook for Organic Photochemistry and Photobiology*, W. Horspool, Ed., CRC Press, Boca Raton, Fl. **2003**; (c) Shiraki, S.; Garcia-Garibay, M. A. in *Handbook of Synthetic Photochemistry*, Albini, A., Ed., John Wiley, New York, **2010**, 25-66.
- 9). a) Cozens, F. L.; Garcia, H.; Gessner, F.; Scaiano, J. C., *J. Phys. Chem.*, **1994**, *98* (34), 8494–8497. (b) Garcia, H.; Scaiano, J. C., *Acc. Chem. Res.*, **1999**, *32* (9), 783–793; (c) Jockush, S.; Hirano, T.; Liu, Z.; Turro, N. J., *Phys. Chem. B*, **2000**, *104* (6), 1212–1216;. (d) Kantor, S. W.; Hauser, C. R. *J. Am. Chem. Soc.*, **1950**, *72* (7), 3290–3291. (e) Hirano, T.; Li, W.; Abrams, L.; Krusic, P. J.; Ottaviani, F.; Turro, N. J. *J. Org. Chem.*, **2000**, *65* (5), 1319–1330.
- 10). Park, J. H.; Hughs, M.; Chung, T. S.; Ayitou, A. J.-L.; Breslin, V.M.; Garcia-Garibay, M. A. *J. Am. Chem. Soc.* **2017**, *139*, 13312–13317.
- 11). (a) Kasai, H.; Nalwa, H. S.; Oikawa, H.; Okada, S.; Matsuda, H.; Minami, N.; Kuakuta, A.; Ono, K.; Mukoh, A.; Nakanishi, H. *Jpn. J. Appl. Phys.* **1992**, *31*, 1132.

- 12). (a) Desiraju, G. R. *J. Am. Chem. Soc.*, **2013**, *135* (27), 9952–9967; (b) Eleguero, J. *Cryst. Growth & Design*, **2011**, *11* (11), 4731–4738.
- 13). (a) Turro, N. J.; Weed, G. C. *J. Am. Chem. Soc.*, **1983**, *105* (7), 1861–1868. (b) Garcia-Garibay, M. A.; Zhang, Z.; Turro, N. J. *J. Am. Chem. Soc.* **1991**, *113* (16), 6212–6218. (c) Turro, N. J.; Zimmt, M. B.; Gould, I. R. *J. Phys. Chem.*, **1988**, *92* (2), 433–437
- 14). (a) Keating, A.E.; Garcia-Garibay, M.A. in *Organic and Inorganic Photochemistry*; Ramamurthy, V., Schanze, K., Eds.; Marcel Dekker: New York, 1998, Vol. 2, pp. 195-248; (b) de Loera, D.; Stopin, A.; Garcia-Garibay, M. A. *J. Am. Chem. Soc.* **2013**, *135*, 6626–6632.
- 15). Weiss, D. *Org. Photochem*; Padwa, A., Ed.; Marcel Dekker: New York, 1981; Vol. 5, 347-420.
- 16). (a) Steiner, U. E.; T. Ulrich, T. *Chem. Rev.*, **1998**, *89*, 51–147. (b) Harbron, E. J.; Forbes, M. D. E. *Encyclopedia of Chem. Physics and Phys. Chemistry*; Moore, J. H., Spencer, N. D., Eds.; Institute of Physics Publishing: Philadelphia, **2001**; Ch. B1.16, 1389– 1417.
- 17). Wang, X.; Qiu, R.; Yan, C.; Reddy, V. P.; Zhu, L.; Xu, X.; Yin, S.-F. *Org. Lett.*, **2015**, *17* (8), 1970.
- 18). Rajca, A.; Tolbert, L. M. *J. Am. Chem. Soc.*, **1988**, *110*, 871.
- 19). (a) Barton, D. H. R.; Finet, J.; Giannotti, C.; Halley, F. *J. Chem. Soc. Perkin. Trans.*, **1987**, *1*, 241. (b) Barton, D.H.R.; Papoula, M. T. B.; Guilhem, J.; Mortherwell, W. B.; Pascard C.; Tran Huu Dau, E. *J. Chem. Soc. Chem. Comm*, **1982**, 732.
- 20). Wakui, H.; Kawasaki, S.; Satoh, T.; Miura, M.; Masakatsu, N., *J. Am. Chem. Soc.*, **2004**, *126*, 8658.
- 21). Popielarz, R.; Arnold, D. R., *J. Am. Chem. Soc.*, **1990**, *112*, 3068.

## **Chapter 5:**

### **Laser Flash Photolysis studies of a Photo-Induced Aryl-Acyl Radical Pair's Recombination Rates in Nanocrystalline Suspensions**

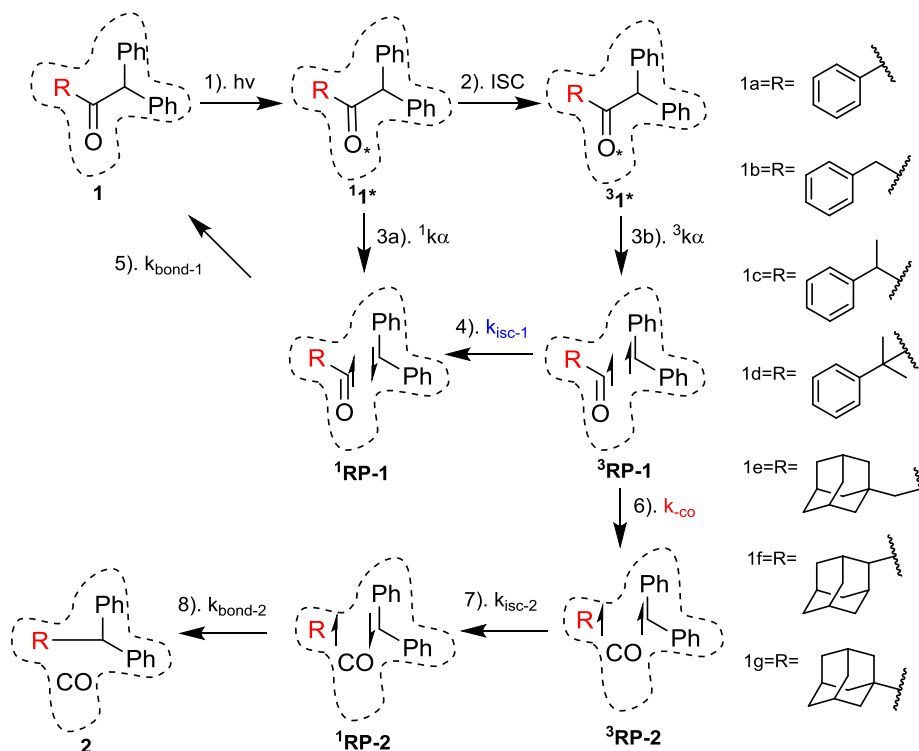
## 5.1 Introduction

Photochemical reactions in the solid-state have gained much interest from the chemical society due to their ability to control regioselectivity as well as stereoselectivity in certain contexts.<sup>1</sup> Reactions in the solid state force molecules to react in their defined crystal cavity, making it difficult for the reactants to explore multiple chemical pathways.<sup>2</sup> This limitation of dictating molecules to react in a specific manner has granted chemists a tool to explore chemically challenging syntheses of natural products<sup>3</sup> as well as other challenges in chemistry.<sup>4</sup> The effectiveness of solid-state photochemical reactions is well demonstrated<sup>5</sup> but its utility is considered marginal because the depth of research in solid-state photochemistry is limited.<sup>6</sup> In comparison to photochemical reactions in solution, photo-induced reactions in the solid state are less prevalent because analytical instrumentation to understand solid-to-solid transformation was considered less than ideal.<sup>7</sup> Since Schmitt and Cohen's report of the topochemical postulate<sup>8</sup>, X-ray crystallography has paved the way as the leading method for extracting mechanistic information from solid-to-solid transitions.<sup>9</sup> However, this technique is less than ideal because it really only provides the chemical structure of the reactant and the product. However, pump-probe spectroscopy allows detection of rapidly fleeting transients by measuring their absorption spectra and lifetimes.<sup>10</sup> This powerful method is widely utilized in detecting and understanding photochemical reactions in solution.<sup>11</sup> However, directly applying this method to analyze solid-state photochemical reactions was considered impractical due to physical properties of solids such as high optical density and intense light scattering that interfere with optical settings.<sup>12</sup> Fortunately, adopting Kasai and coworker's<sup>13</sup> reprecipitation method to create stable nanocrystalline suspensions, it is possible to create a solid suspension of tiny crystals that are smaller than the incident ray of light which makes it possible to mirror the transmission



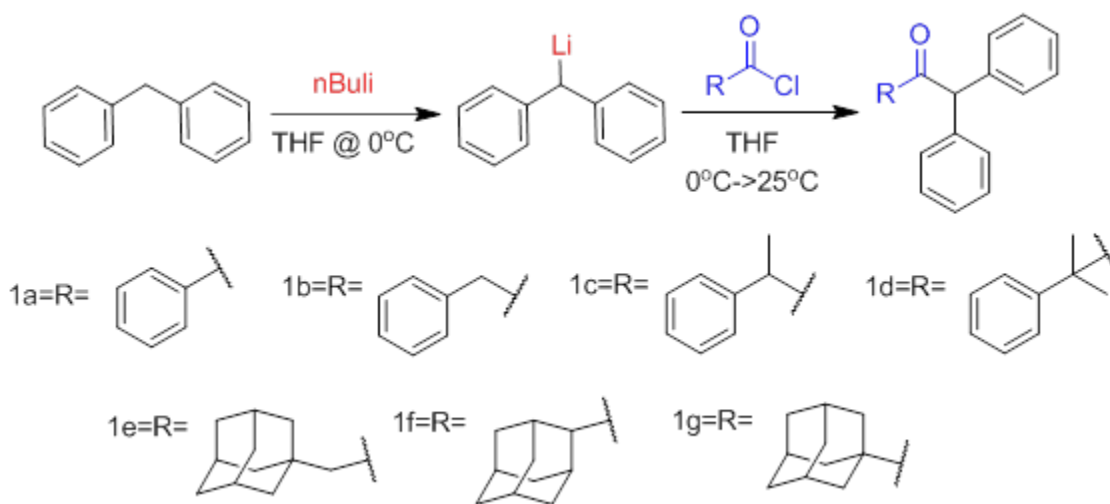
absorption spectroscopy method to study solid-state reactions.<sup>14</sup> With this tool, this paper attempts to further enhance the field of solid-state photochemistry by reporting the ketone kinetics of a solid-state reaction that completely yields the starting material. (Scheme 5.1.1) The irradiation of ketone **1** excites the molecule from the ground state to the excited state  $^11^*$ . Very rapidly the ketone undergoes an intersystem crossing event to yield the triplet ketone  $^31^*$ . The ketone is then able to undergo an initial  $\alpha$ -cleavage to form the triplet radical pair  $^3\text{RP-1}$ . As previously reported in our group, if the rate of the second  $\alpha$ -cleavage is favored, radical pair  $^3\text{RP-2}$  is generated and the lifetime for one of the radicals to spin-flip, ultimately forming product **2**, is measured by the pump-probe spectroscopy method.<sup>15</sup> However, by carefully engineering asymmetric ketones with a stable and detectable diphenylmethane radical handle and a chemically unstable radical substituent upon photolysis show complete recovery of the starting material even after a prolonged irradiation time of 24 hours.

### Scheme 5.1.1



Because of this, product analysis did not provide any new information in determining the existence of the intermediate species. However, our studies reinforce the proposed pathway (Scheme 5.1.1) in the solid-state by reporting lifetimes of the detectable diphenylmethyl transient. We assigned the observed transient absorption to the transition of the initial triplet pair  $^3\text{RP-1}$  to the singlet radical pair  $^1\text{RP-1}$ . Our laser flash photolysis instrument uses a laser with a  $\sim 10$  ns pulse, making it impossible to detect any transients that may form and deplete before this time scale. Therefore, Step 4 ( $k_{\text{isc-1}}$ ) and Step 7 ( $k_{\text{isc-2}}$ ) are the only steps that can be detected by our instrument, but because we observed no product formation, we are ensured that from the projected photochemical pathway detected from our instrument is step 4 ( $k_{\text{isc-1}}$ ). Therefore, we propose lifetimes for an internal conversion further reinforcing the triplet-singlet transition in the solid state. Also, we demonstrate the scope of this chemistry by engineering different ketones to control the kinetics of intersystem crossing.

### Scheme 5.1.2

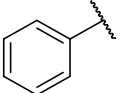
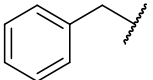
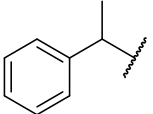
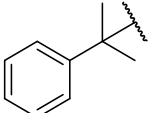
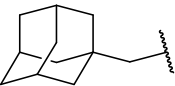

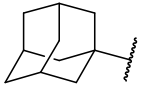


## 5.2 Results and Discussion:

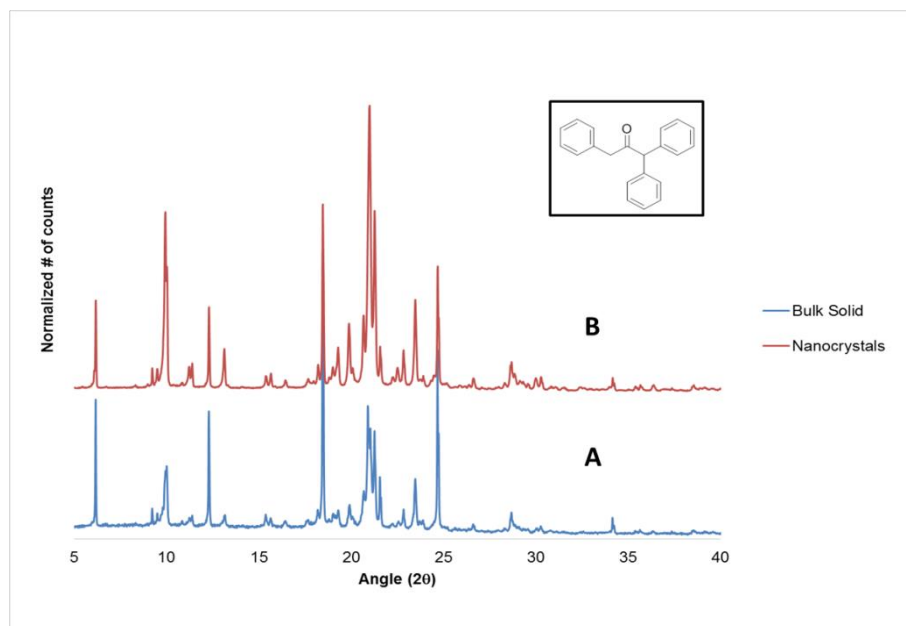
The synthesis of these ketones was performed by lithiating commercially available diphenylmethane with n-butyl-lithium stirring in tetrahydrofuran at  $0^\circ\text{C}$ .<sup>16</sup> After stirring for 30 minutes the respective acid chloride is added drop wise to form the final product. (Scheme 5.2.2)

For commercially unavailable acid chlorides, we opted for the acetic acid and converted it to the acid chloride with oxalyl chloride.<sup>17</sup> It is imperative to test the melting point of these solids to ensure a melting point well above room temperature as the solid state photoreactions tend to melt solids of low melting point. However, all of the tested ketones have a melting point well over 25°C.

**Table 5.2.1:** Solid State Characterization of Ketones for Pre-Decarbonylation Studies

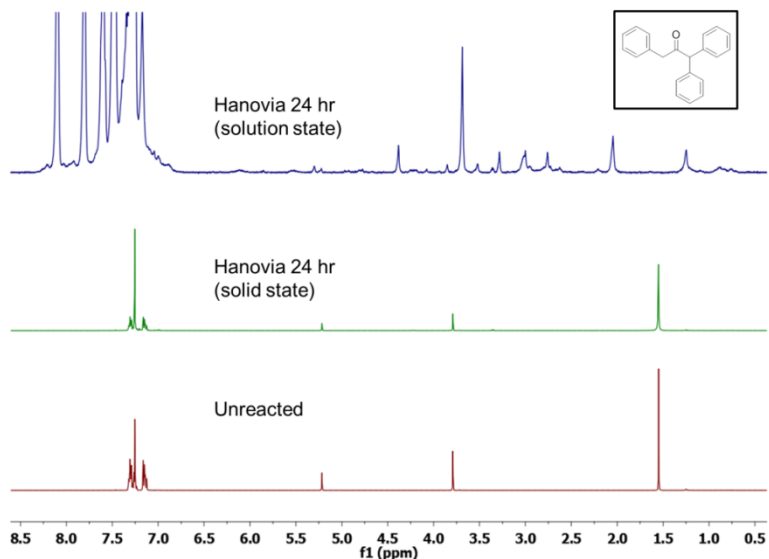
Ketone	R	m.p. (°C)	Biradical Lifetimes, $\mu\text{s}^a$		DLS (nm)
			MeCN	NC	
1a		66 - 67	1.3	1.6, 1.5 (97) <sup>a</sup>	160 ± 70
1b		137 - 138	1.7	0.6, 2.1(98) <sup>a</sup>	250 ± 110
1c		45-46	1.5	2.2, 97 (98) <sup>a</sup>	200 ± 90
1d		75 - 76	0.8	2.6, 27 (95) <sup>a</sup>	220 ± 80
1e		102 - 103	1.2	2.3, 53 (92) <sup>a</sup>	270 ± 110
1f		89 - 90	1.2	3.5, 61 (87) <sup>a</sup>	200 ± 90
1g		104 - 105	1.2	1.8, 63 (87) <sup>a</sup>	220 ± 110

In addition, it is imperative to check the crystallinity of the ketone as the solid may be amorphous which makes it difficult to form nanocrystalline suspensions. However the powdered x-ray diffraction (PXRD) patterns all have sharp and definitive peaks indicating that the ketones are indeed highly crystalline. (Figure 5.2.1)



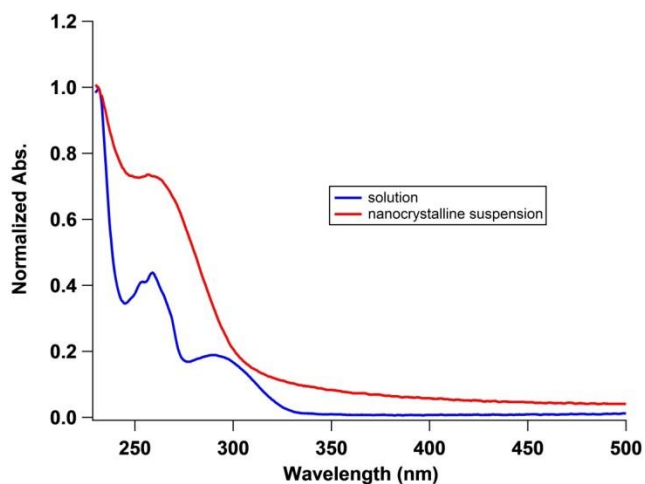
**Figure 5.2.1** Powdered X-Ray Diffractogram of 1,1,3-triphenylpropan-2-one in bulk solid (A) and Nanocrystalline suspensions (B)

Also, the PXRD of the nanocrystalline suspensions indicate that the nanocrystals share the same polymorph as the bulk solid. This information provides assurance that photochemical reactions in the bulk solid are indeed similar to that of nanocrystalline suspensions. With this data in hand, it is important to test the reactivity in the solid state. Depending on the stability of the initial radical pair, <sup>3</sup>RP-1, it has been shown that a second  $\alpha$ -cleavage is likely to occur if the radical that is formed upon the homolytic cleavage is stable.<sup>18</sup> Therefore, we test the photoreactivity of these ketones in solution as well as in the solid state and demonstrate that after 24 hours of irradiation the <sup>1</sup>H NMR shows complete recovery of only the starting material in the solid state where as reactivity in solution gives rise to multiple side products. (Figure 5.2.2)



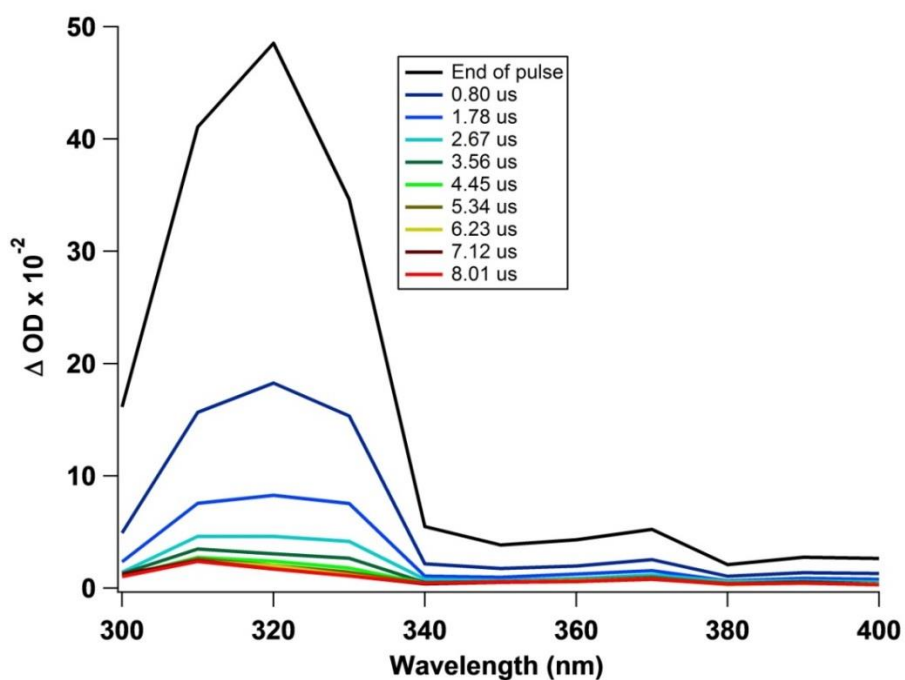
**Figure 5.2.2** Photochemical Product Analysis of 1,1,3-triphenylpropan-2-one in Acetonitrile and in Bulk Solid

This information indicates that in the solid state the reactant is either unaffected by the incident ray of light or the only photoproduct produced from the reaction is the starting material. In order to verify, ultraviolet-visible absorption spectra (UV-Vis) of the ketone in solution and solid state were recorded to indicate strong light absorbance at 266 nm, the laser wavelength of irradiation on the laser flash photolysis instrument. (Figure 5.2.3)



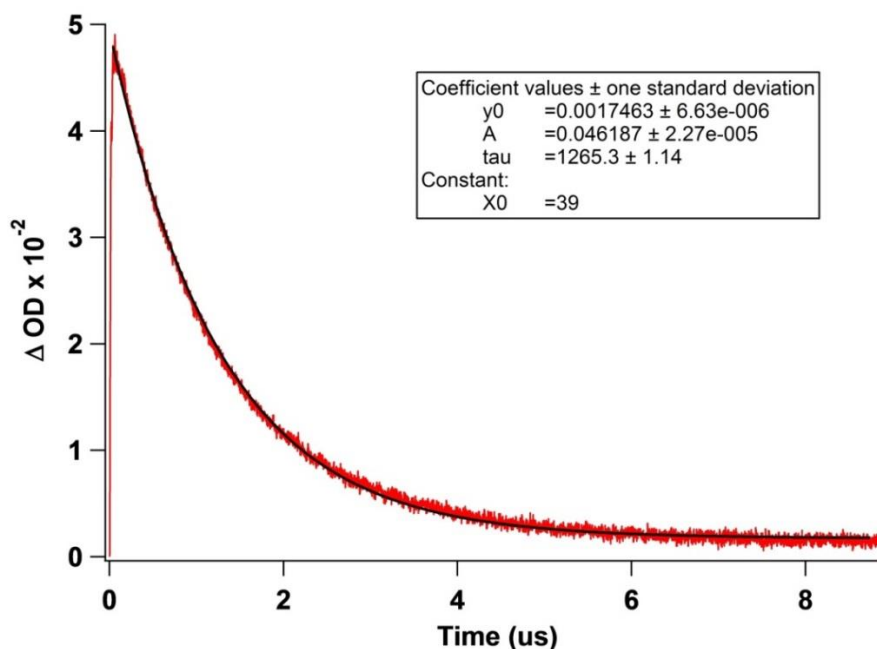
**Figure 5.2.3** UV-Vis of 1,1,3-triphenylpropan-2-one in MeCN solution (blue) and solid state (red)

The UV-Vis absorption spectra not only show a strong absorption at the wavelength of interest but also show marginal light scattering. From our reaction conditions we analyzed that nanocrystalline suspensions that aggregate quickly have UV-Vis absorption spectra with a distinct tail. In order to move onto the pump-probe transmission spectra studies, the UV absorption spectra of the nanocrystalline suspensions were observed for up to ten minutes to verify their stability. (Supplementary Information) Although some aggregation was evident, the level of aggregation in the time frame of ten minutes was minor for all derivatives. Previous reports in literature indicate a  $\lambda_{\text{max}} = 320 \text{ nm} - 340 \text{ nm}$  for the diphenylmethyl radical in solution and in nanocrystalline suspensions.<sup>21</sup> Therefore, taking advantage of the diphenylmethyl radical as a handle, it is possible to detect less stable or shorter living transients that will dictate the kinetics in the photochemical reactivity pathway.



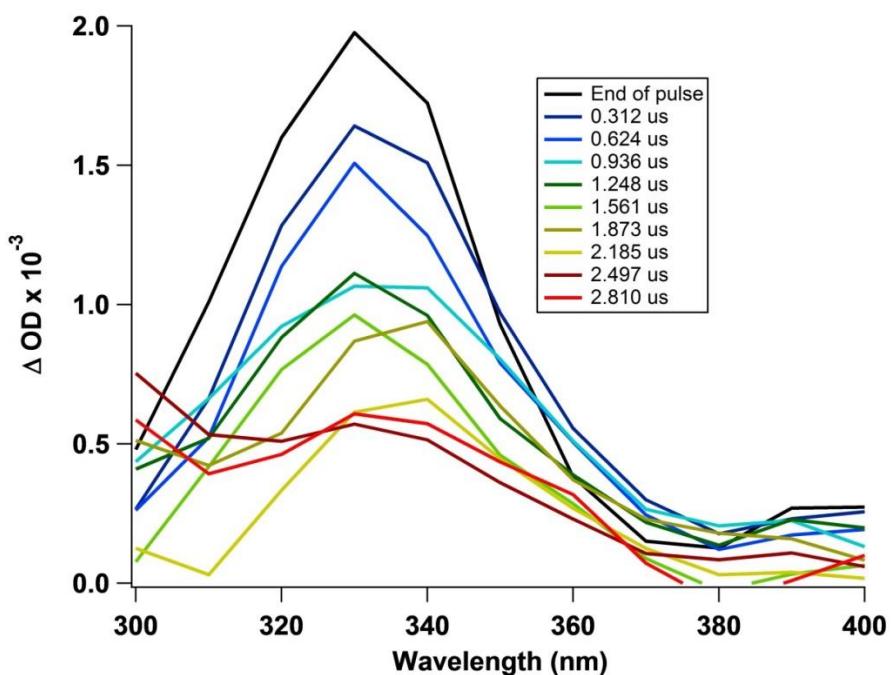
**Figure 5.2.4** Time-dependent spectra of 1,1,3-triphenylpropan-2-one in MeCN solution collected 0 and 8.01 us ( $\lambda_{\text{max}} = 320 \text{ nm}$ )

The operation of the laser flash photolysis instrument begins with making a 100 mL sample of the 1,1,3-triphenylpropan-2-one in MeCN solution which is degassed under argon or nitrogen gas for approximately one hour to get rid of as much ambient oxygen as possible. This is required because oxygen has a triplet state ground state and any reactions mediated by a triplet pathway can easily be quenched by the triplet oxygen.<sup>19</sup> This reservoir of degassed reactant and solution is then subjected to a single path pump that will carry the solution to the cell so that the transients can be generated by the laser and detected. Upon completion of this degassing procedure, a time-dependent spectrum of 1,1,3-triphenylpropan-2-one in MeCN solution is recorded to determine transients of the highest relevance by detecting the  $\lambda_{\max}$ . As predicted, the time-dependent spectra of 1,1,3-triphenylpropan-2-one in MeCN solution reveal a transient with a  $\lambda_{\max} = 320$  nm. (Figure 5.2.4) Assigning this transient as the diphenylmethyl radical, it is possible to pinpoint the kinetics of a particular transient species and probe mechanistic information from the photoreaction.<sup>20</sup>



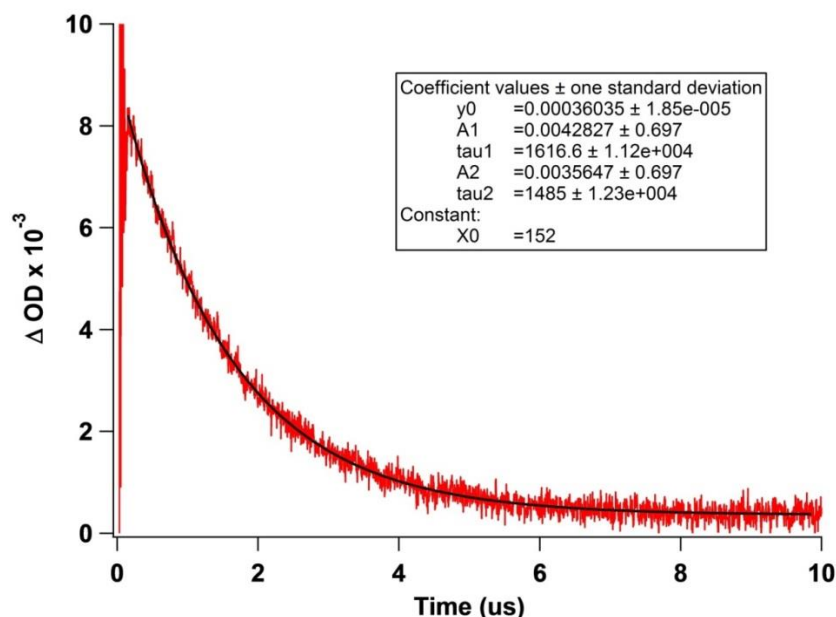
**Figure 5.2.5** Transient decay of 1,1,3-triphenylpropan-2-one in MeCN solution at 330 nm

Therefore, by measuring the decay for the diphenylmethyl transient at the  $\lambda_{\max} = 320$  nm in acetonitrile solution for 1,1,3-triphenylpropan-2-one, we detect that the  $\tau = 1.3$   $\mu\text{s}$ . The decay is most accurate under a monoexponential fit and this is justified by the residual. (Supplementary Information) With this information in hand, we are optimistic in terms of replicating the exact parameters for the nanocrystalline suspensions. Time-dependent spectra of 1,1,3-triphenylpropan-2-one in nanocrystalline suspensions (Figure 5.2.5) reveal that the  $\lambda_{\max} = 330$  nm, indicating a 10 nm red-shift which is common for nanocrystalline suspensions due to low levels of scattering. Upon detecting the transient decay at 330 nm we report a lifetime of  $\tau = 1.6$   $\mu\text{s}$ . (Figure 5.2.7)



**Figure 5.2.6** Time-dependent spectra of 1,1,3-triphenylpropan-2-one in nanocrystalline suspensions collected 0 and 2.8  $\mu\text{s}$  ( $\lambda_{\max} = 320$  nm)





**Figure 5.2.7** Transient decay of 1,1,3-triphenylpropan-2-one in nanocrystalline suspensions at 330 nm

Surprisingly we were able to first detect a lifetime for diphenylmethyl radical, indicating that the generation of this radical is indeed taking place. Also, the bi exponential decay for the diphenylmethyl radical was 50 times faster in the triphenylacetone versus in tetraphenylacetone.<sup>21</sup> In addition we expand the scope of this research by exploring different derivatives such as adamantyl substituted ketones and learn that the lifetimes for the ketones with an adamantyl moiety all exhibit a much longer lifetime ranging in the 50-60  $\mu$ s.

### 5.3 Conclusion

In this paper we demonstrate the feasibility of measuring lifetimes of crystalline compounds by optical methods. The presented method combines known knowledge of transmission absorption spectroscopy along with desirable characteristics of nanocrystalline suspensions to extract mechanistic information of photochemical reactions of crystalline compounds. The study reinforces the projected hypothesis that upon initial  $\alpha$ -cleavage the kinetics for the radical pairs

to recombine through an intersystem crossing to regenerate the starting material. Without any observation of kinetics it is most likely assumed that the reaction did not proceed. However, this finding indicates the reactivity in the solid-state as well as the lifetimes of the photochemical transformation for the short-lived diphenylmethyl radical transient species. In addition, this paper aims to expand the scope of this chemistry by introducing various ketones with an adamantyl moiety attached at the ketone's  $\alpha$ -position to the primary, secondary, and tertiary carbon. The adamantyl moiety was chosen due to their bulkiness and likeliness to form crystalline compounds. Also, the adamantanes are attached at the primary, secondary, and tertiary carbon to ensure that the engineered ketones will not undergo a photodecarbonylation reaction. Upon photolysis of these derivatives, the data indicates that the solid-state lifetime of 1a is similar to that of the solution state  $\tau = 1.4 - 1.6 \mu\text{s}$ . However, the solid-state lifetimes ( $\tau = 50-60 \mu\text{s}$ ) for 1b-1d are much longer than the respective solution state lifetimes ( $\tau = 1.2 \mu\text{s}$ ). It is also possible that this discrepancy exists because of the physical and chemical properties of the adamantyl group. In the midst of growing relevant single crystals for x-ray crystallography to further verify this hypothesis, we are also proposing more derivatives to further explore the internal photochemical reactivity of ketones.

## 5.4 Supplementary Information for Chapter 5

Contents:	Page number
5.4.1). General Methods	222
5.4.2). Experimental Section	224
5.4.3). Spectral data ( $^1\text{H}$ NMR, $^{13}\text{C}$ NMR, UV-VIS)	228
5.4.4). Power X-Ray Diffraction (PXRD) Analysis	253
5.4.5). Solid-State Photochemistry of Dry Powder	257
5.4.6). Laser Flash Photolysis	263
5.4.7). Dynamic Light Scattering	270

**5.4.1 General Methods.** All commercially obtained reagents/solvents were used as received without further purification. Unless stated otherwise, reactions were conducted in oven-dried glassware under argon atmosphere. Proton magnetic resonance spectra were recorded at 500 MHz, and carbon-13 magnetic resonance spectra were recorded at 125 MHz, respectively. All chemical shifts are reported in ppm on the  $\delta$ -scale relative to TMS ( $\delta$  0.0) using residual solvent as reference ( $\text{CDCl}_3$   $\delta$  7.26 and  $\delta$  77.16 for proton and carbon, respectively,  $\text{CD}_3\text{CN}$   $\delta$  1.94 and 1.32, 118.26 for proton and carbon respectively). Standard abbreviations indicating multiplicity were used as follows: s (singlet), b (broad), d (doublet), t (triplet), q (quartet), and m (multiplet). Data for  $^{13}\text{C}$  NMR spectra are reported in terms of chemical shift ( $\delta$  ppm). High-resolution mass spectrum data were recorded on a DART spectrometer in positive (ESI+) ion mode. UV-Vis absorption and transmission spectra were recorded on Ocean Optics spectrometer (DT-MINI-2-GS UV-VIS-NIR LightSource and USB2000+ using SpectraSuite software package). Dynamic Light Scattering (DLS) data were recorded using a Beckman-Coulter N4 Plus particle analyzer with a 10 mW helium-neon laser at 632.8 nm. The particle size was determined using the  $62.6^\circ$  detection angle and was calculated using the size distribution processor (SDP) analysis package provided by the manufacturer. Melting point values were recorded on a Melt-Point II<sup>®</sup> apparatus. Infra-Red spectra were recorded on a PerkinElmer<sup>®</sup> Spectrum Two spectrometer equipped with a universal ATR sampling accessory. Nanosecond transient absorption experiments were performed using Laser Flash Photolysis instrument from Edinburgh Instruments in conjunction with a Nd:YAG laser (Brilliant b, Quantel<sup>®</sup>) with 266-nm output, 4-6 ns pulse width and 36-40 mJ pulse energy. The optical detection is based on a pulsed Xenon arc lamp (450 W), a monochromator (TMS300, Czerny-Turner), a photomultiplier detector (Hamamatsu R928) and a digital oscilloscope (TDS3012C, 100 MHz and 1.25 GS/s from Tektronix). The laser flash

photolysis experiments were performed with 1 cm quartz flow cell mounted on a home-built sample holder that is placed at the cross-section of the laser incident beam and the probe light. Continuously Argon gas purged acetonitrile solutions or crystalline suspensions of ketones (0.0025g/L) were flown through the quartz cell using a peristaltic pump (Masterflex L/S) at a rate of 1.6 – 3.2 mL/min. Due to aggregation fresh samples in batches of 20 mL were made for the crystalline suspensions every 10 minutes. Time-resolved absorption maps were recorded with continuous flow of samples through the quartz cell. Lifetimes at  $\lambda_{\text{max}}$  for end-of-pulse spectra were reproducible and doubly verified/processed with Edinburgh Instruments L900 internal software and Igor Pro (version 6.34A, Wavemetrics) software. The parameters under the detector monochromator settings are as follows: the ketones were observed at the corresponding  $\lambda_{\text{max}}$  in solution (320-330 nm) and in crystalline suspensions (330-340 nm), and the band width was set between 1.00 to 3.00 nm. The flash lamp settings were set where the frequency was at 10 Hz, width at 40  $\mu\text{s}$ , and delay at 4000  $\mu\text{s}$ . The Q-switch settings were set where the frequency was at 1.0 Hz, width at 20  $\mu\text{s}$ , and delay between 260-300  $\mu\text{s}$ .

### 5.4.2 Experimental Section:

Unless reported, all of the substituted ketones were synthesized using commercially available starting materials.

**General Synthesis of Acid Chlorides:**<sup>17</sup> To mitigate costs, the synthesis of these commercially available acid chlorides was synthesized via modified procedure. In an oven flame-dried, argon filled round-bottom flask, carboxylic acid (1 eq) is stirred under dry DCM (15 eq) and is treated with oxalyl chloride (1.1 eq). The reaction is then allowed to stir for 20 minutes and is then treated with dry dimethylformamide (1 eq). After the formation of gas ceases the reaction is further allowed to react for 2 hours. The reaction is quenched with 0.5M HCl and the extracted with DCM (3 X 20mL) and dried over Na<sub>2</sub>SO<sub>4</sub>. The solvents were removed under reduced pressure. The resulting liquid is then stored in a vial for the proceeding steps.

**General Synthesis of ketones:** Following a modified procedure by Rajca *et al.*<sup>16</sup>, in a flame-dried, argon filled round-bottom flask, acid chloride (0.5 eq) in THF (15 eq) was added over 5 minutes to a 5:1 THF/hexane solution of (diphenylmethyl)lithium solution (2.5 eq) stirring at 0 °C. The reaction undergoes a color change from a light orange-red to a deep dark-red. After 1 hour, the remaining acid chloride (0.5 eq) in THF (15 eq) was added over 5 minutes. The reaction is warmed to room temperature and is stirred overnight. The reaction is quenched with 0.5M HCl and the extracted with diethyl ether (3 X 20 mL) and dried over Na<sub>2</sub>SO<sub>4</sub>. The solvents were removed under reduced pressure and was subjected to column chromatography (1:4-9 acetone:hexane). The resulting crystalline solids were further recrystallized via ethanol (19-60% yield).

### Solid-State Photochemistry of Dry Powder:

All solid-state photochemistry product analysis was conducted via a medium-pressure Hg Hanovia lamp with a pyrex emersion well filter with a cutoff of  $\lambda \leq 220$  nm and analyzed by  $^1\text{H}$  NMR (500 MHz,  $\text{CDCl}_3$ ). Samples are grinded between two microscope slides which are then subjected to UV light irradiation inside a chamber. All solution state photochemistry product analysis was conducted in the same setting as the solid state but dissolved in MeCN.

1,2,2-triphenylethan-1-one: Yield 65%; m.p. 66-67 °C; IR(neat)  $\nu_{\text{max}} = 3085, 3060, 3026, 2924, 2854, 1684, 1596, 1495, 1447, 1207, 1007, 745, 696$   $\text{cm}^{-1}$ ;  $\lambda_{\text{max}} = 210-215, 245-250, 270-275$  nm; Using ethyl acetate and hexanes (1:19) ( $R_f = 0.42$ );  $^1\text{H}$  NMR (500 MHz,  $\text{CDCl}_3$ )  $\delta$  8.01-7.99 (d, 2H), 7.51 (m, 1H), 7.42-7.39 (m, 2H), 7.34-7.23 (m, 10H), 6.04 (s, 1H);  $^{13}\text{C}$  NMR (125 MHz,  $\text{CDCl}_3$ )  $\delta$  198.20, 139.08, 136.82, 133.05, 129.15, 128.98, 128.74, 128.63, 127.16, 59.44

1,1,3-triphenylpropan-2-one: Yield 60%; m.p. 137-138 °C; IR(neat)  $\nu_{\text{max}} = 3089, 2925, 3029, 1713, 1492, 1053$   $\text{cm}^{-1}$ ;  $\lambda_{\text{max}} = 260-265, 290-300$  nm; Using ethyl acetate and hexanes (1:19) ( $R_f = 0.348$ );  $^1\text{H}$  NMR (500 MHz,  $\text{CDCl}_3$ )  $\delta$  7.32-7.13 (m, 15H), 5.22 (s, 1H), 3.79 (s, 2H);  $^{13}\text{C}$  NMR (125 MHz,  $\text{CDCl}_3$ )  $\delta$  205.78, 138.04, 134.00, 129.59, 129.07, 128.73, 128.71, 127.28, 127.13, 62.78, 49.68

1,1,3-triphenylbutan-2-one: Yield 25%; m.p. 45-46 °C; IR(neat)  $\nu_{\text{max}} = 3025, 1715, 1599, 1494, 1451, 1028, 727, 695$   $\text{cm}^{-1}$ ;  $\lambda_{\text{max}} = 250-260, 295-305$  nm; Using ethyl acetate and hexanes (1:9) ( $R_f = 0.47$ );  $^1\text{H}$  NMR (500 MHz,  $\text{CDCl}_3$ )  $\delta$  7.37-7.27 (m, 6H), 7.24-7.14 (m, 7H), 6.89-6.87 (m, 2H), 5.17 (s, 1H), 3.92-3.88 (q, 1H), 1.39-1.38 (s, 3H);  $^{13}\text{C}$  NMR (125 MHz,  $\text{CDCl}_3$ )  $\delta$  208.06,

140.20, 138.73, 138.01, 129.13, 129.05, 129.02, 128.77, 128.29, 128.16, 127.41, 127.37, 126.79, 61.94, 52.66, 17.86

3-methyl-1,1, 3-triphenylbutane-2-one: Yield 70%; m.p. 75-76 °C; IR(neat)  $\nu_{\max}$  = 2975, 1710, 1495, 1450, 1078, 1041, 698  $\text{cm}^{-1}$ ;  $\lambda_{\max}$  = 255-265, 290-310 nm; Using ethyl acetate and hexanes (1:9) ( $R_f$  = 0.50);  $^1\text{H}$  NMR (500 MHz,  $\text{CDCl}_3$ )  $\delta$  7.29-7.27 (m, 3H), 7.22-7.14 (m, 8H), 7.03-7.01 (m, 4H), 5.08 (s, 1H), 1.46 (s, 6H);  $^{13}\text{C}$  NMR (125 MHz,  $\text{CDCl}_3$ )  $\delta$  210.04, 142.51, 139.77, 128.66, 128.39, 128.32, 127.17, 126.96, 126.72, 58.68, 53.70, 24.96

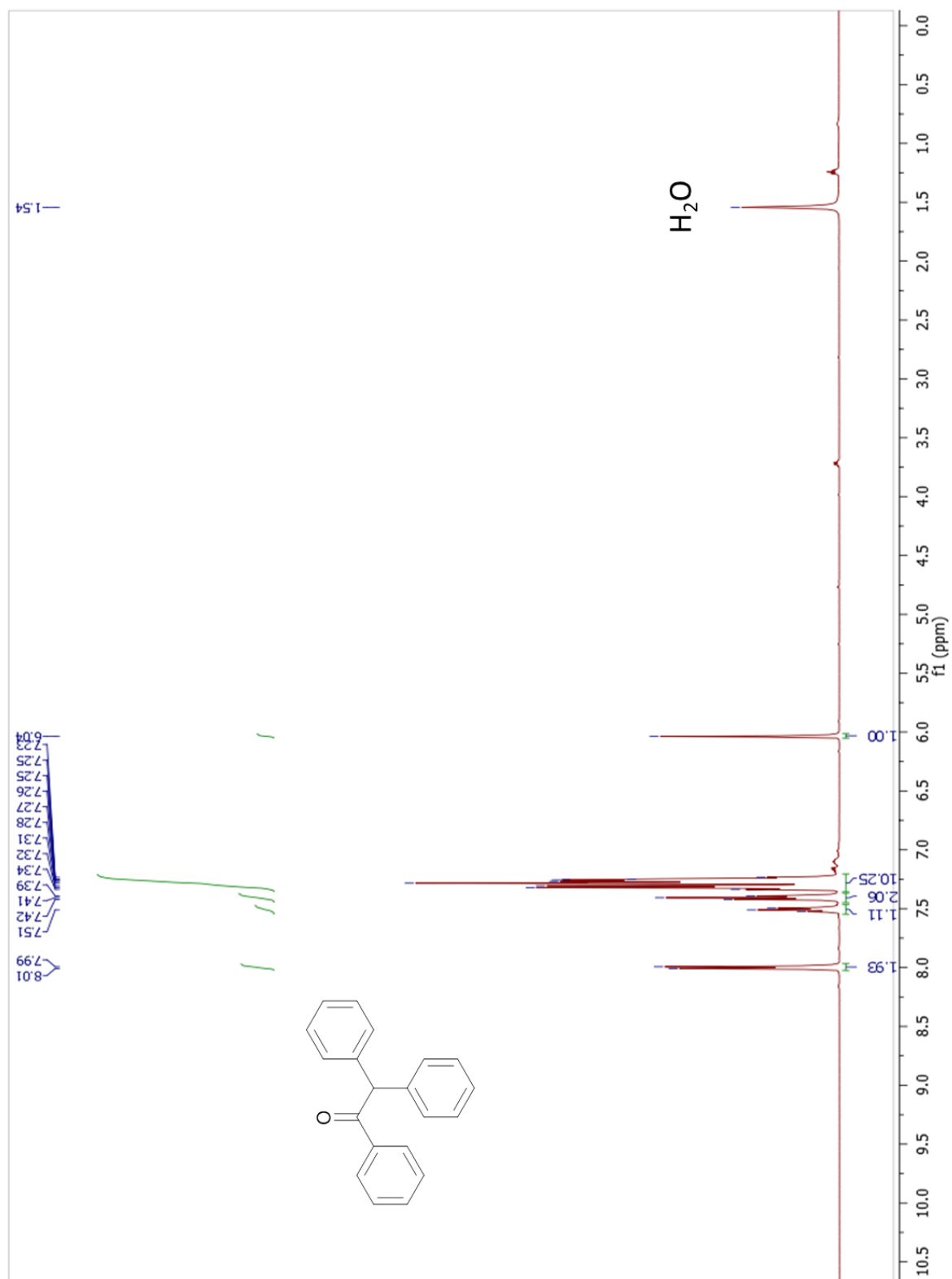
3-((3r,5r,7r)-adamantan-1-yl)-1,1-diphenylpropan-2-one: Yield 40%; m.p. 102.3-103.2 °C; IR(neat)  $\nu_{\max}$  = 3027, 2903, 2841, 1707, 1495, 1450, 1083  $\text{cm}^{-1}$ ;  $\lambda_{\max}$  = 255-260, 290-310 nm; Using ethyl acetate and hexanes (1:19) ( $R_f$  = 0.442);  $^1\text{H}$  NMR (500 MHz,  $\text{CDCl}_3$ )  $\delta$  7.31-7.20 (m, 8H), 5.07 (s, 1H), 2.28 (s, 2H), 1.93 (s, 1H), 1.66-1.64 (m, 12H);  $^{13}\text{C}$  NMR (125 MHz,  $\text{CDCl}_3$ )  $\delta$  207.78, 138.42, 129.08, 128.64, 127.13, 66.20, 55.89, 42.40, 36.78, 33.92, 28.60; HRMS (DART) calcd. for  $[\text{C}_{28}\text{H}_{24}\text{O}+\text{H}]^+$  344.21215, found 344.19249

1-((1r,3r,5r,7r)-adamantan-2-yl)-2,2-diphenylethan-1-on; Yield 19%; m.p. 89.4-89.7 °C; IR(neat)  $\nu_{\max}$  = 3061, 2905, 2848, 1700, 1495, 1447, 1093, 1028  $\text{cm}^{-1}$ ;  $\lambda_{\max}$  = 255-260, 295-305 nm; Using ethyl acetate and hexanes (1:19) ( $R_f$  = 0.442);  $^1\text{H}$  NMR (500 MHz,  $\text{CDCl}_3$ )  $\delta$  7.32-7.22 (m, 8H), 5.39 (s, 1H), 2.75 (s, 1H), 2.38 (s, 2H); 1.89-1.69 (m, 9H), 1.56-1.54 (m, 4H);  $^{13}\text{C}$  NMR (125 MHz,  $\text{CDCl}_3$ )  $\delta$  210.68, 139.09, 128.88, 128.59, 126.99, 60.55, 57.13, 38.54, 38.32, 33.09, 29.59, 27.69, 27.51; HRMS (DART) calcd. for  $[\text{C}_{28}\text{H}_{24}\text{O}+\text{H}]^+$  377.19837, found 330.19239

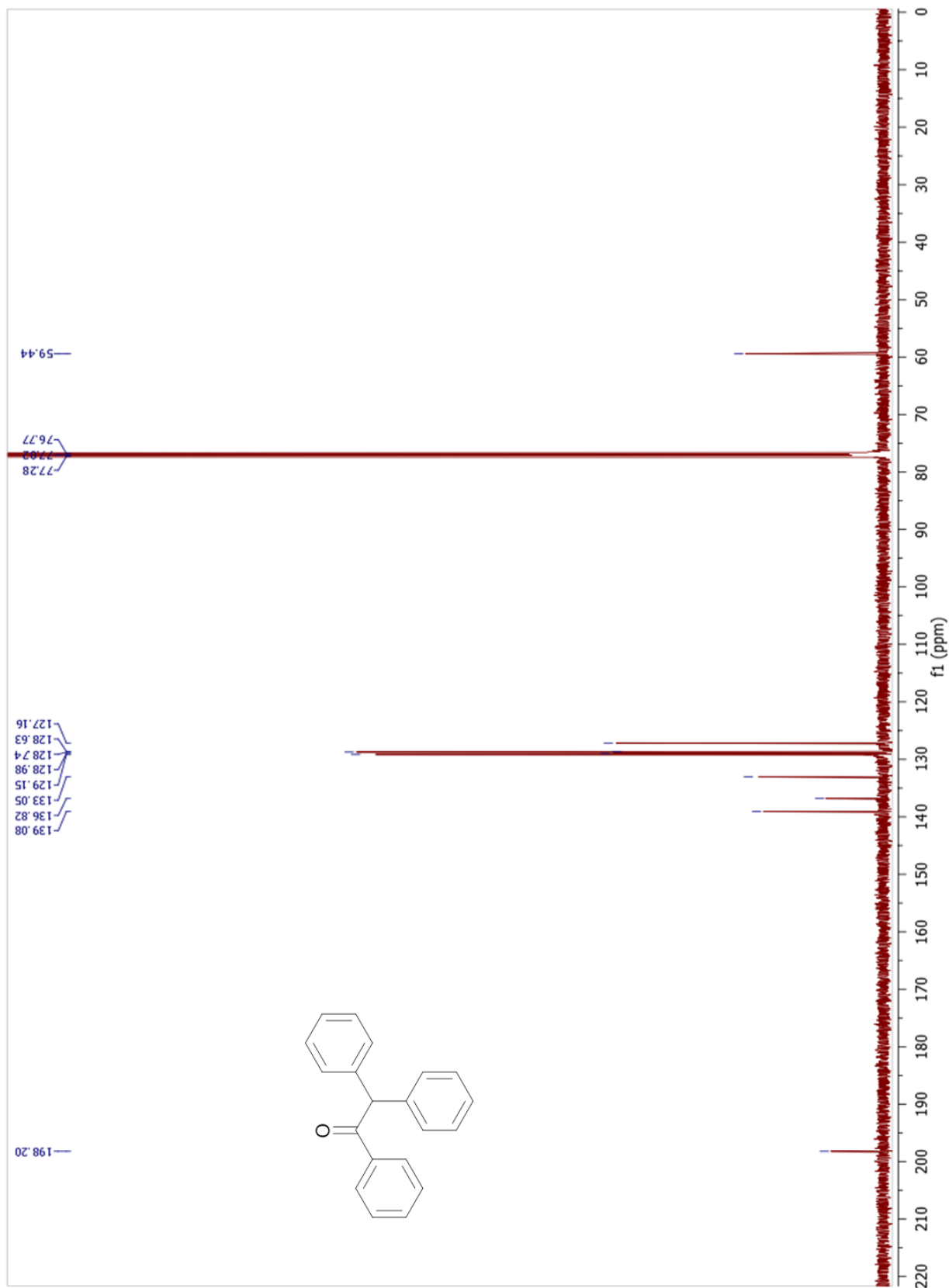


1-((3r,5r,7r)-adamantan-1-yl)-2,2-diphenylethan-1-one: Yield 55%; m.p. 104.4-105 °C;  
IR(neat)  $\nu_{\max}$  = 3051, 2910, 2848, 1700, 1494, 1445, 1348, 1021  $\text{cm}^{-1}$ ;  $\lambda_{\max}$  = 260-265, 295-305  
nm; Using ethyl acetate and hexanes (1:19) ( $R_f$  = 0.414);  $^1\text{H}$  NMR (500 MHz,  $\text{CDCl}_3$ )  $\delta$  7.3-7.19  
(m, 8H), 5.62 (s, 1H), 2.02 (s, 3H), 1.83-1.82 (d, 6H) 1.74-1.64 (dd, 6H);  $^{13}\text{C}$  NMR (125 MHz,  
 $\text{CDCl}_3$ )  $\delta$  212.54, 139.43, 128.92, 128.52, 126.85, 56.71, 47.85, 38.21, 36.47, 27.88. HRMS  
(DART) calcd. for  $[\text{C}_{28}\text{H}_{24}\text{O}+\text{H}]^+$  330.19837, found 330.19249

### 5.4.3 Spectral data ( $^1\text{H}$ NMR, $^{13}\text{C}$ NMR, UV-VIS)



**Figure 5.S1**  $^1\text{H}$  NMR (500 MHz,  $\text{CDCl}_3$ ) of 1,2,2-triphenylethan-1-one



**Figure 5.S2**  $^{13}\text{C}$  NMR (125 MHz,  $\text{CDCl}_3$ ) of 1,2,2-triphenylethan-1-one

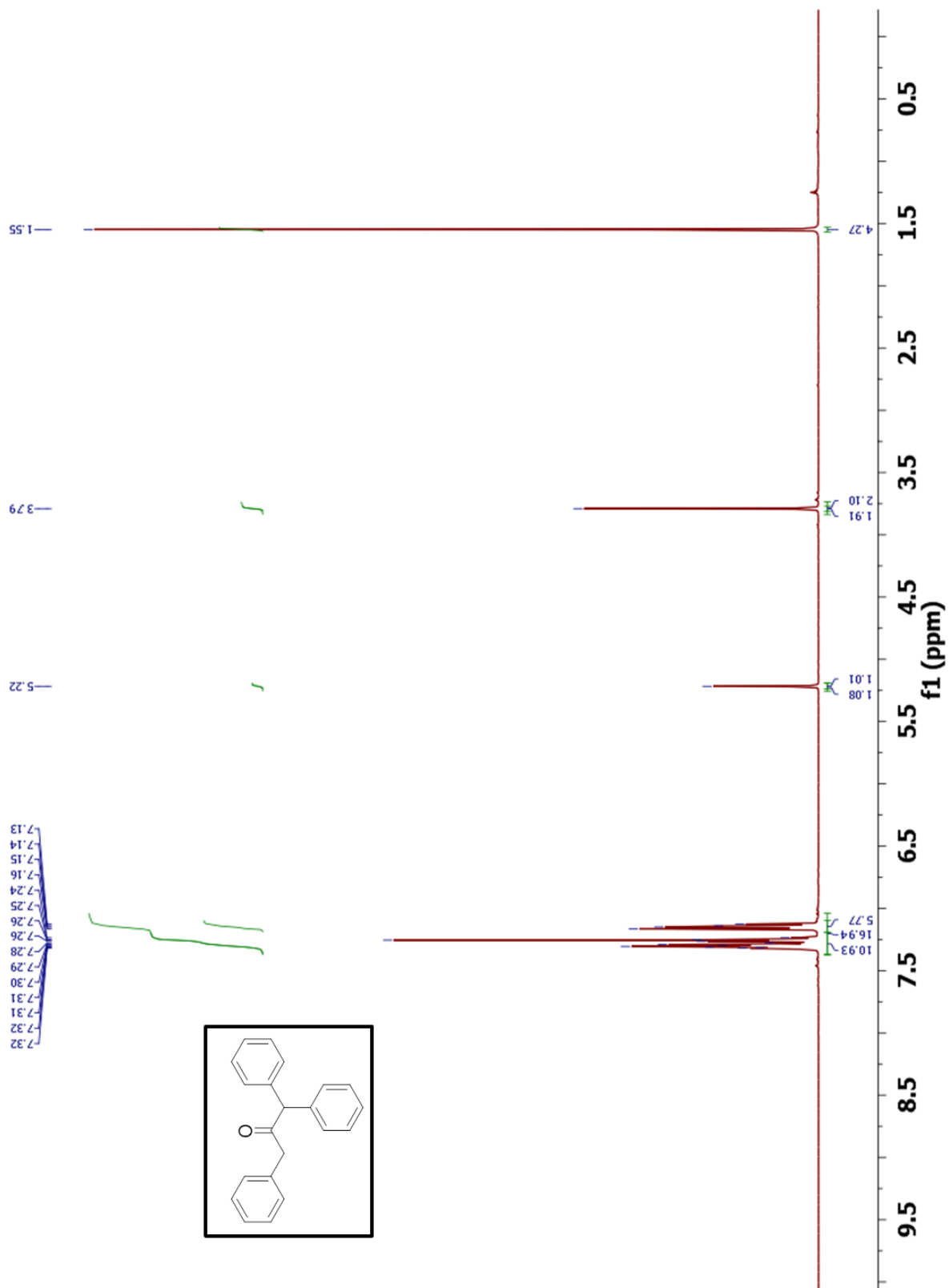
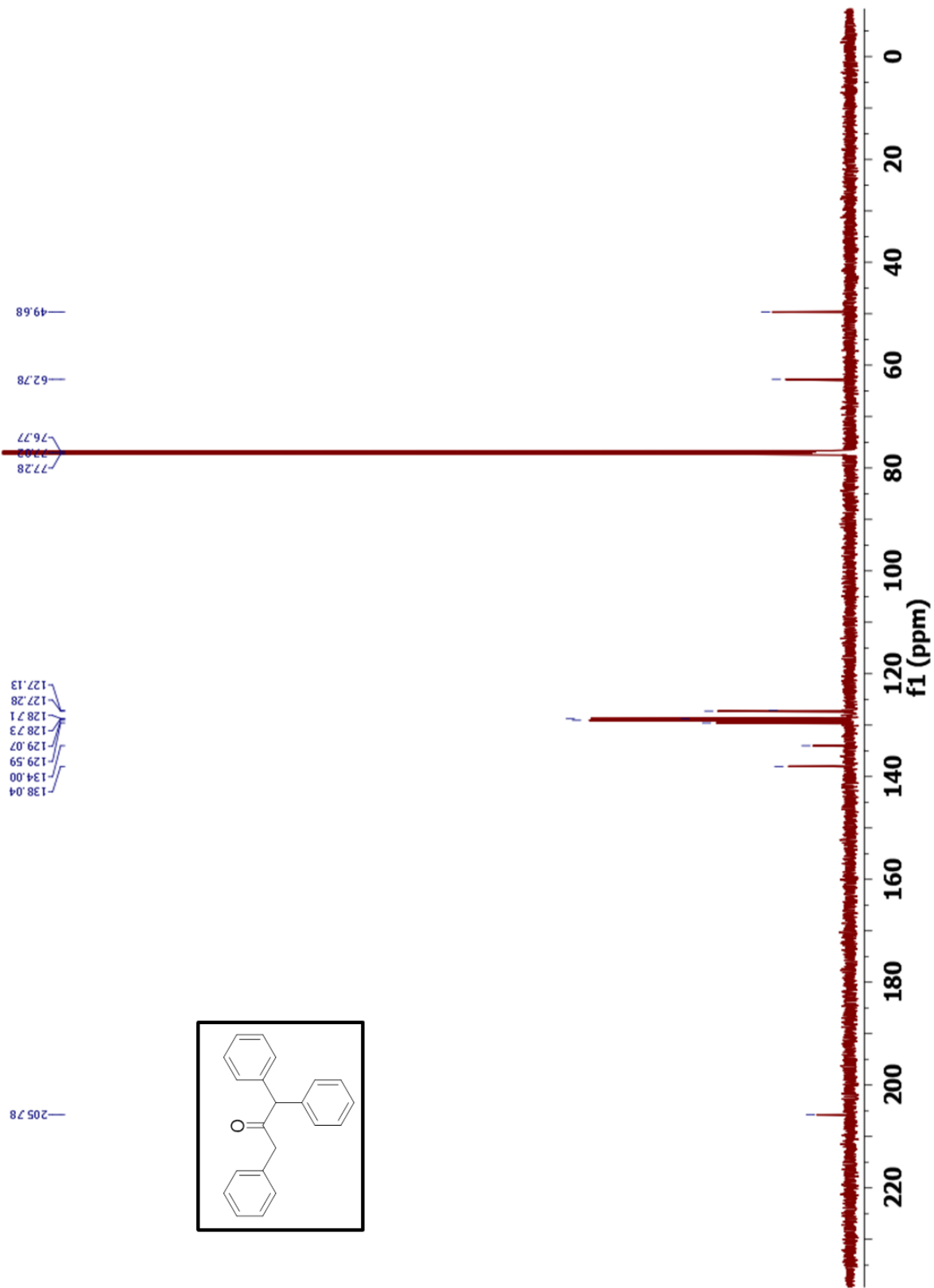
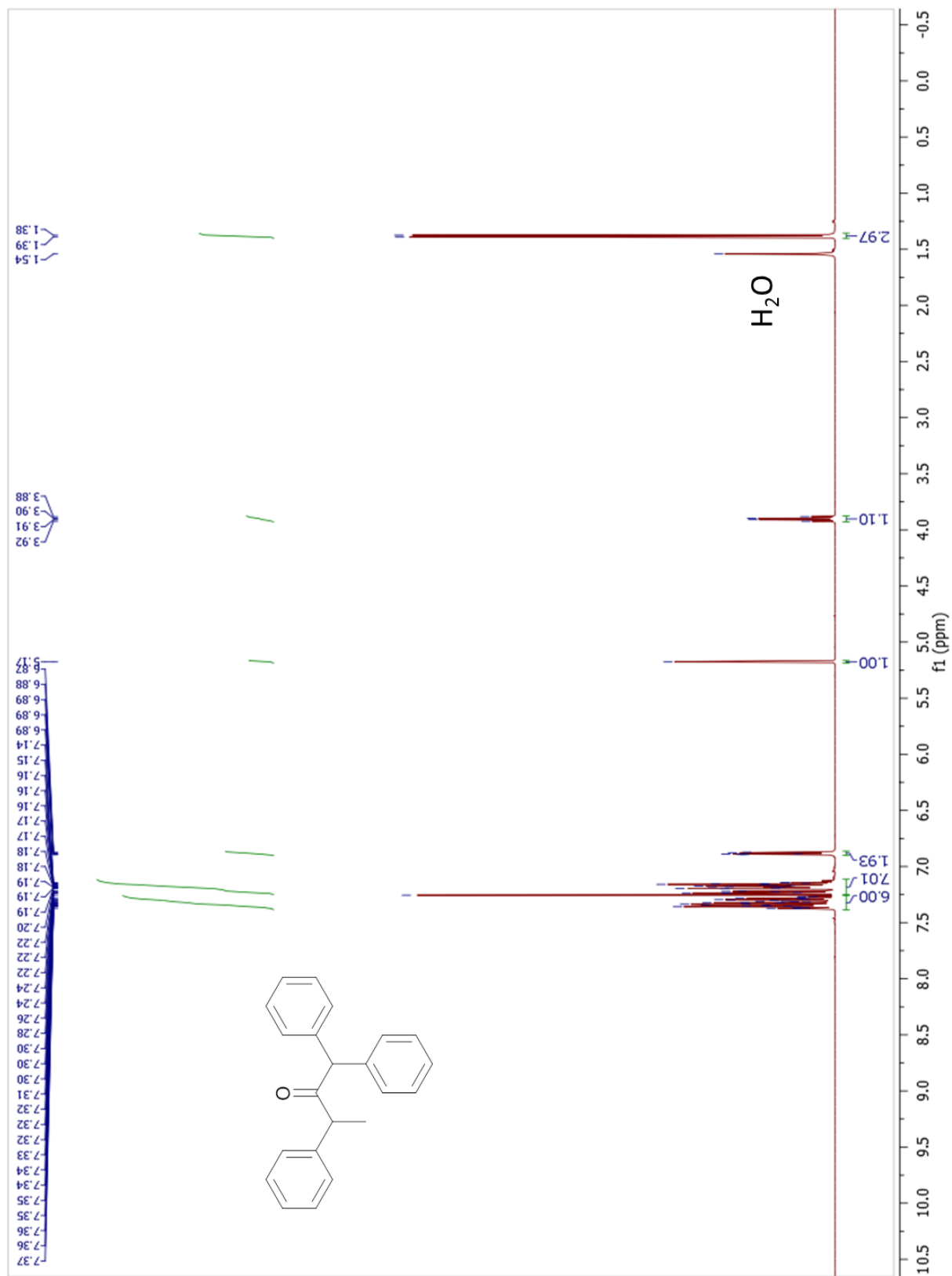


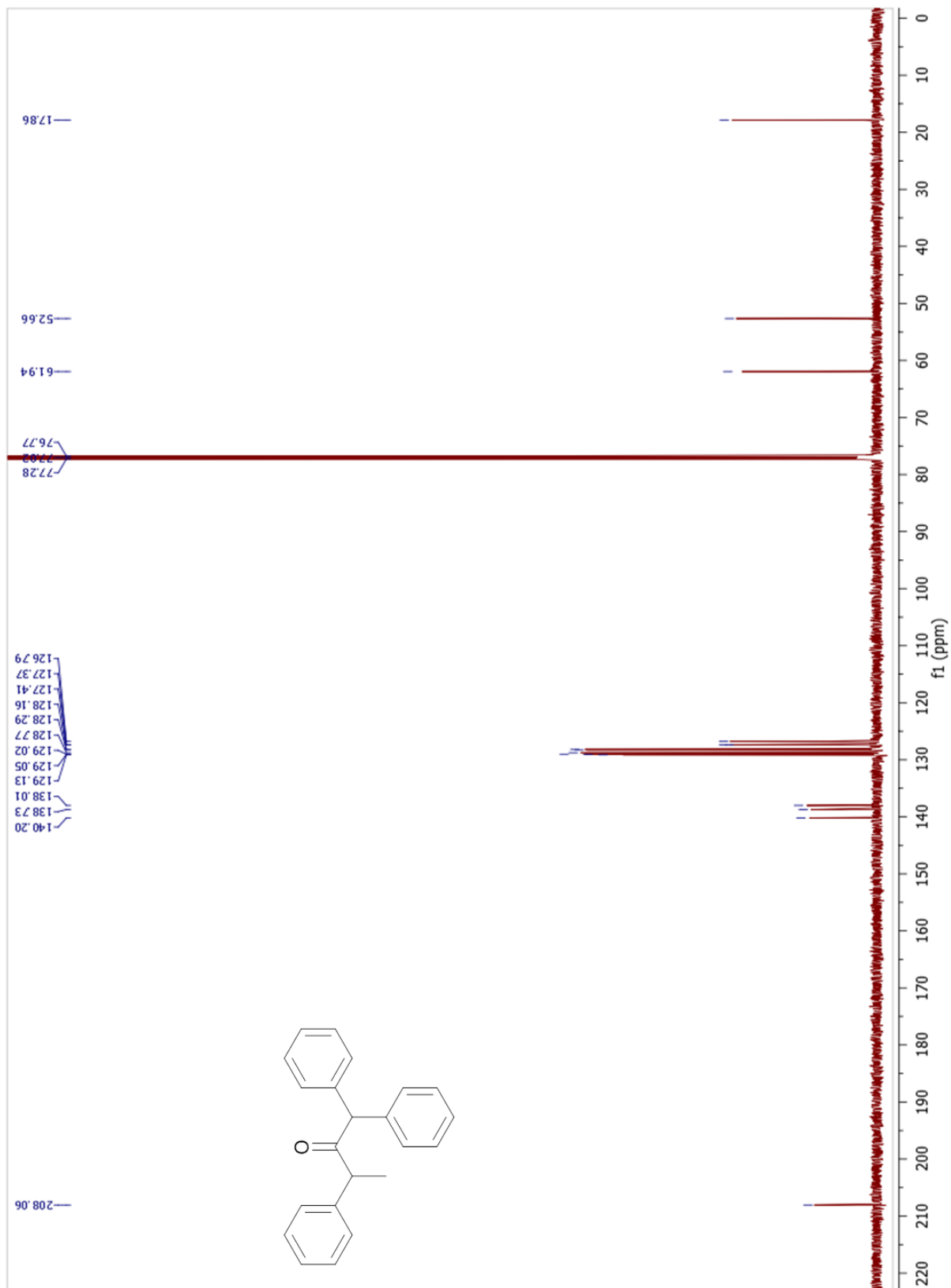
Figure 5.S3 <sup>1</sup>H NMR (500 MHz, CDCl<sub>3</sub>) of 1,1,3-triphenylpropan-2-one



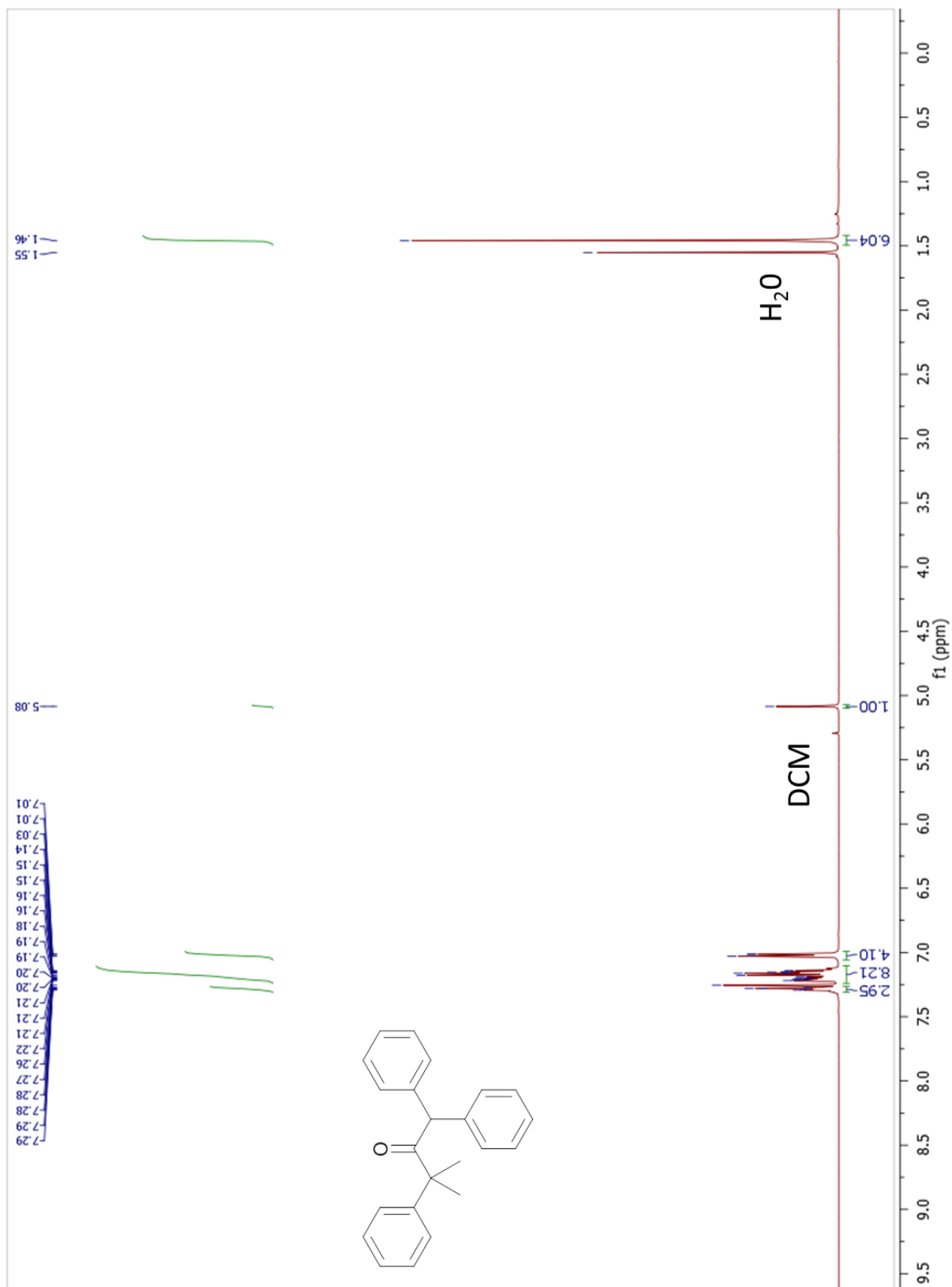
**Figure 5.S4**  $^{13}\text{C}$  NMR (125 MHz, CDCl<sub>3</sub>) of 1,1,3-triphenylpropan-2-one



**Figure 5.S5**  $^1\text{H}$  NMR (500 MHz,  $\text{CDCl}_3$ ) of 1,1,3-triphenylbutan-2-one

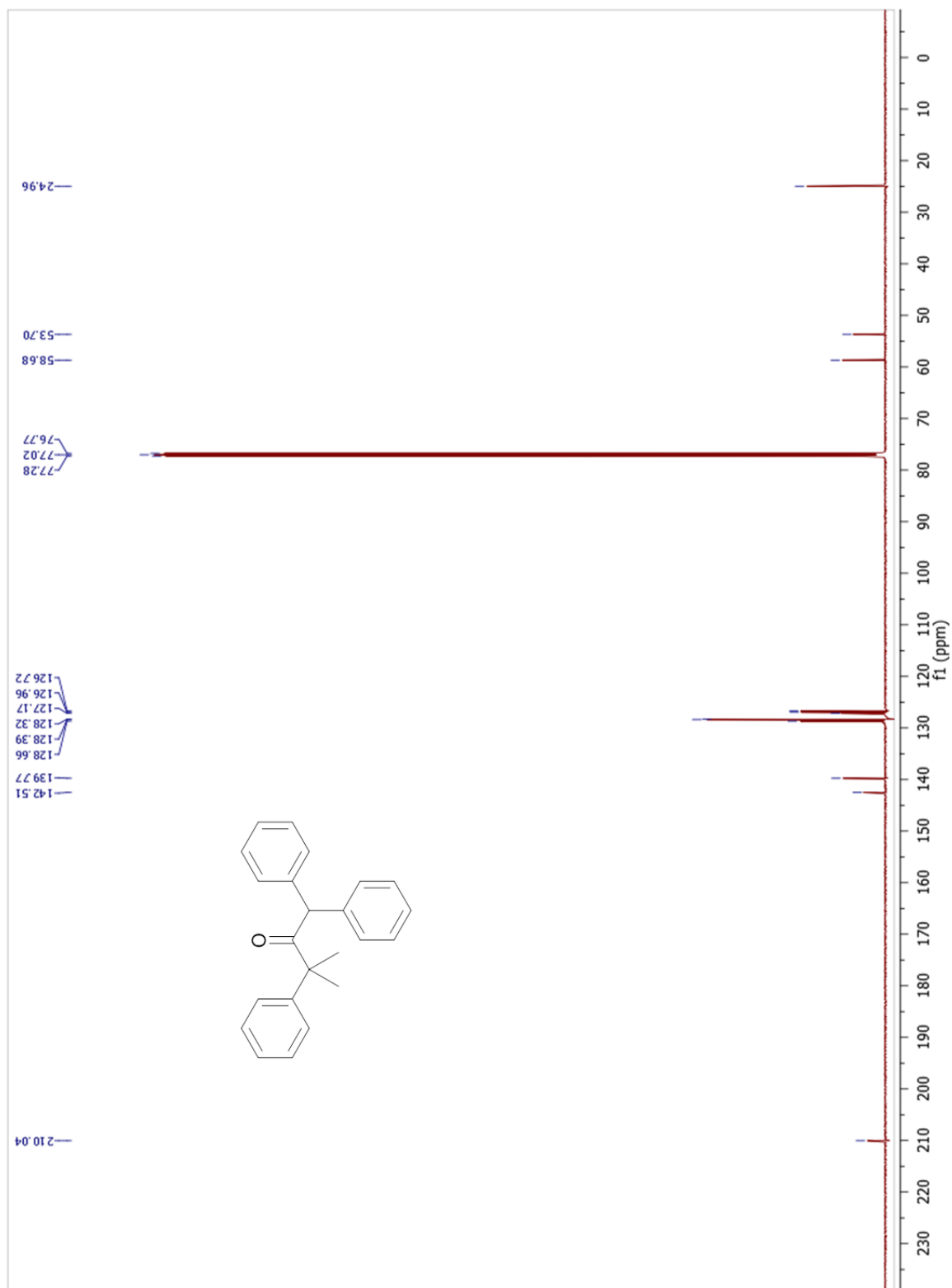


**Figure 5.S6**  $^{13}\text{C}$  NMR (125 MHz,  $\text{CDCl}_3$ ) of 1,1,3-triphenylbutan-2-one

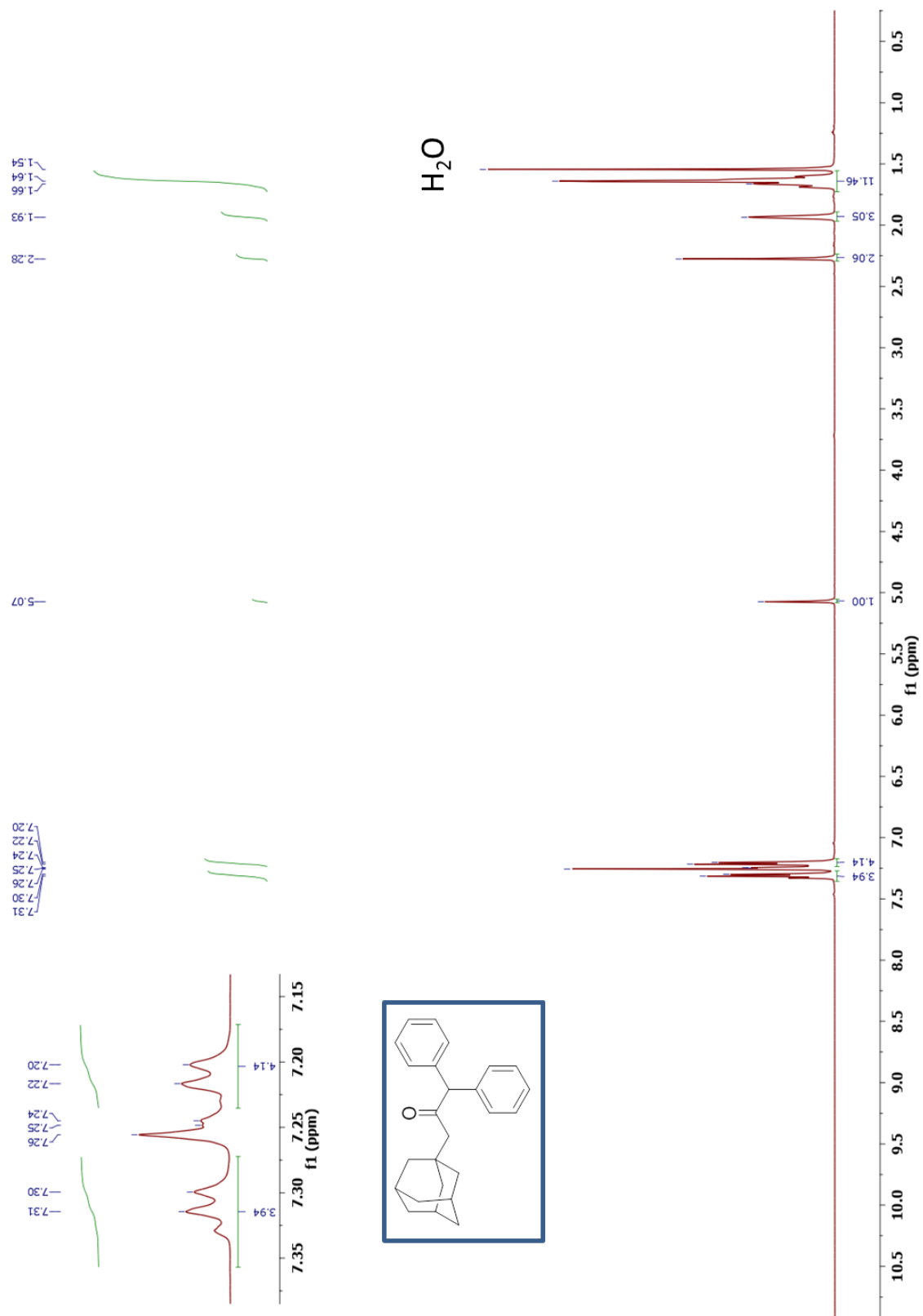


**Figure 5.S7**  $^1\text{H}$  NMR (500 MHz,  $\text{CDCl}_3$ ) of 3-methyl-1,1,3-triphenylbutan-2-one

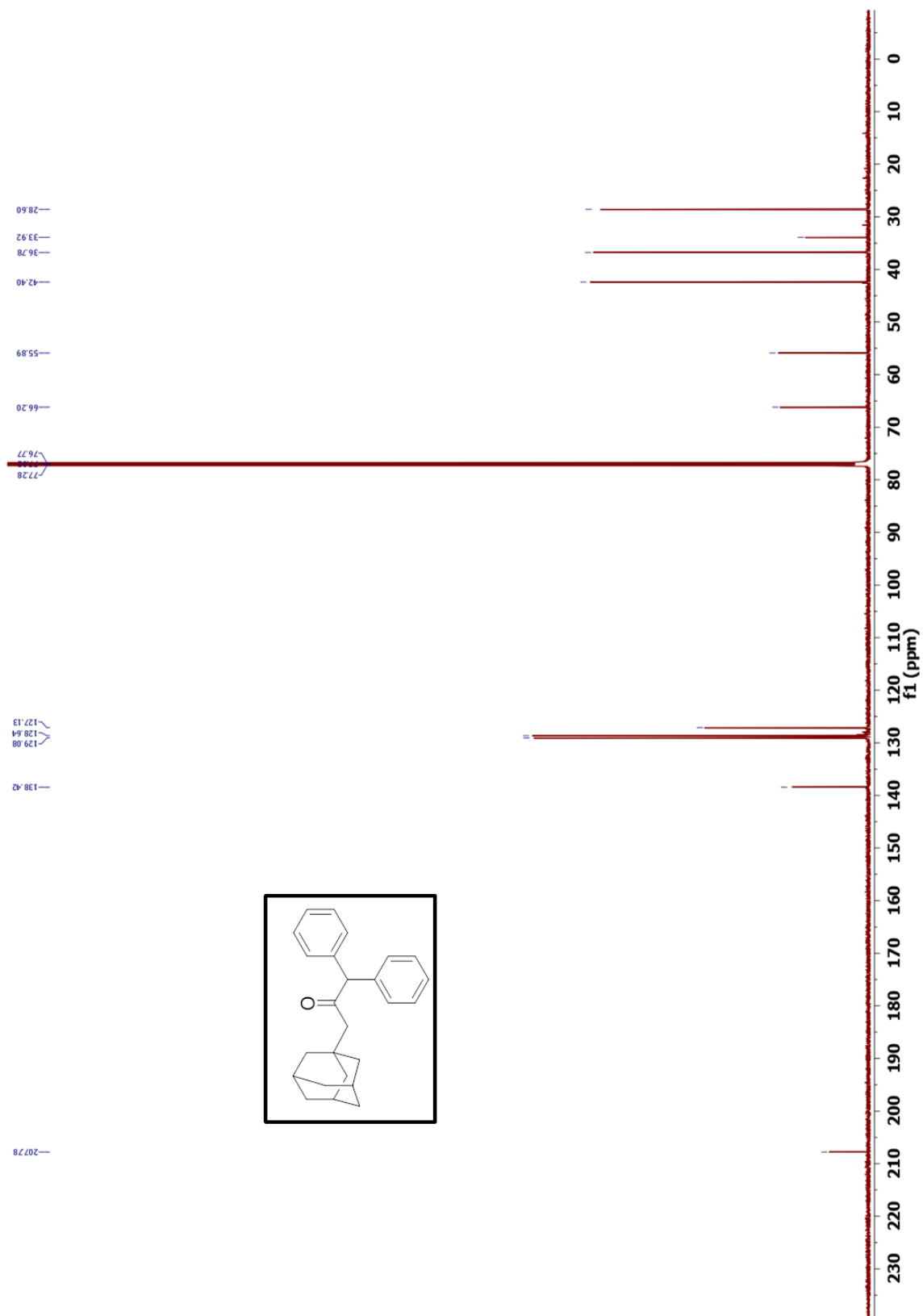




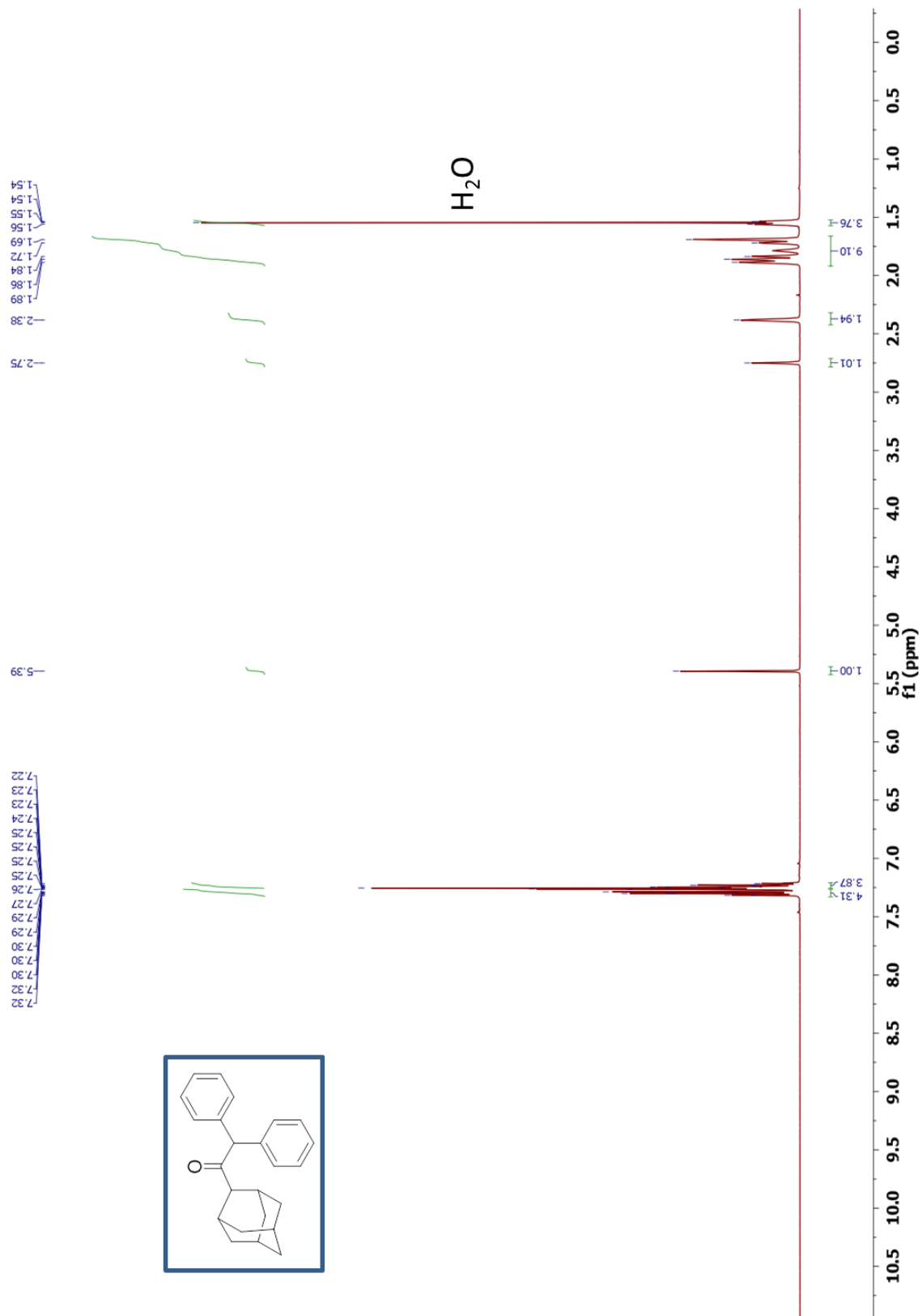
**Figure 5.S8**  $^{13}\text{C}$  NMR (125 MHz,  $\text{CDCl}_3$ ) of 3-methyl-1,1,3-triphenylbutan-2-one



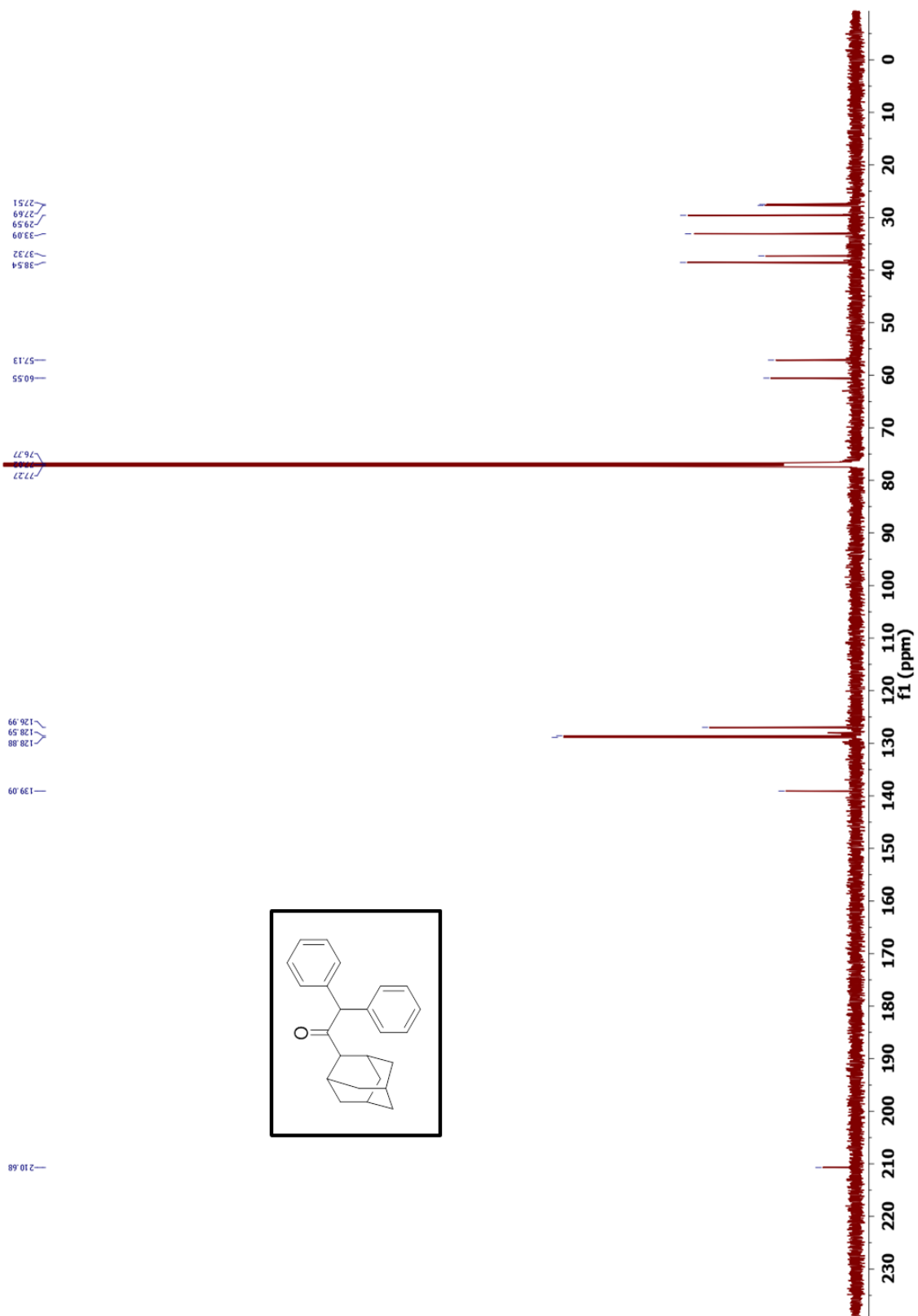
**Figure 5.S9**  $^1\text{H}$  NMR (500 MHz,  $\text{CDCl}_3$ ) of 3-((3r,5r,7r)-adamantan-1-yl)-1,1-diphenylpropan-2-one



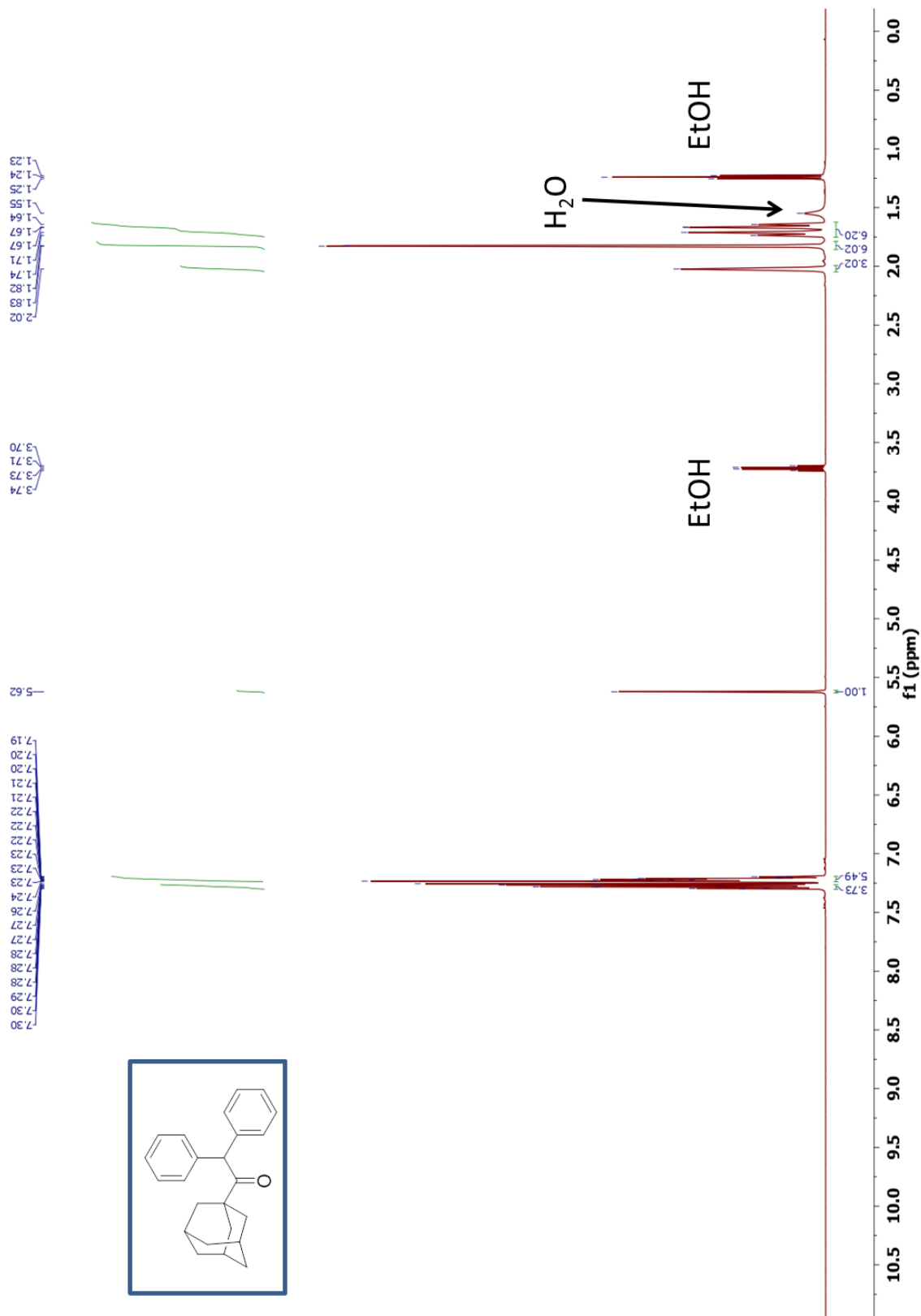
**Figure 5.S10**  $^{13}\text{C}$  NMR (125 MHz,  $\text{CDCl}_3$ ) of 3-((3r,5r,7r)-adamantan-1-yl)-1,1-diphenylpropan-2-one



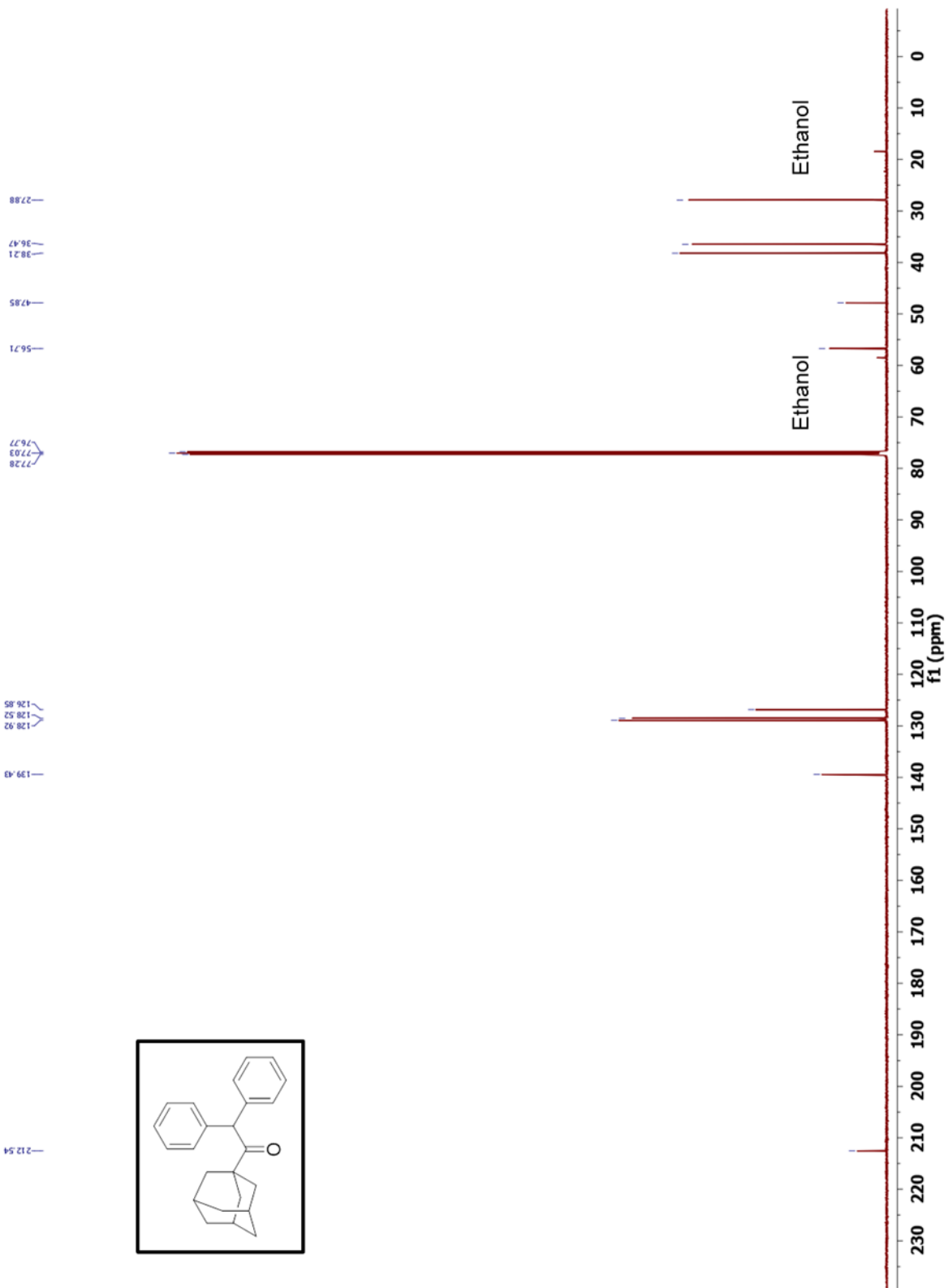
**Figure 5.S11**  $^1\text{H}$  NMR (500 MHz,  $\text{CDCl}_3$ ) of 1-((1r,3r,5r,7r)-adamantan-2-yl)-2,2-diphenylethan-1-one



**Figure 5.S12**  $^{13}\text{C}$  NMR (125 MHz,  $\text{CDCl}_3$ ) of 1-((1r,3r,5r,7r)-adamantan-2-yl)-2,2-diphenylethan-1-one



**Figure 5.S13** <sup>1</sup>H NMR (500 MHz, CDCl<sub>3</sub>) of 1-((3r,5r,7r)-adamantan-1-yl)-2,2-diphenylethan-1-one



**Figure 5.S14** <sup>13</sup>C NMR (125 MHz, CDCl<sub>3</sub>) of 1-((3r,5r,7r)-adamantan-1-yl)-2,2-diphenylethan-1-one

## IR Spectroscopy:

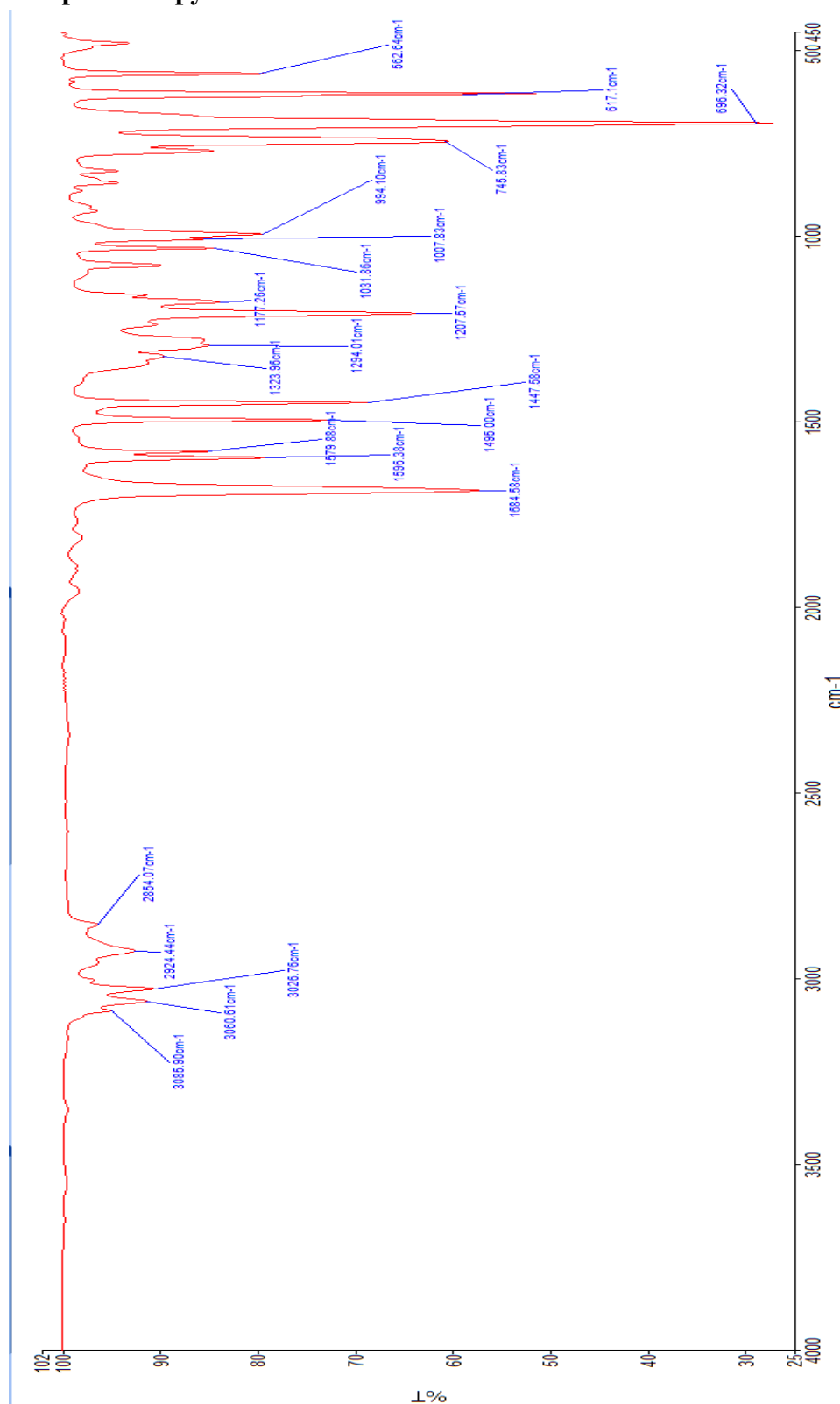


Figure 5.S15: IR(neat)  $\nu_{\max}$  of 1,2,2-triphenylethan-1-one



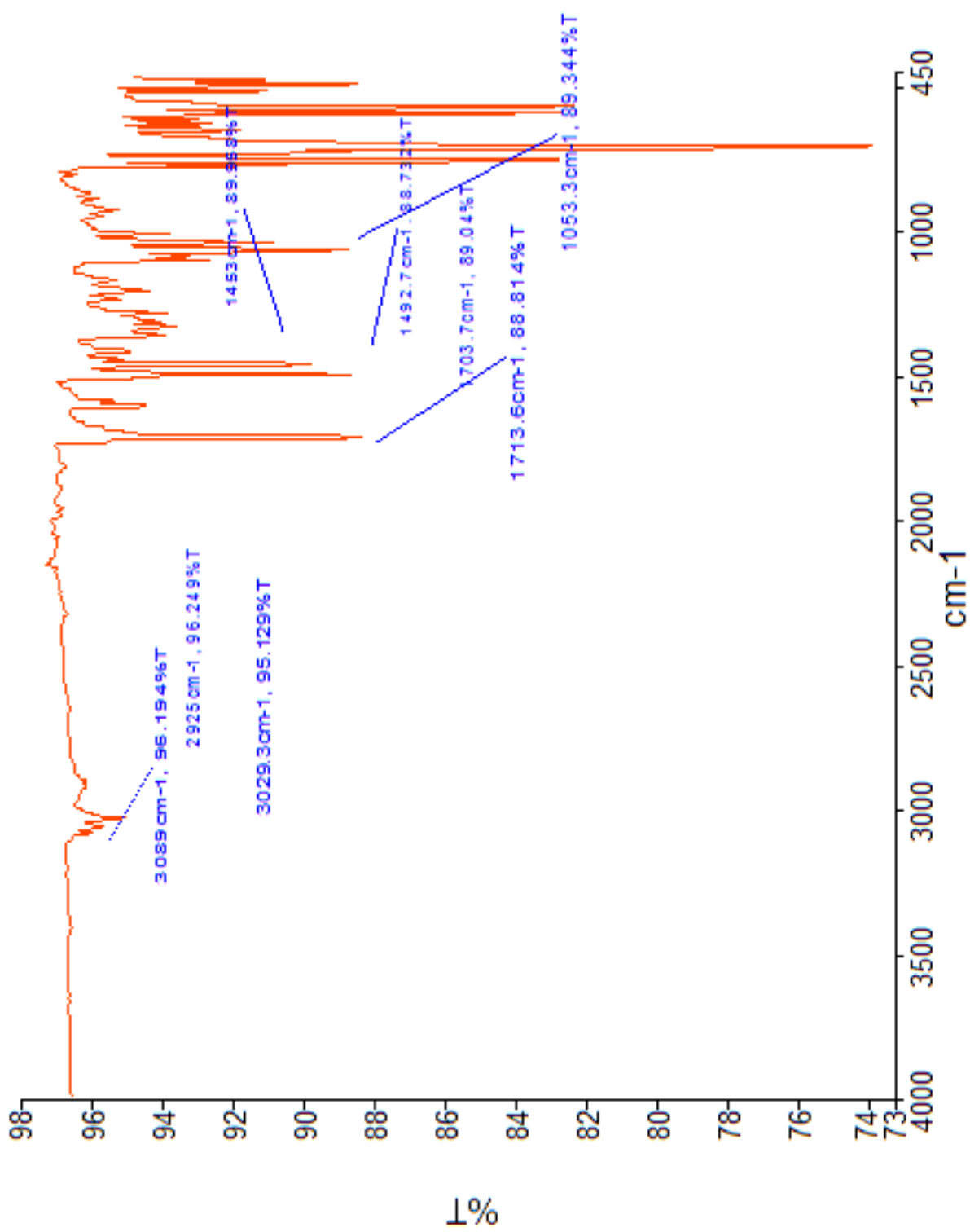


Figure 5.S16: IR(neat)  $\nu_{\max}$  of 1,1,3-triphenylpropan-2-one

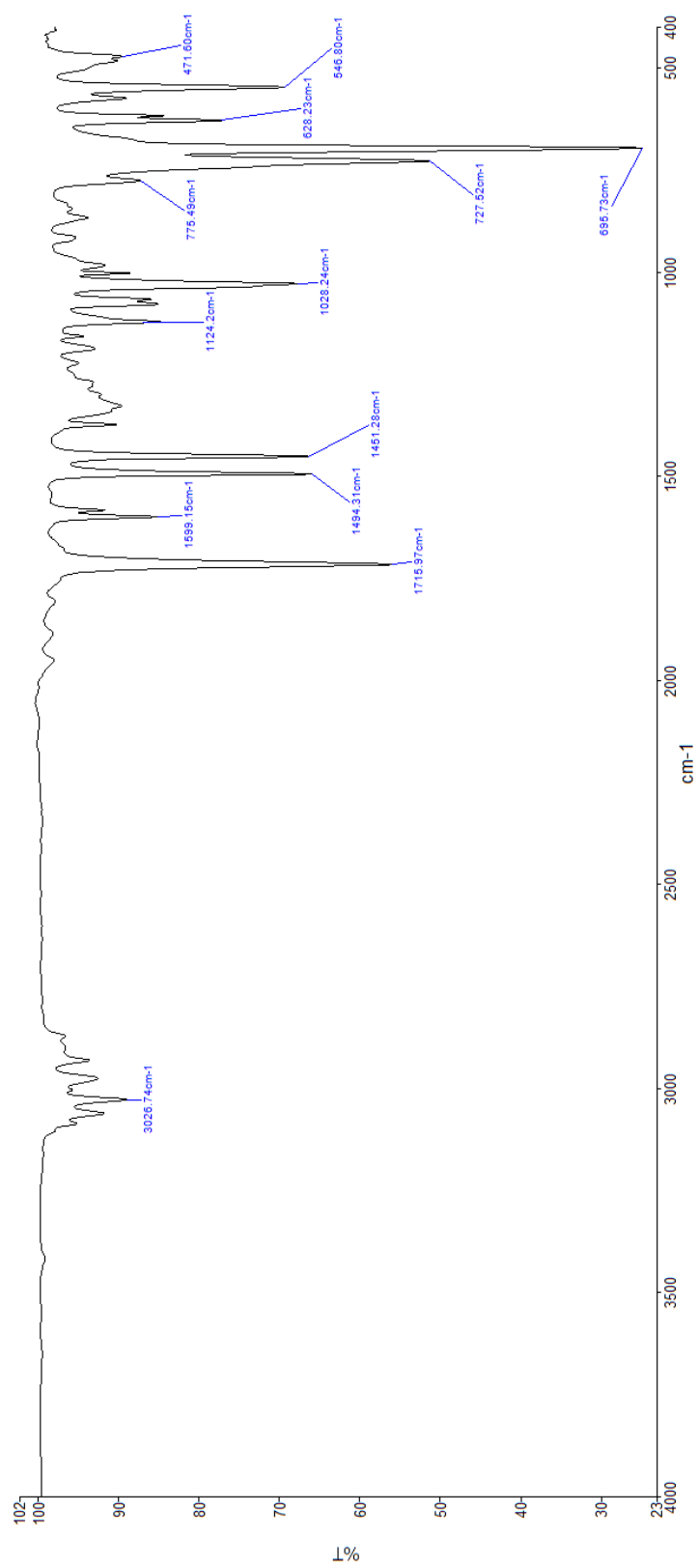
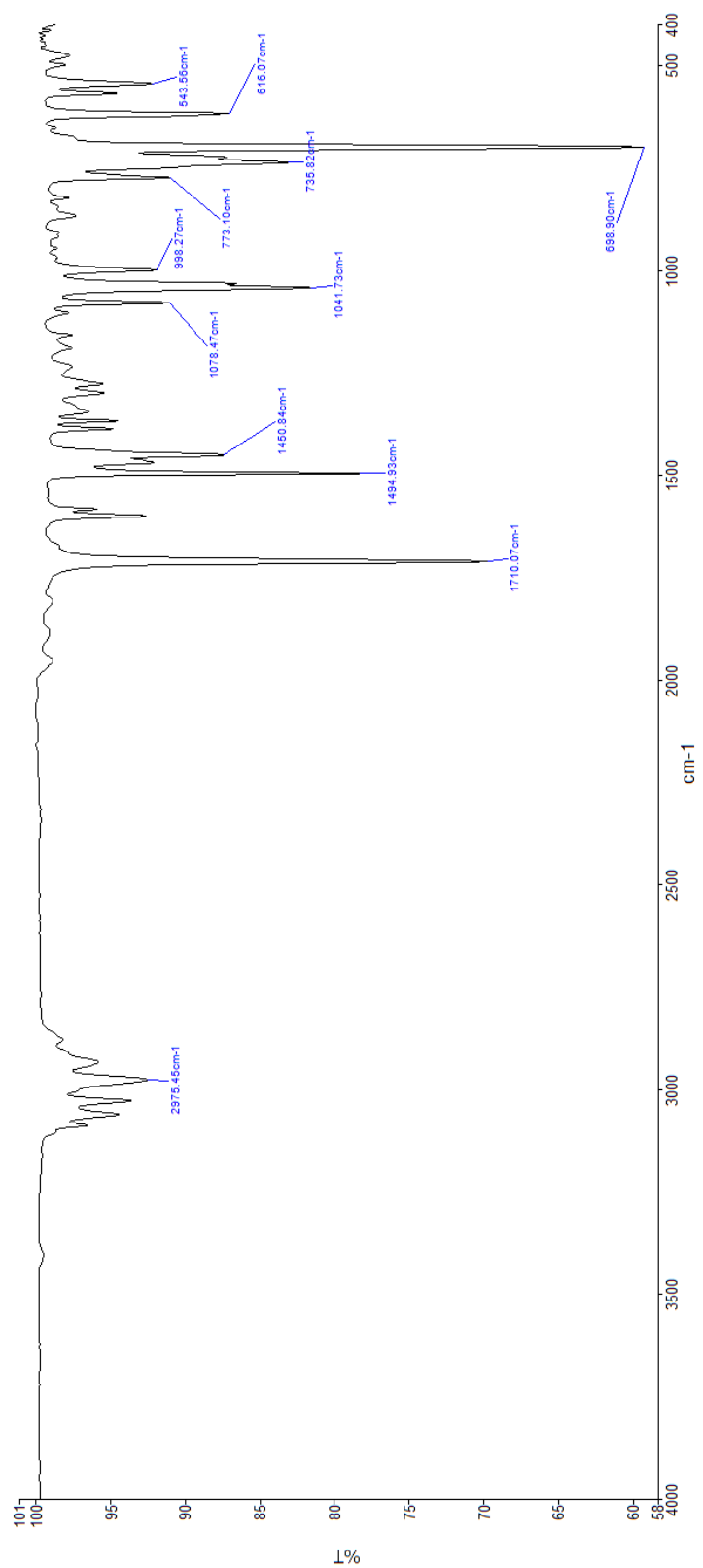


Figure 5.S17: IR(neat)  $\nu_{\max}$  of 1,1,3-triphenylbutan-2-one



**Figure 5.S18:** IR(neat)  $\nu_{\max}$  of 3-methyl-1,1,3-triphenylbutan-2-one

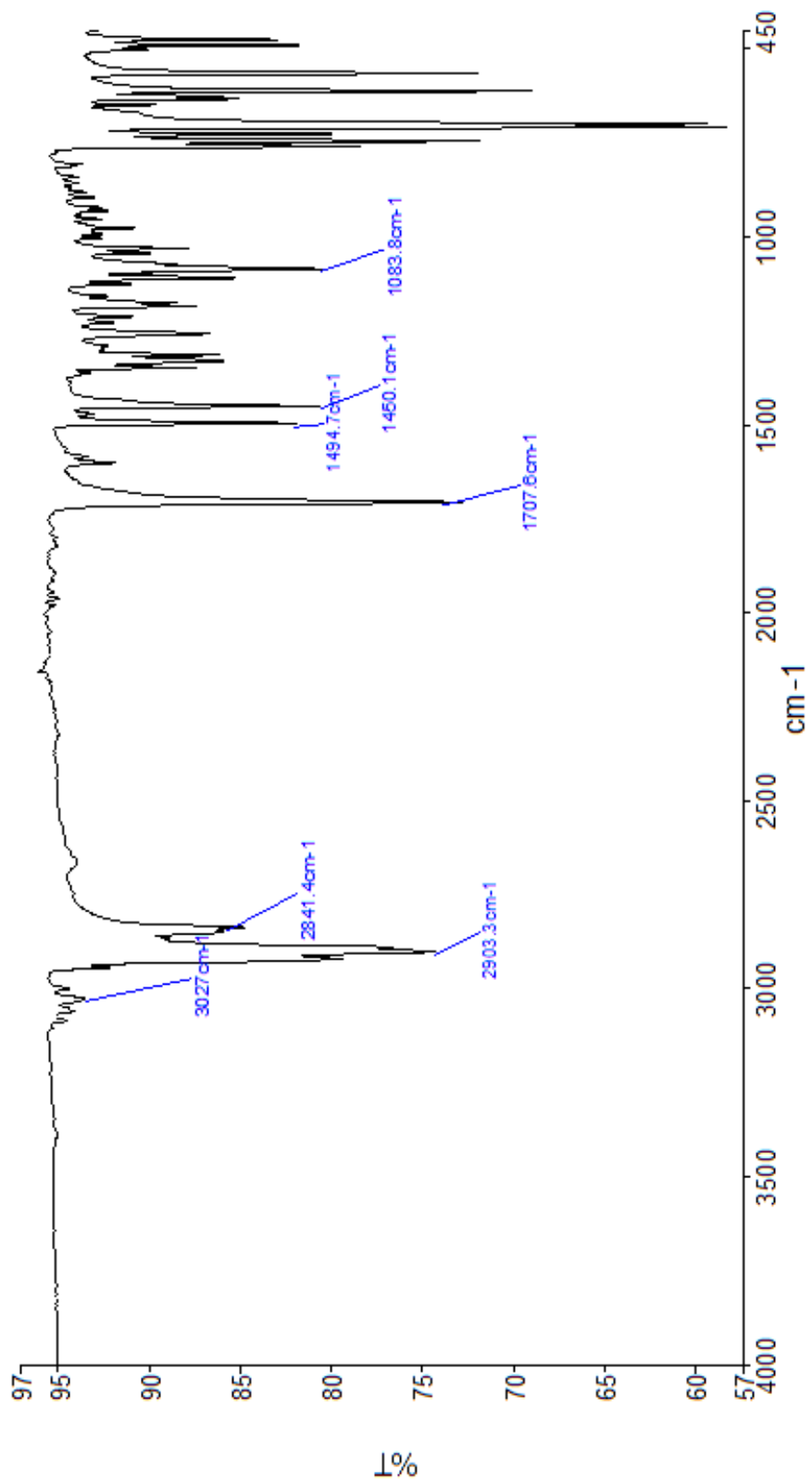


Figure 5.S19: IR(neat)  $\nu_{\max}$  3-((3r,5r,7r)-adamantan-1-yl)-1,1-diphenylpropan-2-one

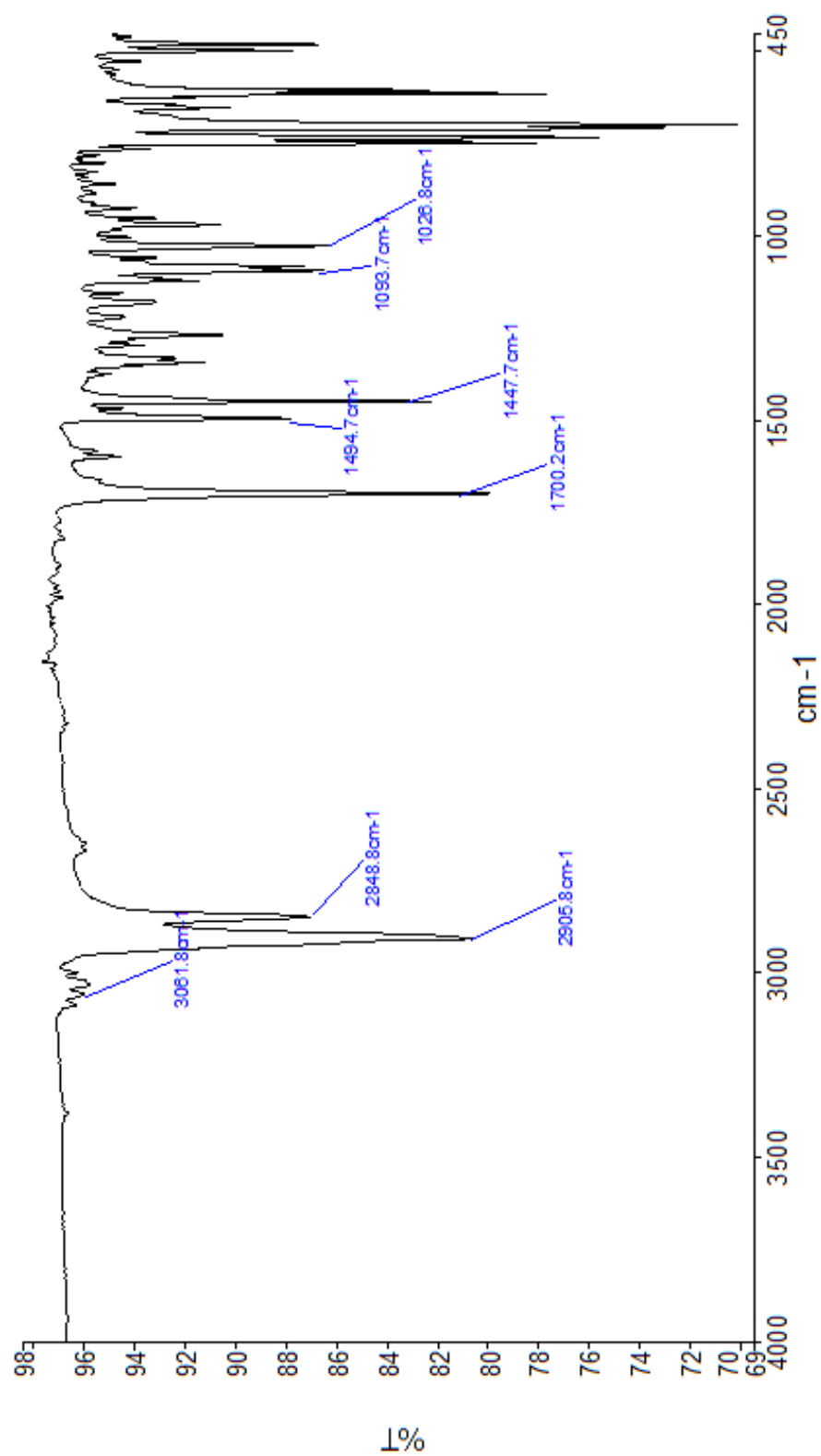
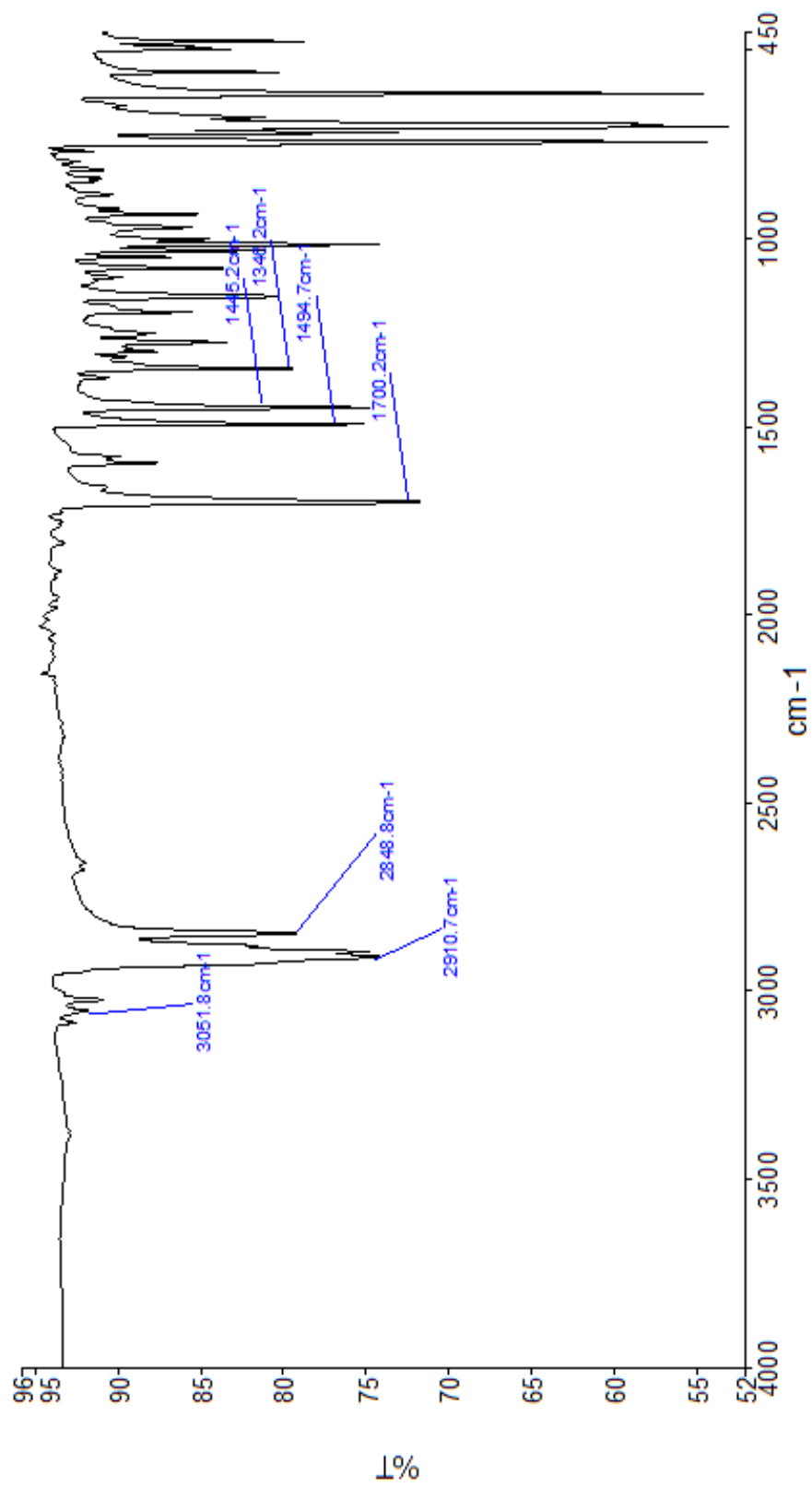
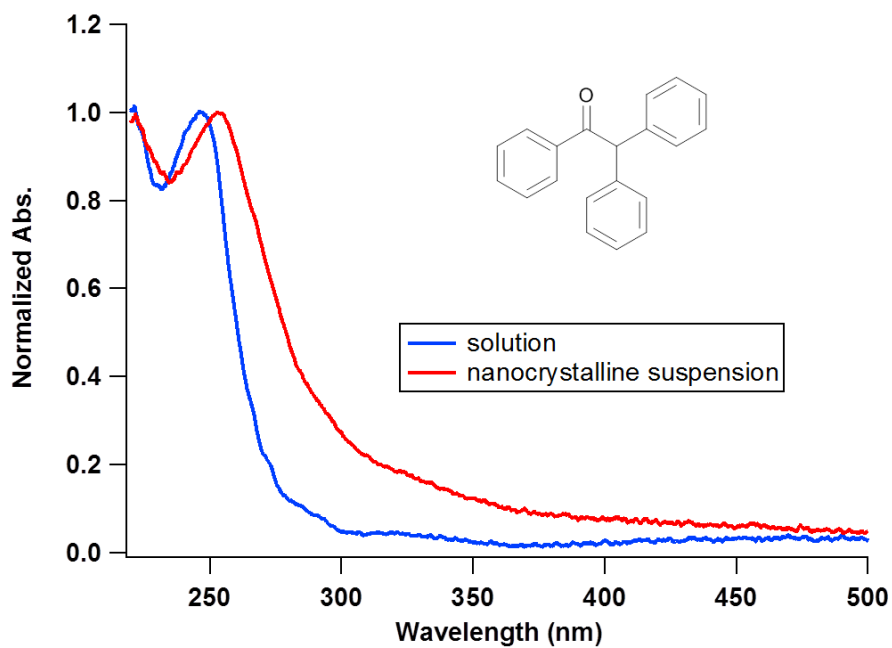


Figure 5.S20 IR(neat)  $\nu_{\max}$  1-((1r,3r,5r,7r)-adamantan-2-yl)-2,2-diphenylethan-1-one

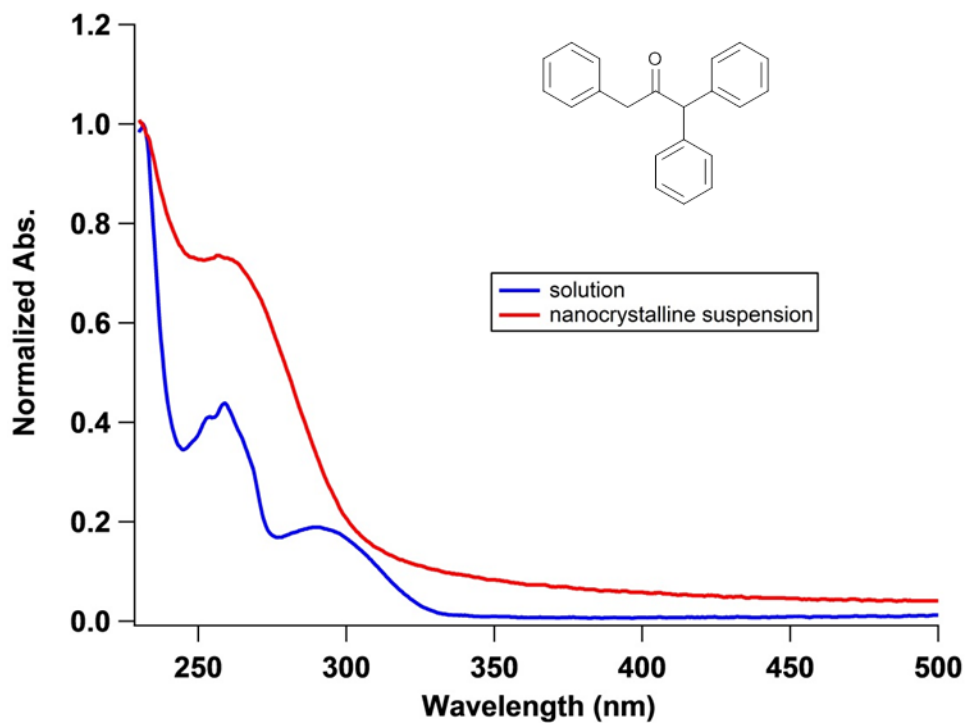


**Figure 5.S21:** IR(neat)  $\nu_{\max}$  1-((3r,5r,7r)-adamantan-1-yl)-2,2-diphenylethan-1-one

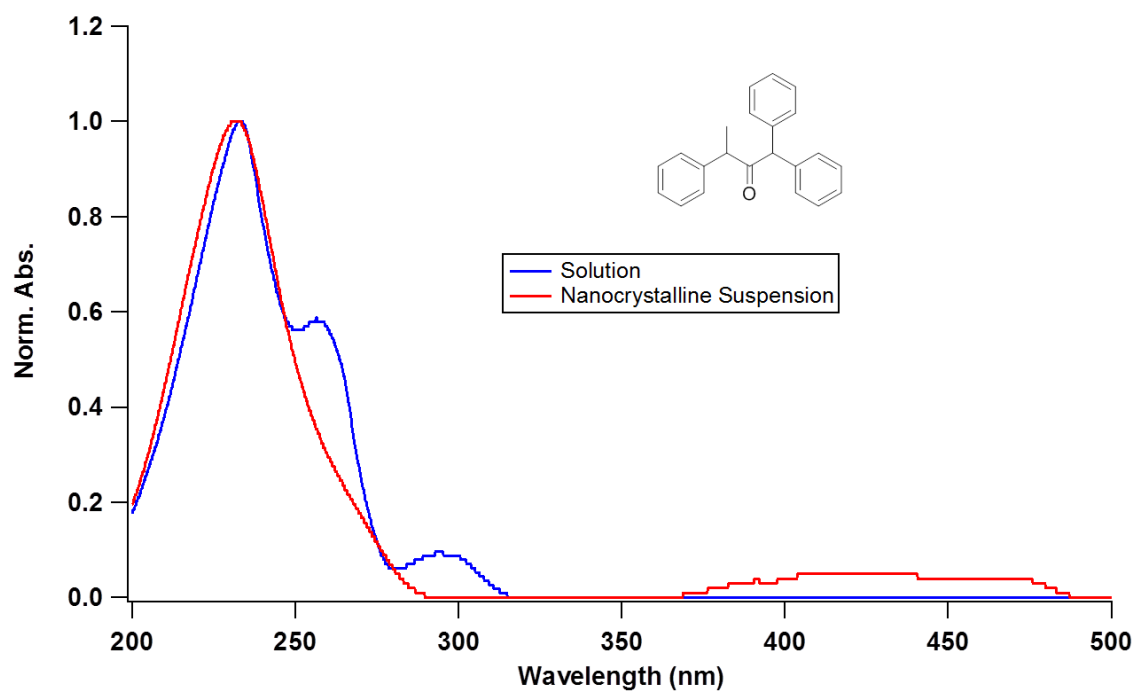
### UV-Vis Spectra:



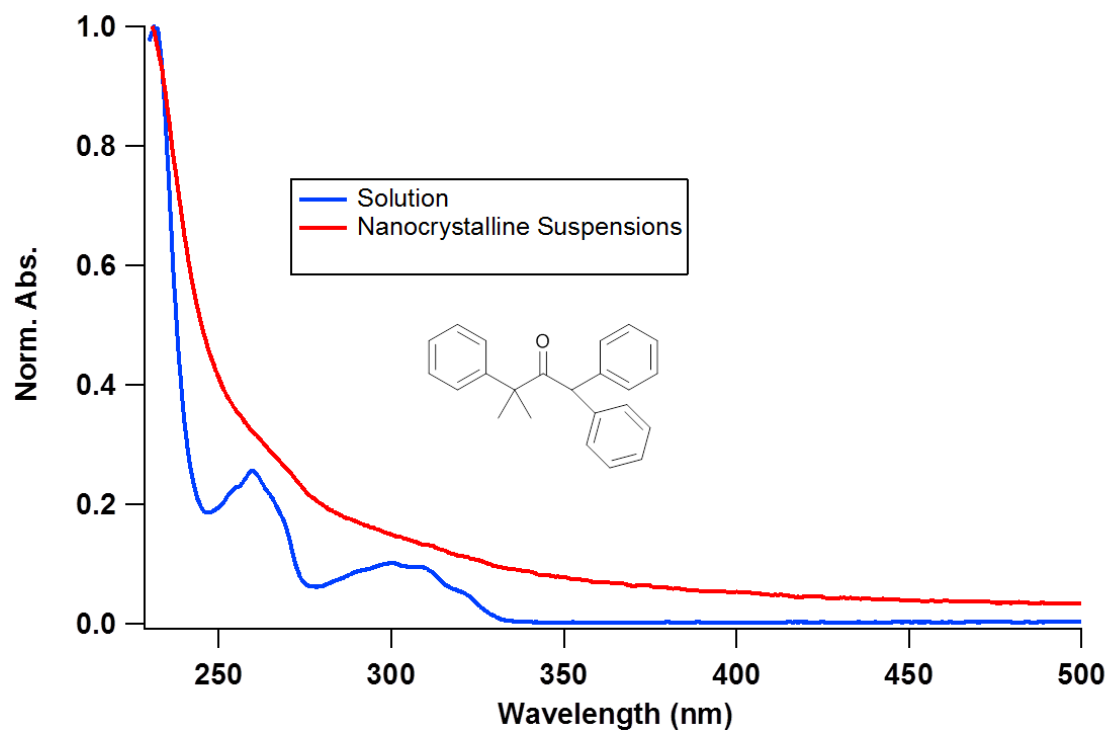
**Figure 5.S22:** UV-vis of ( $3 \times 10^{-5}$  mol/L) of 1,2,2-triphenylethan-1-one in MeCN (blue) and  $2 \times 10^{-5}$  mol/L in nanocrystalline suspensions (red)



**Figure 5.S23:** UV-vis of (0.01 mol/L) of 1,1,3-triphenylpropan-2-one in MeCN (blue) and 0.005 mol/L in nanocrystalline suspensions (red)

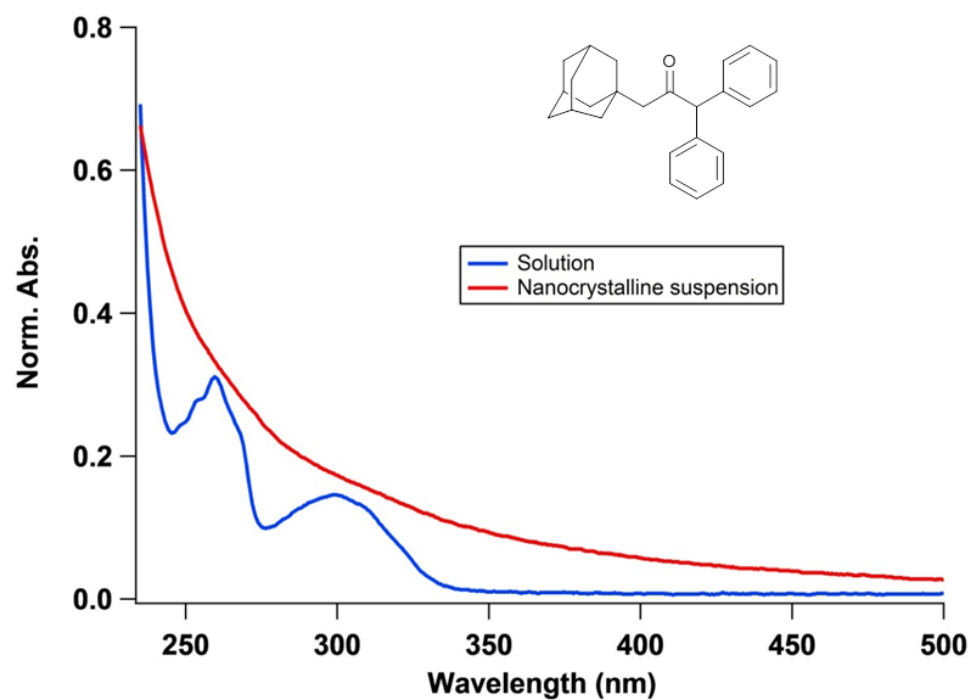


**Figure 5.S24:** UV-vis of (0.01 mol/L) of 1,1,3-triphenylbutan-2-one in MeCN (blue) and 0.005 mol/L in nanocrystalline suspensions (red)

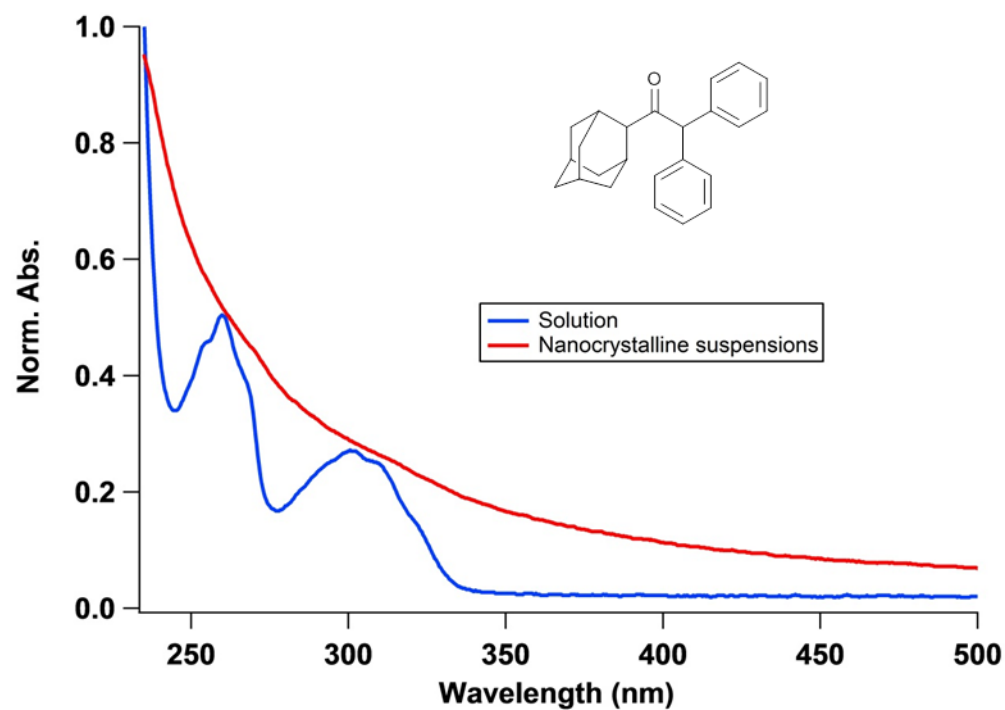


**Figure 5.S25:** UV-vis of (0.01 mol/L) of 3-methyl-1,1,3-triphenylbutan-2-one in MeCN (blue) and 0.005 mol/L in nanocrystalline suspensions (red)

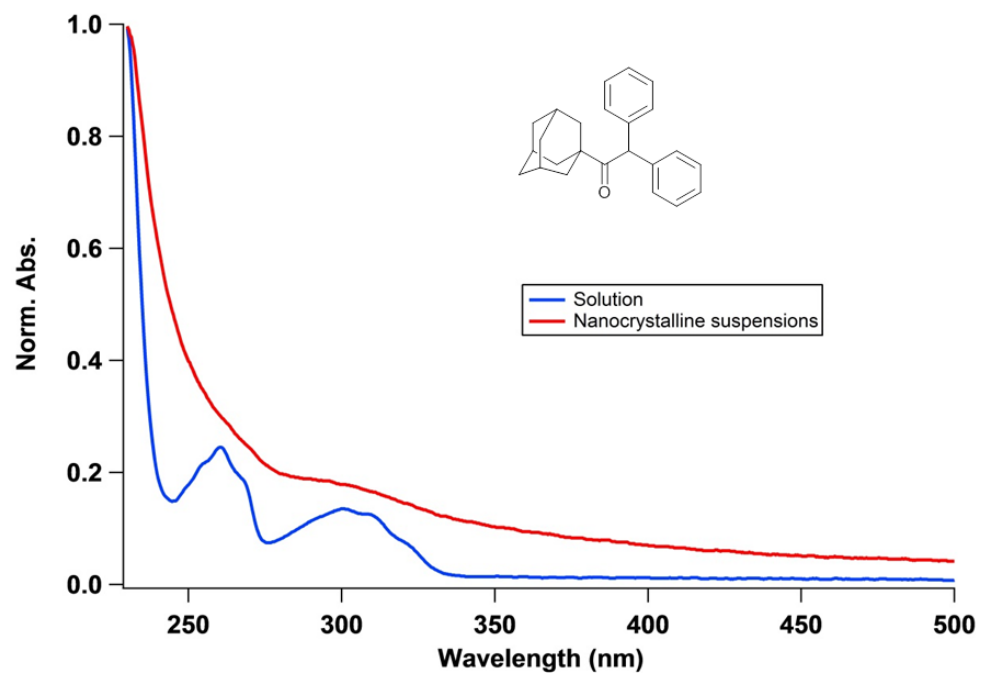




**Figure 5.S26:** UV-vis of (0.01 mol/L) of 3-((3r,5r,7r)-adamantan-1-yl)-1,1-diphenylpropan-2-one in MeCN (blue) and 0.005 mol/L in nanocrystalline suspensions (red)



**Figure 5.S27:** UV-vis of (0.01 mol/L) of 1-((1r,3r,5r,7r)-adamantan-2-yl)-2,2-diphenylethan-1-one in MeCN (blue) and 0.005 mol/L in nanocrystalline suspensions (red)



**Figure 5.S28:** UV-vis of (0.01 mol/L) of 1-((3r,5r,7r)-adamantan-1-yl)-2,2-diphenylethan-1-one in MeCN (blue) and 0.005 mol/L in nanocrystalline suspensions (red)

#### 5.4.4. Power X-Ray Diffraction (PXRD) Analysis

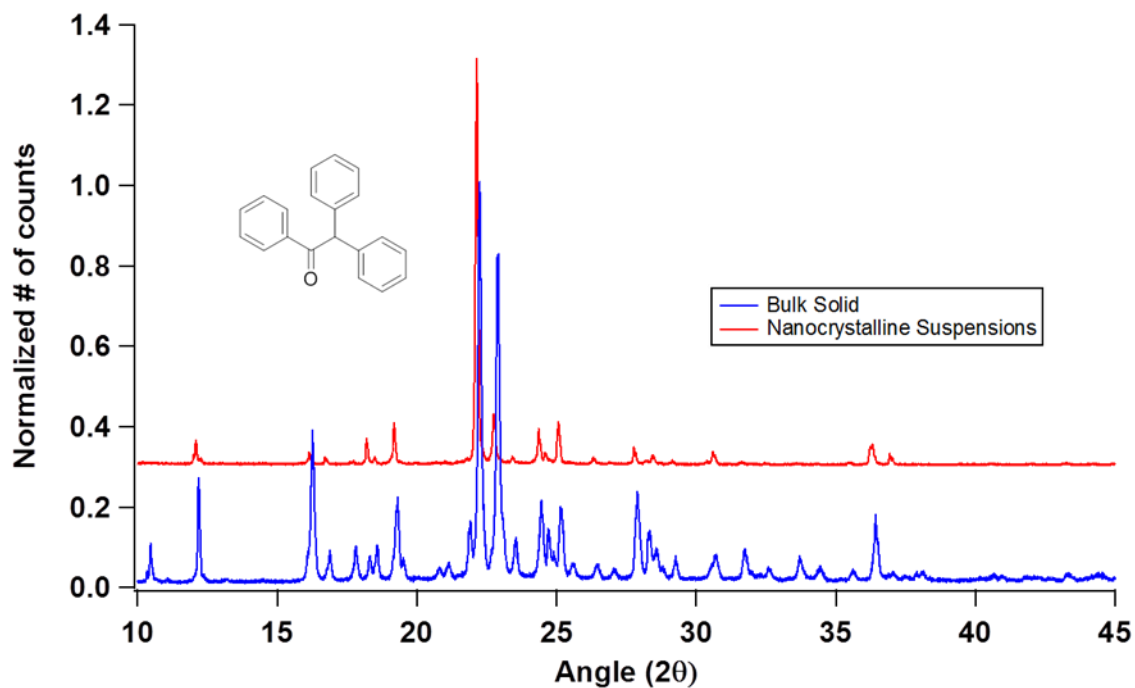


Figure 5.S29: PXRD of 1,2,2-triphenylethan-1-one in the bulk solid and nanocrystalline suspensions

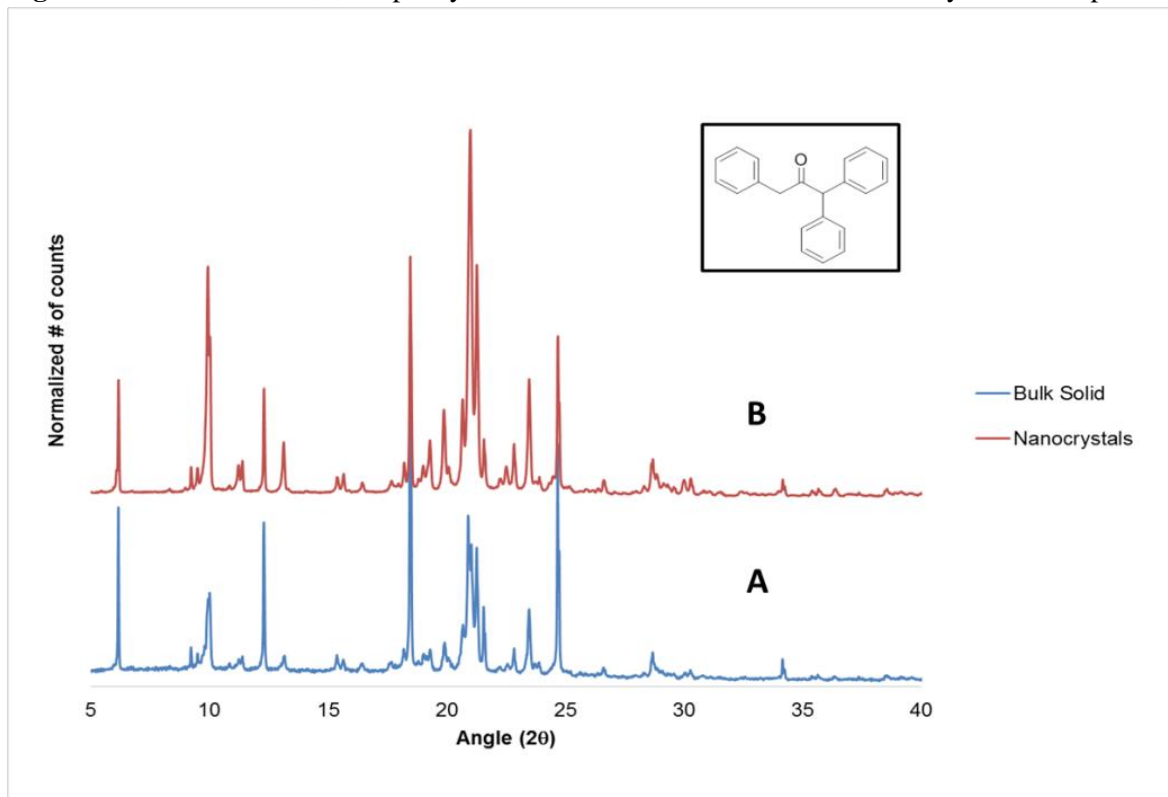


Figure 5.S30: PXRD of 1,1,3-triphenylpropan-2-one in the bulk solid and nanocrystalline suspensions

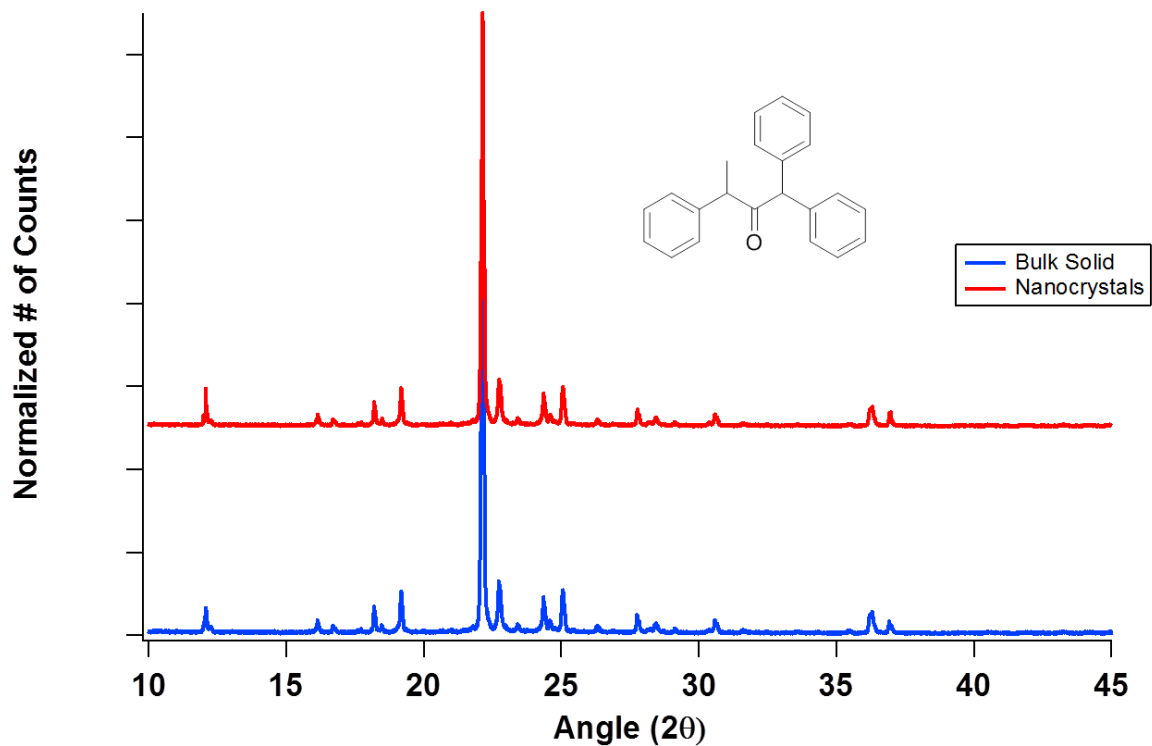


Figure 5.S31: PXRd of 1,1,3-triphenylbutan-2-one in the bulk solid and nanocrystalline suspensions

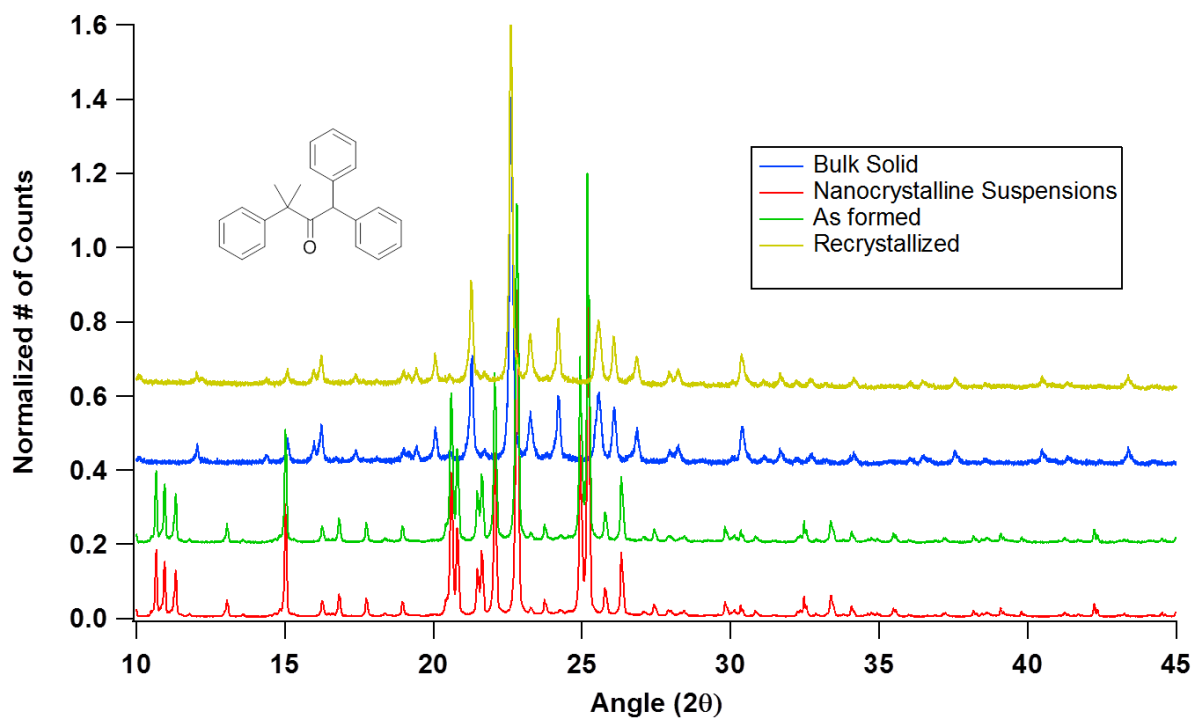
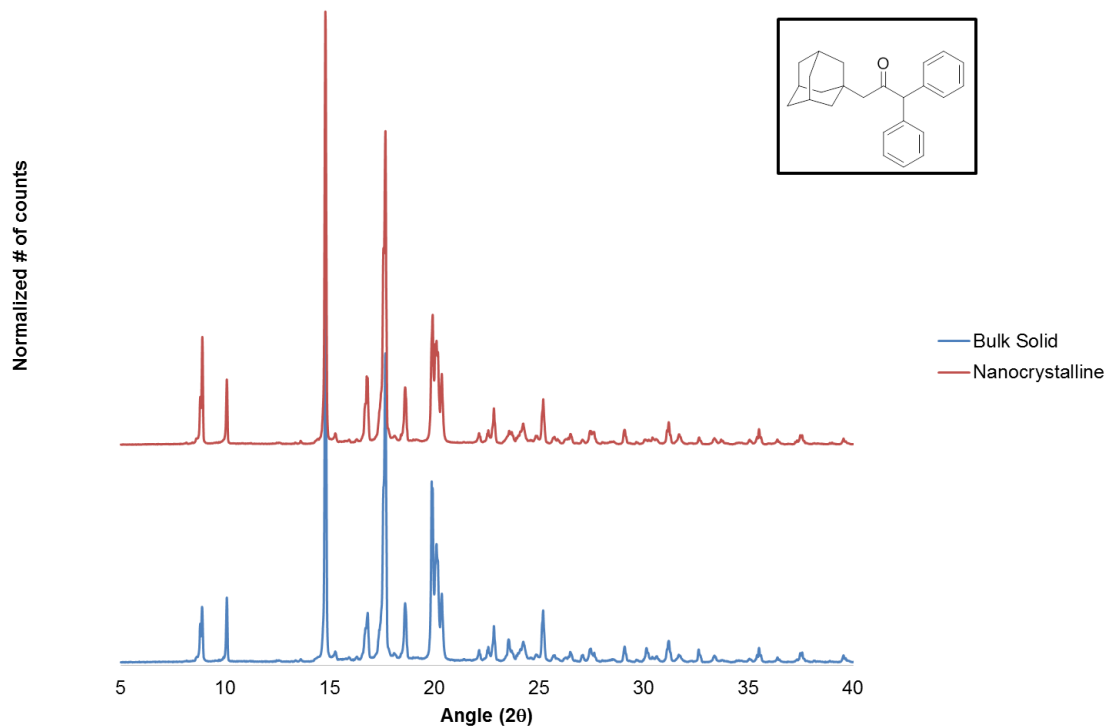
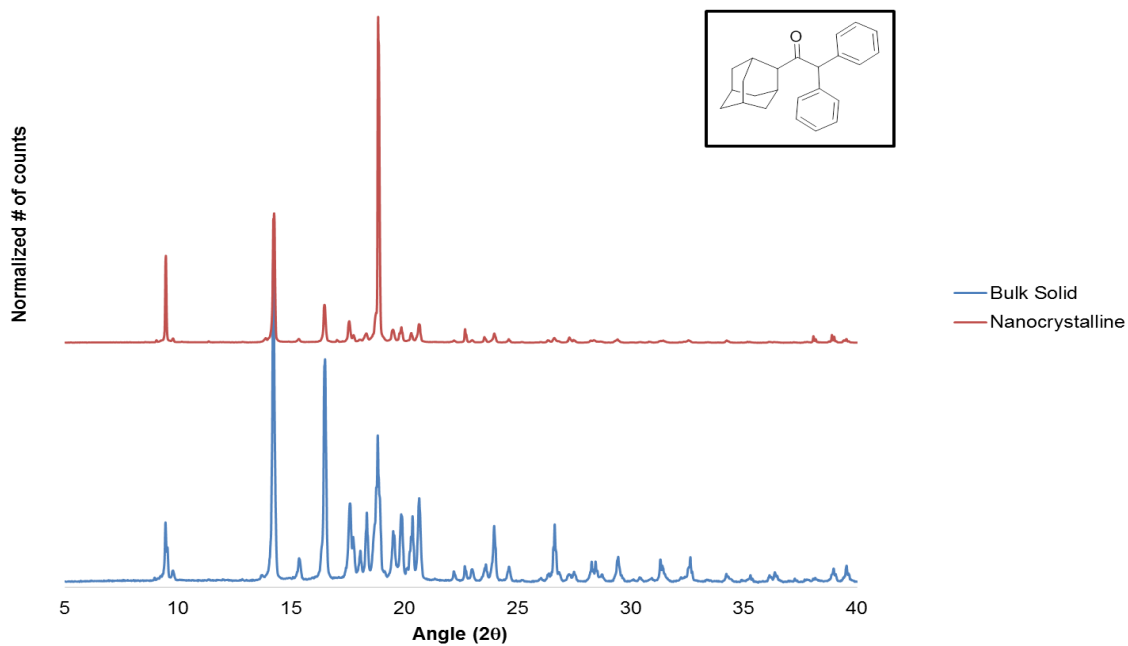


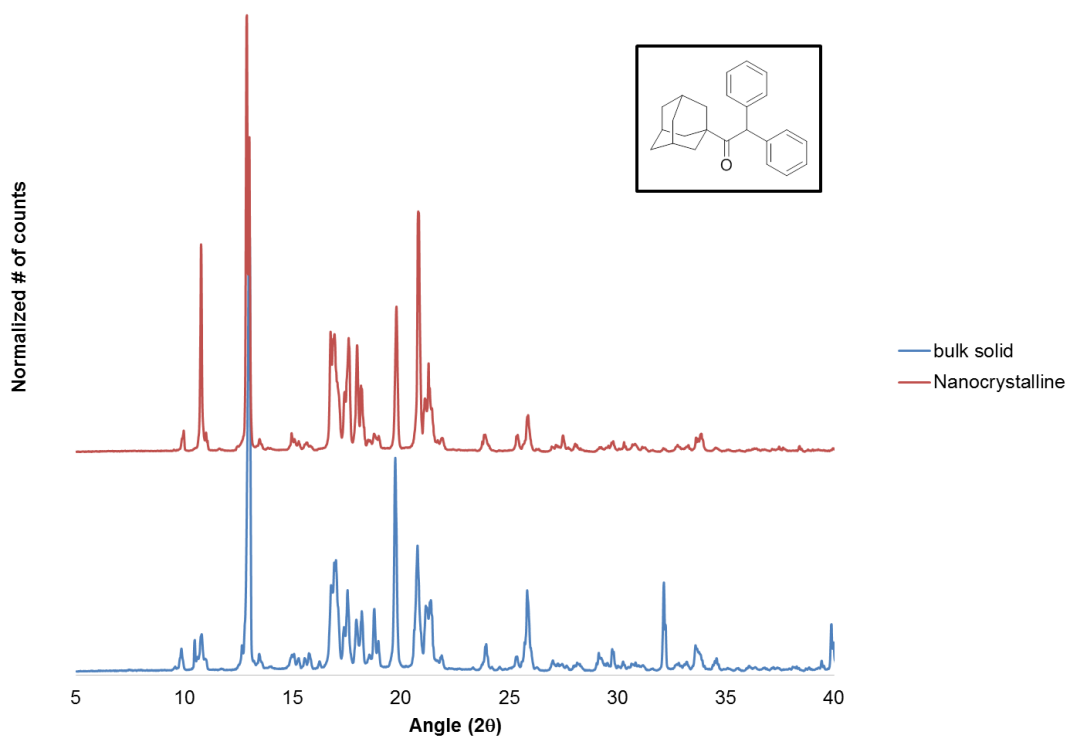
Figure 5.S32: PXRd of 3-methyl-1,1,3-triphenylbutan-2-one in the bulk solid and nanocrystalline suspensions



**Figure 5.S33:** PXRD of 3-((3r,5r,7r)-adamantan-1-yl)-1,1-diphenylpropan-2-one in the bulk solid and nanocrystalline suspensions

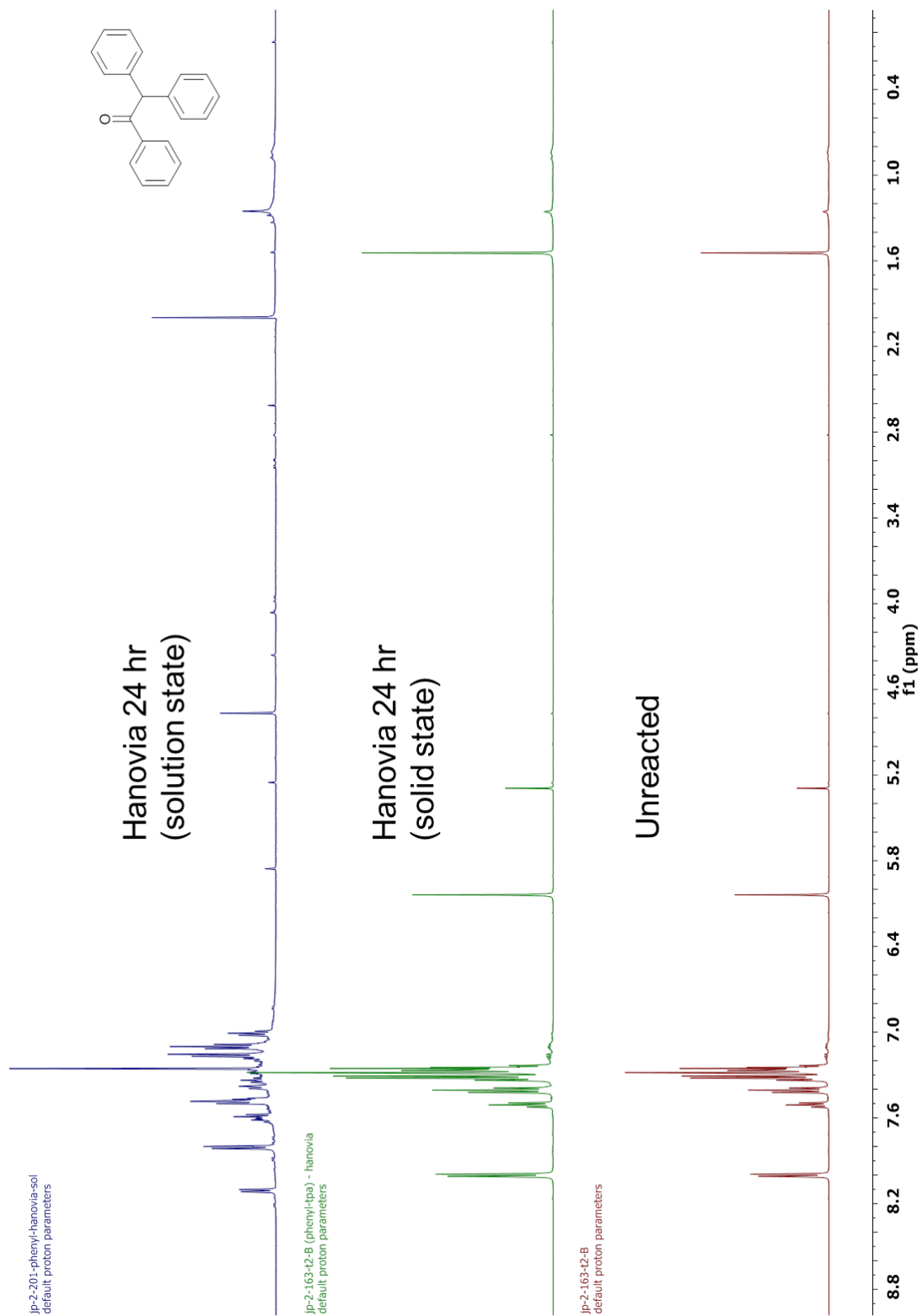


**Figure 5.S34:** PXRD of 1-((1r,3r,5r,7r)-adamantan-2-yl)-2,2-diphenylethan-1-one in the bulk solid and nanocrystalline suspensions

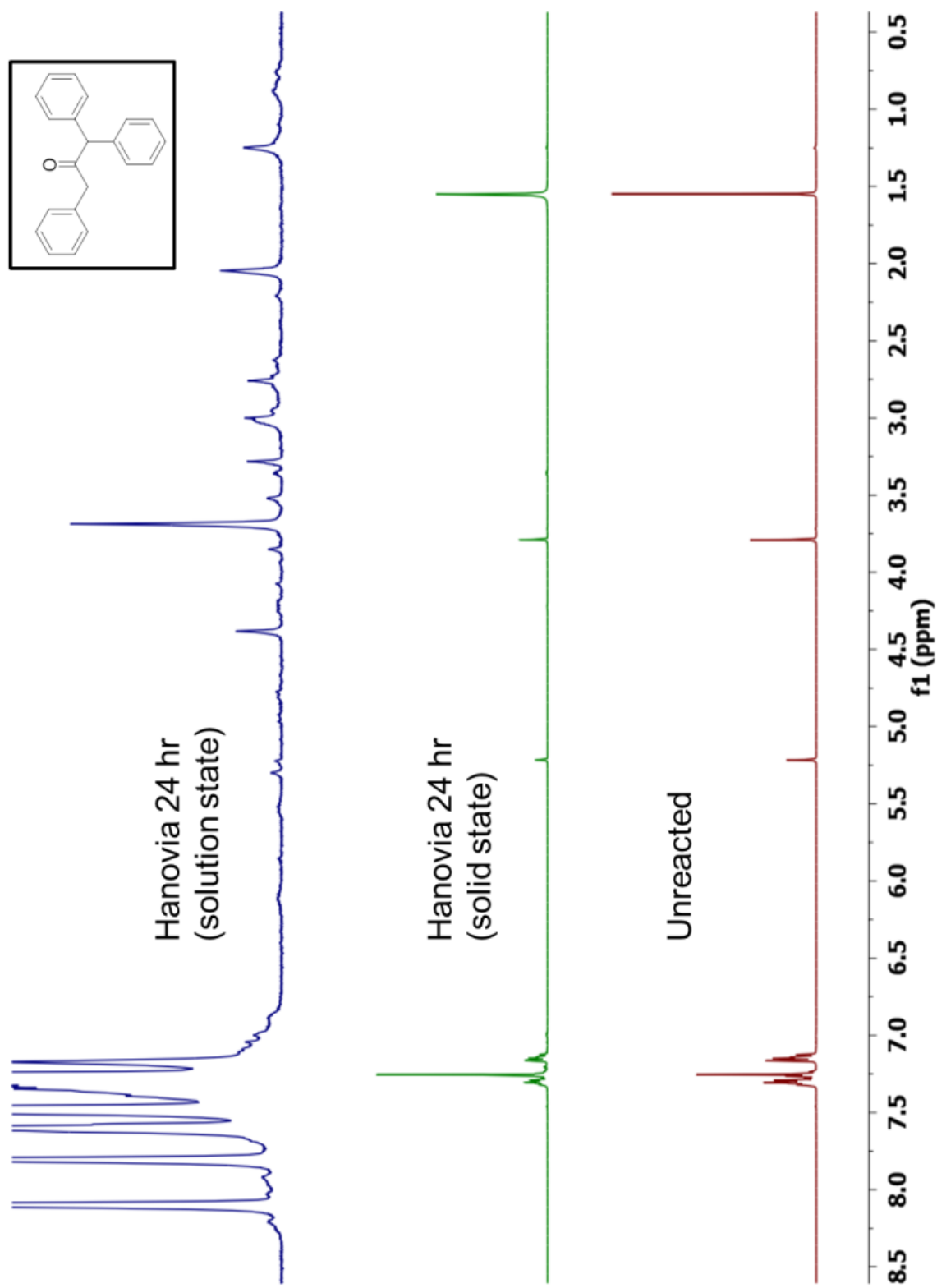


**Figure 5.S35:** PXRD of 1-((3r,5r,7r)-adamantan-1-yl)-2,2-diphenylethan-1-one in the bulk solid and nanocrystalline suspensions

### 5.4.5 Solid-State Photochemistry of Dry Powder

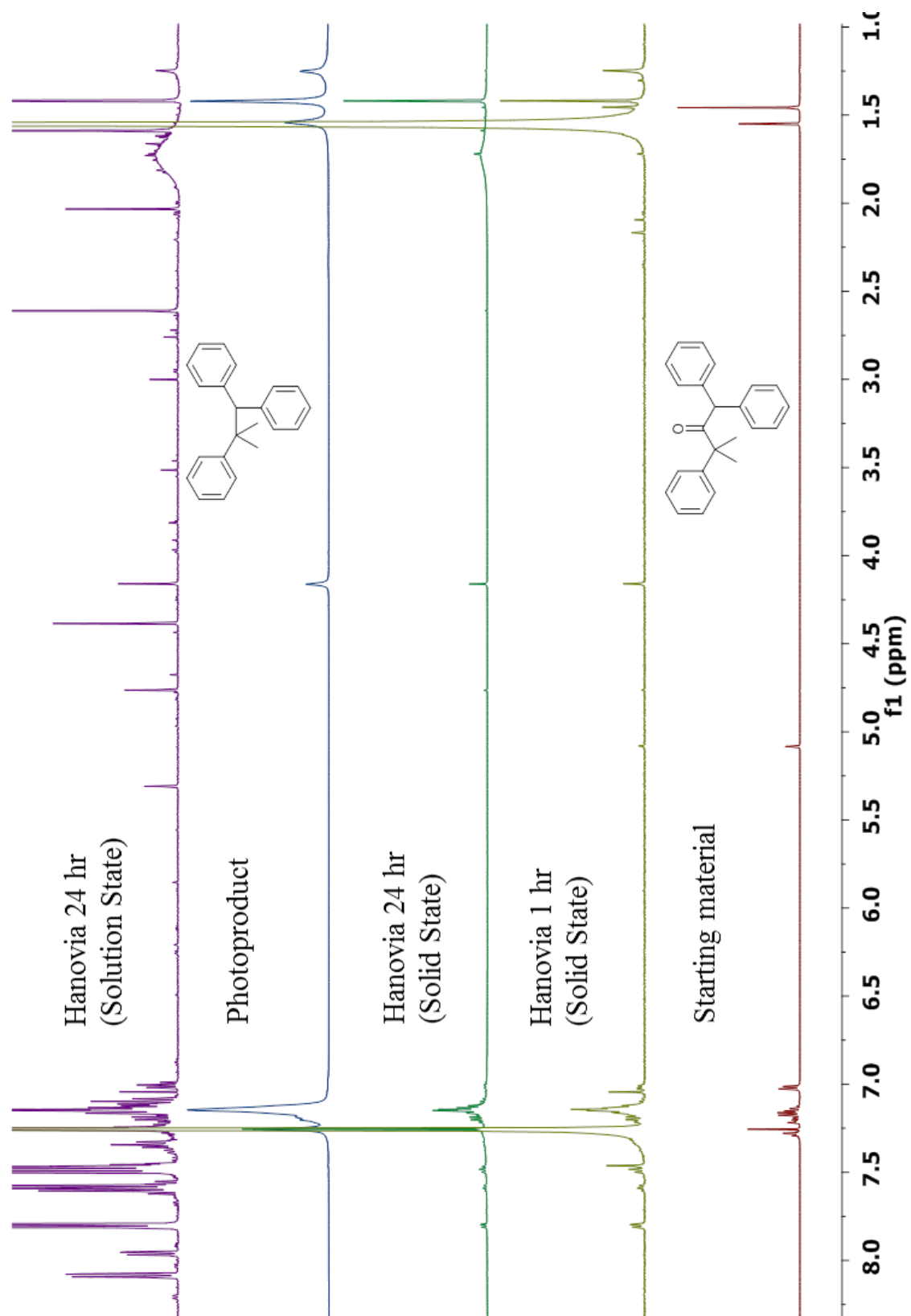


**Figure 5.S36:** <sup>1</sup>H NMR (500 MHz, CDCl<sub>3</sub>) product analysis of 1,2,2-triphenylethan-1-one in MeCN solution and in solid state

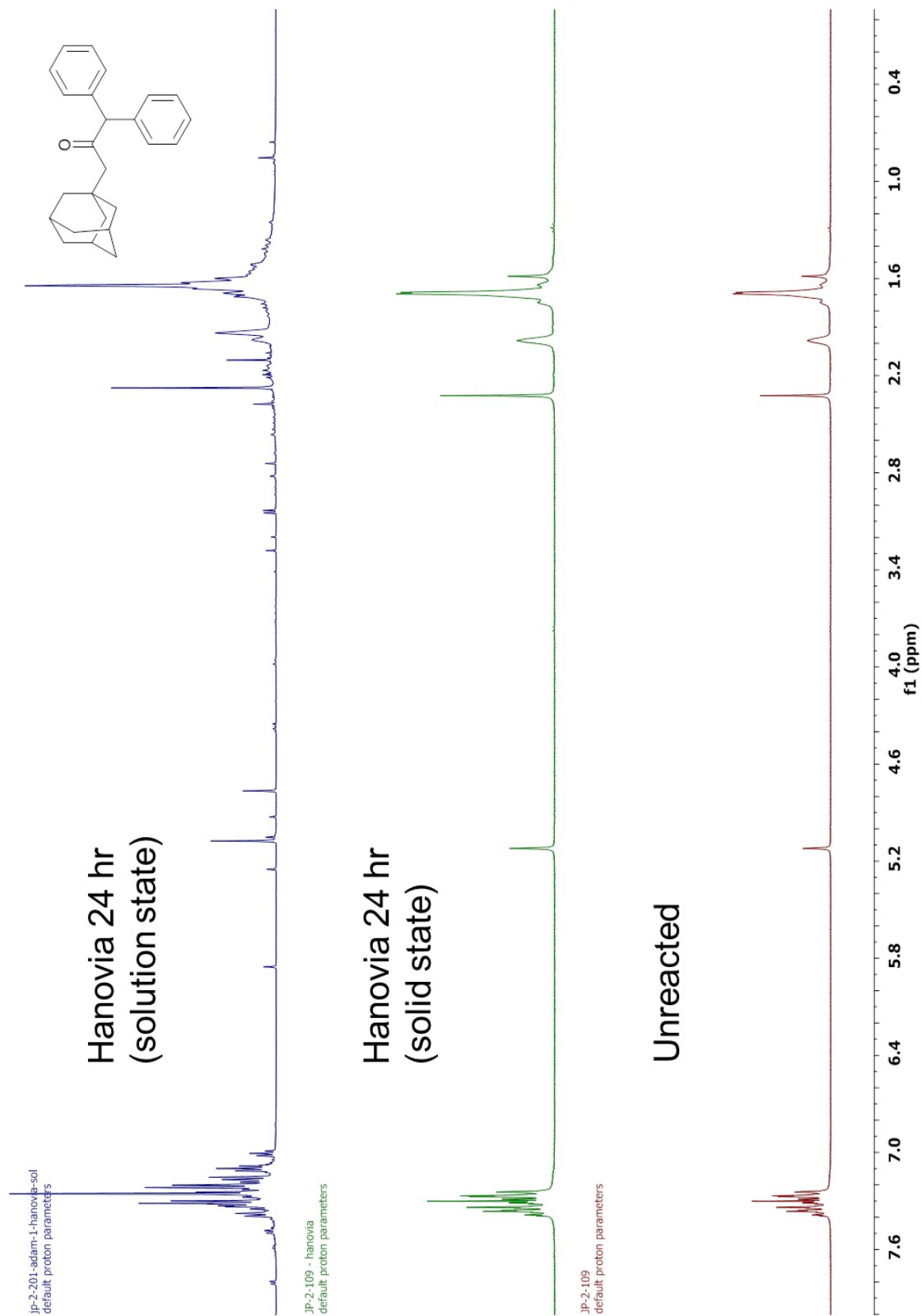


**Figure 5.S37:** <sup>1</sup>H NMR (500 MHz, CDCl<sub>3</sub>) product analysis of 1,1,3-triphenylpropan-2-one in MeCN solution and in solid state

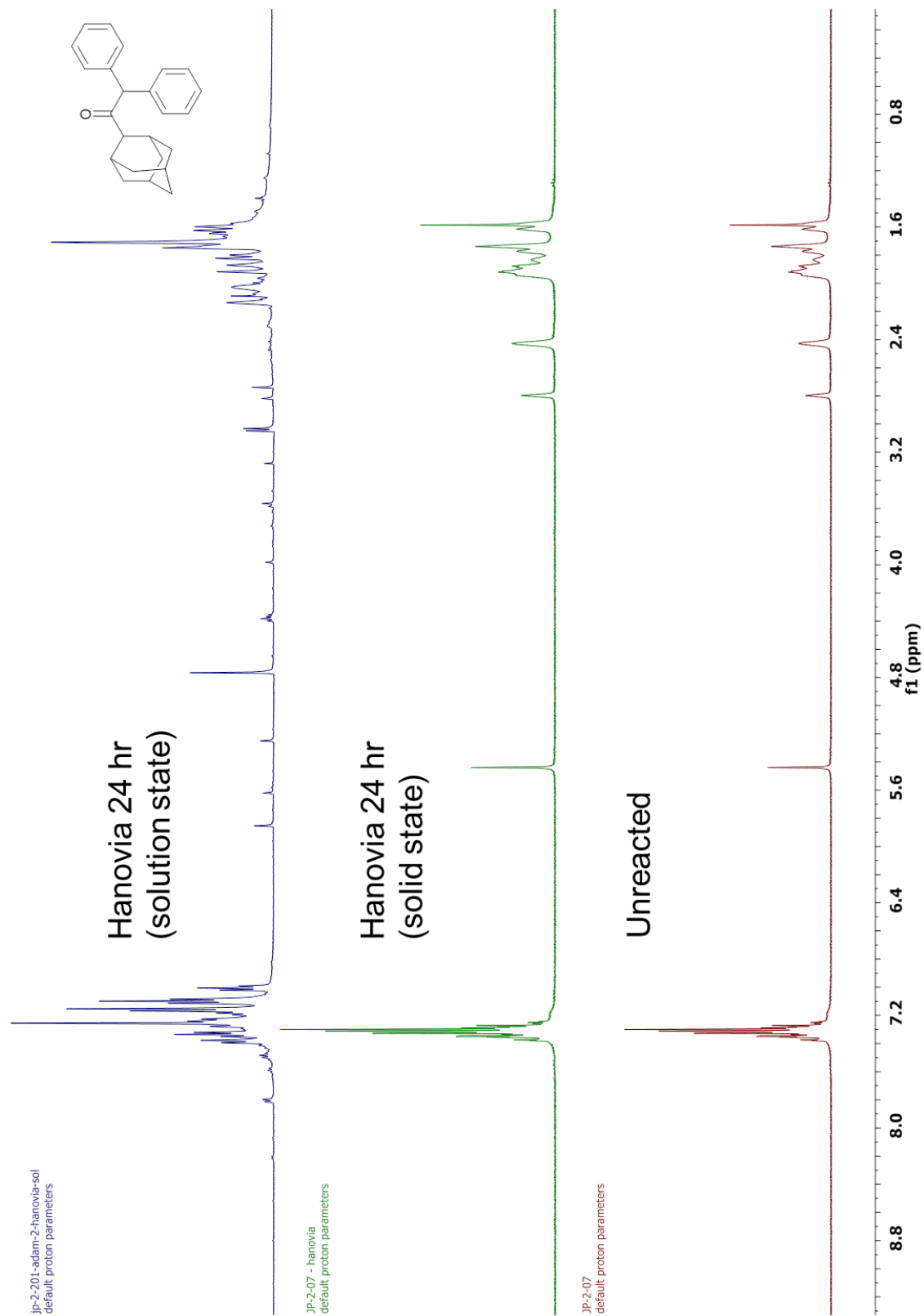




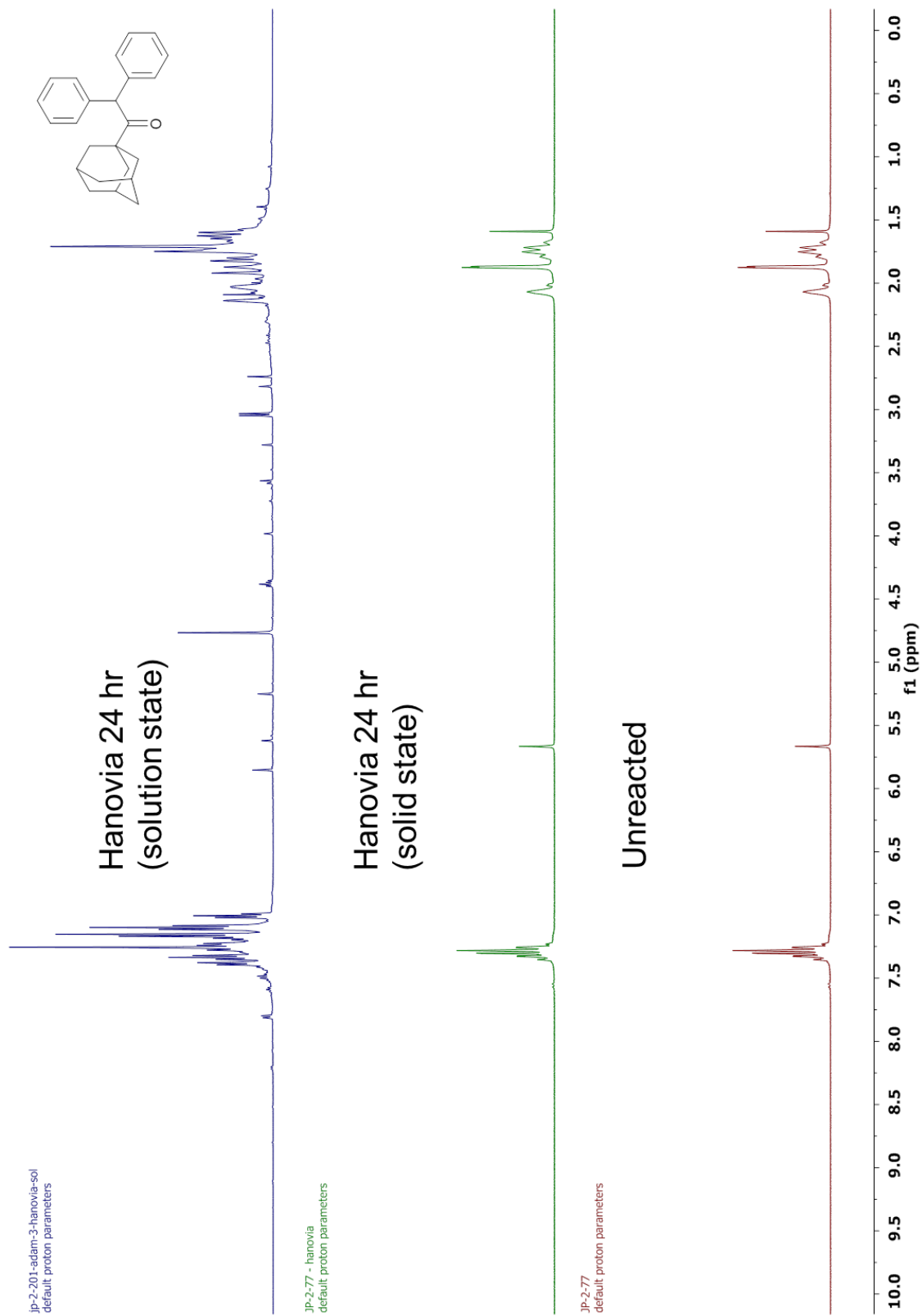
**Figure 5.S38:** <sup>1</sup>H NMR (500 MHz, CDCl<sub>3</sub>) product analysis of 3-methyl-1,1,3-triphenylbutan-2-one in MeCN solution and in solid state



**Figure 5.S39:**  $^1\text{H}$  NMR (500 MHz,  $\text{CDCl}_3$ ) product analysis of 3-((3r,5r,7r)-adamantan-1-yl)-1,1-diphenylpropan-2-one in MeCN solution and in solid state

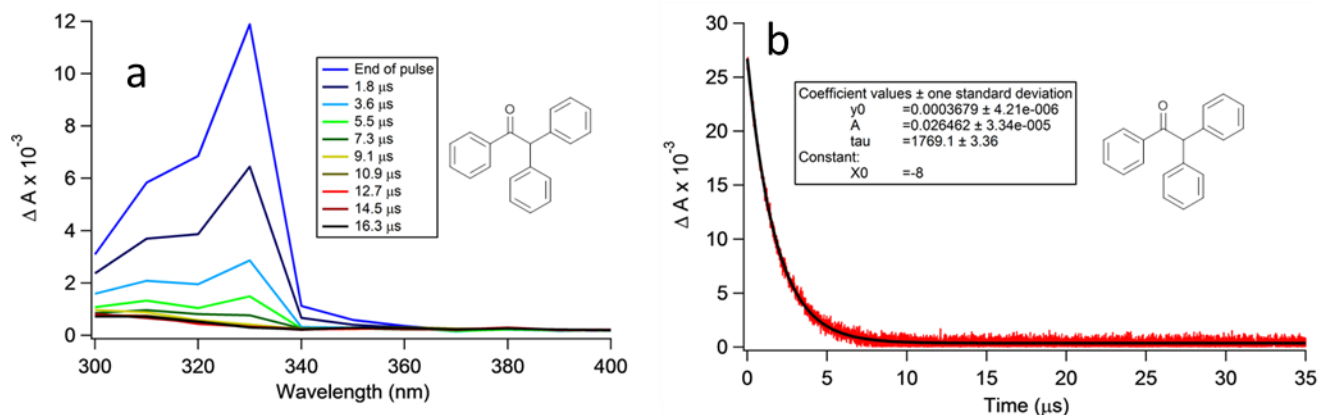


**Figure 5.S40:**  $^1\text{H}$  NMR (500 MHz,  $\text{CDCl}_3$ ) product analysis of 1-((1r,3r,5r,7r)-adamantan-2-yl)-2,2-diphenylethan-1-one in MeCN solution and in solid state

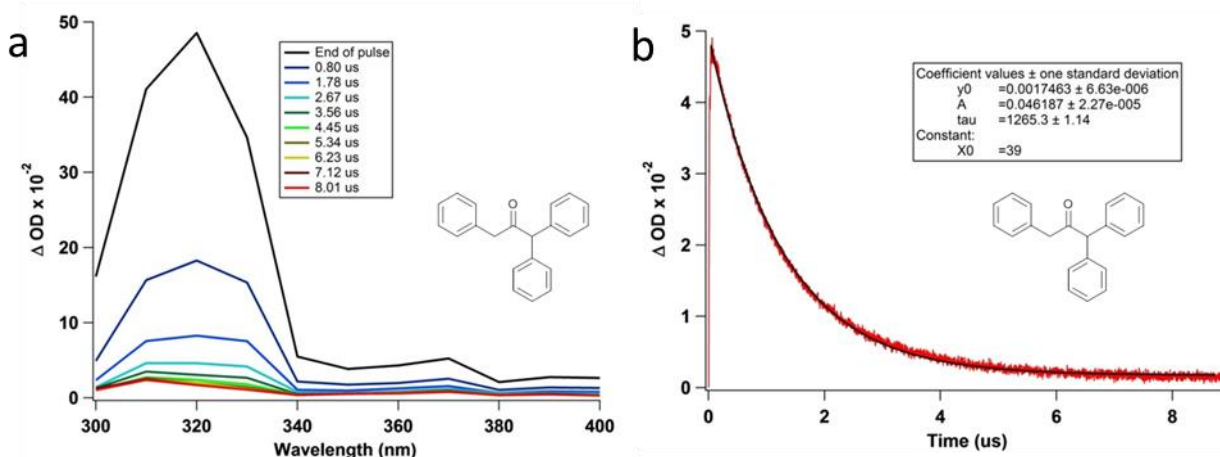


**Figure 5.S41:**  $^1\text{H}$  NMR (500 MHz,  $\text{CDCl}_3$ ) product analysis of 1-((3r,5r,7r)-adamantan-1-yl)-2,2-diphenylethan-1-one in MeCN solution and in solid state

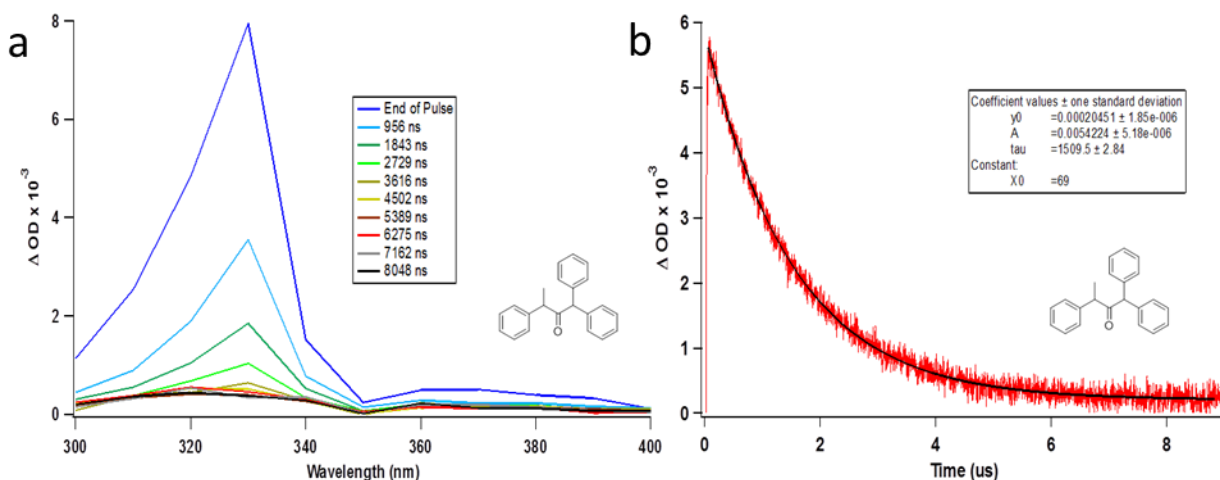
### 5.3.6 Laser Flash Photolysis (solution state)



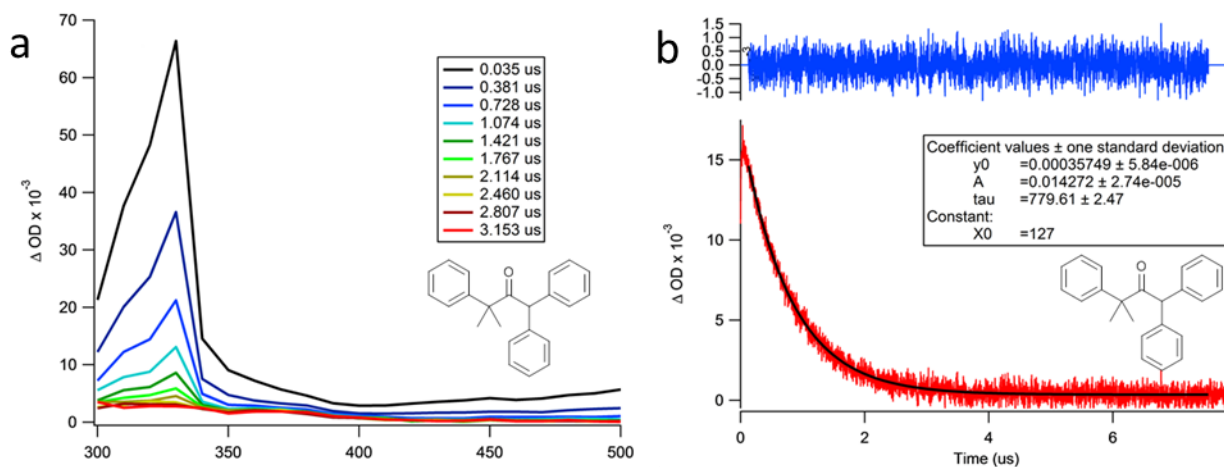
**Figure 5.S42:** (a) Transient Spectroscopy of 1,2,2-triphenylethan-1-one in MeCN ( $\lambda_{\max} = 330$  nm) and (b) transient decay of 1,2,2-triphenylethan-1-one in MeCN ( $\lambda_{\max} = 330$  nm)



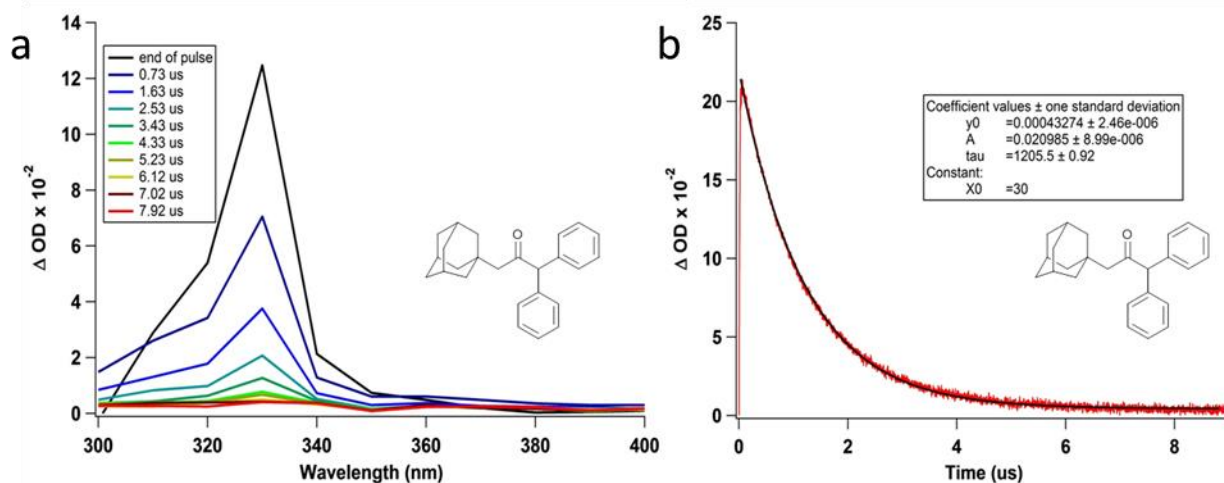
**Figure 5.S43:** (a) Transient Spectroscopy of 1,1,3-triphenylpropan-2-one in MeCN ( $\lambda_{\max} = 320$  nm) and (b) transient decay of 1,1,3-triphenylpropan-2-one in MeCN ( $\lambda_{\max} = 320$  nm)



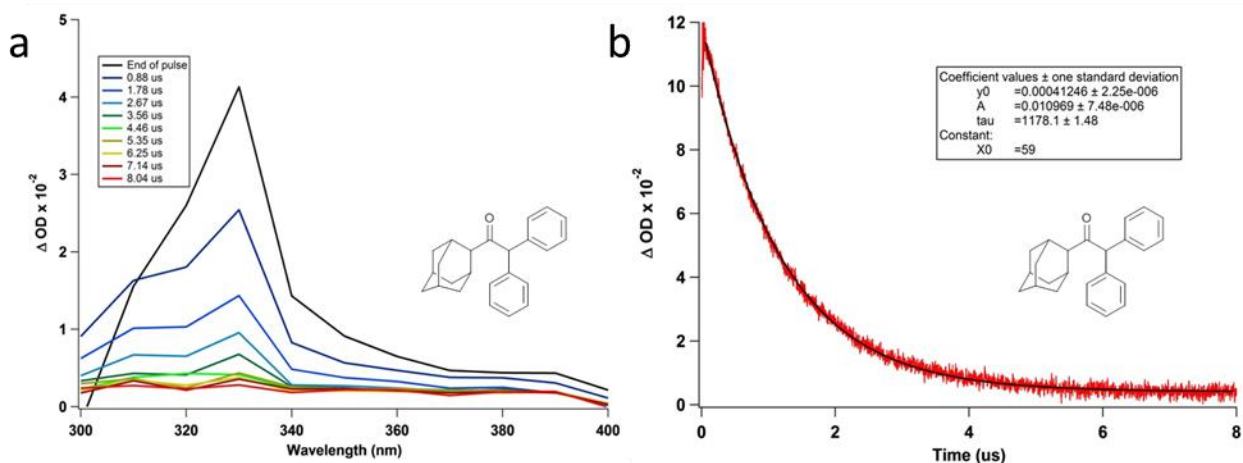
**Figure 5.S44:** (a) Transient Spectroscopy of 1,1,3-triphenylbutan-2-one in MeCN ( $\lambda_{\max} = 330$  nm) and (b) transient decay of 1,1,3-triphenylbutan-2-one in MeCN ( $\lambda_{\max} = 330$  nm)



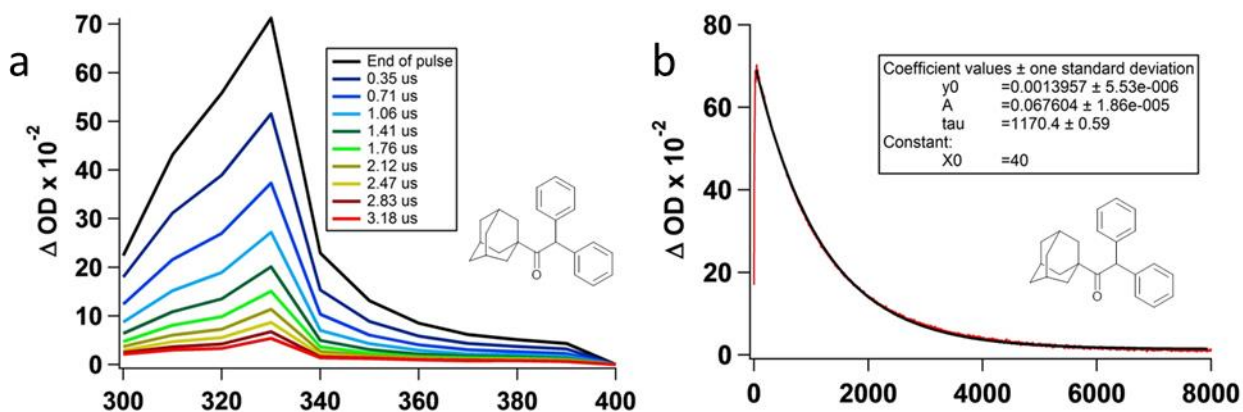
**Figure 5.S45:** (a) Transient Spectroscopy of 3-methyl-1,1,3-triphenylbutan-2-one in MeCN ( $\lambda_{\max} = 330$  nm) and (b) transient decay of 3-methyl-1,1,3-triphenylbutan-2-one in MeCN ( $\lambda_{\max} = 330$  nm)



**Figure 5.S46:** (a) Transient Spectroscopy of 3-((3r,5r,7r)-adamantan-1-yl)-1,1-diphenylpropan-2-one in MeCN ( $\lambda_{\max} = 330$  nm) and (b) transient decay of 3-((3r,5r,7r)-adamantan-1-yl)-1,1-diphenylpropan-2-one in MeCN ( $\lambda_{\max} = 330$  nm)

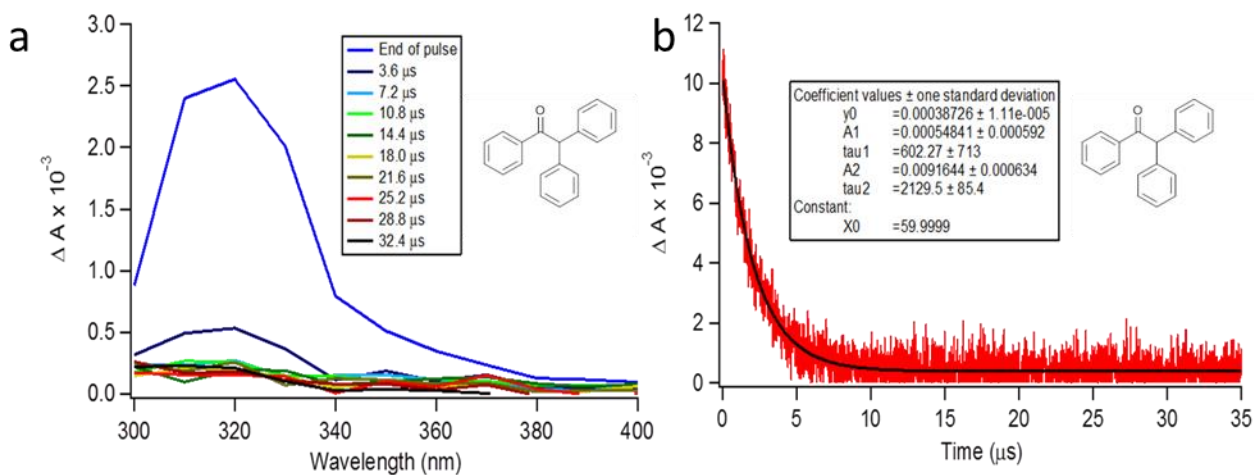


**Figure 5.S47:** (a) Transient Spectroscopy of 1-((1r,3r,5r,7r)-adamantan-2-yl)-2,2-diphenylethan-1-one in MeCN ( $\lambda_{\max} = 330$  nm) and (b) transient decay of 1-((1r,3r,5r,7r)-adamantan-2-yl)-2,2-diphenylethan-1-one in MeCN ( $\lambda_{\max} = 330$  nm)

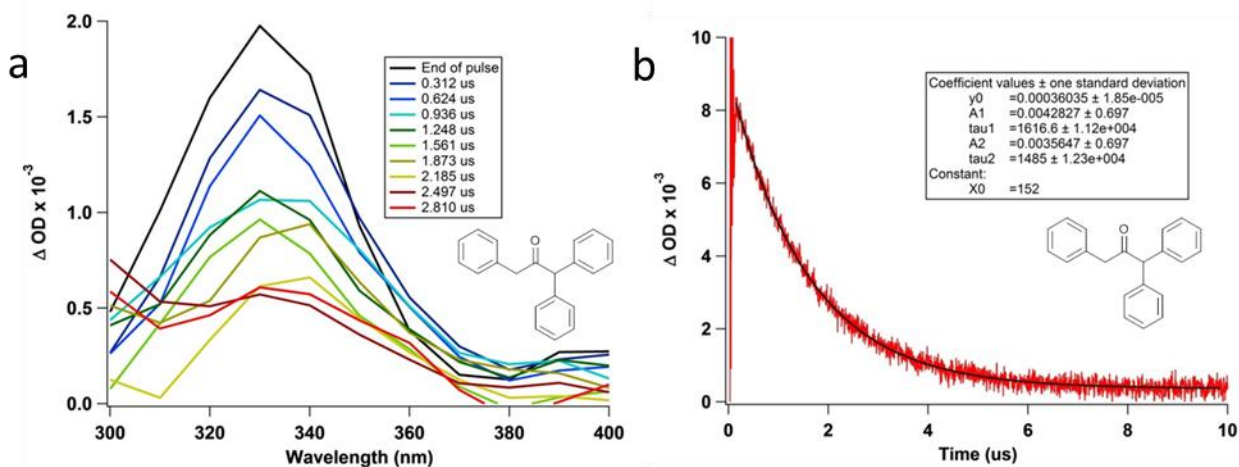


**Figure 5.S48:** (a) Transient Spectroscopy of 1-((3r,5r,7r)-adamantan-1-yl)-2,2-diphenylethan-1-one in MeCN ( $\lambda_{\max} = 330$  nm) and (b) transient decay of 1-((3r,5r,7r)-adamantan-1-yl)-2,2-diphenylethan-1-one in MeCN ( $\lambda_{\max} = 330$  nm)

### 5.3.6 Laser Flash Photolysis (solid state)

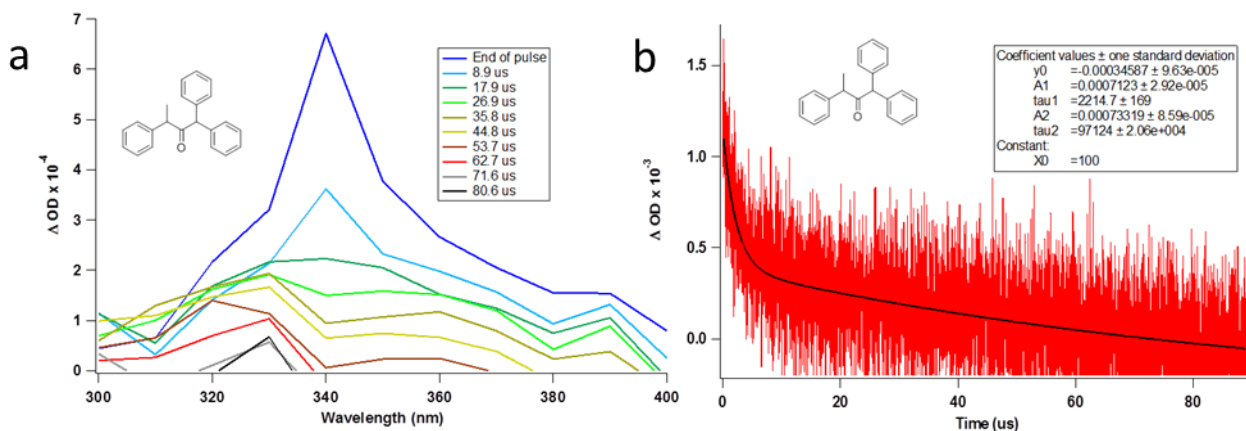


**Figure 5.S49:** (a) Transient Spectroscopy of 1,2,2-triphenylethan-1-one in nanocrystalline suspensions ( $\lambda_{\max} = 320$  nm) and (b) transient decay of 1,2,2-triphenylethan-1-one in nanocrystalline suspensions ( $\lambda_{\max} = 320$  nm)

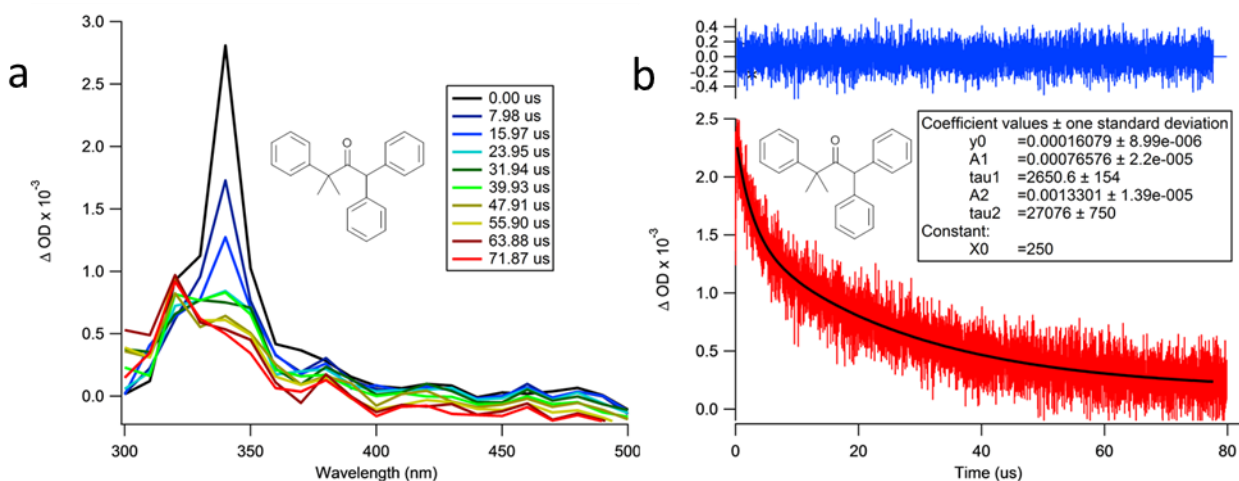


**Figure 5.S50:** (a) Transient Spectroscopy of 1,1,3-triphenylpropan-2-one in nanocrystalline suspensions ( $\lambda_{\max} = 330$  nm) and (b) transient decay of 1,1,3-triphenylpropan-2-one in nanocrystalline suspensions ( $\lambda_{\max} = 330$  nm)

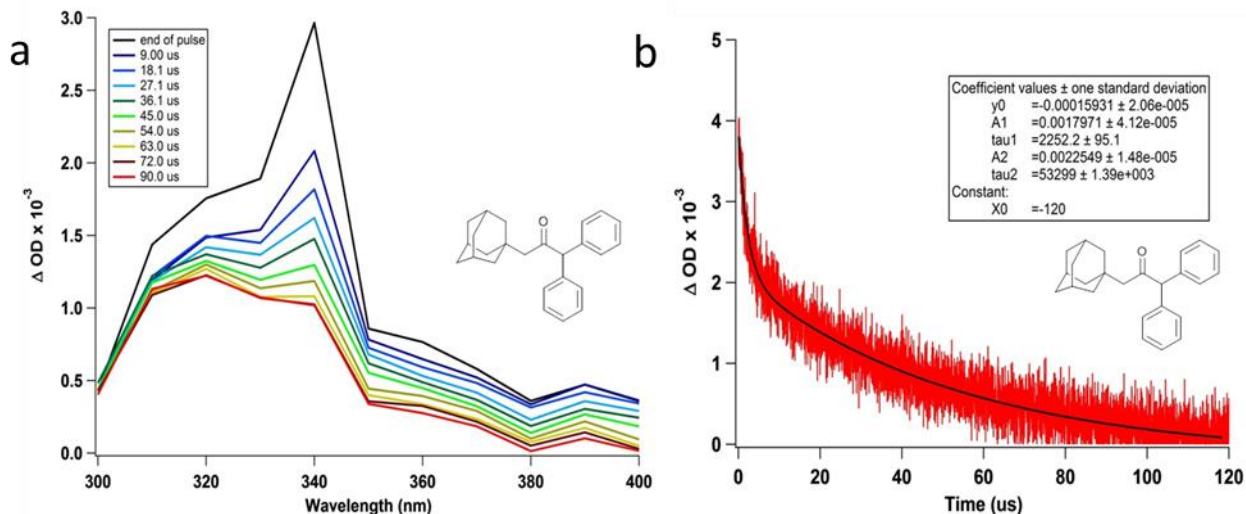




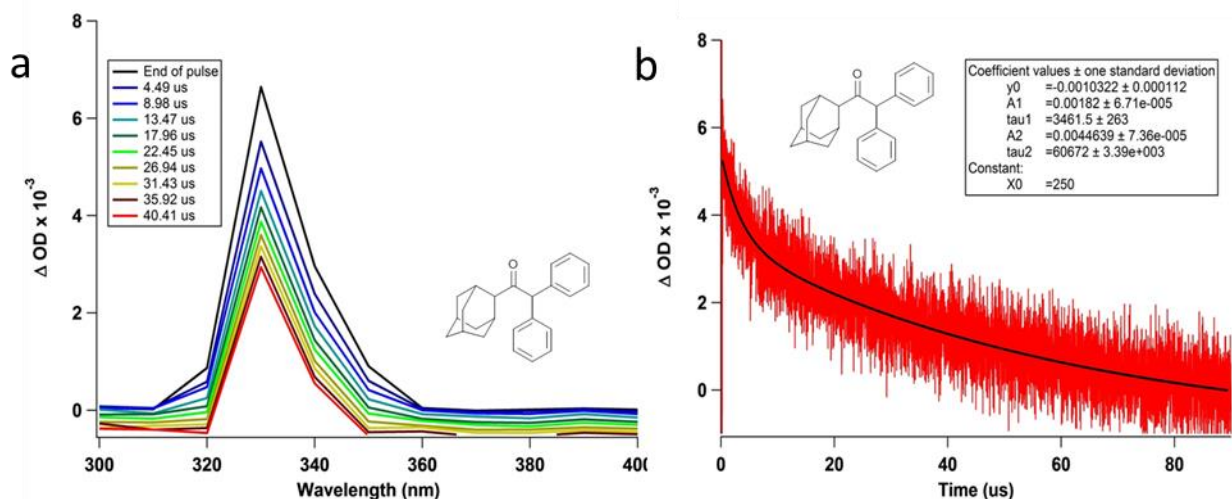
**Figure 5.S51:** (a) Transient Spectroscopy of 1,1,3-triphenylbutan-2-one in nanocrystalline suspensions ( $\lambda_{\text{max}} = 340 \text{ nm}$ ) and (b) transient decay of 1,1,3-triphenylbutan-2-one in nanocrystalline suspensions ( $\lambda_{\text{max}} = 340 \text{ nm}$ )



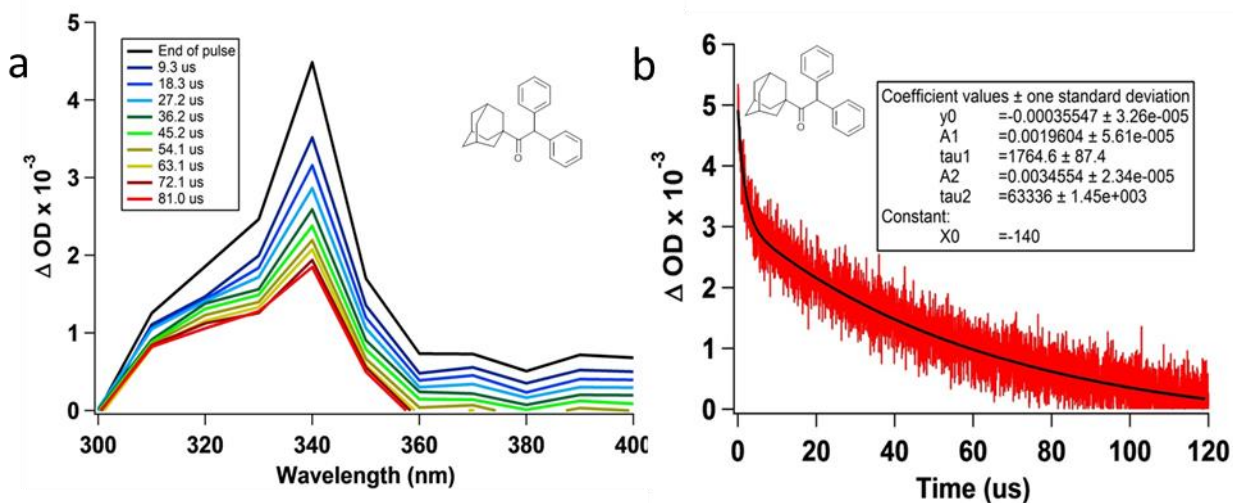
**Figure 5.S52:** (a) Transient Spectroscopy of 3-methyl-1,1,3-triphenylbutan-2-one in nanocrystalline suspensions ( $\lambda_{\text{max}} = 340 \text{ nm}$ ) and (b) transient decay of 3-methyl-1,1,3-triphenylbutan-2-one in nanocrystalline suspensions ( $\lambda_{\text{max}} = 340 \text{ nm}$ )



**Figure 5.S53:** (a) Transient Spectroscopy of 3-((3r,5r,7r)-adamantan-1-yl)-1,1-diphenylpropan-2-one in nanocrystalline suspensions ( $\lambda_{\text{max}} = 330$  nm) and (b) transient decay of 3-((3r,5r,7r)-adamantan-1-yl)-1,1-diphenylpropan-2-one in nanocrystalline suspensions ( $\lambda_{\text{max}} = 330$  nm)

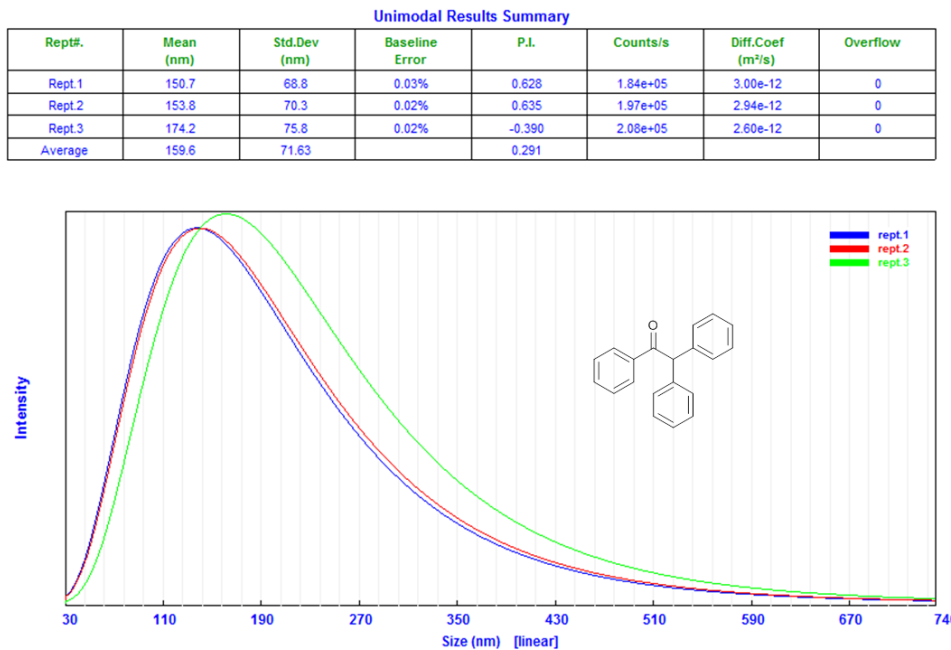


**Figure 5.S54:** (a) Transient Spectroscopy of 1-((1r,3r,5r,7r)-adamantan-2-yl)-2,2-diphenylethan-1-one in nanocrystalline suspensions ( $\lambda_{\text{max}} = 330$  nm) and (b) transient decay of 1-((1r,3r,5r,7r)-adamantan-2-yl)-2,2-diphenylethan-1-one in nanocrystalline suspensions ( $\lambda_{\text{max}} = 330$  nm)

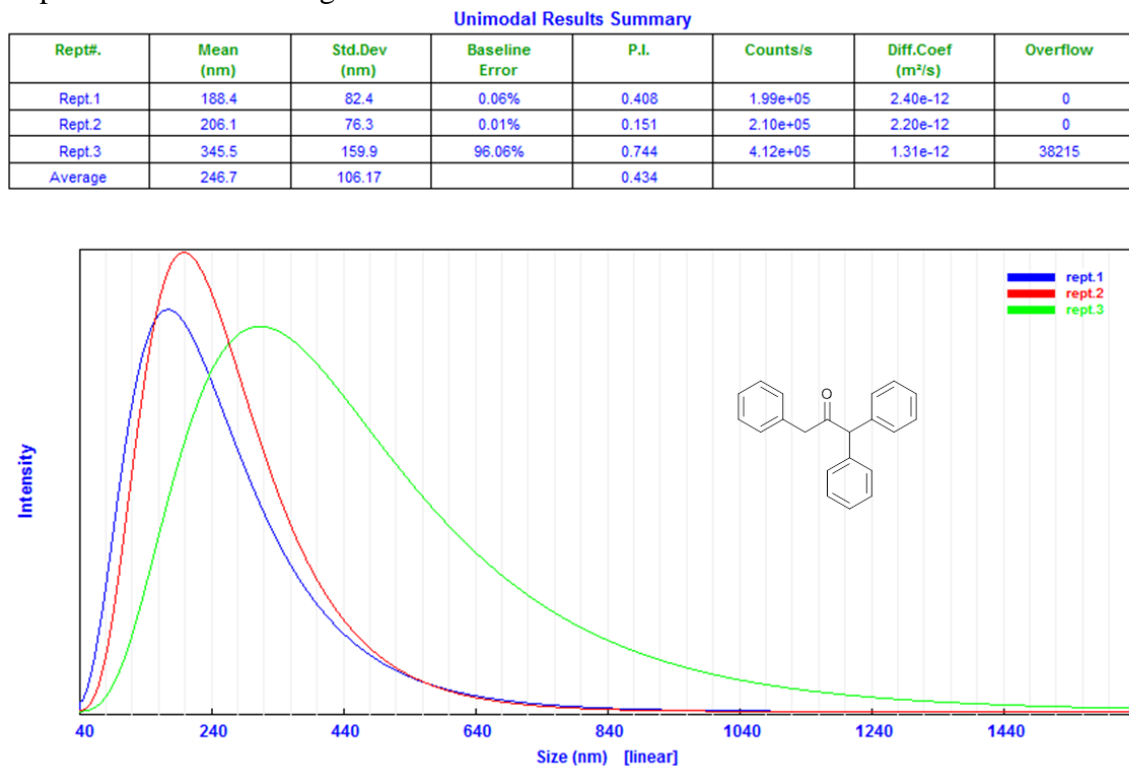


**Figure 5.S55:** (a) Transient Spectroscopy of 1-((3r,5r,7r)-adamantan-1-yl)-2,2-diphenylethan-1-one in nanocrystalline suspensions ( $\lambda_{\text{max}} = 340 \text{ nm}$ ) and (b) transient decay of 1-((3r,5r,7r)-adamantan-1-yl)-2,2-diphenylethan-1-one in nanocrystalline suspensions ( $\lambda_{\text{max}} = 340 \text{ nm}$ )

### 5.4.7). Dynamic Light Scattering



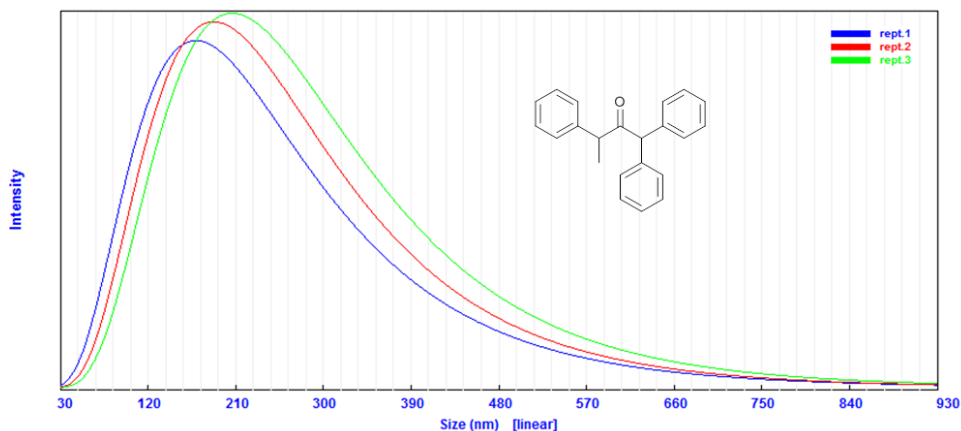
**Figure 5.S56:** Dynamic light scattering results of 1,2,2-triphenylethan-1-one in nanocrystalline suspension with an average value of 160 nm



**Figure 5.S57:** Dynamic light scattering results of 1,1,3-triphenylpropan-2-one in nanocrystalline suspension with an average value of 250 nm

**Unimodal Results Summary**

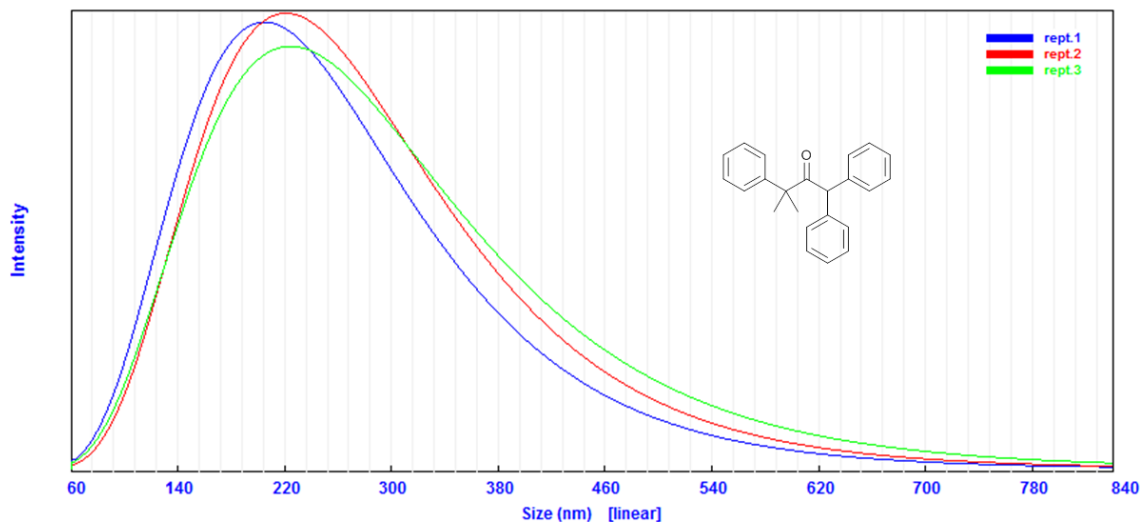
Rept#.	Mean (nm)	Std.Dev (nm)	Baseline Error	P.I.	Counts/s	Diff.Coeff (m <sup>2</sup> /s)	Overflow
Rept.1	187.5	88.7	0.01%	1.064	9.74e+04	2.41e-12	0
Rept.2	203.3	89.7	0.55%	0.439	1.02e+05	2.23e-12	0
Rept.3	221.9	95.0	0.35%	0.343	1.04e+05	2.04e-12	4
Average	204.2	91.12		0.615			



**Figure 5.S58:** Dynamic light scattering results of 1,1,3-triphenylbutan-2-one in nanocrystalline suspension with an average value of 200 nm

**Unimodal Results Summary**

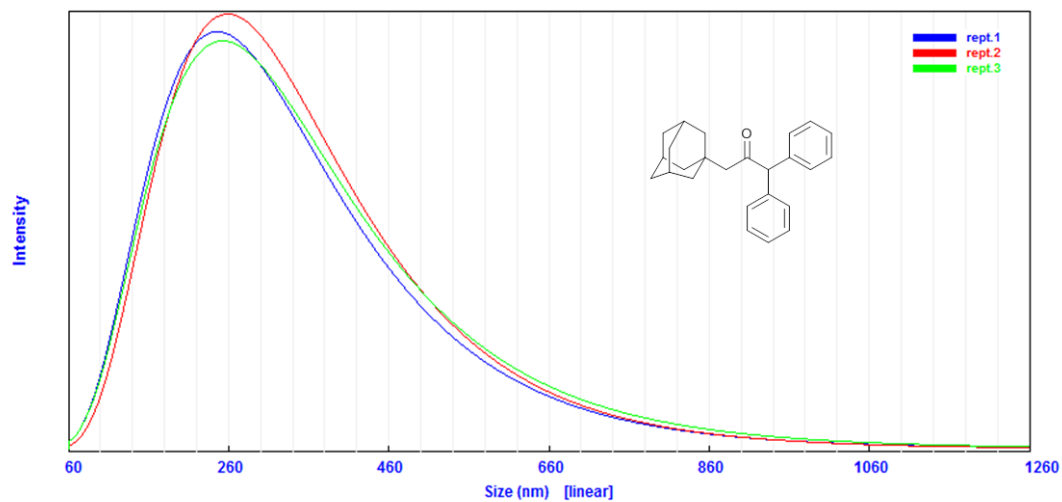
Rept#.	Mean (nm)	Std.Dev (nm)	Baseline Error	P.I.	Counts/s	Diff.Coeff (m <sup>2</sup> /s)	Overflow
Rept.1	210.9	74.1	0.08%	0.122	8.99e+05	2.15e-12	0
Rept.2	226.4	77.7	0.02%	0.111	9.78e+05	2.00e-12	0
Rept.3	233.9	87.9	0.00%	0.162	1.02e+06	1.93e-12	0
Average	223.8	79.91		0.132			



**Figure 5.S59:** Dynamic light scattering results of 3-methyl-1,1,3-triphenylbutan-2-one in nanocrystalline suspension with an average value of 220 nm

Unimodal Results Summary

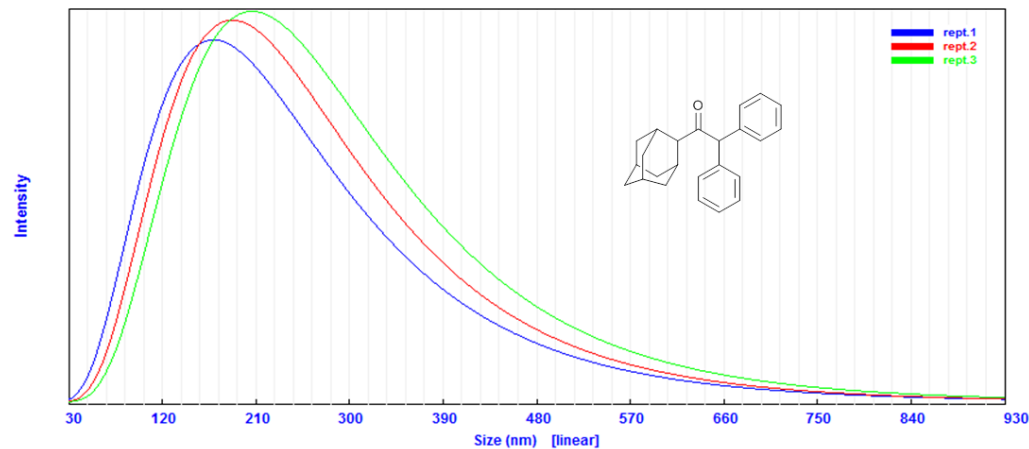
Rept.#	Mean (nm)	Std.Dev (nm)	Baseline Error	P.I.	Counts/s	Diff.Coeff (m <sup>2</sup> /s)	Overflow
Rept.1	261.4	107.1	0.00%	0.256	4.98e+05	1.73e-12	0
Rept.2	271.9	105.8	0.01%	0.192	4.97e+05	1.66e-12	0
Rept.3	270.5	114.0	0.00%	0.308	4.92e+05	1.67e-12	0
Average	267.9	106.98		0.252			



**Figure 5.S60:** Dynamic light scattering results of 3-((3r,5r,7r)-adamantan-1-yl)-1,1-diphenylpropan-2-one in nanocrystalline suspension with an average value of 270 nm

Unimodal Results Summary

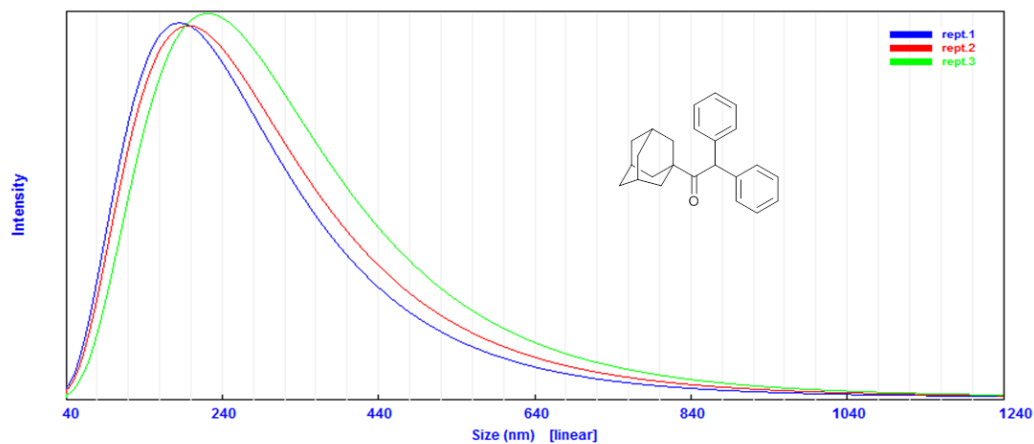
Rept.#	Mean (nm)	Std.Dev (nm)	Baseline Error	P.I.	Counts/s	Diff.Coeff (m <sup>2</sup> /s)	Overflow
Rept.1	187.5	88.7	0.01%	1.064	9.74e+04	2.41e-12	0
Rept.2	203.3	89.7	0.55%	0.439	1.02e+05	2.23e-12	0
Rept.3	221.9	95.0	0.35%	0.343	1.04e+05	2.04e-12	4
Average	204.2	91.12		0.615			



**Figure 5.S61:** Dynamic light scattering results of 1-((1r,3r,5r,7r)-adamantan-2-yl)-2,2-diphenylethan-1-one in nanocrystalline suspension with an average value of 200 nm

Unimodal Results Summary

Rept.#	Mean (nm)	Std.Dev (nm)	Baseline Error	P.I.	Counts/s	Diff.Coeff (m <sup>2</sup> /s)	Overflow
Rept.1	206.2	99.0	0.64%	1.484	3.49e+04	2.19e-12	0
Rept.2	220.4	106.9	0.24%	1.995	3.45e+04	2.05e-12	0
Rept.3	243.9	113.3	0.12%	0.786	3.48e+04	1.86e-12	0
Average	223.5	106.39		1.422			



**Figure 5.S62:** Dynamic light scattering results of 1-((3r,5r,7r)-adamantan-1-yl)-2,2-diphenylethan-1-one in nanocrystalline suspension with an average value of 220 nm

## 5.5 Reference

- 1). (a) Ariel, S.; Askari, S.; Evans, S. V.; Hwang, C.; Jay, J.; Scheffer, J. R.; Trotter, J.; Walsh, L.; Wong, Y.-F. *Tetrahedron*, **1987**, *43* (7), 1253-1272. (b) Aoyama, H.; Hasegawa, T.; Omote, Y. *J. Am. Chem. Soc.*, **1979**, *101*, 5343-5347. (c) Zimmerman, H. E.; Zuraw, M. J. *J. Am. Chem. Soc.*, **1989**, *111* (6), 2358-2561.
- 2). (a) Cerullo, G.; Garavelli, M. *Nature*, **2017**, *9*, 506-507. (b) Shiraki, S.; Natarajan, A.; Garcia-Garibay, M. A. *Photochem. Photobiol. Sci.*, **2011**, *10*, 1480.
- 3). (a) Ng, D.; Yang, Z.; Garcia-Garibay, M. A. *Org. Lett.*, **2004**, *6*, 645-647. (b) Reneta, H.; Zhou, Q.; Baran, P. S. *Science*, **2013**, *339* (6115), 59-63.
- 4). (a) Ramamurthy, V.; Gupta, S. *Chem. Soc. Rev.*, **2015**, *44*, 119. (b) Cole, J. M.; Irie, M. *CrystEngComm*, **2016**, *18*, 7175-7179. (c) Medishetty, R.; Park, I.-H.; Lee, S. S.; Vittal, J. *J. Chem. Comm.*, **2016**, *21*, 3989-4001. (d) Ramamurthy, V.; Venkatesan, K. *Chem. Rev.*, **1987**, *87* (2), 433-481
- 5). (a) Zhang, J.; Zou, Q.; Tian, H. *Adv. Mater.*, **2013**, *25*, 378-399. (b) Warren, M.; Brayshaw, S.; Johnson, A.; Schiffers, S.; Raithby, P.; Easun, T.; George, M.; Warren, J.; Teat, S. *Angew. Chem. Int. Ed.*, **2009**, *121*, 5821-5824. (c) Kim, C. D.; Pillet, S.; Wu, G.; Fullagar, W. K.; Coppens, P. *Acta Cryst. A*, **2002**, *58*, 133-137. (d) Coppens, P. *Angew. Chem. Int. Ed.*, **2009**, *48*, 4280-4281. (e) Hernández-Linares, M. G.; Guerrero-Luna, G.; Pérez-Estrada, S.; Ellison, M.; Ortin, M.-M.; Garcia-Garibay M. A. *J. Am. Chem. Soc.*, **2015**, *137*, 1679.
- 6). (a) Zimmerman, H. E.; Zuraw, M. J. *J. Am. Chem. Soc.*, **1989**, *111*, 2358-2361. (b) Ihmels, H.; Scheffer, J. R. *Tetrahedron*, **1999**, *55*, 885-907. (c) Borecka, B.;



- Gudsmundottir, A. D.; Olovsson, G.; Ramamurthy, V.; Scheffer, J. R.; Trotter, J. *J. Am. Chem. Soc.*, **1994**, *116* (22), 10322–10323.
- 7). (a) Coppens, P.; Novozhilova, I.; Kovalevsky, A. *Chem. Rev.*, **2002**, *102*, 861–884. (b) Dunitz, J. D.; Schomaker, V.; Trueblood, K. N. *J. Phys. Chem.*, **1988**, *92*, 856–867.
- 8). (a) Cohen, M. D.; Schmidt, G. M. J. *J. Chem. Soc.*, **1964**, 1996–2000. (b) Cohen, M. D. *Angew. Chem. Int. Ed.*, **1975**, *14*, 386–393.
- 9). (a) Garcia-Garibay, M. A. *Acc. Chem. Res.*, **2003**, *36*, 491–498. (b) Bragg, W. H; Bragg, W. L. *Proc. R. Soc. London Ser. A*, **1913**, *88*, 428–438. (c) MacGillivray, L. R.; Reid, J. L.; Ripmeester, J. A. *J. Am. Chem. Soc.* **2000**, *122*, 7817–7818. (d) Biradha, K.; Santra, R. *Chem. Soc. Rev.*, **2013**, *42*, 950–967.
- 10). (a) Tsentelovich, Y. P.; Fischer, H. *J. Chem. Soc. Perkin Trans.*, **1994**, *2*, 729–733. (b) Marchioro, A.; Teuscher, J.; Friedrich, D.; Mariunus, K.; Krol, R.; Moehl, T.; Gratzel, M.; Moser, J.-E. *Nature Photonics*, **2014**, *8*, 250–255. (c) Barra, M.; Bohne, C.; Scaiano, J. C. *Photochem Photobiol.*, **1991**, *54*, 1–5.
- 11). (a) Yamaji, M.; Kida, M. *J. Phys. Chem. A*, **2013**, *117* (9), 1946–1951. (b) Gershgoren, E.; Banin, U.; Ruhman, S. *J. Phys. Chem. A*, **1998**, *102*, 9–16. (c) Leyva, E.; Platz, M. S.; Niu, B.; Wirz, J. *J. Phys. Chem.*, **1987**, *91* (9), pp 2293–2298.
- 12). (a) Wilkinson, F.; Kelly, G. Diffuse reflectance flash photolysis. In *Handbook of Organic Photochemistry*; Scaiano, J. C., Ed.; CRC Press: Boca Raton, FL, **1989**; Vol. 1, Chapter 12, pp 293–314. (b) Kessler, R. W.; Krabichler, G.; Uhl, S.; Oelkrug, D.; Hagan, W. P.; Hyslop, J.; Wilkinson, F. *Opt. Acta* **1983**, *30*, 1099.
- 13). Kessler, R.W.; Krabichler, G.; Uhl, S.; Oelkrug, D.; Hagan, W. P.; Hyslop, J.; Wilkinson, F. *Opt. Acta* **1983**, *30*, 1099.

- 14). (a) Polli, D.; Altoe, P.; Weingart, W.; Spillane, K. M.; Manzoni, C.; Brida, D.; Tomasello, G.; Giorgio, D.; Kukura, P.; Mathies, R. A.; Garavelli, M.; Cerullo, G. *Nature*, **2010**, *467*, 440–443. (b) Cerullo, G.; Garavelli, M. *Nature*, **2017**, *9*, 506-507.
- 15). (a) Doan, S.C.; Kuzmanich, G.; Gard, M. N.; Garcia-Garibay, M.A.; Schwarts, B.J. *J. Phys. Chem. Lett.*, **2012**, *3*, 81-86. (b) G. Kuzmanich, M. N. Gard and M. A. Garcia-Garibay *J. Am. Chem. Soc.*, **2009**, *131*, 11606–11614. (c) G. Kuzmanich, A. Natarajan, K. K. Chin, M. Veerman, C. J. Mortko and M. A. Garcia-Garibay *J. Am. Chem. Soc.*, **2008**, *130*, 1140–1141. (c) Kuzmanich, G.; Spanig, F.; Tsai, C.-K.; Um, J. M.; Hoekstra, R. M.; Houk, K. N.; Guldi, D. M.; Garcia-Garibay, M. A. *J. Am. Chem. Soc.*, **2011**, *133*, 2342–2345.
- 16). Rajca, A.; Tolbert, L. M. *J. Am. Chem. Soc.*, **1988**, *110*, 871.
- 17). Adams, R.; Ulich, L. H. *J. Am. Chem. Soc.*, **1920**, *42* (3), 599–611.
- 18). Kuzmanich, G.; Natarajan, A.; Shi, Y.; Patrick, B.O.; Scheffer, J.R.; Garcia-Garibay, M. *A. Photochem. Photobio. Sci.*, **2011**, *10*, 1731-1734.
- 19). (a) Reddy, A. R.; Bendikov, M. *Chem. Commun.*, **2006**, 1179-1181. (b) Rao, V. J.; Uthuramu, K.; Ramamurthy, V. *J. Org. Chem.*, **1982**, *47*, 127-131
- 20). (a) Chung, T. S.; Ayitou, A. J.-L.; Park, J. H.; Breslin, V. M.; Garcia-Garibay, *Phys. Chem. Lett.*, **2017**, *8*, 1845–1850. (b) Chung, T.S.; Park, J.H.; Garcia-Garibay, M. A. *J. Org. Chem.*, **2017**, *82*, 12128–12133.
- 21). Park, J. H.; Hughs, M.; Chung, T. S.; Ayitou, A. J.-L.; Breslin, V. M.; Garcia-Garibay, M. *A J. Am. Chem. Soc.* **2017**, *139*, 13312–13317.